

THE UNIVERSITY *of* EDINBURGH

This thesis has been submitted in fulfilment of the requirements for a postgraduate degree (e. g. PhD, MPhil, DClinPsychol) at the University of Edinburgh. Please note the following terms and conditions of use:

- This work is protected by copyright and other intellectual property rights, which are retained by the thesis author, unless otherwise stated.
- A copy can be downloaded for personal non-commercial research or study, without prior permission or charge.
- This thesis cannot be reproduced or quoted extensively from without first obtaining permission in writing from the author.
- The content must not be changed in any way or sold commercially in any format or medium without the formal permission of the author.
- When referring to this work, full bibliographic details including the author, title, awarding institution and date of the thesis must be given.

An assessment of small vessel disease in human post-mortem tissue through radiology and histology

Catherine Anne Humphreys

Doctor of Philosophy

The University of Edinburgh

2022

TABLE OF CONTENTS

Declaration xi

Abstract xiii

Lay summary xvii

Acknowledgements xix

Publications xxi

List of tables xxiii

List of figures xxv

List of abbreviations xxxi

PART A: UNDERSTANDING THE LANDSCAPE OF SPORADIC HUMAN SMALL VESSEL DISEASE

CHAPTER 1: INTRODUCTION 1

1.1 Background to small vessel disease – how big is the problem? 1

1.2 Structure of the brain 3

1.2.1 Vascular anatomy of the brain 3

1.2.3 The perivascular space 16

1.2.4 The neurovascular unit 20

1.3 Clinical aspects of small vessel disease 24

1.3.1 Epidemiology 25

1.3.2 Diagnosis 26

1.4 Small vessel disease neuroimaging 27

1.4.1 The STandards for Reporting Vascular changes on nEuroimaging guidelines 27

1.4.2 Radiological white matter hyperintensities 31

1.4.3 Lacunes 34

1.4.4 Enlarged perivascular spaces 34

1.4.5 Recent small subcortical infarcts 36

1.4.6 Microbleeds 37

1.4.7 Brain atrophy 38
1.5 The histopathology of small vessel disease 39
1.5.1 Vascular small vessel disease lesions 39
1.5.2 Parenchymal small vessel disease lesions 42
1.5.3 Cerebral amyloid angiopathy 45
1.5.4 Histological examination 45
1.6 Risk factors 47
1.6.1 Hypertension 47
1.6.2 Age 47
1.6.3 Inflammation 48
1.6.4 Salt 49
1.6.5 Cognitive and brain reserve 49
1.7 Pathophysiology of small vessel disease 50
1.7.1 Historical work 50
1.7.2 Vascular dysfunction 51
1.8 Genetics of small vessel disease 55
1.8.1 Monogenic SVD 56
1.8.2 Other single genes 61
1.9 Work in animal models 63
1.9.1 The spontaneously hypertensive stroke-prone rat 63
1.9.2 Vascular mechanisms 65
1.10 Research hypothesis 70
1.11 Justification for this project 70
1.12 Outline methods 73
1.13 Aims 74
1.14 Objectives 74

CHAPTER 2: CORRELATIONS IN POST-MORTEM IMAGING-HISTOPATHOLOGY STUDIES OF SPORADIC HUMAN CEREBRAL SMALL VESSEL DISEASE: A SYSTEMATIC REVIEW 77

2.1 Introduction 77
2.2 Methods 79
2.2.1 Search terms 79

2.2.2 Inclusion and exclusion criteria *80*
2.2.3 Quality of reporting *81*
2.2.4 Data extraction *81*
2.3 Results **83**
2.3.1 Study quality *83*
2.3.2 Study characteristics *89*
2.3.3 Magnetic resonance imaging methods *94*
2.3.4 Autopsy and histological methods *97*
2.3.5 Pathological terminology and definitions *100*
2.3.6 Papers studying white matter hyperintensities *106*
2.3.7 Papers studying enlarged perivascular spaces and lacunes *114*
2.3.8 Magnetic resonance imaging-histopathological correlations on microinfarcts *116*
2.3.9 Cerebral amyloid angiopathy *119*
2.4 Discussion **121**
2.5 Conclusions **126**
2.6 Hypotheses **127**

PART B: METHODS

CHAPTER 3: METHODS **129**

3.1 Developing the cohorts **129**
3.1.1 Background to human tissue donation and brain banking **129**
3.1.2 The MRC Edinburgh Brain Bank **130**
3.1.3 The cohorts used in this thesis **133**
3.1.4 Case selection **138**
3.1.5 In vivo imaging **139**
3.2 Review of cases in the brain bank **140**
3.2.1 Background **140**
3.2.2 Methods used for the retrospective case review **140**

3.3 Constructing histopathological small vessel disease terminology and standards 142

***3.3.1 Background* 142**

***3.3.2 Methods for constructing histopathological small vessel disease terminology and standards* 142**

3.4 Prospective ex vivo imaging 143

***3.4.1 Background* 143**

***3.4.2 Developing the protocol and troubleshooting* 145**

***3.4.3 Methods for prospective ex vivo imaging* 151**

3.5 Grading the burden of SVD on ex vivo MRI 151

***3.5.1 Background* 151**

***3.5.2 Developing the ex vivo MRI assessment* 152**

3.6 Histological SVD assessment 156

***3.6.1 Post-mortem tissue processing* 156**

***3.6.2 Grading SVD on histology* 159**

3.7 Developing the image registration methods 160

***3.7.1 PowerPoint* 160**

***3.7.2 Matlab* 164**

***3.7.3 Methods used to carry out direct lesion comparisons* 171**

PART C: EXPERIMENTAL WORK AND RESULTS

CHAPTER 4: ASSESSMENT OF THE BRAIN BANK CASE REVIEW AND DEFINING THE HISTOPATHOLOGY 173

4.1 The histopathological brain bank case review 173

***4.1.1 Results* 173**

***4.1.2 Discussion* 176**

4.2 Histopathological small vessel disease definitions 179

4.3 Pathological assessment and grading of SVD burden 185

***4.3.1 Histological processing* 185**

***4.3.2 Microscopic assessment and grading* 185**

***4.3.3 Discussion* 192**

CHAPTER 5: A PROTOCOL FOR PRECISE COMPARISONS OF SMALL VESSEL DISEASE LESIONS BETWEEN EX VIVO MAGNETIC RESONANCE IMAGING AND HISTOPATHOLOGY 193

5.1 Introduction 193

5.2 A protocol for precise comparisons of small vessel disease lesions between ex vivo magnetic resonance imaging and histopathology 194

***5.2.1 Background* 194**

***5.2.2 Post-mortem neuropathological examination* 196**

***5.2.3 Post-mortem magnetic resonance imaging* 197**

***5.2.4 Histology* 200**

***5.2.5 Image registration and analysis* 200**

***5.2.6 Study outcomes* 204**

***5.2.7 Estimates of likely numbers of cases* 204**

***5.2.8 Statistical analyses* 205**

5.3 Progress with implementation and discussion 206

5.4 Protocol development 208

5.5 Conclusions 212

CHAPTER 6: RESULTS OF EX VIVO ASSESSMENTS 215

6.1 All scanned cases 215

***6.1.1 Demographics* 215**

***6.1.2 Post-mortem information* 218**

***6.1.3 Medical conditions* 219**

***6.1.4 Discussion* 221**

6.2 Results of SVD burden assessment on ex vivo magnetic resonance imaging 223

***6.2.1 Demographics* 223**

***6.2.2 Ex vivo magnetic resonance imaging assessments* 223**

***6.2.3 Discussion* 226**

6.3 Results of SVD burden assessment on histology 228

***6.3.1 Demographics* 228**

***6.3.2 Histological assessments* 230**

***6.3.3 Discussion* 238**

6.4 Results of direct lesion comparisons **243**

6.4.1 Lesions identified on post-mortem magnetic resonance imaging **243**

6.4.2 Lesions identified on histology **270**

6.4.3 Artefacts **279**

6.4.4 Discussion **279**

CHAPTER 7: PROTEIN ASSESSMENT OF WHITE MATTER DAMAGE IN HUMAN POST-MORTEM TISSUE WITH NEURORADIOLOGICALLY DOCUMENTED SMALL VESSEL DISEASE **287**

7.1 Background **287**

7.1.1 Fiji/Image J **288**

7.1.2 Commercially available tools **288**

7.1.3 Stereology estimation of protein expression **289**

7.1.4 Biochemical protein assessment **289**

7.2 Materials and methods **291**

7.2.1 Stereology methods **291**

7.2.2 Biochemical methods **293**

7.3 Results **303**

7.3.1 Stereology **303**

7.3.2 Biochemical study **308**

7.4 Discussion **324**

7.4.1 Stereology **324**

7.4.2 Biochemical study **326**

PART D: CONCLUSIONS

CHAPTER 8: FINAL DISCUSSION **333**

8.1 The main outputs of this thesis **333**

8.1.1 Systematic review **333**

8.1.2 New methods **335**

8.1.3 Experimental findings **338**

8.1.4 How this data contributes to our understanding of SVD **339**

8.2 Recent relevant findings in SVD **340**

8.3 Future work needed in SVD research **342**

8.3.1 Developing the work in this thesis **343**

8.4 Relevance of human tissue studies **346**

8.4.1 The need to understand a human disease using human tissue **346**

8.4.2 Brain banking **347**

8.5 Final conclusion **348**

PART E: APPENDICES AND REFERENCES

APPENDICES **351**

APPENDIX 1: Library of histological terminology used to describe SVD-related histological lesions and the definitions used for these terms 351

APPENDIX 2: MRC Edinburgh Brain Bank Information booklet 369

APPENDIX 3: Ex vivo MRI tissue block SVD assessment 373

APPENDIX 4: Ex vivo MRI tissue block SVD assessment – Infarcts and lacunes 375

APPENDIX 5: H&E staining protocol 376

APPENDIX 6: Additional immunohistochemical stain details 377

APPENDIX 7: Histological SVD grading proforma 378

APPENDIX 8: Demographic data for cases used to assess SVD burden on ex vivo imaging and histopathology 380

APPENDIX 9: Individual scores for grading SVD burden on ex vivo MRI 385

APPENDIX 10: Individual scores for grading SVD burden on histology 387

APPENDIX 11: Standard curves for biochemical studies 389

APPENDIX 12: Scatterplots showing MAG:PLP1 values according to histological SVD scores 391

APPENDIX 13: Scatterplots showing exploratory analysis of fibrinogen relationship with markers of hypoxia 392

APPENDIX 14: Angiotensin-II level in the white matter did not differ between controls, SVD and AD 393

APPENDIX 15: Scatterplots showing no correlation between histologically assessed SVD and levels of VEGF, VWF, fibrinogen, PDGFRB, AngII or Aβ42 394

REFERENCES **397**

Declaration

I confirm that this thesis was written by myself and that the work contained herein is my own original work except where explicitly stated otherwise in the text. All sources of data and information have been specifically referenced. I have not submitted this work for any other degree or professional qualification.

Catherine Anne Humphreys

2022

Abstract

Sporadic human cerebral small vessel disease (SVD) is a significant problem in our aging population. It is the most common cause of haemorrhagic stroke, causes one quarter of all ischaemic strokes, causes vascular dementia and synergistically worsens other dementias. It also causes a range of other psychological and physical problems and is increasingly common with increased age. SVD is well characterised on neuroimaging, with lesions throughout the brain, and particularly in the white matter. The cause(s) and pathophysiological mechanisms underlying the development of SVD, however, remain poorly understood with poor correlations between the abnormalities seen at the cellular level, on neuroimaging, and clinically.

There are many theories as to the cause of SVD. However, observational studies and experimental evidence point towards an abnormality in the small vasculature of the brain initiating a cascade of events leading to a variety of vascular and brain parenchymal lesions. What these abnormalities are, and how exactly they result in the pathology seen, is unknown. Different structural components of the vessel wall and parenchymal brain cells appear to be involved, as well as functional abnormalities such as abnormal vascular reactivity. Risk factors also play a role, hypertension being the most significant, but how these interact with the normal vasculature is not fully understood.

To provide an overview of our current understanding of SVD in human tissue I first completed a systematic review of the literature comparing the appearances of SVD on post-mortem imaging and histology. This revealed the inconsistency in methods and reporting in these studies and the lack of histopathology agreement on SVD terminology and definitions.

I then studied the histological appearances of the lesions identified by post-mortem imaging to provide a reliable precise histological-imaging correlation. I developed a new protocol for *ex vivo* 7 Tesla magnetic resonance imaging

(7T MRI) scanning of human brain tissue on post-mortem material and developed a grading system to assess SVD burden on MRI and histology with histological definitions, to try to encourage standardised, comprehensive and transparent reporting so that results in small studies can be more easily compared. I studied human post-mortem brain tissue to better investigate the disease in the appropriate context.

In our cases from individuals with haemorrhagic SVD, normal aging and young controls, the most severe SVD pathology on *ex vivo* imaging and histology was, as expected, in the haemorrhagic SVD group. The normal aging group also had significant levels of pathology, perhaps representing the increasing burden of disease present but not necessarily detected clinically with increased age. It is possible the underlying pathophysiology in this group might develop by different mechanisms compared to the haemorrhagic group. Directly comparing the imaging and histological lesions confirmed the histological appearances of some lesions on imaging such as enlarged perivascular spaces, lacunes, microinfarcts and microbleeds. However, making direct comparisons is complex. Some lesions, such as small vessel fibrinoid necrosis, presumed to be below the resolution for detection on 7T MRI, were identified on both histology and imaging. Some features seen on histology in association with recognised SVD lesions, such as perivascular inflammation in an area of white matter rarefaction, were present in a variety of different histological contexts with no apparent correlation on imaging. And some lesions, such as white matter rarefaction around enlarged perivascular spaces, were present often on both imaging and histology, but their significance and contribution to SVD is unknown.

To try to further understand the mechanisms underlying SVD and the lesions seen on imaging I undertook biochemical studies of protein expression in the deep white matter of the haemorrhagic SVD group, young controls and an Alzheimer's disease group, who also have white matter pathology on neuroimaging. Increased fibrinogen levels suggested vascular leakage in both disease groups. However, haemorrhagic SVD had more severe white

matter hypoxic changes and increased vasoconstrictor levels while in Alzheimer's disease there was increased amyloid β42 and levels of a pericyte marker, possibly reflecting different pathophysiological mechanisms causing the similar appearing radiological changes.

When assessing radiologically defined white matter hyperintensities (WMH) I found hypoxic-induced changes throughout brains with WMH, including in normal appearing areas of white matter. This suggests these brains have abnormalities in areas that appear radiologically normal, as found in *in vivo* imaging studies.

To conclude, this work has confirmed the importance of reaching a consensus in histopathological reporting, terminology and definitions which is a basic requirement before we can better understand the pathophysiology of SVD. This has led to the formation of definitions and a practical grading system that could be used as a basis upon which to build a future agreement. The complexity of the histological lesions underlying radiological SVD changes was apparent, and the frequency with which some other potentially important histological changes were identified suggests these have not, to date, been fully appreciated. Investigating the underlying mechanisms of white matter hyperintensities showed vascular leakage was a shared abnormality in two different diseases with white matter changes on imaging, suggesting it may be a common factor upon which variable pathways converge. Future work is needed to further understand the importance of these less well characterised histological features. Investigating the role of vascular leakage and exploring drugs that maintain or improve vascular integrity could be a potential route for helping to treat SVD. Studies into underlying transcriptomic abnormalities around vascular leakage in human tissue may be informative.

Lay Summary

Small vessel disease (SVD) is an important cause of dementia and stroke and becomes more common with age. In our aging population it will become an increasingly important cause of illness. We do not, however, understand how or why it develops, and because of this, we do not know how to prevent or treat it.

SVD affects the microscopic blood vessels within the brain and causes a range of abnormalities on brain scans of people while they are alive. However, the actual changes to the cells of the brain are not understood; that is, although we can see changes in the brain on a scan, we do not know what these changes actually mean for the cells of the brain. I reviewed published scientific articles and found that the language and definitions used to describe the microscopic changes seen in the cells are complicated and confused. If we are to make progress to better understand SVD and enable development of drugs to better treat or prevent it, as researchers we need to first of all be talking the same language. Then we can be sure we are describing the same things and would be able to compare our findings. After reviewing nearly 200 cases by microscopically examining the cells and studying brain scans, I have proposed definitions and a system for grading SVD such that changes seen down the microscope can be compared to the changes on brain scans.

To find out what is happening in the cells where the brain scan shows abnormalities, I devised a method to perform brain scanning on small pieces of brain tissue donated for research from people who have died. I used this to compare the appearances of abnormalities on these scans with those of the cells down the microscope, precisely comparing the exact same lesions to see what is happening in them at the cellular level. I found that some lesions match up well between the brain scan and microscopic appearances. Some however, are more complex, with a range of different appearances,

and some changes that were often seen in the cells have not previously been considered part of SVD, so their role is unknown.

Cells are made of many different proteins, which have different roles in helping cells survive and communicate with each other. I looked at some of the proteins involved in the healthy brain and found changes in SVD that indicate the brain cells are not receiving enough oxygen and that the blood vessels become leaky. I also found that in the brains of people with SVD, changes may be present throughout the whole of the brain, not just the areas where abnormalities are seen on the scans.

To improve our knowledge of SVD in the future, pathologists who carry out microscopic examination of cells need to agree on the language and definitions they use to describe SVD. More research is needed specifically into the role of the lesser-known cellular abnormalities. Genes tell cells how and when to make proteins, and changes in genes can result in abnormal proteins, ultimately causing diseases such as some kinds of cancer, dementia, and possibly SVD. In the future, I would like to carry out further investigations into the role of the leaky blood vessels by looking for changes in the genes of the cells that make up the blood vessels. If we can one day pinpoint changes in the cells or genes that cause SVD, then this may enable us to develop appropriate drugs to treat it.

Acknowledgements

I have many people to thank for their help and support in carrying out this work. I must firstly thank my supervisors, Colin Smith and Joanna Wardlaw for their guidance and wisdom. As a general histopathology trainee at the start of this I required training and patience to get up to speed in neuropathology and neuroimaging techniques and assessment. Their expertise and constructive advice has been immensely useful and will stand me in good stead well beyond the end of this PhD.

I worked with a number of collaborators throughout the project. In the imaging team, Victor González-Castro was the first to attempt to understand what we were trying to do in registering the images, with advice from Cyril Pernet. Susana Muñoz Maniega came in later and developed it further so that the final registration system in this thesis could not have happened without her time, dedication and understanding. The *ex vivo* imaging required the cooperation and efforts of the preclinical imaging team; Maurits Jansen and Ross Lennen went out of their way to optimise our images and ensure the tissue was where it needed to be when it needed to be there. Aidan Hutchison was always there to support the imaging and logistics.

This thesis has centred around the use of human tissue. The brain bank and neuropathology lab staff supported me all the way through and always worked with me, even when I came with slightly ridiculous requests, to make the project happen and obtain the best quality, most precise tissue samples I could ask for. Judith Pate and Karina McDade were invaluable in the lab and I am grateful for their lending me an ear and entertaining me when I needed it. I would like to thank Chris-Anne Mackenzie for keeping me right in all matters brain bank related, and Tracey Millar for her support and always having the answers I needed. Jamie Rose and Beverly Notman spent many hours in a dark room to make the histological slide digitisation possible. Kate Britton kept me right with expenses and admin. Francesca Chappell and

Emily Evans advice and statistical genius were invaluable in making sure I kept on the right track with the analyses.

These tissue samples would not have been available without the ultimate generosity of the cohort participants of LBC1936, LINCHPIN, the sudden death cohort and the SDBTB. I am immensely grateful to them and their families, friends and next of kin who made, and continue to make, this kind of research possible. The cohort coordinators for allowing me to access their tissue and data; Ian Deary, Simon Cox, Rustam Al-Shahi Salman and Tom Russ, and Mark Rodrigues and Tom Moullaali for providing *in vivo* imaging ratings.

I would like to thank Chris Henstridge for his expertise and access to the stereology facility. In Bristol I collaborated with Seth Love and Scott Miners, who took me as a novice in the lab and gave me their time, knowledge and expertise, both in person and remotely, to enable the biochemical analysis.

I would like to express my gratitude to the Stroke Association, who supported the development of this work through the Princess Margaret Research Development Fund, and to the Alzheimer's Society who funded my clinical academic fellowship and the research in this thesis.

Finally, I want to thank my friends for providing motivation and support, in particular Daisy, who understood what I was going through when it really mattered. And to my family; my parents and parents-in-law who gave me precious time to get this done. My girls, who inspire me to work hard every day, and Chris – I can't list everything you have done but this could not have happened without you.

Publications

Published papers

Humphreys CA, Smith C, Wardlaw JM. (2021) Correlations in post-mortem imaging-histopathology studies of sporadic human cerebral small vessel disease: a systematic review. *Neuropathology and Applied Neurobiology*. 47 (7): 910-930.

Humphreys, C. A., Jansen, M. A., Munoz Maniega, S., Gonzalez-Castro, V., Pernet, C., Deary, I. J., Al-Shahi Salman, R., Wardlaw, J. M., Smith, C. (2019) A protocol for precise comparisons of small vessel disease lesions between ex vivo magnetic resonance imaging and histopathology. *International Journal of Stroke*. 14 (3): 310-320.

Manuscript in preparation

Humphreys, C.A., Miners, J.S., Wardlaw J.M., Smith, C.S., Love, S. Biochemical assessment of white matter damage in human post-mortem tissue with neuroradiologically documented small vessel disease.

List of tables

Table 2.1 Systematic review search strategy 79

Table 2.2 Quality assessment 82

Table 2.3 Summary of papers studying non-haemorrhagic SVD 84

Table 4.1 Demographic details and scores of cases used for grading of SVD and neurodegenerative pathology in the brain bank case review 174

Table 4.2 Inter-rater agreement for pathological assessment of SVD and neurodegenerative pathology burden 177

Table 4.3. Histopathological definitions used to assess small vessel disease 180

Table 5.1 Areas affected by maximal radiological SVD in life selected for MR-histology comparison 196

Table 5.2 MR imaging sequences and their parameters 198

Table 5.3 Special stains and immunohistochemical stains used for assessment of SVD, vascular and neurodegenerative pathology 199

Table 5.4 Updated MR imaging sequences and their parameters 209

Table 5.5 Comparison of image registration methods 211

Table 6.1 Summary demographic details for all cases undergoing post-mortem MRI scanning with subsequent grading of SVD burden 216

Table 6.2 Summary of SVD grading burden by cohort on *ex vivo* MR 224

Table 6.3 Summary of cortical thickness measured on *ex vivo* 7T magnetic resonance imaging 225

Table 6.4 Summary of Histological grading of SVD burden by cohort 229

Table 6.5 Summary of cortical thickness measured on histology 232

Table 6.6 Results of paired t-tests comparing cortical thickness measurements at the three different sulcal depths in the three areas 233

Table 6.7 Results of paired t-tests comparing cortical thickness measurements in the three areas at the three different depths 234

Table 6.8 SVD features on histology and MRI considered to be equivalent 240

Table 6.9 Summary of the histological features underlying the radiological lesion appearances 244

Table 6.10 Summary of additional histological features seen in association with radiological enlarged PVS 251

Table 6.11 Summary of the radiological appearances of additional lesions identified on histology and then searched for retrospectively on post-mortem imaging 271

Table 7.1 Stereology individual case details 305

Table 7.2 Individual subject data for the biochemical study of markers comparing ICH-SVD, AD and controls 310

Table 7.3 Individual subject data for biochemical study investigating protein expression in white matter hyperintensities, normal appearing white matter and controls 314

List of figures

Figure 1.1 Schematic of cerebral vascular supply and the blood brain barrier 4

Figure 1.2 The structure of the perivascular space 5

Figure 1.3. Cerebrovascular basement membrane 14

Figure 1.4 The glymphatic pathway 19

Figure 1.5 MRI appearances of SVD-related lesions 29

Figure 1.6 MRI showing atrophy and white matter hyperintensities 30

Figure 1.7 Histological vascular lesions in SVD 41

Figure 1.8 Venous collagenosis 41

Figure 1.9 Parenchymal lesions associated with SVD 43

Figure 1.10 Key SVD mechanisms 57

Figure 2.1 Summary of the literature evaluation 80

Figure 2.2 frequency of reporting features used to measure study quality 89

Figure 2.3 Frequency of SVD risk factor reporting 93

Figure 2.4 Terminology used in histological lesion reporting 103

Figure 2.5 Myelin staining in white matter 104

Figure 2.6 Enlarged perivascular space 105

Figure 2.7 Lacunar infarct 105

Figure 2.8 Cortical microinfarct 106

Figure 3.1 Troubleshooting the MR post-mortem tissue scanning protocol 147

Figure 3.2 Monitoring temperature during MR scanning 150

Figure 3.3 Examples of SVD features on *ex vivo* MR images of small tissue samples 154

Figure 3.4 Image gallery for grading mineralisation in the basal ganglia on *ex vivo* MR images of small tissue samples 155

Figure 3.5 Overlaying images in PowerPoint 161

Figure 3.6 Mismatched image outlines 163

Figure 3.7 MR and histology image registration in Matlab 166

Figure 4.1 Comparing the age of the cohorts used in the brain bank case review 175

Figure 4.2 Histological features of small vessel disease 182

Figure 4.3 Grading histological white matter rarefaction 187

Figure 4.4 Grading histological perivascular space enlargement 188

Figure 4.5 Grading histological arteriolosclerosis 199

Figure 4.6 Grading histological iron deposition in the basal ganglia 190

Figure 5.1 Small tissue samples are placed in plastic cassettes for standard histological processing 197

Figure 5.2 A sample of frontal white matter, where the lack of anatomical landmarks can make comparison difficult. 202

Figure 5.3 The white matter vessel identified in Figure 5.2 is stained to interrogate the gliovascular unit and blood–brain barrier 203

Figure 5.4 High resolution *ex vivo* 7T MRI scans of small brain tissue samples 210

Figure 5.5 Significant cracking artefact sometimes seen on histology, making registration with the post-mortem MR impossible 210

Figure 6.1 Comparisons of cohort features in cases that underwent post mortem MRI 217

Figure 6.2. Scatterplots showing correlations of RIN value and factors that could affect tissue quality 219

Figure 6.3 Frequency of causes of death in cases used to assess SVD burden on imaging and histology 220

Figure 6.4 Frequency of cardiovascular disease in cases used to assess SVD burden on imaging and histology 220

Figure 6.5 Air bubble artefact on *ex vivo* imaging 227

Figure 6.6 Analysis of relationship between histologically graded arteriolosclerosis and hypertension 231

Figure 6.7 Line plots of differences comparing cortical thickness at different sulcal depths in the three brain areas 233

Figure 6.8 Line plots of differences comparing cortical thickness in the three brain areas at different sulcal depths 235

Figure 6.9. Bland Altman plots for the comparison of MR and histological cortical thickness measurements 237

Figure 6.10 Radiological subcortical deep white matter hyperintensity 246

Figure 6.11 Cavitating subcortical white matter hyperintensity 248

Figure 6.12 Radiological periventricular white matter hyperintensity 252

Figure 6.13 Area with multiple enlarged perivascular spaces 254

Figure 6.14 Multiple lesions in the basal ganglia 256

Figure 6.15 A longitudinally sectioned vessel 260

Figure 6.16 Multiple enlarged perivascular spaces 262

Figure 6.17 Enlarged perivascular space with hyperintensity 263

Figure 6.18 Microbleed on T2* 265

Figure 6.19 Superficial siderosis 266

Figure 6.20 T1 hyperintense foci 268

Figure 6.21 Histological arteriolosclerosis not visible on 7T post-mortem MRI 275

Figure 6.22 Perivascular collagenosis not visible on magnetic resonance imaging 276

Figure 6.23 Fibrinoid necrosis visible on 7T post-mortem MRI 278

Figure 7.1 *Ex vivo* MRI assessment of extent of WMHs for selection of tissue for biochemical assessment 295

Figure 7.2 Boxplots showing analysis of protein expression using stereology 306

Figure 7.3 Analysis of differences between amount of staining in WML and areas of NAWM using stereology 307

Figure 7.4 Flowchart illustrating which cases contributed tissue to which study groups 309

Figure 7.5 Boxplots of histological SVD scores in AD and ICH-SVD 316

Figure 7.6 *In vivo* neuroradiological assessment of white matter hyperintensity burden in AD and ICH-SVD 317

Figure 7.7 *In vivo* MRI revealed a greater degree to cortical atrophy in AD compared to ICH-SVD 317

Figure 7.8 Scatterplots comparing atrophy on *in vivo* imaging and histological assessment 318

Figure 7.9 Evidence of cerebral hypoperfusion and white matter ischaemia changes in ICH-SVD 319

Figure 7.10 Scatterplots showing a positive correlation between VEGF and VWF levels 320

Figure 7.11 Fibrinogen is increased in AD and ICH-SVD 321

Figure 7.12 EDN1 is increased in white matter in ICH-SVD 322

Figure 7.13 Increased Aβ42 and pericyte content in white matter in AD 323

Figure 7.14 Protein levels in WMH, NAWM and controls 324

List of abbreviations

Aß = amyloid-beta

A = arachnoid mater

AD = Alzheimer's disease

AD-NC = Alzheimer's disease neuropathological change

AIC = Akaike information criterion

ALB = albumin

angII = angiotensin-II

APOE = apolipoprotein

ARMD = age-related macular degeneration

AVP = arginine vasopressin

BBB = blood brain barrier

BRI2 = Adan gene

BRIC = Brain Research Imaging Centre

CAA = cerebral amyloid angiopathy

CADASIL = cerebral autosomal dominant arteriopathy with subcortical infarcts and leukoencephalopathy

CAPS = capillary

CARASAL = Cathepsin A-related arteriopathy with strokes and leukoencephalopathy

CARASIL = cerebral autosomal recessive arteriopathy with subcortical infarcts and leukoencephalopathy

CNS = central nervous system

COL4 = type 4 collagen

COL4A1 = collagen 4 A1

COL4A2 = collagen 4 A2

CSF = cerebrospinal fluid

CST3 = cystatin C gene

CT = computerised tomography

CTSA = cathepsin A

DAI = diffuse axonal injury

DNA = deoxyribonucleic acid

DTI = diffusion tensor imaging

DWI = diffusion weighted imaging

EDN1 = endothelin-1

ELISA = enzyme-linked immunosorbent assay

eNOS = endothelial nitric oxide synthase

FLAIR = fluid-attenuated inversion recovery

FOXC1 = forkhead box C1

FOXF2 = forkhead box F2

GFAP = glial fibrillary acidic protein

GNAI1 = guanine nucleotide binding protein alpha inhibiting-1

GOM = granular osmiophilic deposits

GRE = gradient echo

GSN = gelsolin gene

GWAS = genome-wide association studies

H&E = haematoxylin and eosin

HIF = hypoxia inducible factor

HRC = histidine rich calcium binding protein

HRP = horseradish peroxidase

HTRA1 = HtrA serine peptidase 1

ICH = intracerebral haemorrhage

IgG = immunoglobulin G

IQR = interquartile range

IRR = inter-rater reliability

ITM2B = Abri gene

LFB = Luxol fast blue

LTBP1 = latent transforming growth factor-ß binding protein-1

MAG = myelin associated glycoprotein

MBP = myelin basic protein

MMP = matrix metalloproteinase

MR = magnetic resonance

MRC = Medical Research Council

MRI = magnetic resonance imaging

MS = multiple sclerosis

NAWM = normal appearing white matter

NHS = National Health Service

NIfTI = Neuroimaging Informatics Technology Initiative

NO = nitric oxide

NOS = nitric oxide synthase

NOTCH3 = notch receptor 3

NVU = neurovascular unit

OPC = oligodendrocyte precursor cell

PACS = picture archive and communication system

PADMAL = pontine autosomal dominant microangiopathy and leukoencephalopathy

PAS = perivascular space

PBS = phosphate buffered saline

PDGF-B = platelet derived growth factor B

PDGFRB = platelet derived growth factor receptor-ß

PITX2 = paired-like homeodomain transcription factor 2

PLP1 = proteolipid protein-1

PMI = post-mortem interval

PRNP = prion gene

PVS = perivascular space

RIN = RNA-integrity number

RNA = ribonucleic acid

RVCL-S = retinal vasculopathy with cerebral leukodystrophy and systemic manifestations

SAS = subarachnoid space

SHRSP = spontaneously hypertensive stroke-prone rat

SLC = solute carrier

SNP = single nucleotide polymorphism

STARD = Standards for the Reporting of Diagnostic Accuracy studies

STRIVE = STandards for Reporting Vascular changes on nEuroimaging

SVD = small vessel disease

SWI = susceptibility weighted imaging

T = Tesla

TGF-ß = transforming growth factor-ß

TIMP3 = tissue inhibitor of metalloproteinases-3

TR = repetition time

TREX1 = three prime repair exonuclease 1

TTR = transthyretin gene

VaD = vascular dementia

VEGF = vascular endothelial growth factor

VCING = vascular cognitive impairment neuropathology guidelines

VHL = Von Hippel-Lindau

VWF = von Willebrand factor

WMH = white matter hyperintensities

WML = white matter lesions

ZCCHC14 = zinc finger CCHC domain-containing 14

PART A: UNDERSTANDING THE LANDSCAPE OF SPORADIC HUMAN SMALL VESSEL DISEASE

CHAPTER 1: INTRODUCTION

1.1 Background to small vessel disease – how big is the problem?

Human cerebral small vessel disease (SVD) is a disorder of intrinsic cerebral blood vessels with both sporadic and genetic forms. Sporadic SVD accounts for the majority of cases and is a disorder associated with aging. Sporadic SVD includes both amyloid (cerebral amyloid angiopathy, CAA) and non-amyloid forms.

Non-amyloid sporadic SVD is the focus of this thesis. It affects all vessel types; arterial, capillary and venous (Wardlaw, Smith et al. 2013, Wardlaw, Smith et al. 2019). It causes defined lesions on neuroimaging, most often white matter hyperintensities (WMH) (Wardlaw, Smith et al. 2013) and has a recognised, if complex, clinical phenotype with several identified risk factors, hypertension being most strongly associated (van Dijk, Prins et al. 2008, Gottesman, Coresh et al. 2010). The pathophysiology, however, is not fully understood. Histological features are not defined or agreed upon in the neuropathological literature (Alafuzoff, Gelpi et al. 2012, Humphreys, Smith et al. 2021), but vascular and parenchymal changes are seen including arteriolosclerosis, enlarged perivascular spaces (PVS), white matter rarefaction, microinfarcts and haemorrhagic lesions of varying sizes. SVD lesions predominantly affect the white matter and deep grey nuclei but can be seen throughout the brain (Pantoni and Gorelick 2014).

There is no single, agreed definition as SVD is a complex disease with varying clinical phenotypes and variable features, on both imaging and histopathology, that do not reliably map onto each other. However, I will use a simple, broad definition that captures current understanding; a “sporadic,

intrinsic process affecting small cerebral arterioles, capillaries and sometimes venules" (Wardlaw, Smith et al. 2013).

CAA has been recognised for many years but is a relatively recent, and important, addition to the SVD spectrum. In CAA, amyloid-beta (Aß) protein is deposited within the walls of leptomeningeal and cortical arteries and capillaries causing visible thickening and weakening of the wall with eventual rupture and haemorrhage (Smith and Eichler 2006, Banerjee, Carare et al. 2017). It is specifically associated with lobar intracerebral haemorrhage (ICH) and there is an increased risk of recurrent bleeding (Charidimou, Imaizumi et al. 2017).

Genetic SVDs are much less common. They are generally more severe with an earlier disease course affecting a younger population. They have provided mechanistic information with regard to the molecular pathological basis of sporadic vasculopathy, although the basic pathophysiology of sporadic SVD remains uncertain. To date at least eleven different mutations have been associated with monogenic SVDs with non-amyloid and amyloid-related pathology (Marini, Anderson et al. 2020). They include:

Cerebral autosomal dominant arteriopathy with subcortical infarcts and leukoencephalopathy (CADASIL) due to notch receptor 3 (NOTCH3) mutation (Di Donato, Bianchi et al. 2017).

Cerebral autosomal recessive arteriopathy with subcortical infarcts and leukoencephalopathy (CARASIL) due to mutations in the HtrA serine peptidase 1 (HTRA1) gene (Uemura, Nozaki et al. 2020).

Cathepsin A-related arteriopathy with strokes and leukoencephalopathy (CARASAL) due to cathepsin A (CTSA) mutation (Finsterer, Scorza et al. 2019).

Type 4 collagen (COL4)-associated angiopathies due to mutations in the collagen 4 A1 and A2 (COL4A1, COL4A2) genes (Zagaglia, Selch et al. 2018), including pontine autosomal dominant microangiopathy and leukoencephalopathy (PADMAL) (Verdura, Herve et al. 2016).

Retinal vasculopathy with cerebral leukodystrophy and systemic manifestations (RVCL-S) due to three prime repair exonuclease 1 (TREX1) mutation (Kolar, Kothari et al. 2014).

Familial amyloid angiopathies linked to mutations in the Aβ, CST3 (cystatin C), TTR (transthyretin), GSN (gelsolin), PRNP (prion) and ITM2B/ BRI2 (ABri and ADan) genes (Biffi and Greenberg 2011).

1.2 Structure of the brain

1.2.1 Vascular anatomy of the brain

To understand how small vessel disease affects the brain it is important to understand the normal vascular anatomy and physiology. The brain is supplied by the internal carotid and vertebral arteries which form the circle of Willis at the base of the brain. From here the three main paired cerebral arteries arise. Smaller deep perforating vessels supplying white matter and deep grey nuclei arise directly from the circle of Willis, the main cerebral arteries, internal carotid arteries and anterior choroidal artery (Djulejic, Marinkovic et al. 2016) (Figure 1.1). Individual variation in the specific vessels that supply precise structures can have clinical significance, for example, in identifying the source of a lacunar stroke or symptoms experienced by a patient.

The cortex and superficial white matter are supplied by superficial perforators that travel over the surface convexity of the brain in the subarachnoid space and turn 90 degrees to penetrate the parenchyma (Reina-De La Torre, Rodriguez-Baeza et al. 1998). At this level, there is a basement membrane on the abluminal aspect of the endothelial cells that also encloses the mural

smooth muscle cells. This is enclosed within pial extensions as the arteriole travels into the brain tissue (Joutel, Haddad et al. 2016). The glia limitans consists of astrocyte processes covered by a basement membrane and covers both the surface of the brain (glia limitans superficialis) and extends around blood vessels (glia limitans perivascularis). The PVS is the space bounded by the glia limitans superficialis and the basement membrane of the vascular wall (Figure 1.2).

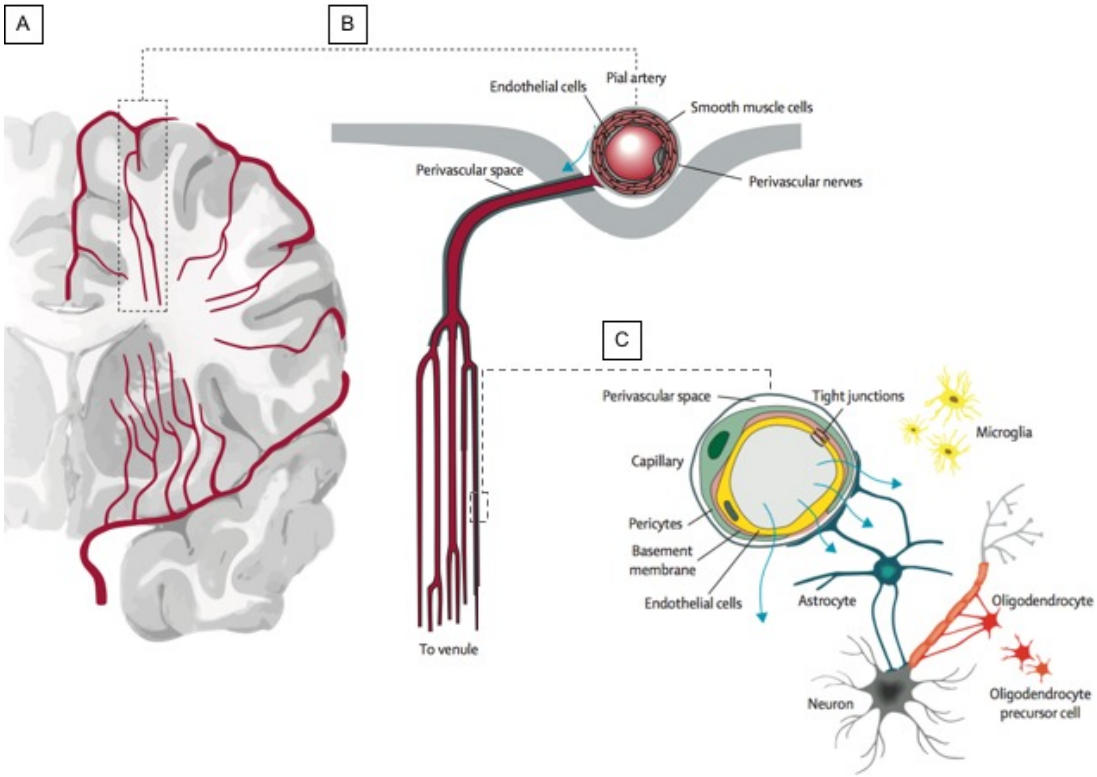


Figure 1.1 Schematic of cerebral vascular supply and the blood brain barrier

A) Superficial cortical vessels from the surface of the brain and deep perforating vessels supply the cerebral parenchyma. B) Larger superficial pial arteries have mural smooth muscle cells. They are surrounded by a single leptomeningeal layer forming the perivascular space as they penetrate the parenchyma, traversing the cortex to supply the white matter. Deep perforating arteries have two leptomeningeal layers. C) At the capillary level pericytes are the contractile cells. Together with endothelial cells, the basement membrane and surrounding astrocyte end-feet they form the blood brain barrier which is in close communication with parenchymal neurons. The functional and structurally dynamic neuro-vascular unit is formed by all of these components plus oligodendrocytes and immune cells. Adapted from (Wardlaw, Smith et al. 2019).

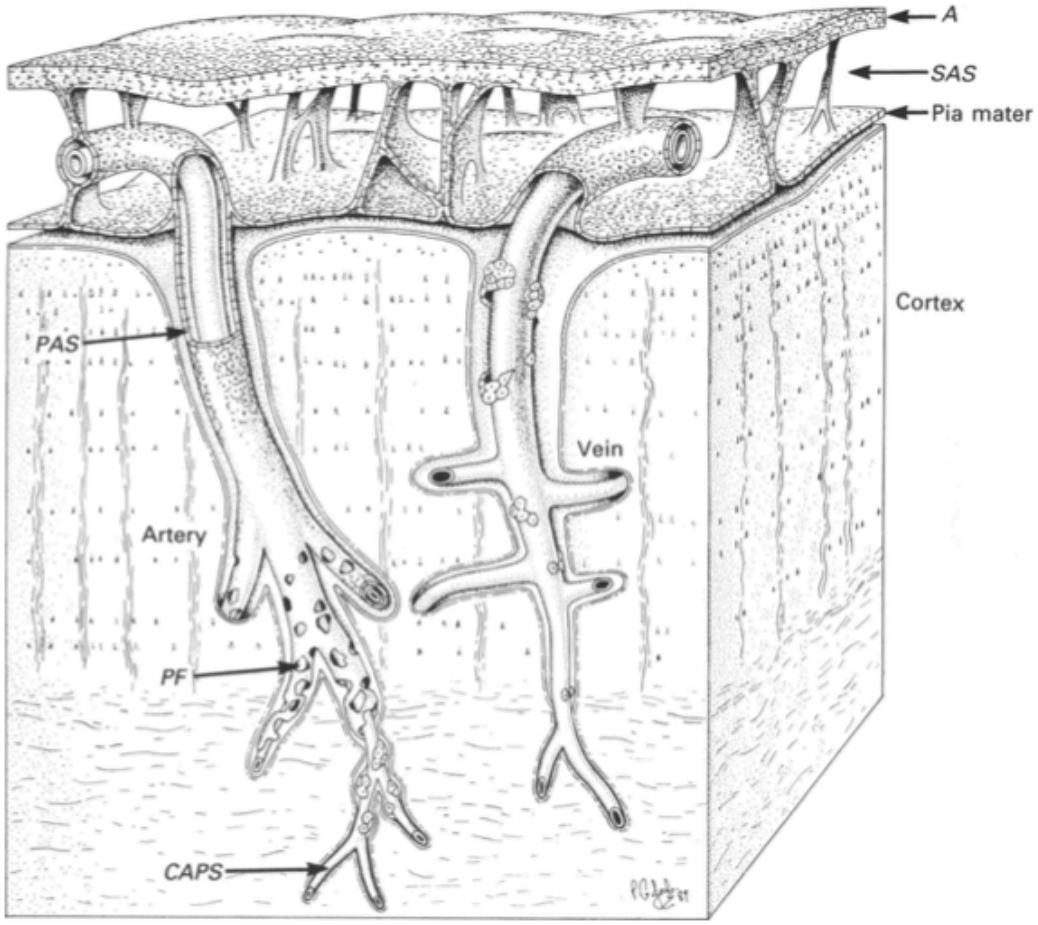


Figure 1.2 The structure of the perivascular space

A diagramatic representation of the perivascular space. Vessels on the surface of the brain travel within the subarachnoid space (SAS) between the arachnoid (A) and the pia mater.The glia limitans superficialis lies immediately below the pia, covering the outer aspect of the brain, which is then continuous with the glia limitans perivascularis surropunding penetrating vessels, the perivascular space (PAS) being the space between the vascular basement membrane and the limiting basement membrane of the glia limitans perivascularis. The space is obliterated at the capillary (CAPS) level. (Zhang, Inman et al. 1990)

The perforators are small arterioles that do not have a continuous elastic lamina, in contrast to the proximal small arteries (Pantoni 2010). As the vessels penetrate further into the brain, the pial extensions are lost and the basement membranes of the vessel and surrounding astrocyte end feet fuse at the capillary level, obliterating the PVS (Krisch, Leonhardt et al. 1984, Zhang, Inman et al. 1990, Joutel, Haddad et al. 2016). The perforators are

terminal vessels with limited anastomoses and overlapping territory, resulting in significant clinical implications in the event of damage or obstruction.

The deep arteriolar vessels run within the subarachnoid space at the base of the brain and are surrounded by two leptomeningeal layers as they enter the parenchyma. On electron microscopy studies the outer layer is continuous with the pia and the inner layer is closely opposed with the vessel adventitia. The PVS is between these two layers and is a continuation of the subarachnoid space at the base of the brain (Pollock, Hutchings et al. 1997, Weller, Djuanda et al. 2009).

Microvascular density in the white matter is lower than that in the grey matter, making it particularly susceptible to damage as a result of vascular compromise (Iadecola 2013). Progressive branching of arterial vessels results in extensive capillary networks throughout the brain which eventually coalesce into venules then veins. The venules have a more sparse elastic lamina and contractile cell coverage but similar basement membrane organisation as proximate arterial vessels (Joutel, Haddad et al. 2016). They eventually drain into venous sinuses (Love, Budka et al. 2015). Typically, arterial vessels have been the focus of SVD research, but it must be remembered that capillaries and venous vessels are also affected.

Vessels may be defined based on size, location and structure. Pial arterioles give rise to the penetrating arterioles as they turn to enter the brain tissue, and they may be called parenchymal arterioles once they are within the parenchyma and almost completely encased by astrocyte end-feet (Cipolla 2009). In practice, this distinction is not necessarily obvious on histological examination. On electron microscopy, intracortical arterioles range from 20-90μm diameter and capillaries measure up to 7μm diameter (Reina-De La Torre, Rodriguez-Baeza et al. 1998, Torres, Loomis et al. 2016). Larger arterial vessel walls contain multiple layers of contractile smooth muscle cells whereas capillary walls have a single contractile pericyte layer (Vanlandewijck, He et al. 2018). There is no agreed definition of the size of

vessels affected by SVD. In a survey of neuropathologists in 2006, less than half agreed on the definition of a small vessel despite almost all of the respondents routinely assessing them. A ‘small vessel’ was reported as less than 500μm diameter (Pantoni, Sarti et al. 2006), significantly larger than the 20-90μm diameter of cortical arterioles seen on electron microscopy (Reina-De La Torre, Rodriguez-Baeza et al. 1998). The same number of respondents defined a small vessel as being in a subcortical location. No consensus has since been reached.

The cerebral vasculature is a uniquely adapted system which regulates and monitors the intraparenchymal environment much more tightly than in any other organ. The vessel wall itself is composed of endothelial and mural cells as in other vascular networks throughout the body, but cerebral arteries have a thinner muscular layer and adventitia and lack an external elastic lamina. The cerebral vascular cells have extensive direct and indirect connections with different cell types in the brain that enable the vasculature to be part of the systems maintaining the homeostasis of the brain parenchymal environment and the normal functioning of neurons and other cells within it. PVS surround some cerebral vessels, and some aspects of their structure and function remain unknown but they are believed to be important in fluid and solute drainage from the brain. They are potentially significant in a variety of neurological disorders including SVD and conditions involving vascular protein deposition (Wardlaw, Benveniste et al. 2020). Cerebrovascular endothelial cells have tight junctions but no fenestrations, forming the basis of the blood brain barrier (BBB) (Love, Budka et al. 2015) which is essential for tight regulation of the interstitial environment. Technical innovations have increased our knowledge and understanding of the brain vasculature at the molecular level but much remains unknown. Studies of brain vessel interactions reveal a variety of significant pathways including angiogenesis, integrin signalling, transforming growth factor-ß (TGF-ß) signalling, calcium regulation, cholecystokinin signalling (a gastrointestinal hormone) and gonadotropin-releasing hormone receptor (Lee, Kwon et al.

2017). Some of these are unsurprising while others suggest there is still much to be learned about brain vasculature interactions. It is helpful to review the structure and function of these vessels in humans in more detail in the context of a range of functional units; the BBB, PVS and neurovascular unit (NVU).

1.2.2.1 The Blood Brain Barrier

The BBB forms a dynamic physical barrier between the systemic vascular circulation and the brain parenchyma. It is a complex system of communication and structure unique from any other vascular lining or structure in the body. Moving outwards from the vascular lumen it consists of endothelial cells, a basement membrane, pericytes (at the capillary level) or smooth muscle cells (at the arteriolar level) (Winkler, Bell et al. 2011), immune cells and astrocytic end-feet. These cells and the connections between them selectively and tightly control the movement of water, cells and solutes through the blood vessel wall (Abbott, Ronnback et al. 2006) to prevent pathogen entry and maintain the optimal environment for neuronal function.

Endothelial dysfunction and BBB leakage are hypothesised to be integral events in the development of SVD (Wardlaw, Sandercock et al. 2003, Farrall and Wardlaw 2009, Wardlaw, Smith et al. 2019). BBB disruption with leakage, structural abnormalities and loss of vascular autoregulation are present in SVD (Farrall and Wardlaw 2009, Wardlaw, Makin et al. 2017, Zhang, Wong et al. 2017).

1.2.2.2 Vascular endothelial cells

Vascular endothelial cells are specialised for their role in the BBB. They are polarised with defined luminal and basolateral faces and differential protein expression on the different aspects to regulate trans-endothelial transport of molecules and cells including, for example, glucose via GLUT-1 (Simpson, Vannucci et al. 2001) and white blood cells via ICAM-1 (Muller 2011). Gene

ontology term studies show endothelial cells are enriched for cell junctions (Vanlandewijck, He et al. 2018). Tight junction proteins between endothelial cells strictly regulate movement across the BBB via para- and trans-cellular routes, (Van Itallie and Anderson 2006, Sharif, Jumah et al. 2018) compared to the relatively permeable barrier in other body systems where looser adherens junctions form the endothelial cell connections. Various proteins with different roles make up the cerebral endothelial cell tight junctions including claudins, junctional adhesional molecule-1 and lipolysis-stimulated receptor (Nitta, Hata et al. 2003, Sohet, Lin et al. 2015). These transmembrane proteins maintain the tight junctions and their barrier ability, while cytoplasmic proteins such as zonula occludens monitor signalling across the BBB (Bazzoni 2006, Abbott, Patabendige et al. 2010) and act as anchors to the cellular cytoskeleton (Tsukita, Katsuno et al. 2009). Claudin-5, in particular, is highly expressed in endothelial cells in all vessel types throughout the brain (Morita, Sasaki et al. 1999, Vanlandewijck, He et al. 2018). It is involved in sealing tight junctions to limit transport through pores to molecules less than 800D (Nitta, Hata et al. 2003). Factor VIII (von Willebrand factor) is also expressed by endothelial cells (Weber, Seitz et al. 1985). Both are used as endothelial markers to identify and quantify endothelial cell content and integrity.

In mice there is a continuous gradation of endothelial cells along the different vessel types (Vanlandewijck, He et al. 2018) with predominance of transcription factors in arterial vessels and transporter proteins in capillaries and veins, particularly transendothelial transport proteins in veins, which are associated with the BBB. A single cell sequencing study has identified 120 transcription factors and 145 transporter proteins that can be used to differentiate endothelial cells in different segments of the vasculature and place them along the arterial/capillary/venous axis (Vanlandewijck, He et al. 2018). Different molecular profiles have also been seen within human capillary endothelial cell populations, particularly in the hippocampus and caudate nucleus compared to the cortex (Lee, Kwon et al. 2017). Differential

expression may be due to cell diversity within the brain, for example between different brain areas or segments, to differing responses to environmental exposures or to species differences between human and animal models. Many proteins are expressed in vascular beds throughout the body while others can be loosely grouped into areas with common expression profiles. However, a small number of proteins (n=8) appear to be expressed only by endothelial cells in the brain (Lee, Kwon et al. 2017) including solute carrier (SLC) transporter proteins involved in transporting glucose and essential amino acids.

Endothelial cells form myoendothelial projections, making direct contact with contractile cells through the basement membrane (Longden, Hill-Eubanks et al. 2016) and also communicate indirectly with other parts of the BBB. For example, they regulate luminal diameter through nitric oxide (NO) release via the action of endothelial nitric oxide synthase (eNOS) which causes vascular smooth muscle and pericyte relaxation and vascular dilatation in response to local metabolic demands (Forstermann, Pollock et al. 1991). In endothelial cell dysfunction this process and many others are disrupted; mural contractile cell proliferation (Mooradian, Hutsell et al. 1995), luminal platelet adhesion (Radomski, Palmer et al. 1991) and increased vascular endothelial growth factor (VEGF) and endothelin-1 (EDN1) release cause dysregulated vasodilation and angiogenesis with potentially leaky new vessels (Lip, Belgore et al. 2000, Rajashekhar, Willuweit et al. 2006). Endothelial cell dysfunction is a common theme in SVD research and is postulated to be the initiating factor in sporadic SVD. In animal models and some human studies, components of the disrupted mechanisms such as NO bioavailability and claudin-5 (tight junctions) can be measured to identify endothelial dysfunction (Bailey, Wardlaw et al. 2011). Further study of these mechanisms may ultimately lead to the identification of biomarkers that could potentially be used to diagnose and monitor endothelial dysfunction *in vivo*.

1.2.2.3 Contractile cells

Contractile cells in the vascular wall regulate blood flow and pressure. Smooth muscle cells in the walls of intracerebral arterial vessels are present in decreasing numbers as the vessels become smaller (Cipolla 2009). Smooth muscle cells are distinct from capillary pericytes but there may be a continuum between them along progressively smaller vessels and a degree of plasticity with one cell type able to change its phenotype to the other as angiogenesis and vascular remodelling occur (Armulik, Abramsson et al. 2005). Smooth muscle cells within small to medium sized arteries express Notch3, mutations of which underlie CADASIL (Joutel, Corpechot et al. 1996), discussed in more detail later. Arterial smooth muscle cells may also be identified by expression of calponin 1 and arteriolar smooth muscle cells by α-smooth muscle actin or smooth muscle protein 22α. A small number of proteins are differentially expressed by human smooth muscle cells in brain vessels, peripheral vessels and non-vascular smooth muscle. Von Hippel-Lindau tumour suppressor (VHL) is specific to cerebral vascular smooth muscle cells. Histidine rich calcium binding protein (HRC) and VHL were the only two brain vascular smooth muscle cell proteins not found in non-vascular smooth muscle cells (e.g. urinary bladder and uterus). (Lee, Kwon et al. 2017). Studies in mice also suggest vascular smooth muscle cells have the ability to respond within seconds to dynamic conditions *in vivo*, partly, at least, due to high expression of immediate early genes (Hall, Reynell et al. 2014, Vanlandewijck, He et al. 2018). Possible interactions between brain endothelial and smooth muscles cells may involve CD34, YES1, TJP1 and B2M proteins. So far, they appear limited, but this may be due to relatively little research into brain smooth muscle cells (Lee, Kwon et al. 2017).

At the capillary and post-capillary venule level the endothelial basement membrane is shared by a surrounding, incomplete layer of contractile pericytes (Sharif, Jumah et al. 2018) (Figure 1.3a) with apparently identical gene expression profiles in both vessel types. Whilst there is a smooth transition of endothelial cell transcripts along the different vessel types, there

is an abrupt transition at the point where smooth muscle cells are replaced by pericytes, from one cell to the next (Vanlandewijck, He et al. 2018). Recently, a new type of contractile mural cell in the 'transitional segment' between arterioles and capillaries has been identified (Ratelade, Klug et al. 2020) which may support the idea of segmentation of contractile cell profiles along the vascular tree. These transitional cells express both smooth muscle cell and pericyte markers and have a unique morphology. Pericytes in the central nervous system (CNS) express a range of markers including platelet derived growth factor receptor-ß (PDGFRB) (Armulik, Genove et al. 2011) and CD13 (Vanlandewijck, He et al. 2018) that can be used to identify them. Genes including ABCC9, have been identified in mice and zebrafish that can distinguish pericytes from other vascular cells (Vanlandewijck, He et al. 2018). The pericyte content of cerebral vessels is significantly higher than in other organ systems (Winkler, Bell et al. 2011). Values vary, but there may be up to 50% more, with a 1:3 ratio to endothelial cells (Shepro and Morel 1993). They are specialised to their role in the CNS (Armulik, Genove et al. 2011) and have a distinct morphology compared to other organ systems, being more flattened with multiple processes extending over a large area of the vessel. They have a range of functions besides regulation and maintenance of the BBB (Armulik, Genove et al. 2010) including vascular contraction, BBB development, transport across the BBB, endothelial cell proliferation, monitoring the extracellular environment, phagocytic and possible stem cell capabilities (Armulik, Abramsson et al. 2005, Collett and Canfield 2005, Peppiatt, Howarth et al. 2006, Bell, Winkler et al. 2010, Armulik, Genove et al. 2011, Vanlandewijck, He et al. 2018). Pericytes and endothelial cells communicate through multiple bidirectional signalling pathways, including platelet derived growth factor B (PDGF-B), Notch-1 and TGF-ß during development, but also for continued maintenance of the BBB in adulthood. Pericytes and endothelial cells also have focal direct communication across the basement membrane via adhesion plaques and peg-socket interactions, with one pericyte connected to multiple endothelial cells (Armulik, Abramsson et al. 2005).

1.2.2.4 The vascular basement membrane

The cerebral vascular basement membrane is a 30-100nm thick, negatively charged layer of extracellular matrix proteins. A remarkably complex structure that has been relatively under-studied, it has been called the 'matrisome' (Joutel, Haddad et al. 2016). In the brain, the basement membrane expresses a number of proteins common to other vascular beds in the body, as well as many unique to it (Naba, Hoersch et al. 2012). It provides physical support to the vessel, is a barrier to large charged molecules and anchors cells (Brightman and Kaya 2000, Sharif, Jumah et al. 2018, Xu, Nirwane et al. 2019). It also helps regulate the BBB, act as a signalling pathway, is involved in angiogenesis and controlling movement of leukocytes into the parenchyma (Thyboll, Kortesmaa et al. 2002, Wu, Ivars et al. 2009). In the brain it is composed of two layers, although in areas without intervening contractile cells it is not possible to tell these layers apart (Figure 1.3). The vascular layer contains α4 and α5 laminins produced by endothelial cells and pericytes. Astrocytes produce α1 and α2 laminins for the parenchymal basement membrane (Wu, Ivars et al. 2009, Sorokin 2010). Other significant extracellular matrix proteins are type IV collagen, laminin, fibronectin, nidogen and heparin sulphate proteoglycans (Hawkins and Davis 2005, Serlin, Shelef et al. 2015) (Figure 1.3c). Together they produce a physically stable barrier of proteins able to interact with the surrounding environment, including cells and chemical factors such as growth factors (Hallmann, Horn et al. 2005).

The importance of the basement membrane is reflected in its involvement in disease. COL4 is the major constituent of the basement membrane and is thought to have a role in maintaining vascular integrity. Of the six identified alpha chains, COL4a1 and COL4a2 are most prominent in cerebrovascular disease. Animal models of gene knock-outs and mutations result in embryonic death, vascular defects and intracerebral haemorrhage (Xu, Nirwane et al. 2019). Breakdown of the basement membrane by matrix metalloproteinases (MMPs), specifically MMP-2 and MMP-9, is implicated in

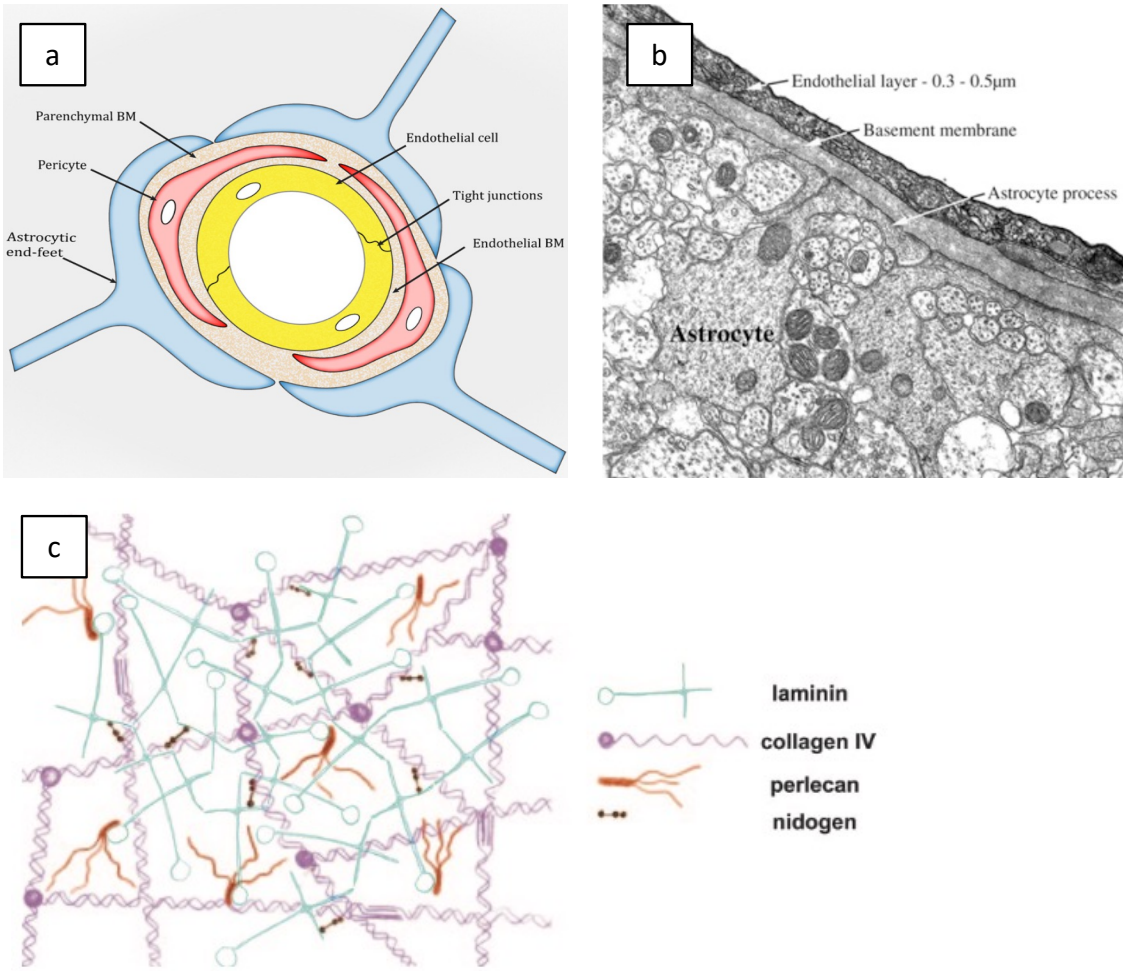


Figure 1.3. Cerebrovascular basement membrane

A) Illustration of pericytes embedded within the endothelial and parenchymal basement membrane layers in capillaries. From (Xu, Nirwane et al. 2019). B) In capillaries, the blood-brain barrier is composed of endothelial cells lining the vessel, the vascular basement membrane and is enclosed by astrocyte end-feet, with an incomplete layer of contractile pericytes (not present in this image) (electron microscopy image. From (Hawkins 2009)). C) Illustration of the proposed structure and interactions of basement membrane proteins. Perlecan is also known as heparin sulphate proteoglycan 2. From (Hallmann, Horn et al. 2005, Xu, Nirwane et al. 2019)

several neurological conditions including stroke, cerebral ischaemia and Alzheimer's disease (AD) (Thomsen, Routhe et al. 2017, Langen, Ayloo et al. 2019). In animal models, there is increased fibronectin and type IV collagen in haemorrhagic and ischaemic stroke in conjunction with BBB leakage (Hamann, Okada et al. 1995, Wasserman and Schlichter 2007, Baumann, Preston et al. 2009, Ding, Feng et al. 2015). In AD, the basement membrane

is thickened with varying amounts of Aß deposition. The mechanisms causing these changes are unknown, but in AD the vascular changes are present in the same areas with parenchymal pathology, suggesting a relationship between them (Thomsen, Routhe et al. 2017). Changes in the basement membrane protein composition and structure are also seen in normal aging resulting in vessel wall thickening and narrowing of the vessel lumen (Uspenskaia, Liebetrau et al. 2004).

Astrocyte end-foot processes provide the outmost layer of the BBB. Gap junctions, looser than those between endothelial cells, are present between adjacent end-feet and contact other cells within the BBB. The end-feet are also polarised by their interactions with pericytes on their vascular aspect (Nedergaard, Ransom et al. 2003). Channels and transporters such as Kir4.1 and aquaporin-4 control the movement of specific molecules, including water, across the BBB (Bernacki, Dobrowolska et al. 2008). Astrocytes communicate with neurons and monitor and maintain the extracellular environment including immune and electrochemical activity and osmolarity (Wong, Ye et al. 2013, Rodriguez-Arellano, Parpura et al. 2016). There are different subtype of astrocytes. At the most basic level they are divided into protoplasmic astrocytes, found in grey matter, and fibrous astrocytes in white matter but recent single cell genetic studies identified gene expression differences in different brain areas alongside regional variations in morphology, cell membrane properties and communication with other cells (Bushong, Martone et al. 2002, Morel, Chiang et al. 2017). In the cortex and hippocampus of animal models each astrocyte occupies its own space without overlapping its neighbours, its distal processes contacting others at the periphery of the territory (Bushong, Martone et al. 2002, Halassa, Fellin et al. 2007). A single hippocampal astrocyte also contacts multiple neurons, and most contact vessels (Bushong, Martone et al. 2002), potentially enabling rapid signal transmission between them. The significance of this is unknown but astrocytes seem to be organised with region-specific functions, which could be important in the regional expression of diseases.

1.2.3 The perivascular space

Immediately outside the basement membrane, the PVS, also known as the Virchow-Robin space, contains cerebrospinal fluid (CSF) and microglia (Sharif, Jumah et al. 2018) and is thought to have a role in fluid and metabolite removal from the brain. First described as early as 1842 (Wardlaw, Benveniste et al. 2020), perivascular spaces in the human brain are seen on *in vivo* imaging studies using magnetic resonance imaging (MRI) and diffusion tensor imaging (Taoka, Masutani et al. 2017, Wardlaw, Benveniste et al. 2020). A comprehensive review of the current state of knowledge around perivascular spaces has recently been published (Wardlaw, Benveniste et al. 2020) and highlights that our knowledge base derives from small studies with diverse populations. The result is that many aspects of the PVS including structure, function and importance in disease, remain under debate. When functioning normally, the PVS remains a 'normal' size and is thought not to be visible. Visible PVS on neuroimaging may also be considered normal with increased age, although how many is acceptable as part of normal aging is not known (Wardlaw, Benveniste et al. 2020).

The structure and form of the PVS is thought to be differ between different vessel types e.g. arteriole and capillary, and also vessel location e.g. deep perforating and superficial cortical arterioles (Wardlaw, Benveniste et al. 2020). On the surface of the brain, the PVS is thought to communicate with the subpial space, but may also have a connection to the subarachnoid space. Studies in rodents are not definitive while histological work shows superficial arterioles communicate with the subpial space only (Weller, Djuanda et al. 2009). Tracers injected into the cisterna magna in imaging studies using live animals reached both deep and superficial arteriole PVS (Iliff, Wang et al. 2012).

In humans, tracers injected into subarachnoid spaces become visible in the cortex and white matter, but less so in the basal ganglia, supplied by the

deep perforating arterioles (Ringstad, Vatnehol et al. 2017, Eide, Vatnehol et al. 2018, Ringstad, Valnes et al. 2018). It is worth noting all of these individuals were being investigated for potential pathology with no completely healthy controls, so it is unknown how accurately they represent the normal physiology. As the arterioles branch and become smaller, the pia is continuous with the basement membrane on the abluminal aspect of the capillaries which is encased by the astrocyte end-feet.

Imaging studies suggest visible PVS and venules are not spatially related and therefore the enlarged PVS are not around venules (Braffman, Zimmerman et al. 1988, Bouvy, Biessels et al. 2014, Jochems, Blair et al. 2020). Histological studies suggest there is a perivenular space continuous with the subpial space at the base of the brain surrounding basal ganglia venules which have just one leptomeningeal layer (Pollock, Hutchings et al. 1997). In these vessels the outer aspect of the PVS is defined by bundles of collagen which are in turn in contact with the glia limitans. It may be that in SVD only periarteriolar PVS are enlarged.

In mice, perivascular fibroblast-like cells have been identified that lie within the PVS, loosely adherent to the vessel wall throughout the vascular tree (Vanlandewijck, He et al. 2018). They appear to form a continuous sheath around intracerebral arterial and venous vessels, but not capillaries. At least two subtypes have been identified but their significance is not known. Genes specifically expressed by these fibroblast-like cells encode proteins significant in the structure and regulation of the extracellular matrix, including fibrillar and non-fibrillar collagens, collagen spacing proteins and collagen-modifying enzymes. They are associated with gene ontology terms for cell adhesion and migration and share many, but not all, characteristics with lung fibroblasts indicating a specialised phenotype within the brain. The role of these fibroblast-like cells in mice remains uncertain (Vanlandewijck, He et al. 2018) although they are involved in stabilising developing blood vessels and are pericyte progenitors in zebrafish (Rajan, Ma et al. 2020). Work to identify a human equivalent has found a cell with a mesenchymal phenotype most

similar to the murine fibroblast-like cell rather than other murine vascular associated cells. They co-express PDGFRA, DCN, COL6A1 and COL3A1, which are all highly expressed in a perivascular distribution in the mouse cells (Liu, He et al. 2021). Further work is needed however, to confirm that these are comparable perivascular cells in humans, rather than other mesenchymal cells or pericytes.

PVS are critical in the so-called 'glymphatic pathway' (Figure 1.4). Approximately 140ml of CSF in the human central nervous system and 280ml of brain interstitial fluid (Bergsneider 2001) may ultimately follow this pathway, although it remains under debate. CSF travels into the brain alongside the perforating arterioles, entering the parenchyma across the glial basement membrane and astrocyte end-feet, which actively transport water via aquaporin-4 channels. Fluid movement within the PVS is not fully understood but believed to depend on a combination of factors. Any changes or problems that disrupt the homeostasis of the system could potentially cause PVS dilation (Wardlaw, Benveniste et al. 2020). Vascular pulsatility is small but measurable in the human brain (Shi, Thrippleton et al. 2020) and may drive PVS fluid movement into the brain along arterioles. Imaging studies in humans (Shi, Thrippleton et al. 2020, Wardlaw, Benveniste et al. 2020) and rodents (Iliff, Wang et al. 2013, Mestre, Tithof et al. 2018) show stagnated flow when vascular pulsatility is abnormal which could result in enlarged PVS and impaired toxin clearance. Aquaporin-4 appears to have an important role in transporting fluid into the interstitial space in mice (Mestre, Hablitz et al. 2018) and possibly in humans, but studies in humans are difficult and to date are not definitive (Wardlaw, Benveniste et al. 2020).

The interstitial fluid moves by bulk flow through the parenchyma towards the venous vessels, where it enters perivenous spaces and moves out of the brain, ultimately draining into the systemic circulation (Iliff, Wang et al. 2012). Movement through the PVS and the parenchyma is particularly active during sleep and is believed to be affected by cardiovascular pulsations, respiratory movements and posture (Iliff, Wang et al. 2012, Xie, Kang et al. 2013, Dreha-

Kulaczewski, Joseph et al. 2015, Lee, Xie et al. 2015, Kiviniemi, Wang et al. 2016).

Intrathecal contrast studies show CSF movement within the PVS in humans is similar to that seen in animals (Ringstad, Vatnehol et al. 2017, Ringstad, Valnes et al. 2018) and relationships between perivascular space dysfunction and sleep disturbance have been found (Ju, Ooms et al. 2017, Shokri-Kojori, Wang et al. 2018). There appear to be specific CSF and PVS dynamics in the brain in life, but we currently do not understand how they work or what drives them. Differing mechanisms may act to remove waste during sleep and wakefulness, although this remains to be proven. Altered protein levels could be due to altered production rather than clearance and there are

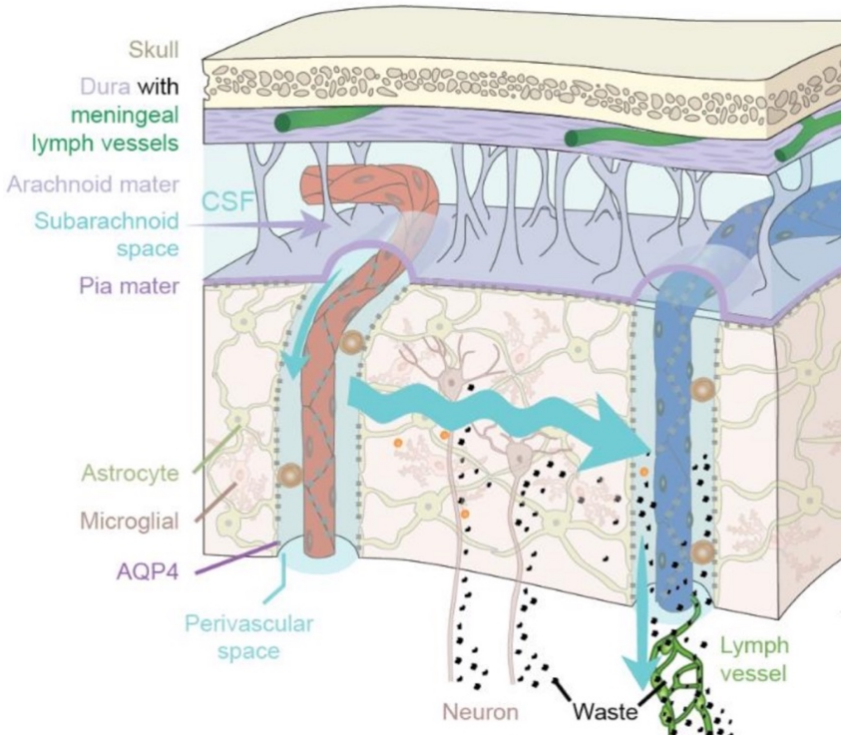


Figure 1.4 The glymphatic pathway

The glymphatic pathway is hypothesised to be a system whereby cerebrospinal fluid (CSF) in the perivascular space can enter the brain parenchyma, contributing to the interstitial fluid (ISF), known as the CSF-ISF interface. The ISF can then be absorbed in to perivenous spaces passing eventually into the venous system (Mogensen, Delle et al. 2021).

inherent complications in performing invasive studies of these mechanisms in humans, particularly in control subjects (Wardlaw, Benveniste et al. 2020).

Studies using tracers in animals show the glymphatic pathway removes toxic metabolites, including Aß, from the brain (Iliff, Wang et al. 2012). Animal models of vascular dementia with multiple infarcts show aquaporin-4 channel mis-localisation and enlarged PVS with impaired glymphatic influx and efflux (Venkat, Chopp et al. 2017, Wang, Ding et al. 2017). There is increased toxin and artificial tracer concentration in the centre of infarcts compared to surrounding viable tissue where PVS are functioning relatively normally (Venkat, Chopp et al. 2017, Zbesko, Nguyen et al. 2018). Together these suggest a critical role for PVS in maintaining normal fluid movement throughout the brain, and that disturbance of this system may lead to imbalance of fluid within different brain compartments and the potential subsequent effects of this, such as increased white matter fluid and enlarged PVS in SVD.

1.2.4 The neurovascular unit

The concept of the NVU was first described in the early 2000's to explain the intricate relationship between the blood vessels and cells within the brain, since then there has been a rapid increase in the number of publications citing the NVU (Iadecola 2017). The exact definition varies, but it generally consists of the BBB components in addition to perivascular and parenchymal cells; including macrophages, microglia, oligodendroglia and neurons. It describes the functional relationship between neuronal requirements and vascular response (Armulik, Genove et al. 2011, Winkler, Bell et al. 2011). There are hundreds of different neuronal subtypes (Peters and Jones 1984). They all work primarily to communicate signals within and beyond the CNS, maintained by the vast array of supporting cells. Neurons are the largest CNS cells with correspondingly large metabolic requirements, but within the CNS there is little capacity to store nutrients and limited numbers of neural stem cells (Hallbergson, Gnatenco et al. 2003, Andreone, Lacoste et al.

2015). Maintenance of homeostasis within the entire system is essential to ensure their proper functioning, and any disturbance can rapidly lead to neuronal dysfunction and demise.

The NVU is involved in development, extracellular matrix maintenance, perivascular clearance, cerebral blood flow and cell mediated immunity. The whole range of interactions within it are, again, not fully understood, but neurovascular coupling has been relatively thoroughly studied. Changes in the level of activity in regional groups of neurons causes changes in local cerebral blood flow (Iadecola 1993, Chaigneau, Oheim et al. 2003, Longden, Hill-Eubanks et al. 2016, Iadecola 2017). The neurons exert their influence through direct axonal connections with astrocyte end-feet and the vascular basement membrane (Hamel 2006), particularly around small arterioles and capillaries. But the whole NVU is involved in flow regulation through complex direct and indirect signalling mechanisms (Iadecola 2017). Vascular responses to neuronal stimulation are reduced when the BBB is damaged (Stanimirovic and Friedman 2012) and the close interrelations within the NVU support a vascular contribution for many neurological conditions including SVD, AD, frontotemporal dementia and Parkinson's disease (Iadecola 2017). Cerebral flow abnormalities have been identified in CADASIL (Chabriat, Joutel et al. 2009) and hypertension (Jennings, Muldoon et al. 2005), and are associated with WMH in sporadic SVD (ten Dam, van den Heuvel et al. 2007, Kraut, Beason-Held et al. 2008, Bernbaum, Menon et al. 2015, van der Veen, Muller et al. 2015) and in a meta-analysis (Shi, Thrippleton et al. 2016), although the results are not uniform suggesting complex mechanisms and relationships.

As the blood vessels branch and traverse the brain, cellular relationships within the NVU change. Peripheral ganglia innervate superficial pial and parenchymal arteriolar vessels (Hamel 2006). As the arterioles become smaller and the smooth muscle cells thin to a single layer there are close associations with dendritic and axonal terminations. Capillary endothelial cells are also closely opposed with surrounding pericytes; both possess

appropriate receptors. One mechanism for neurovascular coupling is thought to involve inwardly rectifying potassium channels. They detect increased extracellular potassium concentration caused by local neuronal activity and initiate local vascular dilatation. The signals rapidly propagate through the endothelium to dilate upstream arterioles, ultimately increasing flow at the capillary level (Looft-Wilson, Payne et al. 2004, Matsushita and Puro 2006, Tallini, Brekke et al. 2007). Local neuronal activity may also drive vascular remodelling throughout life to ensure sufficient blood supply for changing metabolic needs (Andreone, Lacoste et al. 2015).

1.2.4.1 Oligodendrocytes

Oligodendrocytes form the myelin sheath around neuronal axons by extending and wrapping processes to form internodes; increasing axonal signal conduction speed and providing metabolic and trophic support (Wilkins, Chandran et al. 2001). Each oligodendrocyte forms multiple internodes, up to 50 in some areas, contacting and influencing multiple neurons (Chong, Rosenberg et al. 2012). Mature myelin once formed can be detected and assessed histologically and biochemically using antibodies against myelin components including myelin basic protein (MBP), (Sternberger, Itoyama et al. 1978) myelin associated glycoprotein (MAG) (Sternberger, Quarles et al. 1979) and proteolipid protein-1 (PLP1) (Sobel, Greer et al. 1994). A degree of myelin change is seen in normal aging, with thinned, narrowed, loose-appearing internodes (Peters 2007). Myelin loss is seen in SVD on histological examination of WML in human post-mortem brain tissue (Fazekas, Kleinert et al. 1993, Simpson, Fernando et al. 2007) and in rat models (Rajani, Quick et al. 2018) with implications for axonal and neuronal loss, pathway integrity and cellular communication.

Like the other cell types, oligodendrocytes have complex direct and indirect communications with the other cells within the NVU. Oligodendrocytes differentiate from oligodendrocyte precursor cells (OPCs) during development and adulthood for ongoing maintenance and repair of myelin

(Richardson, Young et al. 2011). OPC migration is directed by endothelial cells (Tsai, Niu et al. 2016) and their maturation is inhibited by excess release of heat shock protein 90 α (HSP90 α) from dysfunctional endothelial cells (Rajani, Quick et al. 2018). Myelination and white matter angiogenesis are also dependent upon OPCs via hypoxia inducible factor (HIF) signalling (Yuen, Silbereis et al. 2014). Astrocytes and microglia influence their maturation and myelination (Domingues, Portugal et al. 2016, Miyamoto, Magami et al. 2020) and pericyte-deficient mice show oligodendrocyte, myelin and axonal loss (Domingues, Portugal et al. 2016, Montagne, Nikolakopoulou et al. 2018) which corresponds with the reduced myelin seen in histological studies of WMH (Fazekas, Kleinert et al. 1993, Simpson, Fernando et al. 2007).

1.2.4.2 Microglia

Microglia are specialised immune cells of the CNS that largely communicate with neighbouring cells via paracrine signalling but also by direct communication with other NVU components. Although they are glial cells, they are believed to derive from the embryonic yolk sac, rather than the ectoderm like other glia (Ginhoux, Lim et al. 2013). Microglia maintain a steady-state throughout life and fulfil multiple roles; they are involved in CNS homeostasis through neuronal maintenance and trophic support, phagocytic activity and oligodendroglial regulation (Ueno, Fujita et al. 2013, Tay, Savage et al. 2017, Weinhard, d'Errico et al. 2018), predominantly during development, but also throughout adult life (Sierra, Encinas et al. 2010, Arno, Grassivaro et al. 2014, Hagemeyer, Hanft et al. 2017). They become activated in response to pathogens and can produce pro- and anti-inflammatory cytokines, working as part of both the innate and adaptive immune responses alongside recruited systemic macrophages and lymphocytes (Moisse and Strong 2006). There are multiple microglial phenotypes which are influenced by intrinsic brain conditions, systemic conditions and environmental factors throughout life, in health and disease (Tay, Carrier et al. 2019).

Inflammation is implicated in vascular cognitive impairment. Increased inflammatory cells associated with white matter damage and BBB disruption are uncommon but are seen in histological studies (Tomimoto, Akiguchi et al. 2000, Rosenberg, Sullivan et al. 2001, Simpson, Fernando et al. 2007). Again, their role and the precise mechanisms involved are not fully understood but chronic inflammation may lead to chronic endothelial activation, characterised by increased expression of luminal cell adhesional molecules including VCAM-1, ICAM-1 and E-selectin. Endothelial activation is distinct from endothelial dysfunction, but may play a role in the pathophysiology of SVD (Quick, Moss et al. 2021). Animal models of bilateral carotid stenosis reduce blood flow to the forebrain with resulting adhesion molecule upregulation in endothelial cells (Huang, Zhang et al. 2010), while slowly progressive carotid occlusion produces parenchymal inflammation and loss of myelin (Hattori, Enmi et al. 2016). These studies also suggest a role for vasoconstriction in the pathophysiology of SVD, which could be part of a mechanism involving reduced NO secretion by dysfunctional endothelial cells.

1.3 Clinical aspects of small vessel disease

SVD microvascular pathology affects small blood vessels in all brain regions (Pantoni 2010, Wardlaw, Smith et al. 2019). It is associated with a range of clinical conditions, some more apparent than others, such as lacunar subtype stroke (Bailey, Smith et al. 2012) and vascular dementia (Pasi and Cordonnier 2020). Neuroimaging-identified SVD also increases the risk of future stroke (haemorrhagic and ischaemic) and dementia (Debette, Schilling et al. 2019, Georgakis, Duering et al. 2019). Other clinical expressions are more subtle and may have been previously relatively overlooked. For example, a recent systematic review and meta-analysis found neuropsychiatric symptoms including apathy, fatigue and delirium were associated with more severe radiological WMH (Clancy, Gilmartin et al. 2021). Physical disabilities include gait problems (de Laat, Tuladhar et al.

2011) and extrapyramidal symptoms (van der Holst, van Uden et al. 2015). SVD may also be clinically silent.

CAA usually presents clinically with lobar intracerebral haemorrhage and is particularly associated with increased risk of recurrent ICH (Charidimou, Imaizumi et al. 2017), reduced global cognition (Boyle, Yu et al. 2015) and post-stroke dementia (Moulin, Labreuche et al. 2016).

1.3.1 Epidemiology

SVD is a major healthcare problem. The first detailed descriptions were provided by Fisher in the 1960's (Fisher 1965, Fisher 1968). At this time it was generally assumed to be caused by the same hypertensive atherosclerotic disease processes that affects large vessels and so the pathophysiological causes and consequences of SVD were relatively understudied. Interest revived around the 1990's when the high prevalence of SVD was appreciated on improved MRI techniques. Hypertension is the major risk factor for SVD (discussed later). Current SVD treatment guidelines suggest targeting blood pressure levels below the standard guideline targets in hypertensive patients (Wardlaw, Debette et al. 2021) based on evidence that it reduced growth of radiological WMH and progression of cognitive decline (SPRINT-MIND trial) (Group, Nasrallah et al. 2019, Group, Williamson et al. 2019).

SVD increases with age, predominantly affecting people from middle-age onwards (Inzitari, Pracucci et al. 2009). It is present in over 30% of people aged over 80 years of age (Vermeer, Longstreth et al. 2007). SVD causes 25% of all ischaemic strokes (lacunar type) (Vermeer, Longstreth et al. 2007), 85% of haemorrhagic stroke (Samarasekera, Fonville et al. 2015) and is involved in 45% of all dementias (Gorelick, Scuteri et al. 2011). SVD often exists alongside and complicates other co-morbidities, particularly in the elderly. In at least 56.5% of AD the presence of SVD synergistically worsened symptoms (Jellinger and Attems 2003, Smallwood, Oulhaj et al.

2012), it is commonly seen alongside other dementias, and is a common cerebral co-pathology in the setting of cardiovascular disease (Wardlaw, Smith et al. 2019). CNS arteriolosclerosis has been reported as a significant co-pathology in multiple cohorts looking at cognitive aging (Blevins, Vinters et al. 2021). With the exception of large deep intracerebral or pontine haemorrhages, SVD in itself, however, is usually not fatal. Individuals can live with evolving cognitive problems and functional dependence for many years creating an additional burden on support and healthcare systems. In our aging population SVD will continue to be an increasingly important cause of morbidity and mortality (Hachinski 2002).

1.3.2 Diagnosis

SVD is diagnosed in life clinically, by symptomatic presentation, confirmed by characteristic features on neuroimaging (Potter, Doubal et al. 2010). It is best identified on MRI but also seen on computerised tomography (CT). Mild disease and early disease may go undetected as the small vessels thought to be the origin of SVD are not visualised on clinical neuroimaging. The parenchymal effects are visualised (Pantoni and Gorelick 2014) and are believed to cause the clinical syndrome, or lack thereof, depending on their size and location (Wardlaw, Smith et al. 2013). SVD affects the cerebral white matter, deep grey matter and brainstem on imaging, with relative sparing of the subcortical U-fibres (Revesz, Hawkins et al. 1989, Munoz, Hastak et al. 1993, Wardlaw, Smith et al. 2013, Shi and Wardlaw 2016). In brains with SVD the so-called normal appearing white matter (NAWM) as seen on clinical strength imaging is also affected, changes are identified using advanced functional imaging techniques (Bastin, Clayden et al. 2009, Baykara, Gesierich et al. 2016, Munoz Maniega, Chappell et al. 2017) and on histological studies (Chimowitz, Estes et al. 1992, Bronge, Bogdanovic et al. 2002, Fernando, O'Brien et al. 2004, Simpson, Ince et al. 2007). However, microscopic features of SVD are heterogenous and not fully characterised, with a lack of agreed language, assessment and tissue processing standards. Due to these complexities and our current incomplete

understanding, there are no effective treatment strategies (Bath and Wardlaw 2015).

1.4 Small vessel disease neuroimaging

Previously the language used in SVD neuroimaging was imprecise, but significant advances in MRI terminology, techniques and technology have enabled increasingly detailed and precise assessment of SVD *in vivo*, resulting in the publication of the STandards for Reporting Vascular changes on nEuroimaging (STRIVE) guidelines (Wardlaw, Smith et al. 2013). These have since been adopted by the imaging community and are now widely used for SVD neuroimaging reporting.

1.4.1 The STandards for Reporting Vascular changes on nEuroimaging guidelines

The STRIVE guidelines (Wardlaw, Smith et al. 2013) is a large scale, international consensus document published by an expert working group in response to the need for agreement on standards in SVD neuroimaging reporting. Neuroimaging previously had similar issues to those currently experienced by neuropathology (discussed in Chapter 2), with multiple terms and definitions used for similar lesions without consensus; a systematic review of 1144 papers identified 159 different names given to recent small subcortical infarcts and over 100 different terms used for lacunes of presumed vascular origin (Wardlaw, Smith et al. 2013). STRIVE describes standards for terminology and definitions, image acquisition and analysis, reporting in research and clinical settings as well as reviewing new technology for detecting preclinical SVD. The changes related to SVD on neuroimaging (illustrated in Figures 1.5 and 1.6) seen within the white matter and deep grey matter are:

- WMH of presumed vascular origin
- Lacunae of presumed vascular origin

- Perivascular spaces
- Recent small subcortical infarcts
- Cerebral microbleed
- Brain atrophy

When investigating SVD, STRIVE recommends using optimised MRI sequences with field strength of at least 1.5 Tesla (T) that should ideally include axial diffusion weighted imaging, fluid-attenuated inversion recovery (FLAIR), T2 weighted and T2*-weighted gradient echo (GRE) sequences. Slice thickness should be no more than 5mm with no gap and the in-plane resolution should be at least 1mm x 1mm. Images should be interpreted by readers with a good neuroanatomical knowledge trained using established training sets, in research it should be done by one or only a few individuals for each study. The reporting of discrete lesions which are not numerous (e.g. lacunes) should include the number and location. Ideally, visual rating scales should be established and used.

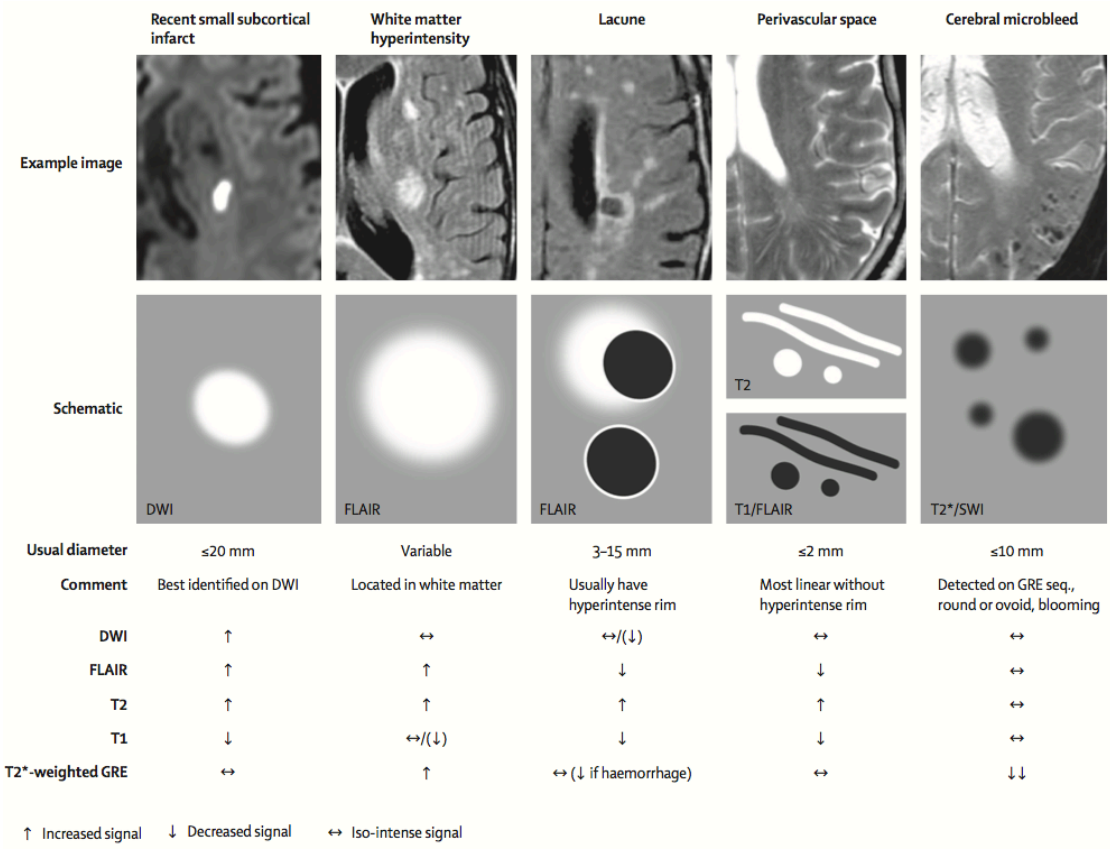


Figure 1.5 MRI appearances of SVD-related lesions

Neuroradiological lesions seen in SVD with schematic representations and summary of size and appearances as identified using different MRI sequences. DWI diffusion weighted imaging. FLAIR fluid-attenuated inversion recovery. SWI susceptibility weighted imaging. GRE gradient-recalled echo. (Taken from (Wardlaw, Smith et al. 2013))



Figure 1.6 MRI showing atrophy and white matter hyperintensities

Coronal T2-weighted MRI with superficial cortical atrophy seen as widening of the sulci (thick arrows) and deep ventricular atrophy (arrowheads) with widening of the ventricles and hyperintense WMH of presumed vascular origin in the periventricular (linear arrows) and deep (asterix) white matter.

The success of STRIVE is reflected in increasing annual citations with over 2300 as of February 2022 (Clarivate 2022). They are regularly referred to at conferences in formal presentations and in conversation (from personal experience). However, these guidelines do not include all lesions that potentially may contribute to SVD. Cortical infarcts are increasingly recognised as potentially significant in the clinical phenotype of SVD, and may present with lacunar syndromes. Conversely, subcortical lacunes may also present with cortical symptoms (Potter, Doubal et al. 2010). Misclassification usually occurs due to a reliance on clinical criteria in the

absence of appropriate neuroimaging. Microinfarcts are visible on high resolution MRI and in my systematic review were most often found in the cortex. However, these papers specifically studied the cortex and looked at microinfarcts in the context of CAA, which predominantly affects the cortex (Humphreys, Smith et al. 2021), so this may not represent the true distribution of microinfarcts. To date, microinfarcts have been mostly observed in autopsy studies (Brundel, de Bresser et al. 2012, Smith, Schneider et al. 2012), but as clinical MRI field strengths increase, they may become more visible and more prominent in SVD reporting.

Deep ICH is associated with SVD-related arteriopathy (Samarasekera, Smith et al. 2012) whereas CAA is associated with lobar ICH. CAA-associated ICH can be diagnosed by the presence of finger-like haemorrhagic projections with subarachnoid haemorrhage on CT and possession of apolipoprotein E4 APOE e4 genotype (Rodrigues, Samarasekera et al. 2018) or by MRI and application of the modified Boston criteria (Linn, Halpin et al. 2010). However, these patients are often too unwell to undergo MRI, and definitive diagnosis is made on post-mortem examination.

Although there is evidence the neuroimaging lesions included here are involved in SVD, it is not fully understood how, or what contribution they each make to the disease. The STRIVE guidelines only require reporting and sometimes counting the features seen. Use of visual scoring and quantification schemes is recommended where possible but specific schemes are not included (Wardlaw, Smith et al. 2013). A future progression based on more complete evidence of the radiological-clinical-pathological associations may involve integrated diagnosis based on clinical and radiological grading systems.

1.4.2 Radiological white matter hyperintensities

WMH of presumed vascular origin are the most common SVD lesions. They are bilateral and of varying sizes and shapes but usually roughly symmetrical

in the deep white and periventricular white matter. They can also occur in the deep grey nuclei and brainstem where they may be called subcortical hyperintensities. Occasionally they show cavitation. WMH appear as hyperintense on T2-weighted MRI sequences, iso- or hypointense on T1 weighted sequences and hypointense on CT (Figures 1.5 and 1.6) (Wardlaw, Smith et al. 2013).

Radiological WMH are seen in up to 21% of people at 64 years and 94% at 82 years (APA 1994) often with carotid atherosclerosis and elevated plasma homocysteine (Bots, van Swieten et al. 1993, Vermeer, van Dijk et al. 2002). Their presence and progression is associated with a variety of obvious and more inconspicuous neurological problems including reduced motor function, cognitive decline, slower information processing, stroke, all types of dementia and increased mortality (van Dijk, Prins et al. 2008, Debette and Markus 2010, Pinter, Ritchie et al. 2017). Confluent (as opposed to punctate) WMH predict progression from mild cognitive impairment to dementia and can be used to estimate the overall SVD burden. WMH were thought to slowly progress with time, but recent studies showed they can decrease in size (van Leijsen, van Uden et al. 2017, Wardlaw, Chappell et al. 2017). They are therefore considered dynamic lesions. Lesions with the appearances of acute ischaemic infarcts on imaging also have several potential fates and can result in cavitation, WMH-like appearances or disappear (Potter, Doubal et al. 2010), suggesting other SVD lesions are also dynamic. The reasons for these differences are currently unknown.

Technological advances in quantitative imaging, such as diffusion tensor imaging, has allowed functional assessment of the brain microstructure, revealing pathology otherwise invisible by conventional imaging methods and suggesting reduced tissue integrity in WMH compared with non-lesional white matter (Munoz Maniega, Chappell et al. 2017), although abnormalities of otherwise NAWM are also seen. In SVD white matter disease increased mean diffusivity reflects increased magnitude of diffusion and decreased fractional anisotropy and is due to decreased directionality (Alexander, Lee et

al. 2007) implying increased interstitial water content and reduced axonal integrity but with generally retained white matter tract directionality (Le Bihan 2003). These are especially useful measures as water content cannot be measured by histopathological analysis, which is otherwise very good for assessing the finer tissue structure and remains able to detect more subtle white matter changes than standard clinical strength MRI (Fernando, O'Brien et al. 2004).

WMH locations are variable but tend to be closely anatomically related to cerebral projection and commissural white matter tracts (Munoz Maniega, Chappell et al. 2017), explaining some of the clinical expression of SVD. However, abnormalities are also found in otherwise NAWM and cortex on imaging, locally and in distant areas (Baykara, Gesierich et al. 2016). BBB leakage is increased in both WMH and NAWM on *in vivo* imaging studies in association with increased WMH burden and with lacunar stroke (Wardlaw, Doubal et al. 2009, Topakian, Barrick et al. 2010, Munoz Maniega, Chappell et al. 2017). Increased white matter interstitial fluid in SVD correlates with clinical measures of cognitive processing speed and disability (Duering, Finsterwalder et al. 2018) and there is increased mean diffusivity and decreased fractional anisotropy in NAWM. NAWM changes are generally not as severe those in the WMH. A gradation of interstitial fluid is seen, highest in WMH and decreasing through adjacent tissue, but increased relative to controls (Munoz Maniega, Chappell et al. 2017, Duering, Finsterwalder et al. 2018). BBB leakage is identified in the apparently unaffected cerebral cortex (Zhang, Wong et al. 2017). Histological examination of NAWM has also found abnormalities, but the gradual zonation of changes from the centre of the WMH to NAWM has not been thoroughly examined microscopically (Humphreys, Smith et al. 2021). Distant secondary SVD-related lesions are also seen due to damage to and ‘die-back’ of these connecting white matter tracts (Duering, Righart et al. 2015, Baykara, Gesierich et al. 2016). WMH are associated with other SVD lesions in imaging studies, such as PVS, but not consistently (Francis, Ballerini et al. 2019).

1.4.3 Lacunes

A lacune of presumed vascular origin is defined on neuroimaging as “as a round or ovoid, subcortical, fluid-filled (similar signal as CSF) cavity, of between 3mm and about 15mm in diameter” (Wardlaw, Smith et al. 2013) (Figure 1.5). They are within the territory of one perforating arteriole and presumed to be the sequalae of small subcortical infarcts or small deep haemorrhages. It may not be possible to know the origin when only imaging from the chronic phase is available.

Lacunes may be identified on neuroimaging in the absence of any clinical signs or symptoms, but they are associated with increased risk of stroke, dementia and cognitive problems (Vermeer, Prins et al. 2003, Vermeer, Longstreth et al. 2007). In the original pathological studies of SVD, an old fluid-filled cavity was called a lacune and was thought to be the consequence of a lacunar infarction. However, lacunes may have heterogenous origins. They can be the result of ischaemic or haemorrhagic foci (Franke, van Swieten et al. 1991) and not all small deep infarcts become lacunes (Moreau, Patel et al. 2012).

1.4.4 Enlarged perivascular spaces

Enlarged PVS may be seen on *in vivo* MRI and are less than 3mm diameter. They appear as circular profiles when imaged perpendicular to the vessel, or linear if the vessel is viewed along its length. They are fluid filled spaces surrounding the vessels with an MRI signal like that of CSF (Figure 1.5). Most often they are seen in the inferior basal ganglia, as well as cerebral white matter and the midbrain (Wardlaw, Smith et al. 2013). Enlarged PVS are somewhat debated as they are not visible on clinical neuroimaging when normally sized. However, the clinical significance and how this may or may not relate to their enlargement is not currently known. Indeed, even when to call a PVS ‘enlarged’ is not well defined.

Enlarged PVS can be seen in normal brains (Groeschel, Chong et al. 2006), but increased numbers have been associated with older age and other neuroimaging features of SVD including WMH and lacunes (Doubal, MacLullich et al. 2010, Zhu, Tzourio et al. 2010, Potter, Doubal et al. 2015) and a range of other neurological conditions (Wardlaw, Benveniste et al. 2020). PVS on neuroimaging have variously been associated positively with reduced cognition (Maclullich, Wardlaw et al. 2004) and dementia (Patankar, Mitra et al. 2005, Beak, Choi et al. 2015), but other studies have only found uncertain associations (Uiterwijk, Huijts et al. 2014) or even no association (Wardlaw, Benveniste et al. 2020). Enlarged PVS are most frequent in the basal ganglia and thalamus, where they are associated with lacunar stroke and increased risk of vascular dementia (Ding, Sigurethsson et al. 2017). They are also found in the white matter and brainstem (Groeschel, Chong et al. 2006, Humphreys, Smith et al. 2021). More numerous visible PVS on neuroimaging have been associated with more severe WMH development, accumulation of lacunes and microbleeds in a study over four years (Ding, Sigurethsson et al. 2017). They may be associated with CAA and have been seen to be enlarged within subcortical white matter adjacent to areas of cortical CAA (Keable, Fenna et al. 2016), but they are also prevalent in non-CAA brains (Wardlaw, Benveniste et al. 2020). Their distribution is linked to that of ICH, with enlarged PVS seen in cerebral white matter in cases of lobar ICH (associated with CAA) and more prominent basal ganglia PVS seen in cases of deep ICH (associated with arteriolosclerotic SVD) (Charidimou, Meegahage et al. 2013, Martinez-Ramirez, Pontes-Neto et al. 2013). Lesion descriptions in older studies may be unreliable as PVS and lacunes may have been confused as they have potentially similar morphology and size as described earlier (Potter, Marlborough et al. 2011). Overall, their clinical significance remains unknown and somewhat controversial.

Perivascular spaces and lacunes may be difficult to distinguish on imaging. No exact size differentiation is known and there is little evidence available,

but the consensus in the STRIVE guidelines is that lacunes are smaller than 15mm (Wardlaw, Smith et al. 2013) and with a current lower limit of 3mm diameter (Hernandez Mdel, Piper et al. 2013). Enlarged PVS are usually maximum 3mm diameter (Wardlaw, Benveniste et al. 2020) although some studies have found 2mm to be the lower limit of lacunes (Braffman, Zimmerman et al. 1988, Bokura, Kobayashi et al. 1998) and upper limit of enlarged PVS (Matsusue, Sugihara et al. 2006). Size variation may be dependent on location, and both are larger in the basal ganglia where enlarged PVS may also be larger than lacunes (Humphreys, Smith et al. 2021). Whichever criteria are used, it seems they should be applied with care in the appropriate context. Lacunes appear as a central hypointense area which may have a surrounding hyperintense ring on FLAIR or T2-weighted sequences. There may also be a similar appearing ring around perivascular spaces, particularly when they are within an area of WMH. At high magnification, the presence of a central vessel may help differentiate PVS from a lacune (Wardlaw, Smith et al. 2013).

1.4.5 Recent small subcortical infarcts

Recent small subcortical infarcts are within the territory of a single penetrating arteriole, measure less than 20mm diameter in the axial plane (Figure 1.5) and are round, oval or tubular shaped. Their recent nature is seen as hyperintensity on T2-weighted, FLAIR and diffusion weighted MRI sequences, being hypointense on T1 sequences. Small lesions may be differentiated from lacunes by diffusion weighted imaging (Wardlaw, Smith et al. 2013).

Recent small subcortical infarcts may be clinically apparent, referred to as lacunar strokes and responsible for 25% of ischaemic strokes. Intrinsic SVD is the most common cause of clinical lacunar stroke (Shi and Wardlaw 2016). Less often, recent small subcortical infarcts may be clinically silent and only found incidentally on imaging, or conversely, they are not always seen in patients presenting with a clinical lacunar stroke and it is believed about 30%

are not identified on imaging (Makin, Doubal et al. 2015). In the chronic phase, recent small subcortical infarcts may cavitate to become lacunes, remain non-cavitated and appear as a WMH, or disappear. The proportions that result in these different outcomes and the reasons why are not known (Wardlaw, Smith et al. 2013).

1.4.6 Microbleeds

Cerebral microbleeds are small, round or oval lesions, measuring less than 10mm. They appear as areas of signal void on paramagnetic sequences, such as T2*-weighted GRE sequences but are not visible on other MRI sequences or CT (Wardlaw, Smith et al. 2013). GRE sequences are sensitive to compounds including haemosiderin, ferritin and deoxyhaemoglobin and identify blood or blood products (among other things) (Schweser, Deistung et al. 2010). Microbleeds are usually found in the cortico-subcortical region, deep white and grey matter, brainstem and cerebellum. Blooming artefact can make them appear larger than they are, but is inconsistent, making it difficult to define size criteria, although it can help to identify small lesions (Mittal, Kalia et al. 2010). Microbleed size may also vary depending on the imaging parameters used (Greenberg, Vernooij et al. 2009). Care must be taken to avoid misinterpretation; blood, blood products or similar radiological appearances can also be seen in chronic foci of haemosiderin-laden macrophages, haemorrhagic malignancies such as metastatic melanoma, as well as calcifications, vascular malformations including aneurysms or cavernous malformations, or diffuse axonal injury (DAI) (Greenberg, Vernooij et al. 2009). The STRIVE guidelines recommend the use of previously published guidelines for reporting and interpreting microbleeds, in the general setting (Greenberg, Vernooij et al. 2009) and in specific clinical settings such as cases of AD and anti-Aß, immunotherapy (Sperling, Salloway et al. 2012).

The importance of microbleeds has only relatively recently been appreciated (Cordonnier, Al-Shahi Salman et al. 2007). Today their presence on

neuroimaging is associated with over 30 different conditions including SVD, AD, vascular dementia and normal aging (Humphries and Mathew 2019). Their interpretation and the clinical relevance of microbleeds on imaging is not completely understood but they have been associated with lacunes and white matter hyperintensities (Cordonnier, Al-Shahi Salman et al. 2007). They have an increased prevalence in haemorrhagic and ischaemic stroke, potentially representing increased risk of recurrent haemorrhage with implications for anti-thrombotic treatment (Cordonnier, Al-Shahi Salman et al. 2007). Microbleeds may be an indicator of more widespread vasculopathy. Like large ICH, their distribution may suggest the underlying pathology. Lobar microbleeds suggest underlying CAA (Vinters and Gilbert 1983) and those in the deep white and grey matter, brainstem and cerebellum indicating so-called arteriolosclerotic arteriopathy (Fazekas, Kleinert et al. 1999).

1.4.7 Brain atrophy

Brain atrophy refers to reduced brain volume, assessed by comparing the brain volume to the inner aspect of the skull and assessing the amount of CSF present. It incorporates generalised global and regional atrophy, but excludes tissue loss secondary to a specific injury. Affected sub-regions should be specified (Wardlaw, Smith et al. 2013). It can be identified by enlargement of superficial sulci or the ventricles (Figure 1.6). Brain atrophy is seen in normal aging, although it is variable and generally of a lesser degree. While the STRIVE guidelines recognise aging as a cause of atrophy, they do not specify how to differentiate between pathological and normal aging.

Brain atrophy may represent a variety of pathological substrates including, cortical or white matter volume loss, neuronal loss and is associated with SVD vasculopathies including arteriolosclerosis and venous collagenosis (Black, Gao et al. 2009). It is associated with reduced global cognitive function, irrespective of periventricular WML, which are associated with compromised executive function (Fein, Di Sclafani et al. 2000, Swartz, Stuss et al. 2008).

1.5 The histopathology of small vessel disease

Pathological substrates of SVD that affect arterial vessels include arteriolosclerosis, lipohyalinosis, fibrinoid necrosis and small vessel atherosclerosis. Venules are also affected by SVD pathology, for example by venous collagenosis, although there is much less literature available around them (Hamilton, Brosnan et al. 2001, Black and Garbutt 2002, Wuerfel, Haertle et al. 2008, Doubal, MacGillivray et al. 2009, Lindley, Wang et al. 2009, Bailey, Smith et al. 2011). The size of affected vessels stated in the literature varies, for example vessels less than 300μm (Rosenblum 2008), vessels between 40-300μm, between 40-200μm (Fisher 1991), between 40-150μm (Deramecourt, Slade et al. 2012), an outer vessel diameter of less than 200μm (Berry, Sidik et al. 2019) or less than 150μm (Skrobot, Attems et al. 2016). There are no agreed histological descriptions of the relevant lesions. Here I provide a brief summary review of terms used in the literature in advance of the systematic review (Chapter 2). Grading systems to assess the severity of small vessel disease burden would be useful but have not been agreed or published.

1.5.1 Vascular small vessel disease lesions

1.5.1.1 Arteriolosclerosis

The most common vascular lesion is arteriolosclerosis. Concentric, eosinophilic hyaline thickening of the arteriolar wall results in narrowing of the lumen (Figure 1.7a). There is loss of the smooth muscle cells and fibrosis (Berry, Sidik et al. 2019) resulting in vessel profiles that often appear circular as the elasticity is lost (personal observation).

1.5.1.2 Lipohyalinosis

Lipohyalinosis is rarely defined in the literature. It is an asymmetric lesion in the vessel wall with fibrosis, hyalinosis and foamy macrophages (McAleese, Alafuzoff et al. 2016) (Figure 1.7b).

1.5.1.3 Fibrinoid necrosis

Fibrinoid necrosis is the result of plasma proteins leaking from the lumen and being deposited in vessel walls (Figure 1.7c), including fibrin and fibrinogen. Fibrinoid necrosis appears similar to hyalinisation on light microscopy, which may account for some of the confusion between them. Both show eosinophilic thickening of the wall with loss of the normal cellular structure, but fibrin stains more intensely, forming visible threads. Fibrin can be identified with various tinctorial stains including a trichrome stain (which would also identify hyaline), phosphotungstic acid or a Putz stain (Rosenblum 2008). Fibrinoid necrosis is segmental along the vessel wall and may not be fully circumferential, so may be missed if under-sampled. The nature of the fibrin deposition has not been comprehensively studied and it is not known if it is a form of true necrosis (Bajema and Bruijn 2000).

1.5.1.4 Small vessel atherosclerosis

Small vessel atherosclerosis is rare in this era of aggressive anti-hypertensive treatment but is still found occasionally (Lammie 2002, Li, Yang et al. 2018). The features are the same as in large vessels with intimal thickening and foamy macrophage accumulation, cholesterol clefts and mural calcification (Figure 1.7d).

1.5.1.5 Venous lesions

Venous lesions are increasingly recognised in SVD, although studies are limited and their nature, pathogenesis and significance remain unknown. Venous collagenosis (Figure 1.8), or venulopathy, is found predominantly in the periventricular area as relatively delicate-appearing collagenous thickening of the venule walls with luminal stenosis and occasional occlusion (Moody, Brown et al. 1995). Venous collagenosis is associated with increased periventricular WMH and increased age in one study (Black, Gao et al. 2009) but another study found no associations between visible venules on 3T MRI and PVS, WMH or hypertension (Jochems, Blair et al. 2020).

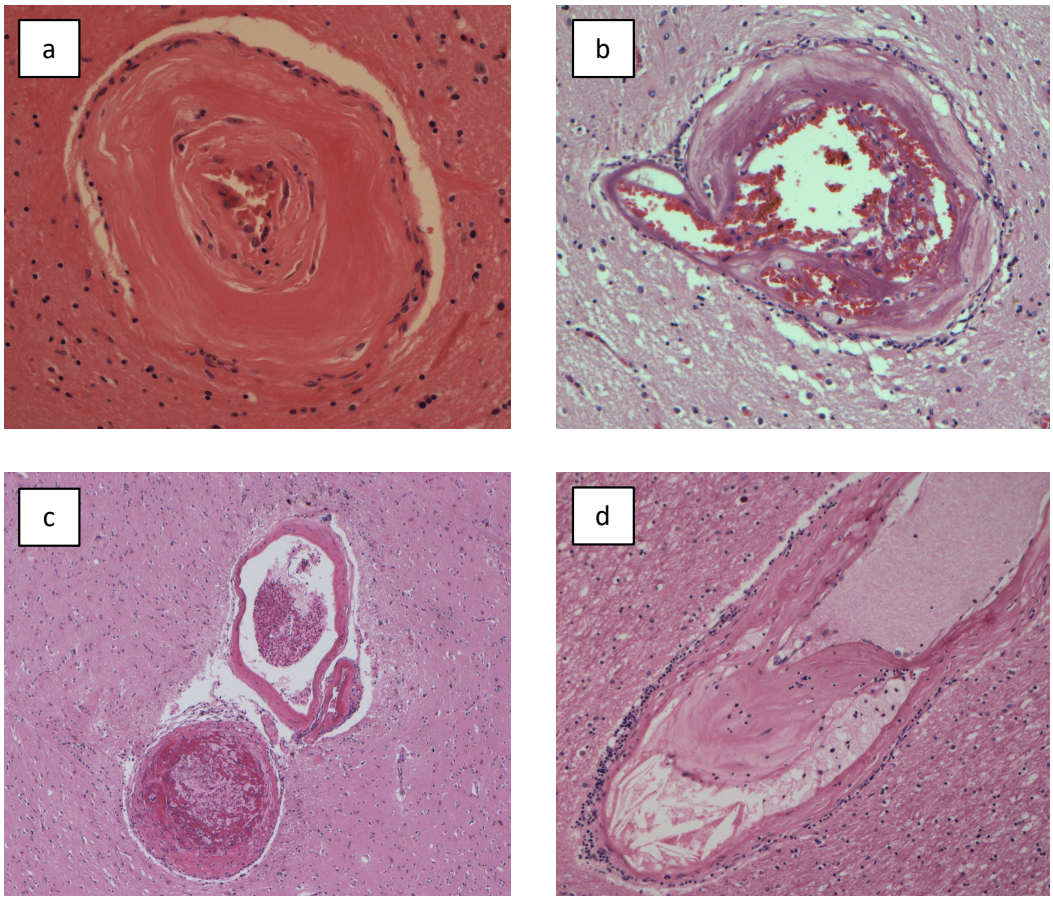


Figure 1.7 Histological vascular lesions in SVD

a) Arteriolosclerosis showing concentric eosinophilic thickening of the vessel wall with narrowing of the lumen is the most common manifestation of SVD (H&E x400). b) In lipohyalinosis there is asymmetrical homogenous thickening of the vessel wall with foamy macrophage infiltration. In this example a small Charcot-Bouchard aneurysm is also seen (H&E x200). c) Fibrinoid necrosis with intensely eosinophilic fibrin deposition in the vessel wall (H&E x100). d) Small vessel atherosclerosis has the same features as that in large vessels with intimal thickening, foamy macrophages and cholesterol clefts. Calcification may also be seen (H&E x200).

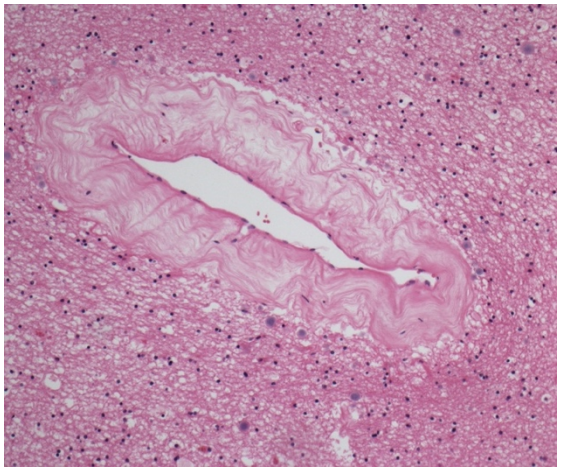


Figure 1.8 Venous collagenosis

Venous collagenosis involving a small venule in the periventricular region. There is fine collagenous expansion of the venular wall (H&E x200)

There may be a relationship between the number of visible venules on imaging and venous sinus pulsatility, but studies have found conflicting results so far (Blair, Thrippleton et al. 2020, Jochems, Blair et al. 2020) and overall there has been very little research into the significance of venules in SVD. One study linked venous collagenosis with WMHs in both AD and aged non-AD brains (Keith, Gao et al. 2017). It is not clear if the collagenosis seen affects exclusively venous vessels.

1.5.2 Parenchymal small vessel disease lesions

Parenchymal damage (Figure 1.9) includes enlarged perivascular spaces, white matter rarefaction, infarcts and haemorrhage. The evolution of the vascular and tissue damage is not clear, but the relative frequency of some lesions such as arteriolosclerosis, perivascular space enlargement and white matter rarefaction might suggest they are core to the disease process and contribute to other forms of damage.

1.5.2.1 Enlarged perivascular spaces

Enlarged PVS can be described as abnormally large areas of perivascular clearing (Figure 1.9a), although a range of varying definitions describing different features are found in the histological literature (Humphreys, Smith et al. 2021). When they were first identified on histology, PVS were attributed to processing artefact or to age-related cell loss (Wardlaw, Benveniste et al. 2020). They are common lesions, but it is not known if, or to what extent, some perivascular clear space is normal and how abnormal or significant perivascular spaces of different sizes or in different locations are. They are prevalent in the deep grey matter and subcortical white matter but not cortex (Braffman, Zimmerman et al. 1988, Zhang, Inman et al. 1990, Bokura, Kobayashi et al. 1998).

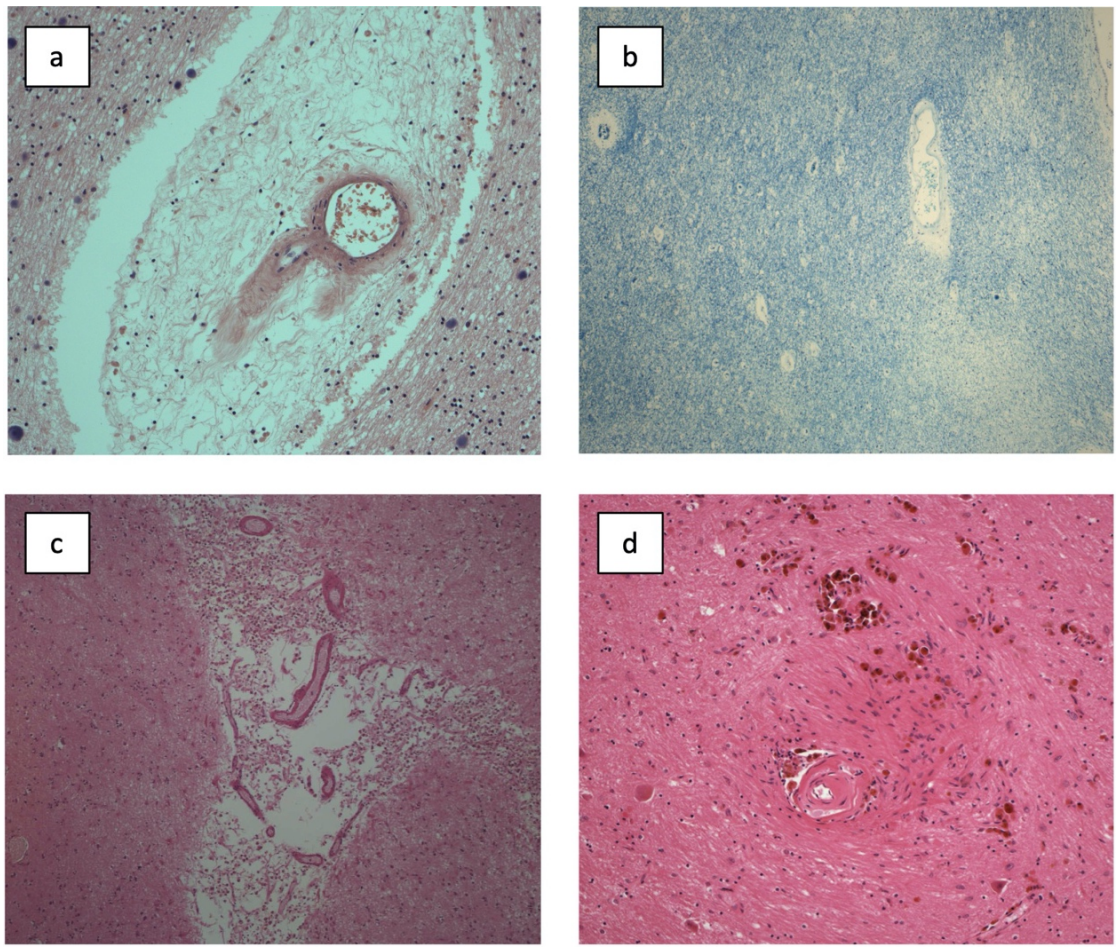


Figure 1.9 Parenchymal lesions associated with SVD

a) Enlarged perivascular spaces can be differentiated from processing artefact by the presence of cellular elements within the perivascular space (H&E x200). b) White matter rarefaction describes an area in which the normal myelin density of the white matter is altered such that an area of pallor can be seen (LFB x10). c) A lacunar infarct with cavitation and surrounding gliosis (H&E x100). d) A subcortical microbleed around an abnormal small vessel, with abundant haemosiderin containing macrophages and reactive gliosis (H&E x200).

1.5.2.2 White matter rarefaction

White matter rarefaction is seen as an area of relatively pale-staining white matter. It can be seen on haematoxylin and eosin (H&E) or myelin stains such as myelin basic protein (MBP) or Luxol fast blue (LFB) (Figure 1.9b) (Bronge, Bogdanovic et al. 2002, Fernando, Simpson et al. 2006, McAleese, Firbank et al. 2013).

1.5.2.3 Lacunar infarct

Infarcts of different sizes are also seen in SVD, although size criteria are not defined. A lacunar infarct is larger than a microinfarct and is said to be due to occlusion of a perforating vessel (Braffman, Zimmerman et al. 1988, van Swieten, van den Hout et al. 1991, Munoz, Hastak et al. 1993) (Figure 1.9c). Sizes of between 1 and 20 mm have been described (Bokura, Kobayashi et al. 1998, Matsusue, Sugihara et al. 2006). Pathological classification of the evolution of lacunar infarcts has been attempted (Poirier and Derouesne 1984) but has not been widely adopted.

1.5.2.4 Microinfarcts

Microinfarcts are only visible microscopically, although sizes up to 5mm have been quoted (Polvikoski, van Straaten et al. 2010). They feature central pallor, cell loss and gliosis and may be cavitated. A lacunar infarct appears similar, with tissue pallor, cell loss or damage and gliosis, which may also be cavitated.

1.5.2.5 Microbleeds

Haemorrhages of all sizes are seen in SVD. Microbleeds are microscopic deposits of haemosiderin within macrophages, usually found adjacent to a vessel (Figure 1.9d). They are associated with so-called hypertensive SVD in the deep grey nuclei, brain stem and cerebellum (Fazekas, Kleinert et al. 1999) and CAA in a lobar distribution (Knudsen, Rosand et al. 2001).

1.5.2.6 Large haemorrhages

Large recent haemorrhages show massive red cell extravasation and tissue necrosis. When older, there is extensive deposition of blood-breakdown products, some within macrophages, with cell loss and gliosis.

1.5.3 Cerebral amyloid angiopathy

CAA generally affects the more superficial aspects of the brain. Aß is deposited in the walls of leptomeningeal, neocortical and superficial white matter arterial vessels and capillaries where it is thought to be phagocytosed by pericytes and smooth muscle cells (Wardlaw, Benveniste et al. 2020). It affects the posterior cerebrum more than the anterior aspects, particularly in the presence of Alzheimer's disease neuropathological change (AD-NC) (Attems, Jellinger et al. 2005). It may also be deposited in the allocortex and cerebellum. CAA is associated with other SVD lesions including microbleeds, microinfarcts, superficial siderosis and enlarged PVS, those in the centrum semiovale and basal ganglia being associated with microbleeds (Linn, Herms et al. 2008, Smith, Schneider et al. 2012, Boulouis, Charidimou et al. 2017), but not associated with hypertension (Biffi and Greenberg 2011). The Aß deposition is seen as acellular eosinophilic thickening of the adventitia and media which shows apple green birefringence on Congo red staining. It replaces smooth muscle cells and eventually extends into the intima, but remains sub-endothelial (Pantoni and Gorelick 2014). CAA-angitis and CAA-related inflammation are rare but may be seen, with lymphocytes, polynuclear giant cells and sometimes granuloma formation within and around the vessel wall (Vinters 1987, Pantoni and Gorelick 2014).

The pathophysiology of CAA is relatively well understood; Aß peptide normally removed from the brain via glymphatic and vascular routes accumulates as abnormal insoluble fibrillar deposits within vessel walls damaging them and eventually leading to microinfarcts, microbleeds and large lobar haemorrhage (Weller, Subash et al. 2008, Miners, Kehoe et al. 2011).

1.5.4 Histological examination

Post-mortem tissue examined for SVD often shows end-stage lesions, akin to a scar, because SVD is often undiagnosed for a long time during life and is

not typically a direct cause of death (Bailey, Smith et al. 2012). It is difficult to unravel pathological mechanisms from end-stage tissue. However, tissue-based studies reflect the multifactorial, complex picture seen clinically and on imaging. This is confounded by the lack of consensus and inconsistent approach to the terminology used for histological SVD lesions, and the relationship between parenchymal and vascular lesions (Grinberg and Heinsen 2010, McAleese, Alafuzoff et al. 2016), which remains a key problem in the pathological literature.

Inter-departmental surveys have identified inconsistencies, including lack of agreement on what the term 'small vessel' actually describes. It is often only to describe arteriolar vessels, neglecting capillary and venule involvement (Pantoni, Sarti et al. 2006, Alafuzoff, Gelpi et al. 2012). Unfortunately, the extent to which this affects the research literature has not been quantified. Various grading systems have been proposed (Deramecourt, Slade et al. 2012, Smallwood, Oulhaj et al. 2012, Skrobot, Attems et al. 2016), but these tend to focus on assessing the contribution of vascular pathology to overall cognitive decline rather than an independent assessment of SVD burden allowing a correlation with non-cognitive clinical phenotypes. In addition, there is limited comparison of SVD histological and imaging appearances and clinical phenotypes, so the concurrence between them is unclear.

Superficially located microbleeds and microinfarcts are seen histologically. Current commonly used clinical imaging thresholds are unable to detect many of them (van Veluw, Charidimou et al. 2016), however they are increasingly recognised and reported as imaging technologies advance. They are considered part of the sporadic SVD spectrum but their pathophysiology is not fully understood and the haemorrhagic pathology may have a different pathophysiology from the so-called 'ischaemic' disease affecting the white matter and deep grey structures. Consensus-based guidelines for histological assessment and grading of CAA have been published and are used by the neuropathological community (Love, Chalmers et al. 2014).

1.6 Risk factors

1.6.1 Hypertension

There is a complex relationship between SVD and risk factors. SVD is associated with traditional vascular risk factors, with hypertension in particular, especially with diastolic blood pressure (van Dijk, Prins et al. 2008, Gottesman, Coresh et al. 2010) and SVD remains prevalent despite relatively aggressive anti-hypertensive therapy. Hypertension has also been linked with BBB leakage (Munoz Maniega, Chappell et al. 2017), although hypertension explains only a proportion of SVD (Jackson and Sudlow 2005). One in three people with SVD have normal blood pressure and not all people with hypertension develop SVD (Lammie, Brannan et al. 1997). Some studies have found previous or current hypertension is associated with WMH (van Dijk, Prins et al. 2008, Marcus, Gardener et al. 2011) but others found no such association (Gouw, van der Flier et al. 2008). As described above, recent guidelines suggest targeting lower systolic blood pressures than those generally recommended may slow progression of sporadic cerebral SVD (Wardlaw, Debette et al. 2021). Microbleeds specifically have been associated with hypertension and other hypertension-associated pathologies including left ventricular hypertrophy (Lee, Park et al. 2004), WMH and lacunes (Jeerakathil, Wolf et al. 2004, Vernooij, van der Lugt et al. 2008). These in turn are associated with larger ICH, providing a link between microbleeds and large ICH. Increased PVS in the basal ganglia on neuroimaging have also been associated with hypertension (Francis, Ballerini et al. 2019).

1.6.2 Age

Increased age is strongly associated with sporadic SVD (Mok, Srikanth et al. 2014) and the prevalence of SVD rises with increasing years. In addition, cigarette smoking and higher disease burden (WML and lacunar infarcts) at baseline are associated with WML progression (van Dijk, Breteler et al. 2004, van Dijk, Prins et al. 2008). Smoking is associated with increased SVD

burden and cortical thinning on imaging, with increased risk of stroke and dementia in sporadic and monogenic SVD (Staals, Makin et al. 2014, Karama, Ducharme et al. 2015, Chabriat, Herve et al. 2016), but not with PVS (Zhu, Tzourio et al. 2010).

1.6.3 Inflammation

Inflammation is implicated in the pathogenesis of SVD and was documented as early as the 1800's (Durand-Fardel 1873) but its full contribution and role is not known. Enlarged PVS and WMH are each associated with raised levels of circulating inflammatory markers (Aribisala, Wiseman et al. 2014, Brown, Benveniste et al. 2018). Chronic inflammatory diseases including multiple sclerosis (MS) (Ge, Law et al. 2005, Wuerfel, Haertle et al. 2008) and systemic lupus erythematosus (Wiseman, Bastin et al. 2016, Miyata, Kakeda et al. 2017), and raised levels of systemic inflammatory markers (Aribisala, Wiseman et al. 2014) have all been associated with visible PVS on neuroimaging studies. In MS, it has been reported that the enlarged PVS are transient, appearing at the periphery of the lesions when acute and active but resolving as the inflammation subsides, and that the visible spaces may be may be perivenular (Ge, Law et al. 2005), although a study specifically looking at the relationship of venules and MRI-visible PVS found the majority of the visible PVS in the centrum semiovale are around arterioles (Jochems, Blair et al. 2020). Inflammatory cells, usually macrophages, may be present within enlarged PVS on histological studies of SVD in humans (Fisher 1982, Kalaria 2012). Inflammation may disrupt PVS function (Wardlaw, Benveniste et al. 2020), but this remains to be proven. Endothelial cells and the BBB are involved in inflammatory signalling processes and regulate inflammatory cell migration into the brain. Activated endothelial cells express increased amounts of inflammatory-related adhesions molecules including VCAM-1 and ICAM-1 (Zhang, Defelice et al. 2010) and mural deposition of proteins such as fibrin extravasated through a dysfunctional BBB can cause localised inflammation with activated microglia and systemic macrophage recruitment (Petersen, Ryu et al. 2018). Parenchymal inflammation is also seen in a

mouse model of progressive carotid occlusion (Hattori, Enmi et al. 2016) and in a rodent model of SVD, the spontaneously hypertensive stroke-prone rat (SHRSP), a high salt diet caused raised serum inflammatory markers, abnormal acute phase response pathways and proteinuria (Sironi, Tremoli et al. 2001). Trials of drugs with anti-inflammatory mechanisms are underway and include colistazol, a phosphodiesterase 3' inhibitor and isosorbide mononitrate, an NO donor (Wardlaw, Smith et al. 2019).

1.6.4 Salt

Excess dietary salt is another modifiable risk factor associated with increased risk of lacunar stroke, WMH and overall severity of SVD (Wardlaw, Smith et al. 2019). In the SHRSP model salt-loading is used to accelerate the onset of SVD-like pathology (Di Nicolantonio and Silvapulle 1988). Both SHRSP and control rats fed a high-salt diet showed decreased endothelial tight junction proteins and increased microglial activation, although tight junction protein reduction was also seen in SHRSP fed a normal diet (Bailey, Wardlaw et al. 2011). The SHRSP animals in these studies also have increased gliosis and hypertension.

1.6.5 Cognitive and brain reserve

Cognitive reserve is a measure reflecting whole life brain function, affected by lifestyle factors including physical and intellectual exercise (Wong, Lau et al. 2016). It refers to how a brain carries out certain tasks and is usually measured clinically by level of education achieved or IQ testing (Wardlaw, Smith et al. 2019). A relatively recent concept, higher cognitive reserve is associated with better cognition after a lacunar stroke (Makin, Doubal et al. 2018) and improved outcomes in SVD; cognition, processing speed and motor function are relatively preserved (Jokinen, Melkas et al. 2016). Brain reserve reflects the structural integrity of the brain in relation to its ability to function in the event of damaging pathology, in terms of, for example, synapse numbers and neuronal quantity and integrity (Stern 2012). It is

further compromised as SVD-related damage accumulates. In stroke, the size and location of the lesion affects the risk of subsequent cognitive impairment. Increased risk is associated with large or strategically located infarcts involving areas including the thalamus, hippocampus and dominant cerebral hemisphere (Pendlebury and Rothwell 2009, Pendlebury 2012). The clinical consequences and individual experience of SVD likewise probably depend on a range of factors beyond the initial insults including, but not limited to, the location affected, severity of disease, presence of co-morbidities, cognitive and brain reserve, secondary effects within the brain and patient age (Wardlaw, Smith et al. 2019).

1.7 Pathophysiology of small vessel disease

1.7.1 Historical work

The first descriptions of SVD date back to 1843 when Durand-Fardel first used the term lacune to describe small lesions “with no associated alteration of colour or consistency” and a “fine meshwork containing very small vessels” extending from them, and état criblé, meaning “riddled with shot or sieve-like”, as “numerous canals or small round holes…from each of which a small vessel projected” (Durand-Fardel 1843). From the 1960’s onwards, Fisher discussed and described the ideas put forward over the years in a series of detailed autopsy studies. He described the “close parallel of [cerebral arterial] atherosclerosis and lacunar disease”, although with exceptions, and a direct association with hypertension, but not diabetes (Fisher 1965), and he brought together many of the terms now used in the histopathological literature. Fisher used état lacunaire for a condition of multiple lacunes at autopsy and described how foci of “segmental arterial disorganization”, with fine connective tissue replacing the vessel wall, sometimes with cholesterol clefts, foamy macrophages or luminal occlusion was the most common cause of lacunar infarction (Fisher 1968). He believed lipohyalinosis to be due to systemic hypertension and lacunes the result of healed lacunar infarcts, appearing as small fluid-filled spaces within the

parenchyma (Fisher 1965, Fisher 1968). However, he appeared to use the terms lipohyalinosis, angionecrosis and fibrinoid necrosis interchangeably, preferring 'lipohyalinosis' as he believed fibrinoid necrosis contained lipidised cells (Fisher 1968, Rosenblum 2008). While he may have intended lipohyalinosis to be distinct from hyalinosis, there seems to be confusion in subsequent literature, with some authors concluding fibrinoid necrosis leads to lipohyalinosis. A review found no evidence to support this and it seems much more likely that they are distinct processes that often occur simultaneously (Rosenblum 2008).

Fisher's original descriptions of lacunes, including morphology (an irregular cavity containing fine fibrillary material), location (deep grey nuclei, base of pons, internal capsule, deep white matter and cerebellar white matter) and size (0.5-15 mm) (Fisher 1968) are remarkably similar to the lesions we see today, despite aggressive anti-hypertensive treatment. This suggests alternative, or at least additional, underlying pathophysiology. The original ischaemic atherosclerotic hypothesis is also no longer supported as histological vascular occlusion and small vessel atherosclerosis are now rarely seen (Lammie, Brannan et al. 1997, Moore, Altarescu et al. 2003). Cardiovascular risk factors, such as hypertension, remain strongly associated with SVD but do not fully account for the risk of developing SVD, and atherosclerotic disease is not associated with SVD burden (Chabriat, Joutel et al. 2009, Wardlaw, Smith et al. 2013). Animal studies do not support cerebral hypoperfusion causing SVD (Joutel, Monet-Lepretre et al. 2010). Only modest associations between imaging and clinical features of SVD have been found (Gouw, Seewann et al. 2011) making it difficult to recognise the relevant risk factors and associations, but there is increasing evidence of a genetic contribution.

1.7.2 Vascular dysfunction

Research supports vascular dysfunction-associated mechanisms initiating sporadic SVD. Heterogenous histological features suggest SVD is due to

multifactorial pathophysiological mechanisms potentially converging on common pathways resulting in a restricted number of outcomes. This could be the result of multiple defects due to genetic predisposition, environmental risk factors, or both. Single or multiple genetic abnormalities could render individuals susceptible to other insults, ultimately leading to vascular malfunction, tissue damage and SVD. Monogenic SVDs have informed potential mechanisms involved in sporadic SVD. Information on genetic abnormalities in sporadic SVDs is less well understood, although, to date, 52 independent genetic loci have been implicated (Bordes, Sargurupremraj et al. 2022), mostly in large-scale genome-wide association studies (GWAS), suggesting common mechanisms and pathways that may be involved in SVD development.

1.7.2.1 Potential mechanisms

Proposed vascular mechanisms underlying the development of SVD include endothelial dysfunction and BBB disruption causing leakage of plasma components out of the vessel lumen, into the vessel wall and brain parenchyma (Wardlaw, Sandercock et al. 2003). GWAS highlight genetic changes involving the extracellular matrix (Haffner, Malik et al. 2016). Vessel wall abnormalities are commonly seen on histology in agreement with these studies, with basement membrane changes, loss of contractile cells and protein deposition (Joutel, Haddad et al. 2016). Presumed ischaemic lesions and haemorrhagic foci in the parenchyma may be consequences of the vascular changes. The endothelium is continuous throughout the brain and so logically could have a role in the global abnormalities seen in SVD, potentially instigating the downstream abnormalities. Endothelial dysfunction has been found before the onset of BBB breakdown in the SHRSP model (Horsburgh, Wardlaw et al. 2018), but the definitive initiating factor(s) remain unknown.

Hypertension-associated consequences, such as increased arteriolar stiffness, could exacerbate or initiate endothelial or other small vessel

damage by exposing intracerebral vessels to pulsations normally absorbed by elastic arterioles. A genetic risk locus for cerebrovascular risk factors including hypertension, type 1 diabetes mellitus and increased cholesterol is associated with small vessel stroke (Kilarski, Achterberg et al. 2014). There are several cross links between hypertension, potential mechanisms and associated genetic changes, highlighting the complexity of associations and possible interactions.

1.7.2.2 Histology

Neuropathological studies support the concept of a global neurovascular dysfunction with increased brain water content and altered perfusion. Immunohistochemical studies of human post-mortem brain tissue have found vascular structural abnormalities with extravasation of plasma components in both WML and NAWM (Tomimoto, Akiguchi et al. 1996, Young, Halliday et al. 2008, Simpson, Wharton et al. 2010), but this is not a universal finding (Bridges, Andoh et al. 2014, Hainsworth, Minett et al. 2017). It is not possible to directly assess water content using histological assessment as with advanced imaging techniques. However, tissue rarefaction and vacuolation used as surrogates (Guimiot, Garel et al. 2008) are associated with radiological WML and increased SVD burden (Lammie, Brannan et al. 1998).

Increased venous pulsatility is positively associated with WMH volume and number of basal ganglia PVS in *in vivo* phase-contrast MRI (Shi, Thrippleton et al. 2020). Abnormal pulsatility could also have implications for normal PVS function and glymphatic fluid movement. Studies of normal aging show vascular basement membrane alterations involved in vessel ‘stiffening’ with increased proportions of collagen and reduced smooth muscle and elastin content (Hajdu, Heistad et al. 1990). Abnormalities of the vascular endothelium could have important consequences for the many direct and indirect interactions the endothelium has with the components of the different functional units within the brain, including the BBB. Damage to different components of the vessel wall and interrupted communication between the

vessel and the parenchyma could alter the ability of vessels to respond to requirements and direct flow appropriately, causing the flow and reactivity abnormalities identified (Sam, Crawley et al. 2016, Shi, Thrippleton et al. 2016, Promjunyakul, Dodge et al. 2018, Blair, Thrippleton et al. 2020).

1.7.2.3 Neuroimaging

Human imaging studies further support the concept of endothelial failure directly causing pathology in SVD; abnormal arterioles are seen within areas of presumed lacunar infarction, rather than being situated proximally (Wardlaw, Dennis et al. 2001). Increased BBB permeability is seen in humans using advanced neuroimaging techniques, as previously described, and is associated with increased age and SVD (Gouw, Seewann et al. 2011, Wharton, Simpson et al. 2015, Wardlaw, Makin et al. 2017), vascular dementia (Farrall and Wardlaw 2009) and monogenic SVD such as CADASIL (Ghosh, Balbi et al. 2015). BBB leakage is associated with cognitive problems (Makin, Turpin et al. 2013) and hypertension clinically (Maillard, Seshadri et al. 2012), and also with prominent PVS and lacunar stroke, on imaging and histology of both animal models and humans (Bailey, McCulloch et al. 2009, Wardlaw, Doubal et al. 2009).

An *in vivo* imaging study found BBB leakage in normal-appearing white matter with increasing leakage closer to the WMH, and maximal leakage in the WMH. BBB leakage was worst in the brightest (most intense) WMH compared to less intense WMH. Interstitial water content and axonal disruption were also seen in NAWM, following the same pattern of increasing towards, and being maximal in, the WMH (Wardlaw, Makin et al. 2017). BBB leakage also predicted declining cognition at 1 year after mild stroke (Wardlaw, Makin et al. 2017).

1.7.2.4 Haemorrhagic small vessel disease

Different mechanisms are suggested in haemorrhagic SVD, but they are not clear. Similar vessel wall defects are seen, in particular loss of vascular

smooth muscle cells and the vessel wall becomes fibrotic, or hyalinised or otherwise weakened and prone to rupture and haemorrhage. In humans and mice with COL4 mutation there is spontaneous deep haemorrhage, without hypertension. Dual vascular defects, each with different underlying mechanisms, may be the result of the genetic mutation and responsible for the propensity to bleed. In the mouse model, smooth muscle cell loss and increased intraluminal pressure in arterioles is associated with hypermuscularisation and mural thickening of the transitional segment between the arteriole and capillary due to increased Notch3 activity (Ratelade, Klug et al. 2020). The thickened vessel wall in the transitional segment might cause the increased arteriolar pressure, which is vulnerable to rupture due to the loss of the smooth muscle cells. Similar hypermuscularisation was found in post-mortem brain tissue from humans who had had sporadic deep intracerebral haemorrhage in life. However, in CADASIL, a monogenic SVD with significant loss of cerebrovascular smooth muscle cells, cerebral haemorrhage is uncommon (Chabriat, Joutel et al. 2009).

1.8 Genetics of small vessel disease

Various genetic changes are associated with SVD features and they may render an individual more likely to develop SVD. Vascular basement membrane abnormalities are seen in both monogenic and sporadic SVD and argue for shared downstream mechanisms, possibly with a genetic contribution. Proteomic studies support a multifaceted pathogenesis involving smooth muscle and basement membrane abnormalities (Martinez-Lemus, Zhao et al. 2011). Acquired matrisomal abnormalities in cerebral vessels, especially due to hypertension, have not been particularly well investigated but cannot be excluded (Joutel, Haddad et al. 2016).

Genetic changes in BBB components have been associated with the presence of SVD features on neuroimaging including the pericyte associated Foxf2 (Malik, Chauhan et al. 2018) and NOTCH3, expressed by smooth

muscle cells (Schmidt, Zeginigg et al. 2011). Most genetic associations have been with radiological WMH, including three loci implicated in inflammatory and glial proliferation pathways (Verhaaren, Debette et al. 2015) but genes involved with osmotic regulation, neurodevelopmental problems, cognitive impairment and oxidative phosphorylation have also been identified (Anderson, Biffi et al. 2013, Lopez, Hill et al. 2015).

There is also an interesting relationship with APOE. The e4 allele is commonly associated with AD but also has been found associated with increased WMH. The e2 allele, protective against AD, is associated with increased risk of CAA, intracerebral haemorrhage (McCarron and Nicoll 2000, Biffi, Sonni et al. 2010, Biffi, Anderson et al. 2011), increased WMH in CADASIL (Gesierich, Opherk et al. 2016) and histological vasculopathies seen in CAA including fibrinoid necrosis, microaneurysms and double barrelling of the vessel wall (Greenberg, Vonsattel et al. 1998).

1.8.1 Monogenic SVD

The identification of causative mutations in human monogenic small vessel diseases has enabled further understanding of specific mechanisms that may be involved in sporadic SVD. Although rare, several monogenic forms of SVD with different genetic causes but similar pathological features occur in younger people (Marini, Anderson et al. 2020), reinforcing the concept of SVD as a distinct disease, as opposed to an inevitable consequence of old age (Haffner, Malik et al. 2016) and allowing study of cellular and molecular disease mechanisms in single-gene SVD in a younger patient group who often have fewer confounding co-morbidities. They have also led to studies looking for a common downstream mechanism upon which the different disease pathways converge, to understand the ultimate abnormality in SVD and potentially be a therapeutic target (Figure 1.10) (Tan and Markus 2015, Joutel, Haddad et al. 2016).

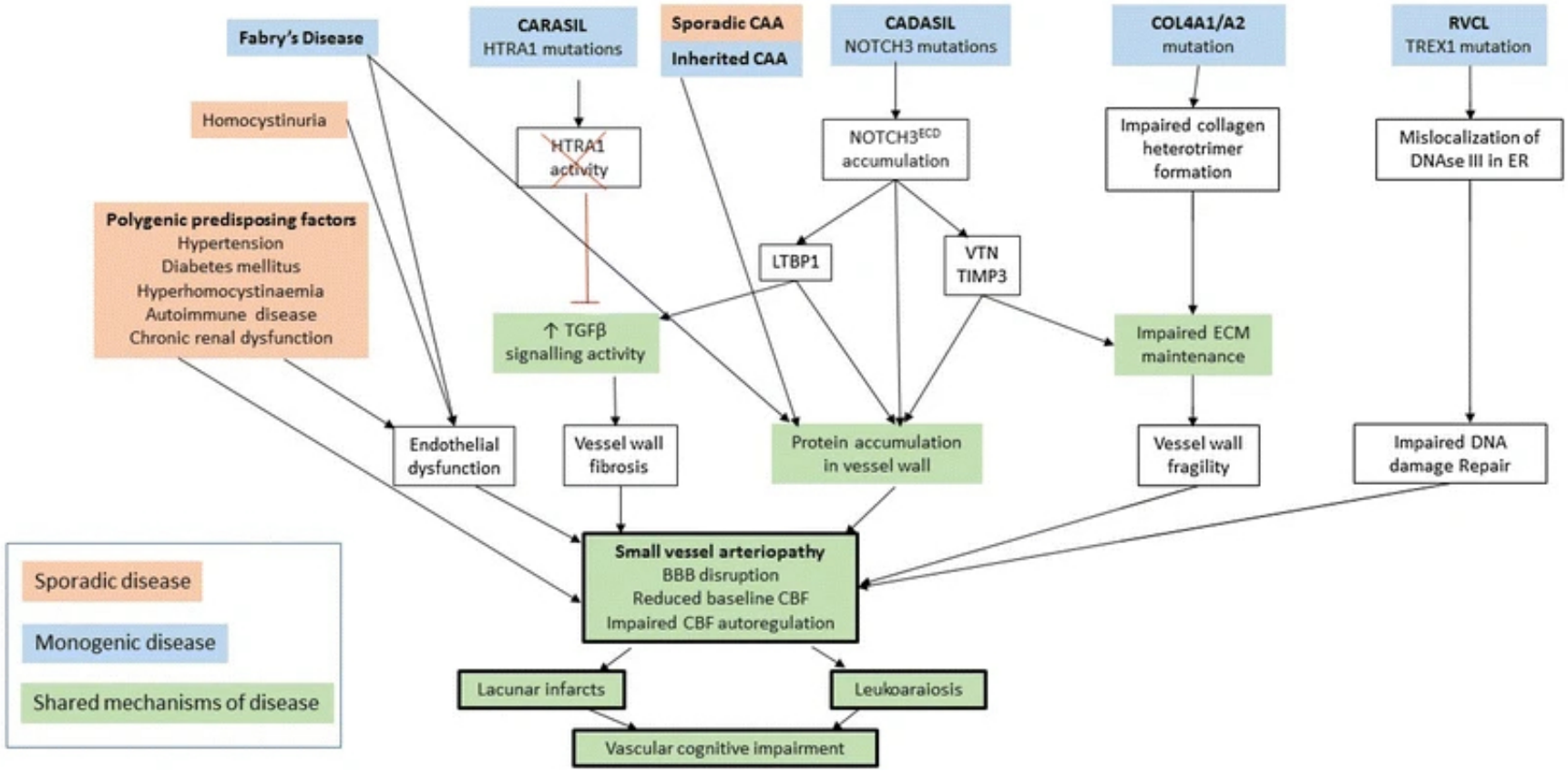


Figure 1.10 Key SVD mechanisms

Key mechanisms involved in some of the monogenic forms of small vessel disease (blue) sporadic small vessel disease (orange), and areas in which there may be overlap with sporadic SVD (green), from (Tan and Markus 2015).

Alterations in cerebrovascular perfusion have also been found in biochemical studies of human brain tissue in vascular dementia where it is associated with increased levels of the potent vasoconstrictor EDN1 and with Aß-42 (Miners, Palmer et al. 2015).

1.8.1.1 Cerebral autosomal dominant arteriopathy with subcortical infarcts and leukoencephalopathy

The most common monogenic SVD is CADASIL, an autosomal dominant inherited SVD. The mean age of onset is before 50 years, usually with ischaemic stroke as well as cognitive problems, migraine and psychiatric symptoms (Chabriat, Joutel et al. 2009). *In vivo* MR imaging shows lesions similar to those seen in sporadic SVD but in a different distribution, which can assist with the diagnosis; WMH and lacunar infarcts are most often seen in the anterior temporal lobe and external capsule and usually present by age 30, before the onset of detectable symptoms (O'Sullivan, Jarosz et al. 2001). Cerebral microbleeds are also seen. Quantitative MRI identifies abnormalities in white matter in areas that otherwise appear normal (Holtmannspotter, Peters et al. 2005), as in sporadic SVD. In contrast, however, CADASIL is not associated with hypertension (Chabriat, Joutel et al. 2009).

CADASIL is caused by a NOTCH3 mutation. NOTCH3 encodes a vascular smooth muscle cell transmembrane receptor expressed in pericytes (Dziewulska and Lewandowska 2012). Notch protein signalling during angiogenesis is believed to be required for arterial and venous differentiation (Lawson, Scheer et al. 2001), initiating expression of endothelial arterial markers and repressing venous markers. In Notch null animal models, the endothelium retains the appropriate phenotype, but arterial smooth muscle cells may have problems defining arterial/venous types and acquire venous features (Joutel, Corpechot et al. 1996, Domenga, Fardoux et al. 2004). In adult humans NOTCH3 is required for ongoing vascular development and

remodelling. Mutations cause accumulation of the extracellular domain of the NOTCH3 transmembrane receptor with vascular smooth muscle cell degeneration (Joutel, Andreux et al. 2000), although the precise mechanism of degeneration is unknown. The abnormal protein multimerizes and recruits other extracellular matrix proteins that would normally be excreted from the brain into large aggregates, proteins such as tissue inhibitor of metalloproteinases-3 (TIMP3), latent TGFß binding protein-1 (LTBP1) and vitronectin. Histologically there is thickening of the media and adventitia of penetrating and cortical arteries with smooth muscle cell degeneration and loss associated with granular deposits that stain for the NOTCH3 extracellular domain. Electron dense granular osmiophilic deposits (GOM) are visible on electron microscopy (Love, Budka et al. 2015). There are currently no effective treatments for CADASIL. Therapy is symptomatic, with appropriate genetic counselling.

1.8.1.2 Cerebral autosomal recessive arteriopathy with subcortical infarcts and leukoencephalopathy

CARASIL is caused by at least four different mutations in the HTRA1 gene (Hara, Shiga et al. 2009). Histological changes include arteriolosclerosis, loss of smooth muscle cells and vascular basement membrane abnormalities. WMH, lacunar infarction and progressive cognitive decline with vascular dementia are common (Oide, Nakayama et al. 2008, Fukutake 2011, Nozaki, Nishizawa et al. 2014, Mancuso, Arnold et al. 2020). The HTRA1 protein is involved in supressing TGF-ß activity (Shiga, Nozaki et al. 2011, Beaufort, Scharrer et al. 2014) and is implicated in endothelial dysfunction through decreasing nitric oxide synthase (NOS) in vascular smooth muscle cells (Schini, Durante et al. 1992). Increased pericyte-derived TGF-ß alters BBB integrity by increasing VEGF (Shimizu, Sano et al. 2013).

1.8.1.3 Cathepsin A-related arteriopathy with strokes and leukoencephalopathy

In CARASAL, a CTSA mutation causes increased cathepsin A levels. Cathepsin A normally degrades EDN1 a potent vasoconstrictor and inhibitor of OPC maturation (Hammond, Gadea et al. 2014). However, in CARASAL, increased EDN1, produced predominantly by dysfunctional endothelial cells (Kowalczyk, Kleniewska et al. 2015), is seen in astrocytes throughout the white matter with increased OPC numbers and decreased myelin (Bugiani, Kevelam et al. 2016).

1.8.1.4 Type 4 collagen-associated angiopathies

Abnormalities in vascular basement membrane type IV collagen α1 and α2 chains cause COL4-associated angiopathies due to mutations in the COL4A1 and COL4A2 genes respectively. Both genes are expressed by cerebrovascular endothelial cells (Zhang, Chen et al. 2014). SNPs in COL4A2 have been associated with WMH volume in GWAS in ischaemic stroke (Traylor, Zhang et al. 2016), and with SVD and deep intracerebral haemorrhage, in a meta-analysis (Rannikmae, Davies et al. 2015). Vessel and white matter alterations are variable but in animal and human studies they are similar to those in sporadic SVD with haemorrhagic and ischaemic stroke, WMH and lacunes (Gould, Phalan et al. 2006, Vahedi and Alamowitch 2011, Verbeek, Meuwissen et al. 2012). Lacunar subtype stroke on neuroimaging has been associated with single nucleotide polymorphisms (SNPs) associated with WMH, one of which was in COL4A2, suggesting potentially common mechanisms (Traylor, Rutten-Jacobs et al. 2016).

1.8.1.5 Retinal vasculopathy with cerebral leukodystrophy-like syndromes

RVCL-S is caused by mutations in the TREX1 gene (Mancuso, Arnold et al. 2020). Different mutations are associated with innate immunity in several studies, although in RVCL-S the initiating factor may be within vessels with an immune mechanisms contributing downstream (Stam, Kothari et al.

2016). Decreased TREX1 activity is associated with multiple human autoimmune diseases (Lee-Kirsch, Chowdhury et al. 2007, Lee-Kirsch, Gong et al. 2007, Rice, Newman et al. 2007) and knock-out mouse models show multi-system inflammation (Morita, Stamp et al. 2004, Yang, Lindahl et al. 2007, Stetson, Ko et al. 2008). There is overlap with sporadic SVD symptoms, but with additional features. Cognitive impairment with focal neurological and psychiatric symptoms manifest clinically, and WMH, mass lesions and calcification on neuroimaging. A micro-vasculopathy affects cerebral and retinal vessels and other organ systems, with fibrosis, hyalinosis, fibrinoid necrosis and perivascular chronic inflammation extending into the parenchyma where there is ischaemic necrosis, reactive gliosis and focal calcification (Stam, Kothari et al. 2016).

1.8.2 Other single genes

1.8.2.1 Forkhead box C1

Forkhead box C1 (FOXC1) is a transcription factor expressed in the neural crest and pericytes during development. The downstream signalling involves PDGF (French, Seshadri et al. 2014). Loss results in fewer pericytes and fragile vessels prone to bleeding (Siegenthaler, Choe et al. 2013, French, Seshadri et al. 2014). Mutations were known to cause Axenfeld-Reiger syndrome (ARS), an autosomal dominant inherited disorder with characteristic eye abnormalities (Ito and Walter 2014), but have also relatively recently been found to cause a familial SVD. Stroke, memory problems and neuroimaging SVD features are present and have been seen in a patient as young as 1 year old (French, Seshadri et al. 2014, Kumar, Chambers et al. 2017). Targeted GWAS identified three SNPs that affected FOXC1 transcription, resulting in ARS and SVD. Paired-like homeodomain transcription factor 2 (PITX2) is also expressed in the neural crest and interacts with FOXC1. Mutation causes ARS and has been associated with atrial fibrillation and cardioembolic stroke (Gudbjartsson, Arnar et al. 2007, Gretarsdottir, Thorleifsson et al. 2008). In a GWAS, nine PITX2 SNPs were

associated with WMH (French, Seshadri et al. 2014). In knock-out mouse models interaction with FOXC1 causes reduced vascular density and fewer contractile cells (French, Seshadri et al. 2014). Knock out animal models have also associated Pitx2 mutations with increased damage from oxidative stress in the heart (Tao, Kahr et al. 2016, Li, Tao et al. 2018). FOXC1 appears to have a developmental role, problems with which could cause BBB compromise and be relevant in sporadic SVD.

1.8.2.2 Forkhead box F2

Forkhead box F2 (FOXF2) is adjacent to FOXC1 in the human genome. It is also expressed in the neural crest and by pericytes during development, and is involved with vasculogenesis (Siegenthaler, Choe et al. 2013). Mutations are associated with increased risk of ischaemic stroke and WMH in a GWAS (Chauhan, Arnold et al. 2016). BBB abnormalities are seen in knock out mouse models and SVD lesions with reduced vascular contractile cells in zebrafish. Silencing the gene in older animals also causes BBB breakdown and subsequent SVD-related pathology with ischaemic appearing neurons, gliosis and microhaemorrhage (Reyahi, Nik et al. 2015, Chauhan, Arnold et al. 2016). One study found that two patients under 35 years of age with large mutations incorporating both FOXC1 and FOXF2 had confluent radiological WMH over ten-times greater in volume than patients with smaller mutations of FOXC1 alone (Chauhan, Arnold et al. 2016).

1.8.2.3 Zinc finger CCHC domain-containing 14

Another gene lying upstream and close by in the genome is zinc finger CCHC domain-containing 14 (ZCCHC14). Highly expressed in the brain and arteries, it is the closest gene to a SNP associated with small vessel stroke in people aged less than 70 years. Plasma levels of the protein have been associated with haemorrhagic stroke where it is correlated with systemic levels of both pro- and anti-inflammatory cytokines, and it has been suggested ZCCHC14 has an anti-inflammatory role (Li, Ye et al. 2019),

possibly in responses to viral infection (Hyrina, Jones et al. 2019), although little has been published regarding its function.

1.9 Work in animal models

1.9.1 The spontaneously hypertensive stroke-prone rat

Few animal models have been used to study SVD (Bailey, McCulloch et al. 2009). One of the most widely used is the SHRSP model. It develops hypertension at 6 weeks of age and stroke around 20 weeks, predominantly small subcortical strokes. It has proved particularly useful in studying early changes in SVD pathophysiology. The structural and white matter pathology is similar to that in human SVD, including lipohyalinosis, fibrinoid necrosis, microinfarcts, white matter pathology and haemorrhage (Yamori, Horie et al. 1976, Bailey, Smith et al. 2011) mostly in vessels less than 150μm (Bailey, Smith et al. 2011) with microvascular disease suggesting BBB failure (Mustapha, Nassir et al. 2019).

Endothelial cell changes can be identified as early as 3 weeks in rodent models of SVD, although BBB leakage is not seen at this stage (Rajani, Quick et al. 2018). The alterations in endothelial cell signalling affect other cells of the NVU; there is increased endothelial production of HSP90 α, decreased NO and claudin-5 production, with increased numbers of OPCs due to reduced maturation and increased proliferation. Elevated plasma ICAM-1 indicates endothelial increased activation in SVD (Fassbender, Bertsch et al. 1999) and is associated with *in vivo* WMH progression (Markus, Hunt et al. 2005). Two drugs with different mechanisms of action, simvastatin and perindopril, improve endothelial dysfunction and reverse the OPC changes. Simvastatin also reduces the histological white matter pathology. Studies in humans with lacunar stroke have found no effects on cognitive decline or WMH progression (Bath and Wardlaw 2015) but they could be reduced by treatment post-stroke (Xiong, Wong et al. 2014, Bath, Scutt et al. 2017).

Gene expression studies at 5 weeks identified alterations present before the onset of stroke symptoms further suggesting an inherent genetic susceptibility could lead to the development of SVD pathology in the context of hypertension. The genetic changes in the SHRSP model reflect reduced endothelial tight junction integrity (reduced claudin 5 and matrix metalloproteinase 14, MMP-14), NO availability (up-regulated guanylate cyclase soluble subunit alpha-3, Gucy1a3), myelination (decreased myelin basic protein, Mbp), vascular reactivity (reduced arginine vasopressin, Avp, and guanine nucleotide binding protein alpha inhibiting-1, Gnai1) and albumin (decreased albumin, Alb) a plasma protein, reduced levels of which increase the likelihood of cerebral parenchymal oedema. Increased astrocytic (increased glial fibrillary acidic protein, Gfap) and microglial activity and alterations in several complement pathway proteins, suggest lifelong abnormal inflammatory responses, not just an acute response to pathological processes (Bailey, Wardlaw et al. 2011, Bailey, McBride et al. 2014). These genetic alterations are reflected by similar findings in immunohistochemical studies of protein expression in the SHRSP model at the same age (Bailey, Wardlaw et al. 2011).

Studies also show structural and cellular changes reflecting BBB dysfunction and inflammation before hypertension is established using a variety of methods including immunohistochemical staining (Yamori, Horie et al. 1975, Fredriksson, Auer et al. 1985, Blezer, Schurink et al. 1998, Mies, Hermann et al. 1999, Michihara, Sawamura et al. 2001, Sironi, Tremoli et al. 2001, Guerrini, Sironi et al. 2002, Sironi, Guerrini et al. 2004, Bailey, Wardlaw et al. 2011). Many of these studies, however, were confounded by the effects of additional salt intake in the experimental animals, administered to make the development of pathology more consistent. Salt loading itself causes more severe hypertension in the SHRSP and affects the BBB with reduced claudin-5 reflecting reduced tight junction protein, increased parenchymal inflammation and reactive gliosis (Bailey, Wardlaw et al. 2011).

Deletion of the ATP11B gene in the SHRSP causes loss of the ATPase Phospholipid Transporting protein 11b and increased endothelial cell production of HSP90 α . A SNP in the ATP11B gene has also been identified in humans with radiological WMH, supporting a genetic predisposition. Electron microscopy studies show endothelial cell dysfunction in SHRSP at 13 weeks with abnormal distribution of tight junction proteins and cell polarity (Lippoldt, Kniesel et al. 2000), required for normal BBB maintenance. These abnormalities potentially lead to oedema and stroke. MRI studies identified focal vascular leakage two weeks before stroke occurred in the same area (Lee, Zhai et al. 2007).

1.9.2 Vascular mechanisms

1.9.2.1 Nitric oxide

NO is involved in many physiological pathways and is produced by several different cell types. Endothelial NO produced by eNOS in particular is involved in reactive vasodilation, regulating platelet adhesion (Moncada, Palmer et al. 1991), maintaining tight junction integrity in the cerebral vasculature (Daneman and Prat 2015), anti-inflammatory and anti-platelet effects (Bath and Wardlaw 2015). NO bioavailability and eNOS levels are commonly used markers of endothelial dysfunction in animal studies. Reduced NO levels have also been found in lacunar stroke patients (Rashid, Whitehurst et al. 2003) and reduced CSF eNOS in SVD patients in life (Deplanque, Lavallee et al. 2013, Lavallee, Labreuche et al. 2013).

NO has been studied more extensively in animals than in humans. NO donors are associated with improved learning and memory in rat models, possibly related to aging (Pitsikas, Rigamonti et al. 2005). While inhibition of NO synthesis is associated with cognitive impairment (Asif, Soiza et al. 2013). Increased microglial activity as seen in the SHRSP can cause increased NO breakdown by reactive oxygen species formed, and an increase in the NO receptor Gucy1a3 may reflect decreased NO levels

(Bailey, McBride et al. 2014). Multiple mechanisms are implicated but NO is repeatedly seen as a common factor. NO-targeting therapies are already widely used in humans and have wide ranging effects including on BBB integrity, endothelial cells, smooth muscle cells, platelets, leukocytes and fibroblasts. For example, glyceryl trinitrate as a NO donor reduces systemic blood pressure and increases cerebral perfusion in acute ischaemic stroke (Bath, Pathansali et al. 2001, Ankolekar, Fuller et al. 2013). Several clinical trials of therapeutic NO donors such as glyceryl trinitrate, isosorbide mononitrate and dietary sources of NO are now in progress. They are specifically targeting pathways involved in cerebral SVD and include cohorts with lacunar subtype stroke (Bath, Woodhouse et al. 2015, Blair, Appleton et al. 2019).

Oxidative damage occurs in the brain due to production of reactive oxygen species during normal cellular metabolism (Floyd 1999). It is normally balanced by ongoing DNA repair, such as repairing strand breaks or removing oxidised bases (Floyd, West et al. 2001). However, when this balance is disturbed there is potential for excessive damage. Oxidative stress can be measured by homocysteine levels and is associated with reduced NO levels, cognitive decline, stroke, atherosclerosis, normal aging and inflammation. NO bioavailability (Tschudi, Barton et al. 1996) and eNOS expression (Hoffmann, Haendeler et al. 2001) are reduced with age and may be associated with vascular dysfunction including endothelial cell apoptosis and systemic vascular reactivity (Hoffmann, Haendeler et al. 2001, Matsushita, Chang et al. 2001).

1.9.2.2 The endothelium

Endothelial activation can lead to an inflammatory response. BBB leakage of harmful plasma proteins such as fibrinogen may cause cellular damage resulting in the activation and recruitment of inflammatory cells including microglia and macrophages (Streit, Xue et al. 2014, Hainsworth, Oommen et al. 2015). In addition, there may be direct damage, for example when

fibrinogen is cleaved to fibrin, which recruits and activates inflammatory cells. Perivascular fibrinogen is seen in AD, it also interacts with OPCs to inhibit their maturation and forms complexes with Aß (Petersen, Ryu et al. 2018), potentially further exacerbating vascular amyloid pathology. Increased numbers of microglia (Akiguchi, Tomimoto et al. 1997, Simpson, Fernando et al. 2007) and increased microglial activation are seen in immunohistochemical studies of SVD (Fernando, Simpson et al. 2006, Bailey, Wardlaw et al. 2011) and histological microglial activation is associated with WMH (Fernando, Simpson et al. 2006). A knock-out mouse model of the tight junction protein claudin-5 produced selective BBB leakage of small tracer molecules <800Daltons in otherwise morphologically normal vessels (Nitta, Hata et al. 2003).

1.9.2.3 Inflammation

Inflammation results in increased production of reactive oxidative species, and more easily occurs in the aging brain (Durany, Munch et al. 1999). Inflammation also activates the inducible NO gene in microglia and astrocytes leading to increased NO production and far higher than normal levels, which, like low levels, is also harmful, particularly to neurons (Floyd 1999, Robinson, Stewart et al. 1999).

1.9.2.4 Vascular flow

Abnormalities in cerebral vascular flow are seen in animal models of SVD. Capillary transit time heterogeneity is a measure of abnormal capillary flow seen in animal models which could be due to shunting or abnormal vasoreactivity mis-directing flow (Ostergaard, Engedal et al. 2016). Although difficult to measure *in vivo*, cerebrovascular reactivity in response to neuronal demand is abnormal in CADASIL (Huneau, Houot et al. 2018) and decreases with age, hypertension lacunar stroke and increased WMH burden (Wardlaw, Smith et al. 2019). Abnormal cerebrovascular responses may be associated with WMH formation as an indicator of endothelial dysfunction.

1.9.2.5 Pericytes

Pericyte deficient mouse models have endothelial abnormalities; decreasing levels of tight junction proteins with increased age correlate with increased BBB permeability to neurotoxic molecules, including blood-derived proteins. In parallel, fewer capillaries result in reduced perfusion, chronic hypoperfusion and tissue hypoxia (Bell, Winkler et al. 2010), with subsequent neuronal damage and inflammation. PDGFRB mutant mice are pericyte-deficient and have increased BBB permeability to molecules of different sizes, including immunoglobulin G (IgG). An increased inflammatory response is seen in aged pericyte-deficient mice and pericyte abnormalities effect changes in other BBB components with loss of astrocyte end-feet polarity, reduced endothelial cell receptors and irregular endothelial cell junctions (Armulik, Genove et al. 2010). Knock out models of Pdgf-b and Pdgfrb lack pericytes, resulting in perinatal mortality (Leveen, Pekny et al. 1994, Lindahl, Johansson et al. 1997). A FOXF2 ortholog knockout zebrafish model has reduced pdgfrb and reduced acta-2 (a smooth muscle cell marker) on larger vessels, indicating FOXF2 may act upstream as part of the same pathway (Chauhan, Arnold et al. 2016).

As contractile cells, pericytes normally respond to stimuli through close connections within the BBB and NVU to regulate capillary diameter. Stimuli include angiotensin II (Kawamura, Kobayashi et al. 2004), EDN1 (Schonfelder, Hofer et al. 1998) and NO (Haefliger, Zschauer et al. 1994), which may be abnormally regulated in SVD (see below) (Love and Miners 2015). Pericyte loss is seen in CADASIL (Dziewulska and Lewandowska 2012), diabetic (McCuskey and McCuskey 1984) and hypertensive animal models (Tagami, Nara et al. 1990), in Aß transgenic mice (Bell, Winkler et al. 2010), in in vitro studies (Verbeek, de Waal et al. 1997) and in humans associated with CAA (Farkas and Luiten 2001) and aging (Kalaria 1996). There are many similarities between pericytes and vascular smooth muscle cells in larger arterial vessels which are also affected (Joutel, Andreux et al. 2000, Attwell, Buchan et al. 2010).

1.9.2.6 Other studies

Other, more general SVD animal models have been less successful. In a primate model of lacunar stroke synthetic emboli injected into the carotid arteries predominantly travel to superficial cortical arteries, with only a minority of the smaller emboli entering lenticulostriate arteries where they would cause a lacunar stroke (Macdonald, Kowalczuk et al. 1995). Murine models of chronic hypoperfusion can be induced by partial or complete surgical carotid occlusion, including models that undergo gradual occlusion over three days. They develop cognitive impairment and white matter pathology but lack the vascular changes and focal lesions (Jiwa, Garrard et al. 2010, Kitamura, Fujita et al. 2012). Hypertensive primate animal models have not successfully reproduced human SVD. Some features are replicated but they lack similar histological vascular pathologies and white matter damage (Kemper, Moss et al. 1999, Kemper, Blatt et al. 2001).

At this stage, studies in humans are potentially most informative in the understanding of the mechanisms underlying human SVD pathological processes and could inform the development of useful animal models to further study the precise molecular mechanisms and therapeutic targets. There is currently no effective treatment for SVD. Traditional antihypertensive therapy has reduced the frequency of pathological small vessel atherosclerosis since the original SVD descriptions by Fisher (Fisher 1968), but the rest of the SVD spectrum remains prevalent. A number of trials using drugs already approved for human use in other applications have been carried out but so far have been unsuccessful (Floyd and Hensley 2002). Others that may target more recently identified pathways potentially involved in SVD are also underway (Wardlaw, Smith et al. 2019).

1.10 Research hypothesis

The hypothesis I will address in this thesis is that the underlying pathophysiology of human SVD is due to diverse, multi-level abnormalities in the neurovascular unit, starting with the endothelium and with common downstream disease pathways.

1.11 Justification for this project

There has been relatively little research into the pathophysiology of SVD over the years for several reasons. Initially it was assumed to be caused by occlusive vascular pathology, similar to atherosclerosis. However, there is little evidence to support this, and instead it seems to be due to a multifactorial, complex range of processes with common outcomes including diffuse white matter pathology, cortical thinning and focal lesions, for example lacunes, microinfarcts and microbleeds (Wardlaw, Smith et al. 2019). Many different cells, molecules, genes and mechanisms are implicated in SVD pathogenesis. However, initial endothelial and BBB dysfunction are prominent within the literature.

A number of animal models, mostly rats and mice, have been used to study SVD. Animal models are generally useful, especially as human tissue is difficult to manipulate. Genetic differences, molecular and cellular processes and pathophysiological pathways can be examined in detail and potentially manipulated to study the consequences of abnormalities. Rats in particular potentially share pathways for related phenotypes with human diseases (Atanur, Diaz et al. 2013) while mouse embryonic stem cells are easily cultured for genetic studies and mice produce abundant offspring (Patil and McCarroll 2013). However, significant inherent differences between animal models and humans mean they cannot fully reproduce or represent the human pathology, particularly when the white matter component is so critical. Compared to rats and mice, humans live longer, have larger brains and blood vessels. The middle cerebral artery of a rat is of a similar size (about

200μm diameter) (Nordborg, Fredriksson et al. 1985) to a typical human small vessel affected by SVD. The composition of our brains is different with a much higher ratio of grey to white matter (Mustapha, Nassir et al. 2019). I*n vitro* work has proved informative, although *in vitro* systems are not able to replicate the intricacies or accurate spatial relations of the *in vivo* BBB or NVU. While models enable interrogation of specific cellular or molecular mechanisms, they currently lack an identified pathological mechanism to mimic. These substantial differences mean that animal models cannot fully reproduce the complete human SVD phenotype, as reflected in systematic reviews (Hainsworth and Markus 2008, Bailey, McCulloch et al. 2009, Bailey, Smith et al. 2011), and so are arguably poor research choices to study SVD pathophysiology.

Human studies, predominantly utilising advanced neuroimaging techniques and histopathological examination have been informative in further understanding the BBB and NVU in the normal brain and how they are affected in SVD, but also further reveal how complex and inter-related the mechanisms and processes are. Individuals often live with SVD for a long time. It is typically asymptomatic in the early stages and advances in a chronic, progressive manner, rather than being rapidly fatal. Lesions studied directly in human brain tissue obtained at autopsy often show end-stage pathology (Bailey, Smith et al. 2012), and it can be difficult to work back from these lesions, using fixed tissue, to unravel and understand the interwoven mechanisms and process that brought them about.

The range of terms used to describe the radiological appearances of SVD have been agreed upon and defined in an international consensus (Wardlaw, Smith et al. 2013), reflecting the growing significance and recognition of SVD. However, the terminology and definitions used to describe the histopathological SVD lesions have been used inconsistently making the identification and assessment of relevant literature difficult (Alafuzoff, Gelpi et al. 2012, Bailey, Smith et al. 2012). For example, even the term ‘small vessel’

itself is often used to describe only small arteries and arterioles, although SVD affects all small vessels in the brain including capillaries and venous vessels (Pantoni 2010). A multi-centre review of pathological practices in 2012 found variation across all aspects of the post-mortem examination, from the autopsy itself through to histological assessment of relevant vascular lesions and the interpretation of their presumed clinical significance (Alafuzoff, Gelpi et al. 2012). It revealed that there had been little advance in unifying examination techniques or terminology since 2006, when a similar survey was carried out (Pantoni, Sarti et al. 2006). It also highlighted the variability in terminology used to describe the same lesions across the clinical, radiological and pathological fields. This is again reflected in the systematic review I conducted as part of this thesis, and I have, I believe for the first time, compiled a list reflecting the variability in terminology and definitions used in histological SVD reporting. While a number of grading systems with associated definitions have been suggested (Deramecourt, Slade et al. 2012, Smallwood, Oulhaj et al. 2012, Skrobot, Attems et al. 2016), these are predominantly focused around vascular contributions to cognitive decline and do not fully reflect the whole spectrum of SVD related pathology. Whilst there are accepted definitions and terminology for neuroimaging SVD lesions, there are no strong correlations with the lesions seen by neuroimaging and those seen on histopathology. Comparisons are generally based on assumptions and there have been relatively few attempts in the published literature to make precise comparisons of the lesion appearances (McAleese, Alafuzoff et al. 2016, Humphreys, Smith et al. 2021).

With this in mind, I aimed to study the pathogenesis of SVD using human post-mortem brain tissue from carefully selected and well characterised cohorts. My aim was to initially study and compare the better-defined neuroimaging and less well-defined histopathological appearances, to develop a more harmonised neuropathological approach to cerebral SVD assessment.

1.12 Outline methods

This thesis is written to explore and further understand the cellular basis of the relationship between the appearances of SVD lesions on neuroimaging and histopathology and explore some of the suggested underlying mechanisms.

In Chapter 2 I systematically reviewed the available literature comparing the appearances of radiological and histological lesions in human sporadic SVD. My primary aim was to understand what methods have been used before and how accurately they were able to identify lesions of interest. I also wanted to appreciate how the pathological terminology was used in these studies and what were the ultimate findings and knowledge gained. The systematic review then informed the development of the methods to enable direct comparison of the appearances of common SVD lesions which would allow confidence in understanding the cellular basis of SVD lesions reported on clinical neuroimaging.

In Chapter 3 I describe the general methods used including the three cohorts from within the Medical Research Council (MRC) Edinburgh Brain Bank representing SVD cases with primarily haemorrhagic pathology, normally aged cases with a lesser amount of primarily presumed ischaemic pathology and controls. In Chapter 4 I undertook a histological review of all relevant cases already held in the brain bank and used this to develop histopathological SVD definitions and a grading system which I then applied in the prospective cases.

I describe the development of the protocol for precise comparison of post-mortem imaging and histopathology in Chapter 5 and the results of this process in Chapter 6.

To further investigate the underlying mechanisms, I collaborated with another research group, developing their biochemical methods for comparing protein

expression in different groups of patients, described in Chapter 7. I established the methods in our laboratory, then expanded and applied them to my specific questions regarding relevant mechanisms in SVD in the context of the disease seen on neuroimaging. For this biochemical work I additionally used a cohort of AD cases to enable comparison against previous studies. AD is commonly seen alongside vascular pathology and may involve similar, if not identical, mechanisms, including BBB leakage (Kalaria 1999, Farrall and Wardlaw 2009, de la Torre 2010).

1.13 Aims

- To better understand the pathological lesions of SVD.

- To make accurate, objective pathological-radiological-clinical correlations of human SVD lesions.

- To study the mechanisms underlying these lesions using targeted protein studies.

1.14 Objectives

- Systematically review the methods and terminology used in studies making imaging and histological comparisons of sporadic SVD lesions in humans.

- Develop a grading system and definitions to be used in the assessment of histological SVD.

- Develop and establish a protocol for precise comparison of SVD lesions on post-mortem neuroimaging and histopathology.

- Use this method to directly compare lesion appearances using standard imaging sequences and histological investigations.

- Develop and establish appropriate biochemical testing protocols in our laboratory to study lesions of interest in sporadic SVD.

- Carry out biochemical studies of protein expression to investigate pathophysiological mechanisms in targeted SVD lesions

CHAPTER 2: CORRELATIONS IN POST-MORTEM IMAGING-HISTOPATHOLOGY STUDIES OF SPORADIC HUMAN CEREBRAL SMALL VESSEL DISEASE: A SYSTEMATIC REVIEW

2.1 Introduction

As described in the introduction, the desperate need for harmonisation and standardisation in neuropathological assessment of SVD is widely recognised but has not been objectively assessed (Grinberg and Heinsen 2010, McAleese, Alafuzoff et al. 2016). A previous systematic review in 2011 found limited correlation between histological and neuroimaging appearances with only modest clinical and imaging associations (Gouw, Seewann et al. 2011).

SVD itself is difficult to define, especially in the absence of a more complete understanding of the clinical, imaging and pathological associations. Published literature uses broad descriptive terms in the context of each publication. Given definitions range from descriptive:

> A brain parenchyma injury that is associated with distal leptomeningeal and intracerebral vessel pathology that resides in poorly collateralized subcortical grey and deep white matter. Moreover, it is mainly due to several vasculo-pathological processes that affect and cause occlusion to the small perforating cerebral capillaries (of sizes 50-400μm), small arteries (mostly branches of middle cerebral arteries [MCAs]), arterioles, and venules that penetrate and supply the brain subcortical region (Novakovic 2010, Pantoni 2010, Hinman, Lee et al. 2015, Benjamin, Zeestraten et al. 2016, Mustapha, Nassir et al. 2019).

To brief and concise:

> A syndrome of clinical and imaging findings that are thought to result from pathologies in perforating cerebral arterioles, capillaries and venules (Shi and Wardlaw 2016).

And concise but not very useful:

> A term grouping microangiopathies including CMBs, recent lacunar infarcts (lacunes), and white matter changes (Humphries and Mathew 2019).

Even the STRIVE guidelines, successful in defining neuroimaging signs of SVD, use descriptive terms for the clinical and pathological characteristics, choosing to avoid constructing concise definitions in the absence of robust clinical-imaging-pathological associations (Wardlaw, Smith et al. 2013).

Defining SVD in a meaningful way will remain difficult until the components of the whole disease are more fully understood, with a more comprehensive grasp of the clinical, imaging and pathological features and their interrelations. To more fully understand this, this systematic review aimed to objectively (as far as possible) assess the state of the pathological literature in relation to SVD lesions; to understand what information we have gained from previous imaging-histological studies and how reliable it is and to identify where succinct definitions and standardisation are required.

In this systematic review I identified all studies correlating *ex vivo* medical imaging with histopathology of SVD lesions. Given the dynamic nature of SVD during life, I focused on studies that used *ex vivo* imaging to avoid extended timelines between imaging and histology.

2.2 Methods

2.2.1 Search terms

I searched for the terms 'small vessel disease', 'SVD' and all relevant commonly used neuroradiological (Wardlaw, Smith et al. 2013) and histopathological terms (Table 2.1), in the Medline online database from its inception in 1966 to the 9th September 2020. The search terms were refined through several iterations to ensure all relevant SVD lesions on imaging and histology were included, and that all potential lesion types were included (Table 2.1). We hand searched reference lists in textbooks, review papers and two relevant journals (*Stroke* and *Neuropathology and Applied Neurobiology*) for relevant primary publications.

Table 2.1 Systematic review search strategy

Results	Search
1	exp Brain/pa, pp [Pathology, Physiopathology]
2	*Cerebrovascular Disorders/pa [Pathology]
3	*Stroke, Lacunar/et, pa, pp [Etiology, Pathology, Physiopathology]
4	(cerebrovascular disease or cerebrovascular lesions or cerebrovascular pathology).ti,ab.
5	SVD.ti,ab.
6	small vessel disease.ti,ab.
7	lipohyalinosis.ti,ab.
8	arteriolosclerosis.ti,ab.
9	(atherosclerosis adj3 small*).ti,ab.
10	CAA.ti,ab.
11	cerebral amyloid angiopathy.ti,ab.
12	(WMH or white matter hyperintensit$).ti,ab.
13	(WML or white matter lesion$).ti,ab.
14	((lacune or lacunar) adj2 (stroke or infarct$)).ti,ab.
15	microbleed.ti,ab.
16	perivascular space.ti,ab.
17	leukoaraiosis.ti,ab.
18	small deep infarct.ti,ab.
19	fibrinoid necrosis.ti,ab.
20	(histopatholog$ or histolog$ or patholog$).ti,ab.
21	(IHC or immunohistochemi$).ti,ab.
22	(ICC or immunocytochemi$).ti,ab.
23	1 or 2 or 3
24	4 or 5 or 6 or 7 or 8 or 9 or 10 or 11 or 12 or 13 or 14 or 15 or 16 or 17 or 18 or 19
25	20 or 21 or 22
26	23 and 24 and 25
27	limit 26 to humans

2.2.2 Inclusion and exclusion criteria

We included all studies published in full which carried out post-mortem CT or MR imaging and histological examination of adult human brain tissue to study sporadic SVD (Figure 2.1). We excluded: studies reporting only biopsy material; studies performing post-mortem imaging but no histopathology or vice versa; studies not reporting on human sporadic SVD; non-English publications; and studies of haemorrhagic SVD lesions only as these were reviewed recently (Cordonnier, Al-Shahi Salman et al. 2007, Kakar, Charidimou et al. 2012). We excluded all duplicate publications, editorials and conference abstracts. Where studies came from the same groups and it was not clear which, if any, cases were included more than once, we included only the largest study for subject characteristics and results, and only distinct individual findings from the other papers.

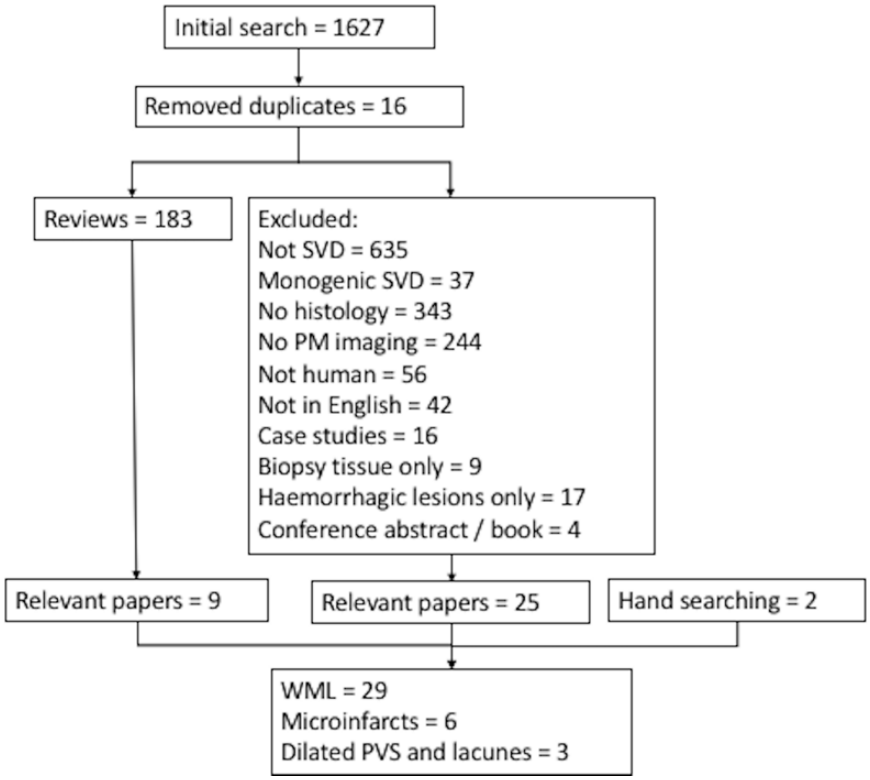


Figure 2.1 Summary of the literature evaluation

PVS perivascular spaces, SVD small vessel disease

2.2.3 Quality of reporting

To assess methodology quality, we adapted the Standards for the Reporting of Diagnostic Accuracy studies (STARD) criteria (Bossuyt, Reitsma et al. 2004) for observational studies to give a score out of 25. Information was extracted regarding authors expertise, aims, the study population, study dates, data collection, participant recruitment, pathological and radiological methods, blinding, analysis, results reporting and discussion of findings (Table 2.2). Each individual feature could gain one point, or part thereof if only part of the criteria was met. The authors discussed and resolved uncertainties regarding inclusion, exclusion and scoring when required.

2.2.4 Data extraction

Data were extracted on study characteristics including study design and dates, prospective or retrospective recruitment, data collected, sample size, blinding and analysis methods. Subject data included demographic and clinical data including cognitive status, *in vivo* investigations, age, gender, ethnicity.

Radiological specifics included scanner field strength, sequence resolution, tissue scanned, measures to avoid artefact and involvement of neuroradiologists. We collected details of pathological processing, assessment of tissue quality, macroscopic examination, staining, grading systems used, terminology and definitions and involvement of neuropathologists.

All three authors read the papers and had regular meetings to agree a consistent approach and achieve a consensus through discussion.

Table 2.2 Quality assessment

Adapted from the Standards for the Reporting of Diagnostic Accuracy studies checklist. Each feature assessed could gain 1 point, or a part thereof if the only part of the data was reported up to a total score of 25.

Title	Neuropathologist and neuroradiologist in the authors
Introduction	State the research questions or study aims
Methods	Describe the study population: inclusion and exclusion criteria, setting and locations where the data were collected
Participants	Report when the study was done, including beginning and ending dates of recruitment
	Describe participant recruitment
	Describe data collection: prospective or retrospective
Pathology	Describe the pathological methods: rationale, technical specifications (and/or cite references)
	Define pathological lesions and criteria used for assessments
	Describe the number and expertise of the persons executing the macroscopic and microscopic neuropathological assessment
	Were the individuals carrying out the macroscopic and microscopic assessment blinded to the results of other assessments and any other available information?
	Assess PM tissue quality and/or report post-mortem interval
Imaging	Describe the radiological methods: rationale, technical specifications (and/or cite references)
	Define radiological lesions and criteria used for assessments
	Describe the number and expertise of the persons executing the radiological assessment
	Were the assessors blinded to the results of other assessments and any other available information?
	Describe measures taken to minimise artefact on MRI
Statistics	Describe statistical methods for calculating or comparing measures of diagnostic accuracy, adjusting for variables, and the statistical methods used to quantify uncertainty (e.g. 95% confidence intervals)
Results	Report clinical and demographic characteristics of the study population (e.g.
Participants	age, sex, race, clinical info etc.)
	Report characteristics for individual subjects
	Report clinical features associated with SVD
Results	Report the distribution of disease severity
	Report a cross-tabulation (including indeterminate and missing results)
Discussion	Discuss the clinical applicability and/or use of the findings
	Discuss the scientific importance use of the findings
	Discuss the future use of the findings

Various pathological terminologies were used in the papers, not always consistently, hence we condensed the information into manageable categories based on the terminologies in each paper. For reference, we provide a full list of the terms encountered and similar expressions in Appendix 1. We recorded the method used to relate tissue locations on

MRI/CT to that on histology, the analyses used and the neuroradiological-neuropathological findings.

2.3 Results

The initial search yielded 1627 articles: 16 duplicates were removed, and we excluded 1403 papers including 37 studying monogenic SVD (reasons detailed in Figure 2.1). For interest, the excluded papers that studied monogenic SVD are listed in the supplement. Searching reference lists of 183 review papers provided nine additional relevant papers, and two further papers were identified from hand-searching journals. This resulted in 38 relevant papers, that reported imaging of at least 1146 individual patients in total, 342 of whom had SVD lesions on imaging. Studies were published between 1986 and September 2020, all using *ex vivo* MRI (Table 3). Of these we created three groups; 29 primarily focused on imaging-identified WML, six studying microinfarcts, and three on PVS and lacunes.

The information provided varied between studies. There were insufficient numerical data to perform a meta-analysis. Only one group clarified subject duplication between papers (Braffman, Zimmerman et al. 1988, Braffman, Zimmerman et al. 1988). We included only the largest study when there was possible duplication and it was not possible to extract precise subject data.

2.3.1 Study Quality

The mean quality score was 14/25 (range 6-19) (Table 2.3, Figure 2.2). Study aims, radiological definitions, statistical analysis, distribution of severity, and discussing the scientific importance, were well reported, and all papers described some degree of radiological methodology. Study dates, participant recruitment methods, tissue quality assessment, blinding of radiological assessment and addressing radiological artefact were not consistently reported. One study reported participants' race (all female and Caucasian) (Smith, Snowdon et al. 2000). None reported tissue quality assessment beyond recording post-mortem interval to autopsy.

Table 2.3 Summary of papers studying non-haemorrhagic SVD

Paper (lead author, year)	Cohort origin	Number of cases with SVD (total scanned)	Number of female subjects in those with SVD (in total)	Mean age (range) (unless otherwise stated)	Data collection	MRI field strength	Tissue scanned (medium)	Quality score
WML								
Awad 1986	Arizona, US	7 (7)	2 (2)	72 (61-84)	Not stated	1.5T	Whole brain (2 fresh in isotonic saline, 8 fixed in formaldehyde solution)	16.75
Braffman 1988	Philadelphia, US	X Duplicated subjects used in Braffman 1988 (33)	X	67 (60-78)	Not stated	1.5T	Whole brain (water)	10.50
Marshall 1988	California, US	6 (18)	- (-)	>60 (-)	Not stated	0.35T	Whole brain (-)	7.75
Revesz 1989	UK	4 (6)	2 (-)	52 (40-68)	Retrospective	0.5T	Slices (-)	12.00
Fazekas 1991	Austria	4 (4)	0 (0)	59 (52-63)	Not stated	1.5T	Whole brain (-)	11.00
Grafton 1991	Seattle, US	5 (7)	- (-)	77 (69-88)	Retrospective	0.5T	Whole brain (air)	15.75
Van Swieten 1991	Netherlands	10 (40)	- (19)	76 (-)	Retrospective	1.5T	Whole brain (formalin)	12.50
Chimowitz 1992	Ohio, US	7 (7)	4 (4)	68 (64-74)	Retrospective	1.5T	Whole brain (water)	12.25
Munoz 1993	Canada	13 (15)	- (11)	69 (47-87)	Not stated	1.5T	Whole brain (air)	14.00
Scarpelli 1994	Italy	17 (21)	7 (9)	74 (65-94)	Retrospective	1T	Whole brain, slices scanned if MR lesions but macroscopically normal (water)	15.25
Scheltens 1995	Netherlands	- (15)	- (9)	73 (60-83)	Retrospective	0.6T	Whole brain (-)	15.75

Fazekas 1999	Austria	9 (11)	4 (5)	72 (45-90)	Not stated	1.5T	Slices (-)	17.00
Smith 2000	Kentucky, US	X Can't be sure subjects not same as those in Smith 2000 (63)	X	- (83-99)	Prospective	-	Whole brain (-)	15.50
Smith 2000	Kentucky, US	52 (54)	52 (54)	89 (SD 4.8)	Prospective	-	- (-)	13.50
Bronge 2002	Sweden	6 (6)	3 (3)	87 (81-101)	Retrospective	1.5T	Whole brain (air)	13.25
Fernando 2004	UK CFAS	X Can't be sure subjects not same as those in Fernando 2006 (58)	X	85 (median) (70-97)	Prospective	1T	Slices (in plastic bag)	19.00
Moody 2004	N Carolina, US	12 (21)	6 (9)	72 (58-90)	Not stated	1.5T	Slices (between cooled plastic sheets)	14.25
Fernando 2006	UK CFAS	- (456) [$]	- (-)	Over 77% >80 years (-)	Prospective	1T	Slices (sealed in polythene)	12.75
Matsusue 2006	Japan	- (-)	- (-)	- (-)	None given	1.5T	Whole brain (-)	6.00
Simpson 2007	UK CFAS	X Can't be sure subjects not same as those in Fernando 2006 (58)	X	Median ages of cohorts range 84-87 (68-95)	Prospective	1T	Slices (plastic bag)	16.00
Simpson 2007	UK CFAS	X Can't be sure subjects not same as those in Fernando 2006 (58)	X	Median ages of cohorts range 80-87 (68-100)	Prospective	1T	Slices (plastic bag)	14.50
Young 2008	Australia	20 (20)	8 (8)	76 (61-94)	Prospective	3T	Whole brain (agar)	18.50

Polvikoski 2010	Finland	132 (132)	114 (114)	91* (85-105)	Not stated	1.5T	Whole brain (0.1mM MnCl2)	16.00
Auriel 2011	Hungary	-	-	64 (-)	Retrospective	1.5T	Whole brain (-) Ex vivo scanning only of brains with poor quality in vivo MRI and control cases	15.50
Murray 2012	Florida, US	- (4)	- (2)	85 (74-90)	Prospective	3T	Hemisphere (distilled water)	14.75
McAleese 2013	UK NBTR	- (40)	- (25)	83 (68-98)	Not stated	4.7T	Hemisphere (air)	14.25
Hainsworth 2017	UK CFAS	X Can't be sure subjects not same as those in Fernando 2006 (58)	X	86 (SD 7.7)	Prospective	1T	Slices (in polythene bag)	14.75
Van Veluw 2019	Massachusetts, US	9 (11)	2 (3)	75 (64-95)	Not stated	3T	Hemisphere (plastic bag filled with periodate-lysine-paraformaldehyde fixative)	18.75
Waller 2019	UK CFAS	X Can't be sure subjects not same as those in Fernando 2006 (58)	X	- (71-101)	Prospective	1T	Slices (in plastic bag)	15

PVS and lacunes								
Bokura 1998	Japan	- (12)	- (2)	76 (61-90)	Retrospective	1.5T	Whole brain (-)	12.25
Braffman 1998	Philadelphia, US	9 (36)	5 (18)	66 (37-78)	Not stated	1.5T	Whole brain (water with very dilute amount of formalin)	10.50
Van veluw 2016	Netherlands	1 (1) 4 additional cases appear to be used in van Veluw 2015 (37)	1 (1)	76 (68-84)	Retrospective	7T	Slices (10% formalin)	14.50
Microinfarcts								
Van Veluw 2013	Netherlands	X Can't be sure cases not used in van Swieten 1991 (48)	X	74 (64-87)	Retrospective	7T	Slices (formalin)	16.75
De Reuck 2014	France, Belgium	- (175)	- (76)	Median ages of cohorts range 65-84 (-)	Not stated	7T	Slices (physiological saline)	16.00
De Reuck 2015	France, Belgium	X Can't be sure cases not used in De Reuck 2014 (33)	X	Median ages of cohorts range 65-82 (-)	Not stated	7T	Slices (salt-free water)	14.50
Van Veluw 2015	Netherlands	9 (11)	6 (8)	72 (65-88)	Retrospective	7T	Slices (10% formalin)	16.75

Van Veluw 2016	Massachusetts, US	X Can't be sure cases not used in van Veluw 2019 (67)	X	85 (77-93)	Retrospective	7T	Slices (10% formalin)	17.25
Niwa 2017	Japan	10 (16)	6 (8)	82 (62-98)	Not stated	3T	Tissue blocks (water at 37°C)	13.5

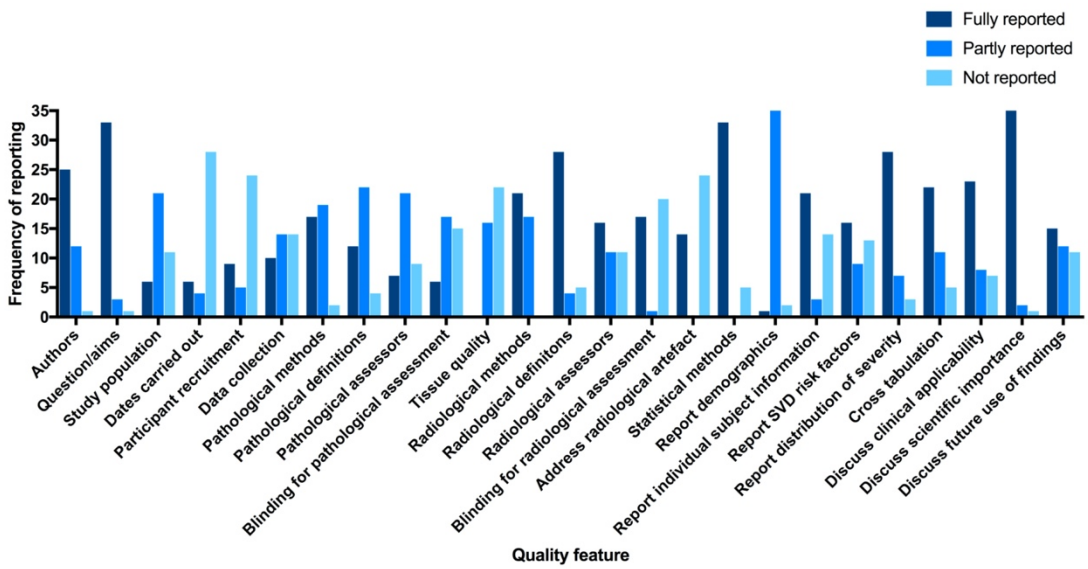


Figure 2.2 frequency of reporting features used to measure study quality

Bar chart showing how often the features used to measure study quality (detailed in Table 2.3) were reporting in the studies included. Bars indicate the number of papers reporting each feature. The number that reported and fully met the criteria in Table 2.2 (dark blue), partly met the criteria (middle blue) and did not report that feature (light blue).

2.3.2 Study characteristics

2.3.2.1 Subjects and small vessel disease lesions

Of the 38 papers identified, 28 studied WML based on the MRI-identified WMHs, one additional study compared white matter MRI diffusion tensor image (DTI) changes with histological measures and was included here. Six studied microinfarcts, and three studied PVS and lacunes.

The WMH/WML studies were from 21 groups in 11 countries (Table 2.3). They included at least 895 subjects, (at least 277 of whom were female) aged 45-101, at least 313 of these had SVD on imaging.

The microinfarct studies were from four groups in different countries, including at least 202 subjects (van Veluw, Zwanenburg et al. 2013, De Reuck, Deramecourt et al. 2014, De Reuck, Deramecourt et al. 2015, van

Veluw, Zwanenburg et al. 2015, van Veluw, Charidimou et al. 2016, Niwa, Ii et al. 2017). Four papers directly compared lesions identified on MRI with histology (van Veluw, Zwanenburg et al. 2013, van Veluw, Zwanenburg et al. 2015, van Veluw, Charidimou et al. 2016, Niwa, Ii et al. 2017). At least 19/202 subjects had microinfarcts although it was not possible to determine how many had lesions in two papers (De Reuck, Deramecourt et al. 2014, De Reuck, Deramecourt et al. 2015). The age range was 62-98 years in the three papers where age could be calculated or was given (van Veluw, Zwanenburg et al. 2015, van Veluw, Charidimou et al. 2016, Niwa, Ii et al. 2017).

The studies reporting on PVS and lacunes were from different groups (Braffman, Zimmerman et al. 1988, Bokura, Kobayashi et al. 1998, van Veluw, Biessels et al. 2016) and included 53 subjects in total, although four subjects (van Veluw, Biessels et al. 2016) also appear to have been reported in a paper studying microinfarcts (van Veluw, Zwanenburg et al. 2015). Ten subjects had PVS and/or lacunes, six of these were female. Ages ranged from 37-90 years.

Haemorrhagic pathology identified within the studies included is not reported here because it was not consistently reported, particularly where it was not the focus of a paper. Recent detailed reviews of haemorrhagic SVD pathology have been published and better serve to describe the relevant lesions (Cordonnier, Al-Shahi Salman et al. 2007, Kakar, Charidimou et al. 2012).

2.3.2.2 Data collection

12 studies collected subjects' data retrospectively (Table 2.3, Figure 2.2) from different, often multiple, sources including medical notes (Revesz, Hawkins et al. 1989, Grafton, Sumi et al. 1991, Chimowitz, Estes et al. 1992, Scarpelli, Salvolini et al. 1994, Scheltens, Barkhof et al. 1995, Bokura, Kobayashi et al. 1998, Bronge, Bogdanovic et al. 2002, Auriel, Bornstein et

al. 2011, van Veluw, Zwanenburg et al. 2013, van Veluw, Zwanenburg et al. 2015, van Veluw, Biessels et al. 2016, van Veluw, Charidimou et al. 2016), cause of death (not specifically stated where these data were obtained)(van Swieten, van den Hout et al. 1991, Scarpelli, Salvolini et al. 1994, Scheltens, Barkhof et al. 1995, Bronge, Bogdanovic et al. 2002, van Veluw, Charidimou et al. 2016), autopsy reports (Chimowitz, Estes et al. 1992, Bronge, Bogdanovic et al. 2002, van Veluw, Zwanenburg et al. 2013, van Veluw, Zwanenburg et al. 2015) and interviewing relatives (Grafton, Sumi et al. 1991). Many did not report how or when subject data were collected (Awad, Johnson et al. 1986, Braffman, Zimmerman et al. 1988, Braffman, Zimmerman et al. 1988, Marshall, Bradley et al. 1988, Fazekas, Kleinert et al. 1991, Munoz, Hastak et al. 1993, Fazekas, Kleinert et al. 1999, Moody, Thore et al. 2004, Polvikoski, van Straaten et al. 2010, McAleese, Firbank et al. 2013, De Reuck, Deramecourt et al. 2014, De Reuck, Deramecourt et al. 2015, Niwa, Ii et al. 2017). Ten studies collected clinical information prospectively (Smith, Snowdon et al. 2000, Smith, Snowdon et al. 2000, Fernando, O'Brien et al. 2004, Fernando, Simpson et al. 2006, Simpson, Fernando et al. 2007, Simpson, Ince et al. 2007, Young, Halliday et al. 2008, Murray, Vemuri et al. 2012, Hainsworth, Minett et al. 2017, Waller, Baxter et al. 2019), and one provided no subject information (Matsusue, Sugihara et al. 2006).

2.3.2.3 Reporting subject data

Reporting of SVD risk factors and conditions affecting subjects in life was variable. 21 papers reported individual subject data for each subject with SVD (Awad, Johnson et al. 1986, Braffman, Zimmerman et al. 1988, Braffman, Zimmerman et al. 1988, Revesz, Hawkins et al. 1989, Fazekas, Kleinert et al. 1991, Grafton, Sumi et al. 1991, Chimowitz, Estes et al. 1992, Scarpelli, Salvolini et al. 1994, Scheltens, Barkhof et al. 1995, Bokura, Kobayashi et al. 1998, Fazekas, Kleinert et al. 1999, Bronge, Bogdanovic et al. 2002, Young, Halliday et al. 2008, Murray, Vemuri et al. 2012, McAleese, Firbank et al. 2013, van Veluw, Zwanenburg et al. 2013, van Veluw,

Zwanenburg et al. 2015, van Veluw, Biessels et al. 2016, van Veluw, Charidimou et al. 2016, Niwa, Ii et al. 2017, van Veluw, Reijmer et al. 2019), 13 of which included SVD risk factors (Figures 2.2, 2.3) (Braffman, Zimmerman et al. 1988, Revesz, Hawkins et al. 1989, Fazekas, Kleinert et al. 1991, Grafton, Sumi et al. 1991, Chimowitz, Estes et al. 1992, Scarpelli, Salvolini et al. 1994, Bokura, Kobayashi et al. 1998, Fazekas, Kleinert et al. 1999, Bronge, Bogdanovic et al. 2002, Young, Halliday et al. 2008, Murray, Vemuri et al. 2012, van Veluw, Zwanenburg et al. 2013, van Veluw, Charidimou et al. 2016). SVD risk factors were not reported in some or all of the subjects in 13 studies (Table 2.3, Figures 2.2, 2.3) (Marshall, Bradley et al. 1988, Scheltens, Barkhof et al. 1995, Smith, Snowdon et al. 2000, Fernando, O'Brien et al. 2004, Fernando, Simpson et al. 2006, Matsusue, Sugihara et al. 2006, Polvikoski, van Straaten et al. 2010, McAleese, Firbank et al. 2013, van Veluw, Biessels et al. 2016, Hainsworth, Minett et al. 2017, Niwa, Ii et al. 2017, van Veluw, Reijmer et al. 2019, Waller, Baxter et al. 2019), mostly community-based cohorts of older subjects with dementia or other neurodegenerative conditions and controls, or unselected subjects. The presence of hypertension, stroke, ischaemic heart disease and conditions predisposing to thrombus formation were reported most often (Figure 2.3).

2.3.2.4 Radiological-histological correlation

A range of methods were used to compare imaging and histological lesions. Attempts to make the lesion comparisons more precise involved using computer software to guide brain cutting, using topographical features to select lesions (Awad, Johnson et al. 1986), or software aligning the MR image to histology then overlaying the images to identify areas of interest (Murray, Vemuri et al. 2012). One study described specifically using only samples where the precise matching sulcal pattern could be identified (Munoz, Hastak et al. 1993). Ferrous (Grafton, Sumi et al. 1991) and plastic (Polvikoski, van Straaten et al. 2010) markers were also used to increase the precision of cutting planes.

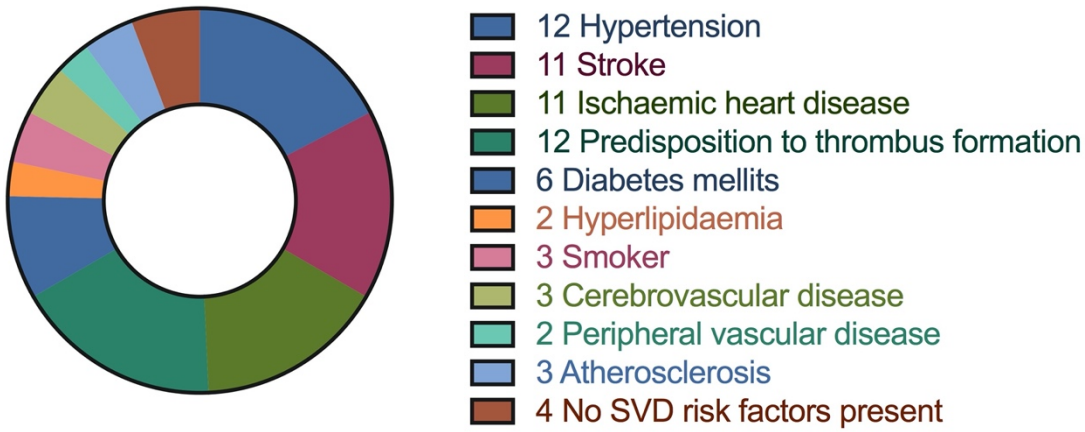


Figure 2.3 Frequency of SVD risk factor reporting

SVD risk factors and associated clinical diagnoses for individual subjects were reported in only 13 of the papers in this study. Some papers reported more than one risk factor, some only one. This figure shows the frequency with which each risk factor was reported. Hypertension, a predisposition to thrombus formation, stroke and ischaemic heart disease were reported most often. The block indicating hypertension begins at 12 o'clock and proceeds clockwise in the same order indicated in the key. SVD small vessel disease.

Most frequently, MRI was used to guide sampling for histological examination (Fazekas, Kleinert et al. 1991, Chimowitz, Estes et al. 1992, Fazekas, Kleinert et al. 1999, Bronge, Bogdanovic et al. 2002, Fernando, Ince et al. 2004, Simpson, Ince et al. 2007, Young, Halliday et al. 2008, Auriel, Bornstein et al. 2011, Hainsworth, Minett et al. 2017, Waller, Baxter et al. 2019). Where the whole brain was scanned, radiologists were sometimes present at the brain cut (Braffman, Zimmerman et al. 1988, Scheltens, Barkhof et al. 1995), with additional brain slice scans after cutting in one paper (Scarpelli, Salvolini et al. 1994). Brain slices were imaged then sampled in some studies (Revesz, Hawkins et al. 1989, Fernando, O'Brien et al. 2004, Moody, Thore et al. 2004, Simpson, Ince et al. 2007, Waller, Baxter et al. 2019), three also described measures to slice the brain at the same thickness as the MR slice (Grafton, Sumi et al. 1991, Scheltens, Barkhof et al. 1995, Bronge, Bogdanovic et al. 2002). The whole brain was scanned and assessed with routine pre-defined samples taken for histology in five studies (Marshall, Bradley et al. 1988, van Swieten, van den Hout et al. 1991, Smith,

Snowdon et al. 2000, Smith, Snowdon et al. 2000, Polvikoski, van Straaten et al. 2010). One study imaged hemispheres then carried out whole hemispheric histological sampling (McAleese, Firbank et al. 2013), another imaged hemispheres and chose MR regions of interest corresponding to the histological samples taken (van Veluw, Reijmer et al. 2019), and one scanned individual histological tissue blocks that were processed afterwards (Niwa, Ii et al. 2017). No description of the correlation technique was given in one paper (Matsusue, Sugihara et al. 2006) while one reflected that 10mm MR slices were not comparable to the micron scale of histological slices (Revesz, Hawkins et al. 1989).

One paper that included both *in vivo* and *ex vivo* imaging without clarifying which results were obtained from which method (Auriel, Bornstein et al. 2011) was included as the imaging was of high quality. One subject in one paper underwent imaging 11 days prior to death and although imaging could not be undertaken post-mortem, this case was included in the results without distinction from those with *ex vivo* MRI (Awad, Johnson et al. 1986). We felt this paper provided unique and important data and should be included within our review despite this. One paper reported two studies that were undertaken, but only the second study used post-mortem MRI and is included here (Young, Halliday et al. 2008).

2.3.3 Magnetic resonance imaging methods

2.3.3.1 Ex vivo scanning

All used MRI, most at 1.5T (Awad, Johnson et al. 1986, Braffman, Zimmerman et al. 1988, Braffman, Zimmerman et al. 1988, Fazekas, Kleinert et al. 1991, van Swieten, van den Hout et al. 1991, Chimowitz, Estes et al. 1992, Munoz, Hastak et al. 1993, Bokura, Kobayashi et al. 1998, Fazekas, Kleinert et al. 1999, Bronge, Bogdanovic et al. 2002, Moody, Thore et al. 2004, Matsusue, Sugihara et al. 2006, Polvikoski, van Straaten et al. 2010, Auriel, Bornstein et al. 2011), with the majority scanning the whole brain

(Awad, Johnson et al. 1986, Braffman, Zimmerman et al. 1988, Braffman, Zimmerman et al. 1988, Marshall, Bradley et al. 1988, Fazekas, Kleinert et al. 1991, Grafton, Sumi et al. 1991, van Swieten, van den Hout et al. 1991, Chimowitz, Estes et al. 1992, Munoz, Hastak et al. 1993, Scarpelli, Salvolini et al. 1994, Scheltens, Barkhof et al. 1995, Bokura, Kobayashi et al. 1998, Smith, Snowdon et al. 2000, Bronge, Bogdanovic et al. 2002, Matsusue, Sugihara et al. 2006, Young, Halliday et al. 2008, Polvikoski, van Straaten et al. 2010, Auriel, Bornstein et al. 2011). One study used a diffusion weighted sequence at 3T (van Veluw, Reijmer et al. 2019). Several scanning mediums were used, including water (Braffman, Zimmerman et al. 1988, Braffman, Zimmerman et al. 1988, Chimowitz, Estes et al. 1992, Scarpelli, Salvolini et al. 1994, Murray, Vemuri et al. 2012, De Reuck, Deramecourt et al. 2015, Niwa, Ii et al. 2017), formalin (Awad, Johnson et al. 1986, van Swieten, van den Hout et al. 1991, van Veluw, Zwanenburg et al. 2013, van Veluw, Zwanenburg et al. 2015, van Veluw, Biessels et al. 2016, van Veluw, Charidimou et al. 2016), sealing the tissue in plastic (Fernando, O'Brien et al. 2004, Fernando, Simpson et al. 2006, Simpson, Fernando et al. 2007, Simpson, Ince et al. 2007, Hainsworth, Minett et al. 2017, Waller, Baxter et al. 2019) or placing between plastic sheets (Moody, Thore et al. 2004). However, most studies did not state which scanning medium was used (Marshall, Bradley et al. 1988, Revesz, Hawkins et al. 1989, Fazekas, Kleinert et al. 1991, Scheltens, Barkhof et al. 1995, Bokura, Kobayashi et al. 1998, Fazekas, Kleinert et al. 1999, Smith, Snowdon et al. 2000, Smith, Snowdon et al. 2000, Matsusue, Sugihara et al. 2006, Auriel, Bornstein et al. 2011). Tissue was scanned in air in four papers (Grafton, Sumi et al. 1991, Munoz, Hastak et al. 1993, Bronge, Bogdanovic et al. 2002, McAleese, Firbank et al. 2013), but some specifically avoided air due to artefact. 11 studies took measures to avoid introducing MR artefact, usually by restricting tissue movement (Young, Halliday et al. 2008, De Reuck, Deramecourt et al. 2014, De Reuck, Deramecourt et al. 2015, van Veluw, Reijmer et al. 2019) (for example by wrapping in cling film (Fernando, O'Brien et al. 2004, Simpson, Fernando et al. 2007, Simpson, Ince et al. 2007, Waller, Baxter et

al. 2019)), or artefact due to air bubbles (van Veluw, Zwanenburg et al. 2013, van Veluw, Zwanenburg et al. 2015), by running a hand over the tissue (Murray, Vemuri et al. 2012), shaking the tissue, (van Veluw, Charidimou et al. 2016) tilting to eliminate air from the ventricles (Chimowitz, Estes et al. 1992) or vacuum sealing (van Veluw, Reijmer et al. 2019). One study tested a variety of methods to reduce artefact, concluding water at 37°C was optimal and that embedding in agar, extended washing to remove formalin and removing the pia had no effect (Niwa, Ii et al. 2017).

2.3.3.2 Establishing ex vivo MR parameters

One brain was scanned ante-mortem and post-mortem after fixation, and the same areas of hyperintensity were identified without obvious differences (Marshall, Bradley et al. 1988). Two post-mortem brains scanned before and after fixation had identical WML appearances (Awad, Johnson et al. 1986). Three studies used clinical scanning protocols at post mortem (Fazekas, Kleinert et al. 1991, Chimowitz, Estes et al. 1992, Niwa, Ii et al. 2017) and some described using optimised sequences, but without giving details (Revesz, Hawkins et al. 1989, Fernando, O'Brien et al. 2004, Fernando, Simpson et al. 2006, Simpson, Fernando et al. 2007, Simpson, Ince et al. 2007, van Veluw, Zwanenburg et al. 2015, van Veluw, Charidimou et al. 2016, Hainsworth, Minett et al. 2017, Waller, Baxter et al. 2019). T2-weighted sequences were said to be best for visualising WML *ex vivo* (Fazekas, Kleinert et al. 1991) while nine studies performed *ex vivo* fluid attenuated inversion recovery (FLAIR) (Revesz, Hawkins et al. 1989, Grafton, Sumi et al. 1991, van Swieten, van den Hout et al. 1991, Fernando, Simpson et al. 2006, Auriel, Bornstein et al. 2011, van Veluw, Zwanenburg et al. 2013, van Veluw, Zwanenburg et al. 2015), two of which described protocol optimization (Young, Halliday et al. 2008, Murray, Vemuri et al. 2012).

One study found a diluted formalin/water scanning medium was hyperintense on short repetition time (TR) sequences, compared to hypointense cerebrospinal fluid (Braffman, Zimmerman et al. 1988) and another stated

that changes in signal intensity due to fixation made identification of lacunar infarcts difficult (Fazekas, Kleinert et al. 1999). Only one study described optimisation of a T1 sequence (van Veluw, Zwanenburg et al. 2013).

2.3.3.3 In vivo imaging

105 subjects in five papers primarily studying WML had *in vivo* MRI available (Awad, Johnson et al. 1986, Braffman, Zimmerman et al. 1988, Fazekas, Kleinert et al. 1991, Fazekas, Kleinert et al. 1999, Auriel, Bornstein et al. 2011), of which at least 17 subjects also underwent *ex vivo* MRI and 15 additionally had *in vivo* CT (Braffman, Zimmerman et al. 1988). In two papers studying PVS and lacunes, nine subjects underwent *in vivo* MR imaging and 20 had *in vivo* CT (Braffman, Zimmerman et al. 1988, Bokura, Kobayashi et al. 1998). In one paper studying microinfarcts, although 12 subjects had both *in vivo* and *ex vivo* MRI carried out, comparison of the microinfarcts was possible in only one subject (van Veluw, Charidimou et al. 2016).

2.3.4 Autopsy and histological methods

2.3.4.1 Post-mortem

The post-mortem interval (PMI) was reported in 14 studies and ranged from less than 24 hours (Grafton, Sumi et al. 1991, Scarpelli, Salvolini et al. 1994, Scheltens, Barkhof et al. 1995, Smith, Snowdon et al. 2000, Bronge, Bogdanovic et al. 2002, Simpson, Ince et al. 2007, Young, Halliday et al. 2008, McAleese, Firbank et al. 2013, Niwa, Ii et al. 2017, van Veluw, Reijmer et al. 2019, Waller, Baxter et al. 2019) to seven days (Simpson, Ince et al. 2007). Most studies had multiple cases, and PMIs would vary considerably within each study. The most common method of fixation was to fix the whole brain in a variety of formalin solutions (Awad, Johnson et al. 1986, Braffman, Zimmerman et al. 1988, Braffman, Zimmerman et al. 1988, Marshall, Bradley et al. 1988, Revesz, Hawkins et al. 1989, Fazekas, Kleinert et al. 1991, Grafton, Sumi et al. 1991, van Swieten, van den Hout et al. 1991, Chimowitz, Estes et al. 1992, Munoz, Hastak et al. 1993, Scarpelli, Salvolini et al. 1994,

Scheltens, Barkhof et al. 1995, Bokura, Kobayashi et al. 1998, Smith, Snowdon et al. 2000, Smith, Snowdon et al. 2000, Bronge, Bogdanovic et al. 2002, Fernando, O'Brien et al. 2004, Moody, Thore et al. 2004, Fernando, Simpson et al. 2006, Matsusue, Sugihara et al. 2006, Simpson, Fernando et al. 2007, Young, Halliday et al. 2008, Polvikoski, van Straaten et al. 2010, Auriel, Bornstein et al. 2011, Murray, Vemuri et al. 2012, McAleese, Firbank et al. 2013, van Veluw, Zwanenburg et al. 2013, De Reuck, Deramecourt et al. 2014, De Reuck, Deramecourt et al. 2015, van Veluw, Zwanenburg et al. 2015, van Veluw, Biessels et al. 2016, van Veluw, Charidimou et al. 2016, Hainsworth, Minett et al. 2017, van Veluw, Reijmer et al. 2019, Waller, Baxter et al. 2019) although one study did not describe how the tissue was fixed (Simpson, Ince et al. 2007). The duration of tissue fixation ranged from slices in a formalin solution overnight (Moody, Thore et al. 2004) to slices formalin fixed for 12 years (Revesz, Hawkins et al. 1989). One study noted that the MR image quality was not affected by different fixation periods from nine to 35 days (Grafton, Sumi et al. 1991) and when time between death and scanning was controlled for statistically it did not alter the results obtained by DTI in cases ranging from 27-498 days (van Veluw, Reijmer et al. 2019). Assessment of post-mortem tissue quality using methods such as pH or ribonucleic acid (RNA) integrity number (RIN) measurement was not reported. Three papers commented on storage temperatures; one cooled brains after autopsy (Moody, Thore et al. 2004), one stored them at room temperature (Smith, Snowdon et al. 2000) and the third stored hemispheres at 4°C until the day before scanning when they were transferred to room temperature (van Veluw, Reijmer et al. 2019).

2.3.4.2 Macroscopic examination

19 studies described macroscopic examination (Awad, Johnson et al. 1986, Braffman, Zimmerman et al. 1988, Braffman, Zimmerman et al. 1988, Marshall, Bradley et al. 1988, Revesz, Hawkins et al. 1989, Fazekas, Kleinert et al. 1991, Grafton, Sumi et al. 1991, van Swieten, van den Hout et al. 1991, Chimowitz, Estes et al. 1992, Munoz, Hastak et al. 1993, Scarpelli, Salvolini

et al. 1994, Scheltens, Barkhof et al. 1995, Bokura, Kobayashi et al. 1998, Smith, Snowdon et al. 2000, Smith, Snowdon et al. 2000, Bronge, Bogdanovic et al. 2002, Polvikoski, van Straaten et al. 2010, Murray, Vemuri et al. 2012, De Reuck, Deramecourt et al. 2014) including photography (Awad, Johnson et al. 1986, Braffman, Zimmerman et al. 1988, Braffman, Zimmerman et al. 1988, Marshall, Bradley et al. 1988, Revesz, Hawkins et al. 1989), brain weight (Awad, Johnson et al. 1986, Revesz, Hawkins et al. 1989, Fazekas, Kleinert et al. 1991, Chimowitz, Estes et al. 1992, Scarpelli, Salvolini et al. 1994, Scheltens, Barkhof et al. 1995, Smith, Snowdon et al. 2000, Smith, Snowdon et al. 2000, Polvikoski, van Straaten et al. 2010, Murray, Vemuri et al. 2012) or describing some general aspect of macroscopic inspection (Awad, Johnson et al. 1986, Marshall, Bradley et al. 1988, Revesz, Hawkins et al. 1989, Grafton, Sumi et al. 1991, van Swieten, van den Hout et al. 1991, Munoz, Hastak et al. 1993, Scheltens, Barkhof et al. 1995, Bokura, Kobayashi et al. 1998, Smith, Snowdon et al. 2000, Smith, Snowdon et al. 2000, Bronge, Bogdanovic et al. 2002, Polvikoski, van Straaten et al. 2010, Murray, Vemuri et al. 2012, De Reuck, Deramecourt et al. 2014).

2.3.4.3 Staining and special techniques

All papers described using special tinctorial or immunohistochemical staining to characterise tissue lesions. Haematoxylin and eosin (H&E) was most often used for general tissue architecture (Awad, Johnson et al. 1986, Braffman, Zimmerman et al. 1988, Braffman, Zimmerman et al. 1988, Marshall, Bradley et al. 1988, Revesz, Hawkins et al. 1989, Fazekas, Kleinert et al. 1991, Munoz, Hastak et al. 1993, Scarpelli, Salvolini et al. 1994, Scheltens, Barkhof et al. 1995, Bokura, Kobayashi et al. 1998, Bronge, Bogdanovic et al. 2002, Fernando, O'Brien et al. 2004, Fernando, Simpson et al. 2006, Simpson, Fernando et al. 2007, Simpson, Ince et al. 2007, Young, Halliday et al. 2008, Polvikoski, van Straaten et al. 2010, Auriel, Bornstein et al. 2011, Murray, Vemuri et al. 2012, McAleese, Firbank et al. 2013, van Veluw, Zwanenburg et al. 2013, van Veluw, Zwanenburg et al. 2015, van Veluw, Charidimou et al.

2016, Niwa, Ii et al. 2017, van Veluw, Reijmer et al. 2019) followed by myelin stains, particularly LFB (Awad, Johnson et al. 1986, Marshall, Bradley et al. 1988, Revesz, Hawkins et al. 1989, Fazekas, Kleinert et al. 1991, Grafton, Sumi et al. 1991, Chimowitz, Estes et al. 1992, Scarpelli, Salvolini et al. 1994, Bokura, Kobayashi et al. 1998, Smith, Snowdon et al. 2000, Bronge, Bogdanovic et al. 2002, Fernando, O'Brien et al. 2004, Moody, Thore et al. 2004, Fernando, Simpson et al. 2006, Simpson, Fernando et al. 2007, Simpson, Ince et al. 2007, Auriel, Bornstein et al. 2011, Murray, Vemuri et al. 2012, McAleese, Firbank et al. 2013, van Veluw, Zwanenburg et al. 2013, van Veluw, Zwanenburg et al. 2015, van Veluw, Reijmer et al. 2019), glial stains (Awad, Johnson et al. 1986, Marshall, Bradley et al. 1988, Grafton, Sumi et al. 1991, Chimowitz, Estes et al. 1992, Scarpelli, Salvolini et al. 1994, Matsusue, Sugihara et al. 2006, Simpson, Fernando et al. 2007, Simpson, Ince et al. 2007, Auriel, Bornstein et al. 2011, Murray, Vemuri et al. 2012, van Dalen, Scuric et al. 2015, van Veluw, Zwanenburg et al. 2015, van Veluw, Reijmer et al. 2019) and a variety of neuronal, microglial, endothelial and amyloid stains. More recently, papers trying to assess specific mechanisms such as inflammation, hypoxia and BBB, have used a wider range of markers to assess the different pathways (Marshall, Bradley et al. 1988, Fernando, O'Brien et al. 2004, Fernando, Simpson et al. 2006, Simpson, Fernando et al. 2007, Simpson, Ince et al. 2007, Young, Halliday et al. 2008, Hainsworth, Minett et al. 2017, Waller, Baxter et al. 2019).

2.3.5 Pathological terminology and definitions

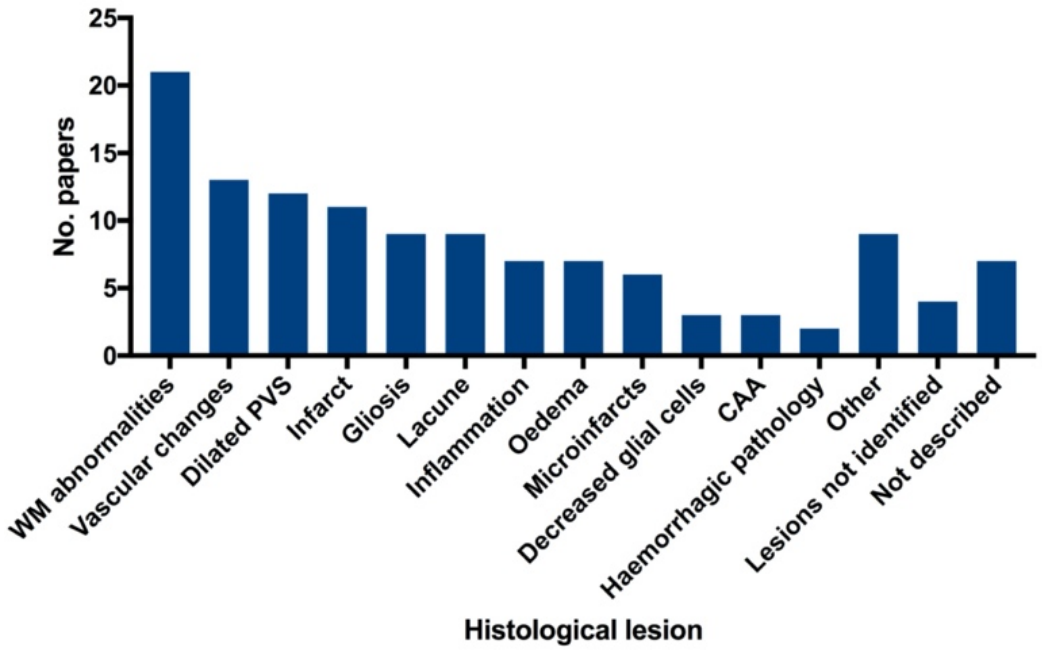
Pathological lesions were less well defined than MRI lesions (Figure 2.2). The histopathological definitions and terminology used were variable between papers (see Appendix 1 for full library of terms), so we have had to apply a degree of interpretation, aiming to group lesions as objectively as possible by their morphological appearance and staining characteristics rather than the presumed underlying cause.

A range of histological findings were described corresponding to radiological SVD (Figure 2.4a), most often a variety of white matter changes including myelin and axon pallor (Figure 2.5), microscopic 'abnormalities', rarefaction and degeneration. Radiological WMH corresponded to several histological appearances (Figure 2.4b), typically more than one. In particular, the range of terminology describing vascular pathology of radiological WMH was wide and often poorly defined (Figure 2.4c).

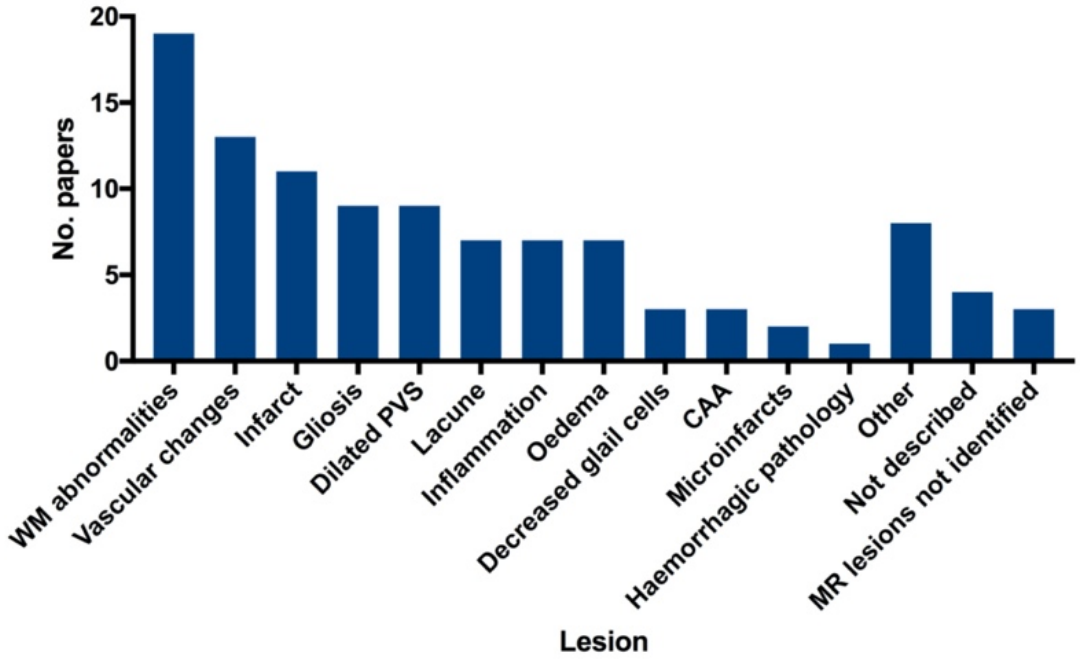
PVS, also known as Virchow-Robin spaces, (Figure 2.6) were defined in two of the three papers studying them specifically as the subarachnoid space around small vessels in the brain excluding capillaries (Braffman, Zimmerman et al. 1988, Bokura, Kobayashi et al. 1998). Enlarged PVS were described as a marker of SVD and defined as spaces filled with interstitial fluid surrounding these vessels (van Veluw, Biessels et al. 2016). État pre-criblé was described as thin, pale and sinuous myelin in surrounding parenchyma, without PVS enlargement. Subsequent rarefaction and disintegration of the perivascular parenchyma (Braffman, Zimmerman et al. 1988) resulting in état criblé in which PVS are enlarged. Associated surrounding changes may be present, including a narrow border of fibrillary gliosis or demyelination (Braffman, Zimmerman et al. 1988).

Lacunes (Figure 2.7) were "a lesion surrounded by gliosis and myelin loss" histologically (Bokura, Kobayashi et al. 1998) or more mechanistically as "infarctions caused by perforating branch occlusion" in white and deep grey matter (Braffman, Zimmerman et al. 1988). They were also called penetrating branch occlusions and lacunar infarcts. In these studies size was not a criterion (Braffman, Zimmerman et al. 1988). Recent lacunar infarcts showed liquefactive necrosis (Braffman, Zimmerman et al. 1988) and when older form an irregular cavity with fibrillary connective tissue and macrophages, which decrease with time (Braffman, Zimmerman et al. 1988). État lacunaire described the presence of multiple lacunar infarcts (Braffman, Zimmerman et al. 1988) and giant lacunae were defined as greater than 1cm diameter (Braffman, Zimmerman et al. 1988).

a)


25
20
15
10
5
0
No. papers
WM abnormalities
Vascular changes
Dilated PVS
Infarct
Gliosis
Lacune
Inflammation
Oedema
Microinfarcts
Decreased glial cells
CAA
Haemorrhagic pathology
Other
Lesions not identified
Not described
Histological lesion

b)


20
15
10
5
0
No. papers
WM abnormalities
Vascular changes
Infarct
Gliosis
Dilated PVS
Lacune
Inflammation
Oedema
Decreased glail cells
CAA
Microinfarcts
Haemorrhagic pathology
Other
Not described
MR lesions not identified
Lesion

c)

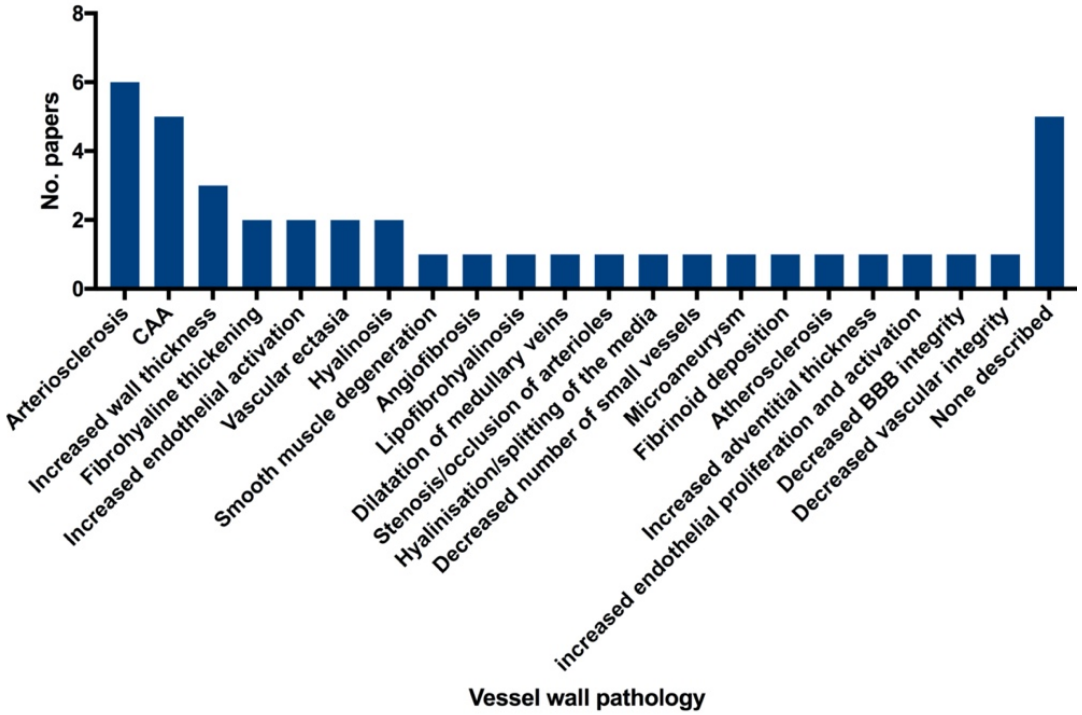


Figure 2.4 Terminology used in histological lesion reporting

For clarity, and to avoid many small groups, some headings contain terms used to describe similar pathologies, some of which were not specifically defined and reflect the variation of terminology summarised in Appendix 1. For example, 'WM abnormalities' include rarefaction, myelin pallor, demyelination, abnormal myelin sheaths, degenerate myeline, decreased axonal staining, decreased axons and Luxol fast blue lesions. a) Histological lesions described microscopically corresponding with all radiological small vessel disease lesions. b) Histological lesions described microscopically corresponding with radiological WM lesions only. c) Histological terminology used to describe the spectrum of vessel wall changes seen in radiological WM lesions. BBB blood-brain-barrier, CAA cerebral amyloid angiopathy, PVS perivascular space, WM white matter.

Six papers studied cortical microinfarcts (Figure 2.8) using a variety of overlapping definitions, but these papers came from only three groups. From defined areas of tissue pallor (van Veluw, Zwanenburg et al. 2015, van Veluw, Charidimou et al. 2016) to "ischaemic necrosis in the territory of a single cortical penetrating vessel" (De Reuck, Deramecourt et al. 2014), ischaemic lesions with cell death or necrosis, sometimes with gliosis, haemosiderin-containing macrophages and cavitation (van Veluw,

Zwanenburg et al. 2013, van Veluw, Zwanenburg et al. 2015) or well defined ischaemia with cell death, necrosis and cavitation (Niwa, Ii et al. 2017). One differentiated acute microinfarcts with tissue loss and gliosis from old microinfarcts with ischaemic or shrunken neurons (van Veluw, Charidimou et al. 2016) but size was not defined in advance. In the others, sizes were described as between 50μm and 2mm depending on the size of the involved vessel (De Reuck, Deramecourt et al. 2014), or from 50μm to a few mm (van Veluw, Zwanenburg et al. 2013, van Veluw, Zwanenburg et al. 2015), but also as almost visible on gross examination (De Reuck, Deramecourt et al. 2014, De Reuck, Deramecourt et al. 2015, van Veluw, Zwanenburg et al. 2015) or microscopic (van Veluw, Zwanenburg et al. 2013). One did not define or describe the histological appearance (De Reuck, Deramecourt et al. 2015).

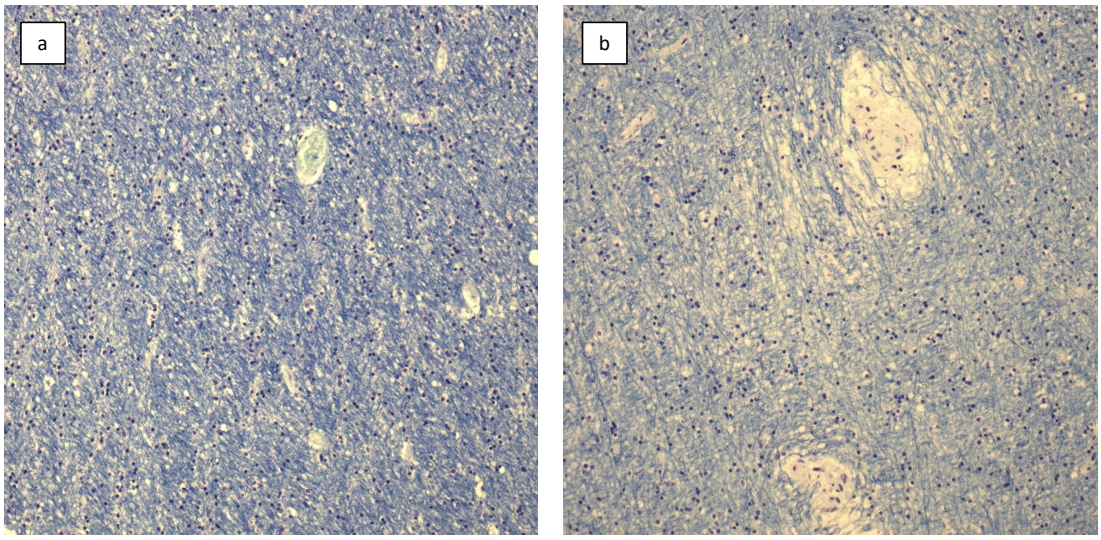


Figure 2.5 Myelin staining in white matter

a) Normal central white matter showing uniform myelin staining (LFB, x100). b) Central white matter from a case with severe small vessel disease, showing pallor and fine vacuolation between axon sheaths (LFB, x100). LFB Luxol fast blue.

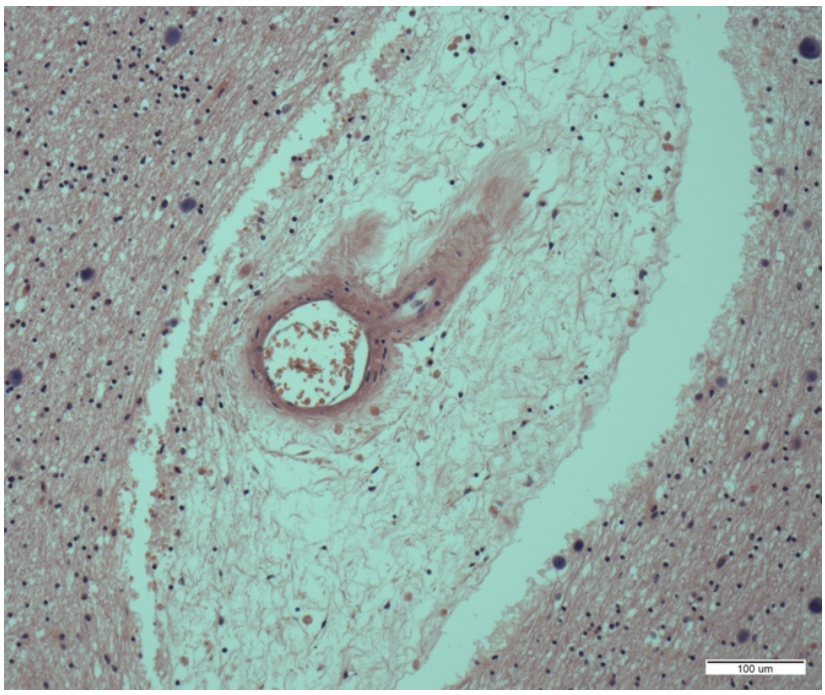


Figure 2.6 Enlarged perivascular space

The space contains a central vessel with marked expansions and fibrillation of the surrounding perivascular space (H&E, x100).

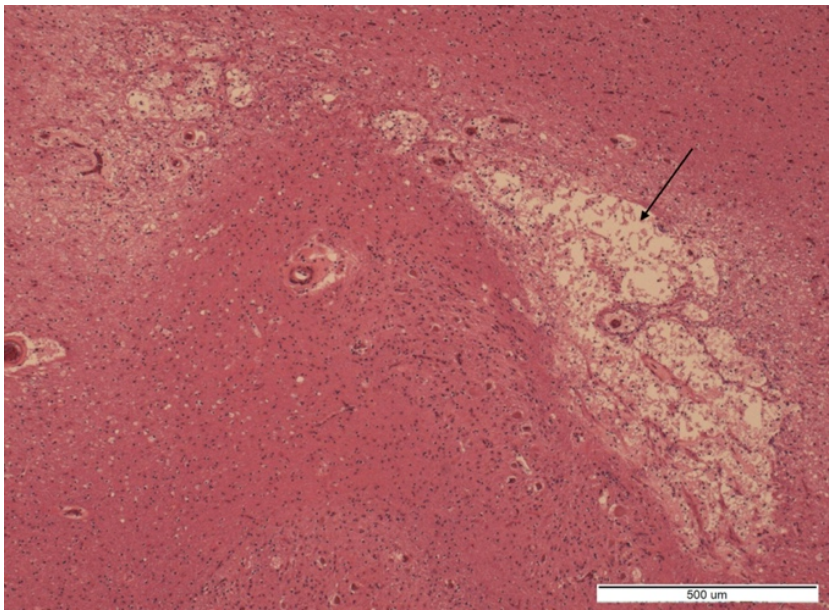


Figure 2.7 Lacunar infarct

A lacunar infarct (arrow) with surrounding gliosis and cystic degeneration, measuring <10mm in maximum diameter (H&E, x40).

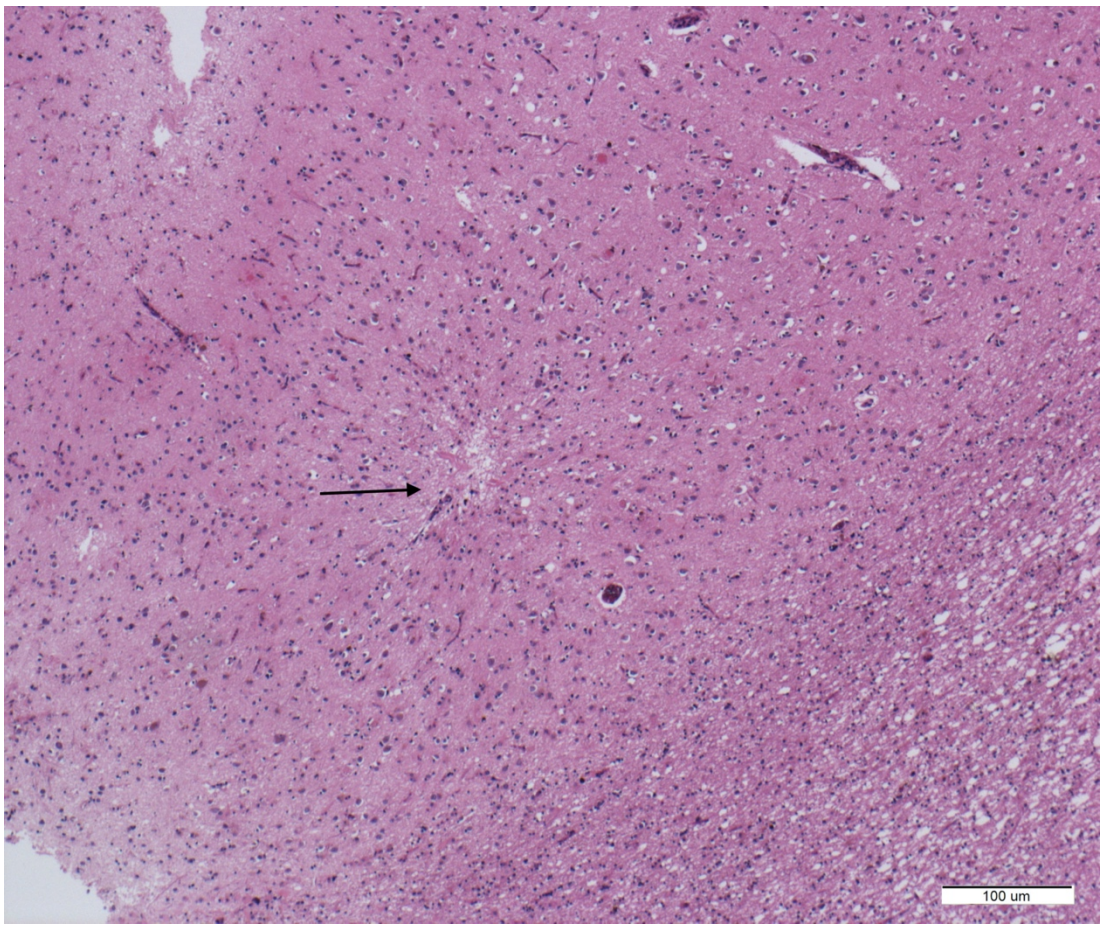


Figure 2.8 Cortical microinfarct

A cortical microinfarct (arrow) with localised tissue loss and reactive gliosis, the lesion being found on microscopic examination but not visible on naked eye examination (H&E, x100).

2.3.6 Papers studying white matter hyperintensities

2.3.6.1 Macroscopic comparisons

Where MR-defined WMH were compared with macroscopic appearances, tissue softening, pallor and loss including infarcts or spaces consistent with lacunes or enlarged PVS (Awad, Johnson et al. 1986, Braffman, Zimmerman et al. 1988, Marshall, Bradley et al. 1988, Revesz, Hawkins et al. 1989, Chimowitz, Estes et al. 1992, Scarpelli, Salvolini et al. 1994) were described most often. However, there were often no obvious macroscopic changes

(Fazekas, Kleinert et al. 1991, Grafton, Sumi et al. 1991, Scarpelli, Salvolini et al. 1994, Scheltens, Barkhof et al. 1995) or only subtle discoloration (Awad, Johnson et al. 1986, Revesz, Hawkins et al. 1989). Macroscopic lesions in one study were on average 54% larger than on MRI (Bronge, Bogdanovic et al. 2002) and were more extensive in another (Munoz, Hastak et al. 1993). A separate study found differences between areas of high signal intensity (discolouration and enlarged PVS) and areas of relatively lower (but still increased) MR signal change, which could not be identified (Murray, Vemuri et al. 2012). Naked eye examination of histological slides stained for myelin or axons described pallor in areas of radiological WMH (van Swieten, van den Hout et al. 1991, Munoz, Hastak et al. 1993).

2.3.6.2 Precise microscopic comparisons

12 papers attempted to make direct comparisons between imaging WMH and corresponding histological lesions, and some described pathology in specific locations. WMH in the centrum semiovale showed variable white matter pathology. WMH in seven brains (five with bilateral discrete WMH, two with ‘diffuse change’) revealed enlarged PVS containing fluid and macrophages, myelin and axonal pallor, and gliosis (Grafton, Sumi et al. 1991). 33 extensive WMH corresponded with poorly defined areas of myelin pallor that appeared larger on histology. They contained axonal swelling and loss and involved subcortical U-fibres when severe with white matter vacuolation (‘spongiosis’), decreased oligodendroglial numbers and dilated PVS throughout. 21% (n=7) of the extensive WMH also contained focal perivascular or scattered diffuse vacuolation. One WMH was close to a small infarct and one contained a small haemorrhage (Munoz, Hastak et al. 1993). WMH corresponded to myelin rarefaction in five brains (three in the centrum semiovale, two periventricular). All five brains had moderate-severe lipofibrohyalinosis and one had diffuse white matter oedema in the centrum semiovale (Fazekas, Kleinert et al. 1999). Seven WMH corresponded with histological infarction, one of which had surrounding gliosis correlating with the WMH, one was recent with early cavitation, macrophages and

surrounding gliosis (Braffman, Zimmerman et al. 1988) and two in the left frontal white matter were old with a 1cm cavity and 3cm of surrounding gliosis. An unspecified number of small intermediate and old infarcts with surrounding isomorphic gliosis were also found in frontal, mid-coronal and occipital WM (Marshall, Bradley et al. 1988). One cerebellar WML corresponded with a 3cm infarct histologically (Marshall, Bradley et al. 1988). 'Isomorphic gliosis' and IgG in astrocytes extended up to 3cm from old infarcts (showing cavitation and minimal gliosis, some with demyelination) and the ventricles (Marshall, Bradley et al. 1988). Pontine WMH revealed severe gliosis and axonal and myelin loss (Revesz, Hawkins et al. 1989). Periventricular WMH contained myelin pallor, enlarged PVS, subependymal gliosis and increased extracellular spaces accompanying disrupted ependyma (Matsusue, Sugihara et al. 2006).

The locations of some lesions and pathologies were not specified. One study sampled 27 radiological WMH from 16 brains (centrum semiovale in two brains, adjacent to the frontal horns of the lateral ventricles in two, optic radiations in five and basal ganglia in three; the number of samples per brain/area is not described). 100% of WMH sampled (n=27) contained at least one severe pathology of arteriolar sclerosis, vascular ectasia or enlarged PVS (Awad, Johnson et al. 1986), 85% (n=23) had two severe changes. 59% (n=16) also showed subependymal gliosis, associated with myelin pallor, axonal loss, enlarged PVS, vascular ectasia and arteriolosclerosis. In 15 control areas sampled, 27% (n=4) had one severe pathology and 7% (n=1) had two severe changes (Awad, Johnson et al. 1986). In another study 141 deep subcortical WMH showed severe myelin pallor and damage (Fernando, O'Brien et al. 2004). Of nine larger (not punctate) subcortical WMHs, 78% (n=7) showed prominent myelin pallor and enlarged PVS with parenchymal oedema, 67% had gliosis (n=6), 44% macrophage infiltration (n=4) and 33% arteriosclerosis (n=3). 26% (n=5) of punctate WMH showed periarteriolar demyelination often surrounding enlarged perivascular spaces and 16% (n=3) had perivenous demyelination.

At least one was in the external capsule (Fazekas, Kleinert et al. 1991). In another paper, deep and subcortical WMH, both punctate and confluent, corresponded with histological myelin pallor and enlarged PVS (Matsusue, Sugihara et al. 2006).

One paper was difficult to interpret but seemed to identify six infarcts, four old and two recent (Scarpelli, Salvolini et al. 1994). Two small areas in the corona radiata showed recent infarction with macrophages and inflammation surrounded by degenerate myelin and one cystic area in the internal capsule corresponded to a enlarged PVS containing an ectatic, sclerotic artery and macrophages with surrounding fibrous gliosis (Scarpelli, Salvolini et al. 1994).

In surrounding, radiologically non-lesional tissue, there were eight areas of enlarged PVS, five parenchymal oedema and four of inflammation (Chimowitz, Estes et al. 1992), and two areas of histological gliosis/non-cavitated minute infarction were adjacent to areas of fibre loss with fibrillary necrosis and cavitated, gliotic infarcts (Braffman, Zimmerman et al. 1988). 11% (n=10) of control samples contained intermediate necrotic lesions with surrounding gliosis (Marshall, Bradley et al. 1988). In tissue adjacent to six punctate WML, 50% (n=3) contained enlarged PVS, 33% (n=2) gliosis, and 17% (n=1) each with arteriosclerosis and myelin pallor (Chimowitz, Estes et al. 1992).

Binswanger's disease described radiologically as 'irregularly distributed WML relatively sparing the temporal lobe' showed histological moderate rarefaction with loss of myelin, axons and oligodendrocytes, and mild gliosis and arteriosclerosis (Matsusue, Sugihara et al. 2006).

Radiological DTI abnormalities replicated those seen *in vivo* and were associated with the presence of microinfarcts in posterior white matter. Abnormal fractional anisotropy was more sensitive to axonal loss while

increased mean diffusivity reflected myelin loss in CAA (van Veluw, Reijmer et al. 2019).

An assortment of other histological lesions appeared as radiological WML. Several so-called lacunae were identified: one with gliosis and myelin pallor surrounding 2mm central area of necrosis (Awad, Johnson et al. 1986); one in the temporo-parieto-occipital deep WM with dense gliosis surrounding a cystic area (Revesz, Hawkins et al. 1989); two WMH in the globus pallidus and putamen corresponded to two lacunar infarcts with the same size on imaging and histology (Marshall, Bradley et al. 1988); a poorly circumscribed, irregular WMH with a halo of signal intensity was a poorly defined cystic cavity with surrounding mild gliosis (Matsusue, Sugihara et al. 2006); a large circumscribed area of low signal in the putamen showed an empty cyst with previous haemorrhage (Revesz, Hawkins et al. 1989) and multiple lacunae were found in the basal ganglia of three brains and the thalamus in two brains (Fazekas, Kleinert et al. 1999). A circumscribed linear WMH smaller than 3mm without surrounding signal change was a enlarged PVS (Matsusue, Sugihara et al. 2006); 88% (n=15) of punctate centrum semiovale WMH contained dilated PVS on microscopy, 6% (n=1) had small infarcts and CAA while no histological abnormality was found in 6% (n=1) (Munoz, Hastak et al. 1993). Punctate WMH additionally represented defined areas of demyelination, two subcortical ganglion cell heterotopias, one periarteriolar fibrosis and one perivenous oedema (Fazekas, Kleinert et al. 1991); one case with telangiectasia (Awad, Johnson et al. 1986); and two areas of demyelination, one cyst and one congenital ventricular diverticulum (Braffman, Zimmerman et al. 1988).

Histological cribriform changes, with a sieve-like pattern of ‘holes’ of varying sizes in the basal ganglia (status cribrosum) were seen in eight subjects; 38% (n=3) in the presence of radiological lacunes, 25% (n=2) with a single radiological lacune but without any MRI correlate in 38% (n=3). This could reflect the low resolution of the MRI with a 1T field strength and 5mm slice thickness (Fazekas, Kleinert et al. 1999).

There were a number of post-mortem imaging-histology mismatches. Radiological lesions not identified on histology included 36 WMH (Braffman, Zimmerman et al. 1988, Fazekas, Kleinert et al. 1991, Fernando, O'Brien et al. 2004) plus multiple lacunes in the centrum semiovale, brainstem, and cerebellum (Fazekas, Kleinert et al. 1999). Histology revealed lesions not seen on imaging; 37 deep subcortical white matter areas with moderate myelin loss and endothelial activation (Fernando, O'Brien et al. 2004), three infarcts (Braffman, Zimmerman et al. 1988, Scarpelli, Salvolini et al. 1994), two basal ganglia lacunes plus one white matter infarct and two small old cortical infarcts, with cribriform change in the cerebellum, basal ganglia and pons (Fazekas, Kleinert et al. 1999).

2.3.6.3 Vascular pathology

A range of vasculopathies were described in MRI WMH (Figure 2.4c) and were often associated with other lesions but not correlated to the other changes. Atherosclerosis was common in periventricular lesions, with vacuolation and gliosis in neurologically normal cases in one study (Scarpelli, Salvolini et al. 1994). WMH in four subjects contained lipofibrohyalinosis and CAA (Fazekas, Kleinert et al. 1999), two subjects additionally showing patchy, rarefied myelin. Lipofibrohyalinosis and CAA were also seen, however, in subjects without MRI WMH. Differing severities of angiofibrosis, hyalinosis and arteriosclerosis were present in 83% (n=5) of six brains in another study, the remaining brain contained angiofibrosis and arteriosclerosis only (Fazekas, Kleinert et al. 1991).

Six punctate WMH examined in deep grey or white matter all showed enlarged PVS and perivascular gliosis. Two thirds of these WMH contained vascular ectasia, one third had perivascular inflammation and half arteriosclerosis (Chimowitz, Estes et al. 1992). Eight linear periventricular WMH, less than 2mm thick, all contained prominent subependymal gliosis (Chimowitz, Estes et al. 1992) and six focal WMH (less than 5mm) at the poles of the lateral ventricles showed myelin pallor with arteriosclerosis and

gliosis. Two thirds of the focal WMH had enlarged PVS, and one each had adjacent arteriolosclerosis, oedema and inflammation (Chimowitz, Estes et al. 1992).

2.3.6.4 In vivo imaging in white matter hyperintensities

Fazekas *et al.* noted many small WMH (less than 5mm diameter) in their study that would not have been identified post-mortem without knowledge of *in vivo* MR (Fazekas, Kleinert et al. 1991). *In vivo* MR also appeared superior at detecting hypointensities (Fazekas, Kleinert et al. 1999). *In vivo* CT did not identify a 4x4mm area of gliosis/infarction, two areas of demyelination and one cyst measuring 6x6mm which were subsequently seen on *ex vivo* MRI (Braffman, Zimmerman et al. 1988).

2.3.6.5 Non-precise white matter hyperintensities comparisons

Deep subcortical WMH showed a range of non-specific changes, particularly myelin pallor, vacuolation, decreased cellularity and enlarged PVS (Grafton, Sumi et al. 1991, Chimowitz, Estes et al. 1992, Munoz, Hastak et al. 1993, Fernando, O'Brien et al. 2004, Matsusue, Sugihara et al. 2006, Simpson, Fernando et al. 2007), with more vasculopathies, including arteriolosclerosis, compared to periventricular WMH (Chimowitz, Estes et al. 1992). Periventricular WMH were associated with disruption of the ependyma (Fernando, Simpson et al. 2006, Simpson, Fernando et al. 2007), abnormalities in myelin, axons and astroglia (Grafton, Sumi et al. 1991, Simpson, Fernando et al. 2007, Murray, Vemuri et al. 2012), and sometimes with increased subependymal gliosis (Chimowitz, Estes et al. 1992, Matsusue, Sugihara et al. 2006). Overall, WMH were larger on MRI than histology (Marshall, Bradley et al. 1988, Bokura, Kobayashi et al. 1998), usually of the order of about 25% with gliosis contributing to the MR appearance (Braffman, Zimmerman et al. 1988, Marshall, Bradley et al. 1988, Matsusue, Sugihara et al. 2006). Some histological studies suggested roles for inflammation, BBB dysfunction and hypoxia in both periventricular

and deep subcortical WMH (Fernando, Simpson et al. 2006, Simpson, Fernando et al. 2007, Simpson, Ince et al. 2007, Young, Halliday et al. 2008, Murray, Vemuri et al. 2012).

Radiologically NAWM in subjects with WMH was studied in some papers. It was histologically abnormal immediately adjacent to lesions (Chimowitz, Estes et al. 1992, Bronge, Bogdanovic et al. 2002, Fernando, O'Brien et al. 2004), where it may represent a transitional zone, but also distant to lesions (Simpson, Ince et al. 2007). However, specific distances from WMH, or graded changes as the distance increased, were not addressed. Suggested mechanisms included a global underlying pathology, possibly involving endothelial activation and inflammation. White matter in subjects without WMH appeared normal with strong myelin staining in several studies (Marshall, Bradley et al. 1988, Bronge, Bogdanovic et al. 2002, Fernando, O'Brien et al. 2004). Microglial staining characteristics and morphology differed between deep subcortical WMH, NAWM and controls (Waller, Baxter et al. 2019).

2.3.6.6 White matter hyperintensities summary

- Macroscopic changes of WMH include discolouration and softening but often no lesion was visible.

- Location of lesions was frequently not described, descriptions were sometimes difficult to interpret and overall difficult to summarise and compare due to differences in terminology and reporting.

- Location of lesions was most often described in the centrum semiovale.

- Microscopy of radiological WMH commonly included myelin pallor (Figure 2.5b), oedema and PVS enlargement (Figure 2.6) as well as

areas of tissue infarction (Figure 2.7) and cavitation. Vascular pathology and inflammation were also seen.

- Gliosis contributes to hyperintensity on imaging.

- Few studies have made precise comparisons of the gradation of histology from lesional to normal appearing tissue, and of radiologically NAWM in lesional brains.

2.3.7 Papers studying enlarged perivascular spaces and lacunes

Three studies specifically reported enlarged PVS and lacunes (Braffman, Zimmerman et al. 1988, Bokura, Kobayashi et al. 1998, van Veluw, Biessels et al. 2016), two of which compared lesions identified on 1.5T MR with histology, on morphology and size (Braffman, Zimmerman et al. 1988). Macroscopic examination confirmed the morphology seen on MR imaging (Braffman, Zimmerman et al. 1988, Bokura, Kobayashi et al. 1998).

2.3.7.1 Precise microscopic comparisons

At least five radiologically identified lacunes corresponded to microscopic cavities with surrounding gliosis and axon loss (Revesz, Hawkins et al. 1989, Scarpelli, Salvolini et al. 1994, Matsusue, Sugihara et al. 2006), two also had perilesional macrophages and lymphocytes with neovascularisation (Scarpelli, Salvolini et al. 1994). Using a 1.5T scanner, one study described the hyperintense halo on MR corresponding with surrounding, partial myelin and axon loss, and gliosis (Matsusue, Sugihara et al. 2006).

2.3.7.2 Vascular pathology

Microscopic vascular wall pathology was not described.

2.3.7.3 Location

Lacunar infarcts and enlarged PVS were both more common in the basal ganglia and thalamus. 82 lacunar infarcts were studied in total; 47 in the basal ganglia and thalamus, 24 in the white matter and nine in the posterior fossa (Braffman, Zimmerman et al. 1988, Braffman, Zimmerman et al. 1988, Marshall, Bradley et al. 1988, Scarpelli, Salvolini et al. 1994, Bokura, Kobayashi et al. 1998, Fazekas, Kleinert et al. 1999). 67 PVS were identified in one paper, 58 within the basal ganglia (Bokura, Kobayashi et al. 1998); a second paper found four areas of dilated PVS in the putamen and white matter (Braffman, Zimmerman et al. 1988).

2.3.7.4 Size and morphology

Studies that compared size and morphology used 1.5T and a 5mm slice thickness (Braffman, Zimmerman et al. 1988, Bokura, Kobayashi et al. 1998) or 0.35T and 0.95mm resolution (Marshall, Bradley et al. 1988). Lacunes were consistently larger than 2mm in their greatest dimension on both MRI and histology (Braffman, Zimmerman et al. 1988, Bokura, Kobayashi et al. 1998), and were largest in the deep grey matter (3x1mm to 14x13mm), followed by posterior fossa (3x1mm to 5x3mm), being smallest in the white matter (2x2mm to 4x2mm) (Braffman, Zimmerman et al. 1988, Marshall, Bradley et al. 1988). Their dimensions were the same on histology and *ex vivo* MRI (Marshall, Bradley et al. 1988) and they were most commonly wedge-shaped, but this was variable with slit-like, round and ovoid morphology also seen (Braffman, Zimmerman et al. 1988, Bokura, Kobayashi et al. 1998). Enlarged PVS were significantly smaller than lacunes in all areas studied except in the most caudal region of the basal ganglia (Bokura, Kobayashi et al. 1998). Enlarged PVS were predominantly round or linear in shape and less than 2x2mm on MRI without perilesional signal change (Matsusue, Sugihara et al. 2006).

2.3.7.5 In vivo imaging

In vivo neuroimaging was performed in 26 subjects; 36 MRI lesions were identified and confirmed on pathology in six subjects (Bokura, Kobayashi et al. 1998). *In vivo* CT identified all six histological lacunar infarcts in the basal ganglia and one of five in the white matter, confirming their morphology, but did not identify any in the brainstem or areas of status cribrosum (Braffman, Zimmerman et al. 1988).

2.3.7.6 Enlarged perivascular spaces and lacunes summary

- Five radiological lacunes were histological cavitated lesions.
- Lacunar infarcts and enlarged PVS were both more common in the basal ganglia and thalamus.
- Radiological lacunes were sometimes surrounded by signal change and were larger than 2mm.
- Enlarged PVS on MRI were smaller than lacunes (less than 2x2mm) without perilesional signal change.

2.3.8 Magnetic resonance imaging-histopathological correlations on microinfarcts

570 microinfarcts were identified on MRI in 202 subjects, 69% (n=396) of these from a single paper (we have calculated this figure from subject numbers and group means) (De Reuck, Deramecourt et al. 2014). The number of microinfarcts per subject ranged from 0 – 72. 67% (n=381) microinfarcts were found on histology. Two papers identified 86% (n=327) of these but compared mean numbers between neurodegenerative disease subgroups only (De Reuck, Deramecourt et al. 2014, De Reuck, Deramecourt et al. 2015). 26 were precisely matched to MR-identified microinfarcts in three papers (van Veluw, Zwanenburg et al. 2013, van Veluw, Zwanenburg et al. 2015, van Veluw, Charidimou et al. 2016). In

another, 49 microinfarcts were initially identified on histology, 35% of these (n=17) were subsequently found on 3T MRI (Niwa, Ii et al. 2017). Those found were all over 2mm in size, but some microinfarcts over 2mm and all less than 1mm could not be seen on 3T MRI.

Seven MRI-identified microinfarcts were searched for on histology but not identified, and one was described as an area of rarefaction (van Veluw, Zwanenburg et al. 2015). 56 additional microinfarcts were identified on histology only (van Veluw, Zwanenburg et al. 2013, van Veluw, Zwanenburg et al. 2015, van Veluw, Charidimou et al. 2016, Niwa, Ii et al. 2017). They measured 0.6mm diameter on average, below the current detection threshold for 7T scanners (van Veluw, Zwanenburg et al. 2015). Nine histological microinfarcts were present in one small sample, none of which had been identified by ultra-high ($100\mu m^3$) resolution MRI, although two identified at $300\mu m^3$ resolution were matched to histology with no additional microinfarcts being identified (van Veluw, Charidimou et al. 2016).

2.3.8.1 Precise microscopic comparisons

Microinfarct histology within the cortex was heterogenous (van Veluw, Zwanenburg et al. 2015). Three studies identified 84 potential microinfarcts as hyperintense cortical lesions on T2 and FLAIR sequences (van Veluw, Zwanenburg et al. 2013) or any lesion smaller than 5mm (van Veluw, Zwanenburg et al. 2015) or both (van Veluw, Charidimou et al. 2016). 26 were confirmed as different types of microinfarcts on histology. 14 with increased signal intensity on T2 and FLAIR sequences revealed histological chronic microinfarcts with pallor, gliosis and neuronal loss (van Veluw, Charidimou et al. 2016), sometimes with incomplete cavitation not visible on MRI (van Veluw, Zwanenburg et al. 2015). Three were hyperintense on T2 and hypointense with a bright rim on FLAIR, histologically revealing fluid filled cavities surrounded by gliosis. Three hypointense lesions on T2, FLAIR and T2* sequences showed histological haemosiderin-laden macrophages, gliosis and neuronal loss (van Veluw, Zwanenburg et al. 2015). Six acute

lesions showed red neurons and pallor of the white matter (van Veluw, Charidimou et al. 2016), and one was hypo-isointense on T2 and FLAIR (van Veluw, Zwanenburg et al. 2015). One study stated microinfarcts and enlarged PVS had similar appearances on MRI, but could be differentiated by their location, enlarged PVS being just below the cortico-medullary junction (Niwa, Ii et al. 2017).

Chronic lesions measured 1.2-2.5mm (van Veluw, Zwanenburg et al. 2013), smaller than the single acute microinfarct measuring 4.4mm. Sizes were not significantly different between MR and histology (van Veluw, Charidimou et al. 2016).

2.3.8.2 Location

Microinfarcts occur throughout the brain (Brundel, de Bresser et al. 2012). However, in the five studies included here, four specifically aimed to study intracortical microinfarcts and one studied them in the context of CAA, which predominantly affects the cortex. It is therefore not unexpected that all microinfarcts identified in these studies were intra-cortical. They were seen in all layers, often in the most superficial layer (De Reuck, Deramecourt et al. 2014) where they sometimes caused a small surface retraction (van Veluw, Zwanenburg et al. 2015), or extended to two or more layers (van Veluw, Zwanenburg et al. 2013, van Veluw, Zwanenburg et al. 2015). They were more commonly seen in parietal and frontal cortex (van Veluw, Zwanenburg et al. 2013) and appeared to cluster on MRI (van Veluw, Charidimou et al. 2016). In both CAA and vascular dementia they were often superficial (De Reuck, Deramecourt et al. 2014). Cerebellar microinfarcts were more common in vascular dementia, where they were also associated with leptomeningeal arteriosclerosis (De Reuck, Deramecourt et al. 2015). Detailed histological assessment of 12 radiological juxtacortical microinfarcts revealed eight PVS, one primary haemorrhage and one venous angioma; two lesions were not identified (van Veluw, Zwanenburg et al. 2015).

2.3.8.3 In vivo imaging

In vivo 1.5T MRI was examined retrospectively in one paper and no microinfarcts were visible (van Veluw, Charidimou et al. 2016). Another study found 15 possible microinfarcts on *in vivo* 7T MRI; four were identified on corresponding *in vivo* 3T T1 and/or T2 sequences but *ex vivo* MRI and histology were not undertaken (van Veluw, Zwanenburg et al. 2013).

2.3.8.4 Non-precise microinfarct comparisons

A number of microinfarcts seen on MR imaging as small, well defined hyperintensities on T2, not visible on T2* were compared but not described histologically in two studies (De Reuck, Deramecourt et al. 2014, De Reuck, Deramecourt et al. 2015). More microinfarcts were identified in cases with neurodegenerative pathology and CAA when compared with non-neurodegenerative brains (De Reuck, Deramecourt et al. 2015).

2.3.8.5 Microinfarcts summary

- 26 histological lesions were precisely matched to MR-identified microinfarcts.

- Histological appearances were variable, most often (in 54%) revealing foci of chronic neuronal loss and gliosis; acute changes with red neurons and white matter pallor were seen in 23%.

- A significant number of microinfarcts identified on histology were too small to be seen on MRI up to 7T.

2.3.9 Cerebral amyloid angiopathy

As stated, we excluded studies of only haemorrhagic pathology, which includes the bulk of reporting on CAA, a major cause of spontaneous intracerebral haemorrhage (Charidimou, Gang et al. 2012). However, many studies did not describe subjects with amyloid and non-amyloid pathology

separately and a number of lesions related to CAA were described within these studies, they are included here.

2.3.9.1 Cerebral amyloid angiopathy and radiological white matter hyperintensities

Most histological studies found no association between cortical or leptomeningeal CAA and radiological WMH (Marshall, Bradley et al. 1988, Chimowitz, Estes et al. 1992, Munoz, Hastak et al. 1993, Scheltens, Barkhof et al. 1995, Moody, Thore et al. 2004, Auriel, Bornstein et al. 2011). One study of WML found no CAA in thickened hyalinised vessels (Marshall, Bradley et al. 1988). Cortical and leptomeningeal CAA correlated with increased levels of the hypoxia marker HIF-1α in deep subcortical WML only (Fernando, Simpson et al. 2006).

2.3.9.2 Cerebral amyloid angiopathy and radiological perivascular spaces

One paper reported a significant positive relationship between severity of histological cortical CAA and of radiological juxtacortical enlarged PVS (van Veluw, Biessels et al. 2016).

2.3.9.3 Cerebral amyloid angiopathy and microinfarcts

Intracortical microinfarcts, rather than juxtacortical and deep white matter infarcts, may be associated with severe CAA (Greenberg, Vernooij et al. 2009, De Reuck, Deramecourt et al. 2014). The number of the smallest superficial cortical microinfarcts were increased in AD with CAA, and in vascular dementia (VaD) (De Reuck, Deramecourt et al. 2014). 72% of microinfarcts in one paper were associated with moderate to severe CAA; one third of these were identified on *ex vivo* MRI. 48/48 cortical microinfarcts in subjects with CAA were associated with vascular abnormalities, 33 were close to Aß-positive vessels and 15 to vessels showing ‘double-barrelling’ arteriopathy associated with CAA.

2.4 Discussion

This review has highlighted the variability in methodology and reporting in radiological-pathological comparisons in sporadic human cerebral SVD. The earliest of these papers were published in the 1980's when MR resolution was much less sensitive than it is today, and SVD knowledge was much less refined. There has since been a consensus on neuroimaging terminology and techniques (Wardlaw, Smith et al. 2013), used in subsequent papers (van Veluw, Zwanenburg et al. 2015, van Veluw, Biessels et al. 2016, van Veluw, Charidimou et al. 2016). However, pathological terminology and reporting remains variable (Pantoni, Sarti et al. 2006), limiting the reproducibility and interrogation of findings (Wardlaw, Valdes Hernandez et al. 2015) and making it difficult to identify and interpret relevant literature (Appendix 1). As such, we recognise that some relevant studies may have been overlooked in this systematic review. Lesions were often poorly defined histologically, and some histological changes with unknown significance overlooked, such as vascular collagenosis and fibrinoid necrosis. In particular, the term 'infarct' is in common use histologically but the precise definition is lacking and, our results indicate, is inconsistent with the term used *in vivo*. Commonly used terms such as 'oedema' and 'lacunar infarction' assume the underlying pathophysiology, when in fact, this remains to be proven in sporadic human SVD.

Tissue 'oedema' and PVS enlargement were frequently observed on histopathology in WMH; although these features have received less attention to date in the pathology literature than myelin loss, the oedema and enlarged PVS correspond with findings on in vivo MRI suggesting that WMH (and the perilesional penumbra) have increased tissue water and increased blood-brain barrier leakage (Cho, Kim et al. 2015, Wardlaw, Valdes Hernandez et al. 2015). It also concurs with the reduction in WMH seen *in vivo* at follow-up in some patients associated with reductions in brain tissue water (Wardlaw, Chappell et al. 2017). Additionally, PVS enlargement n subcortical tissues is associated with increased severity of WMH and other features of SVD, and

may reflect impaired tissue fluid and waste clearance (Wardlaw, Benveniste et al. 2020). Widespread signal changes are seen in post-mortem brains with neurodegenerative pathology, such as altered T2 (Dawe, Bennett et al. 2014) and R2 (transverse relaxation rate) (Yu, Dawe et al. 2017) in multiple areas including white matter that may be associated with mild cognitive decline. However histological correlation is needed in more studies to understand the pathological substrate of these appearances.

Alterations in NAWM adjacent to SVD lesions are seen (Chimowitz, Estes et al. 1992, Bronge, Bogdanovic et al. 2002, Fernando, O'Brien et al. 2004) including specific axonal alterations in nodes of Ranvier and paranodal regions adjacent to lacunar infarcts (Hinman, Lee et al. 2015), but no studies that we are aware of have addressed histological gradients of abnormality around lesions.

Some studies describe risk factors for SVD, but clinical risk factors are generally under-reported and the full association with radiological and pathological burden remains unclear (Shi and Wardlaw 2016). Medical histories were usually collected retrospectively and therefore common vascular risk factors are likely to be under-recognised. Cardiovascular risk factors are the most strongly associated modifiable risk factors for SVD, and WMH were the focus of most radiological-pathological correlation studies assessed in this review. However, it should be noted that cardiovascular risk factors explain only 2% of the variance in WMH on imaging (Wardlaw, Allerhand et al. 2014), and other potentially modifiable risk factors current remain unknown.

The importance of radiological-histological comparisons are well recognised (Wardlaw 2011). However, a significant proportion of lesions, particularly microinfarcts, microbleeds and microvessel pathologies remain undetected on neuroimaging at current clinical field strengths (van Veluw, Charidimou et al. 2016) and this is reflected in the range of field strengths and slice thicknesses used in these studies. Higher field strengths, for example 3T,

reveal lesions for which we currently lack pathological comparative material and technology required to accurately compare radiological and histological lesions.

Tissue storage and fixation times varied from overnight (Moody, Thore et al. 2004) to 12 years (Revesz, Hawkins et al. 1989). Although no formal quality assessments were made, no changes were reported that affected the ability to assess the tissue on post-mortem imaging or histology. Repeated and high field MRI examination of post-mortem tissue does not appear to compromise histological examination but interpretation of post-mortem MR images should consider differences in the superficial and deep aspects of tissue that have been submerged in formalin (Dawe, Bennett et al. 2009, Kotrotsou, Bennett et al. 2014).

There is significant radiological and pathological heterogeneity in SVD. Advances in understanding of the clinical consequences of SVD with ageing have come from imaged cohorts followed over a lifecourse (such as the RUN DMC study (van Norden, de Laat et al. 2011) and Lothian Birth Cohort 1936 (Deary, Gow et al. 2007)), and the introduction of the STRIVE consensus standards for neuroimaging (Wardlaw, Smith et al. 2013) has introduced a standardised approach across neuroimaging SVD studies. Radiological studies now have an established pathway to follow. The number of direct radiological-pathological comparison studies to date are small, and of course pathological studies are, by their nature, static. Radiological studies highlight the dynamic nature of SVD, and therefore the cohorts used to study SVD should be well-characterised clinical and radiological cohorts with brain donation programmes. Making precise comparisons is resource-intensive but possible (Humphreys, Jansen et al. 2018). Initiatives such as the Medical Research Council's (MRC) UK Brain Bank Network is helping to generate an accessible well-characterised brain tissue resource linked to detailed clinical and imaging data. Standardised histological approaches to assessing the contribution of SVD to an overall diagnosis of cognitive impairment have been published (Deramecourt, Slade et al. 2012, Skrobot, Attems et al.

2016), and whilst the need to standardise the basic pathological protocols and descriptions of SVD has been recognised (Alafuzoff, Gelpi et al. 2012), to date no standardised consensus statements have been published. To maximise gain from the valuable brain bank resources, future studies must be of high quality, with subjects characterised as fully as possible *in vivo*, and standardised methods of tissue assessment (both radiologically and histologically), using standardised terminology and reporting.

Standardised methods for processing post-mortem tissue should address artefact, particularly as MRI field strengths continue to increase towards microscopic resolution (van Veluw, Charidimou et al. 2016). These approaches need to account for post-mortem thrombi within vessels and air bubbles that can mimic small haemorrhagic lesions on *ex vivo* MRI (De Reuck, Auger et al. 2011), and the effects of heating during MRI on tissue quality and artefact. Brain tissue absorbs more radiofrequency than other tissue and *in vivo* mechanisms such as vasodilation, which usually dissipate heat (Murbach M 2015), are absent. Tissue quality assessment is important as it reflects the potential for artefact, alters MR imaging properties (Dawe, Bennett et al. 2009) and is essential for further use of tissue, such as genetic assessment, a logical extension of these studies (Tan and Markus 2015).

This review is limited as it does not include individual case studies and abstracts not written in English. It is potentially limited by the search strategy applied and publication bias. However, this is the nature of systematic reviews and we do not believe we have missed any significant publications comparing radiological and histological appearances of SVD lesions. There are several animal models of SVD but they do not fully represent the spectrum of disease, often simplifying the heterogeneity seen in human tissue. By specifying human studies, we have focussed on the disease in the appropriate context. We have concentrated on sporadic SVD rather than monogenic causes which are a distinct subgroup with potentially overlapping pathophysiological mechanisms, but ultimately different phenotypes. We have, however, included CAA as part of the spectrum of SVD, further

increasing the heterogeneity. The lack of precise comparisons combined with sub-optimal MRI resolutions and inconsistent reporting makes it difficult to always be sure the exact same lesions were studied and therefore have confidence in the conclusions drawn. However, we have tried to distinguish comparisons of precise cellular features from more general appearances. Inconsistent reporting also made it difficult to compare the studies, resulting in somewhat lengthy lists and descriptive results which are difficult to read and we were unable to carry out a meta-analysis. This is a further reflection of the variability in SVD terminology and methods.

Recently the dynamic nature of other SVD lesions including microinfarcts and lacunes has been appreciated (van Leijsen, van Uden et al. 2017). WMH are dynamic on *in vivo* neuroimaging with varying outcomes. (Cho, Kim et al. 2015, Schmidt, Seiler et al. 2016, Wardlaw JM 2017) These observations are, to date, not reflected in histological studies which provide only a static assessment of what are, most likely, end-stage tissue changes. In the studies in this review the overall numbers of subjects and lesions is also very small. In future, comprehensive, standardised reporting of clinical and pathological data, with precise comparison methods and advanced neuroimaging technologies are needed to study specific SVD lesions. In particular, attention to changes within and around radiological WMH should be studied; identifying the centre of a lesion and tracking changes in myelin and axons, for example, as it becomes normal appearing white matter; looking carefully for structural changes within normal appearing white matter that may be associated with WMH burden. Comparing lesions in different locations and using prospective, comprehensive medical and lifestyle information will strengthen pathological-radiological-clinical associations, furthering our understanding of the pathological substrates and cellular mechanisms underlying SVD.

In summary, radiological-pathological correlation in human sporadic SVD is important, but standardised protocols and terminology in well-characterised clinical cohorts are required to truly use these correlations to advance our

understanding of the pathophysiology of this common disorder. Using this systematic review and building on important definitions already published (Skrobot, Attems et al. 2016) we plan to undertake a multi-centre work to develop standardised definitions and grading systems that can be used to provide uniformity to future histopathological assessments of elements of sporadic SVD, similar to those developed by neuroimaging (Wardlaw, Smith et al. 2013).

2.5 Conclusions

Definitions and terminology used in SVD pathology have been recognised as problematic for several years (Pantoni, Sarti et al. 2006, Gouw, Seewann et al. 2011, Love, Budka et al. 2015). They continue to be confused and used inconsistently.

In his original studies, Fisher used a variety of terms when trying to understand the cause of lacunes, while summarising previous literature he may have inadvertently contributed to the ensuing confusion (Fisher 1968, Rosenblum 2008). Definitions of SVD lesions also remain unhelpful in neuropathology textbooks published as recently as 2017. For example, arteriolosclerosis defined as ‘arteriosclerosis of perforating and small vessels’ doesn’t explain what arteriolosclerosis is; and lipohyalinosis used synonymously as ‘arteriolar hyalinosis with plasma protein accumulation and fibrinoid necrosis’ (Kovacs, Alafuzoff et al. 2017) confuses a number of lesions.

The histological features underlying radiological lesions in these studies are heterogenous, but specific characteristics that allow the pathological substrates to be identified when reporting neuroimaging remain elusive, as does the relative significance and contribution these other characteristics make to the pathophysiological mechanisms underlying SVD. A systematic review carried out in preparation for the STRIVE guidelines workshop, found the terminology used to describe imaging-related SVD lesions was varied

and inconsistent in a similar way to the current state of the pathological terminology. 159 different names were used for recent small subcortical infarcts, over 100 terms for lacunae, 50 for WMH and 20 for microbleeds. There was also overlap with the same terms being used to describe different lesions, such as recent small subcortical infects referred to as lacunar infarcts (Wardlaw, Smith et al. 2013). By ultimately obtaining a similar, large scale consensus for the pathological terminology we may begin to develop an approach that will enable increased quality of research into SVD including formal meta-analyses of data, leading to more robust and reliable clinical-imaging-pathological associations.

The reporting and methods used to study the lesions are also variable. Future consensus should aim to address tissue sampling, processing and assessment to standardise the procedures, making it as comprehensive as possible, reproducible and easily comparable. Relevant clinical risk factors are relatively simple to collect and record but are under-reported, confounding attempts to make reliable associations. Establishing a minimum clinical dataset required would ensure a thorough assessment is possible. These used strategically in combination with advancing imaging and molecular techniques could significantly advance our understanding and contribute toward unpicking the clinical-imaging-pathological associations.

2.6 Hypotheses

Based on the findings of my systematic review and our current understanding of SVD, the hypotheses I explored in this thesis are:

- SVD lesions identified on MR imaging accurately reflect the underlying cellular lesions.

- Protein expression is altered in brain tissue with SVD compared to controls and other conditions.

I began by identifying appropriate cohorts to investigate SVD in and compare SVD to. As they are currently lacking, I defined a histological grading system and terminology to be used in reporting and grading SVD and I adapted currently used imaging grading systems for use in the small tissue samples I used. I designed a protocol to obtain MR and histological images and register them for accurate lesion comparison and graded the burden of SVD to test the histological grading system and ensure the cohorts used appropriately represented the disease burden expected. I then investigated protein expression in SVD and aimed to investigate gene expression, however this was prevented by Covid-19 and is discussed in Chapter 8.

PART B: METHODS

CHAPTER 3: MATERIAL AND METHODS

3.1 Developing the cohorts

3.1 1 Background to human tissue donation and brain banking

Donated human brain tissue is an invaluable resource for research into neurological disease including SVD, allowing translation from animal and *in vitro* studies for the investigation of human diseases in the right context. It has been fundamental to the work undertaken in this thesis. In recent years, donation of post mortem human tissue has decreased all around the world and particularly in the UK following revelations that many thousands of body parts, organs, still born children and foetuses were retained without permission or informing next of kin by hospitals across the UK, including Alder Hay in Liverpool and Bristol Royal Infirmary in the late 1990's (English and Sommerville 2003). Medical professionals had assumed consent for tissue and organ retention following medical procedures in the face of poor communication and lack of legislation. Public trust was lost, and the medical profession has had to work to rebuild confidence in their procedures and intentions regarding autopsies and retained tissues.

A subsequent inquiry set out the framework for the practice's pathologists follow today. In Edinburgh, we work within the Human Tissue Act (Scotland) 2006 (www.legislation.gov.uk/asp/2006/4/pdfs/asp_20060004_en.pdf). Increased public awareness since the tissue retention scandals and implementation of the new laws and best practice guidance have brought more attention to and better understanding of the importance of tissue donation. Biobanks have been created under strict regulation with transparent procedures and purposes for the collection, storage and provision of human biological resources for use in high quality research projects. These resources can include organs, tissue and cells. Depending on the tissue type and clinical situation, donations can be made in life or post

mortem. In either case, they are usually arranged pre-mortem with fully informed consent from the individual. The programmes running the biobanks today are well adapted to suit the requirements of the research they fulfil. In particular, thorough clinical and background epidemiological information is collected at the point of enrolment into the donation programmes allowing comprehensive characterisation of the groups. These are often accompanied by specialist tests relevant to the investigation, such as serial brain imaging in neurological disease cohorts.

Brain banking is a specialised biobank providing human brain resources for neuroscience research. The UK Medical Research Council (MRC) Brain Bank Network was set up to coordinate brain tissue resources across the UK (MRC 2021). They have established standardised operating procedures with minimum diagnostic datasets, tissue handling and storage protocols, quality assessment and standard ethical, consent, application and governance procedures.

3.1.2 The MRC Edinburgh Brain Bank

The MRC Edinburgh Brain bank was established in 2005 and is part of the UK Brain Bank Network. Several clinical cohorts have individuals from across Scotland who have signed up and consented in life to post mortem brain tissue donation. They include patients with a clinical diagnosis of dementia, intracerebral haemorrhage, MS, amyotrophic lateral sclerosis (motor neuron disease), frontotemporal dementia, progressive supranuclear palsy, corticobasal degeneration, multisystem atrophy, Huntington's disease and Parkinson's disease, cohorts representing normal aging and controls without neurological disease.

3.1.2.1 Ethical approval

Ethical approval is granted by the East of Scotland Research Ethics Service (ref. 16/ES/0084) and the brain bank works within the Human Tissue Act (Scotland) 2006. There is a local management group and steering

committee, both of which have lay members. Requests for tissue for use in research must be approved by the management group.

3.1.2.2 Post mortem authorisation

For all cohort participants who have consented to research autopsy in life, further written authorisation for hospital research autopsy and tissue retrieval is taken after death from the next of kin. Legally, if an individual expresses the desire to donate tissue verbally or in writing, that is all that is required for donation to go ahead. However in the experience of the brain bank, it is received much better by the relatives, friends and carers of the individual if they are involved at the point of donation. It makes for a smoother, less distressing experience for them and makes their interaction with the brain bank more positive.

3.1.2.3 Inclusion and exclusion criteria

The brain bank has conditions for admittance including that the body must be refrigerated within six hours and the autopsy and tissue retrieval must be performed within five days of death. The cohorts within the brain bank each also have their own admission and exclusion criteria and ethical approvals.

The inclusion criteria for the Sudden Death Brain Bank is anyone aged over 16 years with no known neurological disease in life and little or no other significant medical history who has died suddenly and unexpectedly and whose death is reported to the Edinburgh Procurator Fiscal's office. Exclusion criteria include a diagnosis of dementia or other neurodegenerative condition, stroke, epilepsy, homicide, suspicious death or history of alcohol dependence.

3.1.2.4 Admittance to the brain bank

Upon the death of a donor registered to a cohort, Ms Tracey Millar, a senior research nurse, receives notification that a registered donor has died. From

that point the brain bank takes over all arrangements relating to the autopsy and retrieval; liaising with the mortuary, neuropathologists and laboratory to ensure availability, contacting the GP to ensure a death certificate will be issued, having a conversation with the next of kin and obtaining authorisation for autopsy with retention of tissue, transfer of the body to Edinburgh for autopsy and tissue retrieval and returning the body.

In sudden, unexpected deaths, due to the nature of their death, a medicolegal autopsy is ordered by the procurator fiscal and so no written authorisation is required to carry out the autopsy. Cases are identified via the Procurator Fiscal office and the brain bank liaises with the mortuary and forensic pathologists, who conduct the autopsy to ensure they are able to facilitate the research. A cold call is made to the next of kin the day before the autopsy. The need for the autopsy is gently reiterated and the opportunity to authorise the use of tissue samples that would be routinely taken at autopsy for research is presented to the next of kin. If they agree to go ahead, the brain bank coordinates the forensic pathologist, mortuary and laboratory to ensure the samples are retrieved. An information booklet summarising the purpose of the brain bank and what happens to the tissue is provided to the next of kin (Appendix 2).

3.1.2.5 Autopsy

All brain tissue submitted to the MRC Edinburgh Brian Bank from the cohorts studied in this thesis is obtained at research brain post-mortem following standardised procedures including standardised, limited sampling of areas relevant to the diagnosis of SVD and other neurological diseases. The autopsy examination process is detailed in the following chapter.

3.1.2.6 Obtaining tissue for this study

I made separate applications to the MRC Edinburgh Brain Bank for tissue for each stage of my research. These detailed the specific cases, samples and amounts required, the purpose of my project and the specific details of what

the tissue would be used for. I was also involved in brain tissue retrieval and carried out research autopsies.

3.1.3 The cohorts used in this thesis

Four cohorts were used for the experimental work in this thesis. The imaging-histological comparison work was carried out on tissue from the Lothian study of INtraCerebral Haemorrhage, Pathology, Imaging and Neurological Outcome (LINCHPIN), Lothian Birth Cohort 1936 (LBC1936) and controls from the Sudden Death Brain Bank. The biochemical work was carried using tissue from the LINCHPIN cohort, Alzheimer's disease cases from the Scottish Dementia Brain Tissue Bank (SDBTB) and controls.

These cohorts were chosen as they have multiple cases with tissue suitable for the study of SVD using my proposed methods available within the brain bank. They are well characterised through collection of detailed clinical and epidemiological data in life, often with additional investigations such as serial brain imaging or Apolipoprotein E (APOE) genotyping. The extensive additional data is available upon request for use in research, anonymously and with appropriate permissions and approval. The disease cohorts I chose to study represent pathologies relevant to the investigation of the pathophysiology of SVD.

3.1.3.1 Lothian study of INtraCerebral Haemorrhage, Pathology, Imaging and Neurological Outcome

LINCHPIN is a community-based cohort within the Lothian region of Scotland approved by the Scotland A Research Ethics Committee (ref. 10/MRE00/23) (Samarasekera, Lerpiniere et al. 2015). It was established to improve the care of patients with intracerebral haemorrhage (ICH). LINCHPIN includes patients over 16 years of age diagnosed with ICH (first or recurrent) identified by the Lothian Audit of the Treatment of Cerebral Haemorrhage (LATCH, approved by the National Health Service (NHS) Lothian Caldicott Guardian) since the 1st June 2010. LATCH uses multiple sources of information to

capture all individuals diagnosed with ICH, including collaborative networks of physicians and allied medical professionals, daily head CT review, the Scottish Stroke Care Audit and retrospective review of records from secondary care treatment, hospital discharge and sudden deaths (Samarasekera, Fonville et al. 2015).

ICH is defined by LATCH:

> "a symptomatic event (new headache, altered level of consciousness, or neurological symptoms), with or without new neurological signs, referable to a focal collection of blood within the brain parenchyma (seen on brain imaging or at autopsy), with signal characteristics on brain imaging or organization of the hematoma at autopsy consistent with the time of symptom onset, which was not attributable to prior trauma or haemorrhagic transformation of an ischaemic stroke or an alternative explanation." (Samarasekera, Fonville et al. 2015)

Cases with extra-axial ICH only or ICH due to trauma or haemorrhagic transformation of an ischaemic stroke are excluded. ICH is confirmed by CT reviewed by an experienced neuroradiologist. Written informed consent for participation in the cohort is taken from the individual, or their next of kin if the patient does not have mental capacity. Consent for autopsy and tissue retrieval is sought upon enrolment into LINCHPIN. 49% of people approached consent to research autopsy and tissue donation (Samarasekera, Lerpiniere et al. 2015).

Extensive epidemiological data, medical and drug history is collected from interviews with the patients, families and/or carers (as appropriate if the patient lacks capacity), primary care information and hospital records. Follow up data is obtained from multiple sources including questionnaires sent to the individual's general practitioner annually, death certificates and the sources used for the identification of relevant cases.

The LINCHPIN cohort represents severe haemorrhagic SVD. As this work was done prospectively and relatively small numbers of cases are submitted to the brain bank, we have included all cases with primary ICH due to SVD. This encompasses lobar haemorrhage related to CAA in superficial perforating arterioles and deep haemorrhage due to arteriolosclerotic SVD. At the time of writing, there is brain tissue from 161 LINCHPIN participants held in the brain bank.

3.1.3.2 Lothian Birth Cohort 1936

LBC1936 is a community-based cohort that is particularly well studies and characterised. It was established following the discovery of the results of the Scottish Mental Survey of 1947, a cognitive ability test completed by children across Scotland who were then aged 11, and born in 1936. By 2007, 1091 people aged 70 and 71 who took the test in 1947 and were still alive living in the Lothian region had been recruited. LBC1936 aims to study the milder end of the cognitive decline spectrum and normal cognitive aging.

Extensive data has been collected from cohort participants, including detailed clinical, social and demographic histories and physical examination. Extensive cognitive testing includes retaking the same test administered in 1947. Blood sampling has been performed to carry out haematological and biochemical profiling, inflammatory markers and deoxyribonucleic acid (DNA) extraction. Serial vascular ultrasound and brain MR imaging with multiple analyses has also been undertaken to study brain atrophy, white matter lesions, mineralisation and white matter tracts (Wardlaw, Bastin et al. 2011).

Three further waves of testing, history taking and examination have been completed to date with currently around 700 participants (MRC 2021). In combination with the cognitive information from 11 years of age, this provides a unique wealth of available information spanning the lifetime of the participants.

Ethical approval for LBC1936 was granted by the Multi-Centre Research Ethics Committee for Scotland (ref. MREC/01/0/56) and the Lothian Research Ethics Committee (re. LREC/2003/2/29) and LBC1936 works in accordance with the Helsinki Declaration. Written, informed consent is obtained from all participants. Brain tissue donation is not a condition of entry to the cohort, separate written informed consent is obtained.

LBC1936 represents an older cohort with normal aging-related brain changes, including mild cognitive impairment. It was important to include these cases as the non-disease control cases are significantly younger than the disease cases and so I wanted to be able to look at the differences between brains of the same age, with and without severe SVD. At the older ages, completely cognitively and structurally normal brains are not 'normal'. It also allows comparison with the non-diseased, younger cases, who, if they had not died, would potentially have been on a trajectory to either develop severe SVD or progress along the normal aging route. 173 participants from LBC1936 have consented to brain tissue donation. At the time of writing, 25 individuals have donated brain tissue.

3.1.3.3 Scottish Dementia Brain Tissue Bank

The SDBTB is a collaboration between the University of Edinburgh Alzheimer Scotland Dementia Research Centre (ASDRC) and the NHS Research Scotland Neuroprogressive and Dementia Research Network (NRS NDN), initially established as the Scottish Dementia Clinical Research Network in 2008. The tissue bank has ethical approval from the Scotland A Research Ethics Committee (ref. 20/SS/0075). Prospective donors who have a diagnosis of dementia contact the ASDRC and are then put in touch with local NRS NDN clinical studies officers who visit them at home. Informed consent is obtained from the individual or their legal representative where they lack capacity, this includes consent for data linkage. Basic demographic, medical and lifestyle information is obtained at enrolment into the cohort from interview with participants or next of kin as appropriate and health records, a

cognitive screening test is carried out (the Addenbrooke's Cognitive Examination-III), measures of activities of daily living and an assessment of neuropsychiatric symptoms (Russ, Parra et al. 2015). Repeated cognitive assessment to obtain longitudinal data is planned. The cohort is community-based and drawn from across Scotland, covering 75% of the population within both rural and urban settings (Law, Connelly et al. 2013).

I used tissue from the SDBTB for biochemical investigation of changes in the deep white matter. It allowed comparison to previous studies that have used brain tissue with a diagnosis of dementia, and comparison of the changes seen in severe haemorrhagic SVD with those in AD, as both pathologies often coexist. The differences and similarities between the disease processes are not clear and their inclusion enabled examination of them to further clarify the pathophysiology. 120 participants have consented to brain tissue donation and 55 of these have now donated tissue to the brain bank.

3.1.3.4 Control cases – the Edinburgh Sudden Death Brain Bank

The MRC Edinburgh Brian Bank is one of two within the UK Brain Bank Network that collects control tissue samples. This ensures well characterised control material of good quality is available for scientific studies of neurological disease. In the Edinburgh brain bank, control cases are taken from the Sudden Death Brain Bank.

As described, these are cases who have had no known neurological or other significant disease in life. They are approached and recruited post-mortem. Clinical information is obtained from the autopsy report, which, in turn, is informed by the police report (which may include information from the GP, relatives and friends) and medical records available at the time of autopsy. This means these cases have relatively little detailed information available.

As these individuals have been relatively healthy in life and are often younger then the disease cohorts and they usually have no other investigations such

as brain imaging or blood tests available. However, their inclusion is important to allow comparison with normal brains at an earlier time point, many of which would go on to develop SVD.

There are currently 373 sudden death tissue cases held within the brain bank. Recruitment has been on hold since March 2020 due to the Covid-19 coronavirus pandemic.

3.1.4 Case selection

For the prospective post-mortem imaging-histopathology comparison all cases submitted to the LINCHPIN, LBC1936 and sudden death brain banks during the study period from January 2015 – March 2018 were included. Tissue was prepared and scanned immediately following autopsy. Histological slides were prepared routinely and digitally scanned as soon as possible following histological examination and reporting.

For the biochemical assessment, cases were included from the LINCHPIN, SDBRB and sudden deaths cohorts. They were selected based on the availability of frozen tissue from the central white matter and age and sex matched as far as possible. Numbers of available cases in the brain bank were limited and the biological resources are precious, so the number of cases chosen was 78. This maximised the use of two 96-well plates to include eight standards and 40 cases, in duplicate, with 2 carry overs to allow standardisation on the second plate.

For the biochemical assessment with comparison to white matter hyperintensities (WMH) on imaging, cases were chosen from those with post-mortem imaging to include cases with WMH, cases with WMH and distant normal appearing white matter and cases without WMH.

3.1.5 In vivo *imaging*

In vivo imaging has been carried out in LINCHPIN, LBC1936 and SDBTB.

3.1.5.1 Lothian study of INtraCerebral Haemorrhage, Pathology, Imaging and Neurological Outcome

On admission to hospital, if they are well enough, all ICH cases initially undergo diagnostic head CT without contrast. Occasional cases (2% in a sample of 166 cases (Samarasekera, Fonville et al. 2015)) were diagnosed at autopsy. Those that are enrolled in LINCHPIN and are well enough may also undergo brain MRI (18% in the same sample (Samarasekera, Fonville et al. 2015)) carried out at the Brain Research Imaging Centre (BRIC), Neuroimaging Sciences, University of Edinburgh.

3.1.5.2 Lothian Birth Cohort 1936

LBC1936 have completed several waves of investigations including 1.5T brain MRI at BRIC with sequences to enable structural assessment and analysis of biomarkers including fractional anisotropy and magnetic transfer ratio which allow detailed study of white matter including microstructural assessment of myelin and white matter tract integrity. Qualitative visual rating scales have been developed using this population to assess features of normal and pathological aging, as these didn't exist previously. WMH are quantified using a combination of scales that take different aspects into account: the Fazekas scale (Fazekas, Chawluk et al. 1987), Wahlund scale (Wahlund, Barkhof et al. 2001) and Bocti scale (Bocti, Swartz et al. 2005), to enable a comprehensive assessment of WMH. Other features assessed allow a broad assessment of SVD and include infarcts, large haemorrhages, microbleeds, cortical siderosis, basal ganglia mineral deposits and brain tissue volume and loss (Wardlaw, Bastin et al. 2011).

3.1.5.3 Scottish Dementia Brain Tissue Bank

Structural imaging may be carried out as part of the initial dementia diagnostic pathway, if clinically appropriate. This usually takes the form of a CT scan and is carried out under the NHS services. The results are available for use in research under the data linkage approvals and patient consent (Russ, Parra et al. 2015).

3.2 Review of cases in the brain bank

3.2.1 Background

My systematic review (Chapter 2) highlighted the inconsistencies in the histopathological language used in SVD. As there is no agreed terminology for defining the involved vessels or relevant lesions, I, with my supervisor Professor Smith, developed our own based on the best available evidence in published literature and our own experience. First I undertook a review of the cases previously prospectively collected and already held in the brain bank for the cohorts that I intended to study, with several aims; I came from a general histopathology background and had no specific neuropathology experience, so this would provide training in the assessment of histological neurodegenerative disease and SVD. I aimed to use this retrospective case review, along with my systematic review, to inform the construction of objective, useful histological SVD definitions and a grading system for use in the future prospective work (Chapter 6). I also aimed to broadly assess the burden of disease and key demographic characteristics in these cohorts to be sure they would represent the appropriate disease groups and provide a range of pathology for this study.

3.2.2 Methods used for the brain bank case review

An initial review of 20 random cases was undertaken with Professor Smith for training purposes. Following this, all available cases from the LBC1936, Linchpin and sudden death cohorts that were admitted to the MRC

Edinburgh Brain Bank since the cohort inceptions until June 2016 were reviewed separately by each of us (blinded to cohort and clinical information) and graded using published, validated systems to score white matter SVD pathology (Deramecourt, Slade et al. 2012), CAA (Love, Chalmers et al. 2014), parenchymal amyloid ß plaques (Thal, Rub et al. 2002), neurofibrillary tangles (Braak and Braak 1991) and α-synuclein pathology (McKeith, Ballard et al. 2000). An impression of the vascular non-amyloid SVD severity was also assigned as none, mild, moderate or severe. The cases were then reviewed together and any differences resolved.

The gradings for vascular non-amyloid SVD, parenchymal SVD and CAA grading were graded none, mild, moderate, severe. These grades were numericalised 0, 1, 2, 3, respectively, to give an indication of where on the scale of none to severe pathology each cohort lies.

3.2.2.1 Statistical analysis

To investigate the differences in age, Kruskal-Wallis test with Dunn's post-hoc analysis was used to compare groups and there was a statistically significant difference. Ordinal logistic regression was used to study the relationship between vascular and parenchymal scores in the different groups, using age as a covariate. The Akaike information criterion (AIC) was used to check how well the model fit the data. Analyses were carried out in R (version 3.5.0).

Inter-rater reliability (IRR) was assessed using linear weighted Cohen's kappa coefficient. Analysis was carried out using GraphPad Prism version 7.0c for Mac OS X, GraphPad Software, San Diego, California, USA.

3.3 Constructing histopathological small vessel disease terminology and standards

3.3.1 Background

As described, the histopathological literature is hampered by the lack of consensus and confusing use of terminology. It is essential to simplify and define the histopathological features of SVD, and provide a grading system, if progress is to be made correlating SVD histology with the relatively well defined imaging and clinical features.

3.3.2 Methods for constructing histopathological small vessel disease terminology and standards

I initially set out a number of conditions I aimed to adhere to; to be as objective and comprehensive as possible. To make the terminology simple and specific without presuming the underlying pathogenesis of the lesions. I considered the well-established neuroimaging terminology (Wardlaw, Smith et al. 2013) so the histological language would allow useful comparisons to be made. In the future, using terms and descriptors, such as location, which are more comparable to those established in radiological SVD assessment might help strengthen clinical-radiological-pathological correlations.

The vascular cognitive impairment neuropathology guidelines (VCING) (Skrobot, Attems et al. 2016) were recently developed to try to harmonise the reporting of vascular neuropathology in the context of cognitive impairment. To achieve a consensus, a Delphi survey involving 14 UK-based neuropathologists was carried out. Part of this process recognised and attempted to address the lack of histopathological definitions of vascular lesions. Although these guidelines relate to the assessment of vascular lesions in the setting of cognitive impairment, the lesions seen are the same (or at least appear histologically the same, given what little is known about their development). Some of the definitions used in VCING were applied in my study, some were adapted. Other often-used grading systems were also consulted (Deramecourt, Slade et al. 2012, Smallwood, Oulhaj et al. 2012), I

was informed by my systematic review (Chapter 2) and created additional definitions where required (Table 4.3).

3.4 Prospective *ex vivo* imaging

3.4.1 Background

There was no pre-existing standardised protocol for sampling and processing tissue for post-mortem MRI. The post-mortem imaging protocol was developed on the back of pilot work imaging 10 post-mortem brain hemispheres at BRIC (unpublished). MR scanning fixed tissue did not result in useable MR images and frozen tissue is also unsuitable. Movement of water molecules is required to create an MR image, but in frozen tissue the water molecules are fixed in position, because of this, MR scanning results in a 'signal void' devoid of structural detail (Daniel, Butts et al. 1999).

Imaging fresh, unfixed tissue was considered; however post-mortem change begins soon after death, creating artefact and tissue degeneration, potentially compromising the MR images and the subsequent histological examination. To avoid this, tissue must be kept refrigerated after death and processed within 6 days when it is either fixed in preservative or frozen for long term preservation and storage. MR scans also take several hours to complete and so any scanning would need to be carried out in a cool temperature-controlled environment. The post-mortem examination also needs to be carried out as soon as possible so the body can be returned to the next of kin in a timely manner. Due to the demand on MR scanners, inability to control the external environment to that extent and the length of time taken to complete scanning protocols, this would not be practical.

Scanning formalin fixed tissue was undertaken successfully. Initially single hemispheres were scanned, as whole brains do not fit through the 7-Tesla (7T) small-bore MR scanner within the research centre. The resulting images were of good quality. However, a relatively large coil with low sensitivity had to be used, resulting in lower resolution images or longer scan times.

Scanning whole hemispheres also raised potential difficulties in being able to ensure the tissue examined histologically precisely matched that being studied on the post-mortem imaging. Previous attempts are detailed in my systematic review (Chapter 2). The matching and comparison of lesions where whole hemispheres were scanned was not felt to be reliable or precise enough. At autopsy the brain is cut by hand. Even with the use of location markers, slight differences in the location or orientation of the cut relative to the MR slice would result in the small lesions being missed or misidentified. Once cut, the areas corresponding to those seen on the scans would be matched macroscopically by eye, creating an additional opportunity for error in identifying the exact brain area or lesions seen on the scan. Histological sampling of the whole hemisphere was carried out in one study, but without precise examination of individual lesions. Histological examination of the whole hemisphere was not felt to be practical or an appropriate use of time and resources for this work. The hemispheres also needed to be formalin-fixed for three weeks prior to scanning, an unacceptable delay with regards to reuniting the brain with the body and delaying funeral arrangements and resulting in authorisation not being given by next of kin if this protocol was to be applied to many cases over several years.

Imaging the small formalin-fixed tissue samples taken from the brain before they are processed for histology has several important advantages; it will not delay reuniting the brain with the body, the brain is immediately returned and only the small tissue samples, for which authorisation has been given, are retained. Small pieces of tissue are permeated by formalin and fix much faster than relatively large intact cerebral hemispheres, therefore it does not delay the processing of the tissue so the clinical report and diagnosis can be issued in a timely manner. The tissue that undergoes imaging is processed in its entirety and examined histologically, so we can be sure any lesions or features identified on the MR scan are contained within that same piece of tissue.

3.4.2 Developing the protocol and troubleshooting

We initially tested and refined the scanning protocol using small tissue samples in five cases. I worked with the laboratory staff responsible for the tissue preparation and processing and the preclinical imaging staff to establish a scanning and processing protocol that worked for everyone involved, didn't damage or delay the tissue and provided the optimal amount of information with minimal artefact.

At autopsy, the tissue sampled is placed in plastic cassettes for fixation and histological processing. These cassettes are suitable for scanning and could be placed inside a cylindrical plastic container. The tube could fit 13 plastic cassettes and so 13 areas were initially chosen for examination. This tube was filled with formalin as there was minimal adverse effects when scanning formalin-submerged tissue in previous studies (Humphreys, Smith et al. 2021) and it avoids the tissue drying out and compromising the histological examination. Cassette movement within the tube was immediately obvious and so they were held in place by wedging a piece of foam down one side of the length of the container (Figure 3.1).

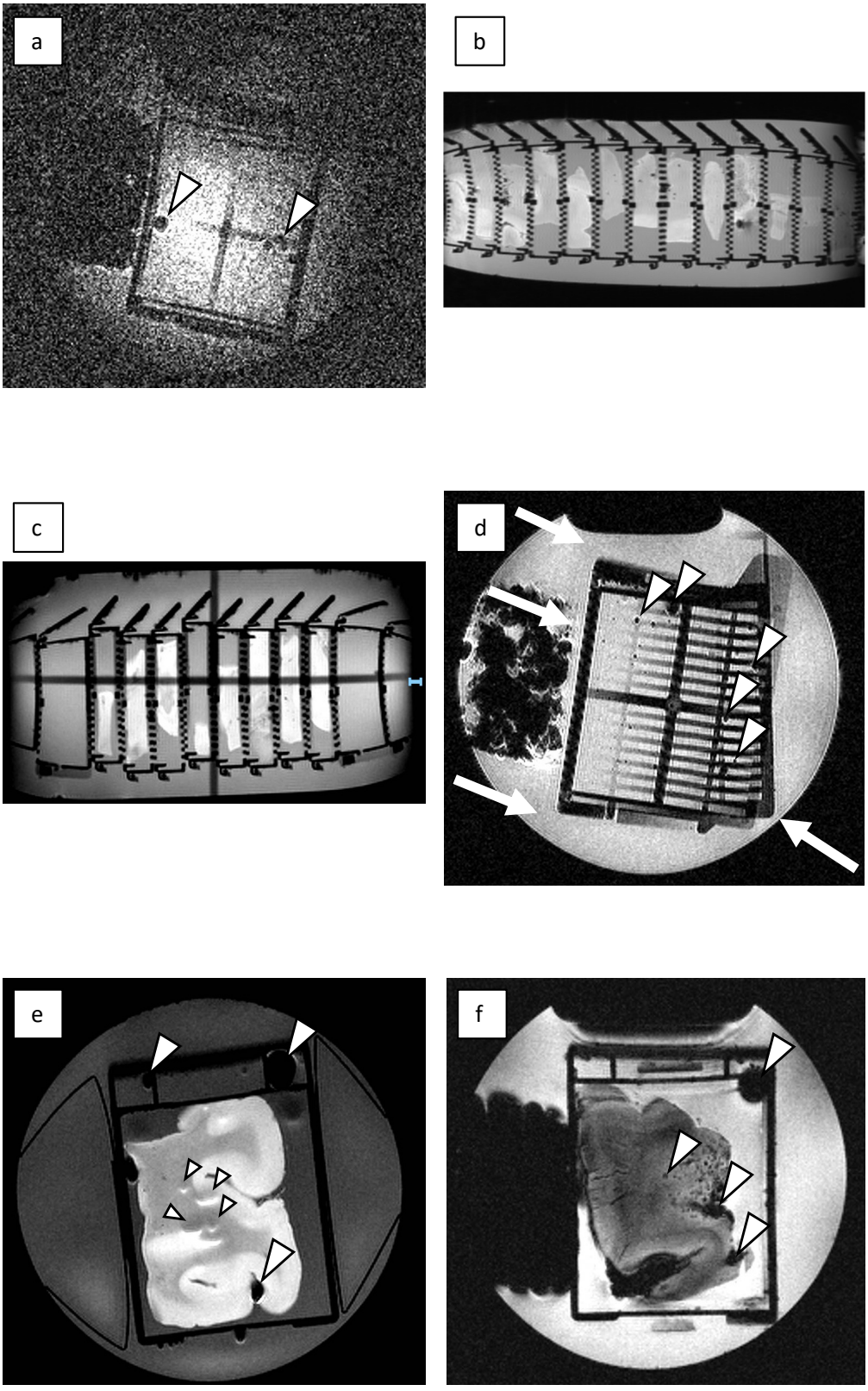
Upon scanning it was apparent that the tissue at the ends of the tube was beyond the linear part of the gradient coil, resulting in a warped image with significant artefact. The images at the ends of the tube were unusable and it would be impossible to take any reliable measurements from it (Figure 3.1a, b). This was addressed by placing empty cassettes at either end of the tube, to hold the cassettes containing tissue in position and ensuring those containing samples are not affected by the artefact (Figure 3.1c). This meant that the tube could only hold eight samples, not enough for the areas we wanted to study. We considered a variety of alternative methods, including separating the tissue using very thin sheets of plastic. This, however would require very careful preparation to not squash the tissue and remove air bubbles and would make it difficult to hold the tissue still in the scanner. Samples of soft, fresh tissue at autopsy are not perfectly cuboidal or uniform.

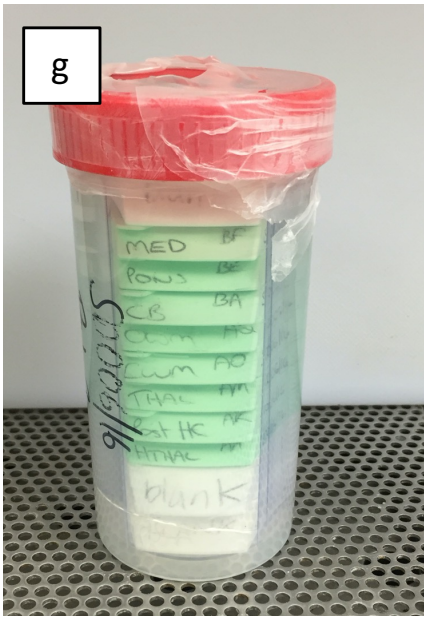
They are then fixed and become firmer but remain non-uniform. MR slices are taken perpendicular to the plastic tube the tissue is in. Separating the tissue with thin plastic sheets would result in samples at random angles relative to each other within the tube, overlap of different samples within the same MR image and slices would not be parallel to the surface of the pieces of tissue. We decided to keep the tissue in the cassettes and use two tubes for each case. we were able to expand the number of areas of interest to 16 tissue samples, and they were held still and in a uniform orientation relative to the scanning plane.

It was apparent that the piece of sponge did not secure the cassettes within the tube to the point that horizontal movement potential was completely eliminated, as gaps around the cassettes remained (Figure3.1d). Placing a piece of folded plastic down each side of the stacked cassettes provided extra stability, the spring loading effect of the folding and ensuring the cassettes are aligned in a stack, removed the possibility of horizontal movement within the tube (Figure 3.1c, e).

Figure 3.4 Troubleshooting the MR post-mortem tissue scanning protocol

a) A section perpendicular to the long axis of the tube shows the cassette held in place by sponge on the left, and air bubble artefact (arrowheads) (T2). b) A section through the length of the tube perpendicular to the tissue shows the stacked cassettes containing tissue samples. The cassettes are identical but are warped by the MRI field at either end of the tube (gradient echo scout). c) Empty cassettes, larger than those containing the tissue, were placed at the ends of the tube, to avoid warping the tissue and prevent vertical movement (gradient echo scout). d) The piece of sponge holding the cassettes in place is visible on the left-hand side of the image. Two cassettes are visible. Gaps around the cassettes (arrows) could result in horizontal movement artefact and the sponge was likely to trap air bubbles that could affect the tissue or move into the tissue (T2). e) Two pieces of plastic, folded and placed down the length of the tube either side of the cassettes hold them in place preventing horizontal movement, although air bubbles were still present (FLAIR). f) Where the sponge was pressed up against the cassette, artefact affecting the adjacent tissue was observed, masking potential pathology (T2*). g) Tube prepared for scanning. Small histology cassettes containing tissue (green) are stacked in the middle of the tube, with empty cassettes at either end (white). Clear plastic supports are folded along the length of the tube, either side of the cassettes. The tube is filled with formalin, air bubbles are evacuated, and the tube is secondarily sealed with Parafilm on the outside. Air bubbles are visible in a,d,e,f) they are too numerous to identify each one, but some are indicated (arrowheads). f) Some are within the tissue and more likely to be mistaken for lesions, e) some are within the cassette and could mask pathology in the tissue (small arrowheads).


a
b
c
d
e
f



Air bubbles were readily apparent within the cassettes and the tissue (Figure 3.1). They were often seen in the small gaps in the cassettes and at the edges of the tissue where they could potentially mask lesions. Bubbles could also be mistaken for pathology, particularly on the T2* sequence where they can mimic microbleeds (Figure 3.1f). To minimise them, the tube was filled with formalin by submerging it in a large amount of formalin and securing the lid under the surface. The tube was left to stand and settle for a few minutes then banged firmly on a hard surface to dislodge any air bubbles. The tube was then re-submerged, the lid removed to release trapped air, and re-secured. This significantly reduced the number of air bubbles so they were only very occasionally seen and could be identified by their MR imaging characteristics.

Other considerations included standardising the procedures so each case was treated as similarly as possible in the context of the process involving several different, busy departments and people. This involved specifying steps such as making sure the tubes were placed in the scanner the same way each time, so the order of the MR images is the same when viewed and

ensuring the steps could be carried out within specified timelines to avoid over-fixing or delaying the tissue.

The tubes are designed to be kept upright, but need to be put through the scanner on their side for several hours, which resulted in formalin leakage. This was resolved by wrapping the tube in Parafilm, a clingfilm-like wrap which stretches over the tube, forming a moisture-barrier and providing a secondary seal (Figure 3.1g).

As described in the following chapter, tissue overheating is a concern as the mechanisms present to dissipate heat in life, such as vasodilation, are not present in *ex vivo* tissue and brain tissue absorbs more radiofrequency than other tissues (Murbach M 2015). Overheating tissue could cause artefact on the MR image, irreversible tissue damage making histological assessment difficult or impossible and compromising the potential for future biochemical or genetic assessment. The MR scanner bore is cooled to 22.6ºC and the protocols were designed to avoid overheating, however they still take several hours to complete. We attached a temperature probe to the tube during scanning to be sure there was no concerning temperature change that could cause thermal damage to the brain tissue. Studies of in vivo temperature exposure in mammals have found histologically visible changes in brain tissue including haemorrhage, necrosis, perivascular oedema, vacuolation, microvascular collapse, neuronal apoptosis, cellular contraction and pyknotic nuclei at temperatures between 38ºC for 4 hours and 43ºC for 30 minutes (Dewhirst, Viglianti et al. 2003, Ahmed 2005). *Ex vivo* studies on human cell lines suggest they can withstand similar, but probably slightly higher temperatures than other animal cell lines before they are killed (Dewhirst, Viglianti et al. 2003). Our monitoring showed a 1.8ºC increase to a maximum temperature of 24.5ºC during scanning (Figure 3.2), well within acceptable limits to avoid tissue damage. It would be much more complicated to measure the temperature in the tissue itself during scanning, there would be potentially significant issues such as causing damage to the tissue and formalin leakage into the MRI scanner.

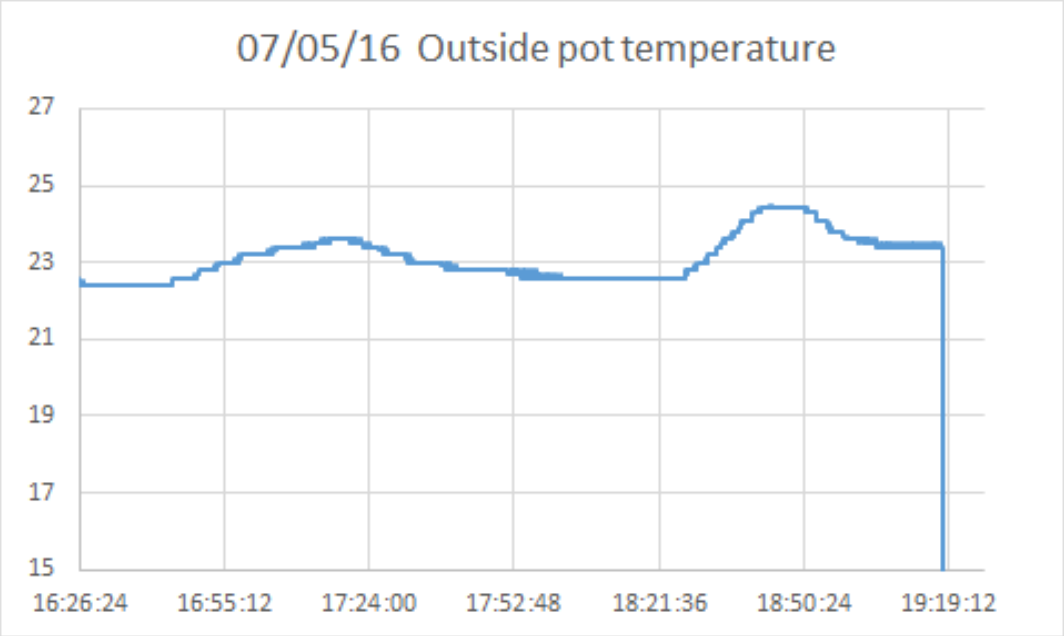


Figure 3.5 Monitoring temperature during MR scanning

This graph was obtained by placing a probe on the pot during scanning and shows the temperature increase was 1.8ºC, from 22.7 to 24.5ºC, much less than that needed to cause damage to the tissue being scanned.

Due to the minimal temperature change observed and the fact that no thermal artefacts or damage have been observed on tissue examination, it was not deemed necessary to establish the precise core tissue temperature during scanning.

We experimented with different MR resolutions to see if we could use a thinner MR slice, closer to the histological tissue thickness. We found 1mm slice thickness and 1mm gap between slices was optimal to balance the best resolution, while minimising signal to noise ratio and time taken to scan. We performed each sequence twice, offset by 1mm to ensure all tissue was scanned. A subsequent scanner upgrade has produced high resolution MR images for analysis with improved detail and lesion visibility (detailed in the following chapter).

3.4.3 Methods for prospective ex vivo imaging

All cases admitted to the brain bank in the LBC1936, Linchpin and sudden death cohorts were prospectively examined. They underwent standardised neuropathological macroscopic examination and sampling, post mortem MR scanning, histological processing and microscopic examination, described in Chapter 5.

Extensive clinical history collected prospectively was available for the well characterised LBC1936 and Linchpin cohorts. Data for the sudden death cohort was obtained from the autopsy report. If the autopsy records stated the medical records were complete, medical conditions not listed were considered not present, otherwise the data was considered incomplete and the presence unknown. Smoking history was included if explicitly stated. A case was included if there was a clinical history of dementia but no neuropathological evidence of dementia pathology.

3.4.3.1 Statistical analysis

To investigate the differences in age, Kruskal-Wallis test with Dunn's post-hoc analysis was used to compare groups.

For burden of SVD, ANOVA with Bonferroni post-hoc test was used to compare cohorts. $P < 0.05$ was considered significant. Correlations were assessed using Pearson's and Spearman's tests. The analyses were performed using GraphPad Prism version7 (GraphPad Software).

3.5 Grading the burden of SVD on *ex vivo* MRI

3.5.1 Background

Accepted, validated grading systems are available for *in vivo* imaging (Wardlaw, Smith et al. 2013), but not *ex vivo* imaging or histology. The *ex vivo* MR SVD grading system developed here was based on the *in vivo* validated visual rating system established in the LBC1936 cohort (Wardlaw,

Bastin et al. 2011) and since applied in many published studies of the cohort involving MRI assessment (Staals, Booth et al. 2015, Ballerini, Booth et al. 2020, Hamilton, Cox et al. 2021).

3.5.2 Developing the ex vivo MRI assessment

I underwent training using the *in vivo* grading systems under the supervision of Professor Wardlaw using LBC1936 *in vivo* whole brain studies using a quantitative analysis based on or similar to a number of previously published and validated systems. It included assessing the presence and location of stroke lesions; infarcts including lacunes, haemorrhages (Wardlaw and Sellar 1994, Potter, Doubal et al. 2010) and microbleeds (Cordonnier, Potter et al. 2009). The amount of enlarged PVS was graded 0-4 in the hippocampus, basal ganglia and centrum semiovale (Maclullich, Wardlaw et al. 2004) and amount of basal ganglia iron deposition graded 1-4 (Casanova and Araque 2003, Penke, Valdes Hernandez et al. 2012). WMH were graded by the Fazekas (Fazekas, Chawluk et al. 1987), Wahlund (Wahlund, Barkhof et al. 2001) and Bocti (Bocti, Swartz et al. 2005) visual rating scales. Deep and superficial atrophy were graded separately by comparison to a validated normative age template on a scale scoring 1-6 (Farrell, Chappell et al. 2009).

The lesions to be assessed in the post-mortem imaging were chosen; infarcts, enlarged PVS, microbleeds, WMH and basal ganglia iron deposition. Cortical thickness in the three cortical samples was measured at the superficial, mid and deep points of a well orientated sulcus. I developed an *ex vivo* MRI proforma for assessing SVD burden in each small tissue specimen that could be applied to the 2x2cm tissue samples imaged *ex vivo*, taking into consideration the small size of each piece of tissue and the limited number of brain areas sampled (Appendix 3). Lesions were defined using the STRIVE guidelines (Wardlaw, Smith et al. 2013) (Figure 1.5). In each case, the MR slice number corresponding to the histological section varies so it was recorded for each sample to enable accurate image registration. It is not

possible to assess atrophy on the limited samples, tissue affected by large haemorrhages was not sampled.

The presence of WMH was recorded in individual tissue samples, rather than by area (Wahlund, Barkhof et al. 2001) or specific pathway (Bocti, Swartz et al. 2005) (example in Figure 3.3a). For each case, a score was assigned based on the number of tissue samples with WMH none=0, 0-5 samples = 1, 6-10 samples = 2, 11-16 samples = 3. The number of enlarged PVS in any area where they were visible were graded 0-4 using the same system as the *in vivo* assessment (Maclullich, Wardlaw et al. 2004) (example in Figure 3.3b). Infarcts were counted and further assessed using the LBC1936 MRI proforma, adapted to include relevant histological information (Appendix 4). Microbleeds were counted and measured. An overall SVD score was assigned as no SVD = 0, mild SVD (PVS 1-2, WMH 1-2) = 1, moderate SVD (PVS 2-4, WMH 2-3), severe SVD (microbleed, infarct, lacune, or PVS 3-4 and WMH 2-3) = 3.

Iron content within the basal ganglia was defined and graded as per the LBC1936 assessment. I constructed a visual rating scale to grade the areas of hypointensity on T2* weighted images: 1 (none), 2 (minimal), 3 (some) or 4 (much) (Figure 3.4). Cortical thickness was recorded in samples containing cerebral cortex where the orientation was sufficient to identify and measure at a superficial gyrus, mid-point and deep aspect of a sulcus on T2 weighted images. The artefact produced by air bubbles was noted as it is a known issue.

I assessed post-mortem MR images according to our devised grading system blinded to all clinical and brain bank details. Any uncertainties were reviewed with Professor Wardlaw and resolved.

3.5.2.1 Statistical analysis

No formal statistical analysis was carried out on the *ex vivo* assessment.

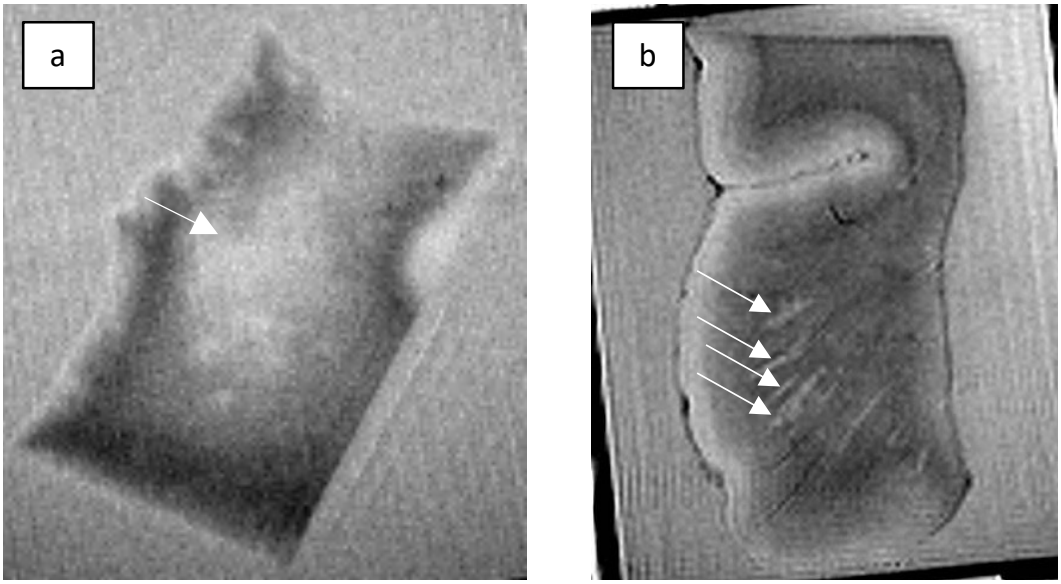


Figure 3.3 Examples of SVD features on *ex vivo* MR images of small tissue samples

a) White matter hyperintensity, T2. b) Multiple perivascular spaces visible on T2, some indicated by arrows.

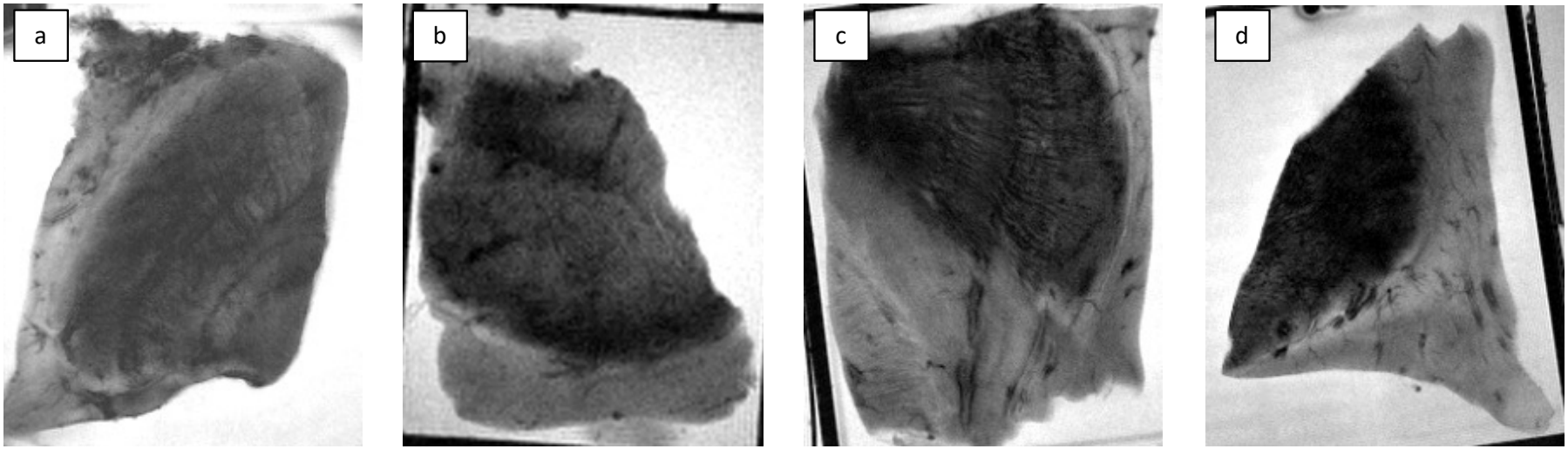


Figure 3.4 Image gallery for grading mineralisation in the basal ganglia on *ex vivo* MR images of small tissue samples

Graded by the increasing depth of hypointensity on the T2* sequence as a) 1 = none, b) 2 = minimal, c) 3 = some, d) 4 = much.

3.6 Histological SVD assessment

3.6.1 Post mortem tissue processing

Procedures for processing and assessing of post mortem human brain tissue using histological and molecular methods are well established at the University of Edinburgh brain bank. The methods we used are detailed in Chapter 5. They needed to be adapted slightly to accommodate the post mortem MR scanning; additional work was created in the preparation of tissue for scanning and a two-day delay in processing while the two overnight scans were carried out. Otherwise the protocols are those used in standard practice.

3.6.1.1 Tissue quality

Human post-mortem brain has relatively stable RNA compared to other body tissues (White, Yang et al. 2018) but can be a challenging tissue in which to study gene expression (Kvastad, Carlberg et al. 2021). The brain tissue quality can be affected by a number of factors that cannot be controlled. The agonal period immediately around the time of death is characterised by hypoxia and acidosis with altered levels of normally tightly regulated metabolites (Donaldson and Lamont 2013). Prolonged agonal state can have a detrimental effect on the quality of tissue subsequently obtained (Preece and Cairns 2003). The duration of the agonal period varies in tissue obtained from humans including in our populations, compared to animal studies where it can be controlled (Monoranu, Apfelbacher et al. 2009). For example, a rapid demise following a cardiac event compared to a prolonged agonal state in an individual with complications of Alzheimer's disease. Therefore an objective assessment of tissue quality was required. Tissue quality is assessed in all cases submitted to the brain bank using the pH of fresh tissue and RIN of frozen tissue.

3.6.1.1.1 pH

pH measurement is a relatively quick and easy way to measure tissue quality. A ‘good ‘pH is considered to be <6.4 (Stan, Ghose et al. 2006). It is potentially worse in the centre of tissue, where measures to preserve tissue such as refrigeration take longer to take effect, although one study found consistency throughout the brain when different regions are tested (Stan, Ghose et al. 2006). We measured the tissue pH at autopsy. The electrode was calibrated in pH 7.01 and pH 4.04 buffers. After removing the brain stem and cerebellar hemispheres, the brain was cut at the level of the mamillary bodies, opening the lateral ventricles. The electrode was inserted into the wall of the lateral ventricle for 30 seconds to provide a stable reading.

pH provides a good indication of tissue quality around the time of death, but has been found to be unaffected by tissue thawing, that can degrade RNA (Stan, Ghose et al. 2006). To provide a complete assessment of the quality of the tissue we also measured the RNA quality.

3.6.1.1.2 RNA integrity number

Good RNA integrity is required for gene expression profiling experiments, a logical continuation of this work beyond histological assessment and protein expression. After death, RNA can degenerate quickly into shorter fragments, catalysed by the presence of RNSase enzymes. The fragmented RNA can hamper efforts to assess the transcriptome, which rely on measuring intact RNA molecules.

The RIN value is a measure of intact RNA transcripts relative to shorter fragments. It reflects the quality of the tissue and its suitability for use in studying gene expression. The PMI is measured from death to autopsy when tissue is retrieved and preserved. It has previously been considered the benchmark for measuring tissue quality. However, the RIN is a more accurate indicator of the suitability of the tissue for further biological studies. Both the pH and RIN are independent of the PMI (Stan, Ghose et al. 2006,

White, Yang et al. 2018). RIN values range from 10 (intact) to 1 (completely degraded) (Schroeder, Mueller et al. 2006). There is no absolute cut off beyond which RIN values exclude the use of brain tissue for molecular study. RIN ≥ 7.5 is considered good while RIN ≤ 5 is considered medium/low and probably not suitable for such experiments (Kvastad, Carlberg et al. 2021), although a RIN value of ≤ 6 is often used as a cut off in practice (White, Yang et al. 2018).

Some factors that affect tissue quality that can be controlled. Particularly repeated freeze/thaw cycles (Monoranu, Apfelbacher et al. 2009). Tissue thawing alone also affects RNA quality as measured by the RIN value but not the pH, emphasising the importance of taking different measurements to fully assess the tissue (Stan, Ghose et al. 2006). We were careful to minimise the effect of freeze/thaw cycles and avoid tissue thawing. Small samples appropriate for a single enzyme-linked immunosorbent assay (ELISA) experiment were aliquoted out and immediately re-frozen at the time of tissue homogenisation for the biochemical studies. This ensured samples are all stored and treated uniformly with respect to the thaw/freeze cycles they undergo and they are not repeatedly thawed and re-frozen. Other factors including tissue source (hospital, community or medicolegal), PMI, age, gender, freezing method, storage duration have not been found to have an effect on tissue quality (Monoranu, Apfelbacher et al. 2009, White, Yang et al. 2018) while in another study PMI did have a significant effect on tissue pH in an AD cohort but not controls (Preece and Cairns 2003). RIN values are calculated for all cases submitted to the brain bank from frozen tissue stored at -80ºC.

3.6.1.2 Histological processing

The histological procedures including processing and staining used to assess the histological appearances of the tissue that underwent *ex vivo* MR scanning are described in full in Chapter 5. The histological slides were digitalised and a range of stains were carried out to assess the

characteristics of the SVD features. In addition to the stains listed in Chapter 5, stains to highlight the vascular endothelium (CD34), activated microglia (CR3-43) and fibrinogen were carried out. The H&E staining protocol and additional immunohistochemical staining information are detailed in Appendices 5 and 6.

3.6.2 Grading SVD on histology

I assessed the histological SVD burden in cases that underwent prospective *ex vivo* MR imaging using the grading system detailed in Chapter 4 (Appendix 7). Cases were graded in batches at a date separate from the *ex vivo* MR assessment and blinded to all clinical and cohort data. 10% were also graded by Professor Smith and any differences were reviewed together and resolved. Clinical neuropathological assessment for routine diagnostic neuropathology and neurodegenerative disease were carried out on all samples from the whole brain by Professor Smith.

I compared the severity of arteriolosclerosis and presence of hypertension to investigate the relationship between them. The clinical history was often incomplete, particularly in the sudden death cohort. Cases with what appeared to be a comprehensive medical history without mention of hypertension or anti-hypertensives listed in the drug history were counted as being normotensive. Cases with no medical history, or a very brief history focused around the cause of death only, were excluded from the analysis.

3.6.2.1 Statistical analysis

In an exploratory assessment, the relationship between hypertension and arteriolosclerosis was examined using scatterplots with linear regression. $P<0.05$ was considered significant. The measurements of cortical thickness on *ex vivo* MRI and histology were compared using the Bland-Altman method. Presuming the histological measurements to be accurate, an exploratory analysis seeking patterns in the cortical thickness related to location or depth within the sulcus was carried out using a series of paired t

tests. The statistical analysis was limited by the small number of cases, age could not be controlled for and so they can only be exploratory. QQ plots and histograms of residuals were used to check for normality.

3.7 Developing the image registration methods

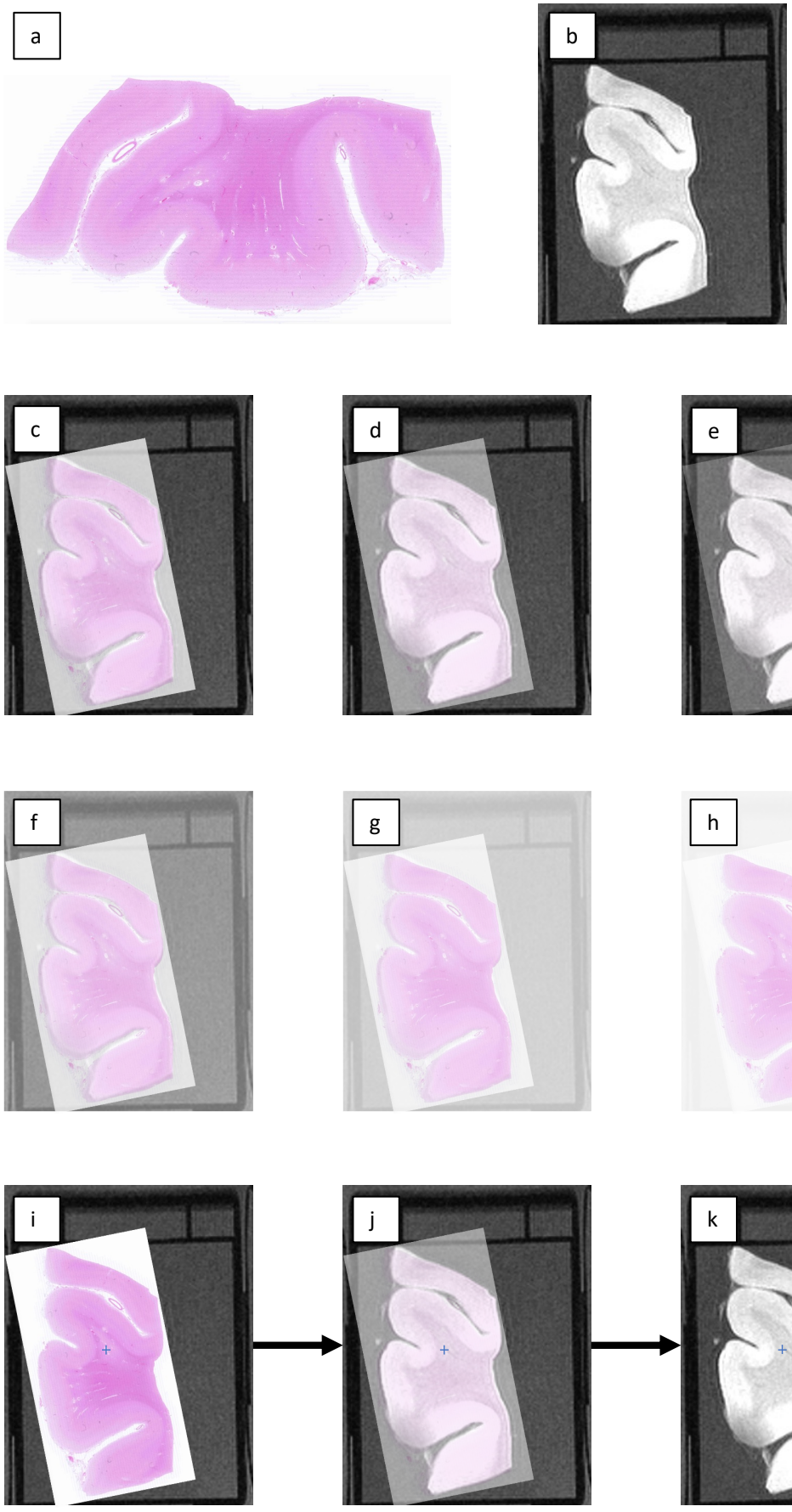
3.7.1 PowerPoint

Overlaying the images initially appeared a relatively simple prospect. Several methods were explored to begin with, including simply overlaying the images and altering the transparency to see the underlying image in PowerPoint (Figure 3.5). When overlaying the images, the histology was orientated to match the MR. then the transparency of the images could be adjusted to examine any lesions (Figure 3.5c-h). A marker could be placed on a lesion on one image, that image then made transparent and that location on the other image examined (Figure 3.5i-k).

During processing, however, the tissue undergoes unpredictable, non-uniform morphological changes which vary in magnitude and direction. These are demonstrated in Figure 3.6. They are only small, the order of mm, but the SVD lesions of interest are mostly in the mm scale, often around 1mm maximum diameter. The tissue changes and shrinkage also affect the whole of the tissue as it is fixed and processed, not just the edges. This method of matching the images does not take any internal features into account and so could not try to compensate for this. Therefore, confidence in the precise identification of the correct lesion and their examination would be compromised by these differences between the images.

Figure 3.5 Overlaying images in PowerPoint

The histological H&E image (a) was orientated to match the corresponding MR FLAIR (b). They could then be overlaid and the transparency adjusted. Histology with c) 25% transparency d) 50% transparency e) 75% transparency overlaid on MR. MR with f) 25% transparency g) 50% transparency h) 75% transparency overlaid on histology. A marker could be placed on a lesion of interest on one image i) then the image made progressively more transparent j, k) to reveal the location on the other image.


a
b
c
d
e
f
g
h
i
j
k

PowerPoint is not intended for this purpose. The image manipulation tools are only very basic and the matching is done by eye. There is no reliable way to ‘fix’ the steps that have been taken to process an image or to save the steps taken to reproduce them. One slight slip and the positioning or resizing that has been done, for example, can be lost.

The histology.czi files are also very large, generally around 2-4 GB each. Powerpoint is unable to cope with these file sizes and often crashes, even when they were saved as other file types, losing work and making the process extremely slow.

The resolution of the MR is 0.23mm and the histology is around 10μm, so it would be also be advantageous to maximise the image registration method to be able to fully exploit the image resolution.

For these reasons, it was obvious that this would not be an appropriate method and something requiring more technical image processing methods would be required.

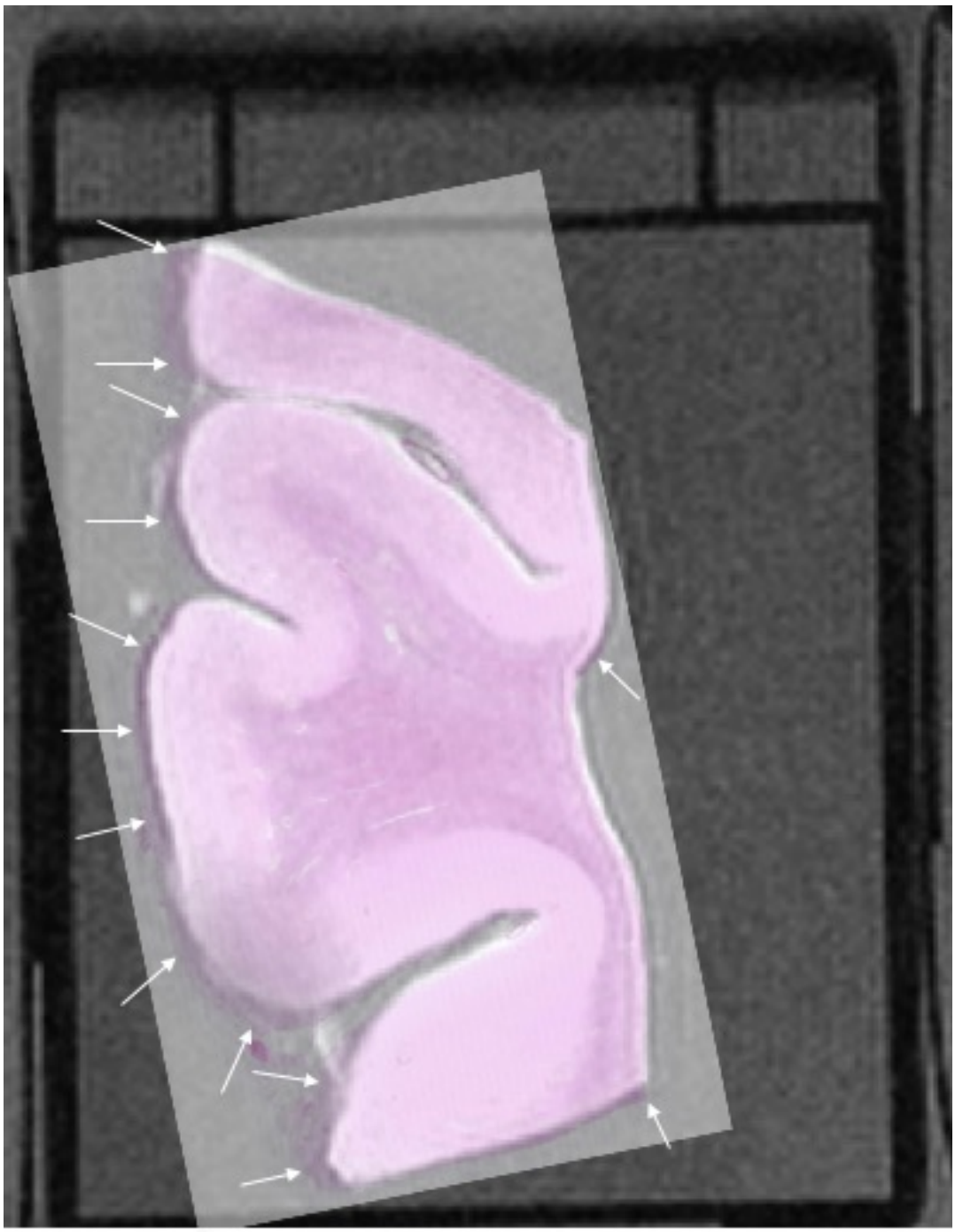


Figure 3.6 Mismatched image outlines

Upon closer inspection the outlines of the two images are mismatched almost entirely around the borders of the tissue. Where the MR outline extends beyond the histology a white line is apparent. The edge of the partially transparent histology is highlighted by arrows where it extends beyond the edge of the MR image. At its maximum in this example the difference is about 2mm. It is also impossible to know how well the internal features map onto each other as this method makes no attempt to match them, but the tissue morphological changes during processing affect the whole tissue in a non-uniform and unpredictable manner. SVD lesions are often only 1mm maximum dimension and so identification would be unreliable using this method. MR FLAIR 0% transparent overlaid by histology H&E 50% transparent.

3.7.2 Matlab

In collaboration with Victor Gonzales-Castro, a neuroimaging sciences researcher at the University of Edinburgh, we developed an image registration method using Matlab 2015a.

The four MR sequence images (FLAIR, T2, T2* and T1, .dcm format) and corresponding histology H&E image (.czi format) were uploaded to the Matlab workspace (Figure 3.7a). Once loaded, an initial affine registration step was carried out to orientate the histology relative to the MR images. Up to five points were placed at corresponding locations in both the MR and histology images. They were points that could be reliably identified by eye, usually macroscopic anatomical landmarks such as extreme points of a particular sulcus or nuclei or distinctive features at the edge of the tissue, either naturally occurring anatomical features or an artefact of cutting at the time of sampling. The images could be enlarged to maximise the accuracy of point placement and the MR sequence could be changed to use the most appropriate one (Figure 3.7b). Landmarks were only selected if they could be identified on both modalities with certainty, the different MR sequences could be used to find the most accurate placing for the points. The resulting histology affine image was oriented correctly ready for the second step (Figure 3.7c).

The second registration step registered the histology affine image to the MR images using multimodal B-spline registration. A sparse set of control points were manually placed uniformly across the orientated images, again using only anatomical or artefactual locations that could be reliably identified by eye (Figure 3.7d) using the different MR sequences to enable the most accurate placement (Figure 3.7e-g). The MR images were the reference image and the histology was the moving image. B-spline registration used B-spline curves to map voxels from the histology to the MR image, defining a continuous 2-dimensional deformation field resulting in a visibly deformed histology image (Figure 3.7h).

The resulting MR and registered histology B-Spline images could then be viewed side by side. An area or lesion of interest selected on one image would then be identified on the other image by the programme for examination of lesions of interest (Figure 3.7i).

This method also had several issues that were inhibitory to continuing to use it. The images would take a long time to load, again predominantly due to the size of the histology image files. The processing of each step was very slow as a result but needed to be done manually and so was extremely time consuming.

If more points could be selected to identify the equivalent locations on the two images in the second registration step, theoretically the accuracy of the registration should be improved. However, in practice, selecting more than four points often led to failure of registration and frequently crashed the system. Four points was not sufficient to account for the complex three-dimensional morphological changes the tissue undergoes during processing.

In the final registered images, points would appear incorrectly on the registered image when chosen on the reference image (Figure 3.7j). Even accounting for the registration deformation, they would be obviously incorrect and were not labelled with the identifier to match up the points locations.

We also assessed the B-spline registration compared to the affine orientated image. The final registered image had obviously undergone stretching and deformation to manipulate it towards matching the MR, but it was often not obviously any more accurate than simply overlaying an unregistered image (Figure 3.7k, l). For these reasons we decided to try an alternative approach to registering the histology and MR images, especially considering the large size of the histology images and the ability to be able to automate the registration to make the process more efficient. The final method is detailed in Chapter 5.

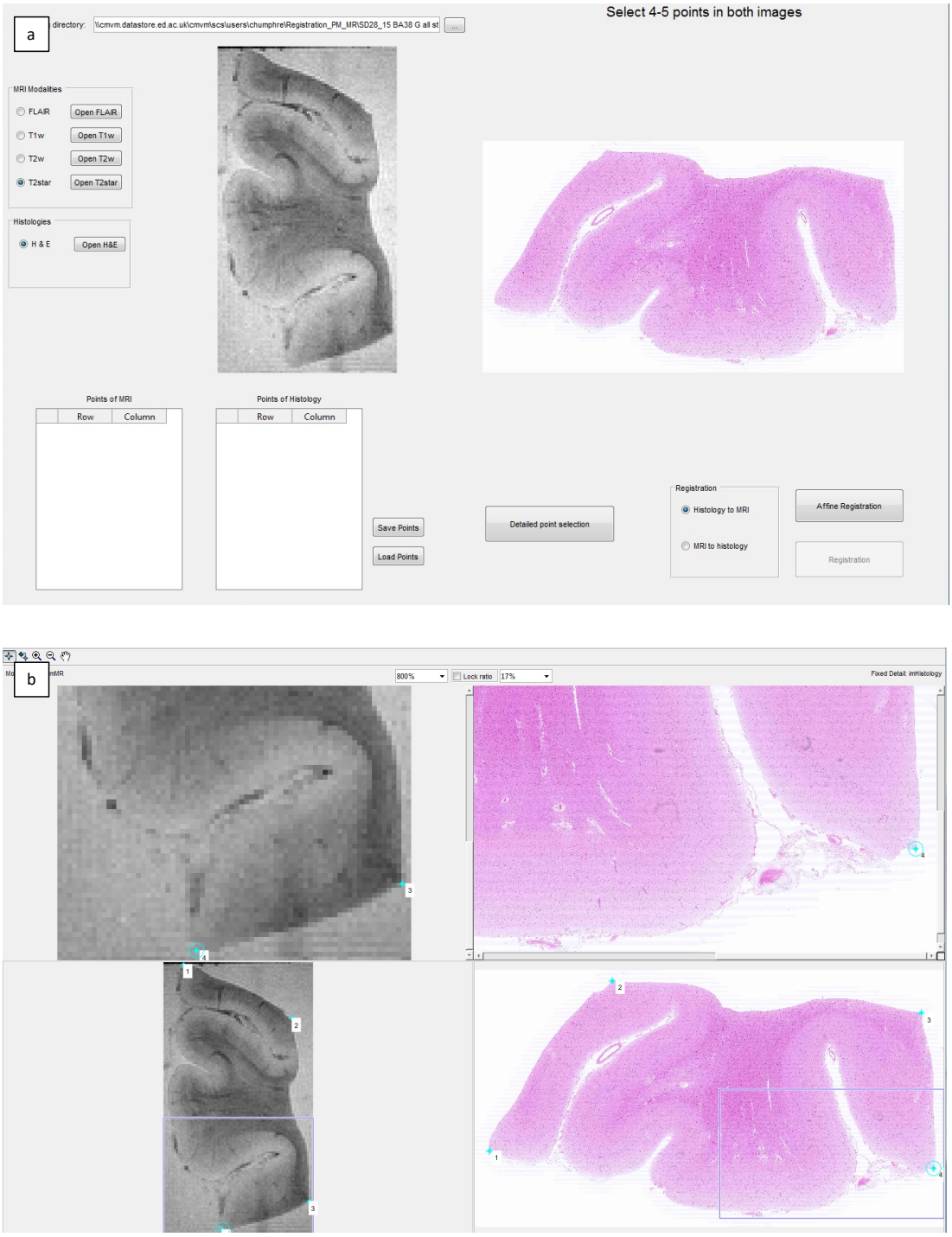
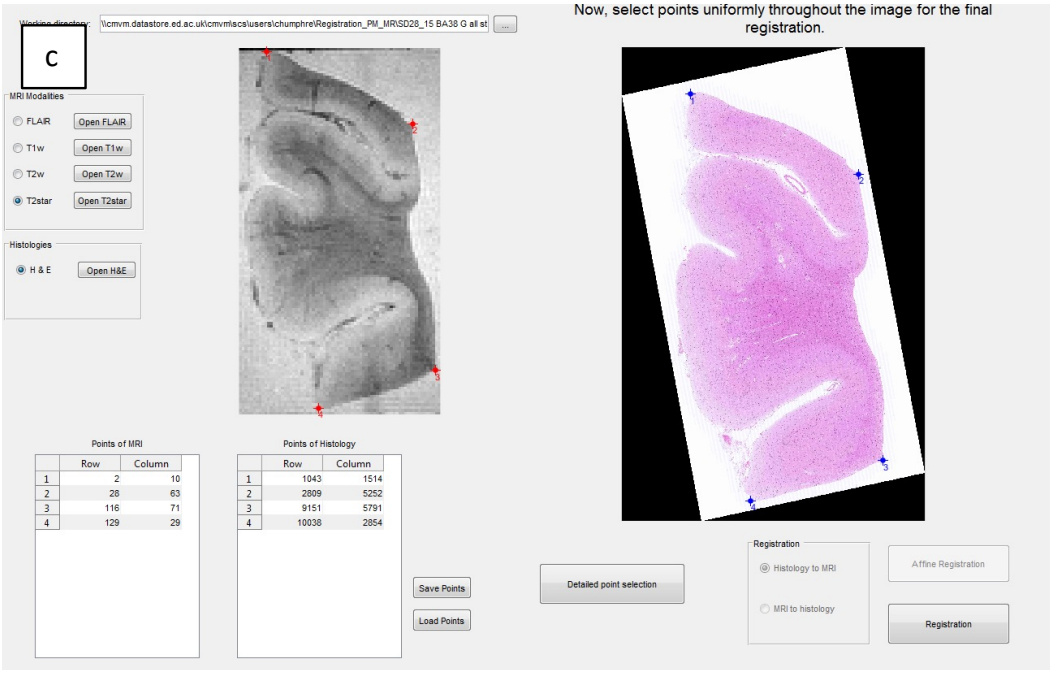
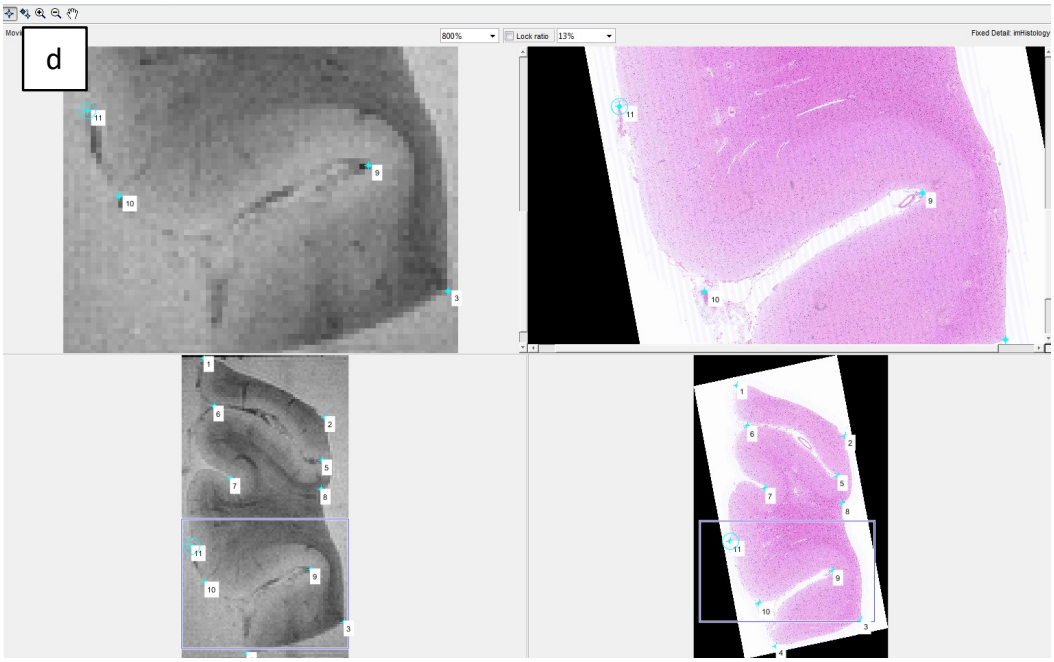
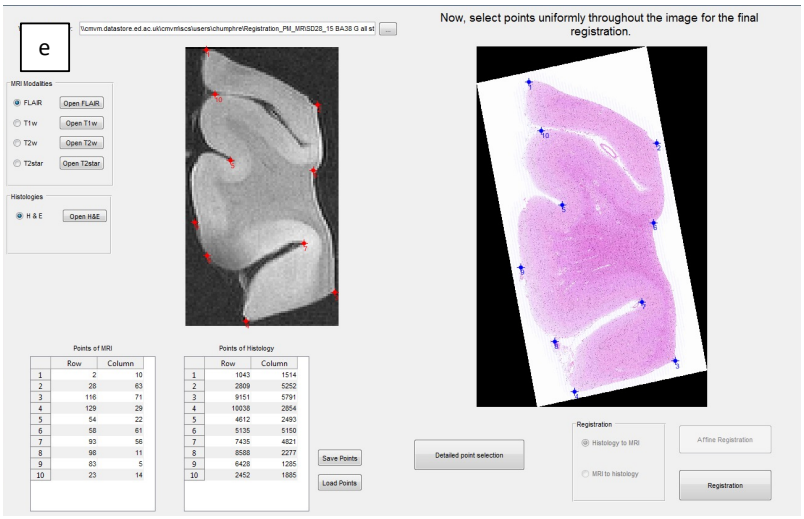
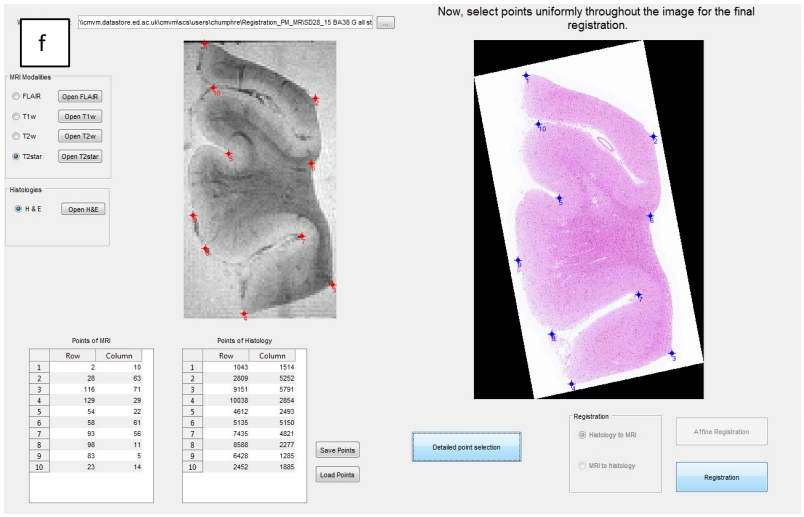


Figure 3.7 MR and histology image registration in Matlab Legend on page 171


c
Working directory:
\\cmvm.datastore.ed.ac.uk\cmvm\scs\users\chumphre\Registration_PM_MRI\SD28_15 BA38 G all st
MRI Modalities
FLAIR
Open FLAIR
T1w
Open T1w
T2w
Open T2w
T2star
Open T2star
Histologies
H & E
Open H&E
Now, select points uniformly throughout the image for the final registration.
Points of MRI
Row Column
1 2 10
2 28 63
3 116 71
4 129 29
Points of Histology
Row Column
1 1043 1514
2 2809 5252
3 9151 5791
4 10038 2854
Save Points
Load Points
Detailed point selection
Registration
Histology to MRI
MRI to histology
Affine Registration
Registration


d
800%
Lock ratio
13%
Fixed Detail: inHistology





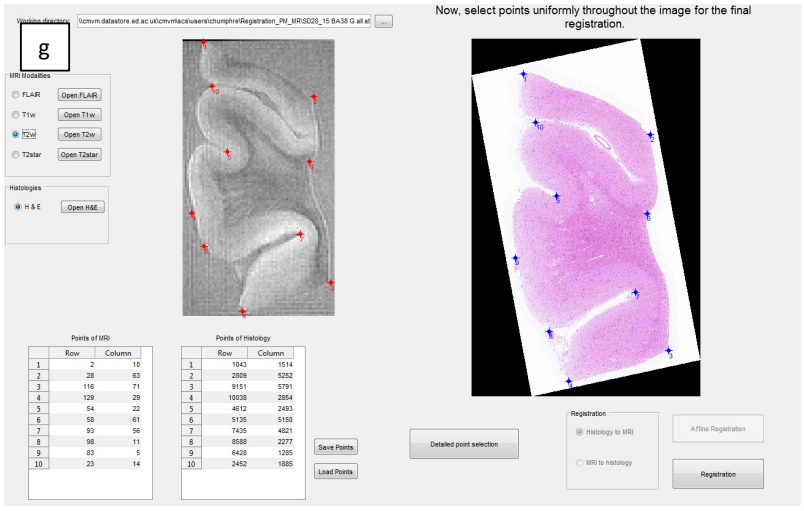
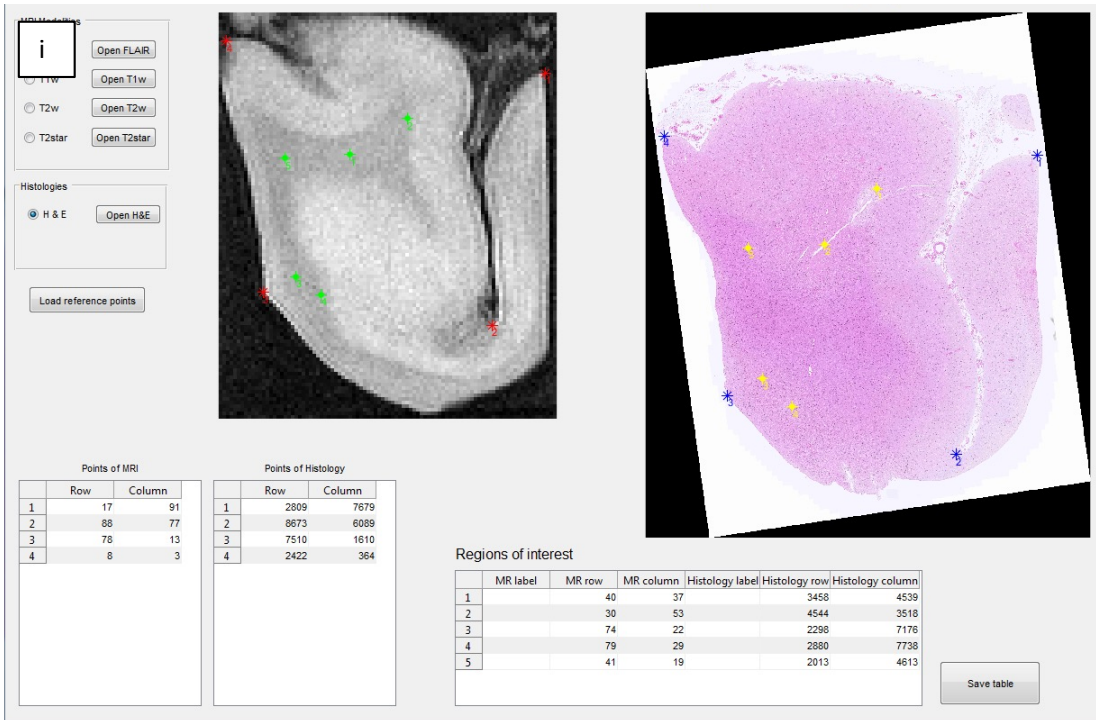
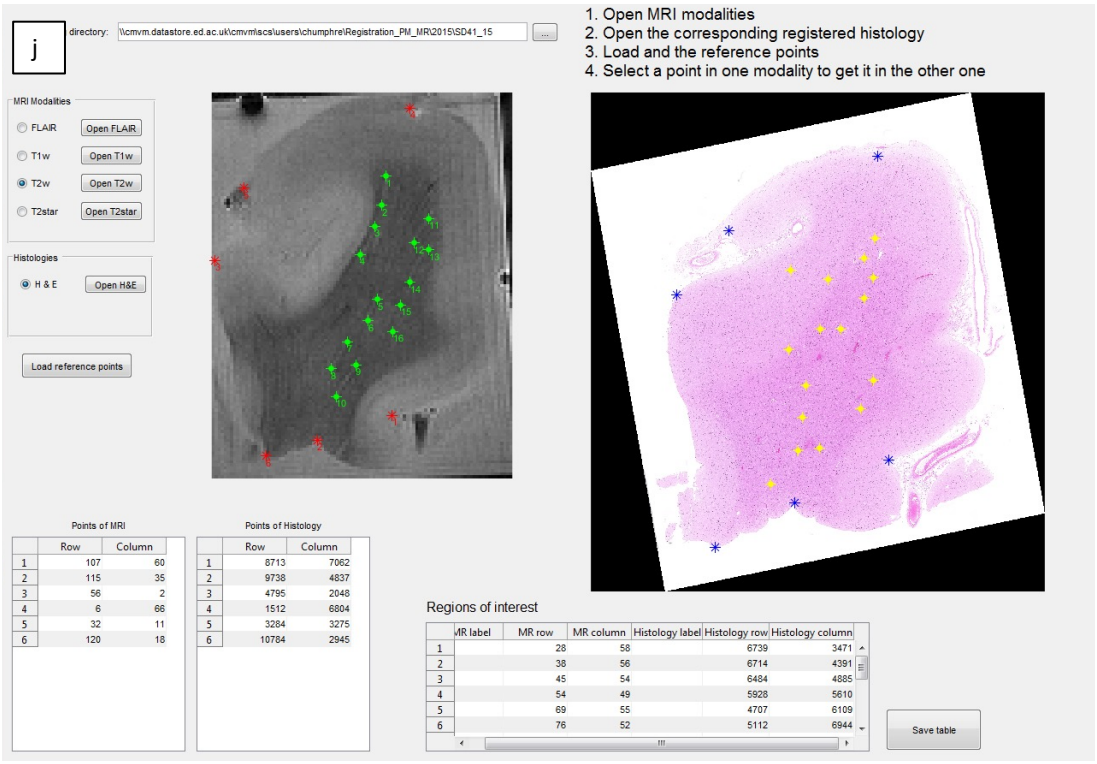
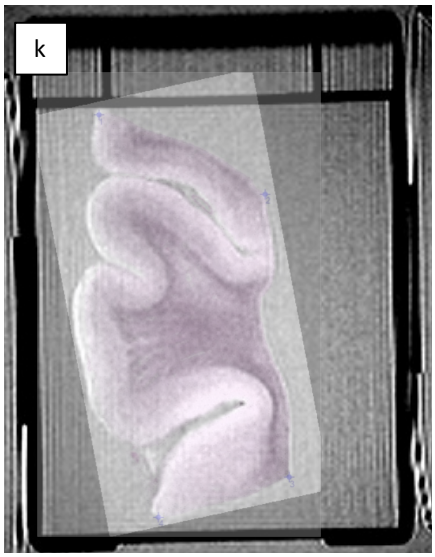


Figure 3.7 MR and histology image registration in Matlab Legend on page 171


h


i
Open FLAIR
Open T1w
T2w
Open T2w
T2star
Open T2star
Histologies
H & E
Open H&E
Load reference points
Points of MRI
Row Column
1 17 91
2 88 77
3 78 13
4 8 3
Points of Histology
Row Column
1 2809 7679
2 8673 6089
3 7510 1610
4 2422 364
Regions of interest
MR label MR row MR column Histology label Histology row Histology column
1 40 37 3458 4539
2 30 53 4544 3518
3 74 22 2298 7176
4 79 29 2880 7738
5 41 19 2013 4613
Save table


j
directory:
\\cmvm.datastore.ed.ac.uk\cmvm\scs\users\chumphre\Registration_PM_MR\2015\SD41_15
...
1. Open MRI modalities
2. Open the corresponding registered histology
3. Load and the reference points
4. Select a point in one modality to get it in the other one
MRI Modalities
FLAIR
Open FLAIR
T1w
Open T1w
T2w
Open T2w
T2star
Open T2star
Histologies
H & E
Open H&E
Load reference points
Points of MRI
Row Column
1 107 60
2 115 35
3 56 2
4 6 66
5 32 11
6 120 18
Points of Histology
Row Column
1 8713 7062
2 9738 4837
3 4795 2048
4 1512 6804
5 3284 3275
6 10784 2945
Regions of interest
MR label MR row MR column Histology label Histology row Histology column
1 28 58 6739 3471
2 38 56 6714 4391
3 45 54 6484 4885
4 54 49 5928 5610
5 69 55 4707 6109
6 76 52 5112 6944
Save table


k

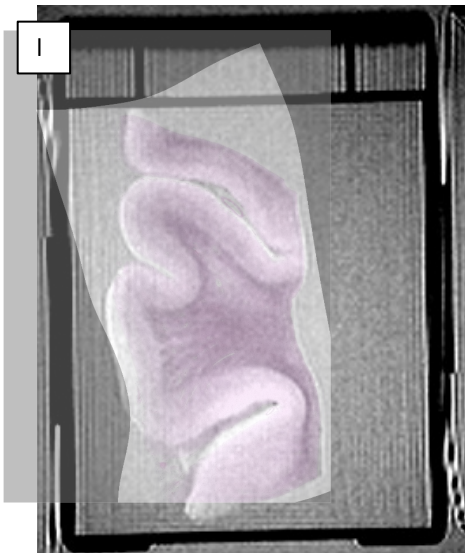

l

Figure 3.7 MR and histology image registration in Matlab

a) The MR and histology images were loaded into the Matlab working space. b) Four to five points were then chosen to perform an initial orientation step. The image could be magnified (at the top of the screen) to ensure the points were placed accurately. c) An Affine image of the histology, orientated correctly relative to the MR, was created. d) Points were then selected to perform a final, detailed registration step. These were also selected using magnified images for accuracy. e) FLAIR, f) T2*, g) T2 and T1 weighted images were available for the registration. h) A B-spline image of the histology was created by the final registration, the 2-dimensional warping across the image is evident at the white border of the original image. i) The fully registered MR and histology could then be viewed alongside each other. Points selected on one image over a lesion of interest would automatically appear on the second image in the correct location for examination. j) An example of an issue with points appearing incorrectly trying to compare the lesion appearances on the registered images. The green points were placed on the MR image on the left in linear patterns along the paths of visible blood vessels to examine the histological appearance of the vessels. The equivalent points should appear in yellow, numbered, in the matched location on the histology image on the right. However, even accounting for deformation due to the registration, the yellow points are obviously in the wrong locations and are not numbered. The k) Affine and l) B-spline registrations were also compared to assess if the B-spline registration improved the accuracy of matching the images. Overall, there was no obvious advantage to performing the B-spline registration compared to simply superimposing the correctly orientated images; small mismatches that would cause lesions to be misidentified remained.

3.7.3 Methods used to carry out direct lesion comparisons

Cases were numbered to mask the clinical and cohort information. Following image registration and grading of the MR and histological burden, at a later date I compared imaging-identified lesions to the histological appearances. I requested the slides randomly as I worked through the cases. At the time of grading, I had annotated screenshots of lesions on the imaging and histology, and used these with the completed grading proformas to identify lesions for comparison and studied them in the registered images viewed in Mango (multi-image analysis GUI, www.ric.uthscsa.edu/mango). I then used the histology annotated image and grading proforma to identify any further lesions not already seen on the imaging. The original histological slides and MR images in the picture archive and communication system (PACS) clinical imaging viewer (Philips) were available to study the appearances in the best resolution possible, as some detail is lost in the registration process.

Due to the amount of time it took to develop and refine the registration methods, there was not as much time to study the lesions as I had intended, so I prioritised making accurate, but potentially fewer comparisons. Chapter 6 contains the results of these comparisons.

PART C: EXPERIMENTAL WORK AND RESULTS

CHAPTER 4: ASSESSMENT OF THE BRAIN BANK CASE REVIEW AND DEFINING THE HISTOPATHOLOGY

4.1 The histopathological brain bank case review

4.1.1 Results

4.1.1.1 Demographics

Five LBC1936, 117 LINCHPIN and 75 sudden death cases (total n=197), all admitted to the brain bank from June 2010-June 2016, were examined (Table 4.1). These represent all cases from these cohorts that were retrieved by the brain bank and where the slides were available in file and had appropriate consent. 41% of individuals were female. Gender differences were most pronounced in the sudden death (23% female) and LBC1936 cohorts (20% female) compared to LINCHPIN (52% female). The average age of the LBC1936 and LINCHPIN cohorts (medians 79 and 81 years, interquartile range (IQR) 1 and 11 respectively) was significantly older than the sudden death cohort (controls, median 53 years, IQR 15, p values 0.011 and <0.0001 respectively) (Figure 4.1).

4.1.1.2 Grading SVD burden

The odds of having a higher vascular SVD score was 26.25 times higher in LINCHPIN than Sudden Death (p=0.0000, 95% CI 9.42-77.75) and 6.44 times higher in LBC1936 than Sudden Death (p=0.0406, 95% CI 1.09-40.33), and both were statistically significant. The LINCHPIN and LBC1936 scores were not significantly different (p=0.084, 95% CI 0.80-20.53). The odds of a higher vascular SVD score was also statistically significant and increased with age by a factor of 1.04 with each year (p=0.013, 95% CI 1.01-1.07). Removing group as a covariate in the model increased the AIC, therefore suggesting that group improves the model fit.

Table 4.1 Demographic details and scores of cases used for grading of SVD and neurodegenerative pathology in the brain bank case review

Number of cases with each pathological severity score by cohort. The non-amyloid SVD score, grade of white matter cerebrovascular pathology (Deramecourt, Slade et al. 2012) and CAA stage (Love, Chalmers et al. 2014). Recorded as none, mild, moderate, severe, they are represented 0-3. Tau pathology is staged 1-6 (Braak and Braak 1991). Amyloid- ß is staged 1-5 (Thal, Rub et al. 2002). α synuclein is recorded by location of deposition, progressing through brainstem, limbic and neocortical (Alafuzoff, Ince et al. 2009). It has been converted to score 1-3 to indicate the average pathology burden. LBC1936 Lothian birth cohort 1936, Linchpin Lothian Study of INtraCerebral Haemorrhage, Pathology, Imaging and Neurological Outcome, IQR inter-quartile range, SVD small vessel disease, SD standard deviation, WM white matter, CAA cerebral amyloid angiopathy, n number.

Cohort	n	Female, n	Age at death, years, median (IQR)	Non-amyloid vascular SVD score = n	WM cerebrovascular pathology score = n	CAA stage = n	Tau stage = n	Amyloid ß phase = n	α synuclein score = n
LBC1936	5	1	79 (78-79)	0 = 0 1 = 2 2 = 2 3 = 1	0 = 0 1 = 3 2 = 0 3 = 2	0 = 2 1 = 1 2 = 2 3 = 0	0 = 0 1 = 3 2 = 2 3 = 0 4 = 0 5 = 0 6 = 0	0 = 1 1 = 2 2 = 2 3 = 0 4 = 0 5 = 0	0 = 5 1 = 0 2 = 0 3 = 0
Linchpin	117	62	81 (75-86)	0 = 0 1 = 16 2 = 36 3 = 65	0 = 1 1 = 16 2 = 35 3 = 65	0 = 36 1 = 22 2 = 11 3 = 48	0 = 14 1 = 16 2 = 39 3 = 13 4 = 11 5 = 4 6 = 20	0 = 26 1 = 27 2 = 39 3 = 15 4 = 2 5 = 8	0 = 105 1 = 7 2 = 3 3 = 2
Sudden death	75	17	53 (46-61)	0 = 47 1 = 17 2 = 10 3 = 1	0 = 52 1 = 19 2 = 3 3 = 1	0 = 69 1 = 4 2 = 2 3 = 0	0 = 61 1 = 6 2 = 5 3 = 1 4 = 1 5 = 0 6 = 1	0 = 66 1 = 5 2 = 3 3 = 0 4 = 0 5 = 1	0 = 74 1 = 1 2 = 0 3 = 0
Total	197	80	75 (57-83)						

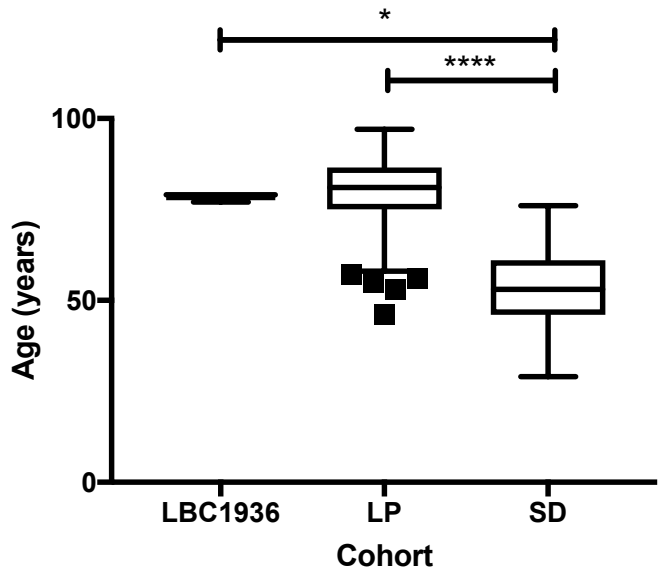


Figure 4.1 Comparing the age of the cohorts used in the brain bank case review

Boxplot of Kruskal Wallis test showing significantly older ages in the LBC1936 and LP cohorts compared to the SD cohort. LBC1936 Lothian birth cohort 1936, LP Linchpin, SD Sudden death. Tukey boxplots indicate the median and inter-quartile range (IQR) with outliers beyond 1.5 IQR plotted individually. * $p < 0.1$, **** $p < 0.000$

The odds of having a higher parenchymal SVD score was 74.4 times higher in LINCHPIN than in Sudden Death (p=0.0000, 95% CI 22.66-285.40) and 18.22 times higher in LBC1936 than Sudden Death (p=0.0057, 95% CI 2.43-156.62), both were statistically significant. The LINCHPIN and LBC1936 scores were not significantly different (p=0.125, 95% CI 0.63-25.30). The odds of a higher parenchymal SVD score increased with age by a factor of 1.03 with each year, but this was not statistically significant (p=0.088, 95% CI 1.00-1.06). Removing group as a covariate in the model increased the AIC, therefore suggesting that group improves the model fit.

4.1.1.3 Grading other neuropathologies

The burden of all other pathologies assessed using the published, validated criteria (CAA, tau fibrillary tangles, Aß plaques and α-synuclein) was greatest in the LINCHPIN cohort (mean score 1.59 (standard deviation 1.30), (2.71

(1.92), 1.69 (1.36), 0.06 (0.33) respectively) followed by LBC1936 (1 (1), 1.4 (0.55), 1.2 (0.84), 0 (0) respectively) which was greater than in the sudden death controls (1.02 (1.27), 1.79 (1.96), 1.12 (1.35), 0.03 (0.25) respectively).

4.1.1.4 Inter-observer agreement

Inter-observer agreement was almost perfect for the assessment of CAA (0.98) and α-synuclein (0.82). Agreement was substantial when grading parenchymal WM SVD pathology (0.77), tau neurofibrillary tangle stage (0.73), non-amyloid vascular SVD (0.66) and amyloid-ß phase (0.65) (Table 4.2).

4.1.2 Discussion

Both the vascular and parenchymal histological SVD scores were significantly higher in the LINCHPIN (haemorrhagic SVD) and LBC1936 (normal aging) cohorts compared to the sudden death controls, controlling for age. This is what we had expected and suggests the grading system provides a reflection of the expected disease burden in the cohorts studied. That there is no significant difference between LINCHPIN and LBC1936 could indicate a significant burden of disease in the normally aged LBC1936, but with a different, underlying pathophysiology and clinical outcomes compared to the group with haemorrhagic disease. It would be expected that the SVD in LBC1936 might be of a more primary arteriolosclerotic type which would fit with these results. However, the underlying pathology in the LBC1936 cohort is likely to be relatively mild within the spectrum of SVD and the use of these cohorts means there is an underrepresentation of patients with severe, predominantly non-haemorrhagic SVD.

The vascular histology SVD score appears to increase with age. The parenchymal histology SVD score showed a trend of increasing with age, but the statistical analysis did not reach significance. This could be a reflection of the small number of cases with mild non-amyloid SVD. The increase with age is in agreement with other studies (Mok, Srikanth et al. 2014).

Table 4.2 Inter-rater agreement for pathological assessment of SVD and neurodegenerative pathology burden

Inter-observer agreement was assessed with linear weighted Cohen's kappa coefficient for the features described in Table 4.1. The results can be interpreted: <0 no agreement, 0.00-0.20 slight agreement, 0.21-0.40 fair agreement, 0.41-0.60 moderate agreement, 0.61-0.80 substantial agreement, 0.81-1.00 almost perfect agreement (Landis and Koch 1977). SVD small vessel disease, WM white matter, CAA cerebral amyloid angiopathy.

Pathological feature	Inter-observer agreement (n = 197)
Non-amyloid vascular SVD score	0.663
WM cerebrovascular pathology	0.773
CAA stage	0.976
Tau stage	0.725
Amyloid ß phase	0.654
α synuclein type	0.816

The results suggest group was a good predictor of vascular and parenchymal score and supports the inclusion of these groups to study SVD. LBC1936 (n=5) is much smaller than LINCHPIN (n=117) and the sudden death controls (n=75), however. It would be desirable to further investigate the relationships between group, score and age, with greater numbers of LBC1936 in the first instance to better understand the burden and nature of SVD in those individuals. As more is understood about SVD pathology, refining the grading systems may also make the relationships clearer. This was one of my aims in the prospective work. However, it is dependent on the number of cases admitted into the brain bank and so a longer period of study may be required to obtain substantial numbers of cases from all cohorts. Larger numbers of cases would also allow the impact of other features, such as cardiovascular disease, particularly hypertension, to be considered.

The relatively large number of cases available for retrospective examination in the case review was an advantage of this work, as histopathological studies can often have very small numbers. This gave a significant amount of practical experience in SVD and related pathologies at the start of this

research and a good basis upon which to build the initial pathological grading proforma and definitions. We also used this study in combination with the clinical, radiological and pathological literature to inform the selection of areas to study that would likely yield the most SVD pathology. During the brain bank case review, two lesions stood out that are referred to in the SVD literature in passing, but have unknown pathogenesis and significance; rarefaction in the immediate surrounding white matter around enlarged PVS and vascular collagenosis. These were then included in our histological assessment of SVD.

The large age difference between the cohorts is unfortunate but unavoidable. Age is one of the few established risk factors for SVD. However, those that die suddenly and unexpectedly with no known neurological disease, the sudden death cohort, are younger. It made age matching subjects in further analyses difficult, especially given the small numbers of subjects available for study, but it highlighted the importance of accounting for the age difference in any statistical analyses. The inclusion of the LBC1936 cohort also aims to help to address this and should be considered when drawing any conclusions.

Analysis of IRR was important to ensure I could reliably proceed with further assessment of disease burden having previous general histopathology experience only. IRR for CAA and α-synuclein were particularly high, although the prevalence of α-synuclein pathology was very low in these cases (11/197, 0.06%).

The rating for our non-CAA vascular SVD pathology rating was also substantial (0.663), and comparable to that for the system published and used to assess white matter parenchymal pathology (0.773) (Deramecourt, Slade et al. 2012). This non-CAA vascular SVD rating was constructed informally, based upon discussion, reading and clinical case review. However, it was constructed specifically with the aim of assessing SVD burden in the context of cognitive impairment compared to previous grading

systems (Deramecourt, Slade et al. 2012, Smallwood, Oulhaj et al. 2012, Skrobot, Attems et al. 2016) and making a system that could be compared against neuroimaging assessment using comparable lesions and grading schemes, given that neuroimaging is the best established and most objective assessment possible currently (Wardlaw, Smith et al. 2013). That the inter-rater scores for this new grading system were significantly comparable was reassuring moving forwards and suggested the system may be reproducible, but this would require validation in other cohorts by different assessors before it could be recommended for wider use in research and clinical settings.

On the basis of this study, I concluded these three cohorts would provide a broad spectrum of SVD pathology including severe haemorrhagic disease, a spectrum of normal aging including arteriolosclerotic pathology and controls. It is important to have this range of pathology included to give a full representation of the range of lesions seen in SVD when comparing the lesion appearances. To do this, however, the histological lesions had to be defined and the grading system formalised.

4.2 Histopathological small vessel disease definitions

Specific lesions were identified by name, e.g. arteriolosclerosis, enlarged PVS. The presence of any individual or combination of these pathologies indicating or resulting from disease of the small vasculature, arterial capillary and venous vessels (Wardlaw, Smith et al. 2013), was referred to as **small vessel disease** (Table 4.3).

Table 4.3. Histopathological definitions used to assess small vessel disease

[1] Taken from/ [2] adapted from (Skrobot, Attems et al. 2016), [3] originally from (Strozyk, Dickson et al. 2010)

Histopathological feature	Definition
General terms	
Small vessel disease	The presence of any individual or combination of pathologies indicating, or resulting from, disease of small intra-parenchymal cerebral vessels.
Infarction	Focal tissue loss and reactive features (variable depending on age of lesion and location, include: gliosis, microglial changes, neuronal changes, inflammatory infiltrate) indicating focal ischaemia.
Haemorrhagic lesion	Focal fresh blood or haemosiderin pigment deposition with tissue loss and reactive features (variable depending on age of lesion and location, include: gliosis, microglial changes, neuronal changes, inflammatory infiltrate) indicating parenchymal haemorrhage.
Gross SVD assessment	
Large haemorrhage	Haemorrhagic lesion visible to the naked eye which is easily identifiable on macroscopic examination. [1]
Large infarct	Focal infarction visible to the naked eye which is easily identifiable on macroscopic examination. [2]
Lacune	Cystic lesion visible to the naked eye but <1cm in diameter, confirmed on histological examination to be an area of infarction, which may contain a cystic cavity. [2,3]
Vessel wall SVD assessment	
Arteriolosclerosis	Hyaline thickening of walls of vessels <150mm in diameter, not associated with lipid-containing cells replacing the tunica media. Diagnosis requires an absence of intramural inflammation, amyloid or fibrinoid necrosis. [1]
Fibrinoid necrosis	Asymmetrical replacement of the vessel wall by amorphous, brightly eosinophilic fibrinoid.
Lipohyalinosis	Asymmetrical vessel wall thickening with hyalinosis, fibrosis and lipid-laden foamy macrophages.
Perivascular collagenosis	Concentric hyaline thickening of the adventitial aspect of vessel walls.
Parenchymal SVD assessment	
White matter rarefaction	Weakly stained/pale and loose appearance of myelinated fibres with reduced white matter myelin staining in Luxol fast blue stained sections. [2]

Enlarged perivascular spaces	Visibly dilated space around parenchymal vessels containing a patent blood vessel.
Perivascular rarefaction	Rarefaction of the parenchyma immediately surrounding an enlarged perivascular space.
Microinfarct	Ischaemic lesion found on microscopic examination but not visible to the naked eye. [2, 3]
Microbleed	Haemorrhagic lesion (with parenchymal involvement) found on microscopic examination only, not visible to the naked eye. [1]
Perivascular haemosiderin	Free haemosiderin and/or haemosiderin laden macrophages in and immediately around the vessel wall without tissue loss or a gliotic reaction.
Perivascular inflammation	An inflammatory cell infiltrate, predominantly lymphocytic, in the parenchyma immediately adjacent to a small vessel in the absence of other SVD-related pathology.

There are multiple references in the literature to various sizes of vessels directly affected by SVD pathology, particularly arteriolosclerosis. Intraparenchymal vessels smaller than approximately 150μm diameter is commonly used (Deramecourt, Slade et al. 2012, De Reuck, Deramecourt et al. 2014, De Reuck, Deramecourt et al. 2015, Skrobot, Attems et al. 2016). In practice, it is not practical to measure the diameter of vessels in every case affected. The size of intracortical arterioles was measured as between 20-90μm on electron microscopy (Reina-De La Torre, Rodriguez-Baeza et al. 1998). Therefore I used a more practical definition of small arterioles completely within the parenchyma.

A **large infarct** (Figure 4.2a) was defined in VCING as greater than 1cm diameter and a microinfarct as not visible to the naked eye. There is an obvious gap between 1cm and 'microscopic' where lesions would not be captured. Similar to haemorrhagic lesions, I used large infarct for those visible macroscopically. Histological **microinfarcts** were identifiable only on microscopy. Cortical microinfarcts are recognised but not as well characterised on neuroimaging due to their small size previously being below

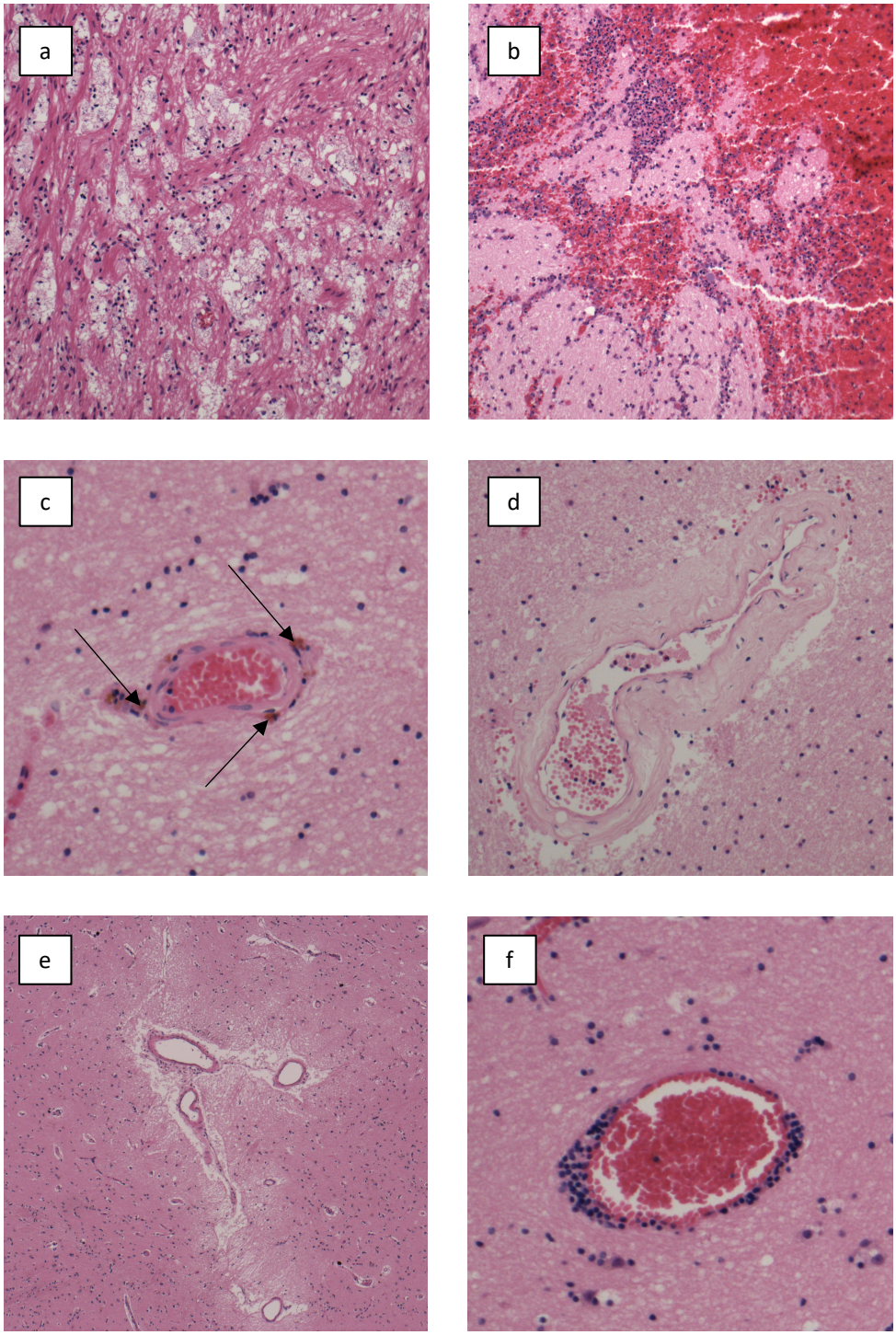


Figure 4.2 Histological features of small vessel disease

a) A large area of infarction with tissue loss and gliosis, x100. b) A relatively acute large haemorrhage with red cell extravasation, inflammatory infiltration and tissue loss, x100. c) Perivascular haemosiderin (arrows) deposited at the vessel adventitia without reactive changes, x200. d) Concentric hyaline thickening of the outer aspect of vessel walls in perivascular collagenosis, x100. e) Perivascular rarefaction in the parenchyma immediately surrounding an enlarged perivascular space, x40. f) Lymphocytic perivascular inflammation immediately adjacent to a small parenchymal vessel, x100. All H&E.

imaging resolution thresholds (Humphreys, Smith et al. 2021). I did not separate the cortical and subcortical locations as there is no histological evidence for doing so. Tissue loss and reactive changes (dependent on lesion age) were required to identify an area of infarction (figure 1.6e).

The features required to identify a **large haemorrhage** (figure 4.2b) or microbleed included parenchymal involvement, namely cell loss and reactive features in addition to blood products or haemosiderin pigment deposition, although the specific features vary depending on the lesion age with more prominent inflammation in more acute lesions and gliosis in more chronic lesions. A **microbleed** is seen on microscopic examination only (figure 1.6c). This allowed separation from **perivascular haemosiderin** deposition, seen as free haemosiderin and haemosiderin laden macrophages in and immediately around the vessel wall in the absence of tissue loss and a gliotic reaction (figure 4.2c).

VCING defined lacunar infarcts as cystic lesions less than 1cm diameter but visible to the naked eye, however, definitions in the literature vary widely (Bailey, Smith et al. 2012). Some enlarged PVS are visible macroscopically where they can appear cystic and empty as the small central vessel may not be visible making them resemble small lacunar infarcts. I adapted the VCING definition to reflect the need for histological confirmation of features suggesting infarction while using the term **lacune** to avoid assuming total knowledge of the underlying pathophysiology (Figure 1.6d).

Arteriolosclerosis was defined as per the VCING definition to describe the hyaline, symmetrical thickening of small vessel walls (Figure 1.5a).

Lipohyalinosis was identified as asymmetrical vessel wall thickening with hyalinosis, fibrosis and foamy macrophages (McAleese, Alafuzoff et al. 2016) (Figure 1.5b).

In **fibrinoid necrosis** the vessel wall is replaced by amorphic, brightly staining eosinophilic fibrinoid (Figure 1.5c). It can be distinguished from hyaline by careful examination on H&E, where hyaline material stains paler. Fibrinoid necrosis is asymmetrical and segmental, meaning it is relatively less often identified on histology (Rosenblum 2008).

In **vascular collagenosis**, concentric collagen deposition thickens the vessel wall with a pale, wispy appearance (Figure 4.2d). It predominantly affects the adventitia, but can be transmural. Venules are thought to be most often affected and it is commonly seen in a periventricular distribution. It is not associated with inflammation and can cause luminal narrowing and obstruction (Black, Gao et al. 2009)

My systematic review found radiological WMH were composed of a variety of lesions (Humphreys, Smith et al. 2021). I described **white matter rarefaction** as loosening of the white matter and pallor on LFB staining (Figure 1.6b), a combination of the separate definitions for white matter rarefaction (loosening) and pallor (on LFB) used by VCING. There may be value in separating these features out, but currently there is no evidence to support this in the context of radiological WMH, one of the hallmarks of clinical SVD (Humphreys, Smith et al. 2021). Other features within radiological WMH included enlarged PVS, infarction, cavitation, vascular pathology and inflammation, these were assessed separately.

Enlarged PVS contained a patent blood vessel and appear visibly dilated relative to the vessel contained within the space (Figure 1.6a). There is no well-defined minimal size on histology at which the space can be called pathological (Humphreys, Smith et al. 2021), but potentially any visible space surrounding a blood vessel is abnormal and so this is how it was defined. As described, rarefaction of the immediately adjacent tissue was sometimes present, I included this **perivascular rarefaction** (Figure 4.2e) in the definitions and grading to try to better understand it's prevalence and significance.

Inflammation is seen in association with other SVD-related lesions, however isolated **perivascular inflammation** consisting of small numbers of lymphocytes can also be seen in SVD (Figure 4.2f).

4.3 Pathological assessment and grading of SVD burden

4.3.1 Histological processing

As described, all cases underwent standardised histological processing, using the same methods applied to all cases in the MRC Edinburgh Brain Bank, with the addition of post-mortem MR imaging (Chapter 5).

For standard assessment, H&E and LFB slides were produced, additional stains were carried out for more detailed assessment of specific features when required; CD34 stains endothelial cells, fibrinogen allows assessment of vascular leakage and CR3-43 activated microglia (Appendices 5 and 6).

4.3.2 Microscopic assessment and grading

Based on the lesions identified and defined, I set out to design a proforma to be applied to the 16 areas identified to assess the extent and grade the burden of SVD to enable comparison to the ex vivo imaging, the result is in Appendix 7.

White matter rarefaction, enlarged PVS, arteriolosclerosis, perivascular haemosiderin, perivascular inflammation and basal ganglia pigment could be assessed on an ordinal scale. Semiquantitative scales of none, mild, moderate and severe are often used in histopathology and should represent the extent of change, to include the amount and severity of disease (Schafer, Eighmy et al. 2018). Given the absence of validated histopathological grading systems, I created grading systems for these lesions to reflect this for white matter rarefaction (Figure 4.3), enlarged PVS (Figure 4.4) and arteriolosclerosis (Figure 4.5). The importance or relative contribution of the extent or severity of these is unknown. Therefore, they were separated to

see if anything could be deduced from the scoring. Basal ganglia pigment deposition was also graded (Figure 4.6).

Examples of the range from normal to most severe SVD-related lesions were selected from within the cases to create a visual grading system; 0 none, 1 mild, 2 moderate, 3 severe, where moderate was the midpoint between mild and severe. These were reviewed and revised with respect to published grading systems, as appropriate (Deramecourt, Slade et al. 2012, Smallwood, Oulhaj et al. 2012, Skrobot, Attems et al. 2016). Use of all visual grading systems is subjective, but to minimise potential for error, the final visual guide of example images accompanied by a written description was created as a frame of reference for each lesion (Figures 4.3-6). These were agreed with Professor Smith.

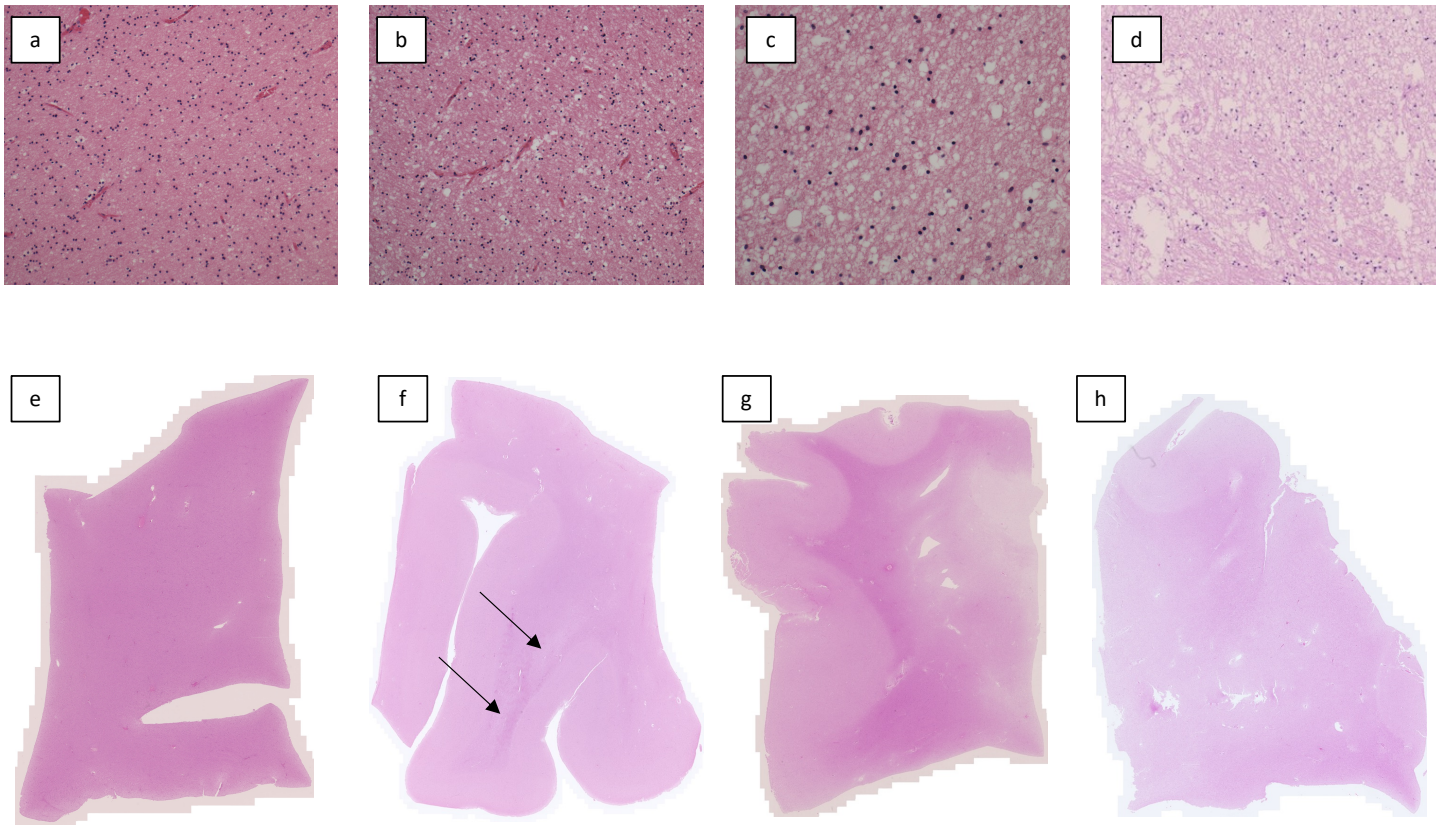


Figure 4.3 Grading histological white matter rarefaction

a-d) By severity a) 0 = normal white matter, b) 1, mild = small uniform vacuolation, c) 2, moderate = larger vacuolation and increasing pallor, d) 3 = severe pallor with large, irregular vacuolation. e-h) By extent of the area of white matter on a histological section e) 0 = none, f) 1, mild = small, focal areas (arrows), g) 2, moderate = up to 50% of the white matter is affected and h) 3, severe = all, or almost all of the white matter is affected. All H&E. a-d) x100 e-f) digitalised whole slides.

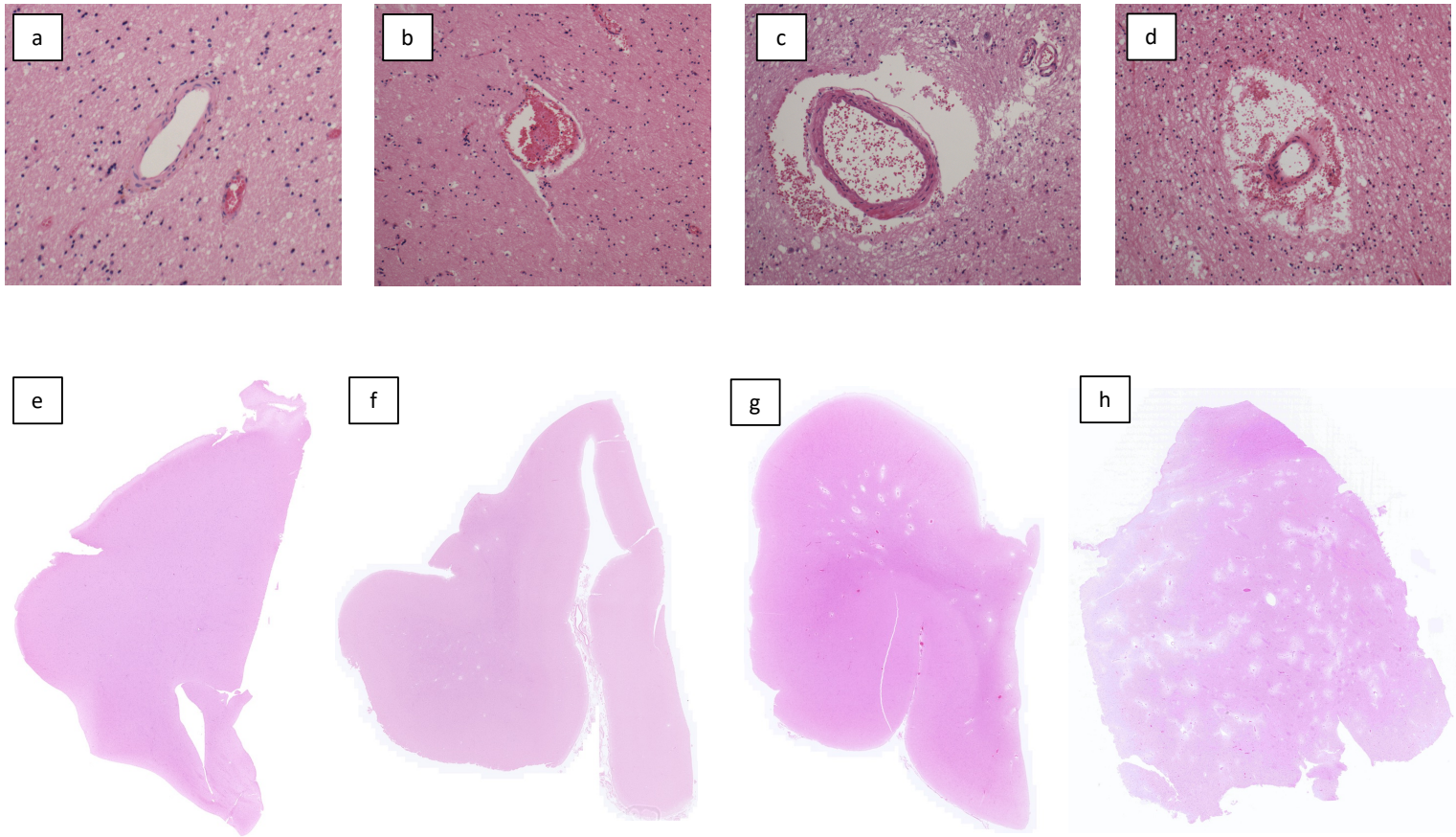


Figure 4.4 Grading histological perivascular space enlargement

a-d) By severity a) 0 = vessels without visibly enlarged perivascular spaces (PVS), b) 1, mild = minimal visible space, c) 2, moderate = the PVS is up to approximately twice the vessel diameter, d) 3, severe = the space is greater than twice the vessel diameter. F-h) By extent throughout the whole slide, e) 0 = none, f) 1, mild = occasional, scattered, g) 2, moderate = significant numbers of visibly enlarged PVS, h) 3 = almost all tissue affected. All H&E. a-d) x100 e-f) digitalised whole slides.

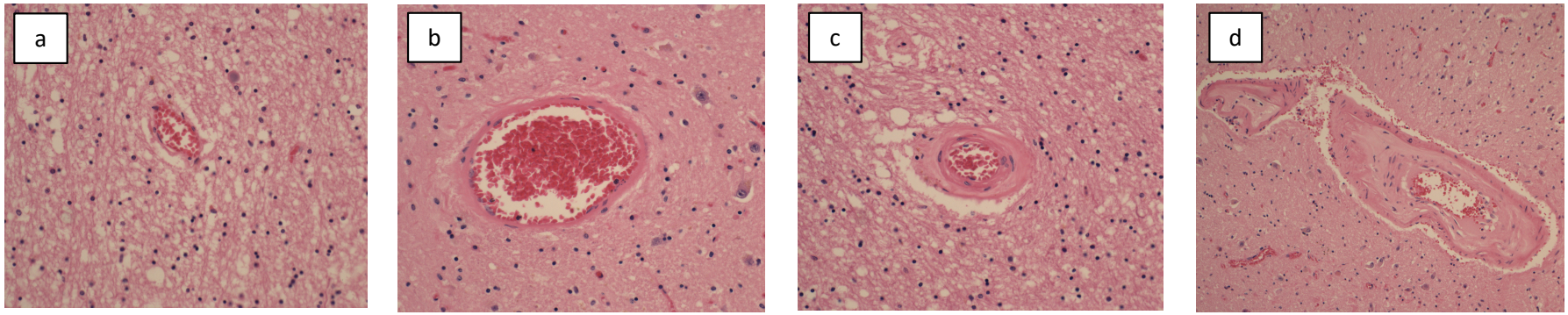


Figure 4.5 Grading histological arteriolosclerosis

a-d) By severity a) 0 = normal arteriole, b) 1, mild = arteriolosclerosis with mild thickening of the wall due to hyaline material deposition not causing luminal compromise, c) 2, moderate = hyaline thickening of the vessel wall with luminal narrowing, d) 3, severe = significant hyaline deposition and luminal compromise greater than approximately 50% of the original diameter. Extent is not shown as the small affected vessels are not visible at low power as for the white matter rarefaction or enlarged perivascular spaces examples. Extent was graded with the same criteria as enlarged perivascular spaces (figure x.4). All H&E, a-c) x100 d) x40.

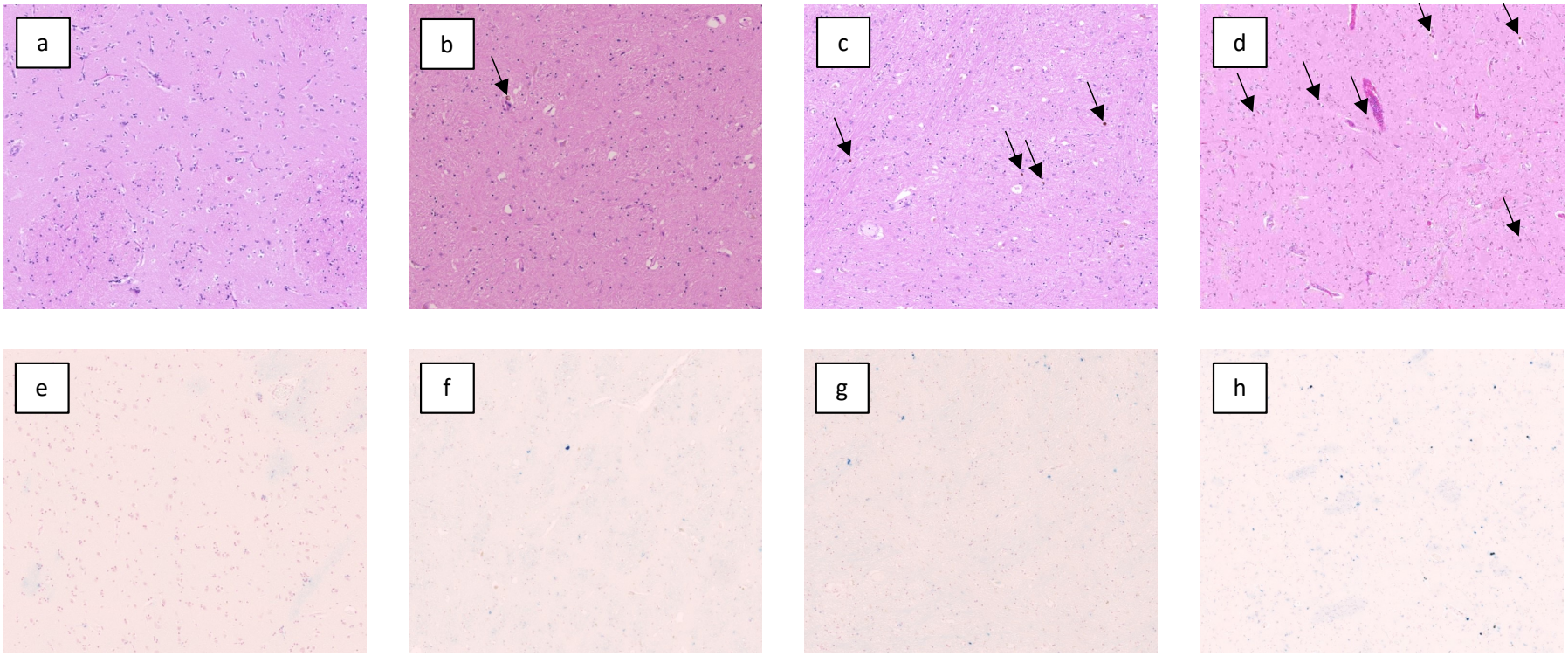


Figure 4.6 Grading histological iron deposition in the basal ganglia

Brown haemosiderin pigment (arrows) can be difficult to discern at low power on H&E: a) 0= none, b) 1, mild = occasional pigmented deposits c) 2 = more extensive deposition d) 3 = the most extensive pigment deposition seen on histology. The iron deposition was confirmed and was easier to identify as and grade as foci of blue material on Perl's stain e) none, f) 1 = mild, g) 2 = moderate, h) 3 = severe. a-d) H&E x40 e-h) Perl's x4

For some lesions it is difficult, not possible or not useful to assign a severity score. These were either recorded as present or absent (large haemorrhage (Figure 4.2b), fibrinoid necrosis (Figure 1.5c), lipohyalinosis Figure 1.5b)) The significance of vascular collagenosis (Figure 4.2d), perivascular vacuolation around enlarged PVS (Figure 4.2e), perivascular haemosiderin (Figure 4.2c) and perivascular inflammation (Figure 4.2f) is unknown. I therefore recorded them as present or absent to understand the prevalence in our population. Focal parenchymal lesions (microinfarcts (Figure 1.6e), lacunes (Figure 1.6d) and microbleeds (Figure 1.6c)) were counted and measured.

I did not apply size criterion to any microscopic lesions such as enlarged PVS, microinfarcts or microbleeds as I found no good evidence to support this histologically and I wanted to approach the assessment with a 'blank slate' without pre-existing expectations or bias.

I attempted to create a grading system for fibrinogen staining, based on the LFB none, mild, moderate, severe system, taking into account the range of staining extent and intensity seen across a variety of cases. However, despite rounds of attempted validation, the fibrinogen staining was too inconsistent between, and within, cases, precluding the production of reproducible scheme and image gallery.

The recording proforma (Appendix 7) was designed to make the assessment process as intuitive as possible, to help compensate for the level of detail required. I initially assessed the extent of white matter rarefaction, enlarged PVS and any large haemorrhage at lower power on H&E and LFB. Parenchymal lesions were then assessed; microinfarcts, lacunes and microbleeds. Finally, the vessels and immediate surrounding areas were studied for further examination of enlarged PVS, arteriolosclerosis, fibrinoid necrosis, lipohyalinosis, venular collagenosis, perivascular haemosiderin and perivascular inflammation.

Cortical thickness was measured from the pia mater to the grey-white matter junction at the superficial aspect of a gyrus, the deepest point of the sulcus and the mid-point, where present and orientated appropriately. This was done with reference to where the measurements were taken on the post-mortem MR image to ensure the same location was measured. I performed the microscopic SVD assessment for each case blinded to the cohort and clinical history. 10% were checked by Professor Smith. Any discrepancies or uncertainties were reviewed together and resolved.

4.3.3 Discussion

I aimed to make these definitions as objective as possible, allowing this work to make comparisons with the lesions identified on neuroimaging without assuming the underlying pathogenesis of the observed lesions and potentially introducing additional bias into these relatively subjective analyses. The histological grading system I have developed and applied here requires validation and application in larger numbers of cases. It is however based on the best available evidence in the neuropathological literature from published grading systems already in use and our systematic review and reflected the expected burden of disease in the brain bank case review, with IRR scores comparable to published systems for other neurodegenerative pathologies. It is intended as a research tool to provide a thorough assessment of SVD in the tissue studied and to be comparable to the imaging assessment of the same tissue to look for associations.

I believe these definitions and grading system represent at least a solid foundation upon which a future, agreed structure of standardised processing protocols, defined pathological lesions and grading system can be built for wider future application. Together with my supervisor, Professor Smith, we will call for such a consensus in the near future and hope to bring experts in neuropathology and related disciplines together to agree a way forward. All aspects of this assessment should be standardised as far as possible if any part of it is to be validated and applied to larger case series.

CHAPTER 5: A PROTOCOL FOR PRECISE COMPARISONS OF SMALL VESSEL DISEASE LESIONS BETWEEN EX VIVO MAGNETIC RESONANCE IMAGING AND HISTOPATHOLOGY

5.1 Introduction

My systematic review (Chapter 2) identified 28 papers comparing the radiological and pathological appearances of WMH, although the exact number of lesions studied could not be counted and many did not describe precise comparisons. Enlarged PVS, oedema and myelin pallor were the most frequent findings histologically. 26 radiological microinfarcts showed variable histological appearances, most often chronic changes with neuronal loss and gliosis. Five radiological lacunes corresponded to cavities on histological examination, with gliosis and axonal loss. Enlarged PVS on imaging are confirmed histologically and described primarily regarding features to enable distinction from lacunes; enlarged PVS were smaller, measuring less than 2x2mm on neuroimaging, without surrounding signal change.

The exact number of lesions compared in ex vivo imaging-histopathology studies is not known, however the overall conclusion from multiple systematic reviews (Gouw, Seewann et al. 2011, Shoamanesh, Kwok et al. 2011, Humphreys, Smith et al. 2021), is that the underlying histology of these radiologically-visible lesions is heterogenous and the underlying mechanisms of their development remain uncertain. My systematic review highlighted inconsistencies in reporting and methodology. If these were addressed, comparisons might be more reliable.

The small vessels affected by SVD are not visualised using standard MRI techniques (van Veluw, Arfanakis et al. 2022). Although perilesional changes, for example around lacunes (Hinman, Lee et al. 2015) and microinfarcts (Coban, Tung et al. 2017), have been described, methodical studies of the microscopic changes from the centre of lesions to distant

normal appearing tissue and of venous changes have not been performed but are needed.

Based on this, the cohorts and tissue available within the remit of the MRC Edinburgh Brain Bank and the resources at the University of Edinburgh, the following protocol was developed and implemented. The aim was to acquire a database of high-resolution MR images of post-mortem human brain tissue with sequences suitable to allow radiological study of SVD and registration with digitalised images of the corresponding histology to enable precise comparisons to be made.

5.2 A protocol for precise comparisons of small vessel disease lesions between ex vivo magnetic resonance imaging and histopathology

5.2 1 Background

Pathological studies are not dynamic, being limited to tissue taken at the time of death. In SVD research much of the pathological literature has focused on the lacune, which is relatively easily identified at autopsy, but is descriptive (Fisher 1982). Attempting to understand the pathophysiology is difficult (Bailey, Smith et al. 2012); pathological studies, especially with imaging correlations, are few (Pantoni and Garcia 1997, Gouw, Seewann et al. 2011), with little information on histopathological changes in and around SVD lesions seen on imaging and whether lesions vary by brain region (Murray, Vemuri et al. 2012). Systematic reviews of studies comparing post-mortem imaging and histology appearances (Gouw, Seewann et al. 2011, Shoamanesh, Kwok et al. 2011) reveal just three studies correlating 79 microbleeds identified on MRI with histopathology in SVD in 15 cases (Fazekas, Kleinert et al. 1999, Tatsumi, Shinohara et al. 2008, Schrag, McAuley et al. 2010), while one other paper described three cases with at least three microbleeds (Tanaka, Ueno et al. 1999). Five papers studied lacunes: two with 59 lacunes in 18 cases (Braffman, Zimmerman et al. 1988, Bokura, Kobayashi et al. 1998), one with four cases and at least four lacunes (Revesz, Hawkins et al. 1989), one with two cases and unknown numbers of

lacunes (Pullicino, Miller et al. 1995) and one study describing lacune appearances without any details of numbers of cases or lesions (Matsusue, Sugihara et al. 2006). There are greater numbers of studies looking at WMH, but their pathophysiology has not yet been fully elucidated (Wardlaw, Valdes Hernandez et al. 2015, Lin, Wang et al. 2017).

All previous post-mortem studies aiming to characterize SVD lesion appearances image whole brains, whole hemispheres or brain slices (Humphreys, Smith et al. 2021). Some studies have attempted to provide more detailed localization by scanning both whole brains and individual macroscopic coronal brain slices (Scarpelli, Salvolini et al. 1994, Murray, Vemuri et al. 2012). This is of value when assessing overall disease burden, but lesion locations are typically approximated using gross landmarks (Awad, Johnson et al. 1986) or tissue is sampled broadly from areas identified on imaging, precluding accurate comparison of individual lesions (Chimowitz, Estes et al. 1992). As such these studies cannot confidently correlate histology with imaging. This may, at least partly, explain the limited understanding of SVD pathogenesis, the lesion heterogeneity at a cellular level, and the modest associations described so far between imaging and clinical features.

The aim of this section was to develop a protocol to precisely compare the histological and radiological features of SVD in human post-mortem brain tissue, to test the hypothesis that different SVD lesions identified and defined on MRI represent specific histological lesions. By defining the histological lesions of SVD I could compare histological observations to clinical and in vivo radiological data. This would facilitate study of the pathophysiological mechanisms with the ultimate goal of defining potential therapeutic targets.

This study used brain tissues from the LINCHPIN intracerebral haemorrhage cohort and LBC1936 as groups with pathological and age-related SVD pathology respectively. These were compared with the sudden death control group.

5.2.2 Post-mortem neuropathological examination

A standard neuropathological post-mortem examination was carried out by at least one neuropathologist according to MRC Edinburgh Brain Bank protocols, extended for this study to include areas typically affected by SVD on MRI. The brain weight was recorded, the cerebellum and brainstem removed, and 1cm thick coronal sections were made. The cerebellum was sliced sagittally and the brain-stem axially. Samples approximately 2x2x1cm are taken from defined neuroanatomical areas (Table 5.1). As SVD is considered to be symmetrical we used tissue from the left cerebral hemisphere only (Wardlaw, Smith et al. 2013). The right hemisphere was also studied in 10% of cases, randomly chosen, to ensure this symmetry was true in our population. Each sample was bisected in the same plane as it was cut; one section was placed in a plastic cassette and fixed in 10% unbuffered formalin in a plastic tube for 24–72 hours before MR scanning and histology (Figure 5.1). The complementary sample is frozen in nitrogen vapor for long-term storage at 150°C to support future research applications.

Table 5.1 Areas affected by maximal radiological SVD in life selected for MR-histology comparison

BA Brodmann area

Area	Brodmann area
Anterior frontal parasagittal cortex	BA9
Broca's area	BA44/45
Temporal tip	BA38
Frontal, temporal, parietal, and occipital white matter	
Caudate nucleus	
Basal ganglia	
Hippocampus	
Hypothalamus	
Thalamus	
Cerebellum	
Pons	
Medulla	

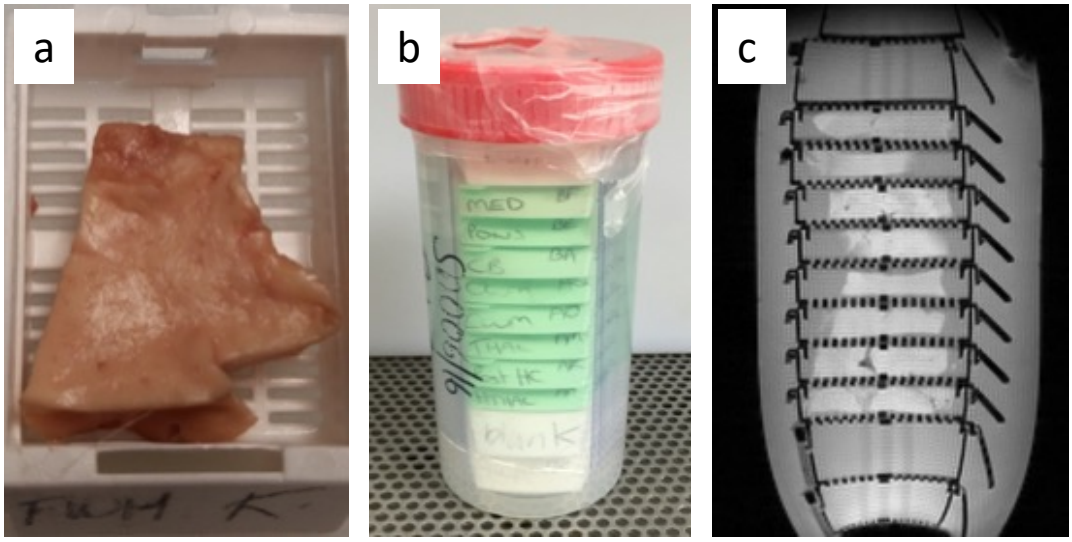


Figure 5.1 Small tissue samples are placed in plastic cassettes for standard histological processing

a) Eight cassettes are stacked in a plastic container and fixed b) before scanning in a small bore 7T MRI scanner c) (gradient echo scout). Tissue is only placed in the cassettes where the gradient coil is mostly linear, empty cassettes at each end and folded plastic along the length of the stack prevent movement within the container.

5.2.3 Post-mortem magnetic resonance imaging

Through pilot work (Chapter 3), we developed the most practical approach to satisfy both our requirements to make precise histopathological comparisons and to obtain excellent quality images. To minimize air bubble artefact, the lid of the container was secured under formalin cover and left to stand for 5 minutes, it was tapped to release trapped air and then the lid re-secured under formalin cover. The cassettes are held by pieces of plastic at the sides with empty cassettes at each end to prevent movement. The tissue is scanned overnight in a 7T small-bore rodent MRI scanner (Agilent Technologies, Yarnton, UK) equipped with a 400 mT/m gradient insert with sequences similar to those used *in vivo* to detect evidence of SVD (Table 5.2). The long acquisition time (135 minutes) increases sensitivity to small, subtle features. For all scans (except the scout), the field of view is 60x60mm, the slice thickness is 1mm with no gap orientated axially,

resolution 0.23x0.23x1.0mm, 30 slices are obtained across the cassettes containing the tissue. For the scout scan, the field of view is 120x120mm, slice thickness 2mm with a 2mm gap in three planes. Shimming is done on the entire plastic container using an automated routine for global shimming followed by manual adjustment of the shim coils. This optimizes the homogeneity of the magnetic field to avoid artefact on images. Quality of shim was checked by measuring the 50% linewidth of the H2O peak in an unlocalized 1H spectrum. Typical values were 50–60Hz. We are not aware of any established systems for grading imaged tissue blocks and the SVD burden therein. We therefore adapted existing protocols for assessing SVD in whole brain MRI which were developed, validated and applied in previous studies of SVD including LBC1936 and LINCHPIN (Wardlaw, Doubal et al. 2009, Wardlaw, Bastin et al. 2011) and have been tested in these studies over the past two decades. These existing protocols for assessing SVD on MRI are now included in international standard definitions (Wardlaw, Smith et al. 2013). MR and histological disease burden assessment was performed independently, blinded to clinical and all other data.

Table 5.2 MR imaging sequences and their parameters

FLAIR: fluid attenuated inversion recovery; GE: gradient echo; FSE: fast spin echo; TE: echo time; TR: repetition time; TI: inversion time; NEX: number of signal averages.

Sequence	Scout	T2	T2*	T1	FLAIR
Type	GE	FSE	GE	FSE	FSE
TE (ms)	3.9	53	22	9.2	40
TR (ms)	23.3	2500	801	700	8000
TI (ms)					1816
Flip angle (º)	20	90/180	20	90/180	90/180
Echo spacing (ms)		13.25			20
Echo train length		4			2
Band width (Hz)	52k	78k	50k	100k	50k
Matrix	256x256	256x256	256x256	256x256	256x256
NEX	2	8	6	4	4
Acquisition time (minutes)	0.2	21.3	20.5	12	68.4

Table 5.3 Special stains and immunohistochemical stains used for assessment of SVD, vascular and neurodegenerative pathology

Stains	Concentration	Antigen retrieval	Manufacturer	Feature assessed
Cut at 4um:				
BA4	1:100	Formic acid	Dako, Glostrup, Denmark, M0872	Amyloid plaques, cerebral amyloid angiopathy
Tau	1:2500	None	Thermo Fisher Scientific, Illinois, US, MN1020	Neurofibrillary tangles
a-synuclein	1:200	Pressure cooker and citric acid	Thermo Fisher Scientific, Illinois, US, AHB0261	Lewy bodies
Myelin basic protein	1:500	Formic acid	Abcam, ab77895	Myelin
Neurofilament heavy	1:500	Citric and formic acid	Abcam, ab8135	Axons
CD163	1:1000	Pressure cooker and citric acid	Abcam, ab87099	Macrophages
Claudin-5	1:250	Pressure cooker and citric acid	Abcam, ab15106	Endothelial tight junctions
Collagen-1	1:1000	Pressure cooker and citric acid	Abcam, ab90395	Vascular media
Platelet derived growth factor receptor ß	1:100	Pressure cooker and citric acid	Abcam, ab32570	Pericytes
Smooth muscle actin	1:1000	Pressure cooker and citric acid	Dako, Glostrup, Denmark, M0851	Vascular smooth muscle
CD68	1:100	Pressure cooker and citric acid	Dako, Glostrup, Denmark, M0876	Activated microglia
Glial fibrillary acidic protein	1:800	None	Dako, Glostrup, Denmark, Z0334	Astrocytes
Cut at 6um:				
H&E				General structure
Masson trichrome				Connective tissue
Luxol fast blue				Myelin
Perl's				Iron

5.2.4 Histology

After scanning, the formalin-fixed tissue was paraffin-embedded in its entirety and sections were stained based on previously published data from histological and imaging literature to assess the gliovascular unit and general neuroinflammatory and glial responses (Table 5.3). SVD burden (Deramecourt, Slade et al. 2012), Alzheimer's disease pathology (Thal, Rub et al. 2002, Braak, Alafuzoff et al. 2006), a-synuclein (Attems, Toledo et al. 2021) and amyloid angiopathy (Love, Chalmers et al. 2014) were graded using published, validated systems. Slides were digitally scanned using the Zeiss Axioscan system.

5.2.5 Image registration and analysis

The MR slice that best matched the histology section was selected visually, and the corresponding slice for each MR sequence was transformed into the Neuroimaging Informatics Technology Initiative (NIfTI) format.

The size of the histology image varies but is of the order of 10–20 thousand pixels in each dimension. To facilitate registration, they are rescaled by a factor of 1/20 using a Mitchell–Netravali kernel and converted to grey levels. To ensure successful registration, the histology images needed to be reoriented to match roughly the position of MR images, which in some cases involved flipping the image around the x or y axis. The histology samples were cut to be approximately rectangular in shape and kept in alignment with the rectangular cassettes. Due to the standardised nature of the histological processing methods, there were only a limited number of opportunities for manipulation and for the image to be rotated away from the position in which it was scanned. Therefore, there were only four possible orientations of the histology sample. The reorientation was done automatically by creating the four possible orientations of the histology image (original, flipped in x, flipped in y, flipped in x and y), registering each to the T1-weighted image (detailed below) and calculating a similarity score (normalised mutual information)

between the histology and MR in each case. The highest similarity score corresponded to the best match between histology and the T1-weighted image and therefore permitted automatic selection of the correct histology orientation. An image with the outline of the MR overlaid on the histology was produced for each sample to enable a rapid visual confirmation of whether the registration had been successful (Figure 5.2c). The automatic reorientation gave a satisfactory registration in >85% of the cases. In the cases where it failed, the histology was reoriented manually before registration, which then completed successfully.

Automatic registration of MR to each histology image was performed as follows. First, the T1-weighted image was used to create a binary mask of the tissue using k-means clustering with three clusters. The binary mask was created by setting the pixels in the cluster of the maximum centre to 1 and the remaining pixels in the image to zero. This mask was applied to all MR images to exclude background signal and then cropped to the minimum field-of-view containing the tissue. Linear registration was then performed between the T1-weighted and histology images using NiftyReg over five levels of progressively finer resolution, with default settings. The transformation obtained was applied to the other MR modalities of the same slice, to obtain their registered versions (Figure 5.2). All registered MR images and the resampled histology were then saved in NIfTI format for visualisation (MRIcro). All processing was performed in R (version 3.4) within RStudio (version 1.0), using the packages ‘‘jpeg’’, ‘‘divest’’, ‘‘mmand’’, ‘‘RNifti’’, and ‘‘RNiftyReg’’. The registered images were visualised and SVD lesions identified and described during grading were selected in one modality and automatically identified in the other, which allowed accurate characterisation and comparison across all MR sequences and histological stains (Figures 5.2 and 5.3).

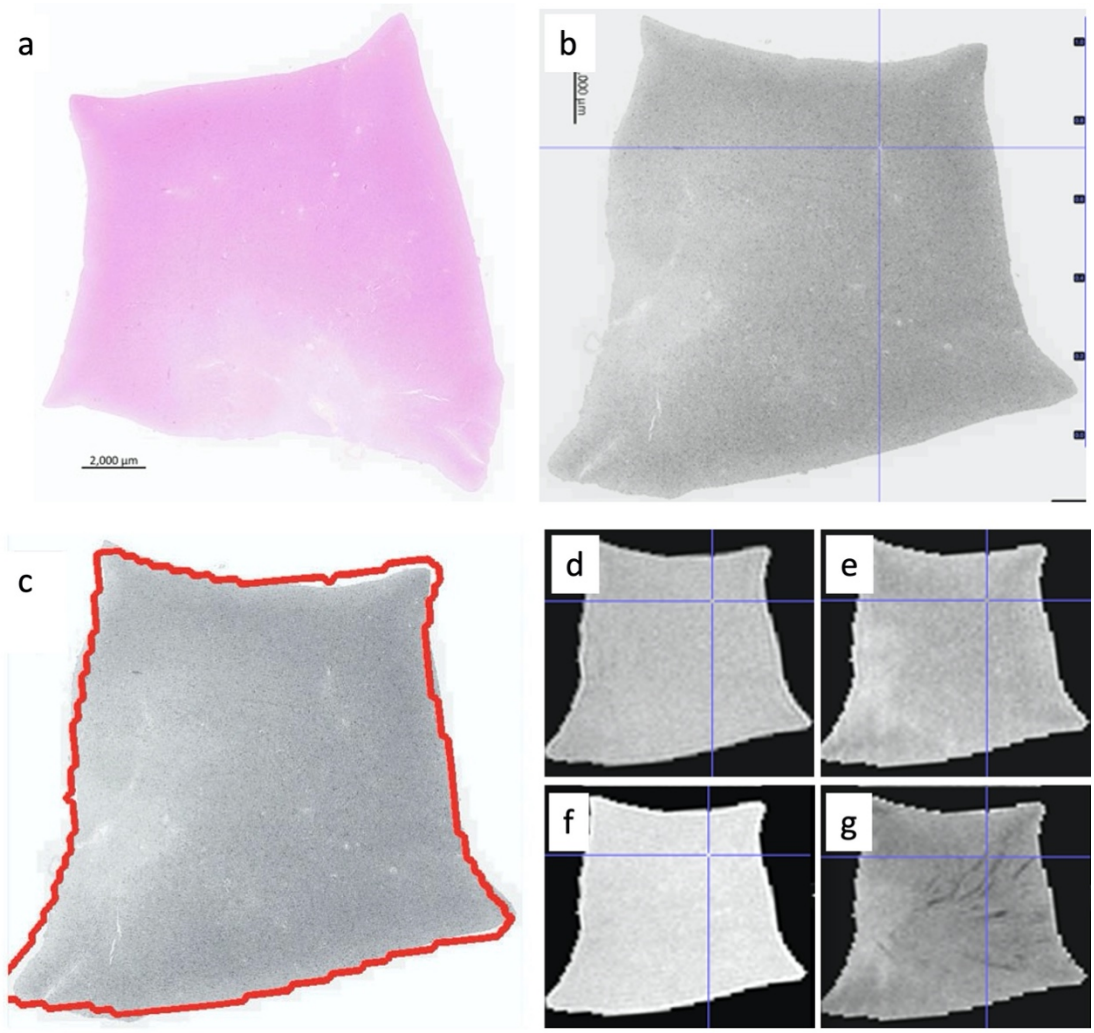


Figure 5.2 A sample of frontal white matter, where the lack of anatomical landmarks can make comparison difficult.

a)The digitalised histology slide (H&E) is b) made black and white, reoriented and registered with the imaging sequences. c) An initial ‘‘quick check’’ image is produced with the MR outline in red overlaid on the registered black and white histology image to confirm successful registration with d) FLAIR, e) T2, f) T1 and g) T2* MR sequences. Features of interest are selected on any image using the blue crosshairs visible in b) and d-g) and the precise corresponding feature on the other images is identified automatically. In this example, a prominent vessel on the MR sequences (d–g) and histology (b) has been identified and is further examined in Figure 5.3. The shape of the tissue sample and any lesions can also help orientate the images, in this case a radiological WMH visible on the left hand side of the tissue in the e) T2 and g) T2* images corresponds with the histological area of white matter pallor at the bottom of a) the unregistered H&E and the left hand side of b) and c) the registered black and white histology images.

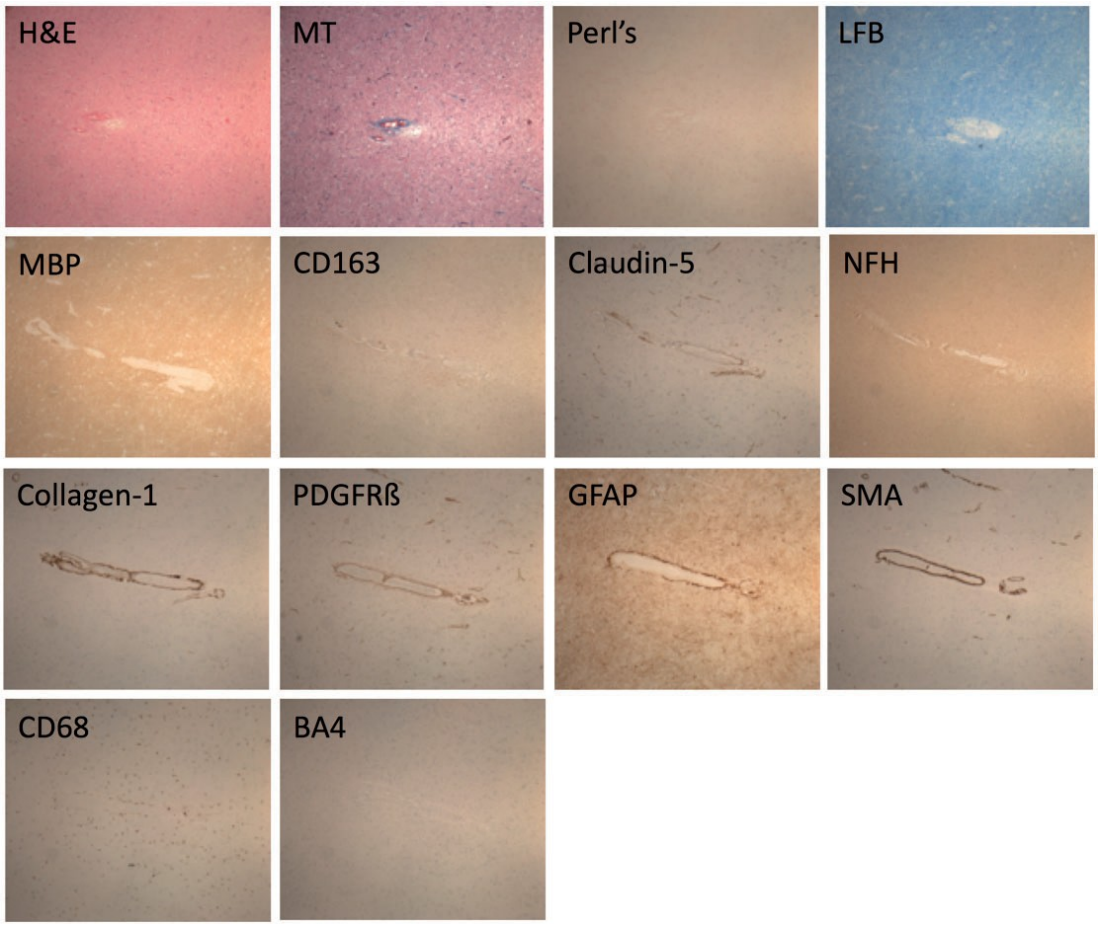


Figure 5.3 The white matter vessel identified in Figure 5.2 is stained to interrogate the gliovascular unit and blood–brain barrier

The course of the vessel identified in the crosshairs in Figure 5.2 b,d-g) is followed on consecutive histological sections enabling the distribution and pattern of protein expression to be described, all x40.

Scanning was done overnight on two consecutive nights. The registration was automated and lesion comparison required several hours, depending on the number of lesions identified. The whole process from autopsy to lesions being compared took about one week.

Both MR and histology quality were excellent; histology, in particular is unaffected by the scanning process (examples in Figures 5.2 and 5.3).

In establishing this protocol, we carefully considered how to minimise bias. All consecutive cases donated to the brain bank that meet the specific cohort and brain bank criteria were coded and processed using standardized procedures. Cases were batched until there are between 5 and 10, then rated at the same time. MR and histology ratings were carried out independently, blinded to cohort, clinical data and all other diagnoses and were based on validated guidelines as far as possible.

5.2.6 Study outcomes

5.2.6.1 Primary outcomes

- Identify and define the pathological lesions of SVD on tissue sections, in relation to the lesions seen on neuroimaging.

5.2.6.2 Secondary outcomes

- Further understanding of gliovascular unit abnormalities from protein expression studies using additional stains and immunohistochemistry.

- Group cases by SVD severity as graded on MRI and histology for future assessment of protein and gene expression.

- Develop a reproducible protocol that can be adapted to study clinical–radiological–pathological correlations in other neurological diseases.

See section 5.4 below for further modifications in practice. The results of the comparisons performed using this protocol are presented in Chapter 6.

5.2.7 Estimates of likely numbers of cases.

We estimated that about 18 brains could be scanned per annum for all three cohorts in total, based on previous years rates of accrual. We began scanning in 2015 and have carried out this protocol in 53 cases to date; 21 LINCHPIN, 9 LBC1936 and 23 controls. Of these, 25 have also had in vivo

MRI or CT brain imaging (17 LINCHPIN, 8 LBC1936). In comparison with existing literature, this sample is one of the largest to date, and the only one to precisely and systematically study the areas most affected by SVD with in vivo imaging. It will allow for much greater depth of analysis regarding, for example, spatial variation in lesions, perilesional changes and severity of lesions. Numbers will increase as we continue to scan cases and include new cohorts.

5.2.8 Statistical analyses.

Specific statistical analyses depend on the distribution of the data and number of cases; they include descriptive statistics for lesion prevalence and appearances, and regression analyses for differences between groups. We assessed a number of relevant features to study from the rich clinical, imaging and histological data available. For example, LBC1936 subjects have serial research-standard MRI in life with detailed assessment of SVD features including quantitative structural and functional analysis, medical histories and cognitive information from age 11 to the 8th decade. Linchpin includes current cognition, medical history and recent in vivo imaging. This will enable associations to be studied where information is currently missing such as the burden of SVD lesions visible in life and the prevalence of matrix protein abnormalities; the relationship between perivascular space visibility on MRI and numbers of active microglia; and confirm if the health of the myelin and axons in apparently normal tissue varies with the severity of WMH as is suggested by in vivo MRI (Maniega, Valdes Hernandez et al. 2015). Control cases have medical and social history available. However, by definition they have had no neurological disease in life, have no cognitive impairment and therefore do not have in vivo imaging. These data can be compared to the extent and severity of SVD assessed on the ex vivo imaging and histology. The extent of the analyses will be decided based on the final number of cases obtained.

After MRI and histology images are fully assessed, I aimed to stratify cases into groups with and without cognitive impairment, by medical history, and SVD burden, from none to severe. The complementary frozen tissue would be used for targeted studies of gene expression differences between the groups. In particular, the short tissue fixation period retains RNA and DNA integrity supporting novel techniques such as BaseScope, a modified, quantifiable in situ hybridization technique identifying transcripts at a single cell level (Mehta, Selvaraj et al. 2020).

5.3 Progress with implementation and discussion

Several issues were encountered while developing this protocol. Air bubbles within the tissue and plastic cassettes caused MR artefact and could be mistaken for, or mask, microbleeds on T2* sequences, making it important to minimise their presence, as described. Previous studies did not precisely match lesions on MR with histological images due to differing slice thicknesses and resolutions. We obtained serial 1mm MR slices through each tissue block, although this is of a different order of thickness to the histological sections (mm versus μm). To make the most accurate comparison, the MR images were compared to corresponding histological images and the most complementary were registered. Formalin fixation of human brain tissue alters the MR properties of the tissue with time as the formalin diffuses into it (Dawe, Bennett et al. 2009). The use of small samples minimizes the difference in fixation between the deep and superficial tissue. T2 values of human brain tissue change with duration of fixation but plateau between 10 hours and five weeks (Dawe, Bennett et al. 2009). We standardized tissue fixation to minimise fixation-induced variability between MR images. At 7T, tissue is vulnerable to overheating, which impairs tissue quality. Brain absorbs more radiofrequency than other tissues and our samples are in a relatively small amount of formalin without in vivo mechanisms, such as vasodilation, to dissipate heat. The scanner bore was cooled to 22.6^{o}C but this may not be sufficient. Our scanning protocols were been designed to maximize anatomic resolution and increase the signal to

noise ratio while avoiding over- heating. Temperature monitoring during scanning showed a maximum 1.8^{o}C rise (Figure 3.2), which would not affect tissue quality and heat artefact was not observed on histological examination.

As with many post-mortem studies, the number of cases available for study was relatively small. However, this is one of the largest detailed post-mortem studies of SVD, and benefited from detailed data linkage and well-characterized cohorts. In addition, we employ extensive sampling of each case, targeting areas particularly affected by SVD and retaining complimentary frozen tissue for further interrogation with genomic technologies. The specific areas studied may be refined in future depending on the specific disease or characteristic under investigation. Pilot work within our laboratory has shown that formalin fixed paraffin-embedded tissue is not suitable for post-mortem imaging so retrospective imaging of cases with paraffin-embedded tissue is not possible. However, the histological protocol developed from the combined radiological–histological assessment could be applied retrospectively to appropriate tissue within a Brain Bank with relevant clinical data, thereby further extending the sample size for future related work using biochemical and genetic methods.

SVD lesions are well characterized on neuroimaging and described on neuropathology (although not consistently (Alafuzoff, Gelpi et al. 2012)); however, attempts to correlate appearances have found only modest associations (Gouw, Seewann et al. 2011). This may reflect variation in methodologies or true variation as suggested in rodent models where it appears SVD may result from multiple minor defects in different components of the neurovascular unit (Bailey, McBride et al. 2014) which we aim to study further with this protocol and future work. As a static assessment of a dynamic disease process, histopathological assessment may be limited; lesions at post-mortem in elderly patients are often end-stage. However, longitudinal assessments in life allow plotting of disease trajectories, and our

initial work suggests a gradation from subclinical, to lesions-in-evolution to severe lesions which will further inform the interpretation of SVD pathophysiology. WMH, in particular, may be more dynamic than previously appreciated (Wardlaw, Valdes Hernandez et al. 2015). Histopathological studies in humans have found protein expression abnormalities within the gliovascular unit in subjects with WMH (Chen, Akinyemi et al. 2016) and in vivo imaging suggests BBB dysfunction and leakiness (Wardlaw, Doubal et al. 2009). Alterations in the gliovascular unit are seen in an animal model prior to the onset of recordable hypertension (Bailey, Smith et al. 2011).

In summary, this protocol describes a new method to precisely assess and compare lesion appearances between brain MRI and histopathology to validate in vivo MRI findings in and around SVD lesions, aiming to increase our understanding of SVD pathophysiology and facilitate a meaningful clinical and radiological diagnosis. These methods and tissue may also be used in other conditions where the pathophysiology is poorly understood and to validate clinical and radiological assessments and diagnoses.

5.4 Protocol development

There have been some minor changes and developments since this protocol was published. It was always intended to be dynamic and responsive in line with the systems it involves – the mortuary, the neuropathology histology laboratory and BRIC. These groups all have other demands upon their time and it is vital everything can work together without compromising any research or clinical work.

The original scanning protocol utilised a 1mm scan thickness and a 1mm gap. However, if the 4μm thick piece of tissue examined on histology is taken from the 1mm gap, none of the lesions within it will be represented on the scan. We reviewed and modified the scanning protocol, and scanning is now performed twice for the four sequences, the second scan being offset by 1mm compared to the first, so that the whole of the tissue is contained within

the MR images. The MR images and the histology are examined by eye and the MR slice that contains the histological section is chosen for the registration.

Since this work was published a new MR scanner (9.4T) has been acquired. This is now used to scan all post-mortem brain tissue resulting in higher resolution sequences (Table 5.4) (Figure 5.4). The field of view is 60x60mm. The FLAIR inversion time (TI) had to be altered as it was not attenuating the signal from the surrounding fluid, most likely due to the strength of the formalin solution. Most often a TI of 1600ms is used.

As we applied the registration method to more cases a number of minor issues became apparent and some improvements have been made to improve the workflow. For example, the mask was sometimes applied to the wrong MR slices in some sequences, or the algorithm chose a different slice to the one specified.

Table 5.4 Updated MR imaging sequences and their parameters

FLAIR fluid attenuated inversion recovery; GE gradient echo; FSE fast spin echo; TE echo time; TR repetition time; TI inversion time; NEX number of signal averages

Sequence	Scout	T2	T2*	T1	FLAIR
Type	GE	FSE	GE	FSE	FSE
TE (ms)	3.9	43	18	9.2	40
TR (ms)	23.3	3500	675	700	8000
TI (ms)					1500-1750
Flip angle (°)	20	90/180	20	90/180	90/180
Echo spacing (ms)		13.25			20
Echo train length		4			2
Band width (Hz)	52k	78k	50k	100k	50k
Matrix	256x256	256x256	256x256	256x256	256x256
NEX	2	8	6	4	4
Acquisition time (minutes)	0.2	21.3	20.5	12	68.4

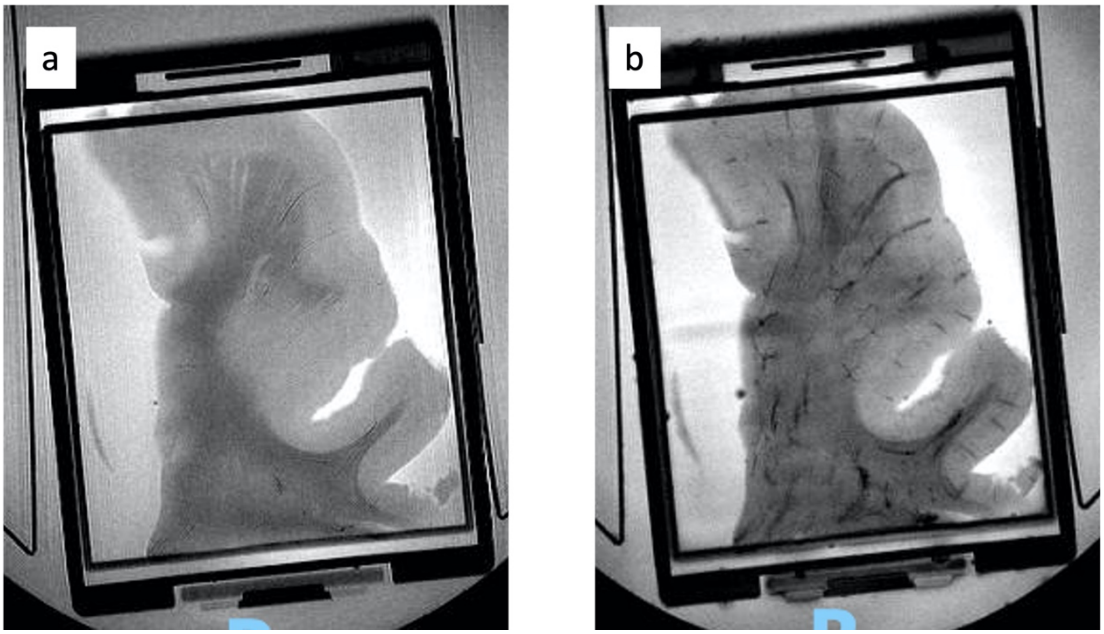


Figure 5.4 High resolution ex vivo 7T MRI scans of small brain tissue samples

a) T2 and b) T2*



Figure 5.5 Significant cracking artefact sometimes seen on histology, making registration with the post-mortem MR impossible

The only way to carry out a precise lesion comparison is to be sure the MR image contains the histological section. We carried out tests on a selection of cases. We used a slice browser to automate the selection of the MR slice that corresponds to the histology (Table 5.5). However, it chose the wrong MR slice in 72% (n=23). This would not be reliable without checking each one, making the automation redundant. It would often choose a nearby slice where the outlines matched better, but it was obvious from the internal detail of the section that they were not the same. It also struggled particularly with sections that lacked distinctive anatomical features, most often white matter tissue blocks with a relatively homogenous internal appearance. We had to find a compromise between the level of automation and accuracy. This has resulted in manual slice selection, with automated orientation which resulted in the correct slice being chosen in 84% (n=27). Of the five not correctly matched, there had been an error in the algorithm in four, which could be fixed manually. In one, significant cracking in the histology meant registration would not work even with manual intervention and it would be excluded (Figure 5.5). In all five, the errors were significant and obvious at the point of lesion comparison, so in subsequent comparisons manual checking of the registration process was not necessary.

Table 5.5 Comparison of image registration methods

Number of correct and useable registered images compared to incorrect and unusable registered images when the MR slice corresponding to the histology was chosen by the algorithm or manually. When the slices were chosen manually, four could be registered with some manual intervention, only in one was the histological artefact too significant (cracked tissue) that the images could not be registered and it had to be excluded. When the slice browser chose the MR slice, 23/32 (72%) were incorrect, rendering the method, and any subsequent lesion comparisons using it, unreliable.

Method	Correct	Incorrect	Reasons
Automated slice browsing	9	23	Wrong slice chosen (19) Histology artefact (2) Incorrect orientation (1)
Slice manually chosen	27	5	Algorithm error (4) could be fixed manually Histology artefact (1) excluded

5.5 Conclusions

The technology involved in these methods is constantly developing and improving and so we have adapted with it. The images obtained from the new 9.4T MRI scanner are much clearer and more detailed, and the improvements made to the registration methods have made it easier and faster to use. The resulting registered images are more accurate and reliable.

There is still room for improvement, particularly in the registration method. Theoretically it could be further automated so it is able to select the corresponding MR and histology images automatically. However, this requires knowledge and experience of neuroimaging, neuroanatomy and histology to interpret subtle features in three dimensions, in the context of external influences such as fixation and artefact due to processing methods. Currently there is no software available that can do this, and I feel we are using the optimum method based on the technology available. However, in the future it may be further improved and could make registration and comparison of lesions in all tissues across imaging and histopathology possible, with potential extension to molecular studies.

The size of the scanned histological images has also hindered our registration, as the file size is often so large that they cause problems running programmes that attempt to open them. The method we have developed uses a compressed black and white histology image for the registration. Lesions can be identified and pinpointed on it but must be examined at high magnification on the glass slide using light microscopy. We explored online slide scanner systems, such as the Philips Digital Pathology platform, that are in clinical diagnostic use. They offer excellent high-resolution viewing of histological slides without compromising the speed of the software, but we were not able to integrate the images and technology to allow us to register them with the MR images. This could be a possible future development, but it would need to be seen to be attractive by the commercial companies developing these systems.

Supplemental funding has been acquired by the MRC Edinburgh Brain Bank since this project was started, to carry out post-mortem scanning on an additional cohort representing mild cognitive dysfunction. The registration methods we developed are now also being applied to study mineralisation such as iron deposition in the basal ganglia in small vessel disease. The appearances on imaging and histology are being compared and quantified to understand the significance of this relatively common finding. Work on these projects is not included in this thesis but they represent an important investment in what this work has established and in developing the application of these methods in the future.

CHAPTER 6: RESULTS OF EX VIVO ASSESSMENTS

6.1 All scanned cases

6.1.1 Demographics

71 cases underwent post-mortem MRI scanning between June 2015, when the scanning protocol was implemented, and May 2018 (10 LBC1936, 26 LINCHPIN; 35 sudden death cohort cases, sudden death cases were scanned from 2016 onwards). 16 cases with Alzheimer's pathology (Braak stage ≥4, Thal phase ≥4), Parkinson's disease pathology, Lewy body pathology or other significant non-SVD neuropathology and those where there was significant scanning artefact or fragmented histology, precluding assessment, were excluded. 55 cases underwent subsequent assessment of SVD burden (10 LBC1936, 20 Linchpin, 25 sudden death) (Table 6.1). Individual subject details are in Appendix 8.

20 of the total cases were female (36%; 4 LBC1936, 10 LINCHPIN, 6 sudden death) (Table 6.1). This amounted to half of the LINCHPIN cases and almost half of the LBC1936 cases, the sudden death cohort had the greatest gender imbalance. The median age overall was 69.56 years, the sudden death cohort (median 57 years) being significantly younger than both LBC1936 (median 79 years, $p = 0.0008$) and LINCHPIN (median 85 years, $p < 0.0001$) (Figure 6.1a).

Table 6.1 Summary demographic details for all cases undergoing post-mortem MRI scanning with subsequent grading of SVD burden

Y years, h hours, n number of cases, IQR interquartile range, LBC1936 Lothian Birth Cohort 1936, LINCHPIN Lothian Study of INtraCerebral Haemorrhage, Pathology, Imaging and Neurological Outcome, SD sudden death cohort

Cohort	n	Female, n	Age at death, y, median (IQR)	Duration of final illness, h, median (IQR)	PMI, h, median (IQR)	pH, mean (SD)	RIN, mean (SD)	Cardiovascular disease, n
LBC1936	10	4	79 (79-79)	120 (36.02-192)	72 (59.75-73.5)	6.08 (0.21)	4.91 (1.17)	9
LINCHPIN	20	10	85 (80-87.25)	120 (48-192)	57.5 (42-83)	6.26 (0.28)	4.97 (0.99)	16
SD	25	6	57 (46-67)	0.96 (0.42-1.63)	94 (71-103)	6.19 (0.19)	6.32 (0.87)	20
Total	55	20	75 (57-81)	6.3 (0.97-120)	74 (58-97.5)	6.19 (0.24)	5.58 (1.18)	45

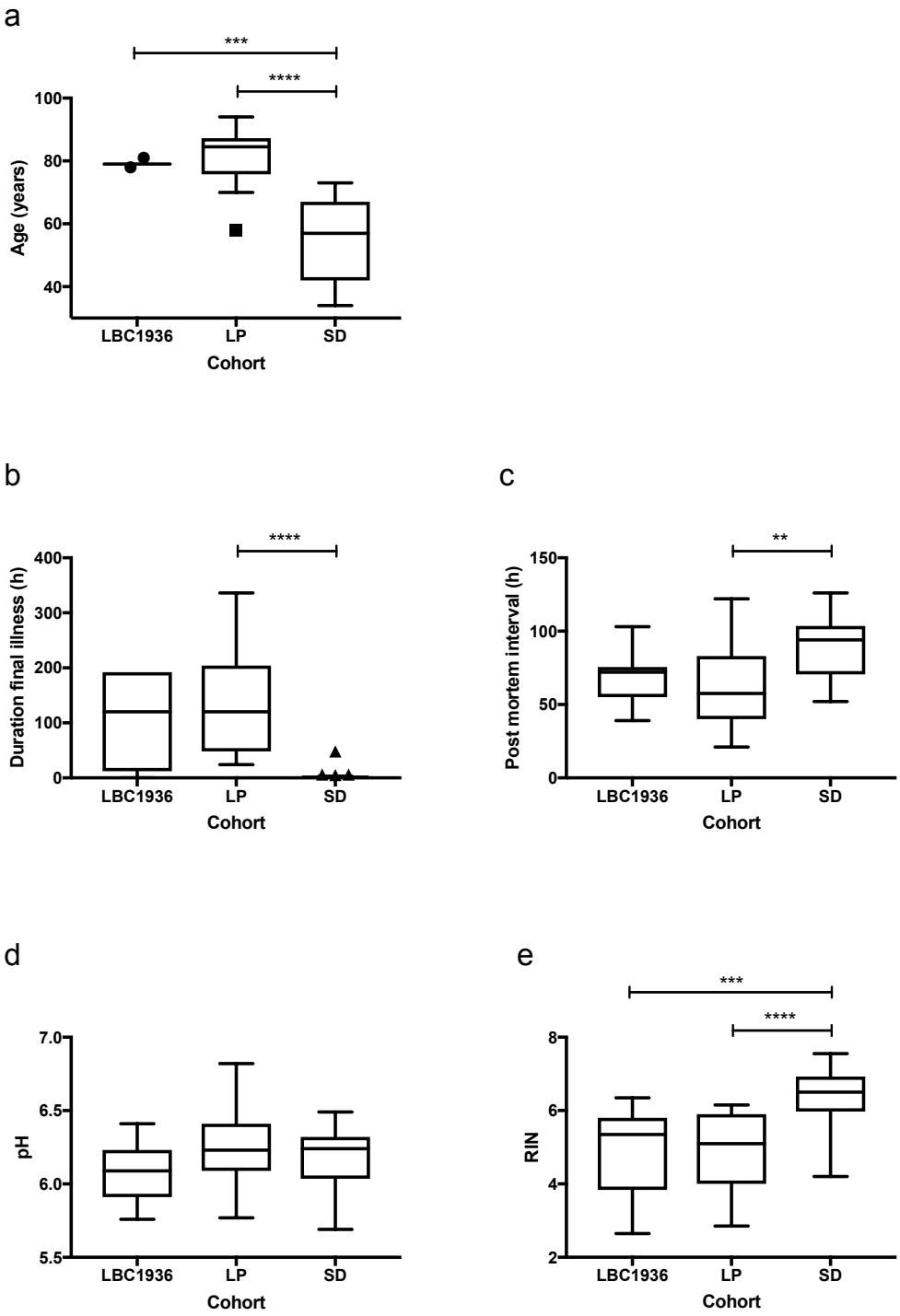


Figure 6.1 Comparisons of cohort features in cases that underwent post mortem MRI

Tukey boxplots showing comparisons of a) age, measures that may affect tissue quality: b) duration of final illness and c) post mortem interval and measures of post mortem tissue quality d) pH and e) RIN. The boxes indicate the median and inter-quartile range (IQR), with outliers beyond 1.5 IQR plotted individually. ** $p < 0.01$, *** $p < 0.001$, **** $p < 0.0001$. LBC1936=Lothian birth cohort 1936; LP=Lothian Study of INtraCerebral Haemorrhage, Pathology, Imaging and Neurological Outcome; SD=sudden death cohort; h=hours; RIN=RNA integrity value.

6.1.2 Post-mortem information

The duration of final illness often needed to be calculated from the clinical history or autopsy report, it was included only where it could be confidently estimated to within 2 hours (n=46; 5 LBC1936, 17 LINCHPIN, 24 sudden death) (Figure 6.1b). The median duration of the terminal illness was 84.23 hours overall, the sudden death cohort had a significantly shorter duration of terminal illness (median 0.96 hours) compared to LINCHPIN (median 120 hours, $p < 0.0001$).

The sudden death cohort (median 94 hours) had a significantly longer PMI compared to LINCHPIN (57.5 hours, $p = 0.009$) (Figure 6.1c). Assessing measures of post-mortem tissue quality showed no difference between the measured pH in the different cohorts (LBC1936 mean 72 hours, Linchpin 57.5, sudden death 6.19) (figure 6.1d) but the RIN value was significantly higher in the sudden death cohort (mean 6.32) compared to both LINCHPIN (4.97, $p < 0.0001$) and LBC1936 cases (4.91, $p = 0.0019$) (Figure 6.1e). The RIN value correlated negatively with both increased age ($r = -0.54$, $p < 0.0001$) (figure 6.2a) and longer duration of final illness ($r = -0.53$, $p = 0.0002$) (Figure 6.2b) but showed a positive correlation with increased PMI ($r = 0.27$, $p = 0.045$) (Figure 6.2c).

The most common cause of death was ischaemic heart disease (n=20) followed by intracerebral haemorrhage (n=9) and pneumonia/pneumonitis due to aspiration (n=8) (Figure 6.3, Appendix 8). The cause of death was not available at the time of autopsy in three cases. The most common cause of death in LBC1936 was pneumonia and metastatic malignancy (n=3 each), in LINCHPIN it was ICH (n=8) and in SD ischaemic heart disease (n=19).

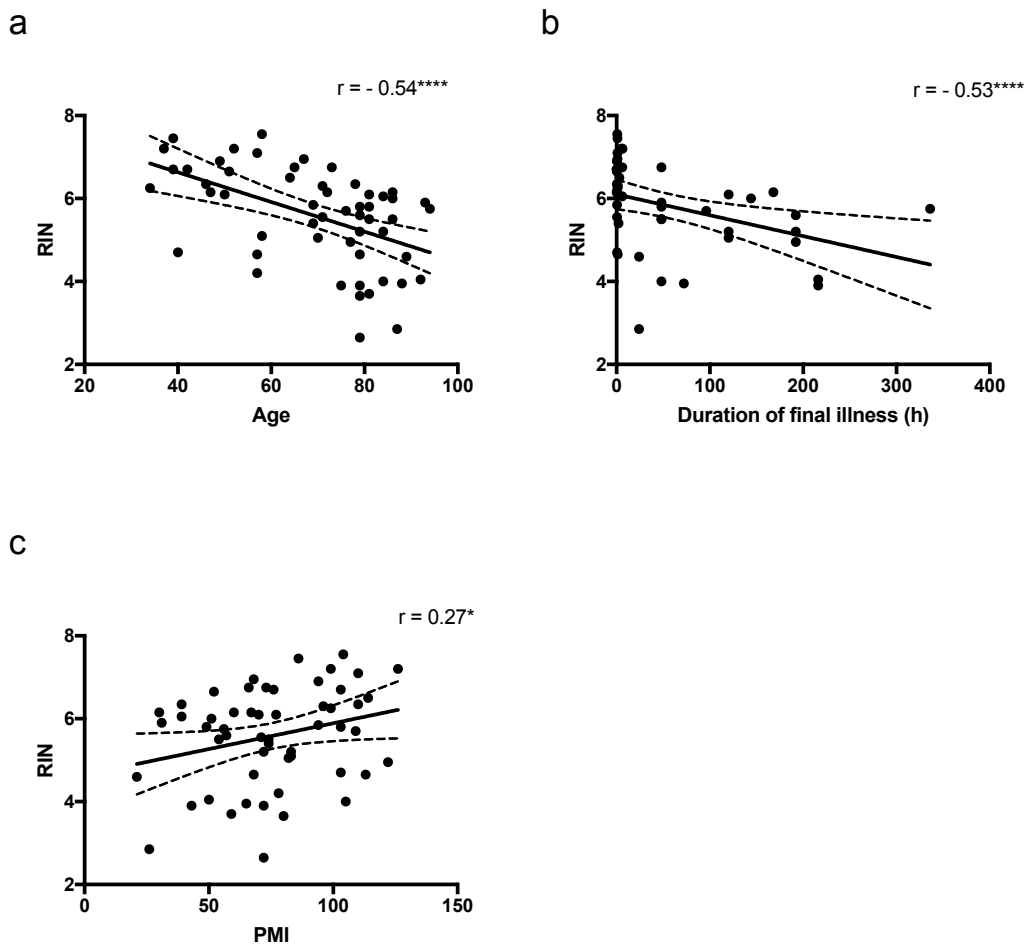


Figure 6.2. Scatterplots showing correlations of RIN value and factors that could affect tissue quality

There was a significant negative correlation with a) increasing age and b) longer duration of final illness and a significant positive correlation with c) post-mortem interval. Each point in the scatterplots indicates a single brain. The best-fit linear regression lines and 95% confidence intervals are superimposed. * $p < 0.1$, **** $p < 0.0001$

6.1.3 Medical conditions

Including autopsy findings, cardiovascular disease was present in 45 individuals, eight had no cardiovascular disease and data was not available in two cases (Figure 6.4). Hypertension (n=24) was most prevalent, followed by ischaemic heart disease (n=23), atrial fibrillation (n=8) and hypercholesterolaemia (n=7).

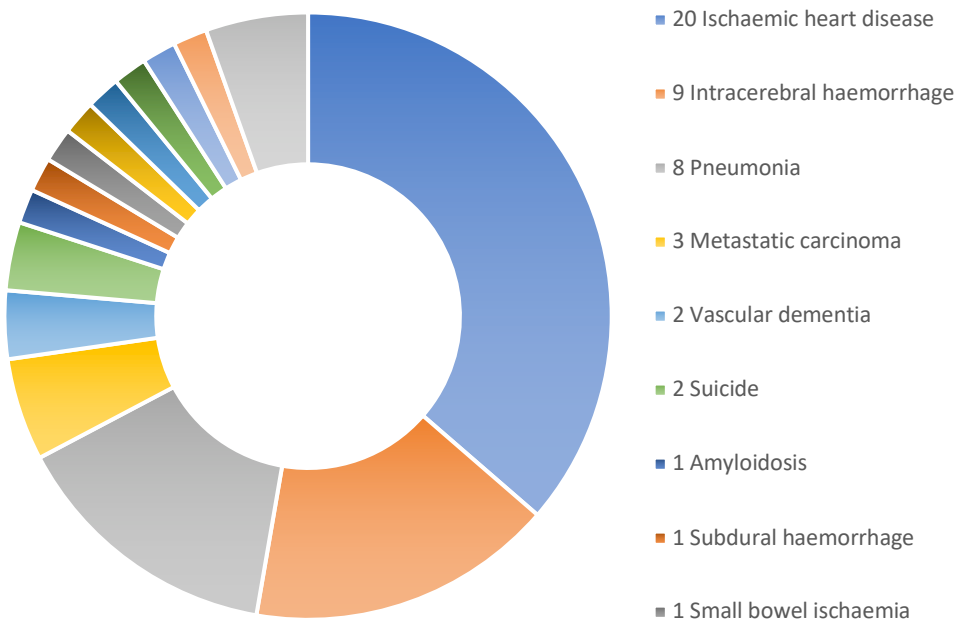


Figure 6.3 Frequency of causes of death in cases used to assess SVD burden on imaging and histology

The key lists the cause of death from section 1a of the medical cause of death certificate. They are show on this doughnut chart in order of frequency beginning at 12 o'clock and proceeding clockwise.

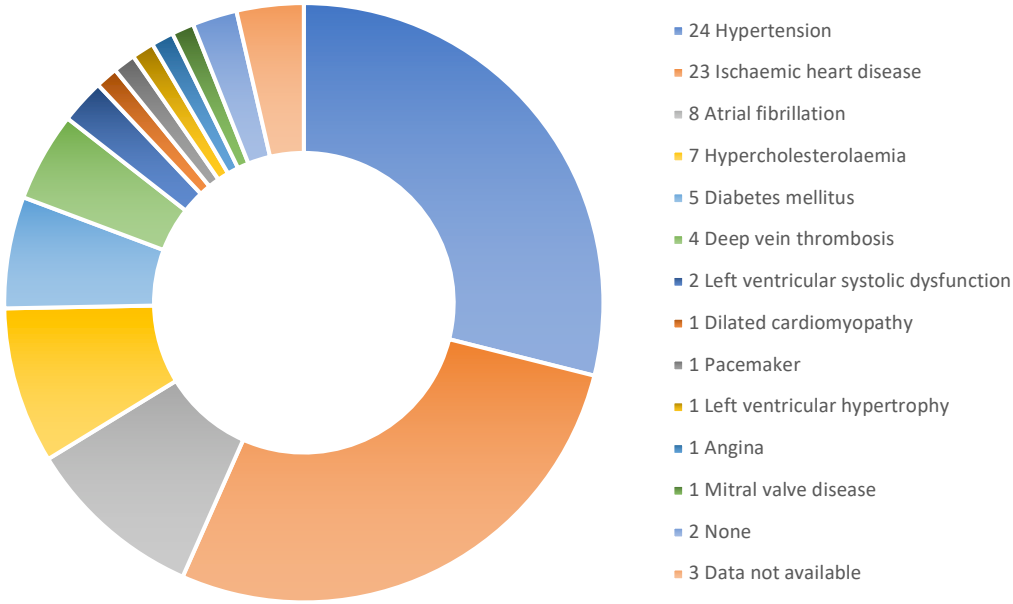


Figure 6.4 Frequency of cardiovascular disease in cases used to assess SVD burden on imaging and histology

Including information from the clinical history and autopsy where available. They are listed on this doughnut chart in order of frequency beginning at 12 o'clock and proceeding clockwise.

At the time of death, 16 individuals were current tobacco smokers, 13 had previously smoked, eight had never smoked. Smoking data was not available for 18 (Appendix 8). Three individuals had no known conditions in life, these all died suddenly of ischaemic heart disease. Full clinical data was unavailable for three sudden death cases, two died of ischaemic heart disease and one of small bowel ischaemia (Appendix 8).

Other, non-cardiovascular conditions were present in 46 individuals, the most common being intracerebral haemorrhage (n=22, 20 of which in LINCHPIN), malignancy in 10, chronic obstructive pulmonary disease in six, stroke events in eight (4 ischaemic stroke, 1 lacunar stroke, 2 transient ischaemic attacks, 1 not otherwise specified) (Appendix 8).

6.1.4 Discussion

As in the retrospective analysis, the greatest difference between the cohorts used is the younger age of the sudden death cases. These cases are important to allow a comparison with 'normal' brains and the inclusion of a 'normally aged' cohort (LBC1936) is also important to be able to consider the changes associated with normal aging.

Tissue quality is important for molecular and genetic experiments. In this study, RIN value seems to be the more sensitive measure of tissue quality, which was greatest in the sudden death cases. The RIN value was negatively correlated with longer duration of final illness and increased age. Prolonged agonal period is recognised as adversely affecting post-mortem brain tissue quality (Tomita, Vawter et al. 2004). It is more often seen in people who die with chronic conditions, often ultimately from pneumonia, for example (the third most common cause of death in these cases, Figure 6.3), compared to cardiac deaths that usually have a shorter agonal period (the most common cause of death in these cases, Figure 6.3). It is possible the positive correlation between RIN value and increased PMI is due to the sudden death cohort who are younger with a shorter duration of final illness,

but longer PMI as a result of undergoing autopsies in the medicolegal system rather than the hospital. I am not aware of any reports of increased age reducing tissue quality, but if this could be confirmed it would be important to consider in future studies.

Only four cases had no cardiovascular disease, and the numbers of other conditions were low so we were unable to further explore the frequency of risk factors in the different cohorts or look for associations. One advantage of this study was that the sudden death cases, which had relatively little clinical data available, underwent a full body post-mortem and so evidence of cardiovascular disease, such as severe coronary atherosclerosis, could be confirmed, even if it had not been diagnosed in life. In future work with greater numbers of cases, it would be useful to be able to investigate more clinical associations using data available in these well characterised cohorts e.g. smoking, obesity, level of education. Some associations are identified in the literature (Chauhan, Adams et al. 2019, Corley, Cox et al. 2019, Wardlaw, Smith et al. 2019, Ballerini, Booth et al. 2020), but no substantial associations beyond vascular risk factors have been established.

This work was limited by the small number of cases involved and that the clinical data is not complete. It was more difficult to get full data for the sudden death cohort, as the only records attached to them are from the autopsy examination report carried out by the forensic pathologists, who have access to police reports and sometimes GP records and hospital medical records. However, their reports are dictated based on their requirements for their own diagnosis and at their discretion. In a busy city mortuary, the report may include what is most accessible and relevant to their examination rather than a fully comprehensive medical history. A minimal dataset for admission to the brain bank could be useful and could include a relatively basic medical summary or list of all known medical conditions.

6.2 Results of SVD burden assessment on *ex vivo* magnetic resonance imaging

6.2.1 Demographics

53/55 cases that were scanned post-mortem underwent *ex vivo* MRI grading of SVD burden (10 LBC1936, 18 LINCHPIN, 25 sudden death) (summarised in Table 6.2, individual scores in Appendix 9). Two cases were not graded due to significant artefact.

6.2.2 Ex vivo magnetic resonance imaging assessments

6.2.2.1 Grading magnetic resonance imaging SVD burden

All of the lesions recorded were most prevalent and scored highest in the LINCHPIN cohort and was least prevalent and scored lowest in the sudden death control cases (Table 6.2). 59 areas of radiological WMH were identified in 39 cases, 14 had no WMH. The amount of individual samples with WMH in each case was graded 0-3, the mean score was 1.10 (SD 0.88) (Table 6.2), being highest in LINCHPIN (mean 1.71, SD 0.98) followed by LBC1936 (mean 1.30, SD 0.67) and was lowest in the sudden death cases (mean 0.60, SD 0.58).

18 infarcts were identified in 14 of the 55 cases that underwent MRI, the maximum number in one case was three. Most were identified in LINCHPIN cases (n=11) followed by LBC1936 (n=5) then sudden death (n=2).

29 microbleeds were identified in 17 cases, the maximum number in one case was eight. There were most in the LINCHPIN cohort (n=19), followed by LBC1936 (n=6) and then sudden death (n=4).

The mean enlarged PVS score was 2.38 (SD 1.29), all cases had at least one enlarged PVS visible. The score was highest in LINCHPIN (mean 3.00, SD 1.12), followed by LBC1936 (mean 2.70, SD 1.25) then sudden death (mean 1.80, SD 1.12)

Table 6.2 Summary of SVD grading burden by cohort on ex vivo MR

Summary of overall SVD grading scores across the whole of each brain in the three different cohorts. PVS enlarged perivascular space, MWH white matter hyperintensity, SVD small vessel disease, BG basal ganglia, SD standard deviation, LBC Lothian birth cohort 1936, LP Lothian Study of INtraCerebral Haemorrhage, Pathology, Imaging and Neurological Outcome, SD sudden death cohort

Cohort	n	Infarcts, n	Enlarged PVS score, mean (SD)	Microbleeds, n	WMH score, mean (SD)	Overall SVD score, mean (SD)	BG mineralisation score, mean (SD)
LBC	10	5	2.70 (1.25)	6	1.30 (0.67)	2.10 (0.89)	2.40 (0.98)
LP	18	11	3.00 (1.12)	19	1.71 (0.98)	2.29 (0.99)	2.53 (1.12)
SD	25	2	1.80 (1.12)	4	0.60 (0.58)	1.56 (0.82)	2.04 (0.84)
Mean overall (SD)			2.38 (1.29)		1.10 (0.88)	1.91 (0.96)	2.31 (0.96)
Total	53	18		29			

The mean overall SVD burden score was 1.90 (SD 0.96) 34 of the 55 cases that underwent post-mortem MRI SVD grading also underwent histological SVD burden grading. The highest SVD score overall was in the LINCHPIN cases (mean 2.29, SD 0.99), followed by LBC1936 (mean 2.10, SD 0.89), the sudden death cohort (mean 1.56, SD 0.82) had the lowest.

6.2.2.2 Basal ganglia mineralisation

The mean intensity grading of basal ganglia mineralisation was 2.31 (SD 0.96). This was also highest in LINCHPIN (mean 2.53, SD 1.12), followed by LBC1936 (mean 2.40, SD 0.98) and then the sudden death cohort (mean 2.04, SD 0.84).

6.2.2.3 Cortical thickness

The cortical thickness on *ex vivo* MRI was measured in 52 cases. 116 measurements were taken from the superficial, 96 from the mid and 90 from the deep point of the gyri. In some cases it was not possible to take all of the measurements. The results are summarised in Table 6.3.

Table 6.3 Summary of cortical thickness measured on ex vivo 7T magnetic resonance imaging

Measured in mm. n number, IQR interquartile range.

		Cortical depth		
Cortical area	n (cases)	Superficial, median (IQR)	Mid, median (IQR)	Deep, median (IQR)
Frontal parasagittal	50	3.12 (2.72-3.48)	2.81 (2.50-3.22)	2.36 (1.93-2.66)
Broca's area	46	3.20 (2.83-3.47)	2.94 (2.65-3.21)	2.27 (2.12-2.66)
Temporal tip	36	3.88 (3.43-4.36)	3.44 (2.92-3.68)	2.66 (2.29-3.13)
Overall	52	3.31 (2.96-3.69)	2.98 (2.66-3.39)	2.42 (2.08-2.80)

Cortical thickness was greatest at the tip of the temporal lobe (BA38) where it was measured in 36 cases; the median thickness on the surface was

3.88mm (IQR 3.43-4.36), at the midpoint 3.44mm (IQR 2.92-3.68) and at deepest point 2.66mm (IQR 2.29-3.13). The cortical thickness in Broca's area (BA44/45) was measured in 46 cases; the median thickness on the surface was 3.20mm (IQR 2.83-3.47), at the midpoint 2.94mm (IQR 2.65-3.21) and at deepest point 2.27mm (IQR 2.12-2.66). The cortex was thinnest in the frontal parasagittal gyrus (BA9) where the cortical thickness was measured in 50 cases; the median thickness on the surface was 3.17mm (IQR 2.72-3.48), at the midpoint 2.81mm (IQR 2.50-3.22) and at deepest point 2.36mm (IQR 1.93-2.66).

6.2.2.4 Air bubbles

Air bubbles caused artefact throughout the images, commonly at the edge of and overlying tissue and in relation to the plastic cassettes holding the tissue (Figure 6.5a-c). They obscured the tissue, potentially masked lesions, and could mimic haemorrhagic lesions (Figure 6.5d). They were confirmed as air bubbles and disregarded if no corresponding lesion within the histological section was subsequently identified.

6.2.3 Discussion

The use of established, validated *in vivo* imaging assessment and grading systems provided a foundation upon which to build the ex vivo imaging SVD assessment. As there is no such agreed system for histological assessment we developed our own based on the best available histological systems and with reference to the features on imaging to try to make the assessments comparable. Although formal statistics could not be carried out, LINCHPIN cases appeared to have the greatest burden of disease on post-mortem MR scanning, suggesting the grading system used does seem to be reflecting the cases where we would expect to see the most pathology. Likewise, as LBC1926 represents normal aging, we would expect there to be some pathology, which we have found.

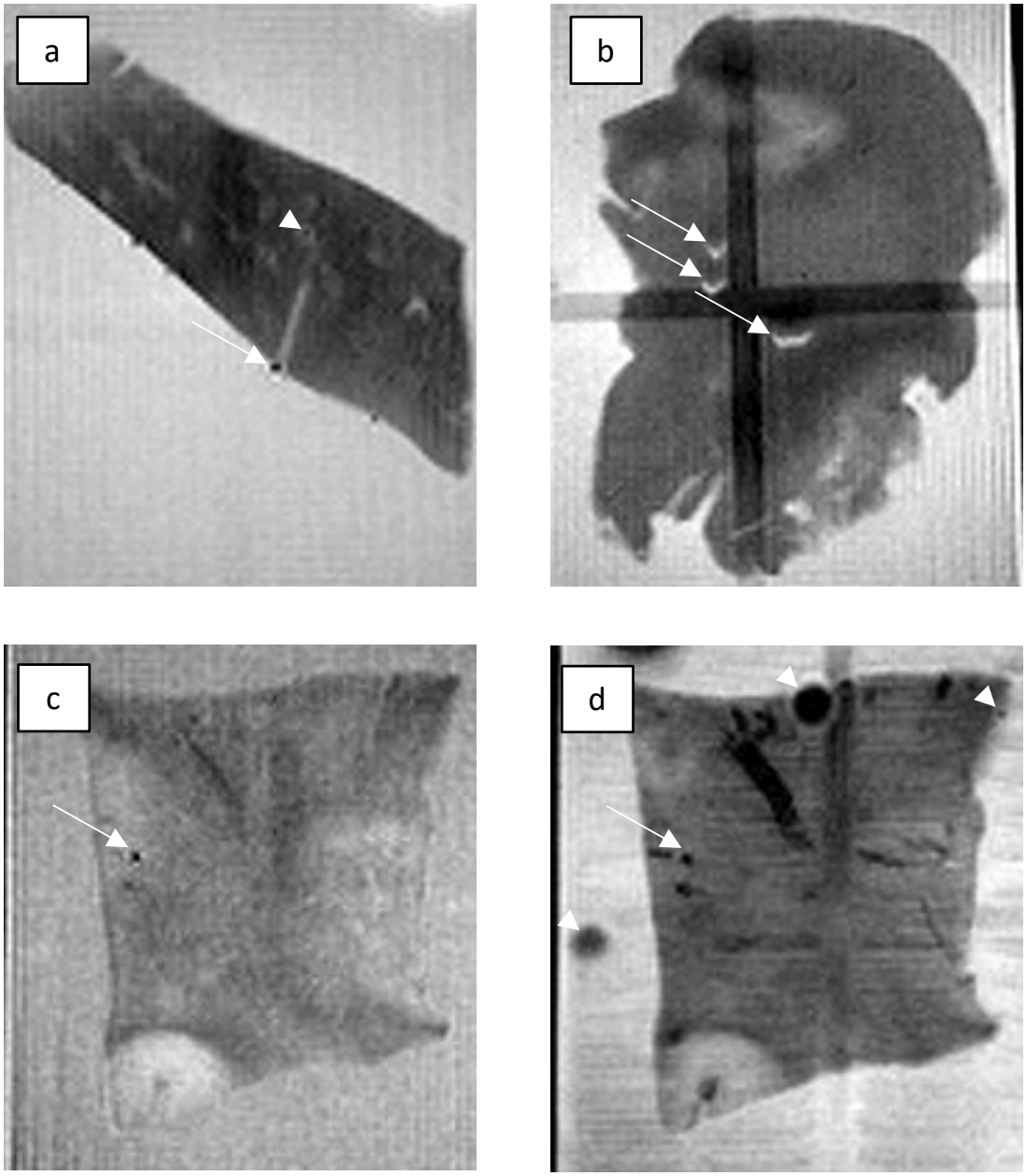


Figure 6.5 Air bubble artefact on *ex vivo* imaging

Air bubbles could be seen as rounded features often a) at the edge of a piece of tissue (arrow) (T2), overlying tissue (arrowhead), which can be difficult to identify, or b) in relation to the plastic cassette the tissue is scanned in (arrows) (T2). An air bubble seen on c) T2 could be mistaken for a haemorrhagic lesion or vessel on d) T2* (arrow), where additional air bubbles could be identified that are not seen on other sequences (arrowheads).

Not knowing the natural history and relative significance of radiological SVD lesions makes it difficult to accurately apply an overall grade for SVD burden. For example, several cases were graded as mild SVD overall, based on very occasional PVS. However, it remains uncertain if these cases should be labelled as SVD, or if perhaps a few enlarged PVS should be considered a normal part of aging. Overall, however, these results suggest the MR SVD grading system applied and the areas assessed, at least partially, give an accurate representation of the burden of SVD in these cases and they could be believed to represent the pathologies and control groups they were chosen for.

The high resolution 7T MRI allowed excellent resolution of the tissue. There were some difficulties initially however, as this kind of grading hasn't been applied to small ex vivo tissue samples and so we had to be wary of any unusual appearances. Air bubbles, in particular, were an issue initially, and remained present but could usually be accurately identified and separated from microbleeds. We also observed a hyperintense artefact at the cut edge of the tissue blocks in some samples, and therefore had to take care to avoid confusing them with WMH.

6.3 Results of SVD burden assessment on histology

6.3.1 Demographics

35 cases underwent grading of SVD burden on histology (8 LBC1936, 18 LINCHPIN, 9 sudden death) (summarised in Table 6.4, individual scores in Appendix 10). Reasons for histological SVD burden not being assessed included extensive haemorrhage and being unable to obtain slides that were required for other purposes in a timely manner to allow assessment.

Table 6.4 Summary of Histological grading of SVD burden by cohort

All features graded 0-3 are presented as mean (standard deviation). WM white matter, PVS perivascular space, CMI cortical microinfarct, SCI subcortical infarct, BG=basal ganglia; SVD=small vessel disease; n=number of cases; LBC=Lothian birth cohort 1936; LP=Lothian Study of INtraCerebral Haemorrhage, Pathology, Imaging and Neurological Outcome; SD=sudden death cohort, parench precnhymal, vasc vascular

Cohort	n	WM rarefaction (0-3)		PVS (0-3)		Infarcts (n)	Lacunes (n)	MB (n)	Arteriolosclerosis (0-3)		Lipohyalinosis (n)	Fibrinoid necrosis (n)	BG pigment (0-3)	Overall (0-3)	
		severity	extent	severity	extent				severity	extent				Parench	Vasc
LBC	8	2.13	2.88	2.50	2.88	2	0	6	1.63	2.50	1	0	1.75	2.63	1.63
		(0.64)	(0.35)	(0.53)	(0.35)				(0.74)	(0.53)			(0.96)	(0.52)	(0.74)
LP	18	2.28	2.61	2.50	2.61	13	9	16	2.00	2.72	6	3	1.18	2.67	2.33
		(0.46)	(0.50)	(0.79)	(0.61)				(0.69)	(0.46)			(0.60)	(0.49)	(0.59)
SD	9	1.11	1.33	1.78	1.78	2	1	0	1.44	2.22	1	1	1.29	1.44	1.56
		(0.60)	(0.71)	(0.83)	(0.67)				(0.53)	(0.67)			(0.95)	(0.44)	(0.44)
Total	35	1.94	2.34	2.31	2.46	17	10	22	1.79	2.59	8	4	1.16	2.34	2.03
		(0.73)	(0.80)	(0.80)	(0.70)				(0.73)	(0.57)			(0.71)	(0.77)	(0.78)

6.3.2 Histological assessments

6.3.2.1 Grading histological SVD burden

In the histological grading of parenchymal pathology, the LINCHPIN cohort had the highest grading for severity of white matter rarefaction (mean 2.28, SD 0.46), and the highest number of focal parenchymal lesions: 13 microinfarcts, 9 lacunes and 16 microbleeds. These were lowest in the sudden death cases (severity of white matter rarefaction mean 1.11 SD 0.60, microinfarcts n=2, lacunes n=1, and microbleeds n=0). The LBC1936 cohort had the highest scores for extent of WM rarefaction (mean 2.88, SD 0.35).

The scores for severity of enlarged PVS was highest in LINCHPIN and LBC1936 (both mean 2.50, SD 0.79 and 0.53 respectively), enlarged PVS extent was greater in LBC1936 (mean 2.88, SD 0.35) compared to LINCHPIN (mean 2.61, SD 0.61). The sudden death cohort had the lowest scores for PVS extent and severity (means 1.78, 1.78, SD 0.67, 0.83).

All aspects of vascular pathology scored highest in LINCHPIN (arteriolosclerosis severity mean 2.00, SD 0.69, extent mean 2.72, SD 0.46, lipohyalinosis n=6, fibrinoid necrosis n=3), while the sudden death cases had the lowest arteriolosclerosis scores (severity mean 1.44, SD 0.53, extent mean 2.22, SD 0.67) and only one case with lipohyalinosis. Fibrinoid necrosis was not seen in any LBC1936 cases.

There was no association between the presence of hypertension and the severity (p=0.537) or extent (p=0.793) of arteriolosclerosis (Figure 6.6) in the 30 cases with sufficient clinical history.

Overall scores for SVD pathology in both the parenchyma and vessels were highest in the LINCHPIN cohort (parenchymal mean 2.67, vascular mean 2.33), although the LBC1936 parenchymal mean score was close at 2.63. The sudden death cohort scored lowest overall (parenchymal mean 1.44, vascular mean 1.56).

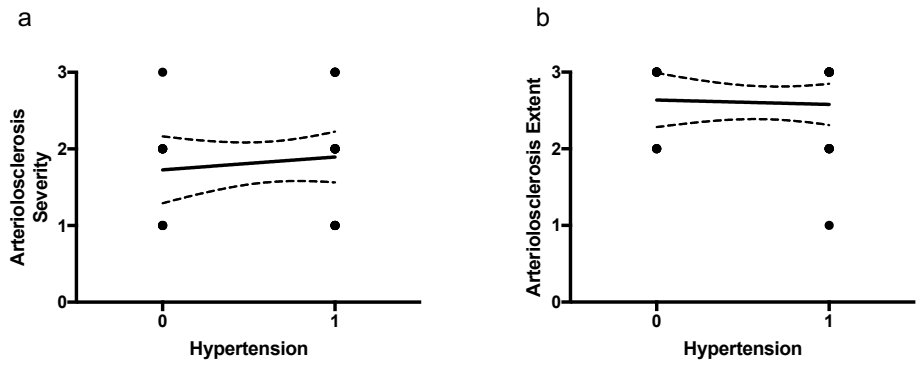


Figure 6.6 Analysis of relationship between histologically graded arteriolosclerosis and hypertension

Scatterplots showing no significant relationship between the histological grading of arteriolosclerosis by a) severity and b) extent, each graded 0-3, compared with the absence (0) or presence (1) of hypertension. There may be a slight positive relationship between the severity of arteriolosclerosis and presence of hypertension in (a). The best-fit regression line and 95% confidence interval are superimposed. Each dot represents one case, multiple dots with the same score are superimposed.

6.3.2.2 Basal ganglia pigment

The amount of basal ganglia pigment deposition was greatest in the LBC1936 cases (mean 1.75) and least in LINCHPIN (mean 1.18).

6.3.2.3 Cortical measurements

The histological cortical thickness was measured in 27 cases. 55 measurement were taken from the superficial, 52 from the mid and 52 from the deep point of the gyri. In some cases it was not possible to take all of the measurements. The results are summarised in Table 6.5. Cortical thickness was greatest at the tip of the temporal lobe (BA38) at all depths and was measured in 19 cases. The median thickness on the surface was 3.50mm (IQR 3.23-3.88), at the midpoint 2.95mm (IQR 2.40-3.15) and at deepest point 2.25mm (IQR 2.10-2.68). The cortical thickness in Broca's area (BA44/45) was measured in 21 cases; the median thickness on the surface was 3.00mm (IQR 2.75-3.35), at the midpoint 2.70mm (IQR 2.40-2.90) and at deepest point 2.00mm (IQR 1.80-2.35). In the frontal parasagittal gyrus

(BA9) the cortical thickness was measured in 25 cases; the median thickness on the surface was 3.30mm (IQR 2.83-3.50), at the midpoint 2.40mm (IQR 2.20-2.90) and at deepest point 2.10mm (IQR 0. 1.85-2.55).

6.3.2.4 Assessing differences between areas and depths

In an exploratory analysis of the histological measurements, comparing different sulcal depths, there were significant differences between the frontal parasagittal superficial (mean 3.148, SD 0.744) and mid (mean 2.638, SD 0.639); superficial and deep (mean 2.258, SD 0.579); mid and deep. In Broca's area between superficial (mean 2.917, SD 0.567) and mid (mean 2.650, SD 0.357); superficial and deep (mean 2.167, SD 0.451); mid and deep. In the temporal tip between superficial (mean 3.262, SD 0.656) and mid (mean 2.882, SD 0.392); superficial and deep (mean 2.414, SD 0.540). There were no significant differences between the temporal tip mid (mean 2.882, SD 0.392) and deep (mean 2.414, SD 0.540) (Table 6.6, Figure 6.7).

Table 6.5 Summary of cortical thickness measured on histology

Measured in mm. n number, IQR interquartile range.

		Cortical depth		
Cortical area	n (cases)	Superficial, median (IQR)	Mid, median (IQR)	Deep, median (IQR)
Frontal parasagittal	25	3.30 (2.83-3.50)	2.40 (2.20-2.90)	2.10 (1.85-2.55)
Broca's area	21	3.00 (2.75-3.35)	2.70 (2.40-2.90)	2.00 (1.80-2.35)
Temporal tip	19	3.50 (3.23-3.88)	2.95 (2.40-3.15)	2.25 (2.10-2.68)
Overall	27	3.30 (02.80-3.50)	2.70 (2.30-3.00)	2.15 (1.88-2.50)

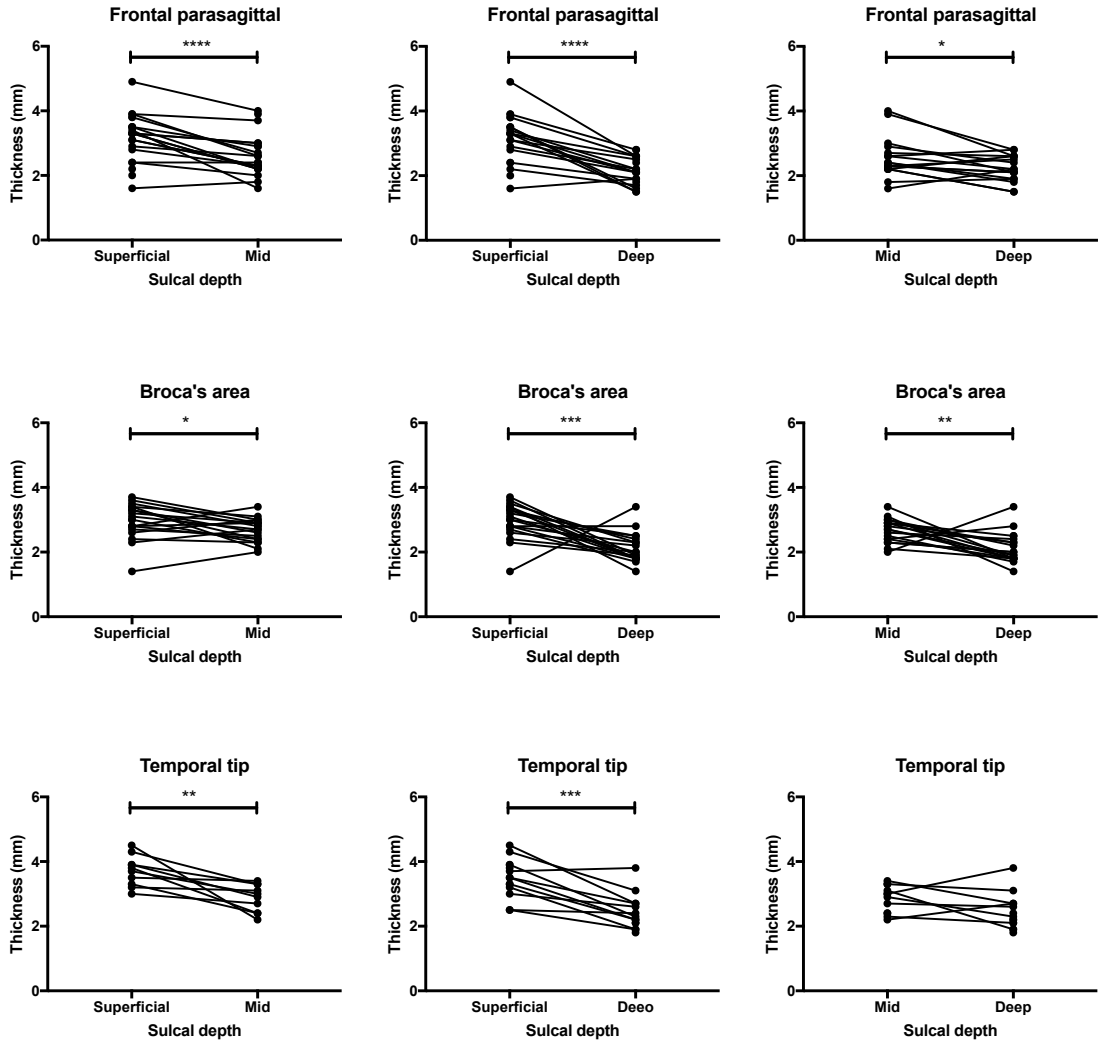
Figure 6.7 Line plots of differences comparing cortical thickness at different sulcal depths in the three brain areas on opposite page

Rows contain the brain areas; top (a-c) frontal parasagittal, middle (d-f) Broca's area, bottom (g-i) temporal tip. Columns each contain a comparison at different depths; left (a, d, g) superficial and mid, middle (b, e, h) superficial and deep, right (c, f, i) mid and deep. In each plot, the more superficial area is on the left. In all except (i), the more superficial area is statistically significantly thicker than the deeper area. Each line represents measurements from one individual.

Table 6.6 Results of paired t-tests comparing cortical thickness measurements at the three different sulcal depths in the three areas

CI confidence interval, df degrees of freedom, t test statistic, p p-value

	Paired differences				
Depths compared	Mean	95% CI	df	t	p
Frontal parasagittal					
Superficial-mid	-0.700	-0.960 - -0.440	17	5.685	<0.0001
Superficial-deep	-1.069	-1.428 - -0.710	15	6.343	<0.0001
Mid-deep	-0.341	-0.620 - -0.062	16	2.959	0.020
Broca's area					
Superficial-mid	-0.294	-0.564 - -0.025	17	2.306	0.034
Superficial-deep	-0.842	-1.271 - -0.413	18	4.129	0.001
Mid-deep	-0.567	-0.916 - -0.218	17	3.424	0.003
Temporal tip					
Superficial-mid	-0.840	-1.315 - -0.365	9	4.003	0.003
Superficial-deep	-0.918	-1.329 - -0.507	10	4.982	0.001
Mid-deep	-0.213	-0.751 - -0.326	7	0.932	0.382



Comparing the three areas sampled, there was only a significant differences in the thickness of the mid sulcus between Broca's area (mean 2.674, SD 0.362) and the temporal tip (mean 2.833, 0.423). There were no significant differences between superficial measurements in the frontal parasagittal (mean 3.177, SD 0.739) and Broca's area (2.963, SD 0.548); parasagittal and the temporal tip (mean 3.493, SD 0.589); Broca's area and the temporal tip. In the mid sulcus between the frontal parasagittal (mean 2.619, SD 0.640) and Broca's area; frontal parasagittal and the temporal tip; in the deepest sulcus between the frontal parasagittal (mean 2.153, SD 0.425) and Broca's area (mean 2.121, SD 0.425); frontal parasagittal and the temporal tip (mean 2.414, SD 0.540); Broca's area and the temporal tip (Table 6.7, Figure 6.8).

Table 6.7 Results of paired t-tests comparing cortical thickness measurements in the three areas at the three different depths

CI confidence interval, df degrees of freedom, t test statistic, p p-value

	Paired differences				
Areas compared	Mean	95% CI	df	t	p
Superficial					
Frontal parasagittal-Broca's area	-0.213	-0.766 – 0.339	14	0.828	0.422
Frontal parasagittal-Temporal tip	0.275	-0.308 – 0.858	11	1.038	0.322
Broca's area-Temporal tip	0.313	-0.378 – 1.003	7	1.071	0.320
Mid					
Frontal parasagittal-Broca's area	0.236	-0.119 – 0.590	13	1.438	0.174
Frontal parasagittal-Temporal tip	0.056	-0.506 – 0.617	8	0.228	0.825
Broca's area-Temporal tip	0.489	0.267 – 0.711	8	5.072	0.001
Deep					
Frontal parasagittal-Broca's area	-0.117	-0.606 – 0.372	11	0.525	0.610
Frontal parasagittal-Temporal tip	0.067	-0.499 – 0.642	11	0.260	0.800
Broca's area-Temporal tip	0.191	-0.410 – 0.792	10	0.708	0.495

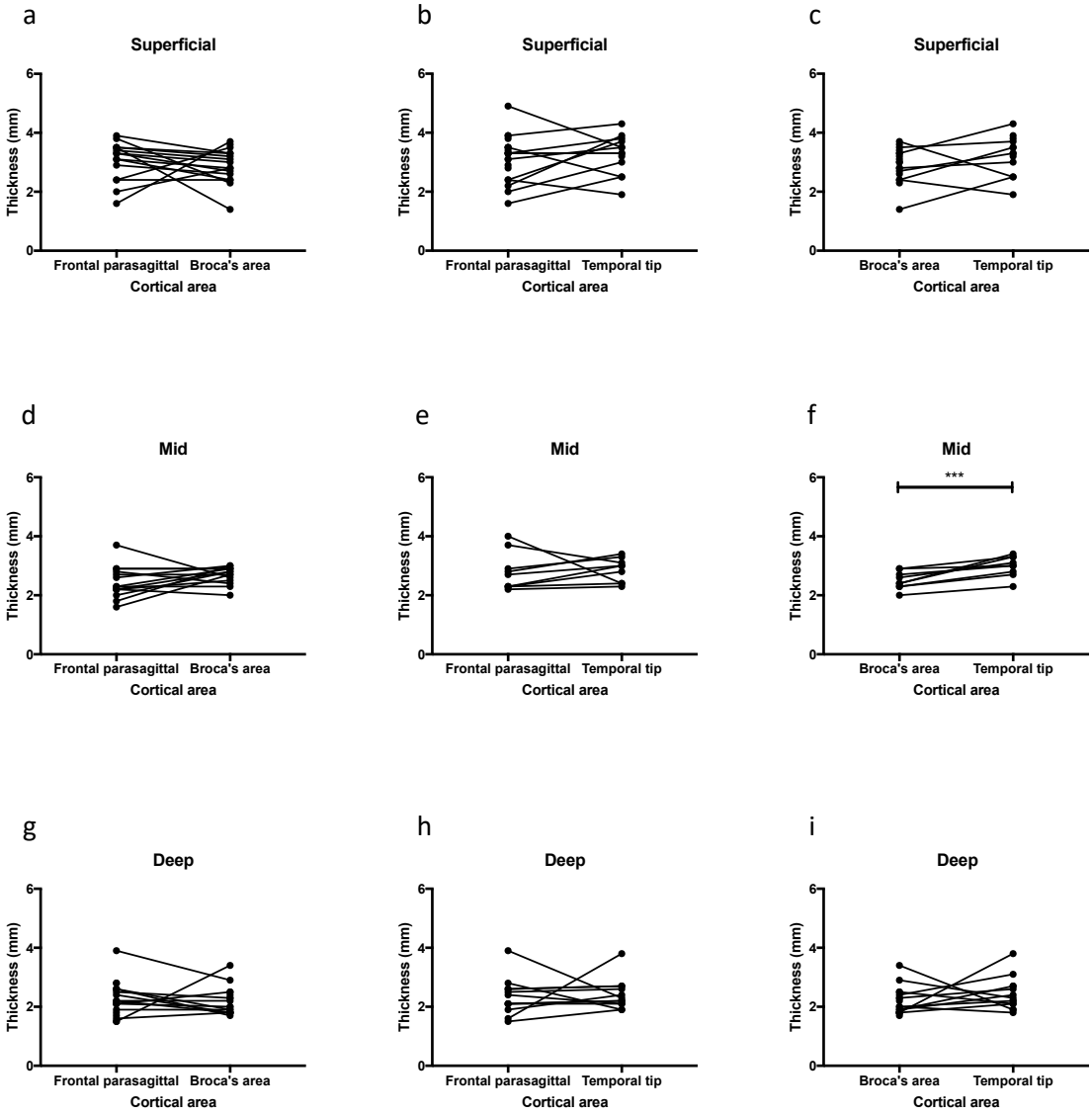


Figure 6.8 Line plots of differences comparing cortical thickness in the three brain areas at different sulcal depths

Rows contain the different sulcal depths; top (a-c) superficial, middle (d-f) mid sulcus, bottom (g-i) deep sulcus. Columns each contain an area comparison; left (a, d, g) frontal parasagittal and Broca's area, middle (b, e, h) frontal parasagittal and temporal tip, right (c, f, i) Broca's area and temporal tip. The only statistically significant difference in cortical thickness between brain areas is f) at the mid depth of the sulcus when comparing Broca's area and the temporal tip. Each line represents measurements from one individual.

6.3.2.5 Comparing measurements on MRI and histology

Scatterplots representing the Bland Altman comparison of cortical thickness measurement on MRI and histology are shown in Figure 6.9.

Comparing *ex vivo* MRI and histology measurements in the frontal parasagittal cortex the mean difference at the superficial aspect was 0.051mm, the limits of agreement were -1.528 and 1.426mm. In the mid sulcus the mean difference was 0.141mm, the limits of agreement were and -1.416 and 1.697mm. In the deep sulcus the mean difference was 0.142mm, the limits of agreement were -0.724 and 1.008mm.

In Broca's area, the mean difference at the superficial aspect was 0.182mm, the limits of agreement were -0.887 and 1.251mm. In the mid sulcus the mean difference was 0.270mm, the limits of agreement were and -0.777 and 1.317mm. In the deep sulcus the mean difference was 0.344mm and the limits of agreement were -0.585 and 1.273mm.

At the temporal tip, the mean difference at the superficial aspect was 0.318mm, the limits of agreement were -0.952 and 1.587mm. In the mid sulcus the mean difference was 0.486mm, the limits of agreement were and -0.436 and 1.408mm. In the deep sulcus the mean difference was 0.218mm and the limits of agreement were -0.780 and 1.235mm.

6.3.2.6 Additional features

White matter rarefaction around enlarged PVS was present in 31 cases. Perivascular collagenosis was present in 33 cases, most often, but not exclusively, in a periventricular location. Perivascular inflammation and haemosiderin were seen in all cases.

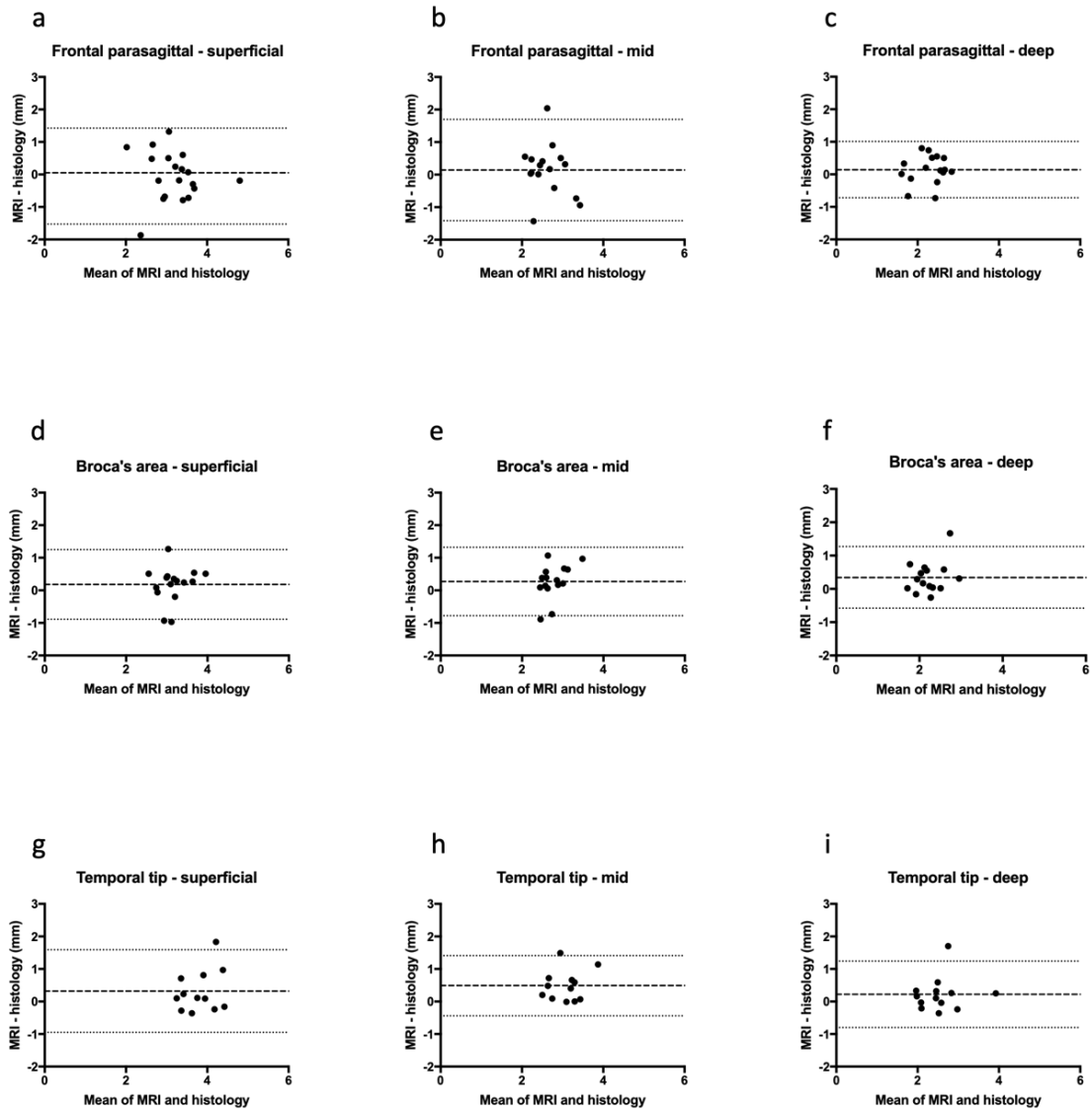


Figure 6.9. Bland Altman plots for the comparison of MR and histological cortical thickness measurements

Horizontal dotted lines represent the limits of agreement, dashed lines show the mean. Each row is a different area; top row (a-c) frontal parasagittal, middle row (d-f) Broca's area and bottom row (g-i) temporal tip. Each column is a different sulcal depth; left (a, d, g) superficial, middle column (b, e, h) is mid sulcus and the right column (c, f, i) is the deep aspect of the sulcus.

6.3.3 Discussion

6.3.3.1 Discussion of the histological grading

Like the *ex vivo* MR grading, the histology results suggest that the severity of histological parenchymal SVD pathology (WM rarefaction, microinfarcts, lacunes and microbleeds) is in keeping with the original retrospective grading carried out and is most severe in the cases with haemorrhagic pathology. Specifically, these cases have more severe and extensive vascular pathology (arteriolosclerosis, lipohyalinosis and fibrinoid necrosis) and more frequent focal parenchymal lesions (infarcts, lacunes and microhaemorrhages). Parenchymal pathology measured by white matter rarefaction and enlarged PVS, however, was more extensive in LBC1936, reflecting the changes seen on *in vivo* imaging in this cohort (Ritchie, Dickie et al. 2015).

If reliable, these results could suggest an extensive but relatively milder parenchymal disease in normal aging in what has been considered to be a relatively ischaemic process. A proportion of these would be expected to have arteriosclerotic pathology, reflected in their scores, which, while generally lower than LINCHPIN, still reflect a significant background burden of disease in an otherwise normal, age matched population. This is compared to the haemorrhagic pathology cases which have more extensive and severe vascular pathology underlying focal vascular rupture and haemorrhage. On *in vivo* imaging, a pattern of more severe WMH and enlarged PVS is seen in LINCHPIN compared to LBC1936 (unpublished), despite them being younger, further suggesting the pathophysiology of these lesions is not necessarily ischaemic. Work to further unpick differential mechanisms would benefit from inclusion of a second SVD group with infarcts, lacunes and more pronounced WM rarefaction, or radiological WMH. A cohort with mild stroke disease is now included in the post-mortem scanning programme to enable this in future.

Lack of complete clinical history did limit some of the analyses. Comparing the presence/absence of hypertension with severity and extent of arteriolosclerosis is probably not as useful as comparing the most recent systolic blood pressure value, but we could not obtain that data. It would also be useful to be able to control for potential confounding variables such as age or antihypertensive therapy. The lack of association seen, however, may reflect the impression from clinical cohort studies that the risk factors for SVD, and arteriolosclerosis in particular, are more complex than vascular risk factors alone (Hamilton, Cox et al. 2021).

White matter rarefaction around enlarged PVS, perivascular collagenosis, perivascular inflammation and haemosiderin were often observed in these cases. We added them to the list of lesions to study specifically using the registered images.

6.3.3.2 Comparison with magnetic resonance imaging grading

Not all of the lesions graded on histology map neatly onto equivalent lesions on MRI, and not all of the grading systems used were equivalent (Table 6.8). Radiological WMH and histological WM rarefaction were considered comparable, but the contribution of other features seen in radiological WMH, such as infarction and enlarged PVS (Humphreys, Smith et al. 2021) is unknown and therefore cannot be considered, although it may be important. It is likely that a more complex interaction between the vascular and parenchymal pathologies combines to cause radiologically and clinically visible disease. Future studies with larger numbers of individuals would have the power to account for different variables that might have an influence. Careful planning of these studies to consider specific mechanisms and interactions of these would be helpful.

The grading I have used for radiological and histological scores produced comparable results in some areas. Severity of WM changes followed the same pattern, with most severe disease in the haemorrhagic SVD cohort and

lowest scores in the young controls, although histology gradings were higher than MRI. The histological extent of disease was also higher scoring, It may be that only more severe histological disease is detectable radiologically and so the radiological grading only represents the more severe end of the histological changes. It is important to remember that all of these studies were done on small tissue samples, which is not usual for radiology and may have caused some differences in interpretation than had they been seen in a whole brain study.

Visible, enlarged PVS are counted on MRI and then graded by amount. There were often too many to realistically count on histology and so our grading was by extent and severity, based on size. These systems are not directly comparable, although the radiological counting method might be more comparable to histological severity rather than extent, because larger PVS, graded as more severe on histology, are more easily identified and counted on MRI. Our results indicate different patterns between the radiological count and histological severity and so our grading systems may need improving.

Table 6.8 SVD features on MRI and histology considered to be equivalent

SVD small vessel disease, MRI magnetic resonance imaging, PVS perivascular space

	MRI lesion	**Histology lesion**
Focal	Infarcts Lacunes Microbleeds	Infarcts Lacunar infarcts Microbleeds
Parenchymal	White matter hyperintensity Enlarged PVS Basal ganglia mineralisation	White matter rarefaction Enlarged PVS Basal ganglia pigment deposition
Vascular		Arteriolosclerosis Lipohyalinosis Fibrinoid necrosis
Overall	SVD score	Parenchymal SVD score Vascular SVD score

Microscopic vessels are not identified on 7T MRI and so vascular pathologies had no direct comparable lesion on imaging. The numbers of focal lesions (infarcts, lacunes, microhaemorrhages, lipohyalinosis and fibrinoid necrosis) are too small to reliably draw conclusions from. Direct comparison of the appearances of these lesions would be more useful.

The overall SVD scores followed the same pattern, with most severe disease in haemorrhagic SVD, followed by normal aging then the young controls. The system I have constructed here means any focal parenchymal lesion is regarded as severe SVD. With better understanding of the pathogenesis of these lesions this may be able to be reclassified and become more accurate. I do however feel separate parenchymal and vascular scores are valuable as there seems to be different patterns of pathology between the haemorrhagic SVD and normal aging cohorts, possibly reflecting different underlying mechanisms, and it would be important to consider these separately, at least until we better understand the origin of these pathologies.

Scores for BG mineralisation were not similar between MR and histology. A more objective assessment would be useful. I have begun work with image analysis experts to carry out quantitative assessment using the post-mortem MR registered with images of histological slides stained with Perl's method for iron to look for correlations.

Accurately measuring the cortex is difficult as it may be cross cut depending on how the brain was cut and sampled, so they should not be taken as absolute measures. However, measurements were taken at the narrowest part each time, as the cortex cannot be made to be artefactually smaller than it is. The same precise point was measured on MR and histology, so they are comparable.

6.3.3.3 Cortical thickness measurements

In all three areas measured, the cortical thickness appears to be greatest in the superficial aspects of the brain, thinning with depth into the base of the sulcus and the thickest cortical area was the temporal tip (BA38). This is supported by the results of the paired t tests using the histological measurements, however it must be noted this is very exploratory and the analyses are limited particularly by the small number of cases. We could not separate out the measurements to study the differences between each cohort but these results suggest it would be interesting in future to conduct more robust studies of differences in cortical depth, and to look further for alterations in other areas of the cortex that may be altered in SVD. This would be particularly interesting in relation to better understanding reports of altered cognitive function in SVD, for example how preserved general cognitive abilities appear to compensate for potential reduction in specific cognitive domains (Hamilton, Cox et al. 2021).

Comparing the measurements obtained by ex vivo MRI and histology, those from the imaging were generally larger with a difference of +/-2.34mm overall. Given the thickness of the cortex being broadly in the range of around 2-4mm, this difference would not be acceptable. However, as stated, this study uses only small numbers of cases and we were not able to control for age, when age is a known risk factor for decreasing cortical thickness (Salat, Buckner et al. 2004).

Making direct comparisons of the lesions studied here on imaging and histology will be useful to try to answer some of the questions about the comparable lesions and important features to include when constructing SVD grading systems.

6.4 Results of direct lesion comparisons

Lesions were studied in 28 cases that had undergone post-mortem MR scanning and grading of SVD burden on MR and histology. The histological features of MRI-identified lesions are summarised in Table 6.9.

6.4.1 Lesions identified on post-mortem magnetic resonance imaging

6.4.1.1 Radiological white matter hyperintensities in the deep white matter

35 areas of WMH in the deep white matter were compared, these were of various sizes, from relatively focal and well defined within a tissue sample, to extending beyond the margin of the sample, to involving the whole of the white matter in a sample. One area was not identified on histology due to artefact caused by a tear. Measurements were not possible because the WMH often extended beyond the edge of the small samples and are not reliable as it is not possible to consistently define the edge of the lesion at the same point, particularly in areas with mild white matter pathology.

White matter pallor was a common histological feature, present in varying degrees in 30 areas of radiological WMH (Figure 6.10). 14 areas had loosening of the white matter, which varied from fine, even background vacuolation to severe loosening that appears to be falling apart with large, irregular holes (Figure 6.11). All had at least one of pallor or vacuolation. Enlarged PVS were present in 29 areas. Most often mild (n=7) or moderate (n=11) but occasionally severe (n=2). In nine areas there were multiple enlarged PVS. In 14 of these the enlarged PVS had white matter vacuolation in the immediate surrounding neuropil. In two areas multiple presumed enlarged PVS were lacking vessels. In one area it was noted there were fewer enlarged PVS than the surrounding normal appearing white matter. Arteriolosclerosis was also common, being seen in 29 areas with a range of mild (n=9), moderate (n=13) and severe (n=7) wall thickening (Figure 6.10e).

Table 6.9 Summary of the histological features underlying the radiological lesion appearances

WMH white matter hyperintensity, PVS perivascular space

Radiology	n	Histology	n
Areas of deep WMH	35	White matter pallor	30
		Enlarged PVS	29
		Arteriolosclerosis	29
		Gliosis	16
		White matter vacuolation	14
		Perivascular haemosiderin	11
		Perivascular inflammation	11
		Perivascular collagenosis	5
		Presumed enlarged PVS	2
		Not identified	1
Areas of periventricular WMH	12	White matter pallor	12
		Focal ependymal loss	10
		White matter vacuolation	7
		Perivascular collagenosis	7
		Gliosis	7
		Enlarged PVS	6
		Decreased cellularity	3
		Perivascular inflammation	3
		Arteriolosclerosis	3
Enlarged PVS	416	Enlarged PVS	297
		Not identified	59
		Presumed PVS	42
		Perivascular vacuolation	5
		Microinfarcts	4
		Linear vacuolation	4
		Ectatic arteriole	2
		Tears	2
		Lacune	1
Enlarged PVS with hyperintense rim	48	Enlarged PVS	33
		Presumed PVS	8
		Not identified	6
		Ectatic venule	1

Areas with multiple enlarged PVS	9	Multiple enlarged PVS	9
Microinfarct	12	Microinfarct	8
		Not identified	3
		Artefact	1
Microbleed	18	Microbleed	3
		Edge of microbleed	4
		Perivascular haemosiderin	4
		Not identified	4
		Enlarged PVS and extravasated red cells	1
		Lipohyalinosis	1
		Pigmented nucleus	1
Superficial siderosis	7	Haemosiderin laden macrophages	7

Astrocytic gliosis, seen as astrocytes with a large amount of eosinophilic cytoplasm with ramified processes, was confirmed on GFAP staining and found in 16 areas. Perivascular haemosiderin and perivascular inflammation were each found in 11 areas, not all the same, although both were present in some areas. Perivascular collagenosis was seen in five areas, some were particularly severe with almost total luminal occlusion. In three areas of WMH the white matter loosening was particularly accentuated around the vessels.

6.4.1.2 Radiological periventricular white matter hyperintensities

12 areas of radiological periventricular WMH were studied. On imaging they were most often seen as a hyperintense periventricular band, sometimes with additional adjacent, reduced hyperintensity. On histology, all areas contained white matter pallor, which appeared more extensive on histology in 10 cases and more extensive on imaging in two. However, this was difficult to assess as the profiles were not the same shape, even taking into account the different sizes. Ten showed focal loss of the ependyma (Figure 6.12), the ependyma was intact in two. Vacuolation of the white matter, perivascular collagenosis and gliosis were each seen in seven areas. Enlarged PVS

(three moderate, three mild) and white matter pallor were present in six cases. There was relative decreased cellularity and foci of perivascular inflammation in three areas each.

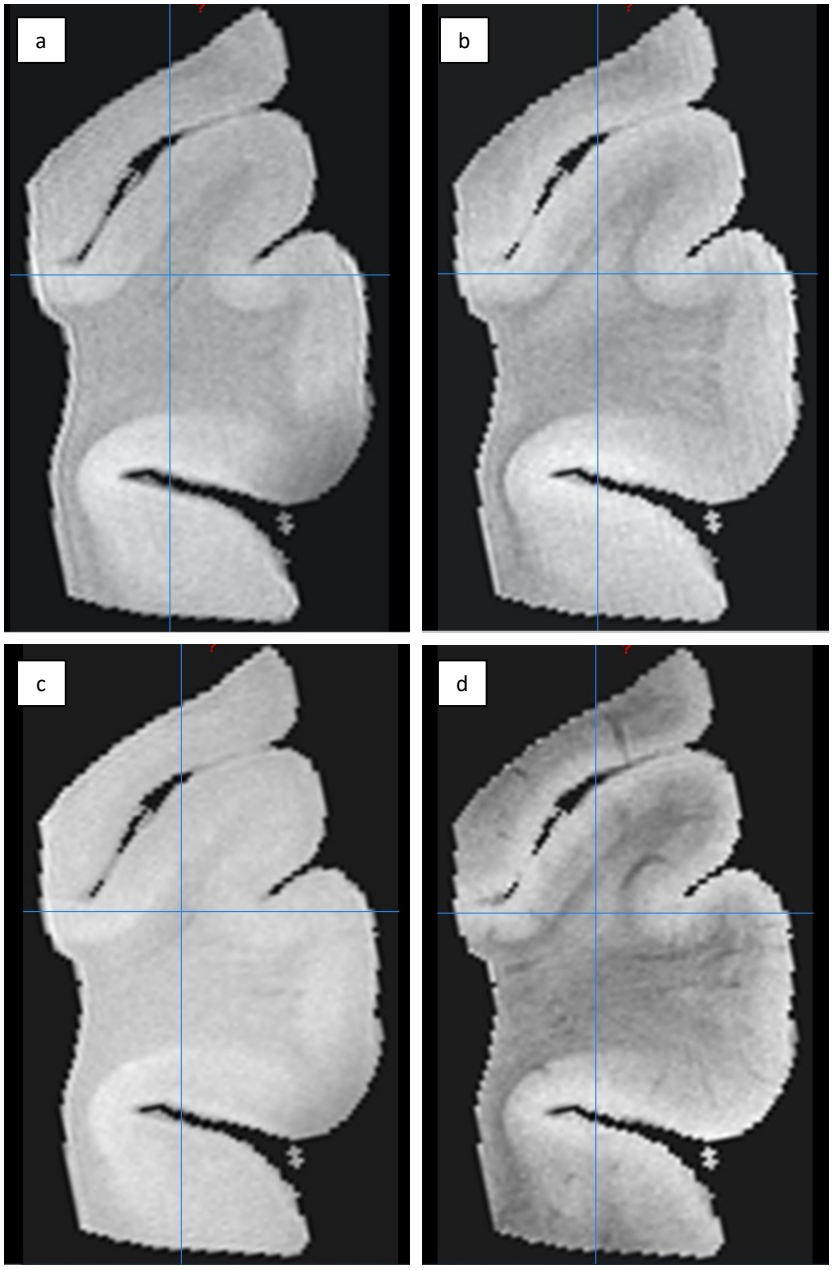
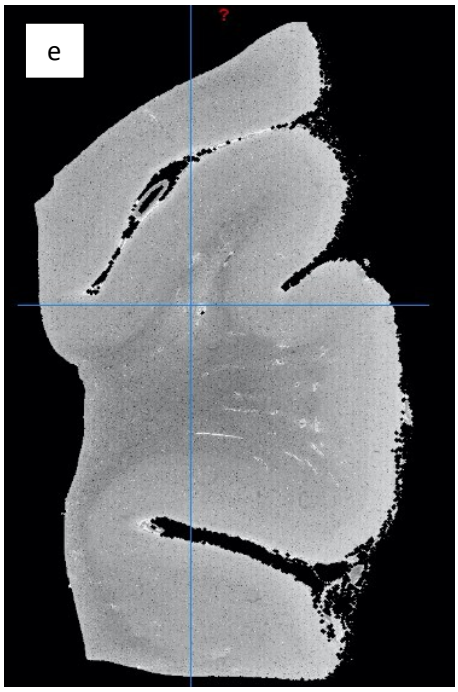
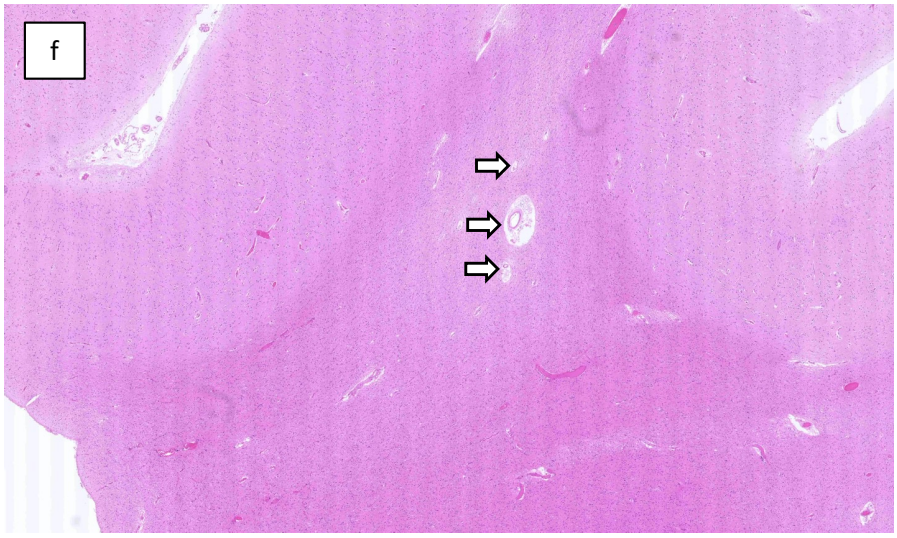
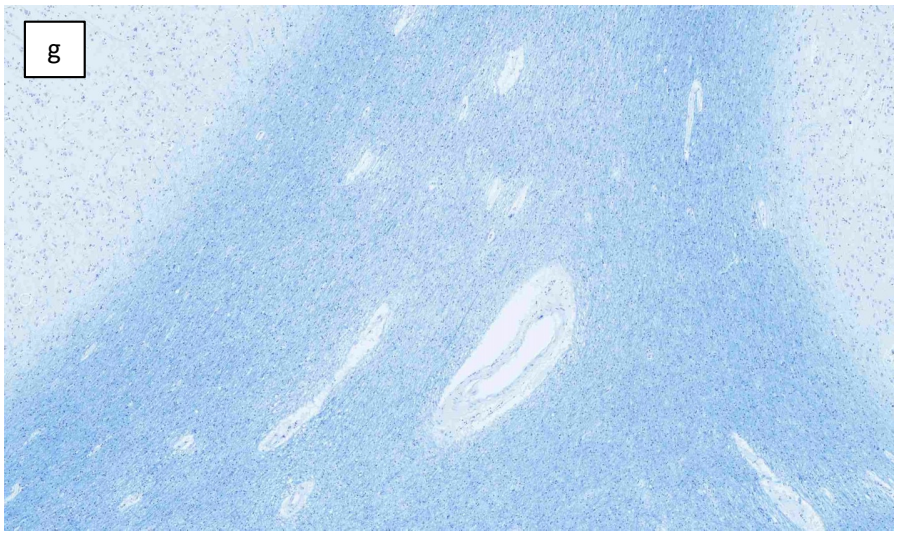


Figure 6.10 Radiological subcortical deep white matter hyperintensity

a) FLAIR b) T2 c) T1 and d) T2* sequences registered with e) greyscale digitalised histology image. The blue crosshairs indicate a subcortical WMH visible on the T2 and T2* sequences. e) This corresponds to an area of pallor on histology containing vessels with arteriolosclerosis and enlarged PVS (some indicated by arrows) (H&E, x20). f) Myelin loss is confirmed by pallor on LFB (x20).


e


f


g

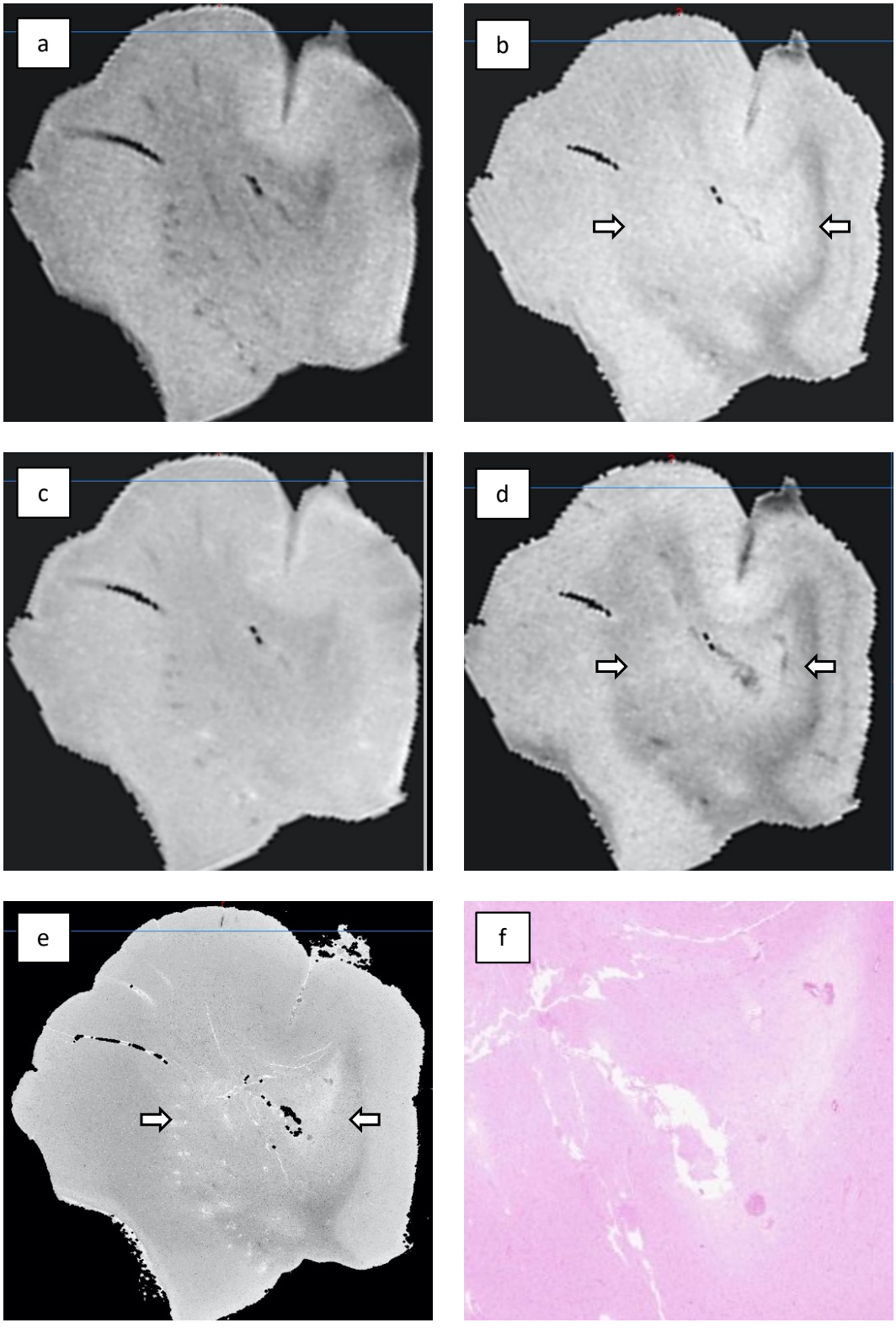


Figure 6.11 Cavitating subcortical white matter hyperintensity

a) FLAIR b) T2 c) T1 and d) T2* sequences registered with e) greyscale digitalised histology image show an area of WMH with central cavitation best identified on the T2 and T2* sequences (between the arrows). f) This corresponds to severe WM rarefaction and cavitation with enlarged PVS on microscopy (H&E x20).

Arteriolosclerosis was present in three areas (two moderate, one mild). Of note, one had a thin hyperintense rim and a wider area of less hyperintense signal change, these corresponded with increased cellularity and white matter vacuolation respectively.

6.4.1.3 Radiological enlarged perivascular spaces

In total, 416 individual enlarged PVS were identified on post-mortem MRI, the underlying histological features are summarised in Table 6.10. 297 of these were confirmed as histological enlarged PVS (Figure 6.13), 59 were not identified on histology and 42 were identified as presumed enlarged PVS but the vessel was missing and they were not assessed further. Five showed vessels surrounded by vacuolated white matter without an enlarged PVS. Four corresponded to linear areas of vacuolation, with the appearances of being adjacent to a vessel that was not included in the section. Two were relatively muscular, ectatic arterioles. Two were artefactual tears.

Four were histological microinfarcts. On imaging they measured from 0.66-1.2mm and were linear or round. On histology they were found to be areas of infarction measuring 0.8-1.4mm with cell loss, white matter vacuolation, vascular loss and gliosis. One measuring 0.9mm was found to be a 2mm lacune histologically (Figure 6.14f).

Of the 297 confirmed enlarged PVS, 110 were mildly enlarged on histology. Of these, 16 contained perivascular haemosiderin and 9 contained perivascular inflammation. The immediate surrounding neuropil was vacuolated in 41 and four contained vessels showing perivascular collagenosis. Mild PVS as small as 0.1mm on histology were identified on post-mortem imaging.

110 of the PVS were moderately enlarged on histology. 12 of these contained perivascular haemosiderin and 11 contained perivascular inflammation. The immediate surrounding neuropil was vacuolated in 42 and

seven contained vessels showing perivascular collagenosis. Four contained congested vessels. Moderate PVS as small as 0.2mm on histology were identified on post-mortem imaging.

77 of the PVS were severely enlarged on histology. 8 of these contained perivascular haemosiderin and 8 contained perivascular inflammation. The immediate surrounding neuropil was vacuolated in 17 and two contained vessels showing perivascular collagenosis. PVS smaller than 0.1mm on histology were identified on post-mortem imaging.

Overall, 147/297 vessels with enlarged PVS showed arteriolosclerosis, 68 mild, 57 moderate and 22 severe. Enlarged PVS were also associated with gliosis, generally in the areas of the enlarged PVS and also focally around individual enlarged PVS with strong staining of the glia limitans (Figure 6.13h, i).

A sample of ten enlarged PVS were measured on post-mortem MR and histology they ranged from 0.37mm-2.47mm on imaging and 0.2-2.1mm on histology. On average, the MR measurements were 1.66 times larger than the equivalent histology.

Often in areas with mildly enlarged PVS and on four occasions in areas with moderately enlarged PVS, multiple other small enlarged PVS were noted in the adjacent tissue that were not visible on MR.

The histological PVS often contained material including delicate collagenous fibres, fibrinoid material, proteinaceous and cellular debris. Some also appeared to contain the glia limitans within the space (Figure 6.15g).

Table 6.10 Summary of additional histological features seen in association with radiological enlarged PVS

Additional histological features seen in association with the 297 radiologically-identified enlarged PVS, the 33 enlarged PVS with a hyperintense rim and the eight enlarged PVS with a hyperintense rim that corresponded to presumed PVS but did not contain a vessel. PVS perivascular space.

PVS enlargement			
Mild	110	Perivascular haemosiderin	16
		Perivascular inflammation	9
		Perivascular vacuolation	41
		Perivascular collagenosis	4
Moderate	110	Perivascular haemosiderin	12
		Perivascular inflammation	11
		Perivascular vacuolation	42
		Perivascular collagenosis	7
Severe	77	Perivascular haemosiderin	8
		Perivascular inflammation	8
		Perivascular vacuolation	17
		Perivascular collagenosis	2
Enlarged PVS with hyperintense rim	33	Perivascular vacuolation	22
		Perivascular inflammation	9
		Perivascular haemosiderin	7
		arteriolosclerosis	7
		Gliosis	3
		Perivascular collagenosis	1
		Congested vessel	5
Presumed PVS	8	Perivascular vacuolation	6

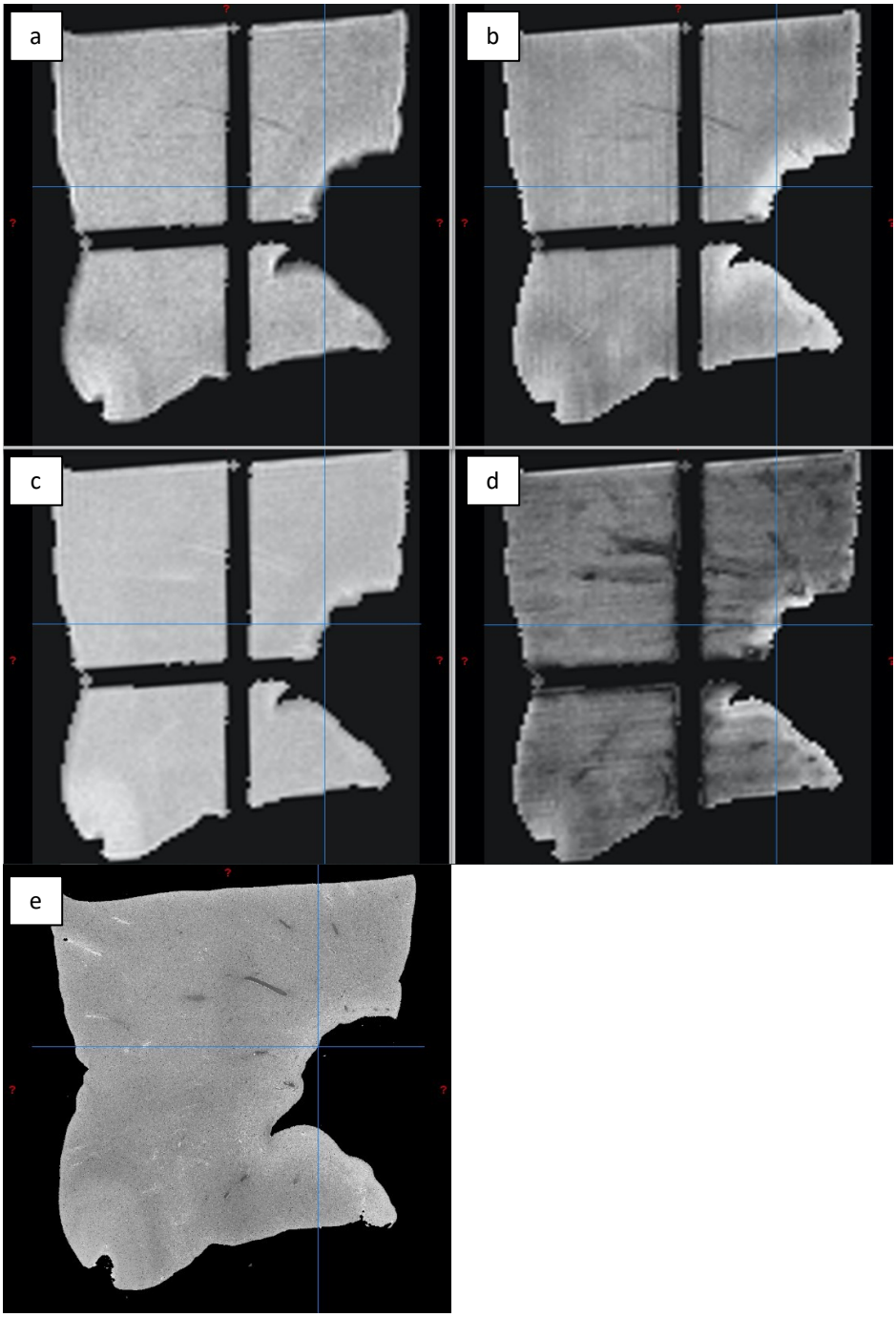
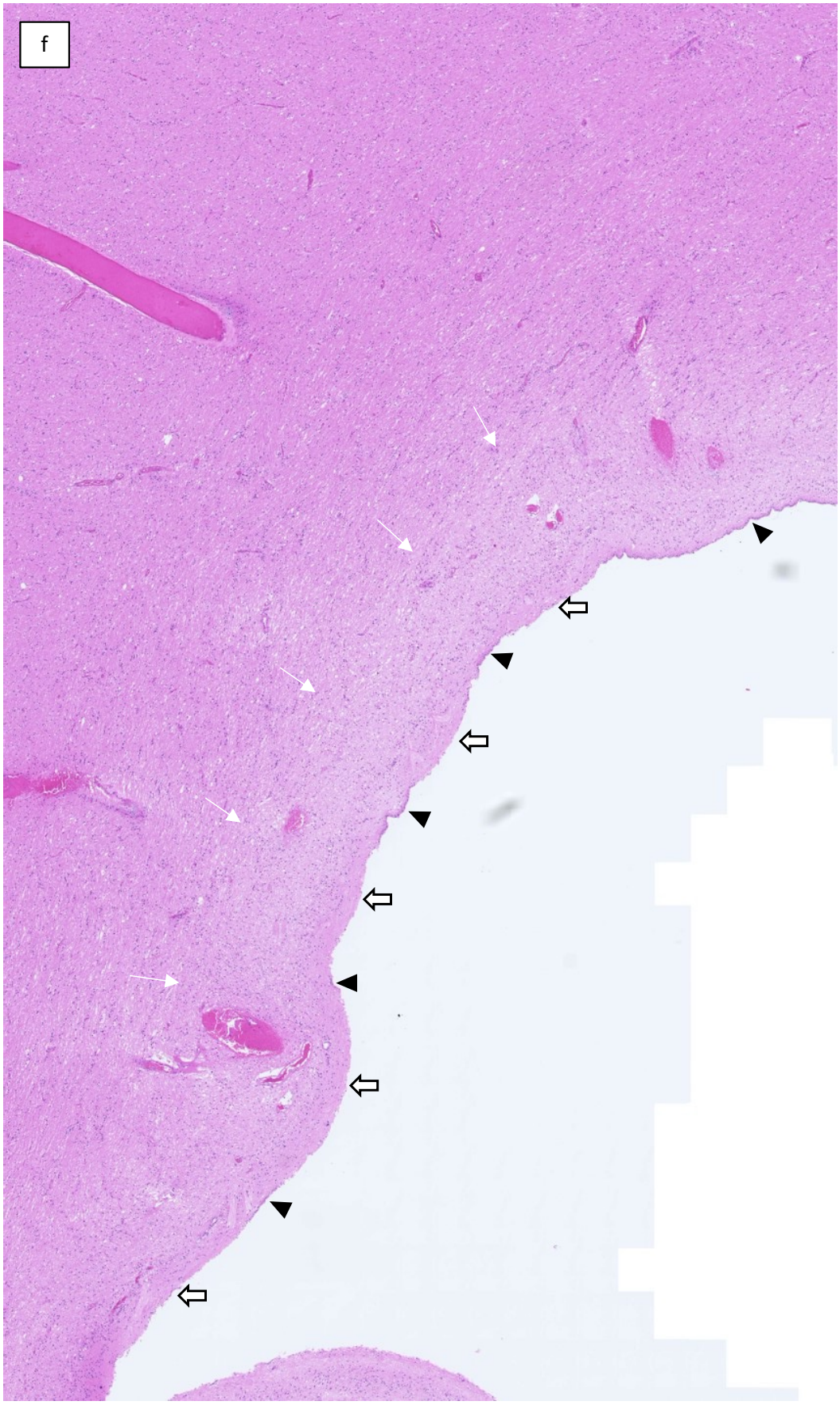


Figure 6.12 Radiological periventricular white matter hyperintensity

a) FLAIR b) T2 c) T1 and d) T2* sequences registered with e) greyscale digitalised histology image. The blue crosshairs are centered on a linear periventricular white matter hyperintensity best seen on T2 and T2* sequences and corresponding with subependymal pallor on histology. f) Closer inspection of the same are on H&E shows histological focal ependymal loss (white arrows) with intervening areas of intact ependyma (black arrowheads). The immediate underlying parenchyma is relatively hypocellular with white matter pallor relative to normal (border roughly marked by small white arrows), focal congested blood vessels, enlarged perivascular spaces and focal perivascular inflammation (x20).


f

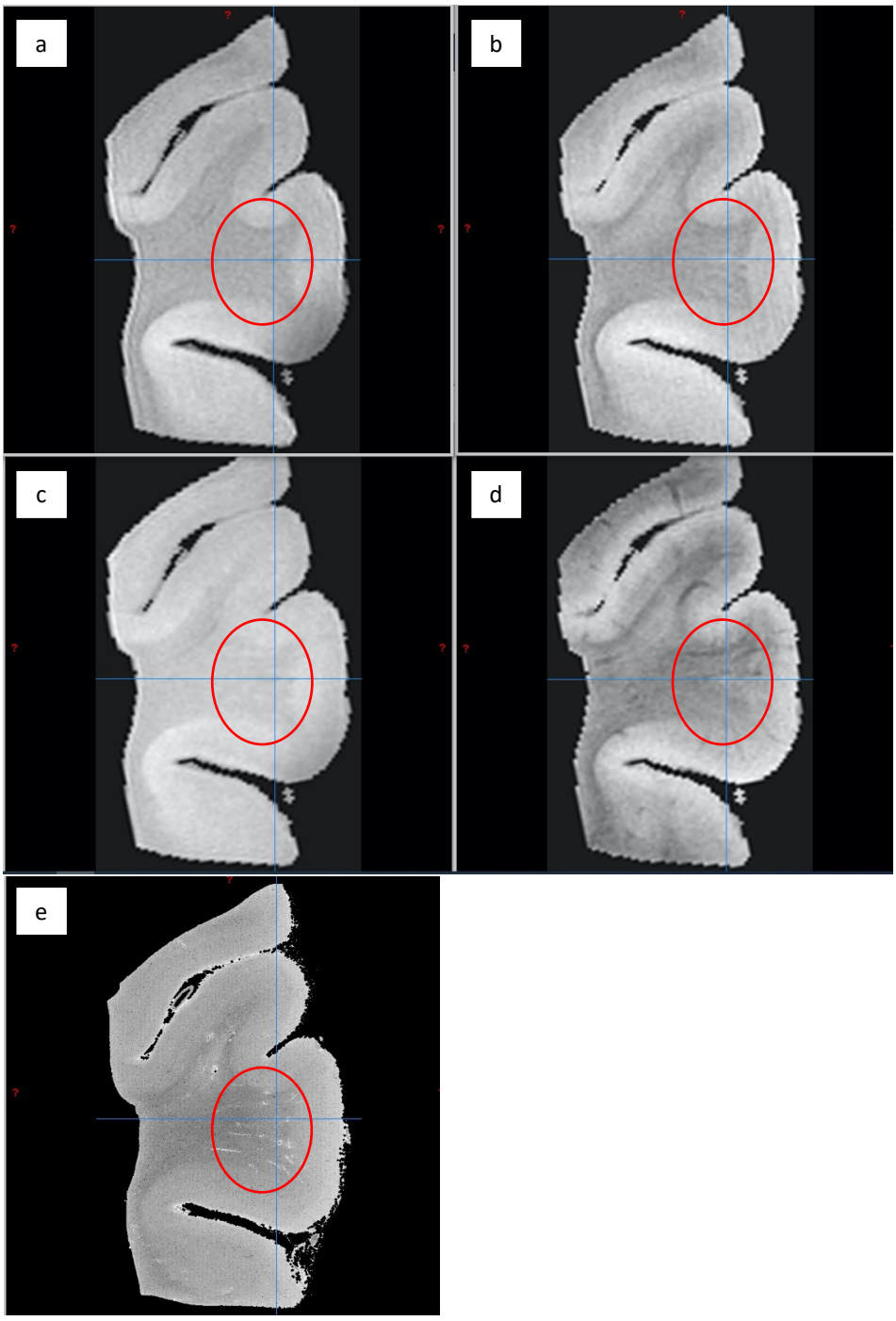
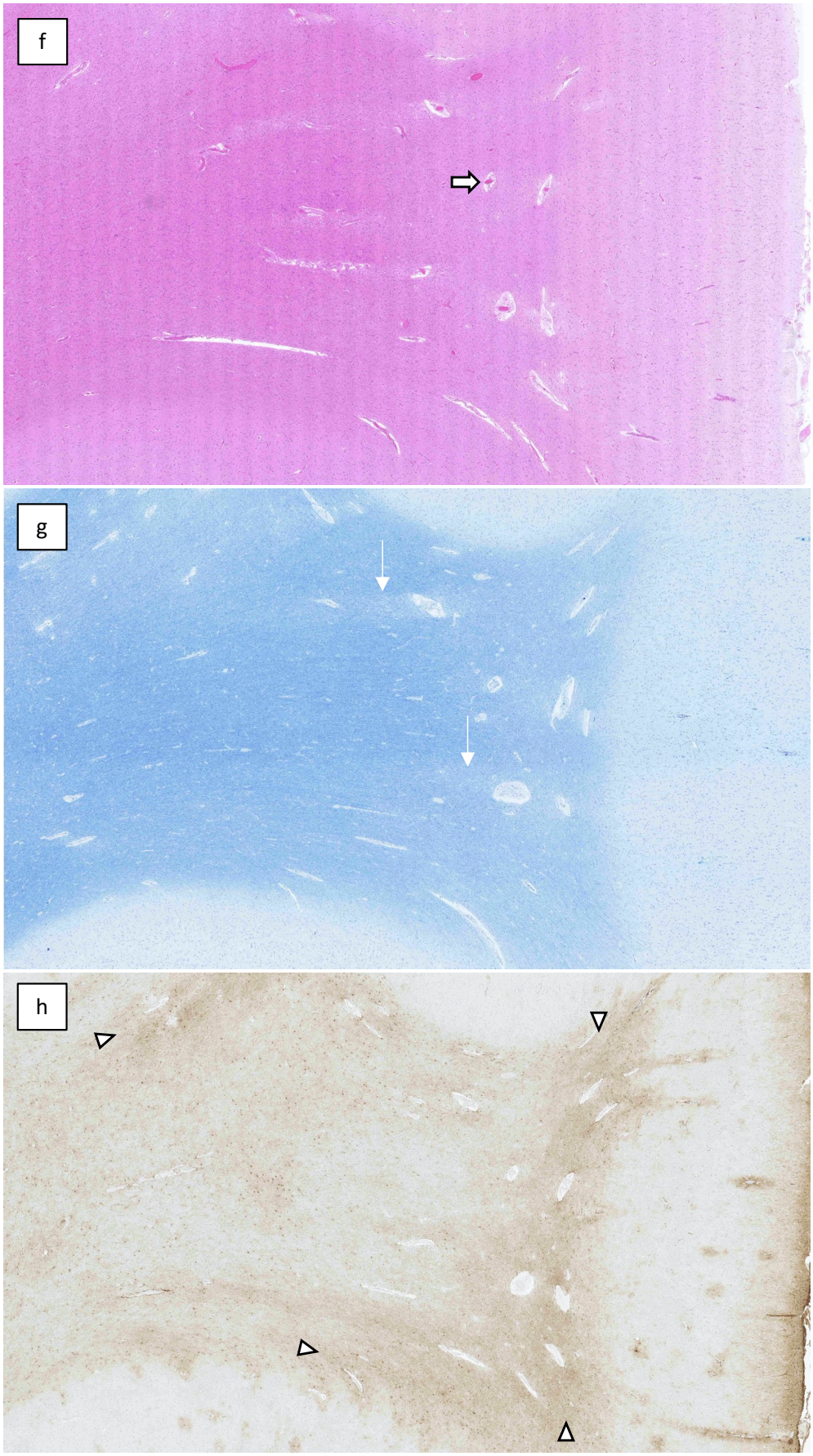


Figure 6.13 Area with multiple enlarged perivascular spaces

a) FLAIR b) T2 c) T1 and d) T2* sequences registered with e) greyscale digitised histology image. The blue crosshairs are centered on an individual enlarged PVS (arrow) on f) the microscopic image (H&E, x20). Some of the enlarged PVS within the area indicated by the red circle show some surrounding hyperintensity. There correspond to perivascular spaces with mild rarefaction of the white matter, seen as pale streaks that follow the course of the vessel on the H&E and g) LFB stain for myelin (white arrows), indicating loss of myelin (x20). h) gliosis is seen in the superficial white matter immediately below the cortex, in the area of enlarged PVS, indicated by increased GFAP staining at low power (indicated by the arrowheads) (GFAP, x20). i) at higher power there is also focal gliosis accentuating the glia limitans around some, but not all, enlarged PVS (GFAP, x40).


f
g
h

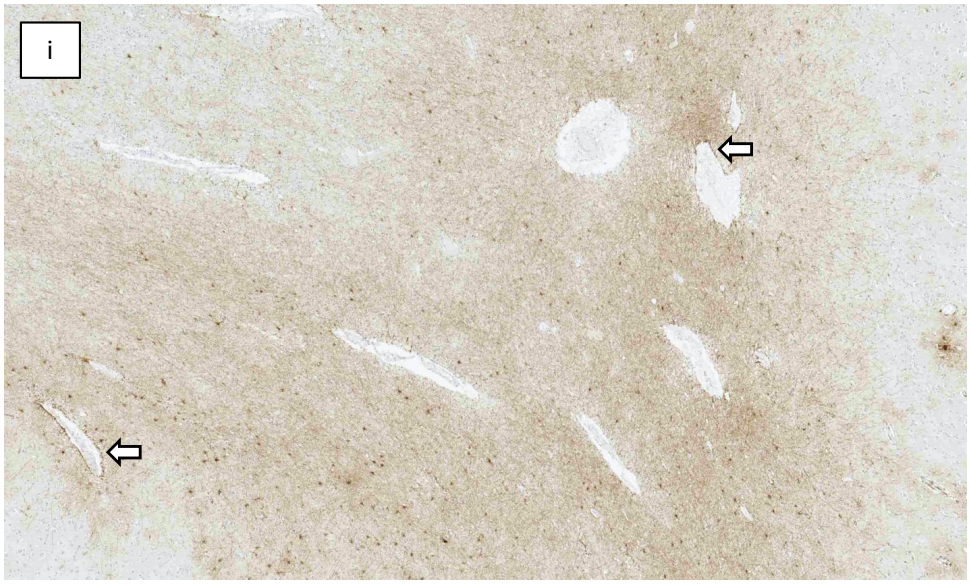


Figure 6.13 Continued from previous page

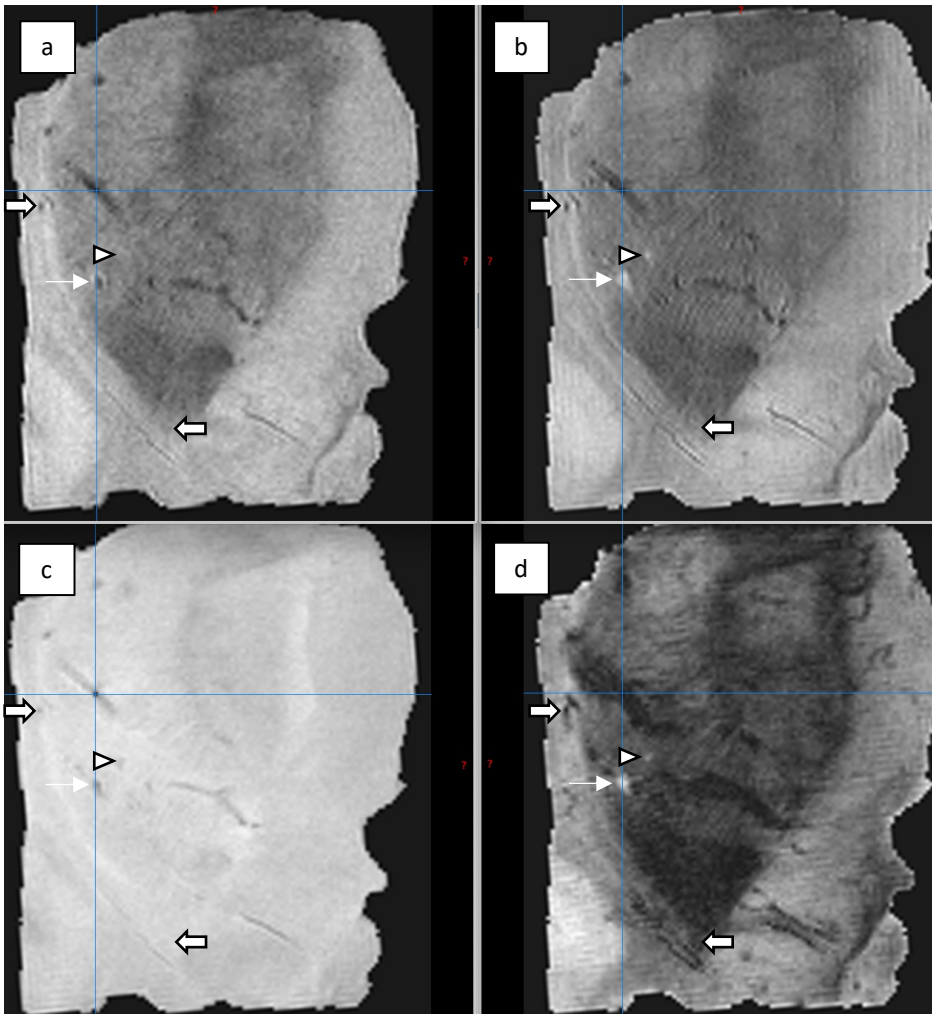


Figure 6.14 Legend on opposite page

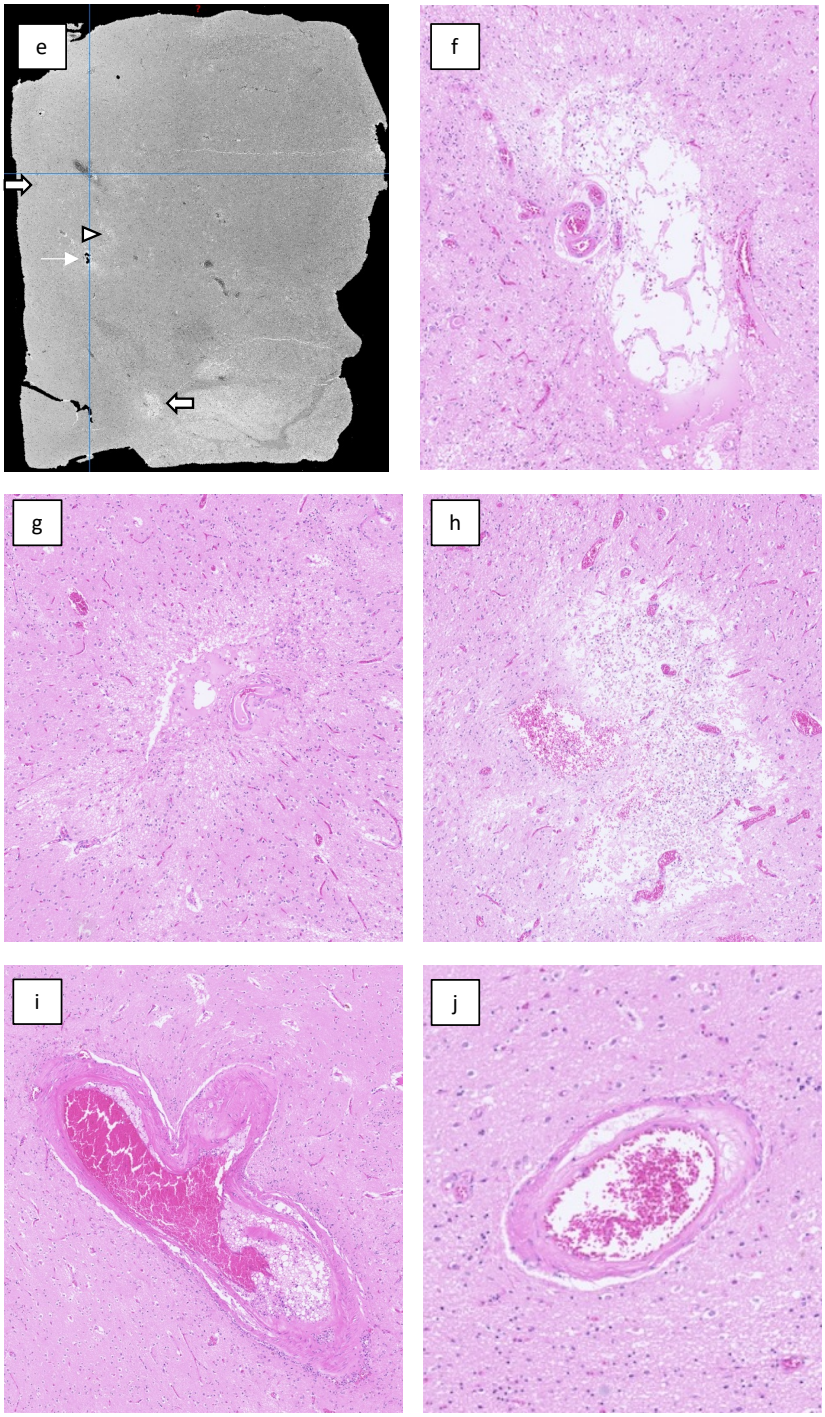


Figure 6.14 Multiple lesions in the basal ganglia

a) FLAIR b) T2 c) T1 and d) T2* sequences registered with e) greyscale digitised histology image. The small white arrows without a black outline indicate a 0.9mm lesion initially called an enlarged perivascular space on MRI but shown to be f) a 2mm lacune on histology. The arrowheads indicate g) a microinfarct measuring 0.8mm on histology, only identified in retrospect on MR imaging. The large left-pointing arrows indicate h) a 3mm histological microbleed not visible on 7T MRI. The blue crosshairs indicate i) a vessel 0.5mm maximum diameter and the large right-pointing white arrows j) a vessel 0.4mm both with lipohyalinosis on histology, not originally identified as lesions on imaging but visible in retrospect as hypointense foci on 7T MRI. All histology H&E x100.

6.4.1.4 Radiological perivascular spaces with a hyperintense rim

48 imaging identified enlarged PVS with a hyperintense rim on FLAIR and/or T2* were studied. Of these, 33 were confirmed as enlarged PVS histologically. Eight were missing a central vessel and were presumed to be PVS (Figure 6.16). Six were not identified on histology and one was an ectatic venule.

22/33 histological enlarged PVS showed perivascular vacuolation in the immediate surrounding neuropil and were associated with pallor on myelin staining (Figure 6.13g), as did 6/8 presumed enlarged PVS. 9/33 enlarged PVS contained perivascular inflammation, seven contained perivascular haemosiderin and seven contained vessels with arteriolosclerosis. The size of the enlarged PVS and the amount of rarefaction varied and it was not possible to identify consistent imaging features to be able to match them to the histology (Figure 6.17).

Gliosis was seen adjacent to three of the enlarged PVS. One contained a vessel with perivascular collagenosis and five contained congested vessels.

Of interest, one vessel sectioned longitudinally showed a branching point (Figure 6.15). Along this vessel on MR, there was an area without a hyperintense rim flanked by areas with hyperintense rims on FLAIR, T2 and T1. On histology, this vessel measured up to 0.5mm maximal diameter and showed mild-moderate enlarged PVS along its course with a small focus of perivascular haemosiderin. The areas with the hyperintensity on imaging showed mild histological perivascular vacuolation. The PVS contained the glia limitans, separated from the parenchyma and proteinaceous material on the parenchymal side of the membrane.

6.4.1.5 Radiological areas with multiple enlarged perivascular spaces

In nine areas multiple enlarged PVS were seen close together, individual vessel comparisons were not carried out but they corresponded to

histological areas of multiple enlarged PVS. In three of these areas the imaging appearances were of patchy hyperintensity (Figure 6.16). Histologically these corresponded to areas of multiple foci of perivascular rarefaction, some of which surround enlarged PVS, many of which directly surround a small vessel. Distinctive imaging features to distinguish those with or without enlarged PVS could not be identified.

Brighter areas of WMH were noted to correspond to more severely enlarged PVS in once example and even in areas of multiple enlarged radiological PVS without hyperintense rims around specific foci, the histological areas of multiple PVS often contained perivascular vacuolation. One area of enlarged PVS was seen within deep grey matter.

6.4.1.6 Radiological microinfarcts

12 radiological infarcts were compared to histology. Eight were confirmed on histology. The largest measuring 3.70mm on *ex vivo* MR in the thalamus was confirmed as 3.6mm infarct with microscopic cell and vessel loss, white matter rarefaction and gliosis. The smallest measuring 1.76mm on MR was a 1.3mm infarct on histology with tissue loss, vacuolation and gliosis. Four were not identified on histology. One measuring 2.94mm was not identified on histology but corresponded to a wider area of white matter vacuolation and pallor with significant numbers of corpora amylacea, one was within an area of radiological WMH corresponding with severe white matter vacuolation. One was in a piece of tissue missing from the histological slide. One measuring 3.11mm was found to correspond with a deep artefactual cut in the edge of the tissue where the superficial aspect had been re-opposed. There were multiple enlarged PVS in the adjacent tissue with vacuolated surrounding white matter. On retrospective examination of the MR, a small cut made during sampling was visible at the edge of the tissue with underlying hypointensity on all sequences, which then changes to hyperintensity on T2 and T2* in the region interpreted as an infarct.

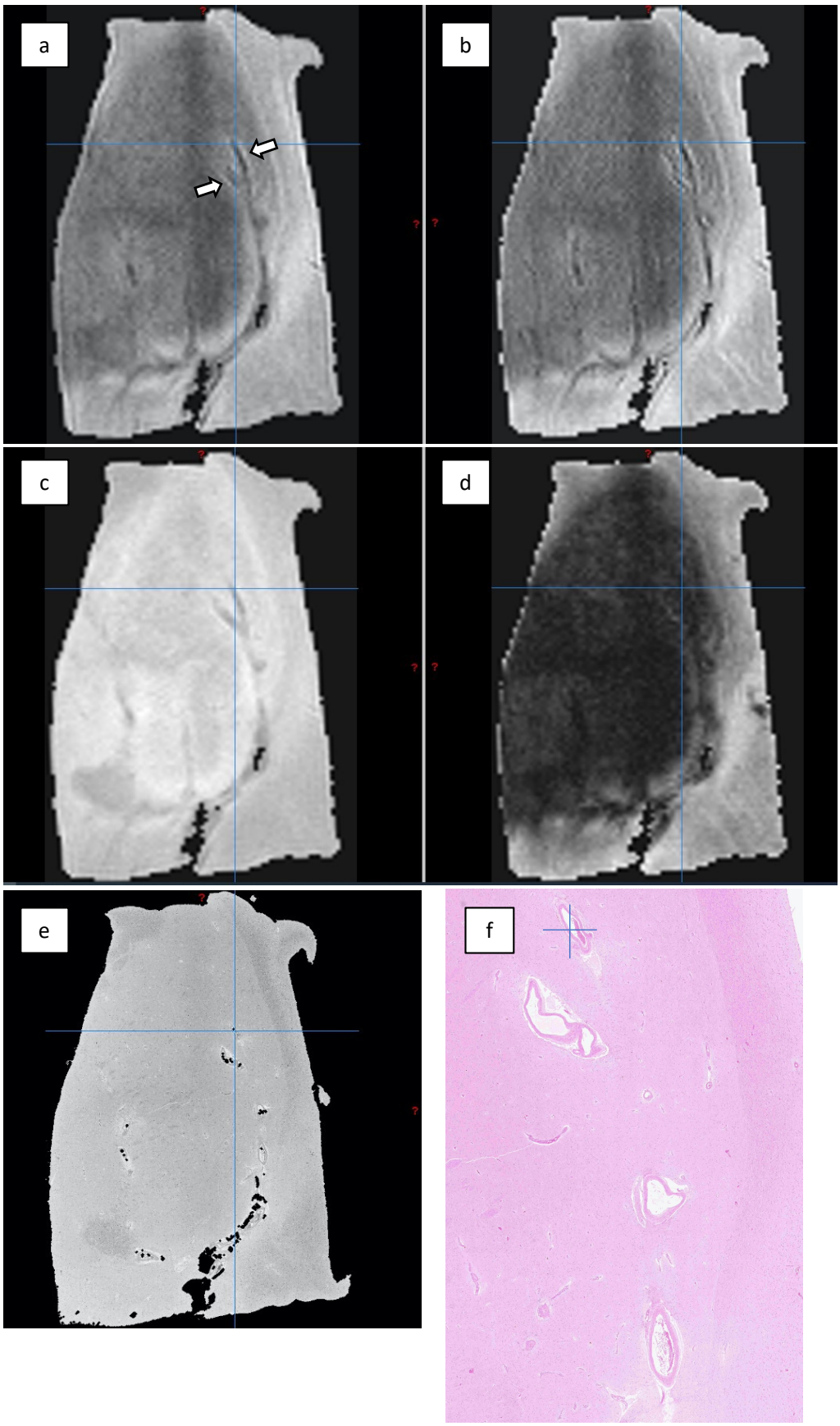


Figure 6.15 Legend on the opposite page

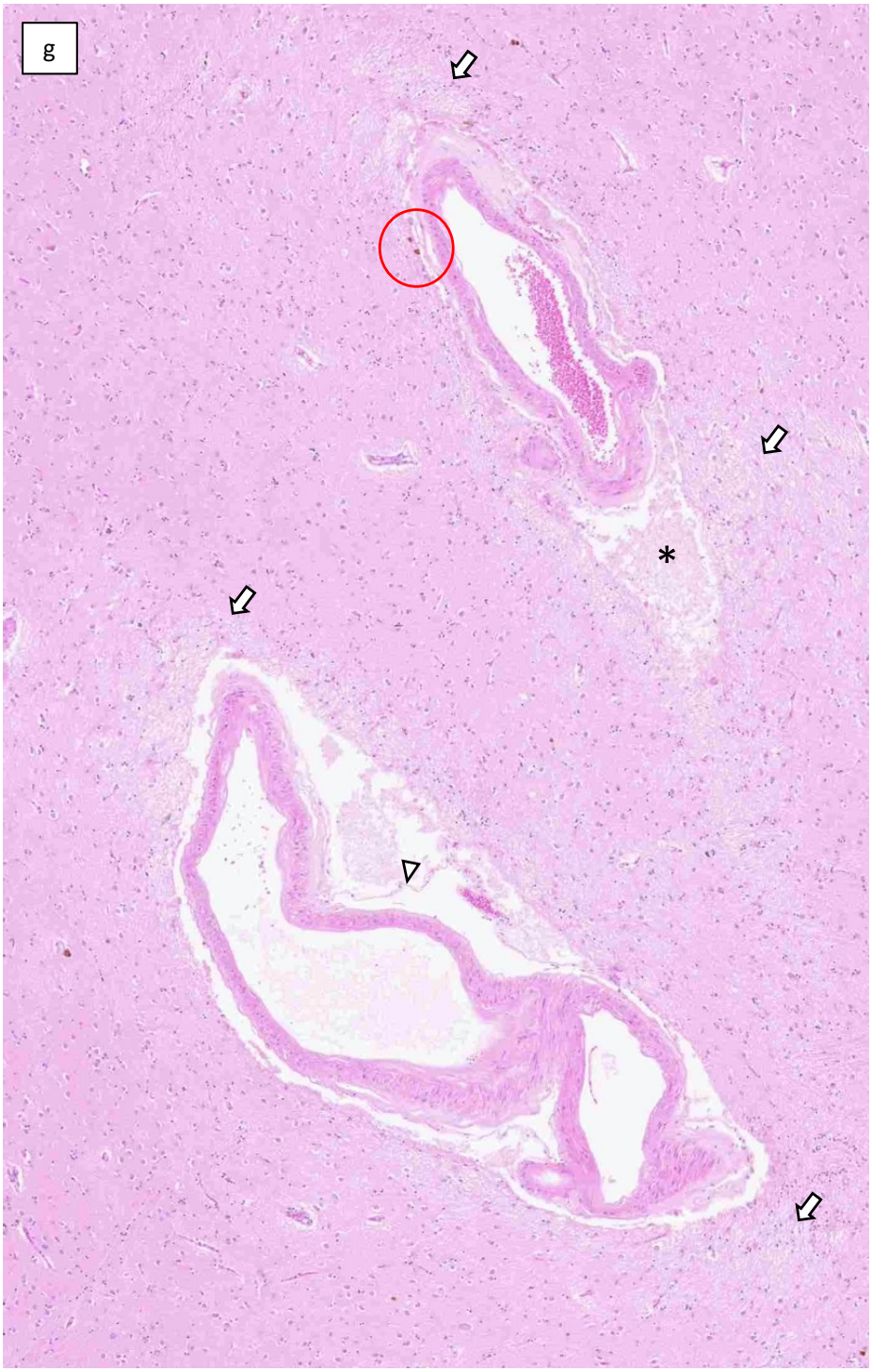


Figure 6.15 A longitudinally sectioned vessel continued

a) FLAIR b) T2 c) T1 and d) T2* sequences registered with e) greyscale digitised histology image. The arrows show a branching vessel imaged longitudinally. The arrows point at sections with a hyperintense rim, which is lacking in other areas. f) On histology, the cross hairs are located at the same point on the superior most part of the vessel. The arrows on histology highlight mild vacuolation, not seen in the areas without MR hyperintensity (H&E x20). g) At higher power, perivascular haemosiderin deposition is present focally (red circle). There is proteinaceous material (*) and glia limitans (arrow head) seen within the enlarged perivascular spaces (H&E x100).

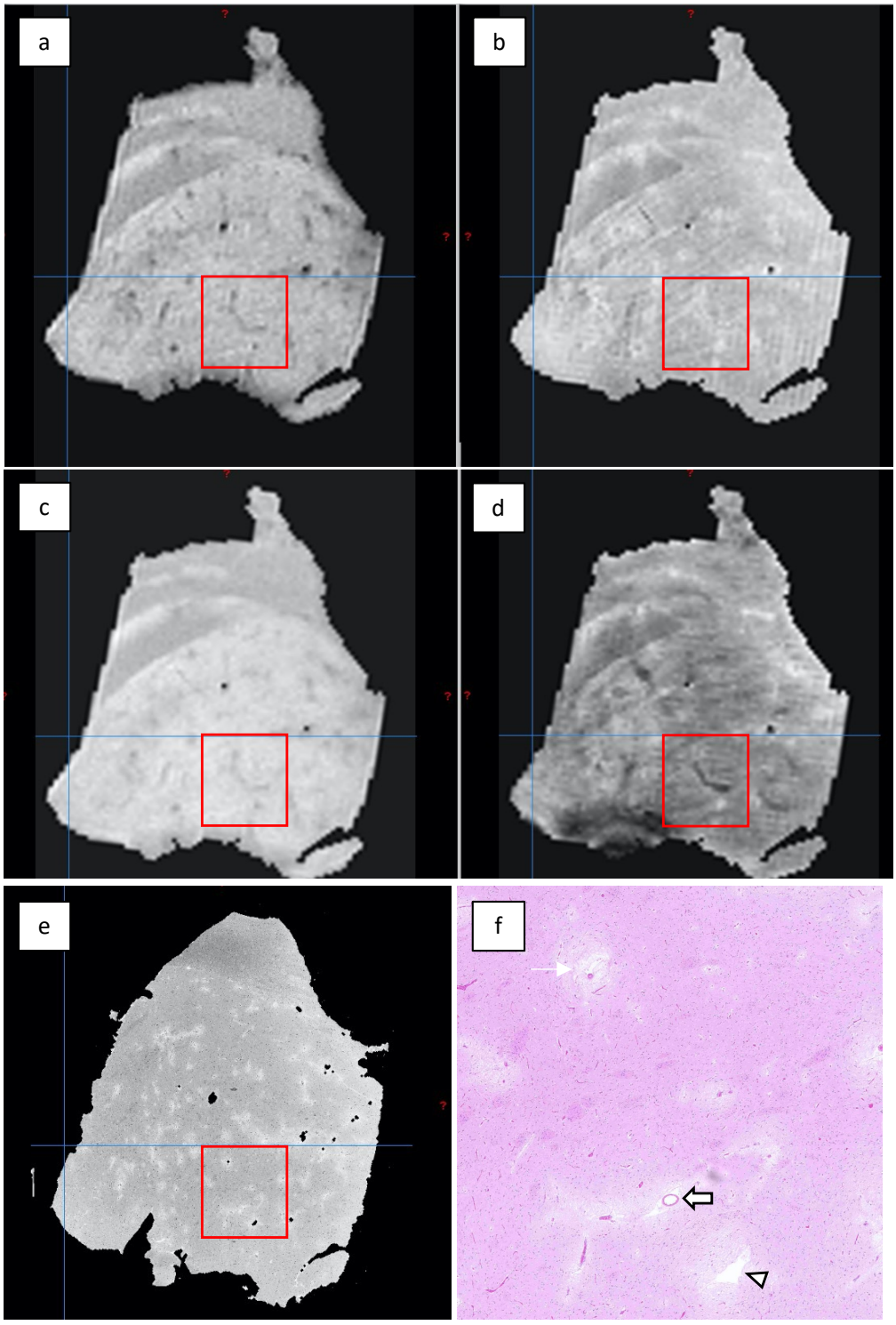


Figure 6.16 Multiple enlarged perivascular spaces

a) FLAIR b) T2 c) T1 and d) T2* sequences of the basal ganglia with multiple enlarged PVS throughout, showing hyperintensity on T2 and T2* and hypointensity on FLAIR and T1. These correspond to e) patchy, ill-defined pale areas throughout the registered histology greyscale image representing multiple foci of perivascular rarefaction. The microscopy of the area within the red box is shown in f), some of the foci of rarefaction surround enlarged PVS (large arrow), some surround vessels without enlarged PVS (smaller white arrow). A presumed PVS, lacking a vessel, is also present (arrowhead). (H&E, x40)

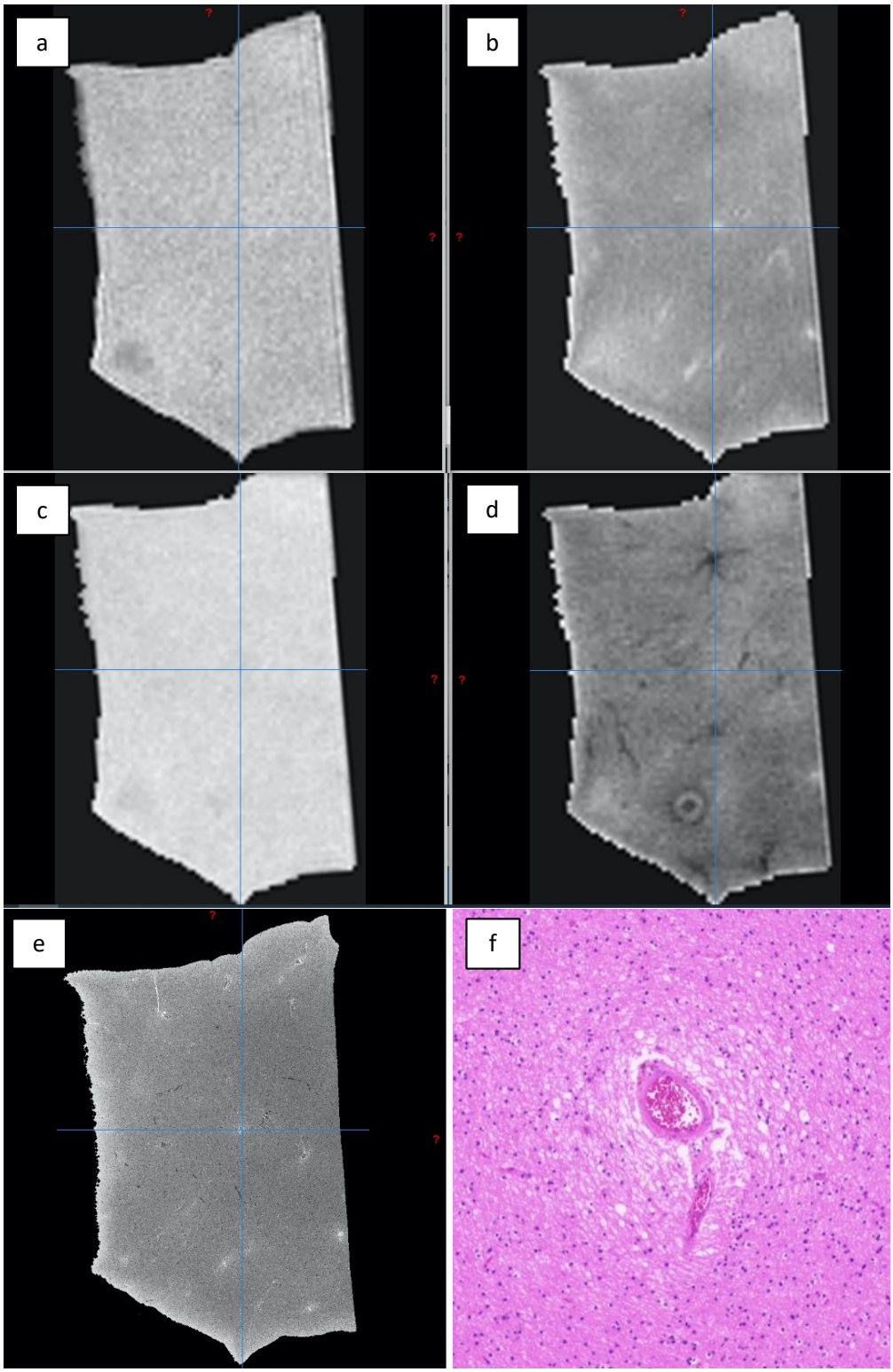


Figure 6.17 Enlarged perivascular space with hyperintensity

a) FLAIR b) T2 c) T1 and d) T2* sequences registered with e) greyscale digitised histology image. The blue crosshairs are centered on an enlarged PVS with focal hyperintensity on the T2 and T2*images and hypointensity on FLAIR. f) On microscopy, the vessel shows arteriolosclerosis and only a very small enlarged PVS with more significant perivascular rarefaction (H&E, x100).

6.4.1.7 Radiological microbleeds

18 potential microbleeds were identified on post-mortem imaging. Three measuring 6.6, 2.56 and 1.39mm were confirmed on histology as microbleeds 1.0, 1.1 and 0.6mm respectively. They showed central tissue loss and vacuolation with haemosiderin-laden macrophages and gliosis in one which corresponded to a rim of hyperintensity on FLAIR and T2. Four radiological microbleeds, three measuring 1.34, 1.23 and 1.07mm corresponded to white matter vacuolation with haemosiderin in the parenchyma and macrophages measuring 0.1, 0.2 and 0.2mm. These were felt to most likely represent the edge of a microbleed that was not fully seen. The fourth was at the edge of the tissue and could not be measured.

Four were found to be areas of perivascular haemosiderin measuring 0.2-0.4mm maximal diameter, one also contained perivascular inflammation. One measuring 0.99mm on MR was a 0.7mm vessel with lipohyalinosis, thrombosis and multiple small recanalised lumens. One measuring 1.09mm was an enlarged PVS containing extravasated red cells (Figure 6.18). One at the edge of the tissue corresponded to the edge of a pigmented nucleus. Four were not identified on histology.

6.4.1.8 Radiological superficial siderosis

Seven radiological areas of superficial siderosis were studied on histology. Two areas showed haemosiderin laden macrophages in the subarachnoid space and superficial cortex. Two showed haemosiderin laden macrophages within the adjacent dura, one of which also contained free haemosiderin. One contained haemosiderin laden macrophages in the dura and superficial cortex and two in the superficial cortex only (Figure 6.19). Cortical haemosiderin was present within macrophages and free in the parenchyma. Several additional areas were not able to be studied as they were lost to masking artefact during the registration process.

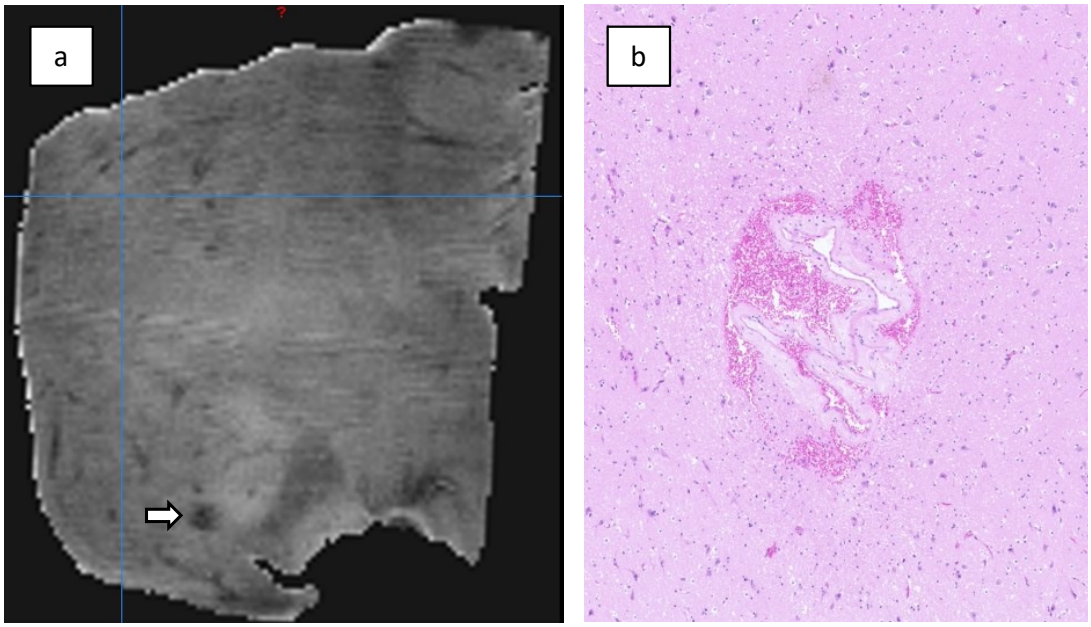


Figure 6.18 Microbleed on T2*

a) T2* sequence with a focal hypointensity and blooming artefact (arrow) called a microbleed but which was found to be b) a focus of extravasated red blood cells on microscopy, surrounding a convoluted venous vessel with perivascular collagenosis (H&E, x100).

6.4.1.9 Radiological foci with T1 hyperintensity

Foci with increased signal on T1 and decreased signal on FLAIR, T2 and T2* were noted on imaging during this study. 38 were compared to histology. 33/38 corresponded to congested vessels with thin walls, as small as 0.2mm histologically, often with red cell extravasation and a narrow rim of condensed neuropil (Figure 6.20). Four had perivascular inflammation, one with mild arteriolosclerosis. An additional two showed arteriolosclerosis. One was an empty venous vessel that may have been previously congested. Perivascular vacuolation was not a feature.

Three of the 38 were not identified on histology and one showed a circular space presumably containing a vessel that had been lost. One corresponded to a severely enlarged PVS containing a large arteriole and mild arteriolosclerosis, mild haemorrhage and moderate-severe perivascular inflammation.

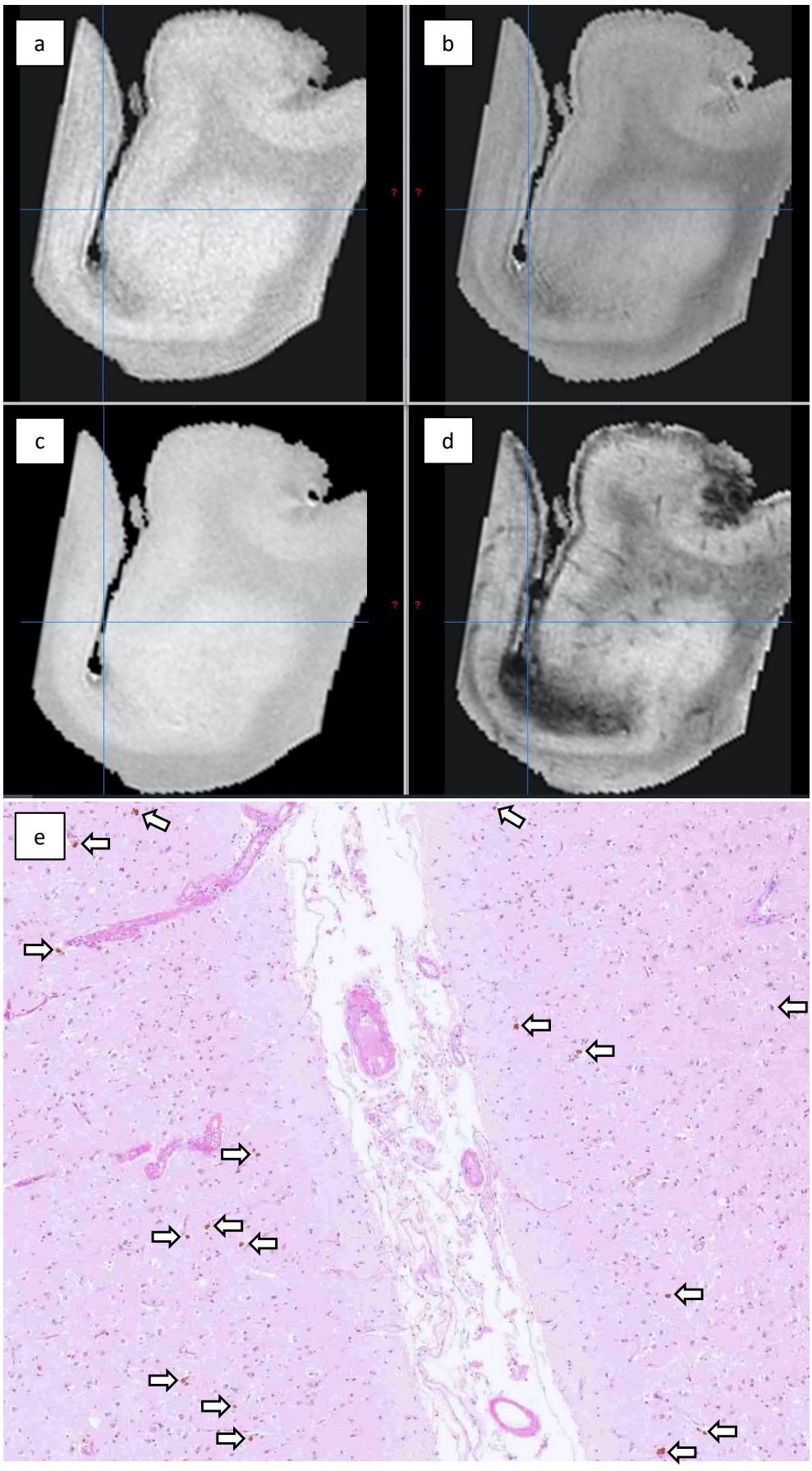

a
b
c
d
e

Figure 6.19 Superficial siderosis

Registered a) FLAIR b) T2 c) T1 and d) T2* sequences with the blue crosshairs centered on a sulcus with superficial siderosis best seen as a hypointense line at the cortical surface on T2*. e) The corresponding histology shows scattered haemosiderin deposits in the parenchyma and within macrophages (arrows), in this case, only in the superficial cortex (H&E, x100).

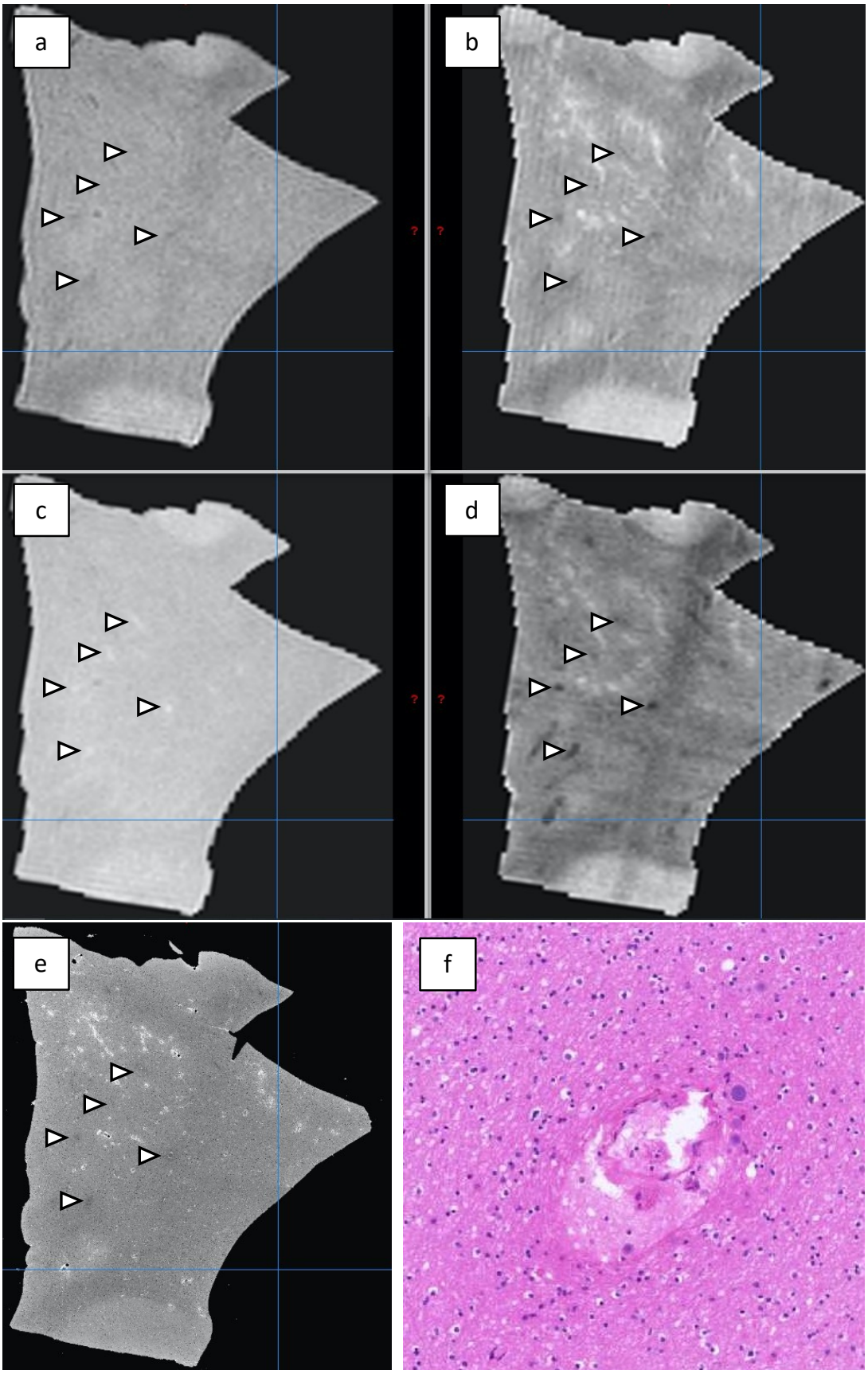


Figure 6.20 Legend on opposite page

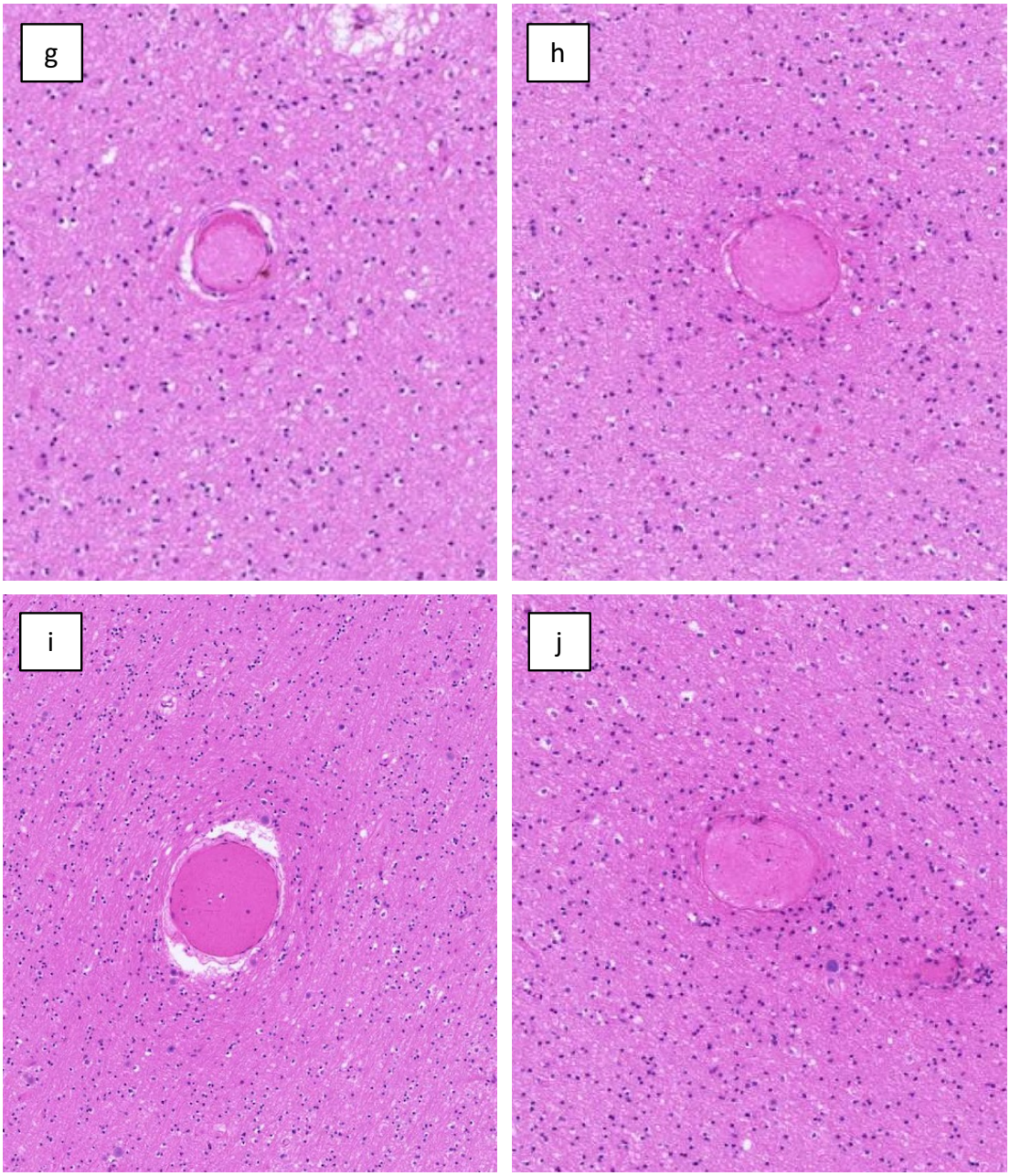


Figure 6.20 T1 hyperintense foci

a) FLAIR b) T2 c) T1 and d) T2* sequences registered with e) greyscale digitised histology image. Multiple foci of T1 hyperintensity were identified with corresponding hypointensity on T2* and more subtle hypointensity on FLAIR and T2 sequences (arrowheads). f-j) These correspond to thin walled vessels (f = top to j = bottom in the MR images). f) Occasionally with extravasated red cells g-j) but more often congested and/or ectatic vessels. Often, the walls appeared densely collagenous with a thin surrounding rim of condensed neuropil.

6.4.2 Lesions identified on histology

Additional lesions identified on histology and sought on the *ex vivo* imaging in retrospect are summarised in Table 6.11.

6.4.2.1 Histological enlarged perivascular spaces

61 additional enlarged PVS were identified on histology and retrospectively searched for on the post-mortem MR. They ranged from <1mm diameter to large and severe PVS. 37 remained not identifiable and it was not possible to find four due to artefact on the MR. On review, 23 were identifiable as enlarged PVS on the MR image, however due to background noise and often being within areas of WMH, they would not have been identifiable without prior knowledge of the histology. One showed only an area of decreased signal on the T2* sequence.

6.4.2.2 Histological infarcts

Eight further infarcts were identified on histological examination. One measured 1.9mm with tissue loss, vacuolation, gliosis in the thalamus and one 0.5mm in the pons also had focal perivascular inflammation. In retrospect, both could be made out on the post-mortem MR scan however they were indistinct and not easily picked out from background patchy WMH. One measuring 0.8mm in the basal ganglia was identified on review of the imaging as a hyperintense focus on T2 and T2* sequences and hypointense on T1 (Figure 6.14g). Five measuring 0.6-2.9mm maximum diameter were not identifiable on ex vivo MR, one was within an area of multiple enlarged PVS and two were hidden by artefact from the plastic cassette.

Three areas containing multiple enlarged PVS were searched for on imaging, one remained unidentifiable. One area within deep grey matter corresponded to a vague area consistent with enlarged PVS signal and one showed a patchy WMH, but neither would not have been identifiable without prior knowledge of the histology.

Table 6.11 Summary of the radiological appearances of additional lesions identified on histology and then searched for retrospectively on post-mortem imaging

Those that were identified would not have been without the guidance of the histology. PVS perivascular space, FLAIR fluid-attenuated inversion recovery.

Histology		Ex vivo imaging	
Enlarged PVS	61	Enlarged PVS	23
		Not identified	37
		T2* hypointensity	1
Areas with multiple enlarged PVS	3	Not identified	1
		Enlarged PVS	1
		Patchy WMH	1
Infarct	8	Not identified	6
		Infarct	2
Lacune	2	Not identified	1
		Lacune	1
Microbleed	9	Not identified	8
		Microbleed	1
Perivascular haemosiderin	13	Not identified	7
		T2* hypointensity	4
		Congested vessel, T1 hyperintensity	2
Perivascular inflammation	6	Not identified	4
		Congested vessel, hypointensity all sequences	1
		Hypointense FLAIR, T1, hyperintense T2, T2*	1
Perivascular haemosiderin and inflammation	5	Not identified	3
		Enlarged PVS	1
		Congested vessel, T1 hyperintensity	1
Arteriolosclerosis	21	Not identified	19
		hypointense FLAIR, T2, T2*	1
Fibrinoid necrosis	4	Not identified	2
		hypointense all sequences	2
Lipohyalinosis	6	Not identified	3
		Congested vessel, T1 hyperintensity	2
		hypointense T2 T2*	1
Perivascular collagenosis	22	Not identified	10
		hypointense all sequences	8
		hyperintense FLAIR, T2	2
		hypointense FLAIR, T2	1
		hyperintense T2	1

6.4.2.3 Histological lacunes

Two lacunes measuring 0.3 and 0.4mm were identified on histology as showing a central cavity with macrophages, tissue loss, gliosis and vacuolation in the surrounding parenchyma. One was visible on MR in retrospect but was within an area of WMH and difficult to identify. One was not visible on the MR.

6.4.2.4 Histological microbleeds

Nine additional microbleeds were identified on histology. One with tissue loss, haemosiderin laden macrophages, extravasated red cells and gliosis was identifiable on retrospective review of the *ex vivo* MR but showed T2* hypointensity with blooming artefact and hyperintensity on FLAIR and T1, which had led it to not be called a microbleed initially. Eight histological microbleeds measuring 0.3-3.0mm were not identified on the MR (3mm microbleed shown in Figure 6.14h), one was within a larger area of T2* hypointensity and one was obscured by cassette artefact.

6.4.2.5 Histological perivascular haemosiderin

The appearances of 13 perivascular haemosiderin foci were compared to imaging. In one, haemosiderin within the wall of a collagenised vessel measuring 0.1mm diameter, with approximately 40 visible hemosiderin laden macrophages, was identified as a 0.42mm T2* hypointensity without blooming. Two further, slightly less severe foci of perivascular haemosiderin corresponded to the radiological appearances of congested vessels, with T1 hyperintensity, one had a branching linear profile. Two severe perivascular haemosiderin deposits were in the vicinity of one moderate deposition. The severe foci had small areas of very hypointense T2* signal, while the less severe focus was also hypointense but less intense. Seven additional foci or moderate-sever histological perivascular haemosiderin measuring from less than 0.1mm up to 0.9mm were not identified on review of the MR.

6.4.2.6 Histological perivascular inflammation

Six moderate-severe histological foci of perivascular inflammation were studied. Two showed subtle MR features that would not have been identified without the histology; one contained a congested vessel and showed hypointensity on all sequences and one with hypointensity on FLAIR and T1 and hyperintensity on T2 and T2*. Four foci measuring from less than 0.1mm to 0.2mm were not identified on imaging.

Five areas with moderate-severe perivascular inflammation and haemosiderin histologically were also compared. One within an enlarged PVS was identified as an enlarged PVS on imaging and one as a congested vessel. Three, measuring from 0.5-0.9mm were not identified.

6.4.2.7 Histological arteriolosclerosis

19 arterioles with moderate-severe arteriolosclerosis on histology were sought on imaging. One congested, moderately arteriolosclerotic vessel with a moderately enlarged PVS and moderate perivascular inflammation was identified as a 0.3mm focus of hypointensity on FLAIR, T2 and T2* with blooming artefact. It was very subtle and would not have been identified without the histology. The remaining 18 vessels ranged in size from less than 0.1mm to 0.3mm and had a range of associated features including perivascular haemosiderin, inflammation, enlarged PVs with surrounding vacuolation and were not identified on MR. Two areas of multiple vessels with arteriolosclerosis measuring 1.5 and 2mm in total, and containing some longitudinally section vessels, were also not identified on imaging (Figure 6.21).

6.4.2.8 Histological perivascular collagenosis

The appearances of 22 vessels with perivascular collagenosis were compared to imaging. Eight of these, ranging in size from 0.2-0.9mm corresponded to hypointense radiological foci on all sequences, the T1 signal was less intense in four and four also had a hyperintense rim on T2, FLAIR and T1. Histologically they had a variety of associated features; enlarged

PVS (n=4), surrounding white matter vacuolation (n=3), perivascular inflammation (n=3), perivascular haemosiderin (n=2) and vascular congestion (n=1). On immunostaining some showed perivascular gliosis and occasional relative myelin preservation when within an area of white matter pallor (Figure 6.23). One with mild surrounding vacuolation corresponded to a very vague area of FLAIR and T2 hypointensity, two to an indistinct focus of area of FLAIR and T2 hyperintensity and one to a focus of T2 hyperintensity only. 10 were not identified on imaging (Figure 6.22).

6.4.2.9 Histological lipohyalinosis

Six foci of histological lipohyalinosis were examined on MR retrospectively. Two, measuring 0.4 and 0.5mm, one of which was associated with a congested vessel showed radiological hypointensity on all sequences (Figure 6.14i, j). One measuring 0.2mm with almost total luminal occlusion and a moderately enlarged PVS with surrounding vacuolation corresponded with a focal hypointensity on T2 and T2*. Three, measuring 0.1-0.2mm were not identified.

6.4.2.8 Histological fibrinoid necrosis

Four foci of fibrinoid necrosis were sought on the post-mortem MR. One measuring 0.3mm was visible as a hypointense foci on all sequences measuring 0.35. It was noted to have similar MR appearances to four other lesions identified histologically as a presumed PVS without a vessel, a congested vessel with mural calcification and two lesions that were not identified on histology. Another 0.3mm focus was just visible as a hypointense (enlarged PVS-like) focus on FLAIR with a bright rim measuring up to 0.37mm, corresponding with the surrounding gliosis (Figure 6.23). Neither would have been distinguished from the background noise without the histology. Two other foci of fibrinoid necrosis measuring 0.1mm and less than 0.1mm were not identified on the *ex vivo* MR.

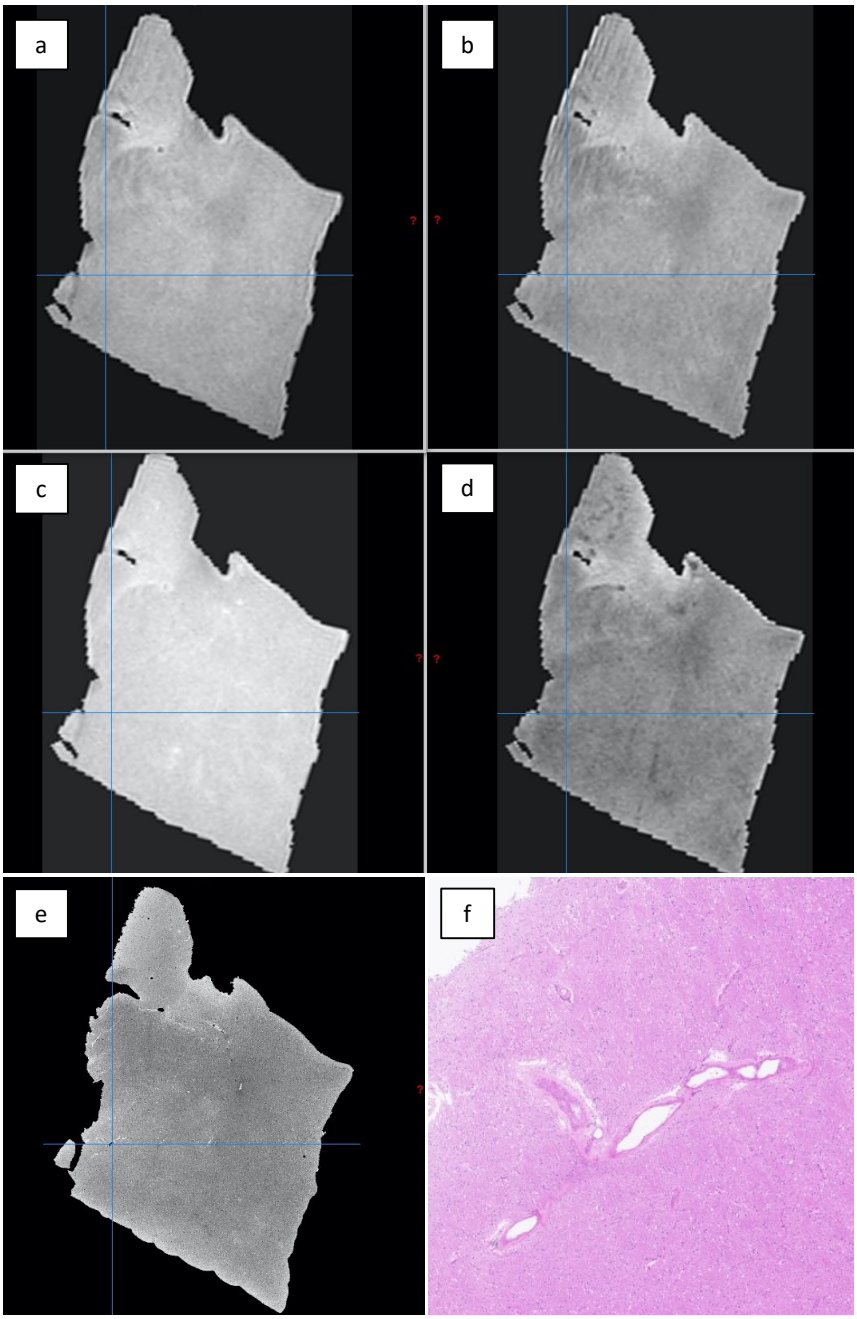


Figure 6.21 Histological arteriolosclerosis not visible on 7T post-mortem MRI

Registered a) FLAIR b) T2 c) T1 and d) T2* sequences registered with e) the digitised greyscale H&E image. The blue crosshairs are centered on f) an area containing several vessels with arteriolosclerosis on histology, shown in part (H&E, x20). The total area measures up to 2mm maximum diameter and is not visible on the MR images.

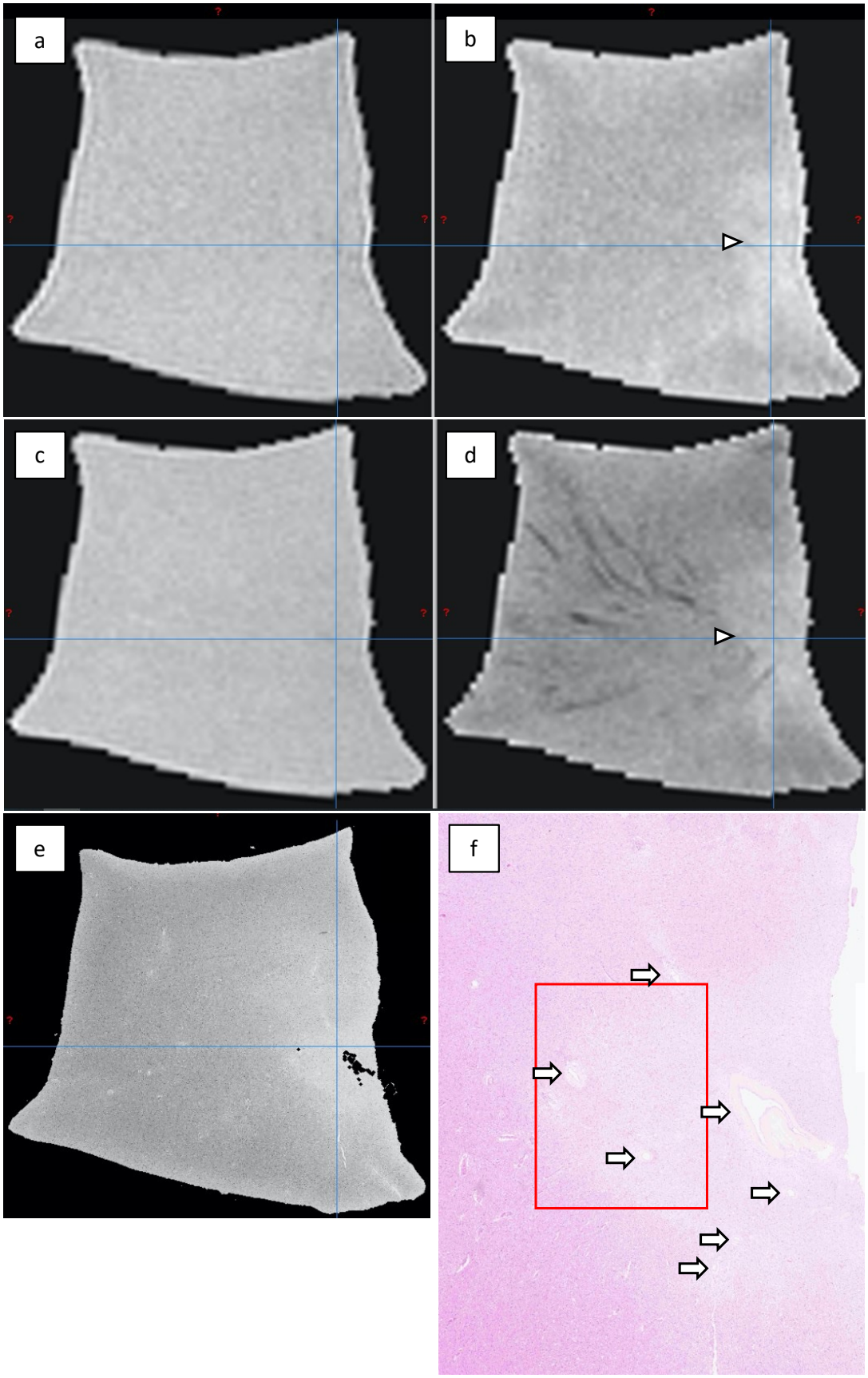


Figure 6.22 Legend on opposite page

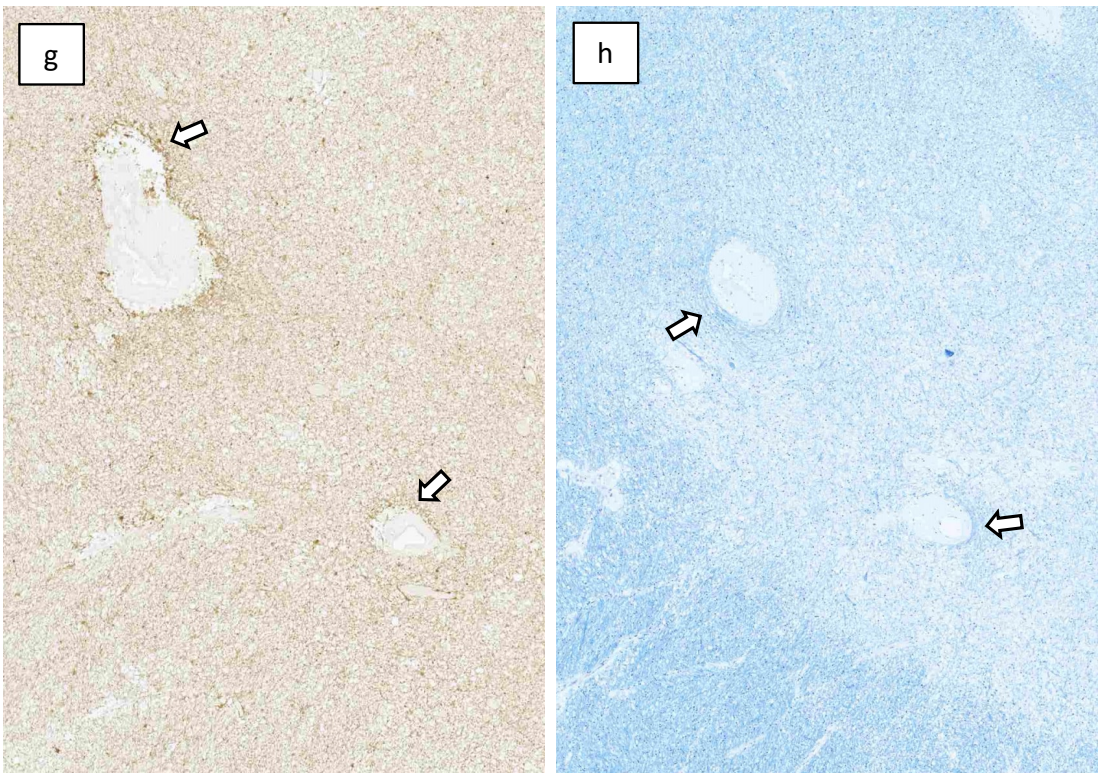


Figure 6.22 Perivascular collagenosis not visible on magnetic resonance imaging

Registered a) FLAIR b) T2 c) T1 and d) T2* sequences registered with e) the digitised greyscale H&E image. The blue crosshairs are centered on f) a focus of several vessels affected by perivascular collagenosis within an area of periventricular white matter rarefaction (arrows) (H&E, x20) The corresponding periventricular WMH is seen on the 7T ex vivo MRI, particularly the T2 and T2* sequences (arrowheads) but the vessels showing perivascular collagenosis are not visible. The area within the red box is shown with an g) LFB stain, confirming the myelin pallor, although with a partial rim of relative myelin preservation (arrows) (x40) and h) GFAP staining which shows a partial, narrow rim of gliosis (arrows) (x40).

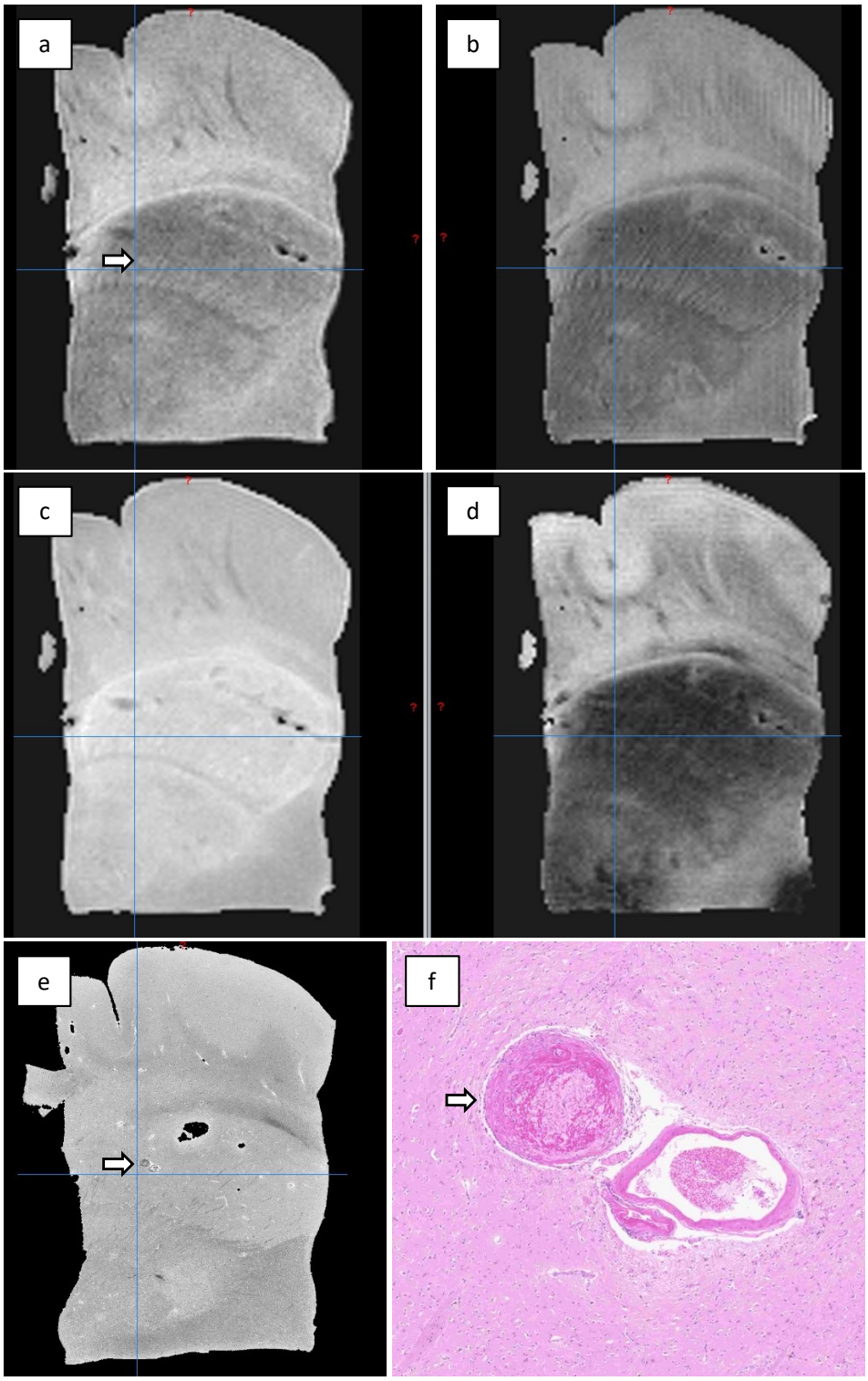


Figure 6.23 Fibrinoid necrosis visible on 7T post-mortem MRI

Registered a) FLAIR b) T2 c) T1 and d) T2* sequences registered with e) the digitised greyscale H&E image. The blue crosshairs are centered below and to the left of f) a focus of fibrinoid necrosis on histology (arrows) (H&E, x40). A corresponding focus with the appearance of a cross-cut enlarged PVS on the FLAIR sequence is visible as a hypointense focus with surrounding hyperintense rim (arrow). This would not have been identified without the corresponding, precisely matched, histology.

6.4.3 Artefacts

The most significant observed artefact was due to trapped air bubbles, these were seen in all spaces of the samples; most commonly at the edge of the tissue, in sulci and overlying tissue (Figure 3.1). They were visible on all MR sequences and identified by their particularly round shape often with a particularly bright border and as having no corresponding histological lesion.

The cassette often caused a cross shaped artefact visible on both the MR and histology and sometime obscured lesions of interest (Figure 6.12). Lesions of interest at the periphery of the sample were also occasionally removed by the tissue masking process. There was often bright signal on FLAIR with the appearance of WMH at the cut edge of the tissue. This had no corresponding lesion on histology and was presumed to be due to formalin.

Due to scanning small pieces of tissue, the wider anatomical association are lost and it was sometimes difficult to orientate the tissue. On one occasion a radiological WMH was found to be an area of cross-cut grey matter and on four occasions possible radiological microbleeds were found to be pigmented nuclei in the region of the thalamus.

6.4.4 Discussion

6.4.4.1 Discussion of lesion comparisons

The main findings of this work are that post-mortem 7T MR correctly predicts the histological pathology of focal lesions only some of the time but is most precise in enlarged PVS and microinfarcts. These focal lesions are also associated with a variety of more subtle features not identified on imaging, particularly perivascular changes including haemosiderin, inflammation, vacuolation and collagenosis. The significance of these perivascular changes and their contribution, or not, to the pathogenesis of SVD is unknown but should be considered in future studies as they may hold further information

on understanding the pathogenetic mechanism underlying SVD. This work also shows there is overlap in the sizes of lacunes and enlarged PVS, and that using size as an identifier on imaging may misidentify them, particularly small lacunes that may be called enlarged PVS.

Some histological features have corresponding radiological appearances, such as the perivascular rarefaction around PVS in both white and grey matter which appeared to contribute to radiological hyperintensity and was sometimes almost continuous with a wider area of white matter rarefaction corresponding to WMH on MRI. Although rarefaction is mentioned in the histological literature, its significance in a perivascular distribution has not been considered in the context of SVD and WMH in particular. Hyperintensity also corresponded to gliosis around a microbleed and was seen in radiological WMH, as in other studies (Simpson, Fernando et al. 2007, Simpson, Ince et al. 2007). However, gliosis around perivascular collagenosis did not, qualitatively, appear to result in brighter radiological WMH. This work does, however, highlight the prevalence of perivascular collagenosis, often in a periventricular location, and the presence of possible associated pathological changes, suggesting in future it should potentially be considered more seriously as a part of the SVD histological spectrum.

This is the first time I am aware of that the histological vascular lesions fibrinoid necrosis, lipohyalinosis and arteriolosclerosis have been identified on 7T MRI. Although they were at the limit of the MR resolution and the appearances were not specific or distinct enough that they would have been identifiable without the histology. Van Veluw et al identified similar vascular pathologies on ultra-high resolution MR (voxel size 100um3) but did not identify any on 7T post-mortem MRI in the same study (van Veluw, Charidimou et al. 2016). In 2001, a targeted study of acute small subcortical infarcts affecting deep perforating vessels found appearances suggesting thrombosed vessels within and adjacent to the areas of infarction (Wardlaw, Dennis et al. 2001). However the vessels on imaging were larger than expected in that area, suggesting there might be additional or alternative

pathology present, within or around the vessel. Histopathological analysis was not carried out in these cases, but a targeted study of these appearances, utilising the methods developed in this thesis would be interesting. Some of the more subtle pathological features such as haemosiderin deposition and perivascular inflammation do not appear to be identifiable on imaging currently, and many questions remain about how they come to be present and what their role is in SVD.

MRI T1 hyperintensity can be due to a number of reasons including blood products (Zaitout, Romanowski et al. 2014). In this series of cases the foci corresponded precisely to congested venules and extravasated red blood cells. As far as I am aware this has not been reported before in SVD, but it is likely a post-mortem artefact due to subacute red cell break down causing the histological and MR appearances seen. As MRI field strengths increase and resolution improves, different kinds of artefact, such as this may become more common. Awareness is needed to avoid misinterpretation.

Strengths of this work included:

- The processing and image registration were developed to exactly meet the needs of the study, prioritising precision, to provide reliable comparisons and conclusions making most efficient use of tissue and resources.

- The use of the three well defined cohorts, representing different aspects of normal, aging and pathological brain tissue, enabling inclusion of the full range of SVD-related pathology including younger as well as more end-stage lesions, although these cannot currently be separated out as we don’t understand the natural history of the disease progression.

- To minimise bias, standardised assessment protocols based on the best available evidence were created and applied.

- Assessments were performed blinded to all clinical, cohort and autopsy data.

- The SVD burden on the *ex vivo* imaging and histopathological assessments in the different cohorts reflect that seen on *in vivo* imaging, supporting their reliability to accurately grade the amount of disease present.

This work also had a number of limitations:

- The number of cases obtained by the brain bank, particularly for the LBC1936 cohort was lower than expected, limiting the potential for analyses comparing normally aged tissue. The intake has increased since this work was completed, however, and post-mortem scanning continues, so the data will be available for future studies and any continuation of this work.

- It took much longer to develop the image registration methods than anticipated, leaving relatively little time to actually perform the precise comparisons. As precision was the priority, a smaller number of accurate comparisons was produced.

- The relatively low number of some lesions, particular infarcts and microbleeds, and the lack of imaging-identified lacunes meant I was unable to carry out really informative comparisons in these lesions. Due to the blinding I did not study all of the focal parenchymal lesions, and no lacunes. In retrospect, someone else could have held the case details and provided random cases, ensuring all focal lesions were included to provide the maximum amount of information about them.

- During the process of carrying out these comparisons, it became apparent that despite using such precise methods, imaging-identified lesions could still be missed on histology due to the differing scales of

slice thickness, for example, a small, sub-millimetre lesion seen on imaging could be deeper within the tissue block that was cut into for histology and so it could be missed. Awareness of this means the number of lesions not identified should be regarded as unresolved, rather than a misleading signal on the MR. Conversely, those seen on histology but not on imaging were almost all ≤2mm and so likely unidentified due to the limit of MR resolution.

- The radiological appearances of the smallest lesions identified often reflected the presence of other features, such as congested vessels or enlarged PVS which could hide any potential unique signal from other, more subtle, histology. It is also possible the variable imaging appearances I saw in these small lesions might be due the presence of multiple subtle pathologies or other associated features such as oedema, not identifiable on histology. These issues may be resolved as higher field strengths with better resolution are used more, but further detailed study and familiarity with their appearances is required before they can be reliably diagnosed. Care must be taken however, as these improved technologies may also result in new and different artefactual issues.

- 0.23mm was the limit of the MR resolution. Measurements and identification of lesions less than this size are not reliable. However, it appears that enlarged PVS appear proportionally bigger on imaging. It is also likely the histological measurements of lesions are not representative of the true maximal size as they may have been seen only at the periphery. Comprehensive histological assessment should involve serially sectioning through the whole lesion. The maximal measurement could then be compared with that on the MR slice.

6.4.4.2 Discussion of the histopathological SVD definitions and grading system

That the histological grading system reflects the expected burden of disease is encouraging, although it needs further study and validation using greater numbers of cases from different cohorts. This grading system applies the definitions developed in this thesis, this supports the potential use of these definitions in histopathological SVD assessment. However wider expert consensus is required if it is to be adopted by the neuropathological community, and we shall undertake a consensus meeting.

We aimed to make the definitions as objective as possible. However, we should remember that some are based on historical assumptions and relatively little is actually known about their development. For example, a focal area of tissue loss and gliosis would be termed an infarct. Given that the brain has a limited number of pathological responses to injury, it is possible several different insults such as ischaemia, haemorrhage or some infections might lead to these appearances, indistinguishable in their end-stage appearance. There is also confusion in the literature regarding a cavitated histopathological 'lacune' and the several different, but very specific, radiological lacunar lesions (Wardlaw 2008). Ideally the terminology used would reflect these uncertainties; however, until these lesions are more fully understood it might not be reasonable to expect such drastic changes.

6.4.4.3 Discussion of cortical thickness measurements

In all three areas measured, the cortical thickness appears to be greatest in the superficial aspects of the brain, thinning with depth into the base of the sulcus and the thickest cortical area was the temporal tip (BA38). The difference in cortical thickness at different sulcal depths is supported by the results of the paired t tests which showed significantly different thicknesses between the different sulcal depths in all three areas measured except between the mid and deep sulcus in Broca's area. In contrast, there were no significant differences between the different areas at the same depth, except

for the mid sulcal measurement in Broca's area and the temporal tip. However it must be noted this is very exploratory and the analyses are limited particularly by the small number of cases and lack of risk factor inclusion. We could not separate out the measurements to study the differences in the difference cohorts but these results suggest it would be interesting in future to conduct more robust studies of differences in cortical depth, and to look further for alterations in other areas of the cortex that may be altered in SVD. This would be particularly interesting in relation to better understanding reports of altered cognitive function in SVD, for example how preserved general cognitive abilities appear to compensate for potential reduction in specific cognitive domains (Hamilton, Cox et al. 2021).

Comparing the measurements obtained by *ex vivo* MRI and histology, it appears in this exploratory analysis that the measurements are unbiased but imprecise and measuring cortical thickness on MRI in this way creates noise in the data, assuming the histological measurements to be accurate. Increasing the sample size would improve the detection of relationships. As age could not be controlled for, including it as a cofactor would also improve the results.

The strengths of this work were the high quality and resolution of imaging available, and availability of precisely matching histology. Although a disadvantage is that cross cutting of the cortex may render it artefactually thicker, the same artefact would be present on both and so they can still be compared. Assuming a similar, random amount of cross cutting throughout the specimens, the measurements can also be used for comparisons across depths and areas in this exploratory analysis. However, this should ideally be controlled for if more robust conclusions are to be drawn, this also means the measurements are not necessarily reliable as indicators of actual thickness.

Cerebral cortical atrophy is variable between individuals but is seen with increased age, although differentially in different areas (McGinnis, Brickhouse et al. 2011). It is also seen in various neurodegenerative

conditions (Walhout, Westeneng et al. 2015, Vuksanovic, Staff et al. 2019, Wilson, Niccolini et al. 2019) including SVD (Jung, Cho et al. 2018). It would be interesting to see if the changes in cortical thickness at different sulcal depths are replicated in larger numbers of cases, where important factors including cohort, age and educational achievement, for example, could be controlled for. In SVD, focal thinning has been associated with underlying focal subcortical infarction (Appelman, Exalto et al. 2009, Aribisala, Valdes Hernandez et al. 2013), and sulcal morphology also changes with age (Jin, Zhang et al. 2018). To explore a relationship between cortical changes in specific areas and focal SVD features in associated functional pathways, particularly focal white matter changes, could be valuable in understanding the pathogenesis and clinical expression of SVD.

6.4.4.4 Conclusion

In the future, it would be interesting to study these lesions in more detail as many unknowns remain. The methods I have used here could be adapted to enable comprehensive assessment of a small number of lesions. Studying the associated histopathological changes around enlarged PVS and focal lesions (infarcts, microbleeds and lacunes), could be informative. Particularly good examples of these lesions, without adjacent pathology, could be identified and sampled, in multiple cohorts. Serial histological sections could be used to enable detailed study of the whole lesion, with protein expression studied and quantified on tinctorial and immunohistochemical stains. Genomic investigation could be carried out on histological sections using spatial transcriptomic methods from the same series to provide an assessment of the amount and location of expression of genes of interest.

A number of features, such as abundance of different cell types and white matter pallor, are difficult to objectively assess on light microscopy. For more accurate understanding I sought to quantify them using alternative methods.

CHAPTER 7: BIOCHEMICAL ASSESSMENT OF WHITE MATTER DAMAGE IN HUMAN POST-MORTEM TISSUE WITH NEURORADIOLOGICALLY DOCUMENTED SMALL VESSEL DISEASE

7.1 Background

As shown so far in this thesis, the cause(s) of SVD are debated and there is limited understanding of the underlying pathology. On in vivo MRI, there is evidence of increased interstitial fluid in WMH but also axon and myelin damage (Fazekas, Ropele et al. 2005, Bastin, Clayden et al. 2009, Maniega, Valdes Hernandez et al. 2015). Microstructural abnormalities are seen in NAWM (Maniega, Valdes Hernandez et al. 2015). The extent of radiological WMH corresponds to a spectrum of histological parenchymal lesions including infarction, vacuolated and degenerate myelin, axonal loss, gliosis, enlarged PVS and a range of vasculopathies including arteriolosclerosis, hyalinisation, vascular ectasia and fibrinoid deposition (Chapter 6) (Awad, Johnson et al. 1986, Braffman, Zimmerman et al. 1988, Braffman, Zimmerman et al. 1988, Marshall, Bradley et al. 1988, Revesz, Hawkins et al. 1989, Fazekas, Kleinert et al. 1991, Grafton, Sumi et al. 1991, van Swieten, van den Hout et al. 1991, Chimowitz, Estes et al. 1992, Munoz, Hastak et al. 1993, Scarpelli, Salvolini et al. 1994, Scheltens, Barkhof et al. 1995, Fazekas, Kleinert et al. 1999, Smith, Snowdon et al. 2000, Smith, Snowdon et al. 2000, Bronge, Bogdanovic et al. 2002, Fernando, O'Brien et al. 2004, Moody, Thore et al. 2004, Fernando, Simpson et al. 2006, Matsusue, Sugihara et al. 2006, Simpson, Fernando et al. 2007, Simpson, Ince et al. 2007, Young, Halliday et al. 2008, Polvikoski, van Straaten et al. 2010, Auriel, Bornstein et al. 2011, Murray, Vemuri et al. 2012, McAleese, Firbank et al. 2013, Hainsworth, Minett et al. 2017). Proposed mechanisms of brain damage focus on microvascular problems including endothelial dysfunction, BBB leakage of neurotoxic proteins such as fibrinogen (Wardlaw, Sandercock et al. 2003, Black, Gao et al. 2009, Wardlaw, Doubal et al. 2013), abnormal arteriolar reactivity to stimuli (Thomas, Miners et al. 2015, Shi, Thrippleton et al. 2016), increased vascular pulsatility, reduced resting

blood flow, ischaemic damage (Markus, Lythgoe et al. 2000, Markus, Hunt et al. 2005) and CAA, which causes about 85% of lobar haemorrhagic pathology (Rodrigues, Samarasekera et al. 2018). Recent MRI studies showed WMH can shrink as well as enlarge (van Leijsen, van Uden et al. 2017, Wardlaw, Chappell et al. 2017) and suggest multiple mechanisms may be involved. The initiating mechanisms, natural history and how these features are related is not understood.

The most common feature of SVD on neuroimaging is WMH in addition to lacunes, enlarged PVS, cerebral microbleeds, atrophy and recent small subcortical infarcts (Wardlaw, Smith et al. 2013, Humphreys, Jansen et al. 2018). To better understand the pathophysiology of WMH I explored how to quantify protein expression in radiological WMH initially by analysing stained paraffin sections. They enable identification and quantification of protein content and are produced routinely for some tissue samples, such as LFB for studying myelin in white matter samples. Other stains not in routine use are readily available and relatively inexpensive.

7.1.1 Fiji/Image J

Image processing and analysis can be carried out in Fiji/ImageJ. It is possible to define regions of interest and segment areas to assess the amount of staining. I undertook training in Fiji/ImageJ and worked with the Imaging Facility Manager in the Centre for Regenerative Medicine at the University of Edinburgh to write a macro script for cases that would quantify the amount of staining, however it proved impossible in these cases due to the large number of samples, the variation in staining and large size of the files.

7.1.2 Commercially available tools

Similar image processing tools are available through commercial companies that are involved in developing slide scanning and digital microscopy using whole slide imaging systems, an area of current development in diagnostic

histopathology and particularly neuropathology. I have previously used Leica Slidepath quantitative software analysis tools successfully to study pleural tumour vascular density in immunostained paraffin sections in a different centre (Tsim, Humphreys et al. 2018). However, upon discussion with the companies, the infrastructure and software was not available to us in Edinburgh. The resources were available in the other centre, however the software was not compatible between the sites to allow digitalisation in Edinburgh and remote analysis and it would not be practical to physically transport slides for digitalisation. Further investigation led me to stereological quantification of stained slides.

7.1.3 Stereology estimation of protein expression

Counting objects in an image can be performed using stereological techniques to provide an unbiased estimate of the number of items within a defined area with a known volume (Geinisman, Gundersen et al. 1996). It has been applied to immunohistochemically stained paraffin sections in LBC1936 to count positive staining and quantify the burden of amyloid plaques and gliosis (Henstridge, Jackson et al. 2015) and would enable me to do an initial assessment and feasibility study in our cohorts.

7.1.4 Biochemical protein assessment

I ultimately collaborated with a group led by Professor Seth Love and Dr Scott Miners at the University of Bristol. We designed a study of protein expression in two cohorts in whom WMH are commonly seen on *in vivo* imaging and controls.

The Bristol group have developed several biochemical methods to investigate the different components of the putative pathophysiology of SVD in human post-mortem brain tissue (Ashby, Kehoe et al. 2010, Barker, Wellington et al. 2013, Thomas, Miners et al. 2015). Markers of chronic and acute ischaemia/reduced tissue oxygenation include decreased MAG to PLP1 ratio (Barker, Wellington et al. 2013) and elevation of VEGF (Thomas,

Miners et al. 2015). These have been validated across independent cohorts (Barker, Wellington et al. 2013, Miners, Moulding et al. 2014). A decline in MAG:PLP1 in parietal cortex and in white matter in AD correlated with the histological severity of arteriolosclerosis and CAA (Barker, Wellington et al. 2013), and with increased VEGF (Miners, Palmer et al. 2015, Miners, Schulz et al. 2018). These might not be strictly transferable to haemorrhagic SVD but were worth investigating.

Vascularity can be quantified biochemically by measurement of von Willebrand factor (VWF) (Ashby, Kehoe et al. 2010). The level of this endothelial cell antigen correlates closely with microvessel density in cerebral cortex and white matter (Barker, Wellington et al. 2013, Barker, Ashby et al. 2014). VWF has been used to assess microvessel density in AD and dementia with Lewy bodies (Miners, Moulding et al. 2014, Thomas TL 2015, Miners, Schulz et al. 2018). Increased fibrinogen within the brain, is a reliable marker of BBB leakage (Petersen, Ryu et al. 2018), as demonstrated in the cerebral cortex and underlying white matter in AD (Miners, Schulz et al. 2018). It was seen as a common finding in older age, but was not associated with SVD (Bridges, Andoh et al. 2014).

The number of pericytes, thought to control vasodilatation, blood flow at microvessel junctions and the blood-brain barrier, can be estimated by measurement of PDGFRB. PDGFRB is decreased in the cortex in AD but not in the underlying white matter; in the cortex the reduced PDGFRB levels are associated with vascular leakage and tissue ischaemia (Miners, Schulz et al. 2018). In SVD and AD there is also evidence of abnormally increased expression of EDN1 and angiotensin-II (angII), two potent vasoconstrictor peptides associated with cerebral hypoperfusion (Miners, Ashby et al. 2009, Miners, van Helmond et al. 2010).

This work aimed to:

1. Establish the biochemical methods in Professor Colin Smith's lab at the University of Edinburgh and validate them in cases from the MRC Edinburgh Brain Bank.

2. Develop the methods to analyse the relationships between neuroradiological and histological white matter abnormalities using biochemical markers of oxygenation, vascularity, BBB function, pericyte content and vasoconstrictor levels.

3. Explore the biochemical marker expression and relationships in WMH and areas of NAWM precisely located on post-mortem imaging, compared to controls without WMH.

Three groups of patients with and without histologically confirmed SVD were prospectively studied; intracerebral haemorrhage (ICH-SVD), AD, and controls (the cohorts are detailed in Chapter 3, Section 3.1.3). These were age-matched as far as possible. This study has revealed similarities but also some striking differences in the biochemical processes associated with white matter abnormalities in ICH-SVD and AD.

7.2 Materials and methods

7.2 1 Stereology methods

Samples were selected from all those cases that had undergone post-mortem *ex vivo* imaging as detailed in Chapter 5. Inclusion criteria for lesional cases was to have at least one area of radiological WMH and at least one area of NAWM on post-mortem imaging, controls had no WMH on *ex vivo* imaging. Cases were age and sex matched. Six lesional cases with areas of radiological WML and separate areas of radiologically NAWM were used, and four controls without WML.

The stains were chosen to measure key aspects of the neurovascular unit thought to be involved in, or affected by, SVD; endothelial cell content (CD34), endothelial tight junctions (claudin-5), pericyte content (PDGFRB) astroglia (GFAP), macrophages (CD163), activated microglia (CD68), inflammatory cells with major histocompatibility complex (MHC) class II activation, including B lymphocytes, microglia and macrophages (CR3-43), vascular leakage (fibrinogen) and myelin (LFB). Tissue was processed for histology as described in Chapter 5, paraffin sections were cut at 4um. Staining details for CD34, CR3-43 and fibrinogen are described in Appendix 6, additional stains in Table 5.3.

Protein expression was estimated in stained paraffin sections using StereoInvestigator software (Micro Bright Field, Zeiss AxioImager Z2). I identified areas of interest on post-mortem MR images and registered digitalised histology images. I outlined the areas at 1.5x magnification on the appropriate stain and scanned tiles at 10x magnification for quantification. A colour-based thresholding algorithm automatically identified positive staining. Exclusion limits for the size of individual stained features were set for each stain to only include the cells of interest and exclude non-specific staining. The area of each region of interest was divided by the area of positive staining to give the percentage of positive staining.

7.2.1.1 Statistical analysis

One-way ANOVA was used to look for differences in staining between the disease groups (WML, NAWM, lesional cases [WML and NAWM combined]) and controls. Paired t tests were used to look for differences between the mean values for areas with WML and NAWM in the same individuals. Additional variables couldn't be controlled for given the small number of cases. Analysis was carried out using GraphPad Prism version 7.0c for Mac OS X, GraphPad Software, San Diego, California, USA.

7.2.2 Biochemical methods

7.2.2.1 Patients used

I used tissue from the three cohorts within the MRC Edinburgh Brain Bank described in Chapter 3; ICH-SVD patients with severe histological features of SVD were obtained from the LINCHPIN cohort (Samarasekera, Fonville et al. 2015, Samarasekera, Lerpiniere et al. 2015), since ICH is a recognised, common presentation of severe SVD in patients aged over 60 years. Cases with AD, diagnosed in life using the Addenbooke's Cognitive Examination (Crawford, Whitnall et al. 2012) and confirmed on post-mortem neuropathology to have Braak tangle stage V-VI disease, were obtained from the SDBTB. Controls had died suddenly and unexpectedly, had no known neurological disease in life, absent neuropathology and came from the sudden death cohort. Subjects were age matched as far as possible but this was difficult between cases and controls as the controls were younger and only relatively small numbers of samples are available.

7.2.2.2 In vivo *imaging*

All patients with *in vivo* imaging had scans rated according to the same standard tools. WMH are readily identified and characterised on MRI (Wardlaw, Smith et al. 2013), however many of the LINCHPIN patients were too unwell to undergo MRI and so only had CT available. WMH are identified as hyperintensities on MRI and hypointensities on CT. Cases with *in vivo* MRI or CT were identified and WMH assessed using validated scores (Wardlaw, Doubal et al. 2009, Wardlaw, Bastin et al. 2011, Valdes Hernandez Mdel, Armitage et al. 2015). Scores for anterior and posterior WMH were combined to give a total WMH score from 0-4. Scans were rated by two independent assessors (myself or a neuroradiology registrar Dr Mark Rodrigues, and checked by an experienced neuroradiologist, Professor Joanna Wardlaw). Any discrepancies reviewed and resolved. Sudden death controls were selected post-mortem (prior to autopsy) and therefore had no *in vivo* imaging.

7.2.2.3 Tissue retrieval

Tissue was obtained at autopsy as described in Chapter 5 (Humphreys, Jansen et al. 2018). The brain was weighed, the brainstem and cerebellum removed and then the cerebrum sectioned coronally. Standardised sampling was used to take tissue specimens measuring approximately 2x2x1cm from defined neuroanatomical regions in the left hemisphere. Deep white matter was taken in the coronal plane of the lateral geniculate body, frontal at the level of the genu of the corpus callosum, periventricular at the level of the mamillary bodies and occipital at the level of the splenium of the corpus callosum. Deep white matter was sampled from the left hemisphere to compare the three cohorts, if this area was affected by a large haemorrhage, tissue from the same area in the right hemisphere was used. The location of the haemorrhage was recorded to indicate its proximity to the sample used (Table 7.2). Tissue to study WMH and NAWM came from different white matter areas depending on the location of the WMH in the subsequent MRI (Table 7.3). Each sample was bisected coronally, half for fixation in buffered formalin, *ex vivo* imaging and histological processing and half for immediate freezing in nitrogen vapour at -80°C.

7.2.2.4 Ex vivo MR imaging

To specifically study tissue with or without WMH, we selected deep WM samples that had had undergone high-resolution *ex vivo* 7T MRI, as detailed in Chapter 5 (Humphreys, Jansen et al. 2018). Tissue sampled for routine histology was formalin fixed for 48-72 h in a plastic container. The container was scanned in a 7T small-bore MRI scanner (Aglient Technologies, Yarnton, UK) with a 400 mT/m gradient coil using sequences adapted from *in vivo* sequences and optimised to detect SVD features.

Protocols validated in large scale studies (Wardlaw, Bastin et al. 2011, Valdes Hernandez Mdel, Armitage et al. 2015) were adapted to grade the radiological WMH burden in the post-mortem tissue samples. WMH were

graded as present/absent on blocks with sufficient white matter, their extent (0 = no WMHs, 1 = some WMHs, 2 = about 50% of white matter lesional, 3 = almost all/all white matter lesional) (Figure 7.1) and location (deep or periventricular) was recorded. Grading was carried out blinded to cohort, clinical data and *in vivo* imaging. Control (no WMH in any blocks) and lesional cases were chosen. Lesional cases donated both WMH (WMH in at least 50% of block, grade 2/3) and NAWM (grade 0) where possible.

7.2.2.5 Histology

AD pathology was staged using standard criteria (Braak and Braak 1991, Thal, Rub et al. 2002). As there remains no general consensus on the significant pathological features of SVD, or grading thereof, we adapted existing published schemes (Deramecourt, Slade et al. 2012, Smallwood, Oulhaj et al. 2012) to grade microvascular and parenchymal pathologies separately as described in Chapter 5, from none to severe (Appendix 7). Assessment was carried out blinded to all clinical and imaging data and to cohort. The relevant vascular lesions include arteriolosclerosis, fibrinoid necrosis, occlusion and recanalisation. Parenchymal changes include rarefaction, PVS dilation, cavitated lesions, large infarcts, microinfarcts and microbleeds as defined in Chapter 4 (Table 4.3).

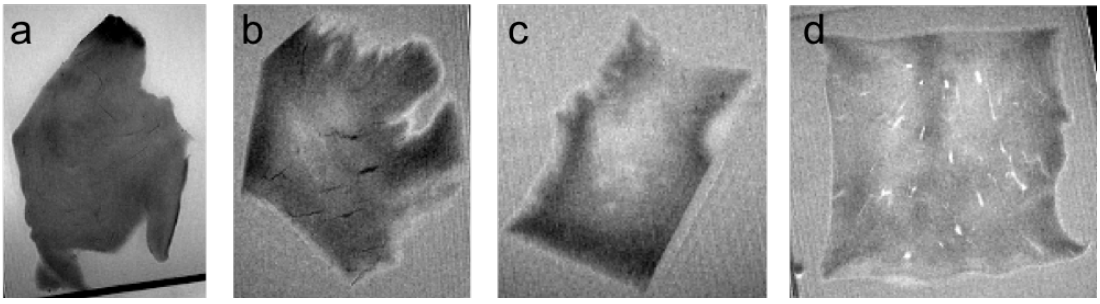


Figure 7.1 Ex vivo MRI assessment of extent of WMHs for selection of tissue for biochemical assessment

a) 0 = no WMH, b) 1 = some WMH, c) 2 = about 50% of WM is hyperintense, d) 3 = almost all of the WM is hyperintense.

7.2.2.6 Biochemical assessment of vascular markers and disease pathology

Tissue preparation and protein measurements were all carried out on the first 40 cases in Bristol in collaboration with Dr Miners for a selection of the experiments (MAG:PLP-1, VEGF, VWF, PDGFRB and fibrinogen). I wrote standard operating procedures for use in Edinburgh for all procedures involved in the preparation and processing of the tissue and established the methods using the same techniques, consumables and equipment as far as possible. I performed all experiments and analyses. Cases were assigned random numbers and analysed blinded to all clinical, cohort, imaging and histological data. In each individual run, cases were further randomised across the plate to avoid experimental bias. The same 40 samples were repeated in Edinburgh for validation initially. The machines, such as the centrifuge, incubator and plate reader, were already available within the University of Edinburgh Centre for Clinical Brain Sciences and so were not identical between the sites. The resulting standard curves and analyses of measured protein levels repeated using the same cases at both centres were compared.

Tissue homogenates were prepared as previously described (Thomas, Miners et al. 2015). In brief; WM for biochemical assessment was taken from frozen samples immediately adjacent to those used for ex vivo MRI. Approximately 200 mg of frozen tissue was defrosted and homogenised in lysis buffer (5 M NaCl, 1 M Tris-HCl pH 7.0, 1 mM phenylmethylsulphonyl fluoride, 1.7 mg/ml aprotinin, 10% sodium dodecyl sulphate), by use of a mechanical Precelleys homogeniser (Bertin Technologies) with 2.3 mm zirconia silica beads (Thistle Scientific). Homogenates were spun at 13,000 rpm for 15 min at 4°C (Eppendorf centrifuge) then supernatants removed and stored at -80°C. Total protein was determined using the Sigma Protein kit following the manufacturer's guidance.

7.2.2.7 MAG direct ELISA

The concentration of MAG was determined by in-house direct ELISA as previously described (Barker, Wellington et al. 2013, Miners, Palmer et al. 2015, Thomas, Miners et al. 2015, Miners, Schulz et al. 2018). Wells of a 96-well clear bottom microplate (R&D Systems) were loaded with brain homogenates diluted 1:10 in phosphate buffered saline (PBS), recombinant human MAG (Abnova) or with PBS only (blanks), in duplicate. They were incubated in a plate-shaker incubator (New Brunswick Scientific) for 2 h at 26°C with shaking at 300 rpm. The plate was washed five times in PBS/0.05% Tween-20 and blocked with 1% bovine serum albumin/PBS for 1 h at 26°C with shaking. The plate was washed five times and incubated for 2 h at 26°C whilst shaking, with 0.5 µg/ml monoclonal mouse anti-MAG (Abcam, ab89780). The plate was washed five times and incubated with biotinylated anti-mouse secondary antibody (Vector labs) diluted 1:4000 for 20 min, at 26oC with shaking. After further washing, 1:500 streptavidin-horseradish peroxidase (HRP) (R&D Systems) was added for 20 min at 26°C. The plate was washed five times then incubated with chromogenic substrate (R&D Systems) for 10 min in the dark before being stopped with 2N sulphuric acid. After the substrate reaction was stopped, absorbance was read at 450 nm in a plate reader (Molecular Devices). Mean values from duplicate measurements are presented. The concentration was interpolated from measurements of serially diluted recombinant human MAG (400-6.25 pg/ml).

7.2.2.8 PLP1 ELISA

The concentration of PLP1 was measured in brain homogenates by commercially available sandwich ELISA (Cloud Clone Corp) following the manufacturer's instructions, as for previous studies (Miners, Palmer et al. 2015, Thomas, Miners et al. 2015, Miners, Schulz et al. 2018). Brain tissue samples diluted 1 in 10 in PBS, recombinant human PLP1, or PBS blanks were incubated for 1 h at 37°C in a plate that had been pre-coated and

blocked. The samples were tipped (not washed) out and the plate was incubated with a detection antibody (antibody A) for 1 h at 37°C. The plate was then washed three times in proprietary wash buffer and incubated with antibody B (streptavidin-HRP) for 30 min at 37°C. The plate was washed five times and incubated in the dark for 15 min then stopped with 2N sulphuric acid. Absorbance was read at 450 nm in a plate reader (Molecular Devices). Mean values from duplicate measurements are presented. The concentration was interpolated from measurements made on serially diluted recombinant PLP1 (10-0.156 ng/ml).

7.2.2.9 VEGF ELISA

The concentration of VEGF was measured using a commercially available duoset ELISA kit (R&D systems) according to the manufacturer's guidelines, as previously described (Barker, Ashby et al. 2014, Miners, Palmer et al. 2015, Thomas, Miners et al. 2015, Miners, Schulz et al. 2018). A plate was incubated overnight at room temperature with mouse capture antibody, washed five times then 1% bovine serum album (BSA) in PBS added for 1 h at room temperature. The plate was washed five times then loaded with brain tissue homogenates diluted 1:5, recombinant human VEGF standards, or 1% BSA in PBS as blanks, and incubated for 2 h at room temperature. After being washed 5 times, the plate was incubated with biotinylated goat VEGF detection antibody for 2 h at room temperature. After washing the plate 5 times it was incubated with streptavidin-HRP in the dark for 20 min, washed 5 times and incubated with substrate solution for 20 min in the dark when the reaction was stopped with 2N sulphuric acid. Absolute VEGF concentration was interpolated from measurements of serial dilutions of recombinant VEGF (2000-31.3 pg/ml).

7.2.2.10 PDGFRB ELISA

PDGFRB concentration was measured using a commercially available duoset ELISA kit (R&D systems) following manufacturer's guidelines, as

previously described (Miners, Palmer et al. 2015, Thomas, Miners et al. 2015, Miners, Schulz et al. 2018). A plate was loaded with mouse anti-human capture antibody and incubated overnight at room temperature. It was washed 5 times (0.05% Tween-20 in PBS) and incubated with homogenised brain tissue samples diluted 1:25, recombinant human PDGFRB standards and PBS blanks for 2 h at room temperature. The plate was washed 5 times then incubated with goat anti-human detection antibody at room temperature for 2 h. After washing the plate 5 times it was incubated with streptavidin-HRP in the dark for 20 min, washed 5 times and incubated with substrate solution for 20 min in the dark. The reaction was stopped with 2N sulphuric acid. Absolute PDGFRB concentration was interpolated from serial dilutions of recombinant human PDGFRB (16,000-250 pg/ml).

7.2.2.11 Fibrinogen ELISA

Fibrinogen level was measured with a commercially available sandwich ELISA kit (FINETEST), following the manufacturer's guidelines, as previously described (Miners, Palmer et al. 2015, Thomas, Miners et al. 2015, Miners, Schulz et al. 2018). A plate preloaded with anti-human fibrinogen capture antibody was washed twice with wash buffer then loaded with recombinant human fibrinogen standards, human brain tissue homogenates diluted 1:3 in the kit sample/standard dilution buffer, which also served as blanks and incubated at 37°C for 90 min. The plate was washed 5 times with 0.05% Tween in PBS then incubated with biotin-labelled antibody for 1 h at 37°C. The plate was washed 5 times then incubated with streptavidin-HRP in the dark at 37°C for 30 min, washed again 5 times and incubated with substrate solution for 20 min in the dark at room temperature. When the colour had developed the reaction was stopped with 2N sulphuric acid. Absolute fibrinogen concentration was interpolated from the serial dilution of recombinant fibrinogen (100-1.56 ng/ml).

7.2.2.12 VWF ELISA

VWF level was measured by commercially available sandwich ELISA kit (Abcam) following manufacturer's guidelines. Homogenised human brain tissue samples diluted 1:11, recombinant human VWF standards and blanks were added to a plate preloaded with a VWF specific antibody and incubated for 2 h at room temperature. The plate was washed 5 times with wash buffer then biotinylated human VWF antibody incubated for a further 2 h at room temperature. The plate was washed as above then incubated with streptavidin-HRP for 30 min at room temperature. After washing 5 times and it was incubated with chromogen substrate for 20 min in the dark at room temperature then stopped. Absorbance was read at 450 nm in a plate reader (Molecular Devices). Average values from duplicate measurements are presented. The concentration of VWF was determined by interpolation from serial dilutions of recombinant human VWF (80-1.25 mIU/mL).

7.2.2.13 EDN1 ELISA

The Quantikine EDN1 ELISA kit (R&D systems) was used to measure EDN1 level according to the manufacturer's guidelines, as previously described (Miners, Palmer et al. 2015, Thomas, Miners et al. 2015, Miners, Schulz et al. 2018). Samples of homogenised human brain tissue containing 1 mg/ml total protein, recombinant human EDN1 standards and blanks were added to a plate precoated with EDN1-specific antibody and incubated at room temperature on a horizontal orbital shaker (Infors HT) at 450 rpm for 1 h. The plate was then washed 5 times and incubated with antibody specific to EDN1 conjugated to HRP for 3 h, at room temperature with shaking. Substrate was added after washing 5 times and the plate incubated for 30 min in the dark without shaking before being stopped with 2N sulphuric acid. EDN1 concentration was interpolated from the serial dilution of recombinant EDN1 (25-0.39 pg/ml).

7.2.2.14 AngII ELISA

The level of angII was measured by in-house direct ELISA as previously described (Kehoe, Al Mulhim et al. 2019). Homogenates diluted 1:20 in PBS, recombinant Ang-II (Enzo Life Sciences) or PBS blanks were incubated for 2 h at 26°C with shaking at 300 rpm (New Brunswick Scientific), after which the plate was washed five times in PBS/0.05% Tween-20 and blocked with 1% bovine serum albumin/PBS for 1 h at 26°C, whilst being shaken. The plate was washed a further five times and incubated with biotin-linked polyclonal rabbit anti-Ang-II (Cloud-Clone-Corp) diluted 1:500 for 2 h at 26°C, whilst being shaken. After another wash step, streptavidin-HRP (1:500) (R&D systems) was added for 20 min at 26°C. The plate was washed then incubated with chromogenic substrate (TMB, R&D systems) in the dark for 10 min and stopped with 2N sulphuric acid.

7.2.2.15 Aβ42 ELISA

The insoluble tissue fraction was prepared and measured as in previous studies (Miners, Palmer et al. 2015, Thomas, Miners et al. 2015, Miners, Schulz et al. 2018). 200 mg of dissected tissue was homogenised in lysis buffer (140 mM NaCl, 25mM TRIS-HCl pH 7.4, KCl, EDTA, 1,10 phenanthroline in 100% ethanol, nonidet P40, 1 mM PMSF, aprotinin), in a mechanical Precelleys homogeniser with 2.3 mm silicon-carbide beads (Thistle Scientific). Homogenates were spun at 13,000 rpm for 15 min at 4°C and supernatants were removed and stored at -80°C . The pellet was washed twice in PBS then re-homogenised in 3:1 guanidine-HCL (Sigma Aldrich):50mM Tris (pH 8) and incubated for 4 h at room temperature before being stored at -80°C.

Aβ42 level was measured by commercially available sandwich ELISA kit (R&D systems) following manufacturer's guidelines. The plate was washed twice then loaded with sample homogenates diluted 1:80, recombinant human amyloid-β42 standards and blanks and incubated at 4°C for 2 hours.

The plate was then washed 4 times and incubated with antibody specific to amyloid-β42 conjugated to HRP for 2 hours, at 4°C. Substrate was added after washing 4 times and the plate incubated for 30 min in the dark at room temperature before being stopped with 2N sulphuric acid. Aβ42 concentration was interpolated from the serial dilution of recombinant Aβ42 (500-7.8 pg/ml).

7.2.2.16 Statistical analyses

To investigate the differences between the cohorts, unpaired two-tailed t tests, ANOVA with Bonferroni post-hoc test, or Kruskall-Wallis test with Dunn's post-hoc analysis were used, as appropriate, to compare groups. Pearson's and Spearman's tests were used to assess correlation. The analyses were performed using GraphPad Prism version7 (GraphPad Software). The cohorts were age-matched as far as possible dependant on the cases available in the Brain Bank. Due to the small sample size, it was not possible to adjust for age or any other demographic or clinical features in the statistical methods. $P<0.05$ was considered significant. In the fibrinogen analysis, an outlier in the control group was noted skewing the data. Analyses were repeated without the outlier to see if it had unduly influenced the results.

To analyse associations with WMH on *ex vivo* imaging, a linear mixed model with subject age as a variable was generated using R (version 2.15.1). All three groups were compared, and cases (lesional white matter and NAWM combined) were compared to controls. QQ plots and histograms of residuals were used to check for normality. Other variables were not able to be included due to the small sample size.

7.3 Results

7.3.1 Stereology

7.3.1.1 Demographics

Tissue from six lesional cases (median age 80 years, interquartile range (IQR) 76.75-84.75, median PMI 57 hours, IQR 54.75-72.00, median brain weight 1340g, IQR 1310.50-1382.00) and four controls (median age 70.5 years, IQR 68.00-73.75, median PMI 73 hours, IQR 69-79, median brain weight 1295g, IQR 1202.50-1386.75) were used (Table 7.1). 50% of lesional cases and 50% of controls were female. All lesional cases provided at least one area of WML and one of NAWM, 16 lesional areas and 13 NAWM areas were studied in total. Control cases each provided four areas of white matter. In the MRC Edinburgh Brain Bank, controls tend to be taken from the sudden death brain bank, where the cases are generally younger, as in other areas of this thesis. However here, due to the small number of cases used here, and that the groups were not limited to specific brain bank cohorts, age and sex matching was more successful.

7.3.1.2 Staining quantification

Quantification of staining revealed no significant differences between the cases compared to controls, or areas with WML or NAWM (from the cases group) compared to controls (Figure 7.2). There appeared to be patterns of narrower spread and less amount of staining in controls compared to lesional samples (combined and separated) in amount of activated microglia (CD68), macrophages (CD163), reactive gliosis (GFAP) and endothelial tight junctions (claudin-5), but these did not reach statistical significance.

Comparing the amount of staining between WML and NAWM within the same cases found no significant differences (Figure 7.3). There did, however, appear to be trends of more inflammation (CR3-43) in areas with

WML, and more activated microglia (CD68), pericyte content (PDGFR) and endothelial tight junction protein (Claudin-5) in NAWM.

It was not possible to analyse two key stains. Myelin content could not be assessed using LFB staining, due to significant background, non-specific staining which could not be excluded from the analysis and made segmentation difficult. Fibrinogen staining was inconsistent between cases and samples within cases making it impossible to define the criteria for the positive staining algorithm.

Table 7.1 Stereology individual case details

PMI post-mortem interval, RIN RNA integrity number, SVD small vessel disease, SD sudden death, LBC Lothian birth cohort 1936, LP Linchpin, ICH intracerebral haemorrhage, ITP idiopathic thrombocytopenic purpura.

						Autopsy and brain bank information					
Case	Sex	Age (y)	Cohort	Cause of death	Medical history	PMI (hours)	Brain weight (g)	RIN	pH	Parenchymal SVD score	Vascular SVD score
Controls											
1	F	65	SD	Ischaemic and hypertensive heart disease	Hypertension Cardiomyopathy Pacemaker Non-smoker	74	1150	6.75	6.35	Mild	Mild
2	F	69	SD	Ischaemic heart disease	Malignancy Hypothyroid	94	1220	5.85	6.25	Mild	Mild
3	M	72	SD	Myocardial infarction	-	60	1370	6.15	6.32	None	Mild
4	M	79	LBC	Pneumonia	Malignancy	72	1437	4.90	6.13	Mild	Mild
Lesional cases											
5	M	76	LP	ICH	Previous ICH	109	1481	5.70	6.26	Severe	Severe
6	M	81	LP	Pneumonia	ICH Hypertension Osteoarthritis Malignancy	77	1339	6.10	6.34	Moderate	Moderate
7	F	86	LP	Pneumonia	ICH	54	1109	5.50	6.60	Severe	Moderate
8	M	79	LBC	Leukaemia	Myelofibrosis ITP Type 2 diabetes	57	1301	5.60	6.11	Moderate	Moderate
9	F	64	LP	Pneumonia	ICH Hypertension Ischaemic heart disease Atrial fibrillation	57	1340	4.45	6.24	Severe	Severe
10	F	87	LP	ICH	Atrial fibrillation	26	1396	2.85	6.41	Severe	Severe

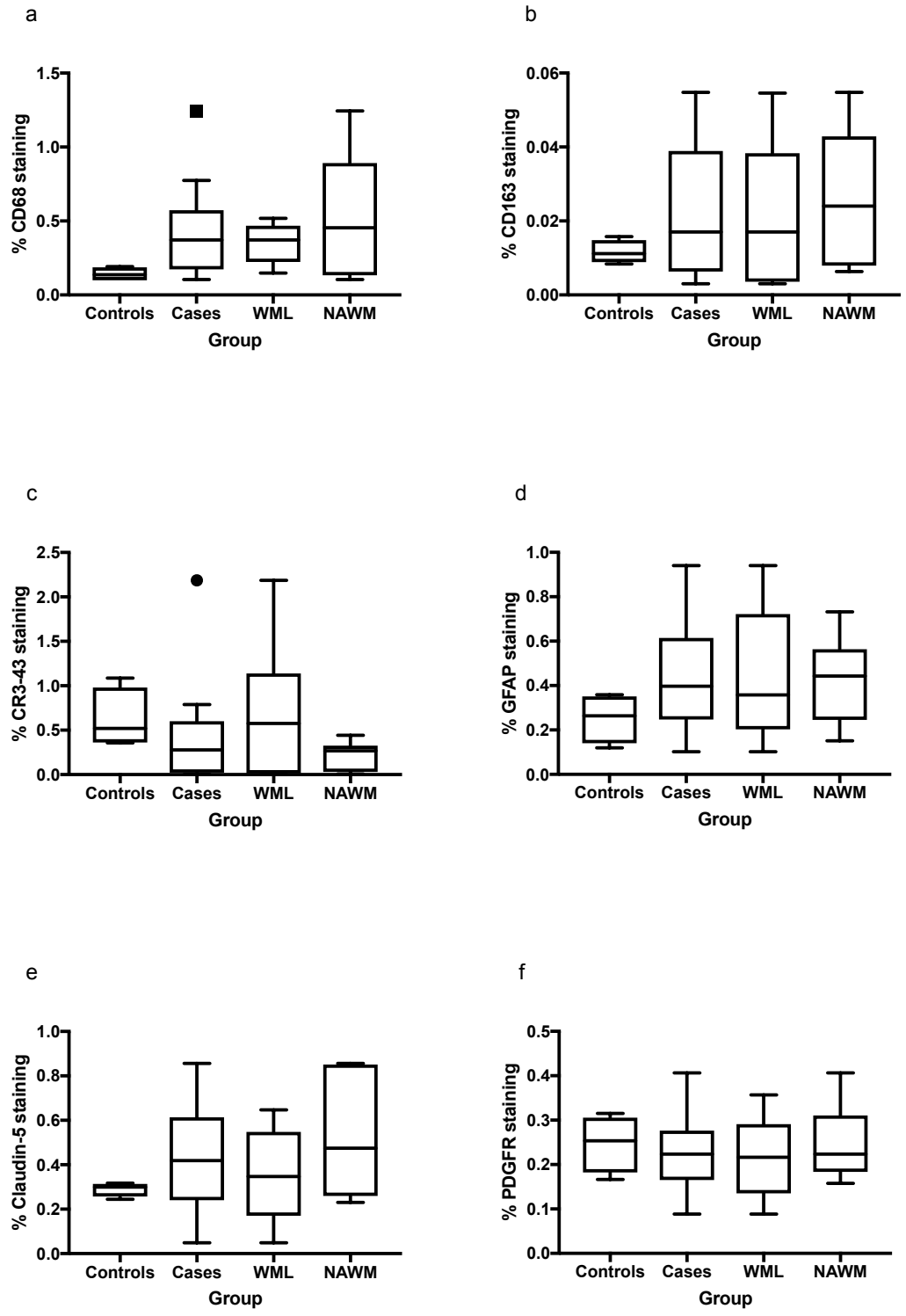


Figure 7.2 Boxplots showing analysis of protein expression using stereology

Immunohistochemical staining was analysed to look for differences between controls (n=4), cases (WML and NAWM combined) and WML and NAWM (from the same cases, separated) (n=6). No significant different were identified. Tukey boxplots indicate the median and inter-quartile range (IQR) with outliers beyond 1.5 IQR plotted individually.

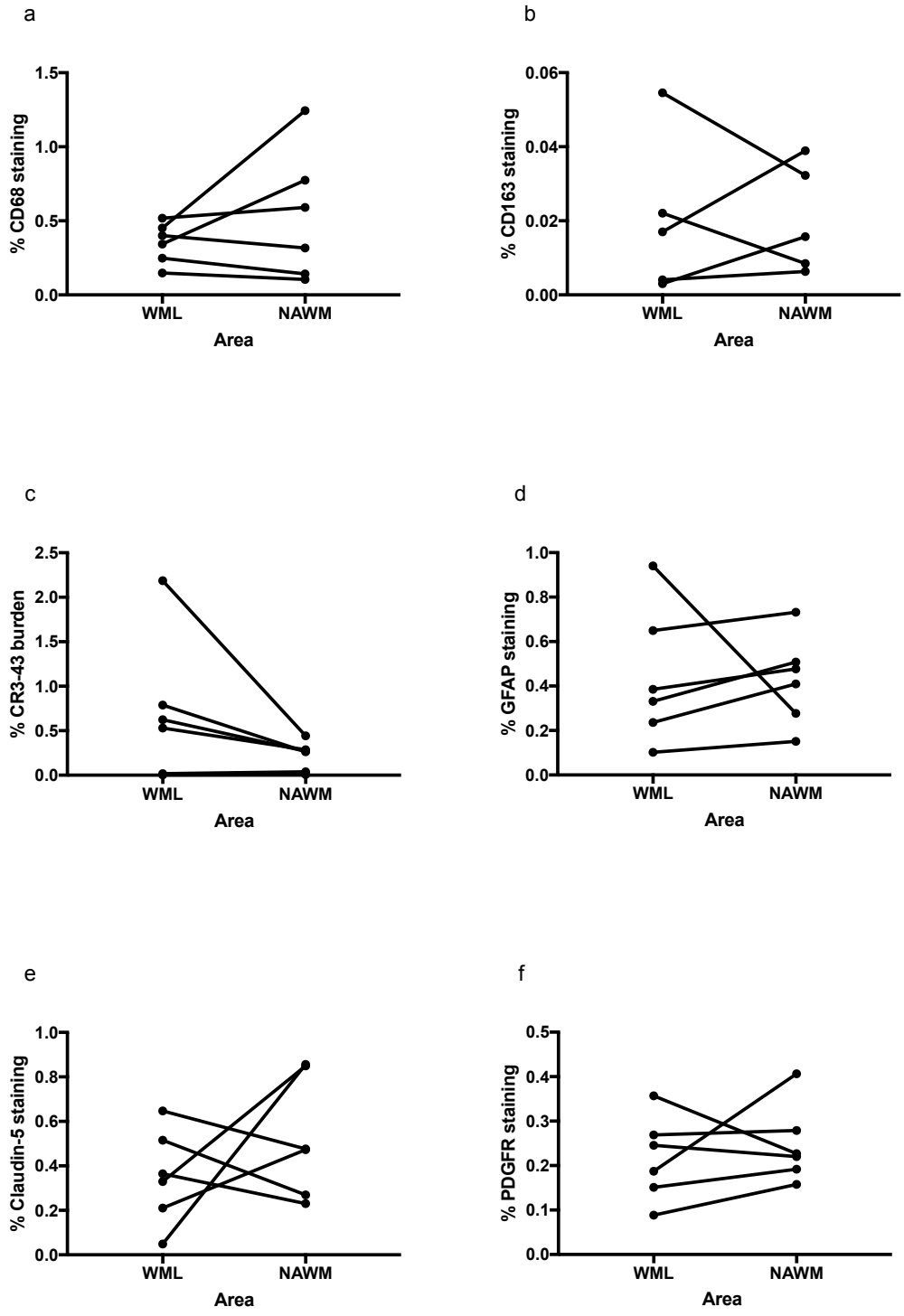


Figure 7.3 Analysis of differences between amount of staining in WML and areas of NAWM using stereology

Each line represents one lesional case and indicates the percentage staining of each protein in the WML area (left) and NAWM area (right) in the same case. Paired t-tests were not significant and no convincing patterns of relative increases or decreases between the areas are seen.

7.3.2 Biochemical study

7.3.2.1 Demographics

To study the levels of biochemical markers, tissue from 18 AD patients (median age 81 years, IQR 69-88; median PMI 79 hours, IQR 67-95), 26 with ICH-SVD (median age 81 years, IQR 73-88; median PMI 62 hours, IQR 37-82) and 35 controls (median age 63 years, IQR 57-71; median PMI 74 hours, IQR 48-96) was used (Table 7.2). In ICH-SVD, no tissue was used that contained macroscopic or microscopic haemorrhage. 12% (n=3) were from the same lobe of the brain as the ICH, 23% (n=6) were from the same hemisphere and 65% (n=17) were from the opposite hemisphere or cerebellum (Table 7.2). The duration of disease from ICH onset to death ranged from 0-1916 days (median 8 days, IQR 3-89) (Table 7.2) The post-mortem interval (PMI) from death to autopsy was similar across the three cohorts (median 74 hours, IQR 50-91 hours). 83% of AD patients (n=15) and 100% of ICH-SVD (n=26) had undergone whole brain imaging in life, no controls had undergone in vivo neuroimaging (Table 7.2).

38 small tissue samples from 25 cases underwent ex vivo MRI and SVD lesion assessment (Table 7.3) with subsequent analysis of biochemical associations. We used tissue from 9 controls (median age 51 years, IQR 49-65; median PMI 76h, IQR 70-99), 16 cases samples with WMH (median age 75 years, IQR 56-79; median PMI 73h, IQR 58-100h) and 13 cases samples with NAWM (median age 72 years, IQR 57-79; median PMI 73h, IQR 50-103). All of the NAWM samples were taken from the cases also contributing WML samples (Figure 7.4).

Three cases donated tissue to both studies of biochemical markers comparing the three disease cohorts and those undergoing post-mortem imaging and subsequent biochemical analysis (Tables 7.2 and 7.3, Figure 7.4)

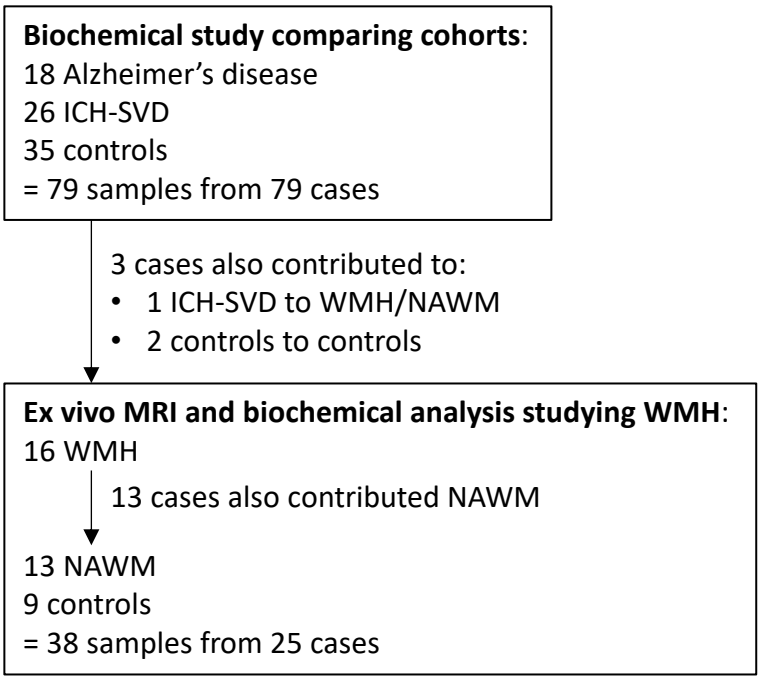


Figure 7.4 Flowchart illustrating which cases contributed tissue to which study groups

Three cases contributed tissue to both studies, one of which contributed tissue to both lesional groups with and without WMH in the study of WML on ex vivo imaging

.

Table 7.2 Individual subject data for the biochemical study of markers comparing ICH-SVD, AD and controls

PMI post-mortem interval from death to autopsy. ICH location is recorded in relation to where the tissue used in this study was sampled from. Duration of disease is from onset of symptoms to death. RIN RNA integrity number, IQR Inter-quartile range, y years, d days, h hours, g grams, WMH white matter hyperintensity, ICH intracerebral haemorrhage, PMI post-mortem interval SVD small vessel disease F female, M male. Blank cells indicate no data available. * data not available ^ subject used in both the biochemical cohort study and the study of radiological WMH.

			In vivo neuroimaging total scores				Autopsy and brain bank information				Neuropathology		
	Age (y)	Sex	WMH score	Atrophy score	ICH location	Duration of disease (d)	PMI (h)	Brain weight (g)	RIN	pH	Parenchymal SVD score	Vascular SVD score	Braak stage
Intracerebral haemorrhage – small vessel disease cohort													
1	85	F	3	2	Same hemisphere	8	87	1265	3	5.64	2	3	IV
2	58	M	1	2	Same lobe	27	83	1437	5.1	6.82	1	2	0
3	81	F	2	2	Same hemisphere	6	77	1339	6.1	6.34	2	1	0
4	64	F	1	1	Same lobe	6	57	1340	4.45	6.25	3	3	0
5	77	F	1	1	Same hemisphere	5	79	1190	4.7	6.4	3	2	0
6	77	M	3	1	Opposite hemisphere	9	122	1329	4.95	5.77	3	3	I
7	74	F	4	0	Opposite hemisphere	946	71	1250	2.85	5.81	2	3	IV
8	63	M	1	3	Same hemisphere	3	28	1235	3.15	6.32	2	2	0
9	77	M	4	1	Opposite hemisphere	10	27	1365	4.45	6.05	3	3	III
10	97	F	3	1	Cerebellum	932	36	1307	6.25	7.2	1	1	II
11	88	F	0	2	Opposite hemisphere	3	65	1383	3.95	6.11	1	2	III
12	89	M	4	0	Same hemisphere	1	21	1272	4.6	6.75	3	3	I
13	67	M	0	3	Opposite hemisphere	7	77	1360	6.05	*	2	3	II
14	93	M	4	2	Opposite hemisphere	478	49	1231	6.65	6.52	2	3	II
15	65	M	2	2	Same hemisphere	1	36	1640	5.65	6.2	3	3	0

16	80	M	0	1	Opposite hemisphere	1916	53	1306	5.5	6.27	3	3	0
17^	70	M	4	1	Opposite hemisphere	8	82	1515	5.05	5.99	3	3	I
18	88	M	2	1	Opposite hemisphere	1	89	1142	5.85	6.07	2	3	II
19	81	M	3	2	Same lobe	4	27	1470	4.7	6.5	3	3	0
20	75	M	3	2	Opposite hemisphere	110	58	1450	5.4	6.5	0	0	III
21	90	F	2	2	Opposite hemisphere	13	91	1420	5.65	6.4	2	3	0
22	83	M	3	3	Opposite hemisphere	0	39	1460	3.6	6.5	3	3	II
23	86	M	3	1	Opposite hemisphere	1422	51	1547	4.5	6.19	1	1	I
24	83	M	3	3	Opposite hemisphere	8	81	1142	2.9	6.06	3	3	I
25	90	F	3	2	Opposite hemisphere	139	90	1302	3.25	6.02	1	1	II
26	72	M	1	2	Opposite hemisphere	0	22	1430	3.75	6.4	3	3	II
Alzheimer's Disease cohort													
27	81	M	3	4			74	1160	6.3	6.1	3	2	V
28	62	F	*	*			109	1029	5	6.04	1	2	VI
29	78	M	3	4			74	1367	3.9	6.13	2	2	VI
30	80	M	0	2			101	1410	5.2	6.1	1	1	VI
31	81	M	4	4			83	1315	5	6.25	3	3	VI
32	96	F	4	4			61	1082	3.8	6.11	2	2	VI
33	57	M	1	3			58	1200	5.05	5.9	1	1	VI
34	79	M	4	4			65	1300	5.8	6.05	2	3	VI
35	85	F	*	*			83	1193	3.65	5.77	2	1	VI
36	88	F	3	3			112	1054	3.7	5.96	3	3	VI
37	60	M	0	3			86	1244	4.15	5.9	2	1	VI
38	66	M	0	2			52	1407	3.05	5.75	1	1	VI
39	85	M	2	2			91	1183	5.6	5.95	2	2	VI
40	86	M	4	3			72	1300	5.8	6.1	3	3	VI

41	90	F	*	*	110	943	3.4	6.06	3	3	VI
42	60	F	3	4	54	1150	4.9	5.95	1	1	VI
43	90	M	3	4	73	943	6.45	6.44	3	3	VI
44	95	M	1	3	96	1221	6.1	6.08	0	1	VI
Controls											
45^	64	F			114	1300	6.5	5.93	1	1	I
46	71	F			41	1210	6	6.5	2	1	0
47	62	M			41	1700	4.95	6.1	2	2	0
48	63	M			76	1680	3.05	5.9	1	1	0
49	75	M			47	1140	2.3	5.4	2	2	0
50	63	M			42	1460	4.5	6.3	0	0	0
51	69	M			49	1370	6.5	5.71	0	0	0
52	61	M			70	1300	4	6.1	1	1	0
53	46	F			49	1210	5.65	6.5	2	2	0
54	60	M			65	1490	5.9	6.3	0	0	II
55	79	F			45	1170	5.8	6.3	2	2	I
56	57	M			113	1820	4.65	6.28	1	1	0
57	68	M			75	1720	4.45	6.7	0	2	0
58	79	F			46	1050	5.3	6.5	3	3	0
59	79	F			100	1190	4	6.3	0	1	0
60	69	M			90	1570	5.43	5.6	2	2	0
61	75	M			78	1580	5.1	6.43	0	0	0
62	57	M			113	1370	5.75	5.76	0	0	0
63	83	F			50	1270	6.1	6.5	3	2	II
64	53	F			40	1680	5	6	3	3	0
65	59	M			74	1500	5.3	6.1	0	0	0
66	53	M			96	1500	6.35	6.37	0	1	0

67	67	M		68	1700	6.95	6.49	1	2	0
68	63	M		42	1480	4.5	6.3	0	0	0
69	54	M		91	1100	4.85	6.28	0	0	0
70	71	F		96	1310	6.3	6.4	0	1	I
71	84	M		23	1365	6.2	6.25	1	1	I
72	69	M		74	1500	5.4	5.92	0	1	II
73	68	M		96	1410	4.85	6.2	0	0	0
74^	51	M		52	1460	6.65	6.38	0	0	0
75	71	F		95	1170	6.25	6.28	1	1	I
76	53	M		97	1520	4.6	6.4	0	1	0
77	52	M		99	1500	7.2	6.3	0	0	0
78	57	M		110	1570	7.1	*	0	1	0
79	57	M		64	1520	5.3	6.41	0	1	0
			Median	74	1339	5.05	6.20			
			IQR	49.5 – 90.5	1210 - 1475	4.45 – 5.89	6.02 – 6.40			

Table 7.3 Individual subject data for biochemical study investigating protein expression in white matter hyperintensities, normal appearing white matter and controls

PMI post-mortem interval from death to autopsy, RIN RNA integrity number, IQR Inter-quartile range, y years, h hours, g grams. * data not available ^ subject used in both the biochemical cohort study and the study of radiological WMH.

Case number	Age (y)	Gender	Deep white matter area used	PMI (h)	Brain weight (g)	RIN	pH
Controls							
1^	64	Female	Frontal	114	1300	6.5	5.93
2^	51	Male	Periventricular	52	1460	6.65	6.38
3	79	Male	Central	72	1437	4.9	6.13
4	50	Male	Central	70	1300	6.1	5.99
5	72	Male	Central	60	1370	6.15	6.32
6	34	Male	Central	99	1530	6.25	6.32
7	46	Male	Frontal	110	1500	6.35	6.23
8	49	Male	Central	94	1530	6.9	6.21
9	65	Female	Frontal	76	1150	6.75	6.35
Normal appearing white matter							
10	42	Male	Central	103	1560	6.7	6.02
11	40	Male	Central	103	1570	4.7	5.69
12	37	Female	Frontal	126	1360	7.2	6.2
13	57	Female	Frontal	73	1320	4.2	6.08
14	84	Male	Frontal	83	1379	5.2	6.41
15	79	Female	Occipital	68	1468	4.65	6.2
16	72	Male	Frontal	71	1300	5.55	5.97
17^	70	Male	Central	82	1515	5.05	5.99
18	84	Male	Central	39	1330	6.05	6.23

19	57	Male	Occipital	110	1640	7.1	*
20	92	Female	Frontal	50	1045	4.05	6.24
21	79	Male	Frontal	49	1503	5.8	6.33
22	78	Male	Central	39	1290	6.35	6.17
White matter hyperintensities							
10	42	Male	Frontal	103	1560	6.7	6.02
11	40	Male	Frontal	103	1570	4.7	5.69
12	37	Female	Occipital	126	1360	7.2	6.2
13	57	Female	Central	73	1320	4.2	6.08
14	84	Male	Central	83	1379	5.2	6.41
15	79	Female	Frontal	68	1468	4.65	6.2
16	72	Male	Occipital	71	1300	5.55	5.97
17^	70	Male	Central	82	1515	5.05	5.99
18	84	Male	Frontal	39	1330	6.05	6.23
19	57	Male	Frontal	110	1640	7.1	*
20	92	Female	Occipital	50	1045	4.05	6.24
21	79	Male	Central	49	1503	5.8	6.33
22	78	Male	Occipital	39	1290	6.35	6.17
23	80	Female	Frontal	61	1289	3.9	5.76
24	79	Female	Frontal	72	1219	2.65	5.95
25	52	Male	Occipital	99	1500	7.2	6.3
			Median	72.5	1379	6.05	6.2
			IQR	54 - 102	1300 - 1503	4.75 – 6.65	6.01 – 6.31

7.3.2.2 Validation of the biochemical methods

Standard curves produced at both sites were replicated. The statistical analyses of the measured proteins in the first 40 cases were also replicated and comparable between the centres (Appendix 11) .

7.3.2.3 Neuroimaging and histological assessments show more severe SVD features in AD and ICH-SVD and more severe atrophy in AD

Histological assessment revealed that histological parenchymal and vascular SVD features were more severe in both the AD (p=0.0018) and ICH-SVD (p<0.0001) groups compared to controls, but did not differ between AD and ICH-SVD (Figure 7.5). In vivo WMH scores did not differ between the AD and ICH-SVD cohorts (Figure 7.6). Total, cortical and central atrophy, assessed by in vivo imaging, was worse in AD than ICH-SVD (p=0.0024, 0.0002, <0.0001 respectively) (Figure 7.7) and worse atrophy correlated with higher Aβ42 level (r=0.39, p=0.016) (Figure 7.7d) but atrophy did not correlate with the severity of histological parenchymal or vascular abnormalities (Figure 7.8). These subjects were age matched, but age was not controlled for statistically.

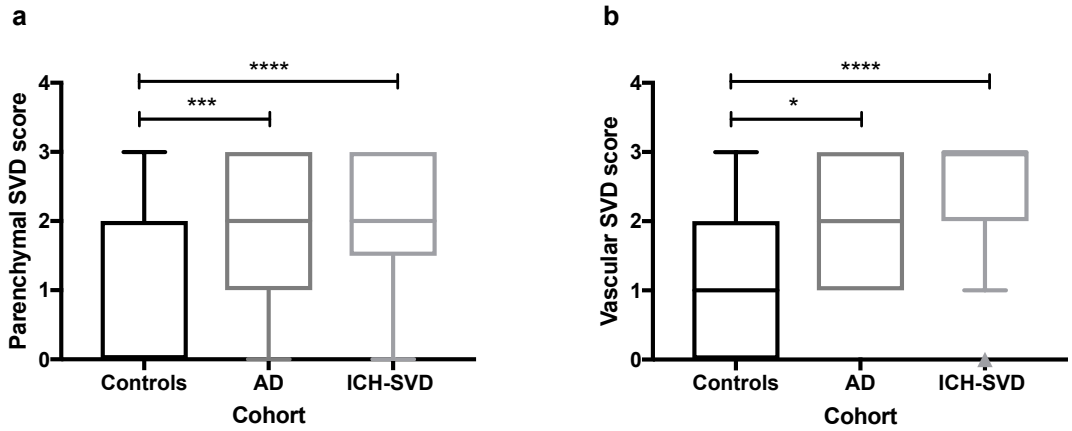


Figure 7.5 Boxplots of histological SVD scores in AD and ICH-SVD

a) parenchymal and b) vascular histological SVD scores were signifcantly higher in the AD and ICH-SVD cohorts compared to controls. Tukey boxplots indicate the median and inter-quartile range (IQR) with outliers beyond 1.5 IQR plotted individually. ** p < 0.01, *** p < 0.001, **** p < 0.0001

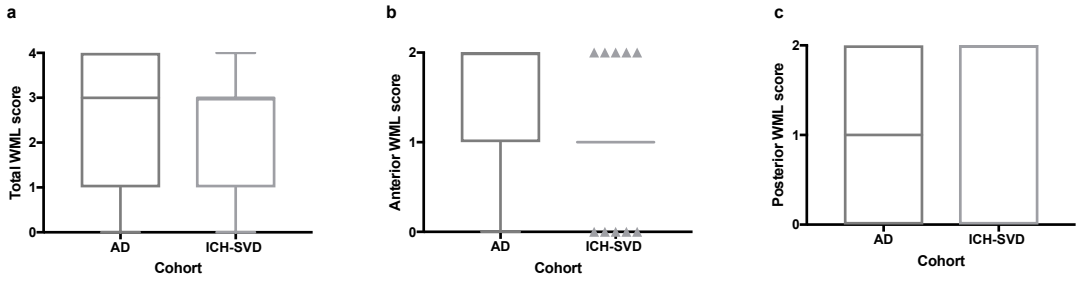


Figure 7.6 *In vivo* neuroradiological assessment of white matter hyperintensity burden in AD and ICH-SVD

Boxplots of Mann Whitney test showing AD and ICH-SVD cohorts had similar white matter lesion scores on *in vivo* whole brain imaging, a) in total, b) anterior scores and c) posterior scores. Tukey boxplots indicate the median and inter-quartile range (IQR) with outliers beyond 1.5 IQR plotted individually.

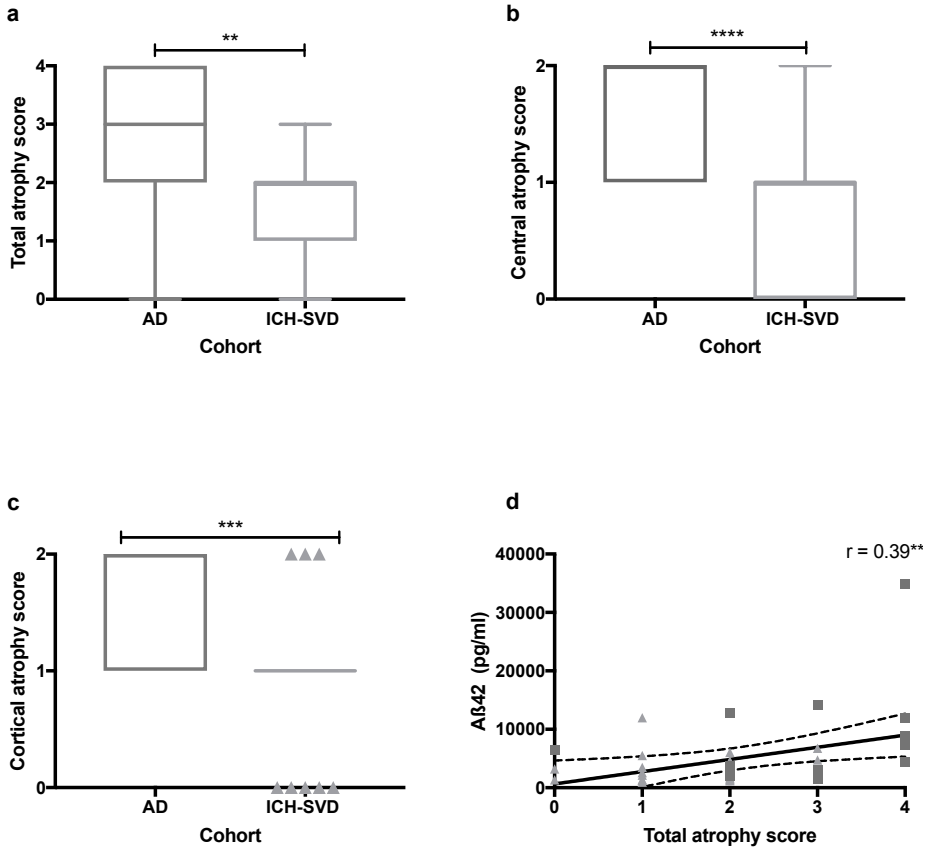


Figure 7.7 *In vivo* MRI revealed a greater degree to cortical atrophy in AD compared to ICH-SVD

a-c) Boxplots of Mann Whitney test showing significant greater atrophy scores in AD compared to ICH-SVD in a) total scores ($p < 0.005$), b) central ($p < 0.0001$) and c) cortical ($p < 0.0005$). d) Scatterplot showing positive correlation between total atrophy score and Aβ42 level in all cases ($r = 0.39$, $p < 0.05$). Tukey boxplots indicate the median and inter-quartile range (IQR) with outliers beyond 1.5 IQR plotted individually. Each point in the scatterplots indicates either a single AD (grey square) or ICH-SVD (pale grey triangle) brain. The best-fit regression line and 95% confidence interval are superimposed. ** $p < 0.01$, *** $p < 0.001$, **** $p < 0.0001$

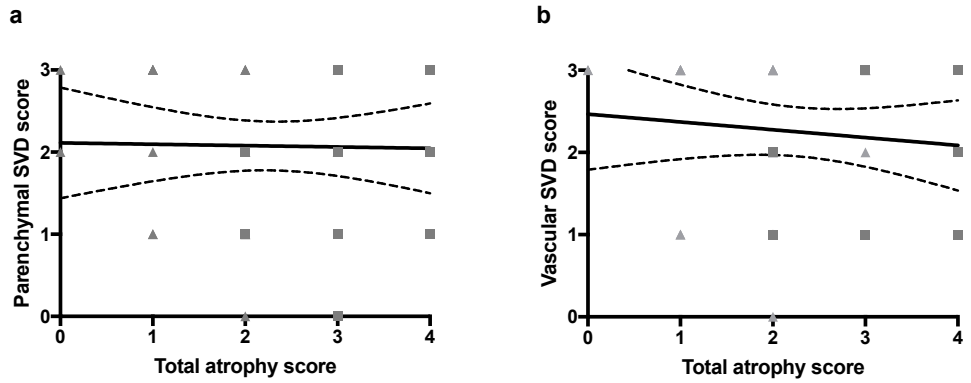


Figure 7.8 Scatterplots comparing atrophy on *in vivo* imaging and histological assessment

Scatterplots show no relationship between a) parenchymal pathology and b) vascular pathology and atrophy measured on *in vivo* imaging for combined AD and ICH-SVD cases. The best-fit linear regression lines and 95% confidence intervals are superimposed. Each point indicates either a single AD (grey square) or ICH-SVD (pale grey triangle) brain.

7.3.2.4 Biochemical assessment indicates reduced tissue oxygenation and increased microvascular density with vascular leakage in ICH-SVD

In deep white matter, tissue oxygenation was significantly reduced, both chronically, indicated by reduced MAG:PLP1, (p=0.0296), and more 'acutely', shown by elevated VEGF (p=0.0001) in ICH-SVD compared with controls (Figure 7.9a, b). The same pattern of reduced MAG:PLP1 and increased VEGF was seen in AD compared to controls but did not reach statistical significance. The level of white matter VWF, a marker of microvascular density, appeared higher in ICH-SVD, but it did reach significance any of the groups (Figure 7.9c). Across the entire cohort, VWF level showed a strong positive correlation with VEGF (r=0.6149, p<0.001) (Figure 7.9d). VWF also correlated with VEGF when the cohort was sub-grouped into ICH-SVD (r=0.52, p=0.045) and control cases (r=0.67, p=0.0002), but not in the AD cases, although they showed the same upward trend but with a much narrower distribution (Figure 7.10). MAG:PLP1 was not statistically significantly related to histological assessment of vascular or parenchymal SVD features in the ICH-SVD and AD groups but showed a decrease with all SVD scores as they increased in the ICH-SVD and AD cases, compared to a

downward trend in the controls (Appendix 12). Fibrinogen level, a measure of BBB leakiness, was significantly elevated in AD compared to controls (p=0.0001) in deep white matter (Figure 7.11a) and there was no difference between fibrinogen levels in AD and ICH-SVD (p=0.0677). However, upon the removal of an outlier in the control group, fibrinogen in both the ICH-SVD and AD groups was significantly elevated compared to controls (p=0.0173, p<0.0001) (Figure 7.11b). In an exploratory analysis, fibrinogen was positively correlated with VEGF and showed a trend of increasing with reduced MAG:PLP1, but no relationship with VWF (Appendix 13).

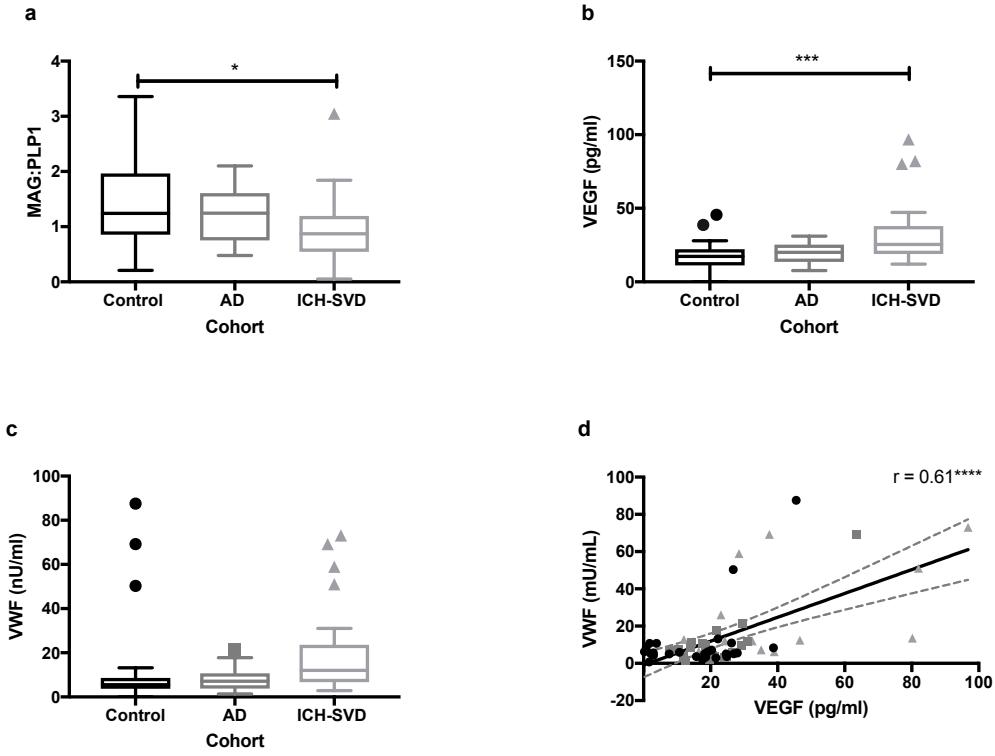
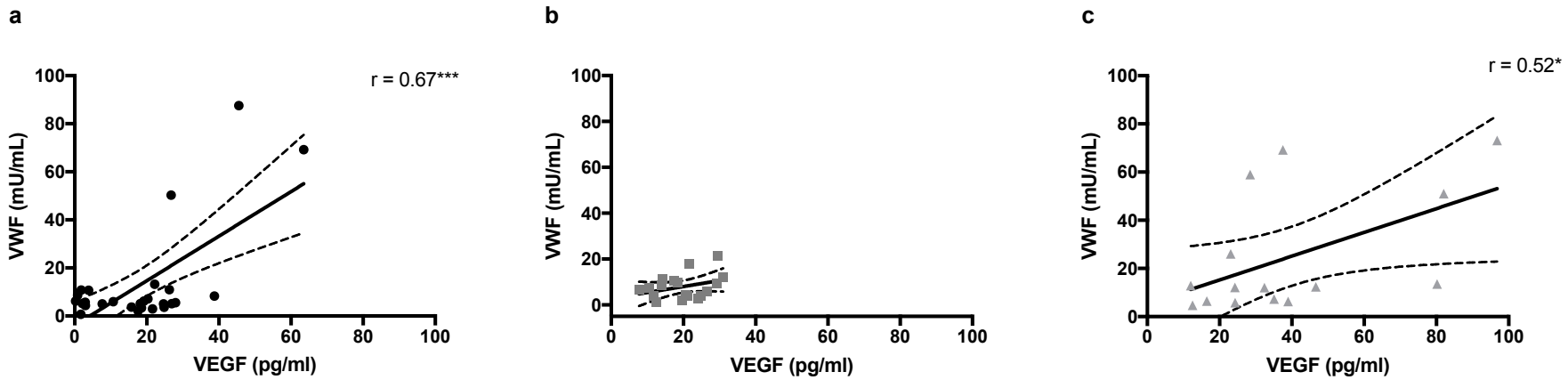


Figure 7.9 Evidence of cerebral hypoperfusion and white matter ischaemia changes in ICH-SVD

Boxplot showing a reduction in the ratio of MAG:PLP1 in ICH-SVD (n = 26) compared to age-matched controls (n = 35) ($p < 0.05$); no change was observed in AD (n = 18) ($p = 0.78$) b) Boxplot chart showing significantly increased VEGF level in ICH-SVD compared to controls ($p < 0.001$). c) Boxplot showing that microvessel density, assessed by VWF level, was unchanged in AD and ICH-SVD. In a-c) Tukey boxplots indicate the median and inter-quartile range (IQR) with outliers beyond 1.5 IQR plotted individually. D) Scatterplot showing a positive correlation between VWF and VEGF in a combined ICH-SVD, AD and control cohort ($r = 0.61$, $p < 0.0001$). Each point in the scatterplot indicates either a single control (black circle) AD (grey square) or ICH-SVD (pale grey triangle) brain. The best-fit linear regression line and 95% confidence interval are superimposed. * $p < 0.05$, *** $p < 0.001$, **** $p < 0.0001$.

Figure 7.10 Scatterplots showing a positive correlation between VEGF and VWF levels

a) the control (r = 0.67, P < 0.05) and c) ICH-SVD cohorts r = 0.67 P < 0.0005) but not b) in the AD cohort. Each point in the scatterplots indicates either a single control (black circle) AD (grey square) or ICH-SVD (pale grey triangle) brain. The best-fit linear regression lines and 95% confidence intervals are superimposed. * p < 0.1, *** p < 0.001



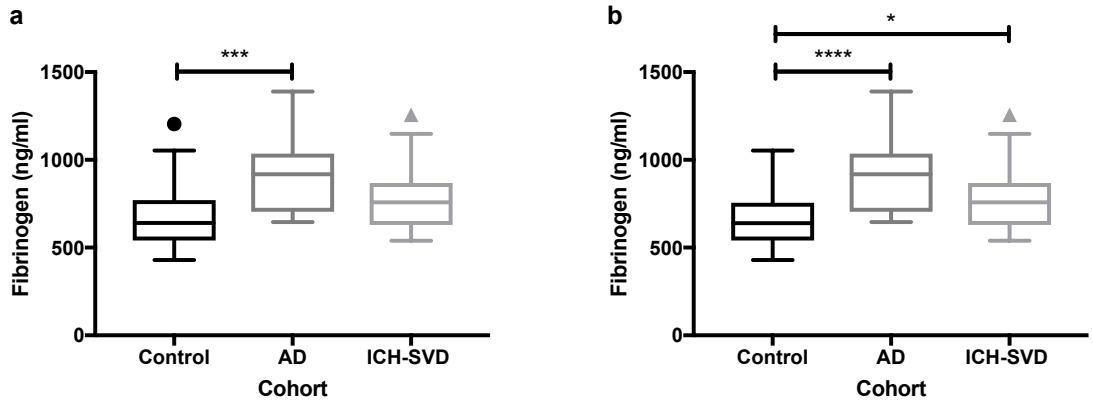


Figure 7.11 Fibrinogen is increased in AD and ICH-SVD
a) Boxplot showing increased concentration of fibrinogen, a marker of blood-brain barrier integrity, in white matter in AD compared to age-matched controls ($p < 0.001$). No difference in fibrinogen or PDGFRB was observed between ICH-SVD and controls or AD cases. b) After the removal of an outlier in the control cases, there was also significantly higher fibrinogen levels in ICH-SVD cases compared to control cases ($p=0.0173$). The Tukey boxplots indicate the median and inter-quartile range (IQR) with outliers beyond 1.5 IQR plotted individually. * $p < 0.05$, *** $p < 0.001$, **** $p < 0.0001$.

7.3.2.5 Biochemical assessment of the pathophysiological processes that mediate hypoxia of white matter may differ between AD and SVD

White matter EDN1 concentration was increased in ICH-SVD compared to controls ($p=0.0003$) and AD ($p=0.0001$) (Figure 7.12a) and showed a trend of increasing with increased histological SVD scores (Figure 7.12b, c). EDN1 was positively correlated with VEGF ($r=0.3747$, $p=0.0019$) in the combined cohort (Figure 7.12d). There was no significant relationship between EDN1 and MAG:PLP1 ratio in the combined cohort (Figure 7.12e). In contrast to EDN1, angII level did not differ between groups (Appendix 14).

Insoluble Aβ42 was significantly elevated in AD compared to controls ($p=0.0003$) and ICH-SVD ($p=0.0011$) in the white matter (Figure 7.13a). No differences were observed between ICH-SVD cases and controls. Pericyte content, indicated by PDGFRB level (Miners, Schulz et al. 2018), was significantly elevated in AD white matter compared to controls ($p=0.0216$) but not ICH-SVD ($p=0.4251$) (Figure 7.13b).

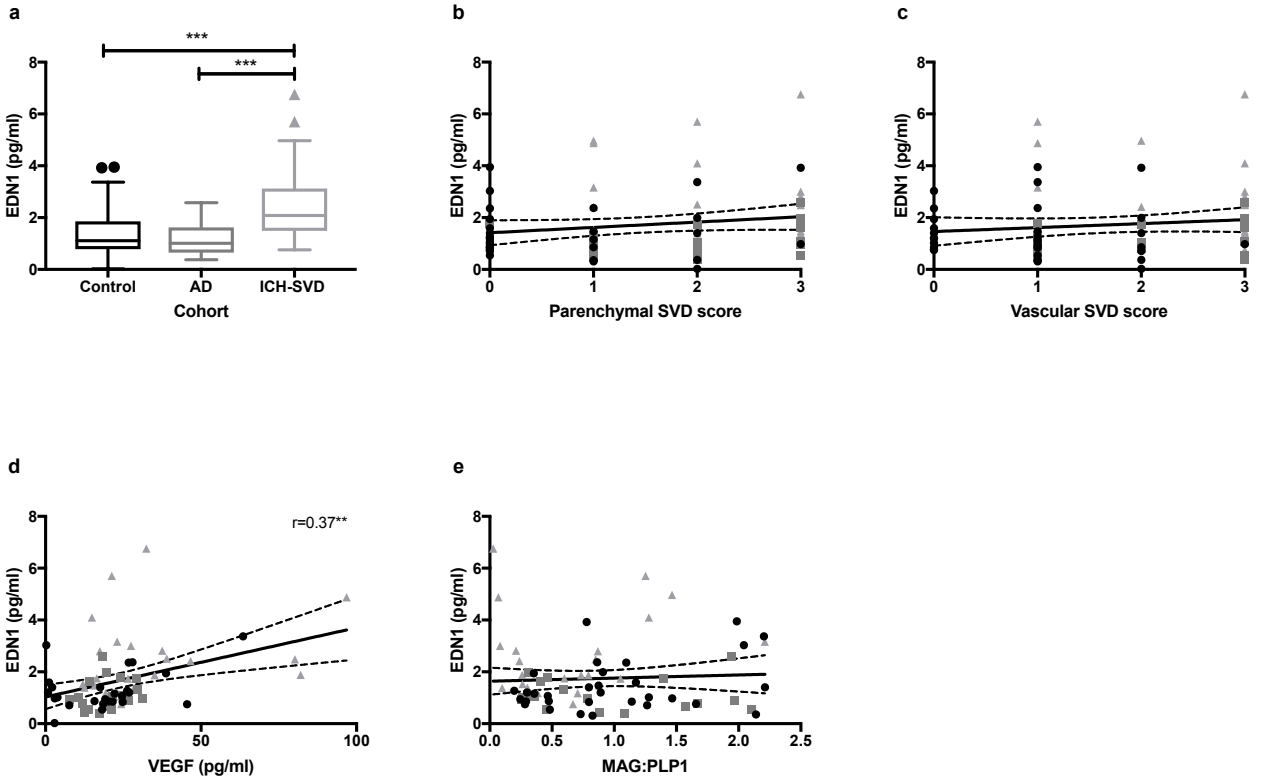


Figure 7.12 EDN1 is increased in white matter in ICH-SVD

a) EDN1 level was significantly elevated in ICH-SVD (n = 26) compared to age-matched controls (n = 35) ($p < 0.0005$); no change was observed in AD (n = 18) compared to controls. b, c) Scatterplots showing no significant correlation between EDN1 level and histological b) parenchymal and c) vascular SVD scores ($p = 0.120$, 0.277 respectively). d) Scatterplot showing a positive correlation ($r = 0.37$, $p < 0.005$) between EDN1 and VEGF in a combined ICH-SVD, AD and control cohort ($r = 0.37$, $p < 0.005$). e) Scatterplot showing no significant correlation between the level of EDN-1 level and MAG:PLP1 ratio ($p = 0.629$). Tukey boxplot indicates the median and inter-quartile range (IQR) with outliers beyond 1.5 IQR plotted individually. Each point in the scatterplots indicates either a single control (black circle) AD (grey square) or ICH-SVD (pale grey triangle) brain. The best-fit linear regression line and 95% confidence interval are superimposed. ** $p < 0.01$, *** $p < 0.001$

We did not find any significant association between the biochemical markers and our assessment of histological vascular or parenchymal SVD features (Appendix 15), although there is a suggestion of increasing VEGF (Appendix 15a, b) and fibrinogen (Appendix 15e, f) with increasing histological SVD score in the upward slope on the scatterplots. Similarly, we found no associations between the biochemical markers and *in vivo* radiological assessment of WMH burden (not shown). The subjects in these analyses were age matched, but age was not controlled for statistically.

7.3.2.6 Relationship between ex vivo MRI findings and biochemical markers of vascular function in ICH-SVD and AD

MAG:PLP1 was significantly lower in lesional cases with WMH than control white matter cases (95% CI -1.605– -0.070, adjusted for subject age). No other differences were found between WMH, NAWM and controls, or lesional brains and controls (Figure 7.14).

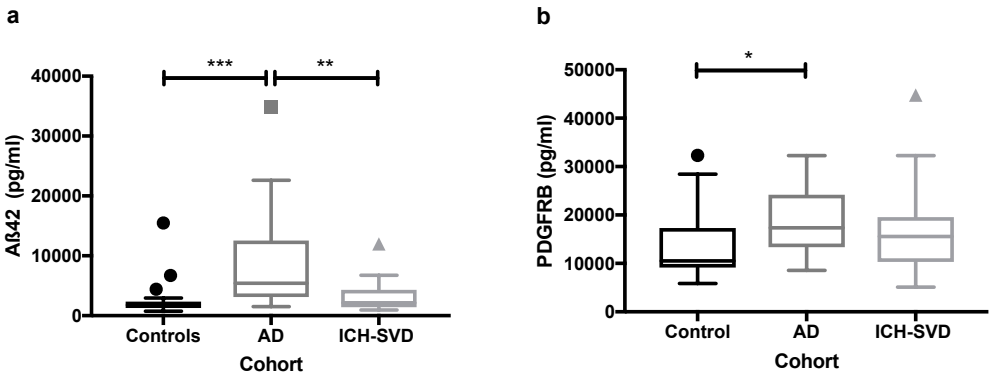


Figure 7.13 Increased Aβ42 and pericyte content in white matter in AD

a) Boxplot showing significantly elevated concentration of Aβ42 within guanidine-extracted extracts representing an insoluble fraction, in AD (n = 18) compared to age-matched controls (n = 35) ($p < 0.001$) and ICH-SVD (n = 26) ($p < 0.01$). b) Boxplot showing a significant elevation in the level of PDGFRB, a pericyte marker, in white matter in AD compared to age-matched controls ($p < 0.05$) and ICH-SVD ($p < 0.01$). The Tukey boxplots indicate the median and inter-quartile range (IQR) with outliers beyond 1.5 IQR plotted individually. * $p < 0.05$, ** $p < 0.01$, *** $p < 0.001$.

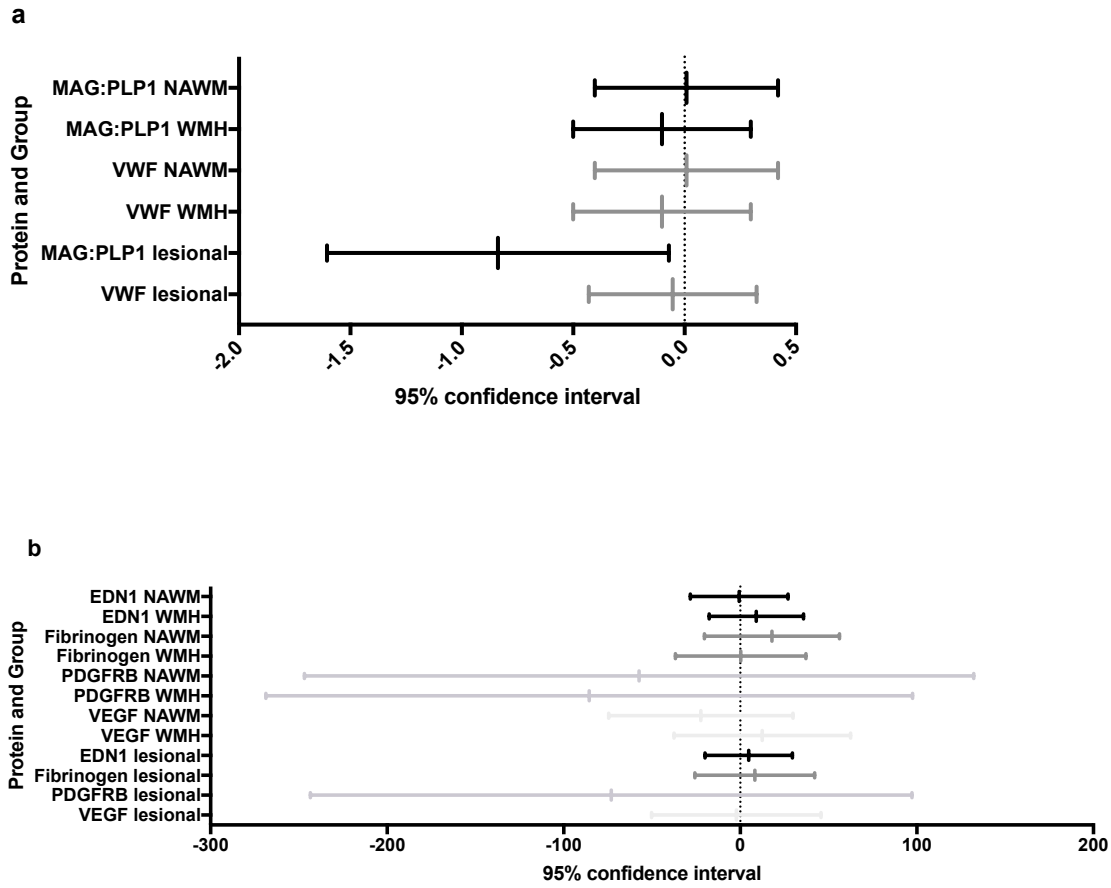


Figure 7.14 Protein levels in WMH, NAWM and controls

Forest plots of linear mixed model 95% confidence intervals comparing measured protein levels in NAWM and WMH on *ex vivo* imaging to controls, and comparing grouped lesional samples (NAWM and WMH) to controls, adjusted for age. Plots are separated to show a) MAG and VWF on a smaller scale around 0 and b) EDN1, fibrinogen, PDGFRB and VEGF on a larger scale for clarity. The only difference identified was lower MAG:PLP ratios in lesional cases than controls. The mean and range are indicated

7.4 Discussion

7.4.1 Stereology

Stereology proved to be the most successful way of measuring protein content in stained paraffin sections. I carried out this pilot study on a small number of cases (n=10) to assess the suitability for quantifying expression of proteins indications relevant in pathways potentially involved in SVD

pathogenesis, specifically vessel structure and function, white matter and inflammatory and reactive changes.

There were no statistically significant differences in measured levels of proteins between visible radiological WML and the white matter areas that appear radiologically normal. However there is a suggestion of increased inflammatory activation in NAWM, potentially suggesting inflammatory activation throughout the brain. This could reflect that pathological features of SVD in these lesional cases may be present throughout brains affected by SVD, reflecting the pattern of 'field change' abnormalities seen on neuroimaging (Bastin, Clayden et al. 2009, Baykara, Gesierich et al. 2016, Munoz Maniega, Chappell et al. 2017) and in some pathological studies (Bronge, Bogdanovic et al. 2002, Fernando, O'Brien et al. 2004, Simpson, Ince et al. 2007). Increased pericyte and endothelial tight junction protein content in NAWM are more difficult to explain, but could represent a compensatory response, or a dysfunctional vasculature which might precede or follow the development of other pathologies. A suggestion of increased inflammatory activation in WML again suggests an inflammatory component, which, while affecting the whole brain might differ between areas with radiological WML and those without. Inflammation is increasingly associated with SVD, one potential initiating factor in SVD could involve fibrinogen entry into the brain via a defective BBB where it can elicit an inflammatory response (Wardlaw, Smith et al. 2019).

Claudin-5 was possibly increased in cases with SVD compared to controls, if correct, this might represent defective or misplaced protein, or increased defective vessels. However this cannot be assessed using these methods. The data also showed a narrower range of staining in controls cases, again the reason is not clear, but these were healthy controls who died suddenly. Gene and protein changes in the perimortem period are affected by factors including agonal factors and disease state in life (Dai, Chen et al. 2021), but also PMI, brain tissue quality measured by pH and RIN value and age at death (Preece and Cairns 2003, Koppelkamm, Vennemann et al. 2011). It

might be suggested that these differences are affecting some of the results seen.

I had initially aimed to identify lesions and features of interest on registered images then obtain serial sections of them with staining quantification to better understand protein expression in the SVD lesions seen on neuroimaging. However my attempts at automating the quantification of staining in these cases failed. I wanted to perform a more comprehensive quantification of protein expression, in particular to include markers reflecting myelin content and vascular leakage. Overall I felt I couldn't reliably use stained paraffin slides to assess protein expression in SVD. I sought an alternative method that would provide an objective, reproducible measure and could be applied in larger numbers of cases to unpick the potential differences between WML, NAWM and controls targeting all specific, relevant proteins of interest, the result is the biochemical analysis described here. Moving forward, I also aimed to increase the number of cases to enable consideration of confounding factors.

7.4 2 Biochemical study

These biochemical techniques had never been carried out in our laboratory in Edinburgh before so it was important initially to validate them to be sure we could produce reliable results. We set out to exclude sources of variability as far as possible; consumables including reagents, ELISA kits and small equipment such as pipettes were sourced to be identical to those used in Bristol. However, there were several variables that could affect the results that cannot be replicated between the sites, particularly the larger and expensive machines used and pipetting technique variation, a recognised significant potential source of error, even when carried out by the same person. The standards provide a defined concentration of protein under identical sample conditions, compared to the samples, which are subject to variable storage, conditions, such as transportation across the country, freezer conditions and thaw-refreeze cycles. And so, during the validation,

particular emphasis was put on reproducing the standard curves when the methods were established in Edinburgh. The experiments carried out in Edinburgh replicated those performed in Bristol and enabled the completion of the biochemical assessment.

This study explored the pathophysiology of deep white matter hypoxia in a subset of SVD with ICH and in AD in relation to lesions observed on histology and neuroimaging. We found markers suggesting acute and chronic reduced tissue oxygenation in deep white matter in ICH-SVD which was less pronounced in AD and controls. Our findings reflect those seen in SVD imaging studies where deep white matter hypoxia (van der Veen, Muller et al. 2014, Shi, Thrippleton et al. 2016), associated with axonal and myelin damage, and oligodendrocyte loss, is commonly observed (Madden, Bennett et al. 2012). We also found reduced MAG:PLP1 in brains with WMH on post-mortem imaging, in lesional and NAWM further supporting tissue hypoxia could as a factor in their development, and reflecting a whole brain-wide field change, as seen in imaging studies (Baykara, Gesierich et al. 2016, Munoz Maniega, Chappell et al. 2017). Radiological WMH are common in SVD, predominantly affecting the deep white matter and deep grey nuclei, which have a different vascular supply from the cortex and superficial white matter, being supplied by deep penetrating vessels from the base of the brain. The biochemical profile of ischaemia-related proteins in deep white matter and pathophysiology of WMH are not fully understood (Wardlaw, Smith et al. 2019). Increased microvascular density (increased VWF) with increased vessel leakiness (increased fibrinogen) and vasoconstrictor levels (increased EDN-1) in our ICH-SVD cohort could suggest the reduced oxygenation is due to a reactive increase in defective vasculature, supported by a lack of concomitant increase in pericyte content. Both EDN-1 and VWF are secreted by endothelial cells (Quick, Moss et al. 2021), abnormalities in their levels could also reflect endothelial dysfunction.

The significance of the differences in these proteins and their potential roles should be considered in the wider context. Increased VEGF, for example,

causes increased compensatory angiogenesis in relatively acute hypoxia. However, VEGF has other roles besides angiogenesis in the brain; it is involved in neurogenesis during development and provides trophic support to neurons and promotes astrocyte mitotic activity in the developed brain (Rosenstein, Krum et al. 2010). Increased production of VEGF can also be pathological, such as in age-related macular degeneration (ARMD) where it causes choroidal neovascularisation and irreversible vision loss. ARMD is now treated with anti-VEGF therapy (Kim 2007, Finger, Daien et al. 2020). Other factors we have not considered here could also be responsible for the increased vascular content seen, such as MMPs (Quick, Moss et al. 2021). Fibrinogen was associated with hypoxic markers in this study but not with vascularity. It increased in AD, in keeping with findings in other studies (Cortes-Canteli, Paul et al. 2010), and showed a positive but less strong association with ICH-SVD. It crosses a dysfunctional BBB from the vessel lumen to enter the brain parenchyma and promotes features associated with SVD including neuroinflammation and further BBB opening. However, like VEGF, it effects a wide range of cells and has roles in many processes including axonal damage, inhibiting OPC differentiation and inducing gliosis (Petersen, Ryu et al. 2018). Fibrinogen is converted into fibrin, seen in MS plaques where there is also BBB breakdown and inflammation, however extravascular fibrin deposition is not a feature of SVD. These examples highlight how we must be cautious in interpreting the roles of proteins and significance of changes detected. However, the findings of this work reflect existing knowledge which provides reassurance about the reliability of the novel findings.

Although we cannot be sure of the significance of all these results in such a small sample, particularly the fibrinogen which was only significantly elevated in ICH-SVD after removal of an outlier. The complexity of the associations found here reflects the heterogeneity seen in the mechanisms and clinical effects associated with SVD. Blood-brain barrier dysfunction and extravasation of neurotoxic proteins has been seen in histological (Simpson,

Fernando et al. 2007), neuroimaging (Vinters, Zarow et al. 2018) and biochemical studies of cerebrospinal fluid and blood in patients with clinical SVD, stroke and cognitive impairment (Wardlaw, Sandercock et al. 2003, Farrall and Wardlaw 2009, Topakian, Barrick et al. 2010, Nation, Sweeney et al. 2019). Impaired oxygenation in SVD and AD (Barker, Ashby et al. 2014, Miners, Palmer et al. 2015, Thomas, Miners et al. 2015) in the cerebral cortex and underlying superficial white matter has also been found with increased white matter EDN1 in SVD (Barker, Ashby et al. 2014) and vascular dementia (Barker, Ashby et al. 2014), compared to EDN1 decrease in AD white matter (Barker, Ashby et al. 2014) and increase in AD cortex (Palmer, Barker et al. 2012), where it also inversely correlated with MAG:PLP1 (Thomas, Miners et al. 2015).

Amyloid deposition is commonly recognised more superficially in AD, but we found increased levels in deep white matter. In vivo imaging assessment in this study confirmed more severe atrophy in AD which correlated with increased levels of insoluble Aβ42 reflecting known changes in global Aβ pathology (Wang, Dickson et al. 1999). Increased fibrinogen in deep white matter in AD may be due to extravasation, possibly associated with blood-brain barrier breakdown. Our findings suggest it may not be due to hypoxia, potentially involving a different disease mechanism to that occurring in the deep white matter in ICH-SVD and different to the superficial cortical and white matter changes (Barker, Ashby et al. 2014, Miners, Palmer et al. 2015, Miners, Schulz et al. 2018). It is unclear whether the increased PDGFRB level seen here reflects elevated pericyte content or a compensatory response of pericytes to injury. But together, these data indicate structurally abnormal vessels within the deep white matter in AD. As we have previously reported, these data also suggest that different pathophysiological processes underpin vascular and ischaemic changes in SVD and AD. They may be region-specific and may be associated with Aβ pathology previously seen in the AD cortex (Miners, Palmer et al. 2015, Thomas, Miners et al. 2015, Miners, Schulz et al. 2018). Amyloid deposits in vessel walls results in

degeneration of smooth muscle cells and pericytes (Thal, Grinberg et al. 2012, Sagare, Bell et al. 2013, Sagare, Sweeney et al. 2015) with blood-brain barrier dysfunction (Sengillo, Winkler et al. 2013) and hypoperfusion (Miners, Palmer et al. 2015, Thomas TL 2015) in animals and human in vitro studies. Levels of the vasoconstrictors EDN1 and angII were unchanged in AD deep white matter suggesting they do not play a role.

We constructed our histological assessment of SVD based on previously published systems and the experience of two neuropathologists. We found substantial inter-rater reliability using it and that it reflected the expected burden of disease in the cohorts examined previously (Chapters 4 and 6). It showed more severe parenchymal and vascular features in the ICH-SVD and AD cohorts compared to controls. There was a suggestion of increased histological SVD scores being associated with hypoperfusion, vascular leakage and vasoconstriction, these did not achieve significance but reflect the biochemical findings in the ICH-SVD cohort. However there were no associations with WMH burden or atrophy on imaging in life. This may reflect again, a relatively small sample or that our histological SVD assessment is suboptimal, at least for a haemorrhagic SVD population. However in the absence of a defined consensus approach in the neuropathological field (Alafuzoff, Gelpi et al. 2012), we felt it appropriate to explore this method. These results further reinforce the need for an expert consensus approach, to ensure future studies are comparable and reproducible, that they are able to identify relevant clinical associations and to be able to understand the contribution of specific pathologies such as arteriolosclerosis.

The main advantages of this study are the prospective design and the use of three well characterised cohorts. If this work can be expanded to include more cases in the future, the data available could be used to make more robust analyses which take more factors relevant to SVD into account such as hypertension, smoking, cardiovascular disease and cognitive function (Wardlaw, Smith et al. 2019).

This study is limited by the relatively small number of available samples, reflecting known difficulties with human post-mortem tissue donation. The small number of cases with in vivo imaging (n=41) may also be the reason we did not find any associations between SVD burden on in vivo imaging and the proteins measured. Age matching was difficult; controls were 18 years younger than the disease cohorts. Within the ICH-SVD group there was variation in proximity of the tissue sample to the ICH, although no areas affected by haemorrhage were included in the study. The duration of disease ranged from less than 24 hours to over 5 years, with a median of 8 days, therefore our results may be affected by acute changes not relevant to chronic disease. Clinical SVD is a spectrum of disease, the cases included here are from the more acute haemorrhagic aspect, rather than the indolent, largely asymptomatic condition commonly thought of as SVD, although these changes may also be present within the ICH cases. Despite these difficulties, this study raises interesting associations and differences, which should be investigated in larger populations where it is possible to have more homogenous cohorts and include an SVD population with more 'typical' pathology.

Our study of biochemical associations is also very small and should be expanded in future to look for further associations and to study variations in WMH. WMH are dynamic lesions (van Leijsen, van Uden et al. 2017, Wardlaw, Chappell et al. 2017), the intensity of which may reflect the progression of the disease or differing underlying pathophysiology, for example, 'more white' lesions being more end-stage and irreversible, compared to 'less white' lesions (Shi and Wardlaw 2016). As we do not understand the natural history of SVD and due to the static nature of histological examination, we have not been able to account for this.

In conclusion, we have found reduced oxygenation in deep cerebral white matter in a haemorrhagic SVD cohort and found reduced oxygenation is associated with the presence of WMH, a common sign of cerebral SVD. Structural and functional abnormalities of the small penetrating vessels within

the deep white matter may involve inappropriate vasoconstriction and blood-brain barrier breakdown, potentially different mechanisms to those involved in AD. Further study of large, well characterised disease cohorts is needed to fully elucidate the underlying mechanisms, in tandem with consensus on histological SVD assessment to establish the histological-radiological-clinical associations in cerebral SVD and AD.

PART D: CONCLUSIONS

CHAPTER 8: FINAL DISCUSSION

8.1 The main outputs of this thesis

8.1.1 Systematic review

Our systematic review found our understanding of human sporadic cerebral SVD is limited by the state of the SVD histopathology terminology. The histopathological language has been consistently inconsistent and confusing since it was first described. There are no agreed, standardised histopathological processing guidelines or grading systems. Such protocols are needed to enable consistent and comprehensive tissue assessment, without presumption of underlying pathophysiological mechanisms to allow useful comparisons with the more established radiological and clinical features, and to ensure quality tissue is obtained for future research using evolving molecular technologies, for example, and in a wide variety of brain regions whereas yet unappreciated pathology might be informative.

While some direct lesion comparisons have been made, many specific features of SVD lesions remain unknown, such as gradation of pathology from the epicentre of a lesion to apparently normal tissue, or the effects of focal lesions on distant connected areas. These have not been investigated using precise imaging-histopathological examination but would lend themselves well to investigation using these methods. They could then be further interrogated by specialised protein and molecular techniques to supplement *in vivo* studies.

We found that the methods used were inconsistent and quality of reporting was suboptimal, in almost all areas including cohort data and demographics, methods used, histopathological assessment and imaging assessment. This inconsistency and lack of transparency makes comparing studies and results

difficult, and this would be particularly valuable given the relatively small numbers of subjects in these studies.

The studies included confirmed that WMH often contain myelin pallor, oedema and enlarged PVS, re-enforcing *in vivo* studies suggesting WMH contain increased water, and that resolution of the oedema may lead to a reduction in WMH size. Distant NAWM showed abnormalities including increased inflammation and axonal alterations but changes away from the lesion in question were relatively understudied. The numbers were small, but lacunes and enlarged PVS showed some overlap of features such as size. Generally enlarged PVS were smaller without perilesional signal change that could be seen in lacunes, and radiological lacunes represented cavitated foci on histology. Microinfarcts were often too small to be identified on *ex vivo* imaging, and most often showed chronic features when examined microscopically. Future applications of these methods should involve protein and molecular analysis to further understand the underlying basis for the development of the features seen, however no studies undertook tissue quality assessment that would be essential to apply such methods.

Following this assessment, I set out to address some of the issues identified, namely the lack of:

- histological SVD definitions and grading system
- transparent and complete reporting
- standardised methods to provide reliable imaging-histological comparisons

I then aimed to use the methods to carry out precise *ex vivo* imaging-histopathology comparisons to better understand the histopathological appearances underlying radiological features in cohorts representing SVD, normal aging and younger controls.

8.1.2 New methods

8.1.2.1 Set out histopathological definitions and grading system for SVD

The histopathological definitions and grading system I developed (Table 4.3) were based on an extensive case review of brain bank cases with varying degrees of SVD histopathology, the expert opinion of a neuropathologist and neuroradiologist, the systematic review and specific papers that have published various grading systems addressing some aspects of SVD.

The definitions were intended to be as objective as possible, to avoid making assumptions about the underlying pathogeneses of the lesions, while also being practical to apply in the context of the existing field of neuropathology. If they were too different or extreme they may not be acceptable to the neuropathological community. They are also intended to enable comparisons with the relatively more established and more widely used radiological definitions (Wardlaw, Smith et al. 2013) to allow the possibility of strengthening histological-radiological correlations. These definitions are an initial attempt intended to set out what we should be aiming for and to stimulate a consensus of terminology by experts across the field.

The histological SVD grading system I developed (Appendix 7) is also intended as a baseline, for use in research. In the absence of any definitive evidence of the relative contribution of specific lesions I included all those identified by the means above with the aim of producing data that would be comparable to the radiological data from the same tissue samples. I separated extent and severity of WM rarefaction, enlarged PVS and arteriolosclerosis, as the significance of each is not understood. In this thesis, it did not appear that there was any obvious benefit to doing this, although the number in my analyses are small so further study is required to be sure what features are important.

Formal statistical analyses in this small study could not be performed, but I applied these definitions and the grading system in the prospectively

collected cases that underwent *ex vivo* imaging. I found that the haemorrhagic SVD cases had more severe vascular pathology, while the normal aging cohort appeared to have more extensive but relatively mild parenchymal disease. The pathophysiological mechanisms underlying these differences could not be assessed on histology alone, and the clinical data was not complete enough to enable identification of clinico-pathological associations. But the results of this grading system, and the *ex vivo* imaging SVD assessment, reflect the burden of disease seen on *in vivo* imaging. Future study with greater numbers of cases and with varied SVD cohorts would help address these issues.

8.1.2.2 Ex vivo tissue protocol and image registration

This protocol standardised tissue sampling, processing and examination conditions to ensure samples from the same brain areas are available for comparison in different brains and that potential external influences are minimised during processing to avoid detrimental effects on tissue quality, protein or gene expression.

Scanning small tissue samples that are processed in their entirety for histology is a particular advantage of our methods, as we can be sure that any lesions seen on the *ex vivo* imaging are contained within the tissue that will be examined microscopically. Imaging small pieces of tissue *ex vivo* enabled the use of a small-bore high-resolution scanner resulting in excellent resolution images and visualisation of lesions within individual small vessels for the first time. They would not be detected without histological guidance at 7T; however, imaging resolution continues to improve and this may change in the future.

Other advantages include these methods being developed following systematic review of the literature. This allowed us to be aware of and avoid or minimise artefacts seen in other studies, such as those from air bubbles, fluid air interfaces and temperature changes. Together, these features

enabled very precise comparisons to be made and reliable conclusions to be drawn.

The main disadvantage was that the registration could not be fully automated. To do this would require computing power and artificial intelligence expertise that we did not have access to. We believe the technologies exist but are currently not easily accessible outside of a more commercial environment. As a result of this, the methods remain time consuming and rather operator dependent. However, on balance, the information they can provide, and the potential to combine detailed clinical data with radiological, pathological and molecular expertise to study SVD in the exact tissue affected is worth the effort.

This protocol was published in full, to promote transparency in reporting and the potential for other groups to reproduce them so the methods applied in the literature might become more streamlined.

8.1.2.3 Established protein analysis methods in Professor Smiths laboratory

I collaborated with Professor Seth Love's research group in Bristol, who developed and have used these methods extensively to study protein expression changes in cortex and subcortical white matter in AD. I was able to establish and validate them in our lab and applied them to study protein expression in deep white matter, significantly affected in SVD. I used three cohorts from within the Edinburgh brain bank to enable meaningful comparisons to be made regarding abnormalities and potential implications in relation to the underlying pathophysiological mechanisms. I was also able to combine the protein analysis with the *ex vivo* imaging protocol methods, to study changes specifically in *ex vivo* imaging-identified WML, NAWM and controls. To increase case numbers for future study and publication, I have also trained a research technician in these methods.

8.1.3 Experimental findings

8.1.3.1 Lesion comparisons

I found that *ex vivo* 7T MRI correctly predicts the underlying histopathological lesion only some of the time. It is most accurate in identifying enlarged PVS and microinfarcts, but that enlarged PVS and lacunar lesions show a size overlap precluding accurate identification all of the time.

Novel vascular lesions could be identified on the *ex vivo* imaging, although their appearances were not specific enough that they could be reliably and consistently identified, but this may change as imaging technologies and resolutions improve.

Additional lesions and histological features, beyond those commonly assessed and included in attempts to make grading scales, such as perivascular collagenosis, perivascular haemosiderin and inflammation are relatively common in SVD, but their development is not fully understood. They are not identifiable on imaging and so require further study and characterisation.

Differences in cortical thickness were identified at different sulcal depths, being thickest on the surface of the brain and thinning towards the depth of the sulcus, although there were no differences in the different areas measured. The reasons for these findings are not fully understood. Differences in areas might be more dependent on the individual's burden of disease and become apparent if cortical areas with distant connections to underlying focal lesions, such as microinfarcts, are studied.

8.1.3.2 Biochemical assessment

Through biochemical analysis of protein expression in human post-mortem brain tissue I found markers suggesting acute and chronic hypoxia in deep white matter in SVD compared to AD and controls. Human post-mortem SVD

compared to AD and controls. I also found reduced MAG:PLP1, a marker of chronic hypoxia, in *ex vivo* imaging-identified WMH and NAWM in brains with distant WMH, compared to control brains without radiological WMH. These findings reflect deep white matter hypoxia seen in *in vivo* imaging studies, and whole brain changes in brains with WMH. I also found that white matter affected by radiological WMH may contain increased amounts of defective vasculature; showing potential leakage and insufficient pericyte content, and that inappropriate vasoconstriction may be involved.

8.1.4 How this data contributes to our understanding of SVD

It confirms hypoxia is involved in radiological WMH, as seen in other studies (van der Veen, Muller et al. 2014), and this confirmation provides support to my more novel findings. Although from this work I cannot say definitively if it is a cause or consequence, the biochemical work suggests it could be related to an increased amount of defective vasculature, the abnormal vessels possibly representing a reactive process to the hypoxia experienced.

Levels of a vasoconstrictor were also increased in the white matter in ICH-SVD, which has also been seen in the cortex in SVD where it was associated with hypoxia (Thomas, Miners et al. 2015), supporting the idea of a whole brain 'field change' in SVD. However, it must be noted, the biochemical significance of these proteins and their roles in normal brain functioning as well as SVD and other pathological processes is not fully understood and requires further study to fully appreciate their contribution to the pathogenesis of SVD.

The lesion comparison work shows that high resolution MRI can identify many SVD lesions, and the application of a grading system based on that used in *in vivo* imaging reflects the severity seen on histological assessment. However, even high resolution imaging, beyond current clinical resolutions, cannot accurately identify all SVD lesions and this may account for some of the relatively poorly understood clinical expressions of radiologically-

assessed SVD. The identification of additional, unexplained but potentially significant pathologies highlights our lack of understanding regarding the pathophysiological mechanisms underlying SVD and the need to utilise histopathological, proteomic and molecular assessment, ideally of human tissue to better understand these mechanisms and inform animal models.

8.2 Recent relevant findings in SVD

Since I started this thesis, the wider field of research into SVD has continued with particular focus on trying to understand the mechanisms underlying the development of SVD. Increasing evidence suggests a role for the BBB and disruption of the complex signalling within the NVU. If different parts of these components and pathways are affected in different individuals, but with common downstream effects, this may explain some of the individual heterogeneity in the underlying mechanisms and risk factors. Endothelial cells, pericytes, astrocytes, microglia and oligodendrocyte precursor cells all have potentially significant interactions and roles (Quick, Moss et al. 2021). Key potential mechanisms involve initial endothelial dysfunction. The precise mechanisms remain unknown, but, for example, endothelial dysfunction causes decreased NO, which could cause loss of tight junctions and increased BBB permeability, leading to increased proliferation and abnormal vascularisation, with effects on the adjacent parenchyma including hypoxia. Abnormalities in matrix proteins related to endothelial dysfunction are also seen (Quick, Moss et al. 2021). Trials of existing drugs, repurposed and aimed at treating the endothelium, are underway (Wardlaw, Bath et al. 2020).

Perivascular spaces as part of the glymphatic system appear to play a role in drainage of fluid, proteins and toxins from the brain. They are implicated in proteinopathies and may be significant in SVD (Benveniste and Nedergaard 2022). Studies in the SHRSP rat model have found transport abnormalities within the perivascular spaces (Mortensen, Sanggaard et al. 2019), possibly associated with altered aquaporin-4 expression (Koundal, Elkin et al. 2020)

or vascular wall stiffening with increased cerebrovascular pulsatility (Shi, Thrippleton et al. 2020).

Microinfarcts are more strongly related to cognition than other SVD lesions (van Veluw, Shih et al. 2017). Cortical microinfarcts are increasingly being studied, whereas previously they were not appreciated to the same degree as they are beyond the resolution of most imaging studies. Functional (Summers, Hartmann et al. 2017) and structural axonal damage (Coban, Tung et al. 2017) seen in a penumbral region beyond the infarct itself has helped explain how such a tiny focus of damage can have pronounced effects on distant brain areas. Depending on the area affected, this enlarged area of damage could affect specific neuronal connections with significant functional consequences. The mechanisms underlying the distant effects are not fully understood, but a mouse study has implicated reactive microglial activation and migration along the tracts connected to cortical microinfarcts (Lubart, Benbenishty et al. 2021). Currently there appear to be no human histopathological, protein or genetic studies that have addressed this.

Evidence based guidelines for management of SVD identified on imaging without overt clinical symptoms has been published recently (Wardlaw, Debette et al. 2021). Overall evidence is lacking, but the strongest recommendations were for blood pressure control, possibly with lower targets than conventional therapy, and for general lifestyle modifications such as regular exercise, healthy diet, good sleep hygiene, weight loss in obesity and avoiding stress. The exact mechanisms underlying how hypertension contributes to SVD remains unknown (Wardlaw, Debette et al. 2021).

A recent systematic review and meta-analysis of 123 studies included 10,938 individuals with moderate to severe SVD found males were more likely to experience more severe disease and more likely to present with stroke (Jimenez-Sanchez, Hamilton et al. 2021). Age in 10 studies showed no difference and other risk factors were not reported sufficiently to draw conclusions. These findings highlight the importance of comprehensive

cohort data collection and integration into tissue studies while the fact that the authors were able to collate and analyse such a large number of studies reenforces the need for high quality, standardised histology reporting so these findings can be assimilated into the general SVD literatures and knowledge base.

8.3 Future work needed in SVD research

Understanding the sequence of events in SVD development is essential to finding effective therapeutic and preventative strategies, particularly understanding more fully the initiating factors and underlying predispositions. Finding robust clinical-imaging-histological associations would help unpick the pathogenesis, supported by target protein and genetic studies.

Understanding the individual lesions would also held understand the development of SVD and the individual variations seen in the type and distribution of disease. As discussed, the origin of some lesions is potentially taken for granted. For example, histological infarcts, may not actually be due to lack of bloody supply, given the limited responses of the brain parenchyma to injury, there could be other underlying mechanisms resulting in those appearances. The evolution of lesions remains poorly understood – for example, why do acute infarcts have multiple sequalae? The changes seen, and the underlying pathophysiology, between the epicentre of a lesion and normal-appearing tissue remain unknown, particularly in more diffuse lesions with less well-defined borders such as radiological WMH or histological white matter rarefaction. The effects of lesions on distant connections, such as through white matter tracts connecting to the cortex, deep nuclei or into the spinal cord are also unknown at the histological level, and could help understand the complex clinical expression of SVD and possibly establish stronger histological-clinical correlations.

The ultimate goal of this has to be the development or identification of effective treatments and/or prevention. I believe addressing some of these

fundamental unknowns will help take a step towards this. Before effective histological work in these areas can be undertaken, however, work towards a consensus on terminology and grading is required.

8.3.1 Developing the work in this thesis

The new methods developed in this thesis could be applied to develop the work I have started to find more robust associations, primarily by increasing subject numbers, or by applying the methods to other cohorts within our groups at the University of Edinburgh or in other centres. I have published the *ex vivo* imaging and registration protocol in detail, the biochemical methods have been published previously and I intend to submit my application of them and my results imminently. I also intend to use the histopathological definitions and grading system with the results obtained from the precise lesion comparisons to host an international consensus meeting, using scanned images for assessment in advance of a physical meeting, as soon as possible to develop a published consensus document accessible to other researchers.

8.3.1.1 SVD histopathology terminology and grading system

The histological definitions and grading system developed in this thesis are an attempt to create an objective means of describing SVD neuropathology. They are intended as a foundation, to highlight the need to use language that can be applied, understood and translated to comparable features in the relatively well-defined neuroimaging initially, but ultimately also to relate to and further enhance understanding of clinical expression of SVD.

After completing the work in this thesis, I have reflected on the aims and requirements for any definitions that might be agreed upon by the neuropathological community. It seems an even more simplified approach may be required to address the existing confusion regarding SVD terminology within neuropathology but also between neuropathology and neuroimaging, particularly relating to infarcts, lacunes and lacunar infarcts. In

neuropathology, a lacune or lacunar infarct is a morphological descriptor, broadly (based on the collected definitions in Chapter 2, Appendix 1) used to describe a focus of infarction with gliosis and central cavitation, macrophages or liquefactive necrosis depending on its age, although age was not often considered. Location is not generally a feature in determining whether a lesion is, or is not, described as a lacune. In neuroimaging, a lacune, lacunar infarct and lacunar stroke have specific definitions. A lacune is a focal, cavitated lesion; lacunar stroke is a clinical stroke subtype attributable to specific locations (subcortical white matter or brainstem); and lacunar infarct refers to a lacunar stroke with an underlying infarct confirmed on imaging (Wardlaw 2008). Neuroimaging defined lacunes may also be the result of focal haemorrhage (Franke, van Swieten et al. 1991), in which case the underlying histopathology would be expected to be different and contain blood breakdown products. If these issues could be addressed and a consensus reached, the definitions and grading system could be applied to make the histopathological literature more easily comparable and to work towards more useful imaging and clinical correlations.

8.3.1.2 Ex vivo imaging protocol

Through developing and applying the *ex vivo* imaging and registration protocol in this thesis, I was able to make broad comparisons of the type and features of the lesions identified. However, it would be interesting and informative to use these methods to address more specific questions about the nature of the lesions we see in SVD. A study of basal ganglia mineralisation, comparing imaging features to histopathological assessment on H&E and special stains, with quantitative assessment is underway. It would also be potentially interesting if a lesion of interest identified on *in vivo* imaging could be flagged and targeted, along with its associated tracts and areas, for sampling at autopsy with subsequent imaging, histopathological examination, protein and genetic analysis maintaining spatial associations. This could all be related back to comprehensive clinical information in the appropriate cohorts. The cases numbers would be small, but a large amount

of precise information could be obtained about specific lesions, their natural history and pathogenesis. The mild stroke cohort now included in the *ex vivo* imaging protocol would likely contain appropriate lesions.

8.3.1.3 Biochemical analysis

The biochemical analysis was limited by time. However, we have started to expand the numbers of cases using the methods described. It would also be interesting to consider additional proteins to measure that might help to explain the role and significance of the changes I identified. As I targeted radiological WML, histological white matter rarefaction, or rarefied enlarged PVS could also be studied to compare any changes seen to those in the imaging lesions.

8.3.1.4 Genetic analysis

At the start of my research, I had intended to carry out transcript analysis using BaseScope (Wang, Flanagan et al. 2012). This enables gene expression analysis, of specified genes of interest on formalin-fixed paraffin-embedded material (i.e. histological slides), at single cell resolution while retaining spatial relations. It has been applied successfully in preserved tissue from the Edinburgh brain bank to study other neurodegenerative conditions (Gregory, McDade et al. 2020). I had identified the genes/ transcripts of interest and completed the probe design input forms that would allow the development of the probes specifically for those genes. However before the order could be fulfilled, all laboratory work was stopped due to the Covid-19 coronavirus pandemic. A lead time of several months combined with a limited probe shelf-life meant I was unable to complete this part of my thesis. However, it remains an aim of my future research as it could be informative in further understanding the roles of the different components of the neurovascular unit in the context of my thesis findings.

8.4 Relevance of human tissue studies

8.4.1 The need to understand a human disease using human tissue

Sporadic human cerebral SVD is a unique disease. The use of human brain tissue was fundamental to the work in this thesis. Animal models have been used to study SVD, and some recapitulate to some degree some of the features of human sporadic SVD, such as the SHRSP. The resulting observations support a multifactorial origin causing global cerebrovascular dysfunction. While animal models may replicate specific features of SVD, they have inherent limitations and do not reproduce the complexity of the human brain or whole organism as discussed earlier in Chapter 1. So far, animal models have not been able to identify the underlying initiating factors of SVD or causative mechanisms that lead to the ultimate pathology and, importantly, have not yet led to the identification of effective therapeutic targets.

Much of our understanding of SVD comes from human neuroimaging studies carried out *in vivo*. Advances in imaging technology have improved imaging resolution to the mm scale, and enabled quantification of some molecular characteristics and monitoring of dynamic processes in real time, such as measuring interstitial fluid content and cerebrovascular reactivity, features that cannot be assessed by pathological tissue studies. However, imaging cannot visualise the microscopic vessels directly and cannot assess cellular morphology, biochemical or genetic alterations; human tissue examination is needed. As the archetypal system it contains the precise features being searched for and so provides advantages over animal models when trying to elucidate the basic underlying mechanisms.

Studying SVD in the appropriate, human, context could enable identification of the precise genetic, mechanistic and cellular abnormalities that ultimately cause SVD. However, it is complex. The origins of SVD do appear to be multifactorial at the individual level and also vary between individuals. The

published literature is hampered by lack of correlations between different modalities and lack of harmonisation in histological terminology, methodology and reporting. Studying post-mortem human brain tissue also has limitations, notably the effects of the perimortem period on gene and protein expression and the fixed nature of the tissue and lesions within it. Future studies using post-mortem human tissue would benefit from greater understanding of the cellular stresses that affect the tissue around the time of death so they can be accounted for in analyses. Autopsy study precludes any longitudinal assessment and many of the lesions may be end-stage, with minimal opportunity to study their evolution. However, once more is understood about the pathophysiology of SVD lesions, it may become apparent that it is possible to identify a proportion that are in evolution at autopsy, and this could be even more informative about the fundamental mechanisms involved.

8.4.2 Brain banking

There is a significant need for high quality brain banking utilising well characterised cohorts, comprehensive sampling of brain tissue and standardised processing and storage methods. This is available in a number of centres across the UK and provides an essential source of human tissue for studies of disease in the appropriate context. The availability of clinical information can be dependent on the individual cohort, so brain banks should seek to require as much information as possible to enable robust assessment of clinical correlations and identification of risk factors.

Frozen tissue with well-preserved (and measured) proteins and both DNA and RNA, as provided by these brain banks, is essential for quality proteomic and genomics studies. Ensuring standardisation of processing is also important to allow results from individual samples and multiple studies to be reliably compared to maximise the yield of this relatively scare, invaluable resource.

There have been few *in vitro* studies using human cell lines. Induced pluripotent stem cells have been generated for several genetic SVDs including hereditary cerebral haemorrhage with amyloidosis-Dutch type (Daoutsali, Buijsen et al. 2019), CADASIL (Ling, Liu et al. 2019) and Fabry disease (Kawagoe, Higuchi et al. 2013). Further use of these techniques using cells derived from patients with sporadic SVD to generate mature vascular or neural cells could also help identify genetic alterations and cellular consequences and potentially identify therapeutic targets.

8.5 Final conclusion

The data within this thesis has confirmed hypoxia in radiological WMH and suggested potential underlying mechanisms that may differ between different radiological and clinical expressions of SVD. It has identified areas and specific features of imaging and histopathological assessment that require further study and a histopathological grading system, based on relatively objective definitions, that reflects the burdens of disease seen on *in vivo* imaging. This has been found within a landscape of confused terminology on a background of complex molecular and pathway interactions with genetic and environmental contributions that are not fully understood. To further our knowledge, agreement on histopathological lesion terminology is first needed, ideally based on objective observations that do not assume the underlying causes.

Brain tissue from well characterised human cohorts could then be used to translate findings from animal models to identify relevant mechanisms, molecules or pathways which could ultimately be translated back into relevant animal models for potential development of effective targeted therapies. Ultimately, histological, proteomic and molecular methods must all be employed to better understand SVD, complemented by comprehensive clinical phenotyping.

PART E: REFERENCES AND APPENDICES

APPENDIX 1: Library of histological terminology used to describe SVD-related histological lesions and the definitions used for these terms

Terms have been grouped in the first column according to the lesions they referred to in the context in which they were used. Relevant associated definitions and descriptions are given in the second column for each groups of terms, again based on the context in which they were used. Horizontal rows are not of relevance. Terms were often used without being defined, or multiple terms for the same lesion used, resulting in the first column containing more items. Alternatively, multiple definitions were given between or within papers, for the same term(s), so there may be more items in the second column. This has required some interpretation of usage and reflects the lack of consensus in histological terminology and reporting of SVD. Descriptive terms are those that did not fit into the groups in the context in which they were used.

Terminology used	Definition/descriptions given
Vessel wall changes	
Small-vessel disease Small-artery disease Small vessel alterations Cerebrovascular disease	Arteriolosclerosis, CAA or other age-related structural changes.(Bronge, Bogdanovic et al. 2002) Includes degenerative lesions of the vessel wall such as fibrosis, arteriosclerosis, arteriolosclerosis, lipohyalinosis and cerebral amyloid angiopathy (CAA).(McAleese, Firbank et al. 2013)
Arteriosclerosis Arteriosclerotic cerebrovascular lesions Arteriosclerotic leptomeningeal vessels Arteriosclerotic disease Angiopathy	Graded: 1 = partly thickened, 2 = increased connective tissue in small arterial walls, 3 = marked vessel wall fibrosis with decreased smooth muscle and severe luminal narrowing, 4 = luminal obliteration and no smooth muscle.(Auriel, Bornstein et al. 2011) If greater than one third of the arterioles within the area of interest had thickened walls with luminal compromise.(Chimowitz, Estes et al. 1992) Thickening of numerous vessels.(Chimowitz, Estes et al. 1992) Concentric, hyaline thickening of small arteries, 40-150μm diameter, causing luminal stenosis.(De Reuck, Deramecourt et al. 2014, De Reuck, Deramecourt et al. 2015) A systemic disorder, thought to cause generalised arteriolar disease, (separated from thickened arterioles).(Fernando, Simpson et al. 2006) Thickened, fibrohyalinised walls of small arterioles, not positive for Congo red.(Marshall, Bradley et al. 1988)

	Arteriosclerosis/atherosclerosis affecting small arteries, 200-800μm diameter. Similar to larger vessels atherosclerosis but lacking calcification.(McAleese, Firbank et al. 2013) Degenerative lesions of the vessel wall.(McAleese, Firbank et al. 2013)
Fibrohyalinosis Fibrohyalinotic arteries Hypertension-induced fibrohyalinosis Fibrohyaline sclerosis of arterioles Hyaline arteriolosclerosis Stenosing fibrohyahne sclerosis, but without hypertensive alterations Angiofibrosis Arteriolar sclerosis	Severe fibrohyalinosis associated with marked ischemic tissue damage.(Fazekas, Kleinert et al. 1999) Severe small vessel sclerosis is associated with marked ischemic tissue damage.(Fazekas, Kleinert et al. 1999) Thickened, fibrohyalinised walls of small arterioles, not positive for Congo red.(Smith, Snowdon et al. 2000)
Fibrosis	Degenerative lesions of the vessel wall.(McAleese, Firbank et al. 2013)
Arteriolosclerosis Hyalinosis	Fibrohyaline thickening of small arteriolar walls within white matter.(Bronge, Bogdanovic et al. 2002) Smooth muscle degeneration without extravasated bleeding or phagocytosis.(Bronge, Bogdanovic et al. 2002) Thickened arteriole wall.(Chimowitz, Estes et al. 1992) Increased mean ratio of cerebral arteriole wall thickness to lumen diameter.(Chimowitz, Estes et al. 1992) Microangiopathy consisting of lipohyalinosis and arteriolosclerosis.(De Reuck, Deramecourt et al. 2013) Concentric, hyaline thickening of small arteries, 40-150 μm diameter.(McAleese, Firbank et al. 2013)

	Intimal proliferation, internal elastic lamina degeneration, and medial hypertrophy with hyalinosis, resulting in thickening of the arteriole wall and narrowing of the lumen.(van Swieten, van den Hout et al. 1991, Scheltens, Barkhof et al. 1995) Measured by mean ratio of wall thickness and the total arteriole diameter.(Scheltens, Barkhof et al. 1995) Fibrohyaline thickening of arteriolar walls on elastic van Gieson staining.(van Swieten, van den Hout et al. 1991)
Atherosclerosis Atherosclerotic vascular lesions Atherosclerotic cerebrovascular disease	Graded macroscopically in the circle of Willis 0-3 and confirmed by elastic van Gieson staining.(De Reuck, Deramecourt et al. 2014) Atherosclerotic changes in large arteries.(Revesz, Holton et al. 1999) Atherosclerotic changes in vessel walls.(Scarpelli, Salvolini et al. 1994)
Lipohyalinosis	Occurs in arteries with a diameter between 40 and 300 µm. Asymmetric areas of fibrosis and hyalinosis, associated with foam cells and accumulation of blood-derived lipids and proteins.(McAleese, Firbank et al. 2013) Degenerative lesions of the vessel wall.(McAleese, Firbank et al. 2013)
Fibrohyalinosis	A vasculopathy, with fibrin in the vessel wall.(van Veluw, Biessels et al. 2016)
Vasculopathies	Morphological changes to small vessels without parenchymal damage, including, microaneurysms, fibrinoid necrosis.(van Veluw, Charidimou et al. 2016)
Blood brain barrier dysfunction	Defined by immunohistochemical labelling for the plasma marker fibrinogen.(Hainsworth, Minett et al. 2017)
Fibrinoid necrosis	CAA-related vasculopathy.(van Veluw, Biessels et al. 2016)
Subcortical arteriosclerotic encephalopathy	Encephalitis subcortical ischronica progressive.(Revesz, Hawkins et al. 1989)
Binswanger's disease	More or less equal loss of axons and myelin in subcortical arteriosclerotic encephalopathy.(Revesz, Hawkins et al. 1989)
Microaneurysms	Often occur at points of bifurcation of otherwise unremarkable small arteries.(Munoz, Hastak et al. 1993)
Afferent vascular density	Area fraction occupied by alkaline phosphatase stained vessels that are smaller than 200 um in

	diameter. Calculated as follows: vessel area (in pixels) divided by total image area (in pixels) multiplied by 100; expressed as a percentage.(Moody, Thore et al. 2004)
Cerebral amyloid angiopathy Degenerated A -positive arterioles	Degenerative lesions of the vessel wall.(McAleese, Firbank et al. 2013)
Double barrel changes	
Capillary endothelial activation	Ratio of intercellular adhesion molecule to basement membrane type IV collagen.(Fernando, Simpson et al. 2006)
Smooth muscle	Graded: 1 = smooth muscle in all vessels (normal), 2 - 3 = lack in some vessels, 4 = none in any vessels.(Auriel, Bornstein et al. 2011)
Periventricular venous collagenosis Venous pathologic changes Dilation periventricular veins Dilation of medullary veins	Non-inflammatory collagenous thickening of the periventricular venous walls.(Auriel, Bornstein et al. 2011) Cerebral venous thickening.(Marshall, Bradley et al. 1988) An age-related degenerative disease. Increased collagen deposition in the walls of veins results in stenosis or occlusion that may restrict venous outflow.(Moody, Thore et al. 2004) Part of periventricular WMH rim pathology.(Matsusue, Sugihara et al. 2006)
Ectatic small arteries and veins Vascular ectasia Ectasia of small arteries and veins	
Descriptive: Occluded disorganised small artery Fibrinoid deposition in the walls of small arteries Thrombosed microaneurysm Hyalinosis of the arteriolar walls Thickening of the arteriolar walls Prominent thickening of the arteriolar walls and hyalinosis	

Splitting of the internal elastic lamina Fibrosis of the wall of small arteries Significant thickening of the wall of small arteries Small arteries presented significant thickening and fibrosis of the wall, and splitting of the internal elastic lamina(Revesz, Hawkins et al. 1989) Vascular ectasia Hyalinization of arterioles Splitting of media of arterioles Splitting of media Hyalinization of vessel walls Occlusive vascular disease Thickened tortuous vessels Vascular degenerative morphology(Fernando, Simpson et al. 2006) Arteries with walls thickened by hyalinosis and fibrosis Thickening of WM arterioles and small arteries Increased wall thickness Increased vessel thickness Increased basement membrane thickness Thickened arterioles Iron and calcium deposits in the walls of deep-perforating vessels Age-related structural changes Wall size thickening that sometimes led to narrowing of the vessel lumen Increased vessels wall thickness Luminal narrowing	

Perivascular changes

Virchow-Robin spaces	The subarachnoid space that surrounds the arteries, arterioles, veins and venules in the CNS.(Bokura, Kobayashi et al. 1998)

	(Separate from enlarged VRS) An invagination of the subarachnoid space that surrounds the vessel wall as it courses form the subarachnoid space through the brain parenchyma. Surround the arteries, arterioles, venules and veins, not the capillaries, of the CNS.(Braffman, Zimmerman et al. 1988, Munoz, Hastak et al. 1993) Graded none / mild / moderate / severe.(Munoz, Hastak et al. 1993) Etat crible without surrounding parenchymal changes.(Braffman, Zimmerman et al. 1988)
Etat crible	Riddled with shot- or sieve-like perforations.(Awad, Johnson et al. 1986, Braffman, Zimmerman et al. 1988) PVS are dilated. Associated surrounding changes may or may not be present, such as a narrow border of fibrillary gliosis, or pale sinuous myelin sheaths in the surrounding parenchyma (gliosis and/or demyelination).(Braffman, Zimmerman et al. 1988) Has surrounding parenchymal changes.(Braffman, Zimmerman et al. 1988) Large fluid-filled space bordered by a rim of compressed tissue.(Scheltens, Barkhof et al. 1995) Riddled with shot or sieve-like. Characterised by arteriosclerosis, dilated PVS and vascular ectasia within the parenchyma. Numerous canals or small holes in the cerebral tissue, each containing a small vessel and located in the striatum, thalamus and cerebral white matter.(Awad, Johnson et al. 1986)
Dilated perivascular spaces Enlarged perivascular spaces Distension of the perivascular space (etat crible of Vogt) Large perivascular spaces	Arteries surrounded by large fluid-filled spaces, bordered by a rim of compressed tissue.(Fazekas, Kleinert et al. 1991) Also called etat crible.(Marshall, Bradley et al. 1988, Fazekas, Kleinert et al. 1991) Contained oedema fluid or macrophages.(Grafton, Sumi et al. 1991) <3mm diameter, sharp margins, no perifocal abnormality.(Matsusue, Sugihara et al. 2006)

Dilatation of perivascular spaces Perivascular spaces dilation Widened perivascular spaces Perivascular spaces Fluid-filled perivascular tunnels Cribriform perivascular enlargement Increased Virchow-Robin space Enlarged Virchow-Robin space Perivascular cavities Dilations of periarteriolar spaces Increased periarteriolar spaces Juxtacortical perivascular spaces dilation	Dilations of medullary arteries.(Matsusue, Sugihara et al. 2006) Increased when the maximum diameter of this perivascular space exceeded thrice the diameter of the vessel contained in it.(Munoz, Hastak et al. 1993, Simpson, Fernando et al. 2007) Perivascular cavities or empty spaces resulting from distortion or elongation of small arteries collectively referred to as etat lacunaire in the grey matter and etat crible in the white matte. May be numerous in older subjects.(Polvikoski, van Straaten et al. 2010) Widened PVS containing an ectatic, sclerotic artery.(Scarpelli, Salvolini et al. 1994) A round regular cavity, the wall consisting of gliosis, and with a patent arteriole.(Smith, Snowdon et al. 2000) A round regular cavity with regular borders and the thickened wall consisting of gliosis, with a patent arteriole. Can be reliably distinguished from an artefactual space, caused by post-mortem retraction of brain parenchyma from the adventitia of the arteriole.(van Swieten, van den Hout et al. 1991) Spaces filled with interstitial fluid surrounding small penetrating vessels, a marker of small vessel disease.(van Veluw, Biessels et al. 2016) No evidence of neuronal death or gliosis.(van Veluw, Zwanenburg et al. 2015)
Etat pre-crible	Myelin sheaths in surrounding parenchyma are thin, pale and sinuous, without PVS dilation. Then, rarefaction and disintegration of the perivascular parenchyma occur.(Braffman, Zimmerman et al. 1988) Similar, if not identical to perivascular atrophic demyelination.(Braffman, Zimmerman et al. 1988)
Perivascular atrophic demyelination	Shrinkage and atrophy of axons and myelin with gliosis surrounding thickened and tortuous vessels (similar, if not identical to etat pre-crible).(Braffman, Zimmerman et al. 1988, Smith, Snowdon et al. 2000)
Perivascular changes	Mildest form of myelin pallor with no loss of fibres or myelin. Often seen around arteries with widened PVS; when more pronounced = vacuolisation.(Bronge, Bogdanovic et al. 2002)

Perivenous damage Atrophic perivascular demyelination Atrophy of perivascular myelin Perivascular tissue changes Perivascular demyelination Perivenous hypomyelination Atrophic Perivascular Demyelination Periarteriolar and perivenous demyelination Perivenous edema and demyelination Perivenous edema Perivenous changes	Ranging from spongiform transformation of neuropil and scattered foci of demyelination to large perivenous areas with marked rarefaction of myelinated fibers.(Fazekas, Kleinert et al. 1991) In regions with WMH etat crible, it was associated with a halo-like area of demyelination extending from a zone of compressed tissue toward the periphery.(Fazekas, Kleinert et al. 1991) Sometimes the reduction of myelinated fibres was even more impressive around venous structures and coexisted with periarterial changes.(Fazekas, Kleinert et al. 1991) Zone of oedema adjacent to a white matter vein leading to spongiform transformation of the tissue.(Fazekas, Kleinert et al. 1991) Rarefaction of myelinated tissue around a large vein.(Fazekas, Kleinert et al. 1991) Halo-like rarefaction of myelinated fibres that surrounded the atrophic neuropil.(Fazekas, Kleinert et al. 1991) Demyelination around arteries.(Fazekas, Kleinert et al. 1991) Small (0.2 - 0.5 cm) perivascular lesions, 'unusually tortuous vessels in the areas had sclerotic thickened walls. Haemosiderin granules were often present in the tissue adjacent to the vessels. They represented chronic, bland atrophy of the perivascular myelin', "Atrophy and shrinkage of axons and myelin; gliosis; probable increased extracellular water content, vasculature always sclerotic.(Munoz, Hastak et al. 1993, Smith, Snowdon et al. 2000) Ranged from spongiform transformation of the neuropil and scattered foci of demyelination to large perivenous areas with marked rarefaction of myelinated fibers.(Smith, Snowdon et al. 2000) Degenerate myelin around the perivascular spaces.(Scarpelli, Salvolini et al. 1994) Areas of reduced myelination with atrophy of the neuropil around fibrohyalinotic arteries.(Fazekas, Kleinert et al. 1991)

	Perivenous oedema causing spongiform tissue transformation.(Fazekas, Kleinert et al. 1991)
Perivascular vacuolation of the white matter Perivascular vacuolisation Vacuolisation of the perivascular neuropil	Vacuolation in a focal area not larger than four times the diameter of the central vessel.(Munoz, Hastak et al. 1993, Smith, Snowdon et al. 2000) Vacuolated myelin around perivascular spaces.(Scarpelli, Salvolini et al. 1994) Causing pale-staining areas surrounding blood vessels.(Scarpelli, Salvolini et al. 1994) Mild widening of the PVS associated with extensive vacuolisation of neuropil and myelin sheaths.(Scarpelli, Salvolini et al. 1994)
Descriptive: Dense periarterial fibrosis	

Parenchymal changes

Demyelination Spongiosis Loss of myelin Loss of myelin fibres Myelin degeneration Myelin damage Myelin pallor Myelin pallor by LFB staining Abnormal myelin Pallor to myelin stain Myelin attenuation Reduced myelin Reduced myelination Myelin changes Partial loss of myelin Decrease in myelin	Graded: 1 = mild pallor, 2 = swollen myelin sheaths, 3 = broken and laminated myelin, 4 = absence of myelin staining.(Auriel, Bornstein et al. 2011) Graded: none, mild, severe.(Awad, Johnson et al. 1986) Lower intensity of myelin staining.(Bronge, Bogdanovic et al. 2002) Area of demyelination.(Bronge, Bogdanovic et al. 2002) Periventricular lesions graded: 0 = no abnormality, 1 = <5mm, 2 = 5-10mm, 3 = >10mm. Deep subcortical lesions graded: 0 = no abnormality, 1 = size < 4mm, number <6, 2 = size <4mm, number >6, 3 = size 4-10mm, number <6, 4 = size 4-10mm, number > 6, 5 = > 10mm, 6 = confluent.(Fernando, O'Brien et al. 2004) Irregularly shaped and fragmented myelin sheaths, reduced density of myelinated fibres.(Fernando, O'Brien et al. 2004) Partial loss of myelin sheaths, pale on myelin stain.(Fernando, Simpson et al. 2006) On myelin and axon stains.(Grafton, Sumi et al. 1991)

Myelin alteration Shrinkage and atrophy of myelin Foci of demyelination Focal rarefaction of the myelin Rarefaction of myelin staining Tissue rarefaction White matter tissue rarefaction Area of demyelination Demyelinating lesions Diffuse myelin pallor Pale myelin Diffuse or patchy myelin loss Diffuse loss of WM Partial loss myelin Diffuse white matter abnormality White matter pathology White matter changes White matter attenuation White matter pallor Lesional white matter Periventricular decrease in myelin White matter rarefaction Tissue rarefaction	White matter with a spongy-appearance, perivascular spaces dilated and contain edema fluid or macrophages.(Grafton, Sumi et al. 1991) White matter pallor on appropriate histochemical stains (for example, Luxol fast blue), sometimes with a bubbly appearance.(McAleese, Firbank et al. 2013) Moderate: pallor on Weil staining involving only some of the white matter. Severe if pallor extends to the subcortical U fibres.(Munoz, Hastak et al. 1993) Variable axonal swelling and loss in severe demyelination.(Munoz, Hastak et al. 1993) Seen in WML, loss of myelin fibres.(Polvikoski, van Straaten et al. 2010) Degree of myelin loss represented pathological change.(Revesz, Hawkins et al. 1989) Graded: normal WM / moderate demyelination / severe demyelination(Scheltens, Barkhof et al. 1995) moderate if the pallor on Weil staining involved only part of the white matter, severe if the pallor extended as far as to the subcortical U fibres.(Smith, Snowdon et al. 2000) Degeneration of myelin sheaths, such as the formation of splits containing electron dense cytoplasm, and the formation on myelin balloons.(Simpson, Fernando et al. 2007) Contained less myelin.(Simpson, Fernando et al. 2007) Graded: mild / moderate / severe demyelination by increasing paleness of Weil staining.(Young, Halliday et al. 2008) Assessed by PLP immunostaining.(Waller, Baxter et al. 2019)

Myelin-depleted deep WM Lesional white matter Lightly stained myelin Degeneration of myelin sheaths Reduced myelin integrity Lower myelin density	
Vacuolated myelin Vacuolated myelin sheaths Spongiform white matter change	Lightly stained myelin in perivascular spaces with vacuoles, not associated with any cellular change.(Scarpelli, Salvolini et al. 1994)
Degenerate myelin	The same features as vacuolated myelin without any obvious relationship to the vessel wall.(Scarpelli, Salvolini et al. 1994) Lightly stained areas.(Scarpelli, Salvolini et al. 1994)
Myelinated fibre loss Shrinkage and atrophy of axons Loss of myelinated axons Axonal loss Axonal changes	
Wide separation of the myelinated fibres	Due to enlargement of the extracellular space and increased volume of intervening astrocytic processes.(Scarpelli, Salvolini et al. 1994)
Normal white matter	Heavily stained by LFB, with densely packed cells.(Bronge, Bogdanovic et al. 2002)
Oligodendrocytes	Identified on the basis of their nuclear morphology.(Simpson, Fernando et al. 2007) Prominent rounded nuclei with tightly compacted basophilic chromatin helping to distinguish them from astrocytes, which tend to be larger, pale, and less compact.(Murray, Vemuri et al. 2012)
Oligodendrocyte loss Abnormal oligodendroglial cell processes and cell bodies	

Degraded MBP-immunopositive oligodendrocytes Loss of oligodendroglial cells Decreased oligodendrocytes Partial loss of oligodendroglial cells	
Oligodendrocyte precursor cells	Immunopositive cells with small, round nuclei, GFAP positive.(Simpson, Fernando et al. 2007)
Remyelinating oligodendrocytes	Dark, round nuclei typically associated with mature oligodendrocytes.(Simpson, Fernando et al. 2007) MAP-2 + MAP-13 immunopositive.(Simpson, Fernando et al. 2007, Simpson, Ince et al. 2007)
Regenerating oligodendrocytes	Larger, open nuclei, microtubule-associated protein-2 expressing exon 13 (MAP-2 +13) immunopositive.(Simpson, Fernando et al. 2007)
Oligodendrocyte apoptosis	Double label with TUNEL and immunohistochemistry for oligodendroglial markers, showing DNA fragmentation occurred. Labelled for DNA fragmentation and apoptosis-regulating proteins. TUNEL-positive nuclei.(Simpson, Fernando et al. 2007)
Descriptive glial terminology: Glial cell pathology Decreased glial density Loss of glial cells (mostly oligodendrocytes) Reduced glial cell density Diffuse loss of glial cells	
PDGFRaR positive oligodendrocyte precursor cells	A round nucleus, compact cytoplasm with no visible staining of processes.(Simpson, Fernando et al. 2007)
Gliosis Reactive glia Reactive astrocytes Astrogliosis	Including the presence of swollen, fibrinogen+ clasmatodendritic astrocytes.(Waller, Baxter et al. 2019)
Germistocytic astrocytes Hyperplastic astrocytes	
Fibrous gliosis	

Fibrous astrocytes	
Ramified microglia	Ramified, bipolar.(Waller, Baxter et al. 2019)
Phagocytic microglia	Increased size and roundness, less ramified, "primed ", amoeboid.(Waller, Baxter et al. 2019)
Microgliosis	
Infarct Infarction Cerebral necrosis Areas of infarction Lesions caused by vascular insufficiency Ischaemic lesions Cerebral infarcts Cerebral infarctions Territorial infarcts Small infarctions Small infarcts True infarct Frank infarctions	Necrosis (shrunken cells and macrophages), demyelination, axonal loss, astrogliosis and cavitation.(Fazekas, Kleinert et al. 1991) Central necrosis, cavitation with surrounding gliosis.(Grafton, Sumi et al. 1991) True infarct: central necrosis, axonal loss and demyelination.(Marshall, Bradley et al. 1988) True infarct: necrosis, axon loss and gliosis.(van Swieten, van den Hout et al. 1991) Infarction: necrosis, demyelination, axonal loss, astrogliosis and cavitation; more prominent in the centre and more subtle at boundary with normal surrounding tissue.(Marshall, Bradley et al. 1988) Generally characterized by necrosis and isomorphic gliosis on H&E, reactive astrocytes were much more apparent on GFAP.(Marshall, Bradley et al. 1988) Necrosis, demyelination, axonal loss, astrogliosis and cavitation.(Munoz, Hastak et al. 1993, Smith, Snowdon et al. 2000) Strictly defined as a delineated lesion consisting of either a cavity with macrophages or a glial scar with loss of oligodendrocytes.(Munoz, Hastak et al. 1993, Smith, Snowdon et al. 2000) Necrosis, demyelination, axonal loss, astrogliosis and cavitation.(Smith, Snowdon et al. 2000)
Necrosis Focal necrosis	Presence of shrunken cells and macrophages.(Marshall, Bradley et al. 1988)
Small infarctions e.g. Watershed infarctions	May resemble lacunae but not caused by branch occlusion of perforating vessels.(Braffman, Zimmerman et al. 1988)
Acute tissue necrosis Recent infarct Recent infarction	Macrophages present and beginning to cavitate, bordered by reactive astrocytes.(Braffman, Zimmerman et al. 1988)

	Recent infarct containing macrophages and inflammatory cells and surrounded by degenerate myelin. No cavitation but with liquefaction necrosis of white matter.(Scarpelli, Salvolini et al. 1994)
Chronic infarct Old infarct	Cavitation and minimal gliosis.(Marshall, Bradley et al. 1988) Cystic region surrounded by intense gliosis.(Revesz, Hawkins et al. 1989) A central cavity surrounded by germistocytic astrocytes, a few inflammatory cells and recently formed capillaries.(Scarpelli, Salvolini et al. 1994) True cystic formation may occur in the chronic stages of infarction.(Braffman, Zimmerman et al. 1988)
Old ischaemic scars	
Cystic infarctions Cystic infarcts	Old infarcts containing a watery substance.(Bokura, Kobayashi et al. 1998) Focal abnormalities accompanying diffuse loss of myelin.(Smith, Snowdon et al. 2000) Focal abnormalities accompanying the diffuse loss of myelin in Binswanger's disease.(van Swieten, van den Hout et al. 1991)
Complete infarction	Similar to centre of larger infarct with cavitation and resolving necrosis.(Marshall, Bradley et al. 1988)
Incomplete infarction:	Diffuse, extensive and not discrete. Spares subcortical U fibres with only slight gliosis. May be artefacts of LFB staining.(Grafton, Sumi et al. 1991) Similar to the periphery of a larger infarct. Ischaemia without infarction, loss of myelin, axons and oligodendroglial cells with mild reactive gliosis, macrophages and arteriolar hyaline fibrosis.(Marshall, Bradley et al. 1988) Enlarged perivascular spaces, lacunes and WML associated with vascular cognitive impairment.(McAleese, Firbank et al. 2013) Similar to "degenerate myelin".(Scarpelli, Salvolini et al. 1994)
'Incomplete' small infarct	Describes the diffuse nature of subtotal ischaemic damage within periventricular and deep white matter, always accompanied by stenosing small-vessel disease in the affected areas.(Simpson, Fernando et al. 2007)
Intermediate (i.e., "resolving") infarction	Necrosis, minimal cavitation and gliosis.(Marshall, Bradley et al. 1988)

Microinfarct Microinfarction Cerebral microinfarct White matter microinfarct	Smaller than lacunar infarcts.(McAleese, Firbank et al. 2013) <5mm, small ischaemic lesions visible only on light microscopy, may have a small vessel at their centre. Pallor, neuronal loss, axonal damage (in white matter) and gliosis, may include regions of incomplete infarction or rarefied (subacute) change. Attenuated lesions seen in cortical or subcortical regions. They should be reported when multiple or greater than three in any region.(Polvikoski, van Straaten et al. 2010) Well defined microscopic ischemic lesion with cell death or tissue necrosis, often with gliosis and cavitation. Can occur in cortical and subcortical areas, presumably more common in watershed areas. Range from 50 um to a few mm.(van Veluw, Zwanenburg et al. 2013) Small delineated region of pallor characterized by neuronal death and gliosis, sometimes with cavitation or macrophages. May contain hemosiderin. Sizes vary between 50 μm and a few mm measured in greatest dimension.(van Veluw, Zwanenburg et al. 2015)
Old microinfarct Chronic microinfarct Chronic gliotic cerebral microinfarct Chronic gliotic cerebral microinfarct with cavitation Chronic gliotic cerebral microinfarcts with haemorrhagic components	Characterized by pallor, tissue loss, and gliosis.(van Veluw, Charidimou et al. 2016) Chronic gliotic cerebral microinfarct: well-defined area of tissue pallor, with neuronal loss and gliosis, a vessel may be present in the centre, mean size 1.7 ± 0.6 mm.(van Veluw, Zwanenburg et al. 2015) Chronic gliotic cerebral microinfarct with cavitation: gliotic cerebral microinfarct with an old, fluid-filled cavity, mean size 1.3 ± 0.4 mm.(van Veluw, Zwanenburg et al. 2015) Chronic gliotic cerebral microinfarct with haemorrhagic components: focal accumulations of hemosiderin-containing macrophages, with gliosis and neuronal loss, and positive for iron, mean size 1.2 ± 0.7 mm.(van Veluw, Zwanenburg et al. 2015)
Acute microinfarcts Acute cerebral microinfarcts.	Characterized by tissue pallor, and ischaemic or shrunken neurons.(van Veluw, Charidimou et al. 2016) Defined by a region of tissue pallor, an area containing red neurons, without astrocytes and macrophages, indicating an acute (less than 24

	hours) ischemic lesion. Mean size 4.4 mm.(van Veluw, Zwanenburg et al. 2015)
Haemorrhagic microinfarcts	Microinfarcts accompanied by multiple haemosiderin deposits.(van Veluw, Charidimou et al. 2016)
Lacunar infarctions Lacunar infarcts Lacunae Lacuna Lacunes Lacuna (cavity) Lacunar lesions Small lacunar infarcts Acute or chronic infarct (lacune) Cystic lacunar infarcts	Lacune: a true infarction.(Awad, Johnson et al. 1986) A lesion surrounded by gliosis and myelin loss measuring 1-10 mm.(Bokura, Kobayashi et al. 1998) Infarction caused by perforating branch occlusion, may occur in deep grey-matter and WM. Size is not a criterion.(Braffman, Zimmerman et al. 1988, Munoz, Hastak et al. 1993) Also called 'penetrating branch occlusions'.(Braffman, Zimmerman et al. 1988) Deep, focal lesions with well-defined margins ranging from 3-4 to 15-20 mm diameter, occasionally part of deep or subcortical WMH.(Matsusue, Sugihara et al. 2006) Small infarcts, histological cavities in the deep grey matter.(McAleese, Firbank et al. 2013) An irregular cavity with dense astrocytic gliosis in the wall; caused by occlusion of a small penetrating artery.(van Swieten, van den Hout et al. 1991)
Recent lacunae Recent lacunar infarcts	Showing early or advanced liquefaction necrosis.(Braffman, Zimmerman et al. 1988) Necrotic debris and foamy macrophages, surrounding reactive gliosis.(Matsusue, Sugihara et al. 2006) Collection of macrophages in an area of coagulative necrosis involving some or all cellular components of the brain parenchyma but without cystic change.(Scarpelli, Salvolini et al. 1994)
Chronic stage of lacunae Old lacunar infarcts	Irregular cavity with a few fine strands of fine fibrillary connective tissue. Fatty macrophages in the cavity decrease with age.(Braffman, Zimmerman et al. 1988) Irregular shape greater than 3 mm diameter, with perifocal myelin pallor and gliosis.(Matsusue, Sugihara et al. 2006)

	Irregular cystic cavity with dense fibrillary gliosis, ill-defined margin and surrounding myelin and axon loss.(Matsusue, Sugihara et al. 2006) A small cavity without a blood vessel inside.(Scarpelli, Salvolini et al. 1994)
Older lacunar infarcts	Less necrotic debris and foamy macrophages, reactive gliosis becomes fibrillary.(Matsusue, Sugihara et al. 2006)
Giant lacunae	1cm or greater.(Braffman, Zimmerman et al. 1988)
Lacunar infarcts seen macroscopically (had different microscopic features)	Small central cyst bordered by macrophages, lymphocytes, newly formed small blood vessels and hyperplastic astrocytes, mainly germistocytic. In one the reactive astrocytes were mainly fibrous.(Scarpelli, Salvolini et al. 1994)
Etat lacunaire Lacunar state	A state of multiple lacunar infarctions.(Braffman, Zimmerman et al. 1988)
Cortical microinfarcts Small superficial infarct Smallest infarcts Laminar infarcts Total cortical infarcts Partial cortical infarcts Ischaemic lesions Intracortical chronic gliotic non-cavitated microinfarct Intracortical chronic gliotic microinfarct with cavitation Intracortical chronic gliotic microinfarct with haemorrhagic components	Ischaemic necrosis in the territory of a single cortical penetrating vessel.(De Reuck, Deramecourt et al. 2014) Intracortical chronic gliotic non-cavitated microinfarct: a region of tissue pallor with neuronal loss and gliosis.(van Veluw, Zwanenburg et al. 2015) Intracortical chronic gliotic microinfarct with cavitation: visible macroscopically as a region of pallor, with neuronal death, gliosis, and accompanied by a cavity surrounded by a rim of gliosis.(van Veluw, Zwanenburg et al. 2015) Intracortical chronic gliotic microinfarct with haemorrhagic components: visible macroscopically as a region of tissue pallor, with neuronal death, gliosis and hemosiderin-containing macrophages.(van Veluw, Zwanenburg et al. 2015) A sharply delineated area of ischemia with cellular death, tissue necrosis, and cavitation.(Niwa, Ii et al. 2017)
Cortical infarct	
Intracortical acute microinfarct	Red neurons, indicative of acute neuronal injury, are present in the area of infarction. Adjacent sections were negative for both CD68 and GFAP indicating a microinfarct approximately 24 hours old.(van Veluw, Zwanenburg et al. 2015)
Cortical watershed microinfarcts	Borderzone (watershed) infarctions, bilateral or unilateral. Develop between two main arterial territories or deep and superficial systems. 5 mm or greater. Wedge-shaped regions of pallor and

	rarefaction extending into the white matter. Areas forming in the white matter are usually larger. The cortical surface develops irregularities due to scar formation. Previously termed granular cerebral atrophy.(Polvikoski, van Straaten et al. 2010)
Deep WM infarction	Attributed to subcortical arteriosclerotic encephalopathy (Binswanger's).(Marshall, Bradley et al. 1988)
Descriptive: Diffuse ischaemic changes Cavitated infarcts with dense gliosis Delicate fibrillary necrosis Chronic cavitated infarct Cystic infarct Cystic cavity Non-cavitated infarcts Infarctions with varying amounts of cavitation White matter infarction Subcortical infarction Areas of necrosis in white matter Ischemic white matter damage Small ischaemic lesions Ischemic change Frank infarction Micro-infarcts Territorial microinfarcts Small deep microinfarcts Small deep white matter microcystic infarcts Microcystic infarcts Discrete infarcts Large-artery territory infarcts Large infarcts Large-artery infarcts	

APPENDIX 2: MRC Edinburgh Brain Bank Information booklet

THE EDINBURGH BRAIN BANK

INFORMATION BOOKLET FOR DONORS AND FAMILIES

Edinburgh Brain Bank
Generic Information Sheet
Version 2: 16th July 2021

Background
We are the only Brain Bank in Scotland.
We retrieve tissue samples from people with different illnesses and diseases, many of which are long-standing and degenerative, and from cases of sudden death.
The tissue donated to the bank is currently supporting research projects in the UK and around the world. In time this research could contribute to greater understanding of these diseases, helping to ultimately find cures and improve the lives of people who suffer from these conditions.
The Edinburgh Brain Bank supplies tissue to researchers all over the world, and operates on a non-profit basis. All processes and procedures have full research ethics approval. A panel of experts has examined the proposal and raised no objections from a medical ethics perspective. It is also a requirement that the medical records of donors are made available for scrutiny by monitors from NHS Lothian and Health Improvement Scotland (HIS). Their role is to check that research is properly conducted and the interests of those involved are adequately protected.

Where does the tissue come from?
Research post-mortem examinations – these are limited post-mortem examinations that are carried out for specific research studies after discussion with, and consent/authorisation from, individuals and their families.

Procurator Fiscal post-mortem examinations – these are full post-mortem examinations instructed by the Procurator Fiscal that are primarily to establish cause of death. In full post-mortem examinations, samples are collected from all organs, including the heart, spleen, liver, lymph nodes and muscle. Authorisation for these samples to be used for research can be obtained from families.

What tissue is collected for research?
We collect a wide range of small tissue samples, depending on specific research studies.
The Brain Bank works closely with specialist medical groups elsewhere in the UK and abroad and small tissue samples may be sent to these other groups to support their ethically approved research.

What do we mean by tissue?
Tissue is the word used for a collection of specialised cells within the human body that perform a specific job. All organs, including the brain and spinal cord, are made up of tissue.

Why is tissue needed for research?
In Edinburgh, all tissue collected is made available for a wide range of research into various illnesses, including conditions such as Multiple Sclerosis, Motor Neurone Disease, Huntington's Disease, Parkinson's Disease, Multiple System Atrophy, Corticobasal Syndrome, Progressive Supranuclear Palsy, dementia, stroke and psychiatric conditions.
Studying tissue samples from people with and without different diseases, results in a collection of a wide variety of samples. Some samples may show early or advanced disease while others may be completely normal. Each of these makes an important contribution to research studies. Often, it is only through the study of large numbers of cases that significant observations can be made, which will increase our understanding of human disease.

Can people with specific illnesses or diseases take part?
Yes. By studying and contrasting tissues from people with and without specific illnesses, we hope to understand what goes wrong in specific diseases. This is vital if any treatments are to be discovered and developed in the future.

Can people who have died suddenly take part?
Yes. Sudden deaths are referred to the Procurator Fiscal who may request a full post-mortem examination. The post-mortem examination and any tests later carried out in the laboratory are undertaken to find the cause of death but this is also an opportunity to collect tissue samples for research.

Will family be able to view the body after full or limited post-mortem examination?
Yes. Your family will be able to view the body either before or after the post-mortem examination if they wish. All post mortem examinations, be they full or limited, are undertaken by highly skilled technicians.

What other information is required?
We request permission to access hospital records where applicable. Having access to detailed information about each donor's medical history means that researchers can match specific symptoms with any changes they see in the tissue samples.

What about confidentiality?
All paperwork and information obtained is stored securely in the Centre for Clinical Brain Sciences, University of Edinburgh where it will be retained indefinitely and remain strictly confidential. Every donor is given a unique identification code and all personal information is removed. Information may be shared in an anonymised form with other researchers, including commercial organisations that perform ethically approved research, but personal details are never shared with anyone.
Regular update training is required for all brain bank staff and local courses are available through NHS Lothian and University of Edinburgh. The University has an ongoing policy for good practice in data protection and the senior member of the brain bank team monitors compliance with data protection.

How will the tissue be made available to researchers?
To help as many research projects as possible, some of the tissue samples will be divided into many sections. These samples and sections are stored safely and securely in the Edinburgh Brain Bank at the Centre for Clinical Brain Sciences, University of Edinburgh.
Researchers from the UK and around the world can request tissue from the Brain Bank to use in their research projects. Our panel of experts reviews each request for tissue before approving the projects we supply tissue to. Tissue is only released to research groups with peer reviewed funding. All tissue released will be completely anonymised to the research group and all identifying data is only known to senior core staff within the Brain Bank.
We cannot predict what type of project the tissue will be used for or where the research will be carried out. However, all research we support is ethically and scientifically approved and will help us to better understand different illnesses and diseases. Tissue may also be used for teaching purposes or in the training of healthcare professionals.

What about genetic research?
Samples of tissue are sometimes used for medical genetic research, which aims to discover the links between genes and disease. Genes can affect health in various ways; a gene abnormality may directly cause illness or more commonly, variations in genes may predispose to illnesses such as high blood pressure and psychiatric disorders. It is important to emphasise that these gene variations do not directly cause illness but in combination with other factors such as diet, smoking etc., they may make a disease more likely.

What about commercial research?
Research groups are sometimes asked by commercial groups if they may obtain samples for ethically approved medical research. This research is usually for the purpose of developing new drug treatments, which could eventually be marketed. Neither relatives nor the research groups profit financially from any developments of this kind. We never release tissues to a "middle man" who can then sell that tissue for profit, and we carefully review the proposed use of all requested tissues.

Are there any costs involved?
No. All costs will be met by the Brain Bank

Can organ and tissue donation for transplant still be done?
Yes. Donation of organs and tissue for transplant will take priority over tissue donation for research but we may be able to arrange research tissue donation after the organ/tissue donation process.

Can a whole body be donated to an Anatomy School after post-mortem examination?
No. Unfortunately, this is not possible as Anatomy Schools require the whole body intact.

What happens when the research is finished?
We carefully preserve the donated tissue samples by embedding them in paraffin wax or freezing them at -80° C. This means the tissue can be used for research for up to ten years or even longer. When the tissue is no longer suitable for research, we dispose of it lawfully.

Will the decision affect the funeral arrangements?
No, the funeral arrangements will not be affected by agreeing to donate tissue for research.

If there is agreement now can this be withdrawn at a later date?
Yes. Giving consent/authorisation for tissue to be used for research is entirely voluntary and withdrawal can be made at any time without giving a reason why. The donated samples will no longer be used for research and education and will be disposed of lawfully.
As regards tissue from post-mortem examinations requested by the Procurator Fiscal, all frozen samples will be lawfully disposed of and all samples embedded in paraffin wax will be retained as part of the deceased's medical record, which is normal practice. They will not be used for research.

Who has reviewed this study?
The East of Scotland Research Ethics Service REC 1, which has responsibility for scrutinising all proposals for research on humans, has examined the proposal and has raised no objections from the point of view of research ethics. It is a requirement that your records in this research, together with any relevant medical records, be made available for scrutiny by monitors from NHS Lothian, whose role is to check that research is properly conducted and the interests of those taking part are adequately protected.

Where are the results of the research?
Researchers often publish their results in scientific journals. Please feel free to ask any questions now or in the future if you wish to find out more.

If there is a belief that any harm has been suffered by taking part in this study, there is a right to pursue a complaint and to seek any resulting compensation through NHS Lothian who is acting as the research sponsor. Details about this are available from the research team. Also as a patient of the NHS, you have the right to pursue a complaint to the Patient Liaison Manager, NHS Lothian Complaints Team, Waverley Gate 2nd Floor, 2 - 4 Waterloo Place, Edinburgh, EH1 3EG (0131 536 3370). Note that the NHS has no legal liability for non-negligent harm. However, if you are harmed and this is due to someone's negligence, you may have grounds for a legal action against NHS Lothian but you may have to pay your legal costs.

Thank you for taking the time to read this Information Sheet and for considering giving consent/authorisation for research

If you require further information or have any queries, please contact:

Tracey Millar
Research Nurse Manager
Academic Department of Neuropathology
Centre for Clinical Brain Sciences
University of Edinburgh
Chancellor's Building
Edinburgh BioQuarter
Edinburgh, EH16 4SB
Telephone: 0131 465 9522 / 07913296845

Professor Colin Smith
Professor of Neuropathology
Academic Department of Neuropathology
Centre for Clinical Brain Sciences
University of Edinburgh
Chancellor's Building
Edinburgh BioQuarter
Edinburgh, EH16 4SB

APPENDIX 3

Ex vivo MRI tissue block SVD assessment Case no: SD……..../…….… Date ……/……/……

Reader …….

Area / MRI slice	Infarct n	EPVS 0-4	MB n	Air bubbles ~ No.	WMH 0-3	Cx thickness (T2) mm	Notes
BA9 (A)						S: M: D:	
BA44/45 (G)						S: M: D:	
BA38 (I)						S: M: D:	
FWM (K)							
Caudate (Q)							
BG (S)						Iron (1-4):	
Ant hip (U)							
PVWM (Y)							
Hypoth (AA)							

Area (Hist)	**Infarct** Y / N	**EPVS** 0-4	**MB** No.	**Air** No.	**WMH** Y / N	**Cx thickness (T2)**	**Notes**
Post hip (AK)							
Thalamus (AM)							
CWM (AO)							
OWM (AQ)							
CB (BA)							
Pons (BE)							
Medulla (BF)							

SUMMARY SD ……..../……..….

Infarcts Y / N *If Y see additional sheet*
Enlarged PVS Y / N
Microbleeds Y / N
Air bubbles Y / N
WMH Y / N
***BG** Y/N *1 = none / 2 = minimal / 3 = some / 4 = much*
Overall SVD severity: *none / mild / moderate / severe*

- Lacune > 3mm
- EPVS </= 3mm *0 = none / 1 = <10 / 2 = 11-20 / 3 = 21-40 / 4 = >40*

- Sequences *T1 T2 T2* FLAIR*
- All measurements in mm

APPENDIX 4

Ex vivo MRI tissue block SVD assessment

Case no:
SD……../…….

Infarcts/Lacunes

	1	2	3	4	5	6	7
Histology block code	☐	☐	☐	☐	☐	☐	☐
MRI slice	☐	☐	☐	☐	☐	☐	☐
Infarct code*	☐	☐	☐	☐	☐	☐	☐
Infarct / **H**aemorrhage	☐	☐	☐	☐	☐	☐	☐
Grey/ **W**hite matter	☐	☐	☐	☐	☐	☐	☐
If lacunar, cavitated (Y/N)	☐	☐	☐	☐	☐	☐	☐
Touches cortex (Y/N)	☐	☐	☐	☐	☐	☐	☐
Max diameter (mm)	☐	☐	☐	☐	☐	☐	☐
Shape (**T**ubular/**O**val-round)	☐	☐	☐	☐	☐	☐	☐
Sequences on which present:							

Histology block Codes

BA9 (histoplogy block A)
BA44/45 (G)
BA38 (I)
FWM (K)
Caudate (Q)
Basal ganglia (S)
Ant hippocampus (U)
PVWM (Y)
Hypothal (AA)
Post hippocampus (AK)
CWM (AO)
OWM (AQ)
Cerebellum (BA)
Pons (BE)
Medulla (BF)

Infarct codes

MCA cortical
1 small cortical
2 basal ganglia
3 subcortical
4 ant half periph MCA
5 post half periph MCA
6 whole periph MCA
7 whole periph+lat BG
8 whole MCA territory

Other cortical
9 anterior ACA
10 posterior ACA
11 anterior PCA
12 posterior PCA
13 anterior BZ
14 posterior BZ

Lacunar**
15 int & ext capsules/lent nucleus
16 internal border zone
17 centrum semiovale
18 thalamus
19 brainstem
20 anterior (mainly) borderzone
21 posterior (mainly) borderzone
27 cerebellum
28 optic radiation

Cerebellum
22 small cortical
23 <1/2 hemisphere
24 >1/2 hemisphere

Brainstem
25 small (i.e. <1/2 medulla)
26 extensive

* Record in the following order: MCA cortical > other cortical > lacunar > cerebellum > brainstem
** Defined as a 'CSF-containing cavity' in an appropriate site, measuring 3-20mm in diameter
*** Defined as high signal on both T2 and FLAIR and of non-CSF signal on T1, and either (1) where no/minimal WMH: typical site, size & configuration (2) where moderate/severe WMH: typical site, size & configuration & very clearly distinct from WMH

Sequences: T1, T2, T2*, FLAIR

APPENDIX 5

H&E staining protocol

1. Sections to be stained are put on slides and dried overnight at 40°C.
2. De-paraffin slides in Xylene x 2, 3 min each.
3. 74 OP industrial denatured alcohol (IDA) x 2, 3 min. each
4. 70% alcohol 3 min.
5. Picric acid 15 min.
6. Wash in running water until sections are clear.
7. Place in Haematoxylin 5 min.
8. Wash in running water 1 min.
9. Blue up slides in lithium carbonate 30 sec.
10. Wash in running water 1 min.
11. Check staining, if it is too pale, replace in haematoxylin for 1 min increments until correct staining is achieved.
12. Dehydrate through alcohols, 2 dips in each 99% IDA, 99% IDA, 99% IDA then absolute alcohol until desired colour is achieved.
13. Clear in xylenes x 4, 2 min in each.
14. Mount slides in cover slipper.

Solutions

Haematoxylin Z: Cellpath (RBA-4201-00A)
Eosin Y: Cellpath (RHS-260-1L)

APPENDIX 6

Additional immunohistochemical stain details

These were used in addition to those in table 3, chapter 4.

Stains	Concentration	Antigen retrieval	Manufacturer	Feature assessed
Cut at 4um:				
CD34	1:100	Citrate	Abcam	Endothelial cells
Fibrinogen	1:4000	Citrate	DAKO	Vascular leakage
CR3-43	1:500	Citrate	DAKO	Inflammatory cells

APPENDIX 7: Histological SVD grading proforma

CB cerebellum, HC hippocampus, haemosid haemosiderin, hypothal hypothalamus, inflamm inflammation, parasag parasagittal, PV perivascular, PVS perivascular space, WM white matter

Case no. ____/____	**WM rarefaction**	**Enlarged PVS**	**PVS rarefaction**	**Large bleed**	**Micro-infarct**	**Lacune**	**Micro-bleed**	**Arteriolo-sclerosis**	**Fibrinoid necrosis**	**Lipo-hyalinosis**	**PV collagenosis**	**PV haemosid**	**PV inflamm**	**Other**
LEFT	Severity, extent	Severity, extent	Present/ absent	Present/ absent	Number size	Number size	Number size	Severity, extent	Present/ absent	Present/ absent	Present/ absent	Present/ absent	Present/ absent	
A Frontal parasag (BA9)														S M D
G Broca's area (BA44/45)														S M D
I Temporal tip (BA38)														S M D
K Frontal WM														
Q Caudate nucleus														
S Basal ganglia														Pigment (0-3)
U Anterior HC														
Y PV WM														

AA Hypothal														
AK Posterior HC														
AM Thalamus														
AO Central WM														
AQ Occipital WM														
BA CB														
BE Pons														
BF Medulla														

Parenchymal SVD: none / mild / moderate / severe **non-CAA vascular SVD:** none / mild / moderate / severe
Rated by:

Grading:

Severity: 0-3
Extent: 0-3
Number: count
Size: measure (mm)

APPENDIX 8: Demographic data for cases used to assess SVD burden on ex vivo imaging and histopathology

Ischaemic heart disease has been used to simplify multiple diagnoses and includes coronary artery atheroma and myocardial infarction where specified. y years, h hours, LBC Lothian Birth Cohort 1936, LP Lothian Study of INtraCerebral Haemorrhage, Pathology, Imaging and Neurological Outcome, SD sudden death cohort, M Male, F female, COPD chronic obstructive pulmonary disease, ICH intracerebral haemorrhage, ADH anti-diuretic hormone, SVD small vessel disease, MRI magnetic resonance imaging, ITP Idiopathic thrombocytopaenic purpura, TIA transient ischaemic attack, - none, * not known.

No.	Cohort	Sex	Age (y)	Graded	Cause of death	Smoking status	Cardiovascular disease	Other Medical Conditions	Place of death	Duration of final illness (h)
1	LBC	M	78	MR & histology	Amyloidosis	Current	-	Alzheimer's disease Stroke COPD	Hospital	1008
2	LP	M	77	MR & histology	Pneumonitis (aspiration)	Current	Hypertension	ICH Microcytic anaemia Chronic kidney disease	Hospital	192
3	LP	F	92	MR & histology	Subdural haemorrhage	*	Atrial fibrillation Hypertension Deep vein thrombosis	ICH	Hospital	216
4	LP	F	81	MR & histology	ICH	*	Hypertension Atrial fibrillation	ICH Asthma	Hospital	-
5	LP	F	75	MR & histology	ICH	*	Hypertension	ICH COPD Osteoporosis Syndrome of inappropriate ADH secretion	Hospital	216
6	LP	F	87	MR & histology	ICH	*	Atrial fibrillation	ICH	Hospital	24
7	LP	M	58	MR & histology	ICH	Current	-	ICH Chronic liver disease Substance abuse	Hospital	*

8	LBC	M	79	MR & histology	Pneumonia	Current	Hypertension Hypercholesterolaemia Left ventricular systolic dysfunction	Chronic liver disease COPD	Hospital	*
9	LP	M	84	MR & histology	ICH	*	-	ICH Lacunar stroke	Hospital	120
10	LBC	M	79	MR & histology	Pneumonia	Current	Hypertension Hypercholesterolaemia	TIA Malignancy COPD Renal failure	Hospital	192
11	LP	M	70	MR & histology	Pneumonitis (aspiration)	Never	Hypertension Hypercholesterolaemia Deep vein thrombosis	ICH Chronic kidney disease Ischaemic stroke Vascular dementia	Hospital	120
12	LP	F	88	MR & histology	ICH	Previous	Atrial fibrillation Pacemaker Hypertension	ICH Ischaemic stroke Osteoarthritis	Hospital	72
13	LP	M	89	MR & histology	ICH	Previous	Hypertension	ICH Ischaemic stroke Renal failure	Hospital	24
14	SD	F	64	MR	Small bowel ischaemia	*	*	Obesity	Home	3
15	LP	M	76	MR & histology	ICH	*	Hypertension	ICH Dementia COPD	Hospital	96
16	LP	M	81	MR & histology	Pneumonitis (aspiration)	Never	Hypertension	ICH Malignancy Osteoarthritis	Hospital	120
17	LBC	F	79	MR & histology	*	Previous	Hypertension Hypercholesterolaemia	Pulmonary fibrosis COPD	Hospice	*
18	LBC	F	79	MR & histology	*	Previous	Hypertension	Metastatic carcinoma	Hospital	*

19	LP	M	86	MR & histology	Pneumonia	*	Atrial fibrillation	ICH	Hospital	312
20	SD	M	39	MR & histology	Ischaemic heart disease	Previous	Ischaemic heart disease	Depression Obesity	Home	1
21	LP	M	86	MR & histology	Pneumonitis (aspiration)	Previous	Ischaemic heart disease Hypertension Deep vein thrombosis	ICH SVD (on MRI 2012) Ischaemic stroke Benign prostatic hypertrophy	Nursing home	144
22	LP	F	86	MR & histology	Pneumonia	*	Left ventricular systolic dysfunction Atrial fibrillation	ICH	Hospital	48
23	LBC	M	79	MR & histology	Chronic lymphocytic leukaemia	Previous	Hypertension Type 2 diabetes mellitus	Myelofibrosis Malignancy Microcytic anaemia ITP ICH	Hospital	192
24	SD	F	37	MR & histology	Myocardial fibrosis	Never	-	Crohn's disease	Home	5
25	LP	F	94	Histology	Vascular dementia	*	-	ICH Multiple TIA	Nursing home	336
26	LBC	F	79	MR & histology	Metastatic carcinoma	Current	Hypertension	Metastatic carcinoma Rheumatoid arthritis Osteoarthritis Chronic liver disease	Hospice	*
27	SD	M	58	MR & histology	Ischaemic heart disease	Current	Ischaemic heart disease	Oesophageal reflux	Home	0.67
28	SD	M	46	MR	Ischaemic heart disease	Current	Ischaemic heart disease	Depression Obesity	Home	0.42
29	LBC	F	79	MR & histology	ICH	Never	Hypertension Hypercholesterolaemia	ICH Hyponatraemia	Hospital	*
30	LP	F	86	Histology	Vascular dementia	Never	Deep vein thrombosis	ICH Malignancy	Nursing home	168

								Coeliac disease		
31	LP	F	84	MR & histology	Ischaemic heart disease	*	Atrial fibrillation	ICH Hypothyroid	Hospital	48
32	SD	M	39	MR	Suicide	Current	*	Depression Chronic pain Alcohol excess	Home	0.17
33	SD	M	57	MR	Ischaemic heart disease	*	Ischaemic heart disease	Obesity	Home	1.3
34	SD	M	52	MR	Ischaemic heart disease	Current	Hypertension Ischaemic heart disease	Rheumatoid arthritis	Home	6.3
35	SD	M	47	MR	Ischaemic heart disease	*	Ischaemic heart disease	*	Home	0.08
36	LP	F	93	MR	*	*	-	Hip fracture ICH	Nursing home	48
37	SD	M	42	MR	Suicide	Current	-	Depression Alcohol excess	Hospital	0.17
38	SD	M	49	MR	Ischaemic heart disease	*	Ischaemic heart disease	Asthma	Home	0.30
39	SD	M	50	MR	Ischaemic heart disease	Current	Ischaemic heart disease	Previous extradural haematoma	Home	1.42
40	SD	M	57	MR	Ischaemic heart disease	Current	Ischaemic heart disease	-	Home	1
41	SD	F	71	MR & histology	Ischaemic heart disease	Previous	Ischaemic heart disease Hypertension Diabetes mellitus	Obesity	Home	1.50
42	SD	M	69	MR & histology	Ischaemic heart disease	Previous	Ischaemic heart disease	Peripheral oedema BPH	Home	2
43	SD	M	51	MR & histology	Ischaemic heart disease	Never	Ischaemic heart disease Hypertension Left ventricular hypertrophy	-	Home	0.42

44	SD	M	67	MR & histology	Ischaemic heart disease	Previous	Ischaemic heart disease Angina	*	Home	0.92
45	SD	M	72	MR & histology	Ischaemic heart disease	Never	Ischaemic heart disease	-	Home	0.25
46	SD	M	73	MR & histology	Ischaemic heart disease	*	Ischaemic heart disease	-	Home	6
47	SD	M	40	MR	Ischaemic heart disease	Current	Ischaemic heart disease	*	Home	0.5
48	SD	M	71	MR	Haemopericardium	Previous	Ischaemic heart disease Hypertension	Depression	Home	0.5
49	SD	M	34	MR	Ischaemic heart disease	*	Ischaemic heart disease	-	Home	1
50	LBC	M	81	MR	Metastatic carcinoma	Previous	Ischaemic heart disease Hypertension Hypercholesterolaemia Type 2 diabetes mellitus	Metastatic carcinoma Pituitary adenoma	Home	48
51	SD	F	57	MR	Cardiomegaly	Current	-	Obesity	Home	*
52	SD	F	65	MR	Ischaemic heart disease	Never	Ischaemic heart disease Dilated cardiomyopathy Hypertension Pacemaker	*	Home	48
53	LBC	M	81	MR	Metastatic carcinoma	Current	Ischaemic heart disease Hypertension Hypercholesterolaemia	Metastatic carcinoma COPD Pulmonary embolus Chronic kidney disease	Hospice	48
54	SD	F	69	MR	Ischaemic heart disease	*	Ischaemic heart disease	Malignancy Hypothyroidism	Home	0.50
55	LP	M	84	MR	Extreme frailty	Previous	Atrial fibrillation Mitral valve disease	Metastatic carcinoma ICH Epilepsy Hip fracture	Nursing home	*

APPENDIX 9: Individual scores for grading SVD burden on ex vivo MRI

***** Denotes case also underwent histological SVD grading, PVS perivascular spaces, WMH white matter hyperintensity, SVD small vessel disease, BG basal ganglia, LBC Lothian birth cohort 1936, LP Lothian Study of INtraCerebral Haemorrhage, Pathology, Imaging and Neurological Outcome, SD sudden death cohort. - not available due to artefact.

Case	Cohort	Infarcts, n	Enlarged PVS (0-3)	Microbleed, n	WMH score (0-3)	Overall SVD score (0-3)	BG iron score (1-4)
1*	LBC	1	4	1	1	3	2
2*	LP	0	4	1	3	3	4
3*	LP	1	4	0	2	3	3
4*	LP	0	4	0	3	3	4
5*	LP	0	2	3	1	3	3
6*	LP	1	4	1	3	3	3
7*	LP	2	4	1	3	3	2
8*	LBC	0	4	0	2	2	3
9*	LP	1	4	2	2	3	4
10*	LBC	3	4	1	1	3	4
11*	LP	0	3	0	0	1	2
12*	LP	0	4	0	1	1	2
13*	LP	0	1	0	0	1	-
14	SD	0	2	0	0	1	3
15*	LP	4	3	8	2	3	3
16*	LP	2	3	0	2	3	2
17*	LBC	0	1	0	1	1	1
18*	LBC	0	1	1	1	1	1
19*	LP	0	2	0	1	1	2
20*	SD	0	2	1	1	3	4
21*	LP	0	2	0	1	1	2
22*	LP	0	4	2	2	3	4
23*	LBC	0	4	0	2	3	3
24*	SD	0	4	0	1	2	1
26*	LBC	1	4	2	2	3	2
27*	SD	1	2	1	0	3	1
28	SD	0	3	0	0	2	1
29*	LBC	1	3	1	2	3	2
31*	LP	1	2	1	2	3	2
32	SD	0	2	0	0	1	1
33	SD	0	2	2	2	3	2
34	SD	0	4	0	1	2	3

35	SD	1	4	0	1	3	2
37	SD	0	2	0	1	1	2
36	LP	0	3	0	1	2	3
38	SD	0	1	0	0	1	1
39	SD	0	1	0	0	1	2
40	SD	0	1	0	1	1	2
41*	SD	0	1	0	1	1	3
42*	SD	0	1	0	1	1	2
43*	SD	0	1	0	1	1	2
44*	SD	0	1	0	0	1	2
45*	SD	0	4	0	1	2	2
46*	SD	0	1	0	1	1	3
47	SD	0	1	0	1	1	2
48	SD	0	1	0	0	1	2
49	SD	1	1	0	0	3	3
50	LBC	0	1	0	0	1	3
51	SD	0	1	0	1	1	1
52	SD	0	1	0	0	1	3
53	LBC	0	1	0	1	1	3
54	SD	0	1	0	0	1	1
55	LP	0	1	0	1	1	0

APPENDIX 10: Individual scores for grading SVD burden on histology

***** Denotes case also underwent histological SVD grading, WM white matter, PVS perivascular spaces, CMI cortical microinfarct, subcortical microinfarct, MB microbleed, BG basal ganglia, LBC Lothian birth cohort 1936, LP Lothian Study of INtraCerebral Haemorrhage, Pathology, Imaging and Neurological Outcome, SD sudden death cohort, SVD small vessel disease,

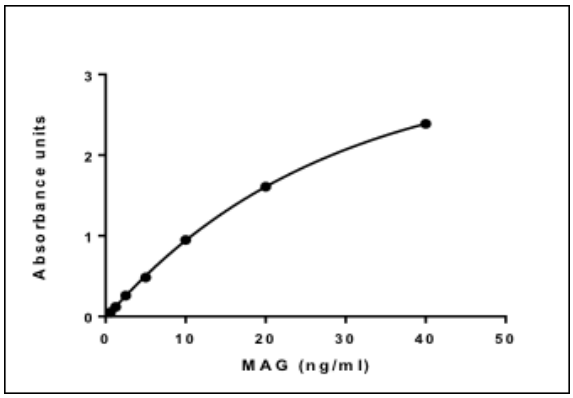
Case	Cohort	WM rarefaction		PVS		CMI	Lacunes	SCI	MB	Arteriolosclerosis		Lipohyalinosis	Fibrinoid necrosis	BG pigment	Overall	
		severity	extent	severity	extent					severity	extent				Parenchymal	Vascular
1*	LBC	2	3	3	3	0	0	0	0	1	3	0	0	2	2	1
2*	LP	2	2	3	3	0	0	1	0	2	3	0	0	1	3	2
3*	LP	2	3	3	3	0	0	1	3	2	3	0	0	1	3	2
4*	LP	2	3	3	3	0	0	0	0	3	2	0	0	2	2	2
5*	LP	2	2	3	2	0	0	1	0	2	2	0	0	1	2	2
6*	LP	3	3	3	3	0	0	0	2	2	3	1	1	1	3	2
7*	LP	2	3	2	3	0	0	0	0	1	3	0	0	1	3	2
8*	LBC	2	3	2	2	0	0	0	0	1	2	0	0	3	2	1
9*	LP	2	3	3	3	0	0	0	0	2	3	0	0	2	2	2
10*	LBC	3	3	3	3	0	0	0	0	2	2	0	0	3	3	2
11*	LP	2	3	3	3	2	0	0	0	2	3	0	0	0	3	3
12*	LP	2	3	3	3	0	0	0	4	3	3	0	0	2	3	3
13*	LP	2	2	1	2	0	0	0	0	1	2	0	0		2	1
15*	LP	3	2	2	2	1	1	1	3	3	3	1	1	1	3	3
16*	LP	2	2	1	2	0	0	0	0	2	3	0	0	1	2	2
17*	LBC	3	3	3	3	0	0	2	2	2	2	0	0	2	3	2
18*	LBC	2	3	3	3	0	0	0	1	1	2	0	0	1	3	1

19*	LP	3	3	3	3	0	1	0	0	1	2	0	0	0	3	2
20*	SD	1	1	1	1	0	1	0	0	1	2	0	0	2	1	1
21*	LP	2	3	2	1	0	0	0	0	1	2	1	0		2	2
22*	LP	3	2	3	3	0	0	1	0	3	3	1	0		3	3
23*	LBC	2	3	2	3	0	0	0	0	1	3	0	0	1	2	1
24*	SD	2	2	1	1	0	0	0	0	2	3	1	1	2	2	3
25	LP	2	2	1	2	1	1	0	2	2	3	1	1		2	2
26*	LBC	1	2	2	3	0	0	0	1	2	3	0	0	1	3	2
27*	SD	1	2	1	2	0	0	0	0	2	2	0	0	0	1	1
29*	LBC	2	3	2	3	0	0	0	2	3	3	1	0		3	3
30	LP	2	3	3	3	1	4	0	1	2	3	0	0	2	3	3
31*	LP	3	3	3	3	1	2	2	1	2	3	1	0	1	3	3
41*	SD	2	2	2	2	0	0	0	0	1	3	0	0		1	1
42*	SD	0	0	3	2	0	0	0	0	1	2	0	0		1	1
43*	SD	1	1	1	1	0	0	0	0	1	1	0	0	0	1	1
44*	SD	1	1	2	2	0	0	0	0	1	2	0	0	1	2	2
45*	SD	1	1	2	2	0	0	0	0	2	2	0	0	1	1	2
46*	SD	1	2	3	3	0	0	2	0	2	3	0	0	1	3	2

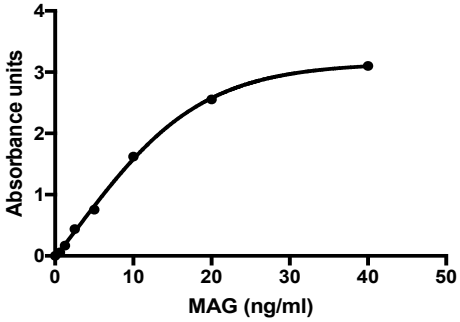
APPENDIX 11

Standard curves for the biochemical studies initially carried out in Bristol (left column, a, c, e, g, I, k) and subsequently carried out in Edinburgh (right column, b, d, f, h, j, l). Each row represents a different protein; a, b) MAG; b, c) PLP-1; e, f) VEGF; g, h) PDGFRB; I, j) VWF; k, l) fibrinogen. MAG myelin associated glycoprotein, PLP-1 proteolipid protein-1, VEG vascaulr endothelial growth factor, PDGFRB platelet derived growth factor receptor β, VWF von Willebrand factor.

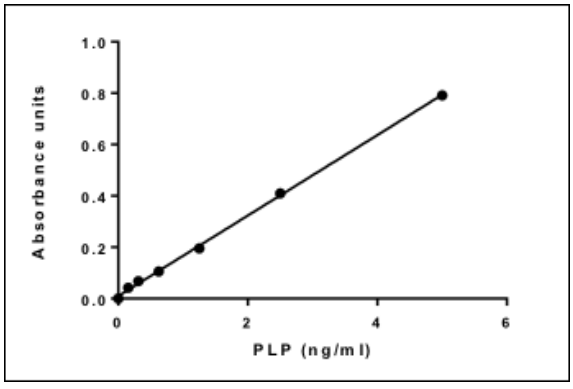
a



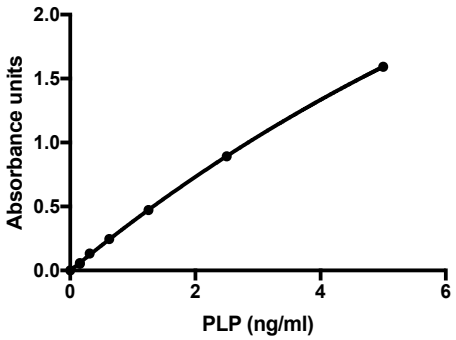
b



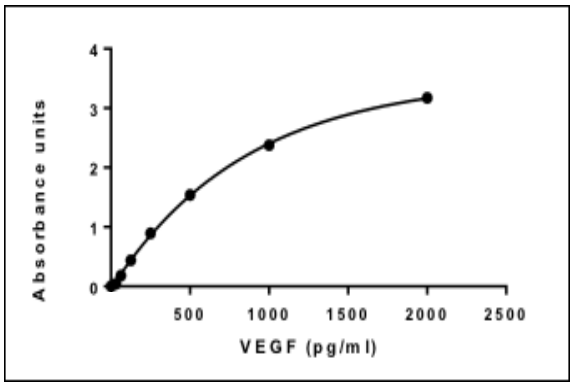
c



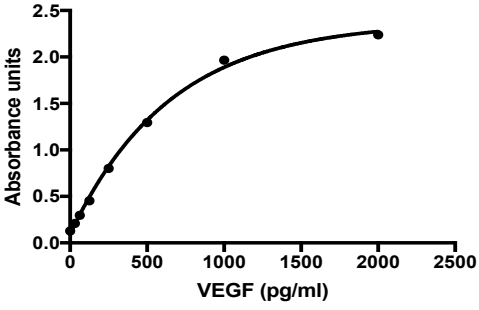
d



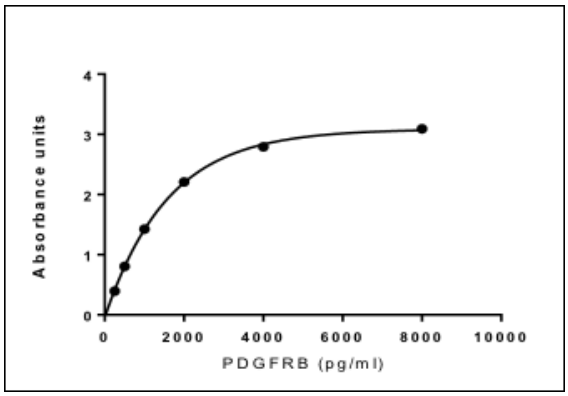
e



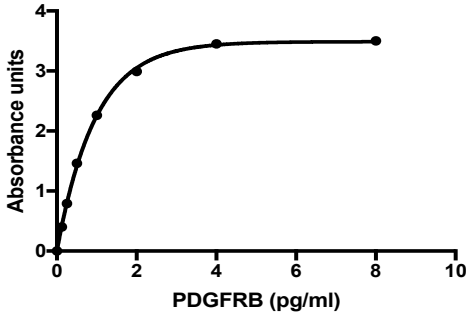
f



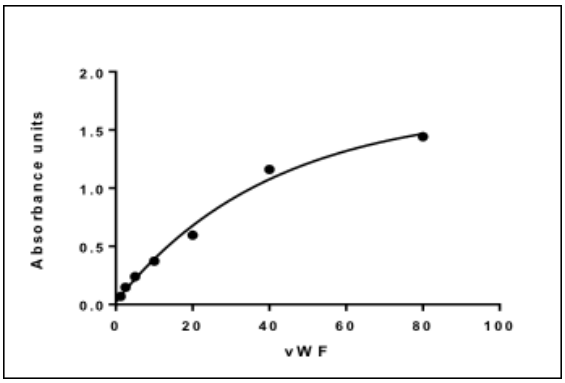
g


Absorbance units
0
1
2
3
4
0
2000
4000
6000
8000
10000
PDGFRB (pg/ml)

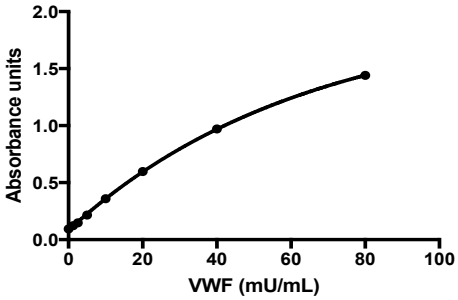
h


Absorbance units
0
1
2
3
4
0
2
4
6
8
10
PDGFRB (pg/ml)

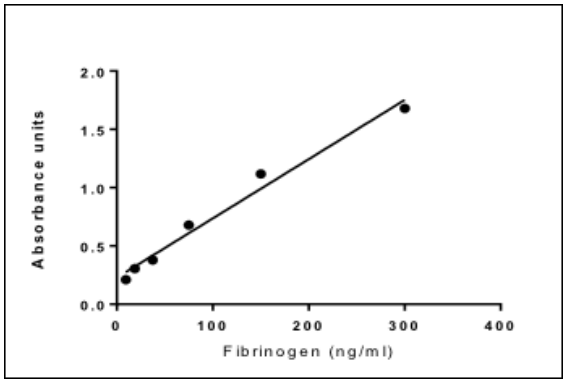
i


Absorbance units
0.0
0.5
1.0
1.5
2.0
0
20
40
60
80
100
vWF

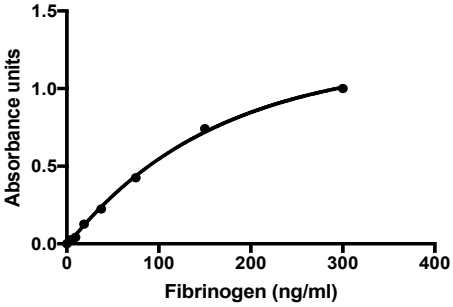
j


Absorbance units
0.0
0.5
1.0
1.5
2.0
0
20
40
60
80
100
VWF (mU/mL)

k

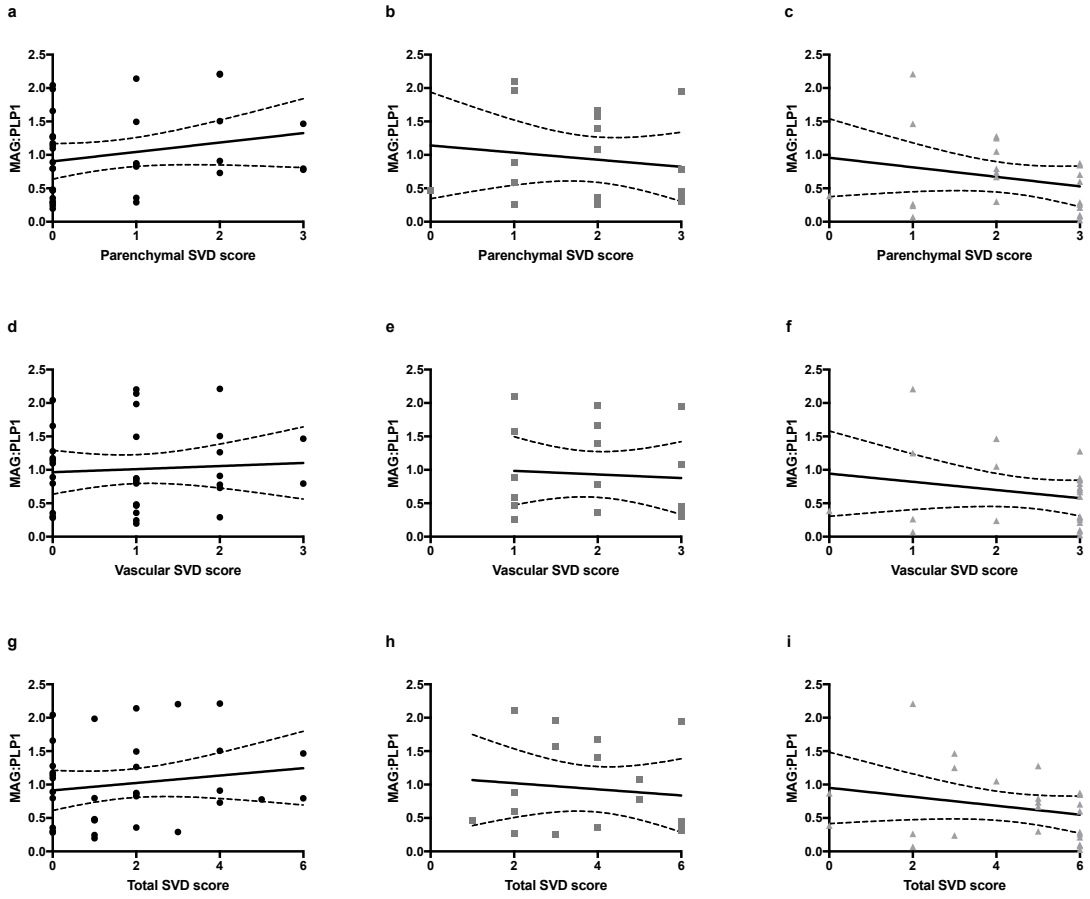

Absorbance units
0.0
0.5
1.0
1.5
2.0
0
100
200
300
400
Fibrinogen (ng/ml)

l


Absorbance units
0.0
0.5
1.0
1.5
0
100
200
300
400
Fibrinogen (ng/ml)

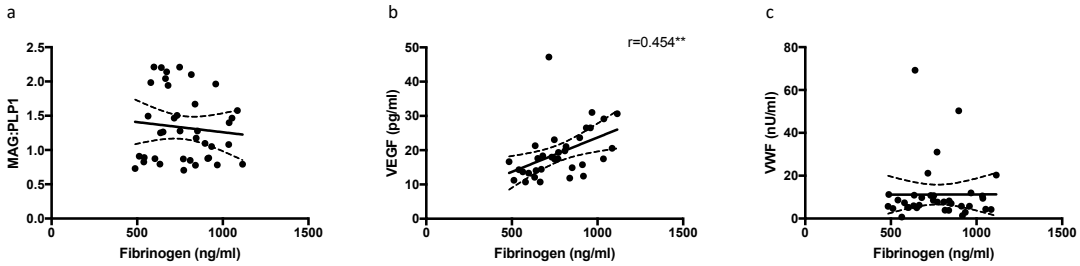
APPENDIX 12

Scatterplots showing MAG:PLP1 values according to histological (a-c) parenchymal damage scores, (d-f) vascular SVD scores and (g-i) total SVD (parenchymal plus vascular SVD) scores in the three cohorts. Although MAG:PLP1 tended to be lower in white matter from AD and ICH-SVD brains with higher scores, the differences were not significant. Each point in the scatterplots indicates either a single control (left column, black circle) AD (middle column, grey square) or ICH-SVD (right column, pale grey triangle) brain.



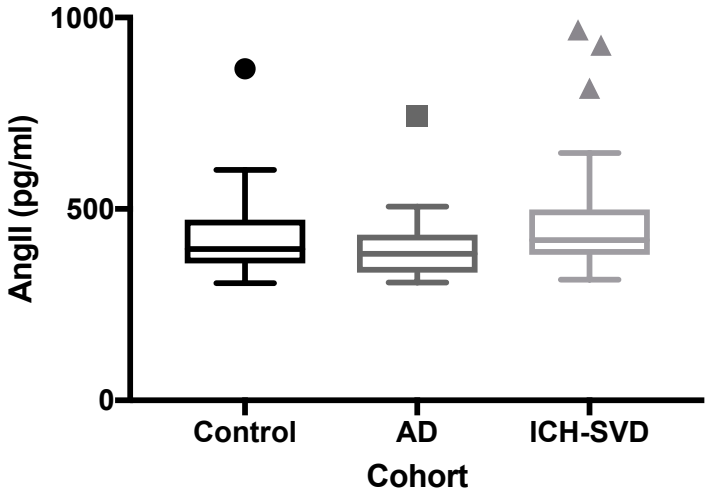
APPENDIX 13

Scatterplots showing exploratory analysis of fibrinogen relationship with markers of hypoxia; a) MAG:PLP1 and b) VEGF, and vascularity; c) VWF. A they show a significant positive association with VEGF and a trend of higher fibrinogen with decreasing MAG:PLP1, supporting an association with hypoxia, but possibly not with vascularity.



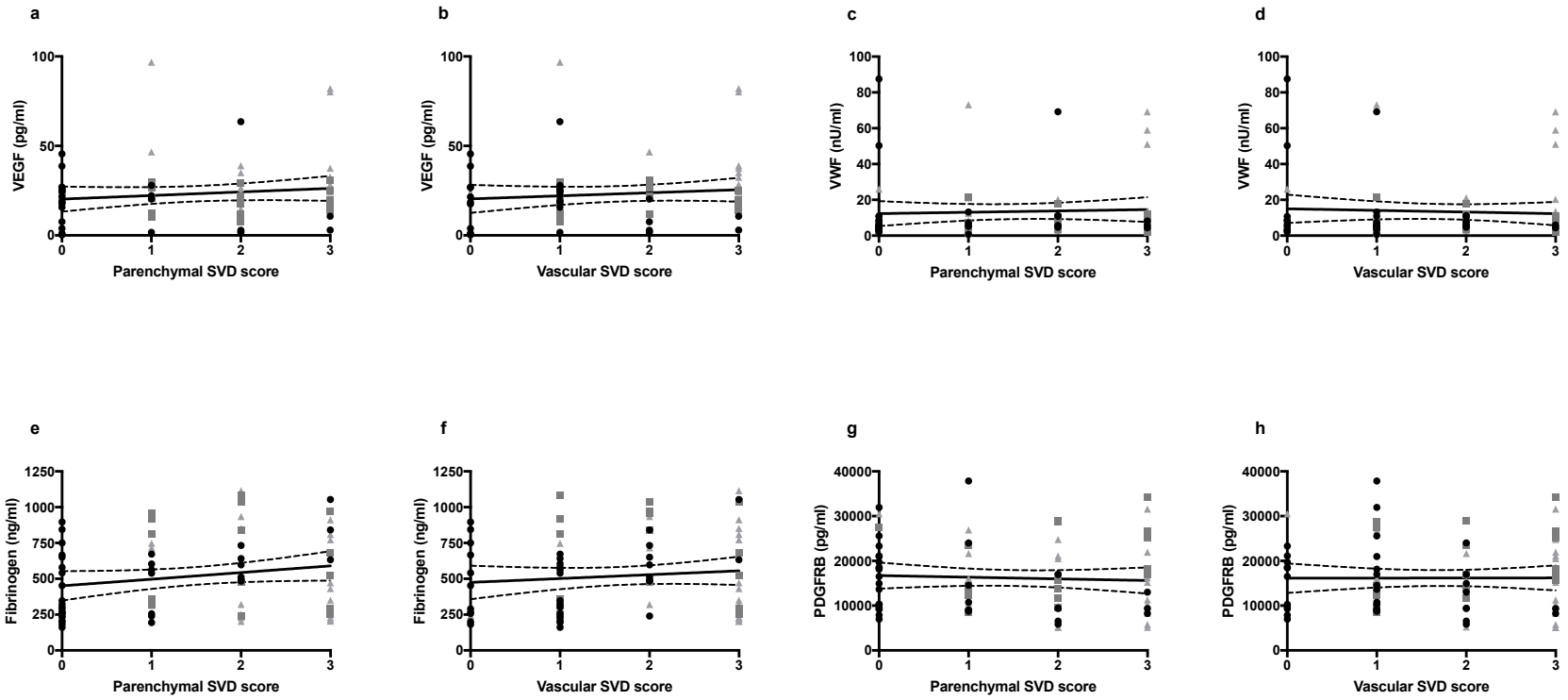
APPENDIX 14

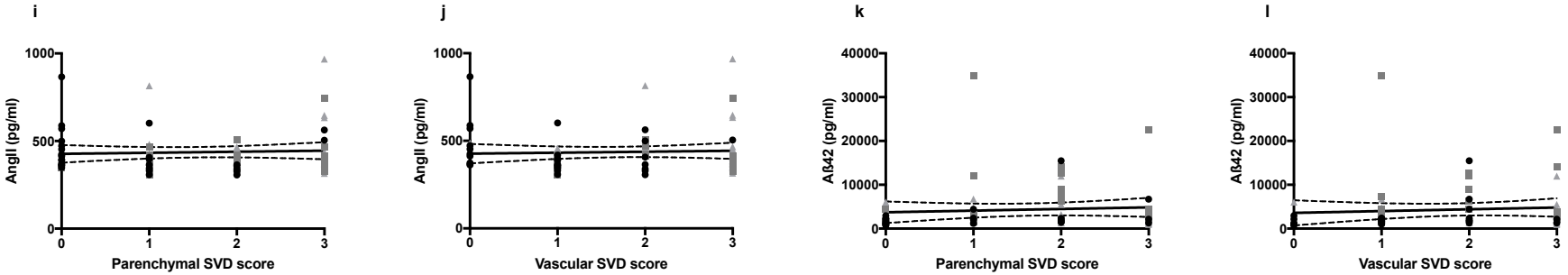
Angiotensin-II (Ang-II) level in the WM did not differ between controls, SVD and AD. These Tukey boxplots indicate the median and inter-quartile range (IQR), with outliers beyond 1.5 IQR plotted individually. Each point indicates either a single control (black circle) AD (grey square) or ICH-SVD (pale grey triangle) brain.



Appendix 15

Scatterplots showing no correlation between histologically assessed parenchymal damage associated with SVD (a, c, e, g, i, k) or severity of SVD features affecting the small vessels (b, d, f, h, j, l) and the levels of VEGF, VWF, fibrinogen, PDGFRB, AngII or Aβ42. The cohorts are combined and each point indicates either a single control (black circle) AD (grey square) or ICH-SVD (pale grey triangle) brain. The best-fit linear regression lines and 95% confidence intervals are superimposed.




i
AngII (pg/ml)
1000
500
0
0
1
2
3
Parenchymal SVD score
j
AngII (pg/ml)
1000
500
0
0
1
2
3
Vascular SVD score
k
Aβ42 (pg/ml)
40000
30000
20000
10000
0
0
1
2
3
Parenchymal SVD score
l
Aβ42 (pg/ml)
40000
30000
20000
10000
0
0
1
2
3
Vascular SVD score

REFERENCES

Abbott, N. J., A. A. Patabendige, D. E. Dolman, S. R. Yusof and D. J. Begley (2010). "Structure and function of the blood-brain barrier." Neurobiol Dis **37**(1): 13-25.

Abbott, N. J., L. Ronnback and E. Hansson (2006). "Astrocyte-endothelial interactions at the blood-brain barrier." Nat Rev Neurosci **7**(1): 41-53.

Ahmed, R. G. (2005). "Heat stress induced histopathology and pathophysiology of the central nervous system." Int J Dev Neurosci **23**(6): 549-557.

Akiguchi, I., H. Tomimoto, T. Suenaga, H. Wakita and H. Budka (1997). "Alterations in glia and axons in the brains of Binswanger's disease patients." Stroke **28**(7): 1423-1429.

Alafuzoff, I., E. Gelpi, S. Al-Sarraj, T. Arzberger, J. Attems, I. Bodi, N. Bogdanovic, H. Budka, O. Bugiani, E. Englund, I. Ferrer, S. Gentleman, G. Giaccone, M. B. Graeber, T. Hortobagyi, R. Hoftberger, J. W. Ironside, K. Jellinger, N. Kavantzas, A. King, P. Korkolopoulou, G. G. Kovacs, D. Meyronet, C. Monoranu, P. Parchi, E. Patsouris, W. Roggendorf, A. Rozemuller, D. Seilhean, N. Streichenberger, D. R. Thal, S. B. Wharton and H. Kretzschmar (2012). "The need to unify neuropathological assessments of vascular alterations in the ageing brain: multicentre survey by the BrainNet Europe consortium." Exp Gerontol **47**(11): 825-833.

Alafuzoff, I., P. G. Ince, T. Arzberger, S. Al-Sarraj, J. Bell, I. Bodi, N. Bogdanovic, O. Bugiani, I. Ferrer, E. Gelpi, S. Gentleman, G. Giaccone, J. W. Ironside, N. Kavantzas, A. King, P. Korkolopoulou, G. G. Kovacs, D. Meyronet, C. Monoranu, P. Parchi, L. Parkkinen, E. Patsouris, W. Roggendorf, A. Rozemuller, C. Stadelmann-Nessler, N. Streichenberger, D. R. Thal and H. Kretzschmar (2009). "Staging/typing of Lewy body related alpha-synuclein pathology: a study of the BrainNet Europe Consortium." Acta Neuropathol **117**(6): 635-652.

Alexander, A. L., J. E. Lee, M. Lazar and A. S. Field (2007). "Diffusion tensor imaging of the brain." Neurotherapeutics **4**(3): 316-329.

Anderson, C. D., A. Biffi, M. A. Nalls, W. J. Devan, K. Schwab, A. M. Ayres, V. Valant, O. A. Ross, N. S. Rost, R. Saxena, A. Viswanathan, B. B. Worrall, T. G. Brott, J. N. Goldstein, D. Brown, J. P. Broderick, B. Norrving, S. M. Greenberg, S. L. Silliman, B. M. Hansen, D. L. Tirschwell, A. Lindgren, A. Slowik, R. Schmidt, M. Selim, J. Roquer, J. Montaner, A. B. Singleton, C. S. Kidwell, D. Woo, K. L. Furie, J. F. Meschia, J. Rosand and C. International Stroke Genetics (2013). "Common variants within oxidative phosphorylation genes influence risk of ischemic stroke and intracerebral hemorrhage." Stroke **44**(3): 612-619.

Andreone, B. J., B. Lacoste and C. Gu (2015). "Neuronal and vascular interactions." Annu Rev Neurosci **38**: 25-46.

Ankolekar, S., M. Fuller, I. Cross, C. Renton, P. Cox, N. Sprigg, A. N. Siriwardena and P. M. Bath (2013). "Feasibility of an ambulance-based stroke trial, and safety of glyceryl trinitrate in ultra-acute stroke: the rapid intervention with glyceryl trinitrate in Hypertensive Stroke Trial (RIGHT, ISRCTN66434824)." Stroke **44**(11): 3120-3128.

APA, A. P. A. (1994). Diagnostic and statistical manual of memntal disorders. 4th ed., APA.

Appelman, A. P., L. G. Exalto, Y. van der Graaf, G. J. Biessels, W. P. Mali and M. I. Geerlings (2009). "White matter lesions and brain atrophy: more than shared risk factors? A systematic review." Cerebrovasc Dis **28**(3): 227-242.
Aribisala, B. S., M. C. Valdes Hernandez, N. A. Royle, Z. Morris, S. Munoz Maniega, M. E. Bastin, I. J. Deary and J. M. Wardlaw (2013). "Brain atrophy associations with white matter lesions in the ageing brain: the Lothian Birth Cohort 1936." Eur Radiol **23**(4): 1084-1092.
Aribisala, B. S., S. Wiseman, Z. Morris, M. C. Valdes-Hernandez, N. A. Royle, S. M. Maniega, A. J. Gow, J. Corley, M. E. Bastin, J. Starr, I. J. Deary and J. M. Wardlaw (2014). "Circulating inflammatory markers are associated with magnetic resonance imaging-visible perivascular spaces but not directly with white matter hyperintensities." Stroke **45**(2): 605-607.
Armulik, A., A. Abramsson and C. Betsholtz (2005). "Endothelial/pericyte interactions." Circ Res **97**(6): 512-523.
Armulik, A., G. Genove and C. Betsholtz (2011). "Pericytes: developmental, physiological, and pathological perspectives, problems, and promises." Dev Cell **21**(2): 193-215.
Armulik, A., G. Genove, M. Mae, M. H. Nisancioglu, E. Wallgard, C. Niaudet, L. He, J. Norlin, P. Lindblom, K. Strittmatter, B. R. Johansson and C. Betsholtz (2010). "Pericytes regulate the blood-brain barrier." Nature **468**(7323): 557-561.
Arno, B., F. Grassivaro, C. Rossi, A. Bergamaschi, V. Castiglioni, R. Furlan, M. Greter, R. Favaro, G. Comi, B. Becher, G. Martino and L. Muzio (2014). "Neural progenitor cells orchestrate microglia migration and positioning into the developing cortex." Nat Commun **5**: 5611.
Ashby, E. L., P. G. Kehoe and S. Love (2010). "Kallikrein-related peptidase 6 in Alzheimer's disease and vascular dementia." Brain Res **1363**: 1-10.
Asif, M., R. L. Soiza, M. McEvoy and A. A. Mangoni (2013). "Asymmetric dimethylarginine: a possible link between vascular disease and dementia." Curr Alzheimer Res **10**(4): 347-356.
Atanur, S. S., A. G. Diaz, K. Maratou, A. Sarkis, M. Rotival, L. Game, M. R. Tschannen, P. J. Kaisaki, G. W. Otto, M. C. Ma, T. M. Keane, O. Hummel, K. Saar, W. Chen, V. Guryev, K. Gopalakrishnan, M. R. Garrett, B. Joe, L. Citterio, G. Bianchi, M. McBride, A. Dominiczak, D. J. Adams, T. Serikawa, P. Flicek, E. Cuppen, N. Hubner, E. Petretto, D. Gauguier, A. Kwitek, H. Jacob and T. J. Aitman (2013). "Genome sequencing reveals loci under artificial selection that underlie disease phenotypes in the laboratory rat." Cell **154**(3): 691-703.
Attems, J., K. A. Jellinger and F. Lintner (2005). "Alzheimer's disease pathology influences severity and topographical distribution of cerebral amyloid angiopathy." Acta Neuropathol **110**(3): 222-231.
Attems, J., J. B. Toledo, L. Walker, E. Gelpi, S. Gentleman, G. Halliday, T. Hortobagyi, K. Jellinger, G. G. Kovacs, E. B. Lee, S. Love, K. E. McAleese, P. T. Nelson, M. Neumann, L. Parkkinen, T. Polvikoski, B. Sikorska, C. Smith, L. T. Grinberg, D. R. Thal, J. Q. Trojanowski and I. G. McKeith (2021). "Neuropathological consensus criteria for the evaluation of Lewy pathology in post-mortem brains: a multi-centre study." Acta Neuropathol **141**(2): 159-172.

Attwell, D., A. M. Buchan, S. Charpak, M. Lauritzen, B. A. Macvicar and E. A. Newman (2010). "Glial and neuronal control of brain blood flow." Nature **468**(7321): 232-243.
Auriel, E., N. M. Bornstein, E. Berenyi, I. Varkonyi, M. Gabor, K. Majtenyi, R. Szepesi, I. Goldberg, R. Lampe and L. Csiba (2011). "Clinical, radiological and pathological correlates of leukoaraiosis." Acta Neurol Scand **123**(1): 41-47.
Awad, I. A., P. C. Johnson, R. F. Spetzler and J. A. Hodak (1986). "Incidental subcortical lesions identified on magnetic resonance imaging in the elderly. II. Postmortem pathological correlations." Stroke **17**(6): 1090-1097.
Bailey, E. L., M. W. McBride, W. Beattie, J. D. McClure, D. Graham, A. F. Dominiczak, C. L. Sudlow, C. Smith and J. M. Wardlaw (2014). "Differential gene expression in multiple neurological, inflammatory and connective tissue pathways in a spontaneous model of human small vessel stroke." Neuropathol Appl Neurobiol **40**(7): 855-872.
Bailey, E. L., J. McCulloch, C. Sudlow and J. M. Wardlaw (2009). "Potential animal models of lacunar stroke: a systematic review." Stroke **40**(6): e451-458.
Bailey, E. L., C. Smith, C. L. Sudlow and J. M. Wardlaw (2011). "Is the spontaneously hypertensive stroke prone rat a pertinent model of sub cortical ischemic stroke? A systematic review." Int J Stroke **6**(5): 434-444.
Bailey, E. L., C. Smith, C. L. Sudlow and J. M. Wardlaw (2011). "Is the spontaneously hypertensive stroke prone rat a pertinent model of sub cortical ischemic stroke? A systematic review." International Journal of Stroke **6**(5): 434-444.
Bailey, E. L., C. Smith, C. L. Sudlow and J. M. Wardlaw (2012). "Pathology of lacunar ischemic stroke in humans--a systematic review." Brain Pathol **22**(5): 583-591.
Bailey, E. L., J. M. Wardlaw, D. Graham, A. F. Dominiczak, C. L. Sudlow and C. Smith (2011). "Cerebral small vessel endothelial structural changes predate hypertension in stroke-prone spontaneously hypertensive rats: a blinded, controlled immunohistochemical study of 5- to 21-week-old rats." Neuropathol Appl Neurobiol **37**(7): 711-726.
Bajema, I. M. and J. A. Bruijn (2000). "What stuff is this! A historical perspective on fibrinoid necrosis." J Pathol **191**(3): 235-238.
Ballerini, L., T. Booth, M. D. C. Valdes Hernandez, S. Wiseman, R. Lovreglio, S. Munoz Maniega, Z. Morris, A. Pattie, J. Corley, A. Gow, M. E. Bastin, I. J. Deary and J. Wardlaw (2020). "Computational quantification of brain perivascular space morphologies: Associations with vascular risk factors and white matter hyperintensities. A study in the Lothian Birth Cohort 1936." Neuroimage Clin **25**: 102120.
Banerjee, G., R. Carare, C. Cordonnier, S. M. Greenberg, J. A. Schneider, E. E. Smith, M. V. Buchem, J. V. Grond, M. M. Verbeek and D. J. Werring (2017). "The increasing impact of cerebral amyloid angiopathy: essential new insights for clinical practice." Journal of Neurology, Neurosurgery & Psychiatry **88**(11): 982-994.
Barker, R., E. L. Ashby, D. Wellington, V. M. Barrow, J. C. Palmer, P. G. Kehoe, M. M. Esiri and S. Love (2014). "Pathophysiology of white matter perfusion in Alzheimer's disease and vascular dementia." Brain **137**(Pt 5): 1524-1532.

Barker, R., D. Wellington, M. M. Esiri and S. Love (2013). "Assessing white matter ischemic damage in dementia patients by measurement of myelin proteins." Journal of Cerebral Blood Flow & Metabolism **33**(7): 1050-1057.
Bastin, M. E., J. D. Clayden, A. Pattie, I. F. Gerrish, J. M. Wardlaw and I. J. Deary (2009). "Diffusion tensor and magnetization transfer MRI measurements of periventricular white matter hyperintensities in old age." Neurobiol Aging **30**(1): 125-136.
Bath, M. W., L. Woodhouse, P. Scutt, K. Kailash and e. al. (2015). "ENOS Trial Invesitgators. Efficacy of nitric oxide, with or without continuing antihypertensive treatment, for management of high blood pressure in acute stroke (ENOS): a partial-factorial randomised controlled trial." Lancet **385**(9968): 617-628.
Bath, P. M., R. Pathansali, R. Iddenden and F. J. Bath (2001). "The effect of transdermal glyceryl trinitrate, a nitric oxide donor, on blood pressure and platelet function in acute stroke." Cerebrovasc Dis **11**(3): 265-272.
Bath, P. M., P. Scutt, D. J. Blackburn, S. Ankolekar, K. Krishnan, C. Ballard, A. Burns, J. Mant, P. Passmore, S. Pocock, J. Reckless, N. Sprigg, R. Stewart, J. M. Wardlaw, G. A. Ford and P. T. Investigators (2017). "Intensive versus Guideline Blood Pressure and Lipid Lowering in Patients with Previous Stroke: Main Results from the Pilot 'Prevention of Decline in Cognition after Stroke Trial' (PODCAST) Randomised Controlled Trial." PLoS One **12**(1): e0164608.
Bath, P. M. and J. M. Wardlaw (2015). "Pharmacological treatment and prevention of cerebral small vessel disease: a review of potential interventions." Int J Stroke **10**(4): 469-478.
Baumann, E., E. Preston, J. Slinn and D. Stanimirovic (2009). "Post-ischemic hypothermia attenuates loss of the vascular basement membrane proteins, agrin and SPARC, and the blood-brain barrier disruption after global cerebral ischemia." Brain Res **1269**: 185-197.
Baykara, E., B. Gesierich, R. Adam, A. M. Tuladhar, J. M. Biesbroek, H. L. Koek, S. Ropele, E. Jouvent, I. Alzheimer's Disease Neuroimaging, H. Chabriat, B. Ertl-Wagner, M. Ewers, R. Schmidt, F. E. de Leeuw, G. J. Biessels, M. Dichgans and M. Duering (2016). "A Novel Imaging Marker for Small Vessel Disease Based on Skeletonization of White Matter Tracts and Diffusion Histograms." Ann Neurol **80**(4): 581-592.
Bazzoni, G. (2006). "Endothelial tight junctions: permeable barriers of the vessel wall." Thromb Haemost **95**(1): 36-42.
Beak, H. W., H. J. Choi, M. S. Byun, Y. M. Choe, D. Yi, J. Y. Han, Y. J. Lee, J. I. Woo and D. L. Lee (2015). "Prevalence of enlarged perivascular spaces in a memory clinic population." Alzheimer's & dementia **11**: 146.
Beaufort, N., E. Scharrer, E. Kremmer, V. Lux, M. Ehrmann, R. Huber, H. Houlden, D. Werring, C. Haffner and M. Dichgans (2014). "Cerebral small vessel disease-related protease HtrA1 processes latent TGF-beta binding protein 1 and facilitates TGF-beta signaling." Proc Natl Acad Sci U S A **111**(46): 16496-16501.
Bell, R. D., E. A. Winkler, A. P. Sagare, I. Singh, B. LaRue, R. Deane and B. V. Zlokovic (2010). "Pericytes control key neurovascular functions and neuronal phenotype in the adult brain and during brain aging." Neuron **68**(3): 409-427.

Benjamin, P., E. Zeestraten, C. Lambert, I. C. Ster, O. A. Williams, A. J. Lawrence, B. Patel, A. D. MacKinnon, T. R. Barrick and H. S. Markus (2016). "Progression of MRI markers in cerebral small vessel disease: Sample size considerations for clinical trials." J Cereb Blood Flow Metab **36**(1): 228-240.
Benveniste, H. and M. Nedergaard (2022). "Cerebral small vessel disease: A glymphopathy?" Curr Opin Neurobiol **72**: 15-21.
Bergsneider, M. (2001). "Evolving concepts of cerebrospinal fluid physiology." Neurosurg Clin N Am **12**(4): 631-638, vii.
Bernacki, J., A. Dobrowolska, K. Nierwinska and A. Malecki (2008). "Physiology and pharmacological role of the blood-brain barrier." Pharmacol Rep **60**(5): 600-622.
Bernbaum, M., B. K. Menon, G. Fick, E. E. Smith, M. Goyal, R. Frayne and S. B. Coutts (2015). "Reduced blood flow in normal white matter predicts development of leukoaraiosis." J Cereb Blood Flow Metab **35**(10): 1610-1615.
Berry, C., N. Sidik, A. C. Pereira, T. J. Ford, R. M. Touyz, J. C. Kaski and A. H. Hainsworth (2019). "Small-Vessel Disease in the Heart and Brain: Current Knowledge, Unmet Therapeutic Need, and Future Directions." J Am Heart Assoc **8**(3): e011104.
Biffi, A., C. D. Anderson, J. M. Jagiella, H. Schmidt, B. Kissela, B. M. Hansen, J. Jimenez-Conde, C. R. Pires, A. M. Ayres, K. Schwab, L. Cortellini, J. Pera, A. Urbanik, J. M. Romero, N. S. Rost, J. N. Goldstein, A. Viswanathan, A. Pichler, C. Enzinger, R. Rabionet, B. Norrving, D. L. Tirschwell, M. Selim, D. L. Brown, S. L. Silliman, B. B. Worrall, J. F. Meschia, C. S. Kidwell, J. P. Broderick, S. M. Greenberg, J. Roquer, A. Lindgren, A. Slowik, R. Schmidt, D. Woo, J. Rosand and C. International Stroke Genetics (2011). "APOE genotype and extent of bleeding and outcome in lobar intracerebral haemorrhage: a genetic association study." Lancet Neurol **10**(8): 702-709.
Biffi, A. and S. M. Greenberg (2011). "Cerebral amyloid angiopathy: a systematic review." J Clin Neurol **7**(1): 1-9.
Biffi, A., A. Sonni, C. D. Anderson, B. Kissela, J. M. Jagiella, H. Schmidt, J. Jimenez-Conde, B. M. Hansen, I. Fernandez-Cadenas, L. Cortellini, A. Ayres, K. Schwab, K. Juchniewicz, A. Urbanik, N. S. Rost, A. Viswanathan, T. Seifert-Held, E. M. Stoegerer, M. Tomas, R. Rabionet, X. Estivill, D. L. Brown, S. L. Silliman, M. Selim, B. B. Worrall, J. F. Meschia, J. Montaner, A. Lindgren, J. Roquer, R. Schmidt, S. M. Greenberg, A. Slowik, J. P. Broderick, D. Woo, J. Rosand and C. International Stroke Genetics (2010). "Variants at APOE influence risk of deep and lobar intracerebral hemorrhage." Ann Neurol **68**(6): 934-943.
Black, P. H. and L. D. Garbutt (2002). "Stress, inflammation and cardiovascular disease." J Psychosom Res **52**(1): 1-23.
Black, S., F. Gao and J. Bilbao (2009). "Understanding white matter disease: imaging-pathological correlations in vascular cognitive impairment." Stroke **40**(3 Suppl): S48-52.
Blair, G. W., J. P. Appleton, K. Flaherty, F. Doubal, N. Sprigg, R. Dooley, C. Richardson, I. Hamilton, Z. K. Law, Y. Shi, M. S. Stringer, M. J. Thrippleton, J. Boyd, K. Shuler, P. M. Bath and J. M. Wardlaw (2019). "Tolerability, safety and intermediary pharmacological effects of cilostazol and isosorbide mononitrate, alone and

combined, in patients with lacunar ischaemic stroke: The LACunar Intervention-1 (LACI-1) trial, a randomised clinical trial." EClinicalMedicine **11**: 34-43.
Blair, G. W., M. J. Thrippleton, Y. Shi, I. Hamilton, M. Stringer, F. Chappell, D. A. Dickie, P. Andrews, I. Marshall, F. N. Doubal and J. M. Wardlaw (2020). "Intracranial hemodynamic relationships in patients with cerebral small vessel disease." Neurology **94**(21): e2258-e2269.
Blevins, B. L., H. V. Vinters, S. Love, D. M. Wilcock, L. T. Grinberg, J. A. Schneider, R. N. Kalaria, Y. Katsumata, B. T. Gold, D. J. J. Wang, S. J. Ma, L. M. P. Shade, D. W. Fardo, A. M. S. Hartz, G. A. Jicha, K. B. Nelson, S. D. Magaki, F. A. Schmitt, M. A. Teylan, E. T. Ighodaro, P. Phe, E. L. Abner, M. D. Cykowski, L. J. Van Eldik and P. T. Nelson (2021). "Brain arteriolosclerosis." Acta Neuropathol **141**(1): 1-24.
Blezer, E. L., M. Schurink, K. Nicolay, P. R. Bar, G. H. Jansen, H. A. Koomans and J. A. Joles (1998). "Proteinuria precedes cerebral edema in stroke-prone rats: a magnetic resonance imaging study." Stroke **29**(1): 167-174.
Bocti, C., R. H. Swartz, F. Q. Gao, D. J. Sahlas, P. Behl and S. E. Black (2005). "A new visual rating scale to assess strategic white matter hyperintensities within cholinergic pathways in dementia." Stroke **36**(10): 2126-2131.
Bokura, H., S. Kobayashi and S. Yamaguchi (1998). "Distinguishing silent lacunar infarction from enlarged Virchow-Robin spaces: a magnetic resonance imaging and pathological study." J Neurol **245**(2): 116-122.
Bokura, H., S. Kobayashi and S. Yamaguchi (1998). "Distinguishing silent lacunar infarction from enlarged Virchow-Robin spaces: a magnetic resonance imaging and pathological study." Journal of Neurology **245**(2): 116-122.
Bordes, C., M. Sargurupremraj, A. Mishra and S. Debette (2022). "Genetics of common cerebral small vessel disease." Nat Rev Neurol **18**(2): 84-101.
Bossuyt, P. M., J. B. Reitsma, D. E. Bruns, C. A. Gatsonis, P. P. Glasziou, L. M. Irwig, J. G. Lijmer, D. Moher, D. Rennie, H. C. de Vet and S. Group (2004). "Towards complete and accurate reporting of studies of diagnostic accuracy: the STARD initiative." Fam Pract **21**(1): 4-10.
Bots, M. L., J. C. van Swieten, M. M. Breteler, P. T. de Jong, J. van Gijn, A. Hofman and D. E. Grobbee (1993). "Cerebral white matter lesions and atherosclerosis in the Rotterdam Study." Lancet **341**(8855): 1232-1237.
Boulouis, G., A. Charidimou, M. Pasi, D. Roongpiboonsopit, L. Xiong, E. Auriel, E. S. van Etten, S. Martinez-Ramirez, A. Ayres, A. Vashkevich, K. M. Schwab, J. Rosand, J. N. Goldstein, M. E. Gurol, S. M. Greenberg and A. Viswanathan (2017). "Hemorrhage recurrence risk factors in cerebral amyloid angiopathy: Comparative analysis of the overall small vessel disease severity score versus individual neuroimaging markers." J Neurol Sci **380**: 64-67.
Bouvy, W. H., G. J. Biessels, H. J. Kuijf, L. J. Kappelle, P. R. Luijten and J. J. Zwanenburg (2014). "Visualization of perivascular spaces and perforating arteries with 7 T magnetic resonance imaging." Invest Radiol **49**(5): 307-313.
Boyle, P. A., L. Yu, S. Nag, S. Leurgans, R. S. Wilson, D. A. Bennett and J. A. Schneider (2015). "Cerebral amyloid angiopathy and cognitive outcomes in community-based older persons." Neurology **85**(22): 1930-1936.

Braak, H., I. Alafuzoff, T. Arzberger, H. Kretzschmar and K. Del Tredici (2006). "Staging of Alzheimer disease-associated neurofibrillary pathology using paraffin sections and immunocytochemistry." Acta Neuropathol **112**(4): 389-404.
Braak, H. and E. Braak (1991). "Neuropathological stageing of Alzheimer-related changes." Acta Neuropathol **82**(4): 239-259.
Braffman, B. H., R. A. Zimmerman, J. Q. Trojanowski, N. K. Gonatas, W. F. Hickey and W. W. Schlaepfer (1988). "Brain MR: pathologic correlation with gross and histopathology. 1. Lacunar infarction and Virchow-Robin spaces." AJR. American Journal of Roentgenology **151**(3): 551-558.
Braffman, B. H., R. A. Zimmerman, J. Q. Trojanowski, N. K. Gonatas, W. F. Hickey and W. W. Schlaepfer (1988). "Brain MR: pathologic correlation with gross and histopathology. 1. Lacunar infarction and Virchow-Robin spaces." AJR Am J Roentgenol **151**(3): 551-558.
Braffman, B. H., R. A. Zimmerman, J. Q. Trojanowski, N. K. Gonatas, W. F. Hickey and W. W. Schlaepfer (1988). "Brain MR: pathologic correlation with gross and histopathology. 2. Hyperintense white-matter foci in the elderly." AJR. American Journal of Roentgenology **151**(3): 559-566.
Bridges, L. R., J. Andoh, A. J. Lawrence, C. H. Khoong, W. W. Poon, M. M. Esiri, H. S. Markus and A. H. Hainsworth (2014). "Blood-brain barrier dysfunction and cerebral small vessel disease (arteriolosclerosis) in brains of older people." J Neuropathol Exp Neurol **73**(11): 1026-1033.
Brightman, M. W. and M. Kaya (2000). "Permeable endothelium and the interstitial space of brain." Cell Mol Neurobiol **20**(2): 111-130.
Bronge, L., N. Bogdanovic and L. O. Wahlund (2002). "Postmortem MRI and histopathology of white matter changes in Alzheimer brains. A quantitative, comparative study." Dement Geriatr Cogn Disord **13**(4): 205-212.
Brown, R., H. Benveniste, S. E. Black, S. Charpak, M. Dichgans, A. Joutel, M. Nedergaard, K. J. Smith, B. V. Zlokovic and J. M. Wardlaw (2018). "Understanding the role of the perivascular space in cerebral small vessel disease." Cardiovasc Res.
Brundel, M., J. de Bresser, J. J. van Dillen, L. J. Kappelle and G. J. Biessels (2012). "Cerebral microinfarcts: a systematic review of neuropathological studies." J Cereb Blood Flow Metab **32**(3): 425-436.
Bugiani, M., S. H. Kevelam, H. S. Bakels, Q. Waisfisz, C. Ceuterick-de Groote, H. W. Niessen, T. E. Abbink, S. A. Lesnik Oberstein and M. S. van der Knaap (2016). "Cathepsin A-related arteriopathy with strokes and leukoencephalopathy (CARASAL)." Neurology **87**(17): 1777-1786.
Bushong, E. A., M. E. Martone, Y. Z. Jones and M. H. Ellisman (2002). "Protoplasmic astrocytes in CA1 stratum radiatum occupy separate anatomical domains." J Neurosci **22**(1): 183-192.
Casanova, M. F. and J. M. Araque (2003). "Mineralization of the basal ganglia: implications for neuropsychiatry, pathology and neuroimaging." Psychiatry Res **121**(1): 59-87.
Chabriat, H., D. Herve, M. Duering, O. Godin, E. Jouvent, C. Opherk, N. Alili, S. Reyes, A. Jabouley, N. Zieren, J. P. Guichard, C. Pachai, E. Vicaut and M. Dichgans (2016). "Predictors of Clinical Worsening in Cerebral Autosomal Dominant Arteriopathy

With Subcortical Infarcts and Leukoencephalopathy: Prospective Cohort Study." Stroke **47**(1): 4-11.
Chabriat, H., A. Joutel, M. Dichgans, E. Tournier-Lasserve and M. G. Bousser (2009). "Cadasil." Lancet Neurol **8**(7): 643-653.
Chaigneau, E., M. Oheim, E. Audinat and S. Charpak (2003). "Two-photon imaging of capillary blood flow in olfactory bulb glomeruli." Proc Natl Acad Sci U S A **100**(22): 13081-13086.
Charidimou, A., Q. Gang and D. J. Werring (2012). "Sporadic cerebral amyloid angiopathy revisited: recent insights into pathophysiology and clinical spectrum." J Neurol Neurosurg Psychiatry **83**(2): 124-137.
Charidimou, A., T. Imaizumi, S. Moulin, A. Biffi, N. Samarasekera, Y. Yakushiji, A. Peeters, Y. Vandermeeren, P. Laloux, J. C. Baron, M. Hernandez-Guillamon, J. Montaner, B. Casolla, S. M. Gregoire, D. W. Kang, J. S. Kim, H. Naka, E. E. Smith, A. Viswanathan, H. R. Jager, R. Al-Shahi Salman, S. M. Greenberg, C. Cordonnier and D. J. Werring (2017). "Brain hemorrhage recurrence, small vessel disease type, and cerebral microbleeds: A meta-analysis." Neurology **89**(8): 820-829.
Charidimou, A., R. Meegahage, Z. Fox, A. Peeters, Y. Vandermeeren, P. Laloux, J. C. Baron, H. R. Jager and D. J. Werring (2013). "Enlarged perivascular spaces as a marker of underlying arteriopathy in intracerebral haemorrhage: a multicentre MRI cohort study." J Neurol Neurosurg Psychiatry **84**(6): 624-629.
Chauhan, G., H. H. H. Adams, C. L. Satizabal, J. C. Bis, A. Teumer, M. Sargurupremraj, E. Hofer, S. Trompet, S. Hilal, A. V. Smith, X. Jian, R. Malik, M. Traylor, S. L. Pulit, P. Amouyel, B. Mazoyer, Y. C. Zhu, S. Kaffashian, S. Schilling, G. W. Beecham, T. J. Montine, G. D. Schellenberg, O. Kjartansson, V. Guethnason, D. S. Knopman, M. E. Griswold, B. G. Windham, R. F. Gottesman, T. H. Mosley, R. Schmidt, Y. Saba, H. Schmidt, F. Takeuchi, S. Yamaguchi, T. Nabika, N. Kato, K. B. Rajan, N. T. Aggarwal, P. L. De Jager, D. A. Evans, B. M. Psaty, J. I. Rotter, K. Rice, O. L. Lopez, J. Liao, C. Chen, C. Y. Cheng, T. Y. Wong, M. K. Ikram, S. J. van der Lee, N. Amin, V. Chouraki, A. L. DeStefano, H. J. Aparicio, J. R. Romero, P. Maillard, C. DeCarli, J. M. Wardlaw, M. Hernandez, M. Luciano, D. Liewald, I. J. Deary, J. M. Starr, M. E. Bastin, S. Munoz Maniega, P. E. Slagboom, M. Beekman, J. Deelen, H. W. Uh, R. Lemmens, H. Brodaty, M. J. Wright, D. Ames, G. B. Boncoraglio, J. C. Hopewell, A. H. Beecham, S. H. Blanton, C. B. Wright, R. L. Sacco, W. Wen, A. Thalamuthu, N. J. Armstrong, E. Chong, P. R. Schofield, J. B. Kwok, J. van der Grond, D. J. Stott, I. Ford, J. W. Jukema, M. W. Vernooij, A. Hofman, A. G. Uitterlinden, A. van der Lugt, K. Wittfeld, H. J. Grabe, N. Hosten, B. von Sarnowski, U. Volker, C. Levi, J. Jimenez-Conde, P. Sharma, C. L. M. Sudlow, J. Rosand, D. Woo, J. W. Cole, J. F. Meschia, A. Slowik, V. Thijs, A. Lindgren, O. Melander, R. P. Grewal, T. Rundek, K. Rexrode, P. M. Rothwell, D. K. Arnett, C. Jern, J. A. Johnson, O. R. Benavente, S. Wasssertheil-Smoller, J. M. Lee, Q. Wong, B. D. Mitchell, S. S. Rich, P. F. McArdle, M. I. Geerlings, Y. van der Graaf, P. I. W. de Bakker, F. W. Asselbergs, V. Srikanth, R. Thomson, R. McWhirter, C. Moran, M. Callisaya, T. Phan, L. C. A. Rutten-Jacobs, S. Bevan, C. Tzourio, K. A. Mather, P. S. Sachdev, C. M. van Duijn, B. B. Worrall, M. Dichgans, S. J. Kittner, H. S. Markus, M. A. Ikram, M. Fornage, L. J. Launer, S. Seshadri, W. T. Longstreth, Jr., S. Debette, t. I. S. G. C. M. A. s. D. G. C. Stroke Genetics Network, H. the Neurology Working Group

of the Cohorts for and C. Aging Research in Genomic Epidemiology (2019). "Genetic and lifestyle risk factors for MRI-defined brain infarcts in a population-based setting." Neurology.
Chauhan, G., C. Arnold, A. Y. Chu, M. Fornage, A. Reyahi and e. al. (2016). "Identification of additional risk loci for stroke and small vessel disease: a meta-analysis of genome-wide association studies." Lancet Neurol **15**(7): 695-707.
Chen, A., R. O. Akinyemi, Y. Hase, M. J. Firbank, M. N. Ndung'u, V. Foster, L. J. Craggs, K. Washida, Y. Okamoto, A. J. Thomas, T. M. Polvikoski, L. M. Allan, A. E. Oakley, J. T. O'Brien, K. Horsburgh, M. Ihara and R. N. Kalaria (2016). "Frontal white matter hyperintensities, clasmatodendrosis and gliovascular abnormalities in ageing and post-stroke dementia." Brain **139**(Pt 1): 242-258.
Chimowitz, M. I., M. L. Estes, A. J. Furlan and I. A. Awad (1992). "Further observations on the pathology of subcortical lesions identified on magnetic resonance imaging." Arch Neurol **49**(7): 747-752.
Cho, A. H., H. R. Kim, W. Kim and D. W. Yang (2015). "White matter hyperintensity in ischemic stroke patients: it may regress over time." J Stroke **17**(1): 60-66.
Cho, A. H., H. R. Kim, W. Kim and D. W. Yang (2015). "White matter hyperintensity in ischemic stroke patients: it may regress over time." J Stroke **17**(1): 60-66.
Chong, S. Y., S. S. Rosenberg, S. P. Fancy, C. Zhao, Y. A. Shen, A. T. Hahn, A. W. McGee, X. Xu, B. Zheng, L. I. Zhang, D. H. Rowitch, R. J. Franklin, Q. R. Lu and J. R. Chan (2012). "Neurite outgrowth inhibitor Nogo-A establishes spatial segregation and extent of oligodendrocyte myelination." Proc Natl Acad Sci U S A **109**(4): 1299-1304.
Cipolla, M. J. (2009). The Cerebral Circulation. San Rafael (CA), Morgan & Claypool Life Sciences.
Clancy, U., D. Gilmartin, A. C. C. Jochems, L. Knox, F. N. Doubal and J. M. Wardlaw (2021). "Neuropsychiatric symptoms associated with cerebral small vessel disease: a systematic review and meta-analysis." Lancet Psychiatry **8**(3): 225-236.
Clarivate, W. o. S. (2022). "Citation report. Web of Science. Clarivate (accessed 28/02/2022)." Retrieved 28/02/2022, from https://www-webofscience-com.ezproxy.is.ed.ac.uk/wos/woscc/citation-report/1dfcf394-7899-434d-b172-c950d02a637d-26c1e05f.
Coban, H., S. Tung, B. Yoo, H. V. Vinters and J. D. Hinman (2017). "Molecular Disorganization of Axons Adjacent to Human Cortical Microinfarcts." Front Neurol **8**: 405.
Collett, G. D. and A. E. Canfield (2005). "Angiogenesis and pericytes in the initiation of ectopic calcification." Circ Res **96**(9): 930-938.
Cordonnier, C., R. Al-Shahi Salman and J. Wardlaw (2007). "Spontaneous brain microbleeds: systematic review, subgroup analyses and standards for study design and reporting." Brain **130**(Pt 8): 1988-2003.
Cordonnier, C., G. M. Potter, C. A. Jackson, F. Doubal, S. Keir, C. L. Sudlow, J. M. Wardlaw and R. Al-Shahi Salman (2009). "improving interrater agreement about brain microbleeds: development of the Brain Observer MicroBleed Scale (BOMBS)." Stroke **40**(1): 94-99.

Corley, J., S. R. Cox, S. E. Harris, M. V. Hernandez, S. M. Maniega, M. E. Bastin, J. M. Wardlaw, J. M. Starr, R. E. Marioni and I. J. Deary (2019). "Epigenetic signatures of smoking associate with cognitive function, brain structure, and mental and physical health outcomes in the Lothian Birth Cohort 1936." Transl Psychiatry **9**(1): 248.
Cortes-Canteli, M., J. Paul, E. H. Norris, R. Bronstein, H. J. Ahn, D. Zamolodchikov, S. Bhuvanendran, K. M. Fenz and S. Strickland (2010). "Fibrinogen and beta-amyloid association alters thrombosis and fibrinolysis: a possible contributing factor to Alzheimer's disease." Neuron **66**(5): 695-709.
Crawford, S., L. Whitnall, J. Robertson and J. J. Evans (2012). "A systematic review of the accuracy and clinical utility of the Addenbrooke's Cognitive Examination and the Addenbrooke's Cognitive Examination-Revised in the diagnosis of dementia." Int J Geriatr Psychiatry **27**(7): 659-669.
Dai, J., Y. Chen, R. Dai, Y. Jiang, J. Tian, S. Liu, M. Xu, M. Li, J. Zhou, C. Liu and C. Chen (2021). "Agonal Factors Distort Gene-Expression Patterns in Human Postmortem Brains." Front Neurosci **15**: 614142.
Daneman, R. and A. Prat (2015). "The blood-brain barrier." Cold Spring Harb Perspect Biol **7**(1): a020412.
Daniel, B. L., K. Butts and W. F. Block (1999). "Magnetic resonance imaging of frozen tissues: temperature-dependent MR signal characteristics and relevance for MR monitoring of cryosurgery." Magn Reson Med **41**(3): 627-630.
Daoutsali, E., R. A. M. Buijsen, S. van de Pas, A. Jong, H. Mikkers, T. Brands, B. Eussen, A. de Klein, L. M. van der Graaf, B. A. Pepers, C. Freund, G. M. Terwindt, V. V. Orlova and W. M. C. van Roon-Mom (2019). "Generation of 3 human induced pluripotent stem cell lines LUMCi005-A, B and C from a Hereditary Cerebral Hemorrhage with Amyloidosis-Dutch type patient." Stem Cell Res **34**: 101359.
Dawe, R. J., D. A. Bennett, J. A. Schneider, S. E. Leurgans, A. Kotrotsou, P. A. Boyle and K. Arfanakis (2014). "Ex vivo T2 relaxation: associations with age-related neuropathology and cognition." Neurobiol Aging **35**(7): 1549-1561.
Dawe, R. J., D. A. Bennett, J. A. Schneider, S. K. Vasireddi and K. Arfanakis (2009). "Postmortem MRI of human brain hemispheres: T2 relaxation times during formaldehyde fixation." Magn Reson Med **61**(4): 810-818.
de la Torre, J. C. (2010). "The vascular hypothesis of Alzheimer's disease: bench to bedside and beyond." Neurodegener Dis **7**(1-3): 116-121.
de Laat, K. F., A. M. Tuladhar, A. G. van Norden, D. G. Norris, M. P. Zwiers and F. E. de Leeuw (2011). "Loss of white matter integrity is associated with gait disorders in cerebral small vessel disease." Brain **134**(Pt 1): 73-83.
De Reuck, J., F. Auger, C. Cordonnier, V. Deramecourt, N. Durieux, F. Pasquier, R. Bordet, C. A. Maurage and D. Leys (2011). "Comparison of 7.0-T T2 -magnetic resonance imaging of cerebral bleeds in post-mortem brain sections of Alzheimer patients with their neuropathological correlates." Cerebrovascular Diseases **31**(5): 511-517.
De Reuck, J., V. Deramecourt, F. Auger, N. Durieux, C. Cordonnier, D. Devos, L. Defebvre, C. Moreau, D. Caparros-Lefebvre, R. Bordet, C. A. Maurage, F. Pasquier and D. Leys (2014). "Post-mortem 7.0-tesla magnetic resonance study of cortical

microinfarcts in neurodegenerative diseases and vascular dementia with neuropathological correlates." J Neurol Sci **346**(1-2): 85-89.
De Reuck, J., V. Deramecourt, C. Cordonnier, F. Auger, N. Durieux, F. Pasquier, R. Bordet, L. Defebvre, D. Caparros-Lefebvre, C. A. Maurage and D. Leys (2013). "Superficial siderosis of the central nervous system: a post-mortem 7.0-tesla magnetic resonance imaging study with neuropathological correlates." Cerebrovascular Diseases **36**(5-6): 412-417.
De Reuck, J. L., V. Deramecourt, F. Auger, N. Durieux, C. Cordonnier, D. Devos, L. Defebvre, C. Moreau, D. Capparos-Lefebvre, F. Pasquier, D. Leys, C. A. Maurage and R. Bordet (2015). "The significance of cortical cerebellar microbleeds and microinfarcts in neurodegenerative and cerebrovascular diseases. A post-mortem 7.0-tesla magnetic resonance study with neuropathological correlates." Cerebrovascular Diseases **39**(2): 138-143.
Deary, I. J., A. J. Gow, M. D. Taylor, J. Corley, C. Brett, V. Wilson, H. Campbell, L. J. Whalley, P. M. Visscher, D. J. Porteous and J. M. Starr (2007). "The Lothian Birth Cohort 1936: a study to examine influences on cognitive ageing from age 11 to age 70 and beyond." BMC Geriatr **7**: 28.
Debette, S. and H. S. Markus (2010). "The clinical importance of white matter hyperintensities on brain magnetic resonance imaging: systematic review and meta-analysis." BMJ **341**: c3666.
Debette, S., S. Schilling, M. G. Duperron, S. C. Larsson and H. S. Markus (2019). "Clinical Significance of Magnetic Resonance Imaging Markers of Vascular Brain Injury: A Systematic Review and Meta-analysis." JAMA Neurol **76**(1): 81-94.
Deplanque, D., P. C. Lavallee, J. Labreuche, F. Gongora-Rivera, A. Jaramillo, D. Brenner, H. Abboud, I. F. Klein, P. J. Touboul, E. Vicaut, P. Amarenco and B. I. Lacunar (2013). "Cerebral and extracerebral vasoreactivity in symptomatic lacunar stroke patients: a case-control study." International Journal of Stroke **8**(6): 413-421.
Deramecourt, V., J. Y. Slade, A. E. Oakley, R. H. Perry, P. G. Ince, C. A. Maurage and R. N. Kalaria (2012). "Staging and natural history of cerebrovascular pathology in dementia." Neurology **78**(14): 1043-1050.
Dewhirst, M. W., B. L. Viglianti, M. Lora-Michiels, P. J. Hoopes and M. Hanson (2003). "Thermal Dose Requirement for Tissue Effect: Experimental and Clinical Findings." Proc SPIE Int Soc Opt Eng **4954**: 37.
Di Donato, I., S. Bianchi, N. De Stefano, M. Dichgans, M. T. Dotti, M. Duering, E. Jouvent, A. D. Korczyn, S. A. Lesnik-Oberstein, A. Malandrini, H. S. Markus, L. Pantoni, S. Penco, A. Rufa, O. Sinanovic, D. Stojanov and A. Federico (2017). "Cerebral Autosomal Dominant Arteriopathy with Subcortical Infarcts and Leukoencephalopathy (CADASIL) as a model of small vessel disease: update on clinical, diagnostic, and management aspects." BMC Med **15**(1): 41.
Di Nicolantonio, R. and M. J. Silvapulle (1988). "Blood pressure, salt appetite and mortality of genetically hypertensive and normotensive rats maintained on high and low salt diets from weaning." Clin Exp Pharmacol Physiol **15**(10): 741-751.
Ding, J., S. Sigurethsson, P. V. Jonsson, G. Eiriksdottir, A. Charidimou, O. L. Lopez, M. A. van Buchem, V. Guethnason and L. J. Launer (2017). "Large Perivascular Spaces Visible on Magnetic Resonance Imaging, Cerebral Small Vessel Disease Progression,

and Risk of Dementia: The Age, Gene/Environment Susceptibility-Reykjavik Study." JAMA Neurol **74**(9): 1105-1112.
Ding, R., L. Feng, L. He, Y. Chen, P. Wen, Z. Fu, C. Lin, S. Yang, X. Deng, J. Zeng and G. Sun (2015). "Peroxynitrite decomposition catalyst prevents matrix metalloproteinase-9 activation and neurovascular injury after hemoglobin injection into the caudate nucleus of rats." Neuroscience **297**: 182-193.
Djulejic, V., S. Marinkovic, B. Georgievski, L. Stijak, M. Aksic, L. Puskas and I. Milic (2016). "Clinical significance of blood supply to the internal capsule and basal ganglia." J Clin Neurosci **25**: 19-26.
Domenga, V., P. Fardoux, P. Lacombe, M. Monet, J. Maciazek, L. T. Krebs, B. Klonjkowski, E. Berrou, M. Mericskay, Z. Li, E. Tournier-Lasserve, T. Gridley and A. Joutel (2004). "Notch3 is required for arterial identity and maturation of vascular smooth muscle cells." Genes Dev **18**(22): 2730-2735.
Domingues, H. S., C. C. Portugal, R. Socodato and J. B. Relvas (2016). "Oligodendrocyte, Astrocyte, and Microglia Crosstalk in Myelin Development, Damage, and Repair." Front Cell Dev Biol **4**: 71.
Donaldson, A. E. and I. L. Lamont (2013). "Biochemistry changes that occur after death: potential markers for determining post-mortem interval." PLoS One **8**(11): e82011.
Doubal, F. N., T. J. MacGillivray, P. E. Hokke, B. Dhillon, M. S. Dennis and J. M. Wardlaw (2009). "Differences in retinal vessels support a distinct vasculopathy causing lacunar stroke." Neurology **72**(20): 1773-1778.
Doubal, F. N., A. M. MacLullich, K. J. Ferguson, M. S. Dennis and J. M. Wardlaw (2010). "Enlarged perivascular spaces on MRI are a feature of cerebral small vessel disease." Stroke **41**(3): 450-454.
Dreha-Kulaczewski, S., A. A. Joseph, K. D. Merboldt, H. C. Ludwig, J. Gartner and J. Frahm (2015). "Inspiration is the major regulator of human CSF flow." J Neurosci **35**(6): 2485-2491.
Duering, M., S. Finsterwalder, E. Baykara, A. M. Tuladhar, B. Gesierich, M. J. Konieczny, R. Malik, N. Franzmeier, M. Ewers, E. Jouvent, G. J. Biessels, R. Schmidt, F. E. de Leeuw, O. Pasternak and M. Dichgans (2018). "Free water determines diffusion alterations and clinical status in cerebral small vessel disease." Alzheimers Dement **14**(6): 764-774.
Duering, M., R. Righart, F. A. Wollenweber, V. Zietemann, B. Gesierich and M. Dichgans (2015). "Acute infarcts cause focal thinning in remote cortex via degeneration of connecting fiber tracts." Neurology **84**(16): 1685-1692.
Durand-Fardel, C. L. M. (1873). "Traité pratique des Maladies des Vieillards." Paris: Baillère.
Durand-Fardel, M. (1843). "Traité du Ramollissement du Cerveau." Baillière, Paris.
Durany, N., G. Munch, T. Michel and P. Riederer (1999). "Investigations on oxidative stress and therapeutical implications in dementia." Eur Arch Psychiatry Clin Neurosci **249 Suppl 3**: 68-73.
Dziewulska, D. and E. Lewandowska (2012). "Pericytes as a new target for pathological processes in CADASIL." Neuropathology **32**(5): 515-521.

Eide, P. K., S. A. S. Vatnehol, K. E. Emblem and G. Ringstad (2018). "Magnetic resonance imaging provides evidence of glymphatic drainage from human brain to cervical lymph nodes." Sci Rep **8**(1): 7194.
English, V. and A. Sommerville (2003). "Presumed consent for transplantation: a dead issue after Alder Hey?" J Med Ethics **29**(3): 147-152.
Farkas, E. and P. G. Luiten (2001). "Cerebral microvascular pathology in aging and Alzheimer's disease." Progress in Neurobiology **64**(6): 575-611.
Farrall, A. J. and J. M. Wardlaw (2009). "Blood-brain barrier: ageing and microvascular disease--systematic review and meta-analysis." Neurobiol Aging **30**(3): 337-352.
Farrell, C., F. Chappell, P. A. Armitage, P. Keston, A. Maclullich, S. Shenkin and J. M. Wardlaw (2009). "Development and initial testing of normal reference MR images for the brain at ages 65-70 and 75-80 years." Eur Radiol **19**(1): 177-183.
Fassbender, K., T. Bertsch, O. Mielke, F. Muhlhauser and M. Hennerici (1999). "Adhesion molecules in cerebrovascular diseases. Evidence for an inflammatory endothelial activation in cerebral large- and small-vessel disease." Stroke **30**(8): 1647-1650.
Fazekas, F., J. B. Chawluk, A. Alavi, H. I. Hurtig and R. A. Zimmerman (1987). "MR signal abnormalities at 1.5 T in Alzheimer's dementia and normal aging." AJR Am J Roentgenol **149**(2): 351-356.
Fazekas, F., R. Kleinert, H. Offenbacher, F. Payer, R. Schmidt, G. Kleinert, H. Radner and H. Lechner (1991). "The morphologic correlate of incidental punctate white matter hyperintensities on MR images." AJNR Am J Neuroradiol **12**(5): 915-921.
Fazekas, F., R. Kleinert, H. Offenbacher, R. Schmidt, G. Kleinert, F. Payer, H. Radner and H. Lechner (1993). "Pathologic correlates of incidental MRI white matter signal hyperintensities." Neurology **43**(9): 1683-1689.
Fazekas, F., R. Kleinert, G. Roob, G. Kleinert, P. Kapeller, R. Schmidt and H. P. Hartung (1999). "Histopathologic analysis of foci of signal loss on gradient-echo T2*-weighted MR images in patients with spontaneous intracerebral hemorrhage: evidence of microangiopathy-related microbleeds." AJNR Am J Neuroradiol **20**(4): 637-642.
Fazekas, F., S. Ropele, C. Enzinger, F. Gorani, A. Seewann, K. Petrovic and R. Schmidt (2005). "MTI of white matter hyperintensities." Brain **128**(Pt 12): 2926-2932.
Fein, G., V. Di Sclafani, J. Tanabe, V. Cardenas, M. W. Weiner, W. J. Jagust, B. R. Reed, D. Norman, N. Schuff, L. Kusdra, T. Greenfield and H. Chui (2000). "Hippocampal and cortical atrophy predict dementia in subcortical ischemic vascular disease." Neurology **55**(11): 1626-1635.
Fernando, M. S., P. G. Ince, M. R. C. C. Function and G. Ageing Neuropathology Study (2004). "Vascular pathologies and cognition in a population-based cohort of elderly people." Journal of the Neurological Sciences **226**(1-2): 13-17.
Fernando, M. S., J. T. O'Brien, R. H. Perry, P. English, G. Forster, W. McMeekin, J. Y. Slade, A. Golkhar, F. E. Matthews, R. Barber, R. N. Kalaria, P. G. Ince and M. C. Neuropathology Group of (2004). "Comparison of the pathology of cerebral white matter with post-mortem magnetic resonance imaging (MRI) in the elderly brain." Neuropathol Appl Neurobiol **30**(4): 385-395.

Fernando, M. S., J. E. Simpson, F. Matthews, C. Brayne, C. E. Lewis, R. Barber, R. N. Kalaria, G. Forster, F. Esteves, S. B. Wharton, P. J. Shaw, J. T. O'Brien, P. G. Ince, M. R. C. C. Function and G. Ageing Neuropathology Study (2006). "White matter lesions in an unselected cohort of the elderly: molecular pathology suggests origin from chronic hypoperfusion injury." Stroke **37**(6): 1391-1398.
Finger, R. P., V. Daien, B. M. Eldem, J. S. Talks, J. F. Korobelnik, P. Mitchell, T. Sakamoto, T. Y. Wong, K. Pantiri and J. Carrasco (2020). "Anti-vascular endothelial growth factor in neovascular age-related macular degeneration - a systematic review of the impact of anti-VEGF on patient outcomes and healthcare systems." BMC Ophthalmol **20**(1): 294.
Finsterer, J., C. A. Scorza, F. A. Scorza and S. M. Wakil (2019). "Update on hereditary, autosomal dominant cathepsin-A-related arteriopathy with strokes and leukoencephalopathy (CARASAL)." Acta Neurol Belg **119**(3): 299-303.
Fisher, C. M. (1965). "Lacunes: Small, Deep Cerebral Infarcts." Neurology **15**: 774-784.
Fisher, C. M. (1968). "The arterial lesions underlying lacunes." Acta Neuropathol **12**(1): 1-15.
Fisher, C. M. (1982). "Lacunar strokes and infarcts: a review." Neurology **32**(8): 871-876.
Fisher, C. M. (1991). "Lacunar infarcts - a review." Cerebrovascular Diseases **1**: 311-320.
Floyd, R. A. (1999). "Antioxidants, oxidative stress, and degenerative neurological disorders." Proc Soc Exp Biol Med **222**(3): 236-245.
Floyd, R. A. (1999). "Neuroinflammatory processes are important in neurodegenerative diseases: an hypothesis to explain the increased formation of reactive oxygen and nitrogen species as major factors involved in neurodegenerative disease development." Free Radic Biol Med **26**(9-10): 1346-1355.
Floyd, R. A. and K. Hensley (2002). "Oxidative stress in brain aging. Implications for therapeutics of neurodegenerative diseases." Neurobiol Aging **23**(5): 795-807.
Floyd, R. A., M. West and K. Hensley (2001). "Oxidative biochemical markers; clues to understanding aging in long-lived species." Exp Gerontol **36**(4-6): 619-640.
Forstermann, U., J. S. Pollock, H. H. Schmidt, M. Heller and F. Murad (1991). "Calmodulin-dependent endothelium-derived relaxing factor/nitric oxide synthase activity is present in the particulate and cytosolic fractions of bovine aortic endothelial cells." Proc Natl Acad Sci U S A **88**(5): 1788-1792.
Francis, F., L. Ballerini and J. M. Wardlaw (2019). "Perivascular spaces and their associations with risk factors, clinical disorders and neuroimaging features: A systematic review and meta-analysis." Int J Stroke **14**(4): 359-371.
Franke, C. L., J. C. van Swieten and J. van Gijn (1991). "Residual lesions on computed tomography after intracerebral hemorrhage." Stroke **22**(12): 1530-1533.
Fredriksson, K., R. N. Auer, H. Kalimo, C. Nordborg, Y. Olsson and B. B. Johansson (1985). "Cerebrovascular lesions in stroke-prone spontaneously hypertensive rats." Acta Neuropathol **68**(4): 284-294.

French, C. R., S. Seshadri, A. L. Destefano, M. Fornage, C. R. Arnold, P. J. Gage, J. M. Skarie, W. B. Dobyns, K. J. Millen, T. Liu, W. Dietz, T. Kume, M. Hofker, D. J. Emery, S. J. Childs, A. J. Waskiewicz and O. J. Lehmann (2014). "Mutation of FOXC1 and PITX2 induces cerebral small-vessel disease." J Clin Invest **124**(11): 4877-4881.
Fukutake, T. (2011). "Cerebral autosomal recessive arteriopathy with subcortical infarcts and leukoencephalopathy (CARASIL): from discovery to gene identification." Journal of Stroke & Cerebrovascular Diseases **20**(2): 85-93.
Ge, Y., M. Law, J. Herbert and R. I. Grossman (2005). "Prominent perivenular spaces in multiple sclerosis as a sign of perivascular inflammation in primary demyelination." AJNR Am J Neuroradiol **26**(9): 2316-2319.
Geinisman, Y., H. J. Gundersen, E. van der Zee and M. J. West (1996). "Unbiased stereological estimation of the total number of synapses in a brain region." J Neurocytol **25**(12): 805-819.
Georgakis, M. K., M. Duering, J. M. Wardlaw and M. Dichgans (2019). "WMH and long-term outcomes in ischemic stroke: A systematic review and meta-analysis." Neurology **92**(12): e1298-e1308.
Gesierich, B., C. Opherk, J. Rosand, M. Gonik, R. Malik, E. Jouvent, D. Herve, P. Adib-Samii, S. Bevan, L. Pianese, S. Silvestri, M. T. Dotti, N. De Stefano, J. van der Grond, E. M. Boon, F. Pescini, N. Rost, L. Pantoni, S. A. Oberstein, A. Federico, M. Ragno, H. S. Markus, E. Tournier-Lasserve, H. Chabriat, M. Dichgans, M. Duering and M. Ewers (2016). "APOE varepsilon2 is associated with white matter hyperintensity volume in CADASIL." J Cereb Blood Flow Metab **36**(1): 199-203.
Ghosh, M., M. Balbi, F. Hellal, M. Dichgans, U. Lindauer and N. Plesnila (2015). "Pericytes are involved in the pathogenesis of cerebral autosomal dominant arteriopathy with subcortical infarcts and leukoencephalopathy." Ann Neurol **78**(6): 887-900.
Ginhoux, F., S. Lim, G. Hoeffel, D. Low and T. Huber (2013). "Origin and differentiation of microglia." Front Cell Neurosci **7**: 45.
Gorelick, P. B., A. Scuteri, S. E. Black, C. Decarli, S. M. Greenberg, C. Iadecola, L. J. Launer, S. Laurent, O. L. Lopez, D. Nyenhuis, R. C. Petersen, J. A. Schneider, C. Tzourio, D. K. Arnett, D. A. Bennett, H. C. Chui, R. T. Higashida, R. Lindquist, P. M. Nilsson, G. C. Roman, F. W. Sellke, S. Seshadri, C. o. E. American Heart Association Stroke Council, C. o. C. N. C. o. C. R. Prevention, Intervention, S. Council on Cardiovascular and Anesthesia (2011). "Vascular contributions to cognitive impairment and dementia: a statement for healthcare professionals from the american heart association/american stroke association." Stroke **42**(9): 2672-2713.
Gottesman, R. F., J. Coresh, D. J. Catellier, A. R. Sharrett, K. M. Rose, L. H. Coker, D. K. Shibata, D. S. Knopman, C. R. Jack and T. H. Mosley, Jr. (2010). "Blood pressure and white-matter disease progression in a biethnic cohort: Atherosclerosis Risk in Communities (ARIC) study." Stroke **41**(1): 3-8.
Gould, D. B., F. C. Phalan, S. E. van Mil, J. P. Sundberg, K. Vahedi, P. Massin, M. G. Bousser, P. Heutink, J. H. Miner, E. Tournier-Lasserve and S. W. John (2006). "Role of COL4A1 in small-vessel disease and hemorrhagic stroke." N Engl J Med **354**(14): 1489-1496.

Gouw, A. A., A. Seewann, W. M. van der Flier, F. Barkhof, A. M. Rozemuller, P. Scheltens and J. J. Geurts (2011). "Heterogeneity of small vessel disease: a systematic review of MRI and histopathology correlations." J Neurol Neurosurg Psychiatry **82**(2): 126-135.
Gouw, A. A., W. M. van der Flier, F. Fazekas, E. C. van Straaten, L. Pantoni, A. Poggesi, D. Inzitari, T. Erkinjuntti, L. O. Wahlund, G. Waldemar, R. Schmidt, P. Scheltens, F. Barkhof and L. S. Group (2008). "Progression of white matter hyperintensities and incidence of new lacunes over a 3-year period: the Leukoaraiosis and Disability study." Stroke **39**(5): 1414-1420.
Grafton, S. T., S. M. Sumi, G. K. Stimac, E. C. Alvord, Jr., C. M. Shaw and D. Nochlin (1991). "Comparison of postmortem magnetic resonance imaging and neuropathologic findings in the cerebral white matter." Arch Neurol **48**(3): 293-298.
Greenberg, S. M., M. W. Vernooij, C. Cordonnier, A. Viswanathan, R. Al-Shahi Salman, S. Warach, L. J. Launer, M. A. Van Buchem, M. M. Breteler and G. Microbleed Study (2009). "Cerebral microbleeds: a guide to detection and interpretation." Lancet Neurology **8**(2): 165-174.
Greenberg, S. M., J. P. Vonsattel, A. Z. Segal, R. I. Chiu, A. E. Clatworthy, A. Liao, B. T. Hyman and G. W. Rebeck (1998). "Association of apolipoprotein E epsilon2 and vasculopathy in cerebral amyloid angiopathy." Neurology **50**(4): 961-965.
Gregory, J. M., K. McDade, M. R. Livesey, I. Croy, S. Marion de Proce, T. Aitman, S. Chandran and C. Smith (2020). "Spatial transcriptomics identifies spatially dysregulated expression of GRM3 and USP47 in amyotrophic lateral sclerosis." Neuropathol Appl Neurobiol.
Gretarsdottir, S., G. Thorleifsson, A. Manolescu, U. Styrkarsdottir, A. Helgadottir, A. Gschwendtner, K. Kostulas, G. Kuhlenbaumer, S. Bevan, T. Jonsdottir, H. Bjarnason, J. Saemundsdottir, S. Palsson, D. O. Arnar, H. Holm, G. Thorgeirsson, E. M. Valdimarsson, S. Sveinbjornsdottir, C. Gieger, K. Berger, H. E. Wichmann, J. Hillert, H. Markus, J. R. Gulcher, E. B. Ringelstein, A. Kong, M. Dichgans, D. F. Gudbjartsson, U. Thorsteinsdottir and K. Stefansson (2008). "Risk variants for atrial fibrillation on chromosome 4q25 associate with ischemic stroke." Ann Neurol **64**(4): 402-409.
Grinberg, L. T. and H. Heinsen (2010). "Toward a pathological definition of vascular dementia." J Neurol Sci **299**(1-2): 136-138.
Groeschel, S., W. K. Chong, R. Surtees and F. Hanefeld (2006). "Virchow-Robin spaces on magnetic resonance images: normative data, their dilatation, and a review of the literature." Neuroradiology **48**(10): 745-754.
Group, S. M. I. f. t. S. R., I. M. Nasrallah, N. M. Pajewski, A. P. Auchus, G. Chelune, A. K. Cheung, M. L. Cleveland, L. H. Coker, M. G. Crowe, W. C. Cushman, J. A. Cutler, C. Davatzikos, L. Desiderio, J. Doshi, G. Erus, L. J. Fine, S. A. Gaussoin, D. Harris, K. C. Johnson, P. L. Kimmel, M. Kurella Tamura, L. J. Launer, A. J. Lerner, C. E. Lewis, J. Martindale-Adams, C. S. Moy, L. O. Nichols, S. Oparil, P. K. Ogrocki, M. Rahman, S. R. Rapp, D. M. Reboussin, M. V. Rocco, B. C. Sachs, K. M. Sink, C. H. Still, M. A. Supiano, J. K. Snyder, V. G. Wadley, J. Walker, D. E. Weiner, P. K. Whelton, V. M. Wilson, N. Woolard, J. T. Wright, Jr., C. B. Wright, J. D. Williamson and R. N. Bryan (2019). "Association of Intensive vs Standard Blood Pressure Control With Cerebral White Matter Lesions." JAMA **322**(6): 524-534.

Group, S. M. I. f. t. S. R., J. D. Williamson, N. M. Pajewski, A. P. Auchus, R. N. Bryan, G. Chelune, A. K. Cheung, M. L. Cleveland, L. H. Coker, M. G. Crowe, W. C. Cushman, J. A. Cutler, C. Davatzikos, L. Desiderio, G. Erus, L. J. Fine, S. A. Gaussoin, D. Harris, M. K. Hsieh, K. C. Johnson, P. L. Kimmel, M. K. Tamura, L. J. Launer, A. J. Lerner, C. E. Lewis, J. Martindale-Adams, C. S. Moy, I. M. Nasrallah, L. O. Nichols, S. Oparil, P. K. Ogrocki, M. Rahman, S. R. Rapp, D. M. Reboussin, M. V. Rocco, B. C. Sachs, K. M. Sink, C. H. Still, M. A. Supiano, J. K. Snyder, V. G. Wadley, J. Walker, D. E. Weiner, P. K. Whelton, V. M. Wilson, N. Woolard, J. T. Wright, Jr. and C. B. Wright (2019). "Effect of Intensive vs Standard Blood Pressure Control on Probable Dementia: A Randomized Clinical Trial." JAMA **321**(6): 553-561.

Gudbjartsson, D. F., D. O. Arnar, A. Helgadottir, S. Gretarsdottir, H. Holm, A. Sigurdsson, A. Jonasdottir, A. Baker, G. Thorleifsson, K. Kristjansson, A. Palsson, T. Blondal, P. Sulem, V. M. Backman, G. A. Hardarson, E. Palsdottir, A. Helgason, R. Sigurjonsdottir, J. T. Sverrisson, K. Kostulas, M. C. Ng, L. Baum, W. Y. So, K. S. Wong, J. C. Chan, K. L. Furie, S. M. Greenberg, M. Sale, P. Kelly, C. A. MacRae, E. E. Smith, J. Rosand, J. Hillert, R. C. Ma, P. T. Ellinor, G. Thorgeirsson, J. R. Gulcher, A. Kong, U. Thorsteinsdottir and K. Stefansson (2007). "Variants conferring risk of atrial fibrillation on chromosome 4q25." Nature **448**(7151): 353-357.

Guerrini, U., L. Sironi, E. Tremoli, M. Cimino, B. Pollo, A. M. Calvio, R. Paoletti and M. Asdente (2002). "New insights into brain damage in stroke-prone rats: a nuclear magnetic imaging study." Stroke **33**(3): 825-830.

Guimiot, F., C. Garel, C. Fallet-Bianco, F. Menez, S. Khung-Savatovsky, J. F. Oury, G. Sebag and A. L. Delezoide (2008). "Contribution of diffusion-weighted imaging in the evaluation of diffuse white matter ischemic lesions in fetuses: correlations with fetopathologic findings." AJNR Am J Neuroradiol **29**(1): 110-115.

Hachinski, V. (2002). "Stroke: the next 30 years." Stroke **33**(1): 1-4.

Haefliger, I. O., A. Zschauer and D. R. Anderson (1994). "Relaxation of retinal pericyte contractile tone through the nitric oxide-cyclic guanosine monophosphate pathway." Invest Ophthalmol Vis Sci **35**(3): 991-997.

Haffner, C., R. Malik and M. Dichgans (2016). "Genetic factors in cerebral small vessel disease and their impact on stroke and dementia." J Cereb Blood Flow Metab **36**(1): 158-171.

Hagemeyer, N., K. M. Hanft, M. A. Akriditou, N. Unger, E. S. Park, E. R. Stanley, O. Staszewski, L. Dimou and M. Prinz (2017). "Microglia contribute to normal myelinogenesis and to oligodendrocyte progenitor maintenance during adulthood." Acta Neuropathol **134**(3): 441-458.

Hainsworth, A. H. and H. S. Markus (2008). "Do in vivo experimental models reflect human cerebral small vessel disease? A systematic review." J Cereb Blood Flow Metab **28**(12): 1877-1891.

Hainsworth, A. H., T. Minett, J. Andoh, G. Forster, I. Bhide, T. R. Barrick, K. Elderfield, J. Jeevahan, H. S. Markus and L. R. Bridges (2017). "Neuropathology of White Matter Lesions, Blood-Brain Barrier Dysfunction, and Dementia." Stroke **48**(10): 2799-2804.

Hainsworth, A. H., A. T. Oommen and L. R. Bridges (2015). "Endothelial cells and human cerebral small vessel disease." Brain Pathol **25**(1): 44-50.

Hajdu, M. A., D. D. Heistad, J. E. Siems and G. L. Baumbach (1990). "Effects of aging on mechanics and composition of cerebral arterioles in rats." Circ Res **66**(6): 1747-1754.
Halassa, M. M., T. Fellin, H. Takano, J. H. Dong and P. G. Haydon (2007). "Synaptic islands defined by the territory of a single astrocyte." J Neurosci **27**(24): 6473-6477.
Hall, C. N., C. Reynell, B. Gesslein, N. B. Hamilton, A. Mishra, B. A. Sutherland, F. M. O'Farrell, A. M. Buchan, M. Lauritzen and D. Attwell (2014). "Capillary pericytes regulate cerebral blood flow in health and disease." Nature **508**(7494): 55-60.
Hallbergson, A. F., C. Gnatenco and D. A. Peterson (2003). "Neurogenesis and brain injury: managing a renewable resource for repair." J Clin Invest **112**(8): 1128-1133.
Hallmann, R., N. Horn, M. Selg, O. Wendler, F. Pausch and L. M. Sorokin (2005). "Expression and function of laminins in the embryonic and mature vasculature." Physiol Rev **85**(3): 979-1000.
Hamann, G. F., Y. Okada, R. Fitridge and G. J. del Zoppo (1995). "Microvascular basal lamina antigens disappear during cerebral ischemia and reperfusion." Stroke **26**(11): 2120-2126.
Hamel, E. (2006). "Perivascular nerves and the regulation of cerebrovascular tone." J Appl Physiol (1985) **100**(3): 1059-1064.
Hamilton, C. A., M. J. Brosnan, M. McIntyre, D. Graham and A. F. Dominiczak (2001). "Superoxide excess in hypertension and aging: a common cause of endothelial dysfunction." Hypertension **37**(2 Pt 2): 529-534.
Hamilton, O. K. L., S. R. Cox, J. A. Okely, F. Conte, L. Ballerini, M. E. Bastin, J. Corley, A. M. Taylor, D. Page, A. J. Gow, S. Munoz Maniega, P. Redmond, M. D. C. Valdes-Hernandez, J. M. Wardlaw and I. J. Deary (2021). "Cerebral small vessel disease burden and longitudinal cognitive decline from age 73 to 82: the Lothian Birth Cohort 1936." Transl Psychiatry **11**(1): 376.
Hammond, T. R., A. Gadea, J. Dupree, C. Kerninon, B. Nait-Oumesmar, A. Aguirre and V. Gallo (2014). "Astrocyte-derived endothelin-1 inhibits remyelination through notch activation." Neuron **81**(3): 588-602.
Hara, K., A. Shiga, T. Fukutake, H. Nozaki, A. Miyashita, A. Yokoseki, H. Kawata, A. Koyama, K. Arima, T. Takahashi, M. Ikeda, H. Shiota, M. Tamura, Y. Shimoe, M. Hirayama, T. Arisato, S. Yanagawa, A. Tanaka, I. Nakano, S. Ikeda, Y. Yoshida, T. Yamamoto, T. Ikeuchi, R. Kuwano, M. Nishizawa, S. Tsuji and O. Onodera (2009). "Association of HTRA1 mutations and familial ischemic cerebral small-vessel disease." N Engl J Med **360**(17): 1729-1739.
Hattori, Y., J. Enmi, S. Iguchi, S. Saito, Y. Yamamoto, M. Tsuji, K. Nagatsuka, R. N. Kalaria, H. Iida and M. Ihara (2016). "Gradual Carotid Artery Stenosis in Mice Closely Replicates Hypoperfusive Vascular Dementia in Humans." J Am Heart Assoc **5**(2).
Hawkins, B. T. and T. P. Davis (2005). "The blood-brain barrier/neurovascular unit in health and disease." Pharmacol Rev **57**(2): 173-185.
Hawkins, R. A. (2009). "The blood-brain barrier and glutamate." Am J Clin Nutr **90**(3): 867S-874S.
Henstridge, C. M., R. J. Jackson, J. M. Kim, A. G. Herrmann, A. K. Wright, S. E. Harris, M. E. Bastin, J. M. Starr, J. Wardlaw, T. H. Gillingwater, C. Smith, C. A. McKenzie, S. R. Cox, I. J. Deary and T. L. Spires-Jones (2015). "Post-mortem brain analyses of the

Lothian Birth Cohort 1936: extending lifetime cognitive and brain phenotyping to the level of the synapse." Acta Neuropathol Commun **3**: 53.
Hernandez Mdel, C., R. J. Piper, X. Wang, I. J. Deary and J. M. Wardlaw (2013). "Towards the automatic computational assessment of enlarged perivascular spaces on brain magnetic resonance images: a systematic review." J Magn Reson Imaging **38**(4): 774-785.
Hinman, J. D., M. D. Lee, S. Tung, H. V. Vinters and S. T. Carmichael (2015). "Molecular disorganization of axons adjacent to human lacunar infarcts." Brain **138**(Pt 3): 736-745.
Hoffmann, J., J. Haendeler, A. Aicher, L. Rossig, M. Vasa, A. M. Zeiher and S. Dimmeler (2001). "Aging enhances the sensitivity of endothelial cells toward apoptotic stimuli: important role of nitric oxide." Circ Res **89**(8): 709-715.
Holtmannspotter, M., N. Peters, C. Opherk, D. Martin, J. Herzog, H. Bruckmann, P. Samann, A. Gschwendtner and M. Dichgans (2005). "Diffusion magnetic resonance histograms as a surrogate marker and predictor of disease progression in CADASIL: a two-year follow-up study." Stroke **36**(12): 2559-2565.
Horsburgh, K., J. M. Wardlaw, T. van Agtmael, S. M. Allan, M. L. J. Ashford, P. M. Bath, R. Brown, J. Berwick, M. Z. Cader, R. O. Carare, J. B. Davis, J. Duncombe, T. D. Farr, J. H. Fowler, J. Goense, A. Granata, C. N. Hall, A. H. Hainsworth, A. Harvey, C. A. Hawkes, A. Joutel, R. N. Kalaria, P. G. Kehoe, C. B. Lawrence, A. Lockhart, S. Love, M. R. Macleod, I. M. Macrae, H. S. Markus, C. McCabe, B. W. McColl, P. J. Meakin, A. Miller, M. Nedergaard, M. O'Sullivan, T. J. Quinn, R. Rajani, L. M. Saksida, C. Smith, K. J. Smith, R. M. Touyz, R. C. Trueman, T. Wang, A. Williams, S. C. R. Williams and L. M. Work (2018). "Small vessels, dementia and chronic diseases - molecular mechanisms and pathophysiology." Clin Sci (Lond) **132**(8): 851-868.
Huang, Y., W. Zhang, L. Lin, J. Feng, F. Chen, W. Wei, X. Zhao, W. Guo, J. Li, W. Yin and L. Li (2010). "Is endothelial dysfunction of cerebral small vessel responsible for white matter lesions after chronic cerebral hypoperfusion in rats?" J Neurol Sci **299**(1-2): 72-80.
Humphreys, C. A., M. A. Jansen, S. Munoz Maniega, V. Gonzalez-Castro, C. Pernet, I. J. Deary, R. Al-Shahi Salman, J. M. Wardlaw and C. Smith (2018). "A protocol for precise comparisons of small vessel disease lesions between ex vivo magnetic resonance imaging and histopathology." Int J Stroke: 1747493018799962.
Humphreys, C. A., C. Smith and J. M. Wardlaw (2021). "Correlations in post-mortem imaging-histopathology studies of sporadic human cerebral small vessel disease: A systematic review." Neuropathol Appl Neurobiol **47**(7): 910-930.
Humphreys, C. A., C. Smith and J. M. Wardlaw (2021). "Correlations in post-mortem imaging-histopathology studies of sporadic human cerebral small vessel disease: a systematic review." Neuropathol Appl Neurobiol.
Humphries, T. J. and P. Mathew (2019). "Cerebral microbleeds: hearing through the silence-a narrative review." Curr Med Res Opin **35**(2): 359-366.
Huneau, C., M. Houot, A. Joutel, B. Beranger, C. Giroux, H. Benali and H. Chabriat (2018). "Altered dynamics of neurovascular coupling in CADASIL." Ann Clin Transl Neurol **5**(7): 788-802.

Hyrina, A., C. Jones, D. Chen, S. Clarkson, N. Cochran, P. Feucht, G. Hoffman, A. Lindeman, C. Russ, F. Sigoillot, T. Tsang, K. Uehara, L. Xie, D. Ganem and M. Holdorf (2019). "A Genome-wide CRISPR Screen Identifies ZCCHC14 as a Host Factor Required for Hepatitis B Surface Antigen Production." Cell Rep **29**(10): 2970-2978 e2976.
Iadecola, C. (1993). "Regulation of the cerebral microcirculation during neural activity: is nitric oxide the missing link?" Trends Neurosci **16**(6): 206-214.
Iadecola, C. (2013). "The pathobiology of vascular dementia." Neuron **80**(4): 844-866.
Iadecola, C. (2017). "The Neurovascular Unit Coming of Age: A Journey through Neurovascular Coupling in Health and Disease." Neuron **96**(1): 17-42.
Iliff, J. J., M. Wang, Y. Liao, B. A. Plogg, W. Peng, G. A. Gundersen, H. Benveniste, G. E. Vates, R. Deane, S. A. Goldman, E. A. Nagelhus and M. Nedergaard (2012). "A paravascular pathway facilitates CSF flow through the brain parenchyma and the clearance of interstitial solutes, including amyloid beta." Sci Transl Med **4**(147): 147ra111.
Iliff, J. J., M. Wang, D. M. Zeppenfeld, A. Venkataraman, B. A. Plog, Y. Liao, R. Deane and M. Nedergaard (2013). "Cerebral arterial pulsation drives paravascular CSF-interstitial fluid exchange in the murine brain." J Neurosci **33**(46): 18190-18199.
Inzitari, D., G. Pracucci, A. Poggesi, G. Carlucci, F. Barkhof, H. Chabriat, T. Erkinjuntti, F. Fazekas, J. M. Ferro, M. Hennerici, P. Langhorne, J. O'Brien, P. Scheltens, M. C. Visser, L. O. Wahlund, G. Waldemar, A. Wallin, L. Pantoni and L. S. Group (2009). "Changes in white matter as determinant of global functional decline in older independent outpatients: three year follow-up of LADIS (leukoaraiosis and disability) study cohort." BMJ **339**: b2477.
Ito, Y. A. and M. A. Walter (2014). "Genomics and anterior segment dysgenesis: a review." Clin Exp Ophthalmol **42**(1): 13-24.
Jackson, C. and C. Sudlow (2005). "Are lacunar strokes really different? A systematic review of differences in risk factor profiles between lacunar and nonlacunar infarcts." Stroke **36**(4): 891-901.
Jeerakathil, T., P. A. Wolf, A. Beiser, J. K. Hald, R. Au, C. S. Kase, J. M. Massaro and C. DeCarli (2004). "Cerebral microbleeds: prevalence and associations with cardiovascular risk factors in the Framingham Study." Stroke **35**(8): 1831-1835.
Jellinger, K. A. and J. Attems (2003). "Incidence of cerebrovascular lesions in Alzheimer's disease: a postmortem study." Acta Neuropathologica **105**(1): 14-17.
Jennings, J. R., M. F. Muldoon, C. Ryan, J. C. Price, P. Greer, K. Sutton-Tyrrell, F. M. van der Veen and C. C. Meltzer (2005). "Reduced cerebral blood flow response and compensation among patients with untreated hypertension." Neurology **64**(8): 1358-1365.
Jimenez-Sanchez, L., O. K. L. Hamilton, U. Clancy, E. V. Backhouse, C. R. Stewart, M. S. Stringer, F. N. Doubal and J. M. Wardlaw (2021). "Sex Differences in Cerebral Small Vessel Disease: A Systematic Review and Meta-Analysis." Front Neurol **12**: 756887.
Jin, K., T. Zhang, M. Shaw, P. Sachdev and N. Cherbuin (2018). "Relationship Between Sulcal Characteristics and Brain Aging." Front Aging Neurosci **10**: 339.

Jiwa, N. S., P. Garrard and A. H. Hainsworth (2010). "Experimental models of vascular dementia and vascular cognitive impairment: a systematic review." J Neurochem **115**(4): 814-828.
Jochems, A. C. C., G. W. Blair, M. S. Stringer, M. J. Thrippleton, U. Clancy, F. M. Chappell, R. Brown, D. Jaime Garcia, O. K. L. Hamilton, A. G. Morgan, I. Marshall, K. Hetherington, S. Wiseman, T. MacGillivray, M. C. Valdes-Hernandez, F. N. Doubal and J. M. Wardlaw (2020). "Relationship Between Venules and Perivascular Spaces in Sporadic Small Vessel Diseases." Stroke: STROKEAHA120029163.
Jokinen, H., S. Melkas, S. Madureira, A. Verdelho, J. M. Ferro, F. Fazekas, R. Schmidt, P. Scheltens, F. Barkhof, J. M. Wardlaw, D. Inzitari, L. Pantoni and T. Erkinjuntti (2016). "Cognitive reserve moderates long-term cognitive and functional outcome in cerebral small vessel disease." J Neurol Neurosurg Psychiatry **87**(12): 1296-1302.
Joutel, A., F. Andreux, S. Gaulis, V. Domenga, M. Cecillon, N. Battail, N. Piga, F. Chapon, C. Godfrain and E. Tournier-Lasserve (2000). "The ectodomain of the Notch3 receptor accumulates within the cerebrovasculature of CADASIL patients." J Clin Invest **105**(5): 597-605.
Joutel, A., C. Corpechot, A. Ducros, K. Vahedi, H. Chabriat, P. Mouton, S. Alamowitch, V. Domenga, M. Cecillion, E. Marechal, J. Maciazek, C. Vayssiere, C. Cruaud, E. A. Cabanis, M. M. Ruchoux, J. Weissenbach, J. F. Bach, M. G. Bousser and E. Tournier-Lasserve (1996). "Notch3 mutations in CADASIL, a hereditary adult-onset condition causing stroke and dementia." Nature **383**(6602): 707-710.
Joutel, A., I. Haddad, J. Ratelade and M. T. Nelson (2016). "Perturbations of the cerebrovascular matrisome: A convergent mechanism in small vessel disease of the brain?" J Cereb Blood Flow Metab **36**(1): 143-157.
Joutel, A., M. Monet-Lepretre, C. Gosele, C. Baron-Menguy, A. Hammes, S. Schmidt, B. Lemaire-Carrette, V. Domenga, A. Schedl, P. Lacombe and N. Hubner (2010). "Cerebrovascular dysfunction and microcirculation rarefaction precede white matter lesions in a mouse genetic model of cerebral ischemic small vessel disease." J Clin Invest **120**(2): 433-445.
Ju, Y. S., S. J. Ooms, C. Sutphen, S. L. Macauley, M. A. Zangrilli, G. Jerome, A. M. Fagan, E. Mignot, J. M. Zempel, J. Claassen and D. M. Holtzman (2017). "Slow wave sleep disruption increases cerebrospinal fluid amyloid-beta levels." Brain **140**(8): 2104-2111.
Jung, N. Y., H. Cho, Y. J. Kim, H. J. Kim, J. M. Lee, S. Park, S. T. Kim, E. J. Kim, J. S. Kim, S. H. Moon, J. H. Lee, M. Ewers, D. L. Na and S. W. Seo (2018). "The impact of education on cortical thickness in amyloid-negative subcortical vascular dementia: cognitive reserve hypothesis." Alzheimers Res Ther **10**(1): 103.
Kakar, P., A. Charidimou and D. J. Werring (2012). "Cerebral microbleeds: a new dilemma in stroke medicine." JRSM Cardiovasc Dis **1**(8): 2048004012474754.
Kalaria, R. N. (1996). "Cerebral vessels in ageing and Alzheimer's disease." Pharmacol Ther **72**(3): 193-214.
Kalaria, R. N. (1999). "The blood-brain barrier and cerebrovascular pathology in Alzheimer's disease." Annals of the New York Academy of Sciences **893**: 113-125.

Kalaria, R. N. (2012). "Cerebrovascular disease and mechanisms of cognitive impairment: evidence from clinicopathological studies in humans." Stroke **43**(9): 2526-2534.
Karama, S., S. Ducharme, J. Corley, F. Chouinard-Decorte, J. M. Starr, J. M. Wardlaw, M. E. Bastin and I. J. Deary (2015). "Cigarette smoking and thinning of the brain's cortex." Mol Psychiatry **20**(6): 778-785.
Kawagoe, S., T. Higuchi, M. Otaka, Y. Shimada, H. Kobayashi, H. Ida, T. Ohashi, H. J. Okano, M. Nakanishi and Y. Eto (2013). "Morphological features of iPS cells generated from Fabry disease skin fibroblasts using Sendai virus vector (SeVdp)." Mol Genet Metab **109**(4): 386-389.
Kawamura, H., M. Kobayashi, Q. Li, S. Yamanishi, K. Katsumura, M. Minami, D. M. Wu and D. G. Puro (2004). "Effects of angiotensin II on the pericyte-containing microvasculature of the rat retina." J Physiol **561**(Pt 3): 671-683.
Keable, A., K. Fenna, H. M. Yuen, D. A. Johnston, N. R. Smyth, C. Smith, R. Al-Shahi Salman, N. Samarasekera, J. A. Nicoll, J. Attems, R. N. Kalaria, R. O. Weller and R. O. Carare (2016). "Deposition of amyloid beta in the walls of human leptomeningeal arteries in relation to perivascular drainage pathways in cerebral amyloid angiopathy." Biochim Biophys Acta **1862**(5): 1037-1046.
Kehoe, P. G., N. Al Mulhim, H. Zetterberg, K. Blennow and J. S. Miners (2019). "Cerebrospinal Fluid Changes in the Renin-Angiotensin System in Alzheimer's Disease." J Alzheimers Dis.
Keith, J., F. Q. Gao, R. Noor, A. Kiss, G. Balasubramaniam, K. Au, E. Rogaeva, M. Masellis and S. E. Black (2017). "Collagenosis of the Deep Medullary Veins: An Underrecognized Pathologic Correlate of White Matter Hyperintensities and Periventricular Infarction?" J Neuropathol Exp Neurol **76**(4): 299-312.
Kemper, T., M. B. Moss, W. Hollander and S. Prusty (1999). "Microinfarction as a result of hypertension in a primate model of cerebrovascular disease." Acta Neuropathol **98**(3): 295-303.
Kemper, T. L., G. J. Blatt, R. J. Killiany and M. B. Moss (2001). "Neuropathology of progressive cognitive decline in chronically hypertensive rhesus monkeys." Acta Neuropathol **101**(2): 145-153.
Kilarski, L. L., S. Achterberg, W. J. Devan, M. Traylor, R. Malik, A. Lindgren, G. Pare, P. Sharma, A. Slowik, V. Thijs, M. Walters, B. B. Worrall, M. M. Sale, A. Algra, L. J. Kappelle, C. Wijmenga, B. Norrving, J. K. Sandling, L. Ronnblom, A. Goris, A. Franke, C. Sudlow, P. M. Rothwell, C. Levi, E. G. Holliday, M. Fornage, B. Psaty, S. Gretarsdottir, U. Thorsteinsdottir, S. Seshadri, B. D. Mitchell, S. Kittner, R. Clarke, J. C. Hopewell, J. C. Bis, G. B. Boncoraglio, J. Meschia, M. A. Ikram, B. M. Hansen, J. Montaner, G. Thorleifsson, K. Stefanson, J. Rosand, P. I. de Bakker, M. Farrall, M. Dichgans, H. S. Markus, S. Bevan, W. T. C. C. C. A. S. G. C. t. M. C. Garnet Collaborative Research Group and C. the International Stroke Genetics (2014). "Meta-analysis in more than 17,900 cases of ischemic stroke reveals a novel association at 12q24.12." Neurology **83**(8): 678-685.
Kim, R. (2007). "Introduction, mechanism of action and rationale for anti-vascular endothelial growth factor drugs in age-related macular degeneration." Indian J Ophthalmol **55**(6): 413-415.

Kitamura, A., Y. Fujita, N. Oishi, R. N. Kalaria, K. Washida, T. Maki, Y. Okamoto, Y. Hase, M. Yamada, J. Takahashi, H. Ito, H. Tomimoto, H. Fukuyama, R. Takahashi and M. Ihara (2012). "Selective white matter abnormalities in a novel rat model of vascular dementia." Neurobiol Aging **33**(5): 1012 e1025-1035.
Kiviniemi, V., X. Wang, V. Korhonen, T. Keinanen, T. Tuovinen, J. Autio, P. LeVan, S. Keilholz, Y. F. Zang, J. Hennig and M. Nedergaard (2016). "Ultra-fast magnetic resonance encephalography of physiological brain activity - Glymphatic pulsation mechanisms?" J Cereb Blood Flow Metab **36**(6): 1033-1045.
Knudsen, K. A., J. Rosand, D. Karluk and S. M. Greenberg (2001). "Clinical diagnosis of cerebral amyloid angiopathy: validation of the Boston criteria." Neurology **56**(4): 537-539.
Kolar, G. R., P. H. Kothari, N. Khanlou, J. C. Jen, R. E. Schmidt and H. V. Vinters (2014). "Neuropathology and genetics of cerebroretinal vasculopathies." Brain Pathol **24**(5): 510-518.
Koppelkamm, A., B. Vennemann, S. Lutz-Bonengel, T. Fracasso and M. Vennemann (2011). "RNA integrity in post-mortem samples: influencing parameters and implications on RT-qPCR assays." Int J Legal Med **125**(4): 573-580.
Kotrotsou, A., D. A. Bennett, J. A. Schneider, R. J. Dawe, T. Golak, S. E. Leurgans, L. Yu and K. Arfanakis (2014). "Ex vivo MR volumetry of human brain hemispheres." Magn Reson Med **71**(1): 364-374.
Koundal, S., R. Elkin, S. Nadeem, Y. Xue, S. Constantinou, S. Sanggaard, X. Liu, B. Monte, F. Xu, W. Van Nostrand, M. Nedergaard, H. Lee, J. Wardlaw, H. Benveniste and A. Tannenbaum (2020). "Optimal Mass Transport with Lagrangian Workflow Reveals Advective and Diffusion Driven Solute Transport in the Glymphatic System." Sci Rep **10**(1): 1990.
Kovacs, G. G., I. Alafuzoff and (Editors) (2017). Handbook of Clinical Neurology. Volume 145. Neuropathology., Elsevier.
Kowalczyk, A., P. Kleniewska, M. Kolodziejczyk, B. Skibska and A. Goraca (2015). "The role of endothelin-1 and endothelin receptor antagonists in inflammatory response and sepsis." Arch Immunol Ther Exp (Warsz) **63**(1): 41-52.
Kraut, M. A., L. L. Beason-Held, W. D. Elkins and S. M. Resnick (2008). "The impact of magnetic resonance imaging-detected white matter hyperintensities on longitudinal changes in regional cerebral blood flow." J Cereb Blood Flow Metab **28**(1): 190-197.
Krisch, B., H. Leonhardt and A. Oksche (1984). "Compartments and perivascular arrangement of the meninges covering the cerebral cortex of the rat." Cell Tissue Res **238**(3): 459-474.
Kumar, M., C. Chambers and R. Dhamija (2017). "Axenfeld-Rieger Syndrome and Leukoencephalopathy Caused by a Mutation in FOXC1." Pediatr Neurol **66**: 113-114.
Kvastad, L., K. Carlberg, L. Larsson, E. G. Villacampa, A. Stuckey, L. Stenbeck, A. Mollbrink, M. Zamboni, J. P. Magnusson, E. Basmaci, A. Shamikh, G. Prochazka, A. L. Schaupp, A. Borg, L. Fugger, M. Nister and J. Lundeberg (2021). "The spatial RNA integrity number assay for in situ evaluation of transcriptome quality." Commun Biol **4**(1): 57.
Lammie, G. A. (2002). "Hypertensive cerebral small vessel disease and stroke." Brain Pathol **12**(3): 358-370.

Lammie, G. A., F. Brannan, J. Slattery and C. Warlow (1997). "Nonhypertensive cerebral small-vessel disease. An autopsy study." Stroke **28**(11): 2222-2229.
Lammie, G. A., F. Brannan and J. M. Wardlaw (1998). "Incomplete lacunar infarction (Type Ib lacunes)." Acta Neuropathologica **96**(2): 163-171.
Landis, J. R. and G. G. Koch (1977). "The measurement of observer agreement for categorical data." Biometrics **33**(1): 159-174.
Langen, U. H., S. Ayloo and C. Gu (2019). "Development and Cell Biology of the Blood-Brain Barrier." Annu Rev Cell Dev Biol **35**: 591-613.
Lavallee, P. C., J. Labreuche, D. Faille, M. G. Huisse, P. Nicaise-Roland, M. Dehoux, F. Gongora-Rivera, A. Jaramillo, D. Brenner, D. Deplanque, I. F. Klein, P. J. Touboul, E. Vicaut, N. Ajzenberg and B. I. C. H. A. T. I. Lacunar (2013). "Circulating markers of endothelial dysfunction and platelet activation in patients with severe symptomatic cerebral small vessel disease." Cerebrovasc Dis **36**(2): 131-138.
Law, E., P. J. Connelly, E. Randall, C. McNeill, H. C. Fox, M. A. Parra, J. Hudson, L. A. Whyte, J. Johnstone, S. Gray and J. M. Starr (2013). "Does the Addenbrooke's Cognitive Examination-revised add to the Mini-Mental State Examination in established Alzheimer disease? Results from a national dementia research register." Int J Geriatr Psychiatry **28**(4): 351-355.
Lawson, N. D., N. Scheer, V. N. Pham, C. H. Kim, A. B. Chitnis, J. A. Campos-Ortega and B. M. Weinstein (2001). "Notch signaling is required for arterial-venous differentiation during embryonic vascular development." Development **128**(19): 3675-3683.
Le Bihan, D. (2003). "Looking into the functional architecture of the brain with diffusion MRI." Nat Rev Neurosci **4**(6): 469-480.
Lee, H., L. Xie, M. Yu, H. Kang, T. Feng, R. Deane, J. Logan, M. Nedergaard and H. Benveniste (2015). "The Effect of Body Posture on Brain Glymphatic Transport." J Neurosci **35**(31): 11034-11044.
Lee, J. M., G. Zhai, Q. Liu, E. R. Gonzales, K. Yin, P. Yan, C. Y. Hsu, K. D. Vo and W. Lin (2007). "Vascular permeability precedes spontaneous intracerebral hemorrhage in stroke-prone spontaneously hypertensive rats." Stroke **38**(12): 3289-3291.
Lee, S. H., J. M. Park, S. J. Kwon, H. Kim, Y. H. Kim, J. K. Roh and B. W. Yoon (2004). "Left ventricular hypertrophy is associated with cerebral microbleeds in hypertensive patients." Neurology **63**(1): 16-21.
Lee, S. J., S. Kwon, J. R. Gatti, E. Korcari, T. E. Gresser, P. C. Felix, S. G. Keep, K. C. Pasquale, T. Bai, S. A. Blanchett-Anderson, N. W. Wu, C. Obeng-Nyarko, K. M. Senagbe, K. C. Young, S. Maripudi, B. C. Yalavarthi, D. Korcari, A. Y. Liu, B. C. Schaffler, R. F. Keep and M. M. Wang (2017). "Large-scale identification of human cerebrovascular proteins: Inter-tissue and intracerebral vascular protein diversity." PLoS One **12**(11): e0188540.
Lee-Kirsch, M. A., D. Chowdhury, S. Harvey, M. Gong, L. Senenko, K. Engel, C. Pfeiffer, T. Hollis, M. Gahr, F. W. Perrino, J. Lieberman and N. Hubner (2007). "A mutation in TREX1 that impairs susceptibility to granzyme A-mediated cell death underlies familial chilblain lupus." J Mol Med (Berl) **85**(5): 531-537.
Lee-Kirsch, M. A., M. Gong, D. Chowdhury, L. Senenko, K. Engel, Y. A. Lee, U. de Silva, S. L. Bailey, T. Witte, T. J. Vyse, J. Kere, C. Pfeiffer, S. Harvey, A. Wong, S.

Koskenmies, O. Hummel, K. Rohde, R. E. Schmidt, A. F. Dominiczak, M. Gahr, T. Hollis, F. W. Perrino, J. Lieberman and N. Hubner (2007). "Mutations in the gene encoding the 3'-5' DNA exonuclease TREX1 are associated with systemic lupus erythematosus." Nat Genet **39**(9): 1065-1067.
Leveen, P., M. Pekny, S. Gebre-Medhin, B. Swolin, E. Larsson and C. Betsholtz (1994). "Mice deficient for PDGF B show renal, cardiovascular, and hematological abnormalities." Genes Dev **8**(16): 1875-1887.
Li, D. L., L. Ye, L. Gao and H. W. Cheng (2019). "Plasma concentration of ZCCHC14 contributes to prognostic efficacy in intracerebral hemorrhage patients." Eur Rev Med Pharmacol Sci **23**(19): 8533-8539.
Li, L., G. Tao, M. C. Hill, M. Zhang, Y. Morikawa and J. F. Martin (2018). "Pitx2 maintains mitochondrial function during regeneration to prevent myocardial fat deposition." Development **145**(18).
Li, Q., Y. Yang, C. Reis, T. Tao, W. Li, X. Li and J. H. Zhang (2018). "Cerebral Small Vessel Disease." Cell Transplant **27**(12): 1711-1722.
Lin, J., D. Wang, L. Lan and Y. Fan (2017). "Multiple Factors Involved in the Pathogenesis of White Matter Lesions." Biomed Res Int **2017**: 9372050.
Lindahl, P., B. R. Johansson, P. Leveen and C. Betsholtz (1997). "Pericyte loss and microaneurysm formation in PDGF-B-deficient mice." Science **277**(5323): 242-245.
Lindley, R. I., J. J. Wang, M. C. Wong, P. Mitchell, G. Liew, P. Hand, J. Wardlaw, D. A. De Silva, M. Baker, E. Rochtchina, C. Chen, G. J. Hankey, H. M. Chang, V. S. Fung, L. Gomes, T. Y. Wong, R. Multi-Centre and G. Stroke Study Collaborative (2009). "Retinal microvasculature in acute lacunar stroke: a cross-sectional study." Lancet Neurology **8**(7): 628-634.
Ling, C., Z. Liu, M. Song, W. Zhang, S. Wang, X. Liu, S. Ma, S. Sun, L. Fu, Q. Chu, J. C. I. Belmonte, Z. Wang, J. Qu, Y. Yuan and G. H. Liu (2019). "Modeling CADASIL vascular pathologies with patient-derived induced pluripotent stem cells." Protein Cell **10**(4): 249-271.
Linn, J., A. Halpin, P. Demaerel, J. Ruhland, A. D. Giese, M. Dichgans, M. A. van Buchem, H. Bruckmann and S. M. Greenberg (2010). "Prevalence of superficial siderosis in patients with cerebral amyloid angiopathy." Neurology **74**(17): 1346-1350.
Linn, J., J. Herms, M. Dichgans, H. Bruckmann, G. Fesl, T. Freilinger and M. Wiesmann (2008). "Subarachnoid hemosiderosis and superficial cortical hemosiderosis in cerebral amyloid angiopathy." Ajnr: American Journal of Neuroradiology **29**(1): 184-186.
Lip, P. L., F. Belgore, A. D. Blann, M. W. Hope-Ross, J. M. Gibson and G. Y. Lip (2000). "Plasma VEGF and soluble VEGF receptor FLT-1 in proliferative retinopathy: relationship to endothelial dysfunction and laser treatment." Invest Ophthalmol Vis Sci **41**(8): 2115-2119.
Lippoldt, A., U. Kniesel, S. Liebner, H. Kalbacher, T. Kirsch, H. Wolburg and H. Haller (2000). "Structural alterations of tight junctions are associated with loss of polarity in stroke-prone spontaneously hypertensive rat blood-brain barrier endothelial cells." Brain Res **885**(2): 251-261.

Liu, J., L. He, L. Muhl, G. Mocci, S. Gustavsson, B. Buyandelger, M. Vanlandewijck, C. Betsholtz, B. Westermark and J. Andrae (2021). "A human cell type similar to murine central nervous system perivascular fibroblasts." Exp Cell Res **402**(2): 112576.
Longden, T. A., D. C. Hill-Eubanks and M. T. Nelson (2016). "Ion channel networks in the control of cerebral blood flow." J Cereb Blood Flow Metab **36**(3): 492-512.
Looft-Wilson, R. C., G. W. Payne and S. S. Segal (2004). "Connexin expression and conducted vasodilation along arteriolar endothelium in mouse skeletal muscle." J Appl Physiol (1985) **97**(3): 1152-1158.
Lopez, L. M., W. D. Hill, S. E. Harris, M. Valdes Hernandez, S. Munoz Maniega, M. E. Bastin, E. Bailey, C. Smith, M. McBride, J. McClure, D. Graham, A. Dominiczak, Q. Yang, M. Fornage, M. A. Ikram, S. Debette, L. Launer, J. C. Bis, R. Schmidt, S. Seshadri, D. J. Porteous, J. Starr, I. J. Deary and J. M. Wardlaw (2015). "Genes from a translational analysis support a multifactorial nature of white matter hyperintensities." Stroke **46**(2): 341-347.
Love, S., H. Budka, J. Ironside and A. E. Perry (2015). Greenfield's Neuropathology. 9th edition. London, CRC Press.
Love, S., K. Chalmers, P. Ince, M. Esiri, J. Attems, K. Jellinger, M. Yamada, M. McCarron, T. Minett, F. Matthews, S. Greenberg, D. Mann and P. G. Kehoe (2014). "Development, appraisal, validation and implementation of a consensus protocol for the assessment of cerebral amyloid angiopathy in post-mortem brain tissue." Am J Neurodegener Dis **3**(1): 19-32.
Love, S. and J. S. Miners (2015). "White matter hypoperfusion and damage in dementia: post-mortem assessment." Brain Pathol **25**(1): 99-107.
Lubart, A., A. Benbenishty, H. Har-Gil, H. Laufer, A. Gdalyahu, Y. Assaf and P. Blinder (2021). "Single Cortical Microinfarcts Lead to Widespread Microglia/Macrophage Migration Along the White Matter." Cereb Cortex **31**(1): 248-266.
Macdonald, R. L., A. Kowalczuk and L. Johns (1995). "Emboli enter penetrating arteries of monkey brain in relation to their size." Stroke **26**(7): 1247-1250; discussion 1250-1241.
Maclullich, A. M., J. M. Wardlaw, K. J. Ferguson, J. M. Starr, J. R. Seckl and I. J. Deary (2004). "Enlarged perivascular spaces are associated with cognitive function in healthy elderly men." J Neurol Neurosurg Psychiatry **75**(11): 1519-1523.
Madden, D. J., I. J. Bennett, A. Burzynska, G. G. Potter, N. K. Chen and A. W. Song (2012). "Diffusion tensor imaging of cerebral white matter integrity in cognitive aging." Biochim Biophys Acta **1822**(3): 386-400.
Maillard, P., S. Seshadri, A. Beiser, J. J. Himali, R. Au, E. Fletcher, O. Carmichael, P. A. Wolf and C. DeCarli (2012). "Effects of systolic blood pressure on white-matter integrity in young adults in the Framingham Heart Study: a cross-sectional study." Lancet Neurol **11**(12): 1039-1047.
Makin, S. D., F. N. Doubal, M. S. Dennis and J. M. Wardlaw (2015). "Clinically Confirmed Stroke With Negative Diffusion-Weighted Imaging Magnetic Resonance Imaging: Longitudinal Study of Clinical Outcomes, Stroke Recurrence, and Systematic Review." Stroke **46**(11): 3142-3148.

Makin, S. D., F. N. Doubal, K. Shuler, F. M. Chappell, J. Staals, M. S. Dennis and J. M. Wardlaw (2018). "The impact of early-life intelligence quotient on post stroke cognitive impairment." Eur Stroke J **3**(2): 145-156.
Makin, S. D., S. Turpin, M. S. Dennis and J. M. Wardlaw (2013). "Cognitive impairment after lacunar stroke: systematic review and meta-analysis of incidence, prevalence and comparison with other stroke subtypes." J Neurol Neurosurg Psychiatry **84**(8): 893-900.
Malik, R., G. Chauhan, M. Traylor, M. Sargurupremraj, Y. Okada, A. Mishra, L. Rutten-Jacobs, A. K. Giese, S. W. van der Laan, S. Gretarsdottir, C. D. Anderson, M. Chong, H. H. H. Adams, T. Ago, P. Almgren, P. Amouyel, H. Ay, T. M. Bartz, O. R. Benavente, S. Bevan, G. B. Boncoraglio, R. D. Brown, Jr., A. S. Butterworth, C. Carrera, C. L. Carty, D. I. Chasman, W. M. Chen, J. W. Cole, A. Correa, I. Cotlarciuc, C. Cruchaga, J. Danesh, P. I. W. de Bakker, A. L. DeStefano, M. den Hoed, Q. Duan, S. T. Engelter, G. J. Falcone, R. F. Gottesman, R. P. Grewal, V. Gudnason, S. Gustafsson, J. Haessler, T. B. Harris, A. Hassan, A. S. Havulinna, S. R. Heckbert, E. G. Holliday, G. Howard, F. C. Hsu, H. I. Hyacinth, M. A. Ikram, E. Ingelsson, M. R. Irvin, X. Jian, J. Jimenez-Conde, J. A. Johnson, J. W. Jukema, M. Kanai, K. L. Keene, B. M. Kissela, D. O. Kleindorfer, C. Kooperberg, M. Kubo, L. A. Lange, C. D. Langefeld, C. Langenberg, L. J. Launer, J. M. Lee, R. Lemmens, D. Leys, C. M. Lewis, W. Y. Lin, A. G. Lindgren, E. Lorentzen, P. K. Magnusson, J. Maguire, A. Manichaikul, P. F. McArdle, J. F. Meschia, B. D. Mitchell, T. H. Mosley, M. A. Nalls, T. Ninomiya, M. J. O'Donnell, B. M. Psaty, S. L. Pulit, K. Rannikmae, A. P. Reiner, K. M. Rexrode, K. Rice, S. S. Rich, P. M. Ridker, N. S. Rost, P. M. Rothwell, J. I. Rotter, T. Rundek, R. L. Sacco, S. Sakaue, M. M. Sale, V. Salomaa, B. R. Sapkota, R. Schmidt, C. O. Schmidt, U. Schminke, P. Sharma, A. Slowik, C. L. M. Sudlow, C. Tanislav, T. Tatlisumak, K. D. Taylor, V. N. S. Thijs, G. Thorleifsson, U. Thorsteinsdottir, S. Tiedt, S. Trompet, C. Tzourio, C. M. van Duijn, M. Walters, N. J. Wareham, S. Wassertheil-Smoller, J. G. Wilson, K. L. Wiggins, Q. Yang, S. Yusuf, J. C. Bis, T. Pastinen, A. Ruusalepp, E. E. Schadt, S. Koplev, J. L. M. Bjorkegren, V. Codoni, M. Civelek, N. L. Smith, D. A. Tregouet, I. E. Christophersen, C. Roselli, S. A. Lubitz, P. T. Ellinor, E. S. Tai, J. S. Kooner, N. Kato, J. He, P. van der Harst, P. Elliott, J. C. Chambers, F. Takeuchi, A. D. Johnson, D. K. Sanghera, O. Melander, C. Jern, D. Strbian, I. Fernandez-Cadenas, W. T. Longstreth, Jr., A. Rolfs, J. Hata, D. Woo, J. Rosand, G. Pare, J. C. Hopewell, D. Saleheen, K. Stefansson, B. B. Worrall, S. J. Kittner, S. Seshadri, M. Fornage, H. S. Markus, J. M. M. Howson, Y. Kamatani, S. Debette, M. Dichgans, R. Malik, G. Chauhan, M. Traylor, M. Sargurupremraj, Y. Okada, A. Mishra, L. Rutten-Jacobs, A. K. Giese, S. W. van der Laan, S. Gretarsdottir, C. D. Anderson, M. Chong, H. H. H. Adams, T. Ago, P. Almgren, P. Amouyel, H. Ay, T. M. Bartz, O. R. Benavente, S. Bevan, G. B. Boncoraglio, R. D. Brown, Jr., A. S. Butterworth, C. Carrera, C. L. Carty, D. I. Chasman, W. M. Chen, J. W. Cole, A. Correa, I. Cotlarciuc, C. Cruchaga, J. Danesh, P. I. W. de Bakker, A. L. DeStefano, M. D. Hoed, Q. Duan, S. T. Engelter, G. J. Falcone, R. F. Gottesman, R. P. Grewal, V. Gudnason, S. Gustafsson, J. Haessler, T. B. Harris, A. Hassan, A. S. Havulinna, S. R. Heckbert, E. G. Holliday, G. Howard, F. C. Hsu, H. I. Hyacinth, M. A. Ikram, E. Ingelsson, M. R. Irvin, X. Jian, J. Jimenez-Conde, J. A. Johnson, J. W. Jukema, M. Kanai, K. L. Keene, B. M. Kissela, D. O. Kleindorfer, C.

Kooperberg, M. Kubo, L. A. Lange, C. D. Langefeld, C. Langenberg, L. J. Launer, J. M. Lee, R. Lemmens, D. Leys, C. M. Lewis, W. Y. Lin, A. G. Lindgren, E. Lorentzen, P. K. Magnusson, J. Maguire, A. Manichaikul, P. F. McArdle, J. F. Meschia, B. D. Mitchell, T. H. Mosley, M. A. Nalls, T. Ninomiya, M. J. O'Donnell, B. M. Psaty, S. L. Pulit, K. Rannikmae, A. P. Reiner, K. M. Rexrode, K. Rice, S. S. Rich, P. M. Ridker, N. S. Rost, P. M. Rothwell, J. I. Rotter, T. Rundek, R. L. Sacco, S. Sakaue, M. M. Sale, V. Salomaa, B. R. Sapkota, R. Schmidt, C. O. Schmidt, U. Schminke, P. Sharma, A. Slowik, C. L. M. Sudlow, C. Tanislav, T. Tatlisumak, K. D. Taylor, V. N. S. Thijs, G. Thorleifsson, U. Thorsteinsdottir, S. Tiedt, S. Trompet, C. Tzourio, C. M. van Duijn, M. Walters, N. J. Wareham, S. Wassertheil-Smoller, J. G. Wilson, K. L. Wiggins, Q. Yang, S. Yusuf, N. Amin, H. S. Aparicio, D. K. Arnett, J. Attia, A. S. Beiser, C. Berr, J. E. Buring, M. Bustamante, V. Caso, Y. C. Cheng, S. H. Choi, A. Chowhan, N. Cullell, J. F. Dartigues, H. Delavaran, P. Delgado, M. Dorr, G. Engstrom, I. Ford, W. S. Gurpreet, A. Hamsten, L. Heitsch, A. Hozawa, L. Ibanez, A. Ilinca, M. Ingelsson, M. Iwasaki, R. D. Jackson, K. Jood, P. Jousilahti, S. Kaffashian, L. Kalra, M. Kamouchi, T. Kitazono, O. Kjartansson, M. Kloss, P. J. Koudstaal, J. Krupinski, D. L. Labovitz, C. C. Laurie, C. R. Levi, L. Li, L. Lind, C. M. Lindgren, V. Lioutas, Y. M. Liu, O. L. Lopez, H. Makoto, N. Martinez-Majander, K. Matsuda, N. Minegishi, J. Montaner, A. P. Morris, E. Muino, M. Muller-Nurasyid, B. Norrving, S. Ogishima, E. A. Parati, L. R. Peddareddygari, N. L. Pedersen, J. Pera, M. Perola, A. Pezzini, S. Pileggi, R. Rabionet, I. Riba-Llena, M. Ribases, J. R. Romero, J. Roquer, A. G. Rudd, A. P. Sarin, R. Sarju, C. Sarnowski, M. Sasaki, C. L. Satizabal, M. Satoh, N. Sattar, N. Sawada, G. Sibolt, A. Sigurdsson, A. Smith, K. Sobue, C. Soriano-Tarraga, T. Stanne, O. C. Stine, D. J. Stott, K. Strauch, T. Takai, H. Tanaka, K. Tanno, A. Teumer, L. Tomppo, N. P. Torres-Aguila, E. Touze, S. Tsugane, A. G. Uitterlinden, E. M. Valdimarsson, S. J. van der Lee, H. Volzke, K. Wakai, D. Weir, S. R. Williams, C. D. A. Wolfe, Q. Wong, H. Xu, T. Yamaji, D. K. Sanghera, O. Melander, C. Jern, D. Strbian, I. Fernandez-Cadenas, W. T. Longstreth, Jr., A. Rolfs, J. Hata, D. Woo, J. Rosand, G. Pare, J. C. Hopewell, D. Saleheen, K. Stefansson, B. B. Worrall, S. J. Kittner, S. Seshadri, M. Fornage, H. S. Markus, J. M. M. Howson, Y. Kamatani, S. Debette, M. Dichgans, A. F. Consortium, H. Cohorts for, C. Aging Research in Genomic Epidemiology, C. International Genomics of Blood Pressure, I. Consortium, Starnet, G. BioBank Japan Cooperative Hospital, C. Consortium, E.-C. Consortium, E. P.-I. Consortium, C. International Stroke Genetics, M. Consortium, C. C. Neurology Working Group of the, N. S. G. Network, U. K. Y. L. D. Study, M. Consortium and M. Consortium (2018). "Multiancestry genome-wide association study of 520,000 subjects identifies 32 loci associated with stroke and stroke subtypes." Nat Genet **50**(4): 524-537.

Mancuso, M., M. Arnold, A. Bersano, A. Burlina, H. Chabriat, S. Debette, C. Enzinger, A. Federico, A. Filla, J. Finsterer, D. Hunt, S. Lesnik Oberstein, E. Tournier-Lasserve and H. S. Markus (2020). "Monogenic cerebral small-vessel diseases: diagnosis and therapy. Consensus recommendations of the European Academy of Neurology." Eur J Neurol **27**(6): 909-927.

Maniega, S. M., M. C. Valdes Hernandez, J. D. Clayden, N. A. Royle, C. Murray, Z. Morris, B. S. Aribisala, A. J. Gow, J. M. Starr, M. E. Bastin, I. J. Deary and J. M.

Wardlaw (2015). "White matter hyperintensities and normal-appearing white matter integrity in the aging brain." Neurobiology of Aging **36**(2): 909-918.
Maniega, S. M., M. C. Valdes Hernandez, J. D. Clayden, N. A. Royle, C. Murray, Z. Morris, B. S. Aribisala, A. J. Gow, J. M. Starr, M. E. Bastin, I. J. Deary and J. M. Wardlaw (2015). "White matter hyperintensities and normal-appearing white matter integrity in the aging brain." Neurobiol Aging **36**(2): 909-918.
Marcus, J., H. Gardener, T. Rundek, M. S. Elkind, R. L. Sacco, C. Decarli and C. B. Wright (2011). "Baseline and longitudinal increases in diastolic blood pressure are associated with greater white matter hyperintensity volume: the northern Manhattan study." Stroke **42**(9): 2639-2641.
Marini, S., C. D. Anderson and J. Rosand (2020). "Genetics of Cerebral Small Vessel Disease." Stroke **51**(1): 12-20.
Markus, H. S., B. Hunt, K. Palmer, C. Enzinger, H. Schmidt and R. Schmidt (2005). "Markers of endothelial and hemostatic activation and progression of cerebral white matter hyperintensities: longitudinal results of the Austrian Stroke Prevention Study." Stroke **36**(7): 1410-1414.
Markus, H. S., D. J. Lythgoe, L. Ostegaard, M. O'Sullivan and S. C. Williams (2000). "Reduced cerebral blood flow in white matter in ischaemic leukoaraiosis demonstrated using quantitative exogenous contrast based perfusion MRI." J Neurol Neurosurg Psychiatry **69**(1): 48-53.
Marshall, V. G., W. G. Bradley, Jr., C. E. Marshall, T. Bhoopat and R. H. Rhodes (1988). "Deep white matter infarction: correlation of MR imaging and histopathologic findings." Radiology **167**(2): 517-522.
Martinez-Lemus, L. A., G. Zhao, E. L. Galinanes and M. Boone (2011). "Inward remodeling of resistance arteries requires reactive oxygen species-dependent activation of matrix metalloproteinases." Am J Physiol Heart Circ Physiol **300**(6): H2005-2015.
Martinez-Ramirez, S., O. M. Pontes-Neto, A. P. Dumas, E. Auriel, A. Halpin, M. Quimby, M. E. Gurol, S. M. Greenberg and A. Viswanathan (2013). "Topography of dilated perivascular spaces in subjects from a memory clinic cohort." Neurology **80**(17): 1551-1556.
Matsushita, H., E. Chang, A. J. Glassford, J. P. Cooke, C. P. Chiu and P. S. Tsao (2001). "eNOS activity is reduced in senescent human endothelial cells: Preservation by hTERT immortalization." Circ Res **89**(9): 793-798.
Matsushita, K. and D. G. Puro (2006). "Topographical heterogeneity of K(IR) currents in pericyte-containing microvessels of the rat retina: effect of diabetes." J Physiol **573**(Pt 2): 483-495.
Matsusue, E., S. Sugihara, S. Fujii, E. Ohama, T. Kinoshita and T. Ogawa (2006). "White matter changes in elderly people: MR-pathologic correlations." Magn Reson Med Sci **5**(2): 99-104.
Matsusue, E., S. Sugihara, S. Fujii, E. Ohama, T. Kinoshita and T. Ogawa (2006). "White matter changes in elderly people: MR-pathologic correlations." Magnetic Resonance in Medical Sciences **5**(2): 99-104.
McAleese, K. E., I. Alafuzoff, A. Charidimou, J. De Reuck, L. T. Grinberg, A. H. Hainsworth, T. Hortobagyi, P. Ince, K. Jellinger, J. Gao, R. N. Kalaria, G. G. Kovacs, E.

Kovari, S. Love, M. Popovic, O. Skrobot, R. Taipa, D. R. Thal, D. Werring, S. B. Wharton and J. Attems (2016). "Post-mortem assessment in vascular dementia: advances and aspirations." BMC Med **14**(1): 129.
McAleese, K. E., M. Firbank, D. Hunter, L. Sun, R. Hall, J. W. Neal, D. M. Mann, M. Esiri, K. A. Jellinger, J. T. O'Brien and J. Attems (2013). "Magnetic resonance imaging of fixed post mortem brains reliably reflects subcortical vascular pathology of frontal, parietal and occipital white matter." Neuropathol Appl Neurobiol **39**(5): 485-497.
McCarron, M. O. and J. A. Nicoll (2000). "Apolipoprotein E genotype and cerebral amyloid angiopathy-related hemorrhage." Ann N Y Acad Sci **903**: 176-179.
McCuskey, P. A. and R. S. McCuskey (1984). "In vivo and electron microscopic study of the development of cerebral diabetic microangiography." Microcirc Endothelium Lymphatics **1**(2): 221-244.
McGinnis, S. M., M. Brickhouse, B. Pascual and B. C. Dickerson (2011). "Age-related changes in the thickness of cortical zones in humans." Brain Topogr **24**(3-4): 279-291.
McKeith, I. G., C. G. Ballard, R. H. Perry, P. G. Ince, J. T. O'Brien, D. Neill, K. Lowery, E. Jaros, R. Barber, P. Thompson, A. Swann, A. F. Fairbairn and E. K. Perry (2000). "Prospective validation of consensus criteria for the diagnosis of dementia with Lewy bodies." Neurology **54**(5): 1050-1058.
Mehta, A. R., B. T. Selvaraj, S. K. Barton, K. McDade, S. Abrahams, S. Chandran, C. Smith and J. M. Gregory (2020). "Improved detection of RNA foci in C9orf72 amyotrophic lateral sclerosis post-mortem tissue using BaseScope shows a lack of association with cognitive dysfunction." Brain Commun **2**(1): fcaa009.
Mestre, H., L. M. Hablitz, A. L. Xavier, W. Feng, W. Zou, T. Pu, H. Monai, G. Murlidharan, R. M. Castellanos Rivera, M. J. Simon, M. M. Pike, V. Pla, T. Du, B. T. Kress, X. Wang, B. A. Plog, A. S. Thrane, I. Lundgaard, Y. Abe, M. Yasui, J. H. Thomas, M. Xiao, H. Hirase, A. Asokan, J. J. Iliff and M. Nedergaard (2018). "Aquaporin-4-dependent glymphatic solute transport in the rodent brain." Elife **7**.
Mestre, H., J. Tithof, T. Du, W. Song, W. Peng, A. M. Sweeney, G. Olveda, J. H. Thomas, M. Nedergaard and D. H. Kelley (2018). "Flow of cerebrospinal fluid is driven by arterial pulsations and is reduced in hypertension." Nat Commun **9**(1): 4878.
Michihara, A., M. Sawamura, Y. Yamori, K. Akasaki and H. Tsuji (2001). "Mevalonate pyrophosphate decarboxylase in stroke-prone spontaneously hypertensive rat is reduced from the age of two weeks." Biol Pharm Bull **24**(12): 1417-1419.
Mies, G., D. Hermann, U. Ganten and K. A. Hossmann (1999). "Hemodynamics and metabolism in stroke-prone spontaneously hypertensive rats before manifestation of brain infarcts." J Cereb Blood Flow Metab **19**(11): 1238-1246.
Miners, J. S., P. Kehoe and S. Love (2011). "Neprilysin protects against cerebral amyloid angiopathy and Abeta-induced degeneration of cerebrovascular smooth muscle cells." Brain Pathol **21**(5): 594-605.
Miners, J. S., J. C. Palmer and S. Love (2015). "Pathophysiology of Hypoperfusion of the Precuneus in Early Alzheimer's Disease." Brain Pathol.

Miners, J. S., I. Schulz and S. Love (2018). "Differing associations between Abeta accumulation, hypoperfusion, blood-brain barrier dysfunction and loss of PDGFRB pericyte marker in the precuneus and parietal white matter in Alzheimer's disease." J Cereb Blood Flow Metab **38**(1): 103-115.
Miners, J. S., Z. van Helmond, P. G. Kehoe and S. Love (2010). "Changes with age in the activities of beta-secretase and the Abeta-degrading enzymes neprilysin, insulin-degrading enzyme and angiotensin-converting enzyme." Brain Pathol **20**(4): 794-802.
Miners, S., E. Ashby, S. Baig, R. Harrison, H. Tayler, E. Speedy, J. A. Prince, S. Love and P. G. Kehoe (2009). "Angiotensin-converting enzyme levels and activity in Alzheimer's disease: differences in brain and CSF ACE and association with ACE1 genotypes." Am J Transl Res **1**(2): 163-177.
Miners, S., H. Moulding, R. de Silva and S. Love (2014). "Reduced vascular endothelial growth factor and capillary density in the occipital cortex in dementia with Lewy bodies." Brain Pathol **24**(4): 334-343.
Mittal, P., V. Kalia and S. Dua (2010). "Pictorial essay: Susceptibility-weighted imaging in cerebral ischemia." Indian J Radiol Imaging **20**(4): 250-253.
Miyamoto, N., S. Magami, T. Inaba, Y. Ueno, K. Hira, C. Kijima, S. Nakajima, K. Yamashiro, T. Urabe and N. Hattori (2020). "The effects of A1/A2 astrocytes on oligodendrocyte linage cells against white matter injury under prolonged cerebral hypoperfusion." Glia **68**(9): 1910-1924.
Miyata, M., S. Kakeda, S. Iwata, S. Nakayamada, S. Ide, K. Watanabe, J. Moriya, Y. Tanaka and Y. Korogi (2017). "Enlarged perivascular spaces are associated with the disease activity in systemic lupus erythematosus." Sci Rep **7**(1): 12566.
Mogensen, F. L., C. Delle and M. Nedergaard (2021). "The Glymphatic System (En)during Inflammation." Int J Mol Sci **22**(14).
Moisse, K. and M. J. Strong (2006). "Innate immunity in amyotrophic lateral sclerosis." Biochim Biophys Acta **1762**(11-12): 1083-1093.
Mok, V., V. Srikanth, Y. Xiong, T. G. Phan, C. Moran, S. Chu, Q. Zhao, W. W. Chu, A. Wong, Z. Hong, X. Liu, L. K. Wong and D. Ding (2014). "Race-ethnicity and cerebral small vessel disease--comparison between Chinese and White populations." Int J Stroke **9 Suppl A100**: 36-42.
Moncada, S., R. M. Palmer and E. A. Higgs (1991). "Nitric oxide: physiology, pathophysiology, and pharmacology." Pharmacol Rev **43**(2): 109-142.
Monoranu, C. M., M. Apfelbacher, E. Grunblatt, B. Puppe, I. Alafuzoff, I. Ferrer, S. Al-Saraj, K. Keyvani, A. Schmitt, P. Falkai, J. Schittenhelm, G. Halliday, J. Kril, C. Harper, C. McLean, P. Riederer and W. Roggendorf (2009). "pH measurement as quality control on human post mortem brain tissue: a study of the BrainNet Europe consortium." Neuropathol Appl Neurobiol **35**(3): 329-337.
Montagne, A., A. M. Nikolakopoulou, Z. Zhao, A. P. Sagare, G. Si, D. Lazic, S. R. Barnes, M. Daianu, A. Ramanathan, A. Go, E. J. Lawson, Y. Wang, W. J. Mack, P. M. Thompson, J. A. Schneider, J. Varkey, R. Langen, E. Mullins, R. E. Jacobs and B. V. Zlokovic (2018). "Pericyte degeneration causes white matter dysfunction in the mouse central nervous system." Nat Med **24**(3): 326-337.

Moody, D. M., W. R. Brown, V. R. Challa and R. L. Anderson (1995). "Periventricular venous collagenosis: association with leukoaraiosis." Radiology **194**(2): 469-476.
Moody, D. M., C. R. Thore, J. A. Anstrom, V. R. Challa, C. D. Langefeld and W. R. Brown (2004). "Quantification of afferent vessels shows reduced brain vascular density in subjects with leukoaraiosis." Radiology **233**(3): 883-890.
Mooradian, D. L., T. C. Hutsell and L. K. Keefer (1995). "Nitric oxide (NO) donor molecules: effect of NO release rate on vascular smooth muscle cell proliferation in vitro." J Cardiovasc Pharmacol **25**(4): 674-678.
Moore, D. F., G. Altarescu, W. C. Barker, N. J. Patronas, P. Herscovitch and R. Schiffmann (2003). "White matter lesions in Fabry disease occur in 'prior' selectively hypometabolic and hyperperfused brain regions." Brain Res Bull **62**(3): 231-240.
Moreau, F., S. Patel, M. L. Lauzon, C. R. McCreary, M. Goyal, R. Frayne, A. M. Demchuk, S. B. Coutts and E. E. Smith (2012). "Cavitation after acute symptomatic lacunar stroke depends on time, location, and MRI sequence." Stroke **43**(7): 1837-1842.
Morel, L., M. S. R. Chiang, H. Higashimori, T. Shoneye, L. K. Iyer, J. Yelick, A. Tai and Y. Yang (2017). "Molecular and Functional Properties of Regional Astrocytes in the Adult Brain." J Neurosci **37**(36): 8706-8717.
Morita, K., H. Sasaki, M. Furuse and S. Tsukita (1999). "Endothelial claudin: claudin-5/TMVCF constitutes tight junction strands in endothelial cells." J Cell Biol **147**(1): 185-194.
Morita, M., G. Stamp, P. Robins, A. Dulic, I. Rosewell, G. Hrivnak, G. Daly, T. Lindahl and D. E. Barnes (2004). "Gene-targeted mice lacking the Trex1 (DNase III) 3'-->5' DNA exonuclease develop inflammatory myocarditis." Mol Cell Biol **24**(15): 6719-6727.
Mortensen, K. N., S. Sanggaard, H. Mestre, H. Lee, S. Kostrikov, A. L. R. Xavier, A. Gjedde, H. Benveniste and M. Nedergaard (2019). "Impaired Glymphatic Transport in Spontaneously Hypertensive Rats." J Neurosci **39**(32): 6365-6377.
Moulin, S., J. Labreuche, S. Bombois, C. Rossi, G. Boulouis, H. Henon, A. Duhamel, D. Leys and C. Cordonnier (2016). "Dementia risk after spontaneous intracerebral haemorrhage: a prospective cohort study." Lancet Neurol **15**(8): 820-829.
MRC. "Medical Research Council. UK Brain Banks Network (accessed 30/01/2021)." Retrieved 30/01/2021, from https://mrc.ukri.org/research/facilities-and-resources-for-researchers/brain-banks/].
MRC. (2021). "Medical Research Council. Research, cohort directory, Lothian Birth Cohort 1936 (accessed 01/09/2021)." Retrieved 01/09/2021, from https://mrc.ukri.org/research/facilities-and-resources-for-researchers/cohort-directory/lothian-birth-cohort-1936-lbc1936/.
MRC. (2021). "Medical Research Council. UK Brain Banks Network (accessed 16/08/2021)." from https://mrc.ukri.org/research/facilities-and-resources-for-researchers/brain-banks/about-the-uk-brain-banks-network/.
Muller, W. A. (2011). "Mechanisms of leukocyte transendothelial migration." Annu Rev Pathol **6**: 323-344.

Munoz, D. G., S. M. Hastak, B. Harper, D. Lee and V. C. Hachinski (1993). "Pathologic correlates of increased signals of the centrum ovale on magnetic resonance imaging." Arch Neurol **50**(5): 492-497.
Munoz Maniega, S., F. M. Chappell, M. C. Valdes Hernandez, P. A. Armitage, S. D. Makin, A. K. Heye, M. J. Thrippleton, E. Sakka, K. Shuler, M. S. Dennis and J. M. Wardlaw (2017). "Integrity of normal-appearing white matter: Influence of age, visible lesion burden and hypertension in patients with small-vessel disease." J Cereb Blood Flow Metab **37**(2): 644-656.
Murbach M, Z. E., Neufeld E, Cabot E, Kainz W, Kuster N (2015). "Heating and Safety Concerns of the Radio-Frequency Field in MRI." Current Radiology Reports **3:45**.
Murray, M. E., P. Vemuri, G. M. Preboske, M. C. Murphy, K. J. Schweitzer, J. E. Parisi, C. R. Jack, Jr. and D. W. Dickson (2012). "A quantitative postmortem MRI design sensitive to white matter hyperintensity differences and their relationship with underlying pathology." Journal of Neuropathology & Experimental Neurology **71**(12): 1113-1122.
Murray, M. E., P. Vemuri, G. M. Preboske, M. C. Murphy, K. J. Schweitzer, J. E. Parisi, C. R. Jack, Jr. and D. W. Dickson (2012). "A quantitative postmortem MRI design sensitive to white matter hyperintensity differences and their relationship with underlying pathology." J Neuropathol Exp Neurol **71**(12): 1113-1122.
Mustapha, M., C. Nassir, N. Aminuddin, A. A. Safri and M. M. Ghazali (2019). "Cerebral Small Vessel Disease (CSVD) - Lessons From the Animal Models." Front Physiol **10**: 1317.
Naba, A., S. Hoersch and R. O. Hynes (2012). "Towards definition of an ECM parts list: an advance on GO categories." Matrix Biol **31**(7-8): 371-372.
Nation, D. A., M. D. Sweeney, A. Montagne, A. P. Sagare, L. M. D'Orazio, M. Pachicano, F. Sepehrband, A. R. Nelson, D. P. Buennagel, M. G. Harrington, T. L. S. Benzinger, A. M. Fagan, J. M. Ringman, L. S. Schneider, J. C. Morris, H. C. Chui, M. Law, A. W. Toga and B. V. Zlokovic (2019). "Blood-brain barrier breakdown is an early biomarker of human cognitive dysfunction." Nat Med **25**(2): 270-276.
Nedergaard, M., B. Ransom and S. A. Goldman (2003). "New roles for astrocytes: redefining the functional architecture of the brain." Trends Neurosci **26**(10): 523-530.
Nitta, T., M. Hata, S. Gotoh, Y. Seo, H. Sasaki, N. Hashimoto, M. Furuse and S. Tsukita (2003). "Size-selective loosening of the blood-brain barrier in claudin-5-deficient mice." J Cell Biol **161**(3): 653-660.
Niwa, A., Y. Ii, A. Shindo, K. Matsuo, H. Ishikawa, A. Taniguchi, S. Takase, M. Maeda, H. Sakuma, H. Akatsu, Y. Hashizume and H. Tomimoto (2017). "Comparative Analysis of Cortical Microinfarcts and Microbleeds using 3.0-Tesla Postmortem Magnetic Resonance Images and Histopathology." J Alzheimers Dis **59**(3): 951-959.
Nordborg, C., K. Fredriksson and B. B. Johansson (1985). "The morphometry of consecutive segments in cerebral arteries of normotensive and spontaneously hypertensive rats." Stroke **16**(2): 313-320.
Novakovic, V. (2010). "Cardiovascular risk factors, white matter abnormalities and dffusion tensor magnetic resonance imaging." Biol. Psychiatry Psychopharmacol. **12**(2): 103-104.

Nozaki, H., M. Nishizawa and O. Onodera (2014). "Features of cerebral autosomal recessive arteriopathy with subcortical infarcts and leukoencephalopathy." Stroke **45**(11): 3447-3453.
O'Sullivan, M., J. M. Jarosz, R. J. Martin, N. Deasy, J. F. Powell and H. S. Markus (2001). "MRI hyperintensities of the temporal lobe and external capsule in patients with CADASIL." Neurology **56**(5): 628-634.
Oide, T., H. Nakayama, S. Yanagawa, N. Ito, S. Ikeda and K. Arima (2008). "Extensive loss of arterial medial smooth muscle cells and mural extracellular matrix in cerebral autosomal recessive arteriopathy with subcortical infarcts and leukoencephalopathy (CARASIL)." Neuropathology **28**(2): 132-142.
Ostergaard, L., T. S. Engedal, F. Moreton, M. B. Hansen, J. M. Wardlaw, T. Dalkara, H. S. Markus and K. W. Muir (2016). "Cerebral small vessel disease: Capillary pathways to stroke and cognitive decline." J Cereb Blood Flow Metab **36**(2): 302-325.
Palmer, J. C., R. Barker, P. G. Kehoe and S. Love (2012). "Endothelin-1 is elevated in Alzheimer's disease and upregulated by amyloid-beta." J Alzheimers Dis **29**(4): 853-861.
Pantoni, L. (2010). "Cerebral small vessel disease: from pathogenesis and clinical characteristics to therapeutic challenges." Lancet Neurol **9**(7): 689-701.
Pantoni, L. and J. H. Garcia (1997). "Pathogenesis of leukoaraiosis: a review." Stroke **28**(3): 652-659.
Pantoni, L. and P. Gorelick (2014). Cerebral Small Vessel Disease. Cambridge, Cambridge University Press.
Pantoni, L., C. Sarti, I. Alafuzoff, K. Jellinger, D. G. Munoz, J. Ogata and V. Palumbo (2006). "Postmortem examination of vascular lesions in cognitive impairment: a survey among neuropathological services." Stroke **37**(4): 1005-1009.
Pasi, M. and C. Cordonnier (2020). "Clinical Relevance of Cerebral Small Vessel Diseases." Stroke **51**(1): 47-53.
Patankar, T. F., D. Mitra, A. Varma, J. Snowden, D. Neary and A. Jackson (2005). "Dilatation of the Virchow-Robin space is a sensitive indicator of cerebral microvascular disease: study in elderly patients with dementia." AJNR Am J Neuroradiol **26**(6): 1512-1520.
Patil, C. K. and S. A. McCarroll (2013). "Of rats and men." Cell **154**(3): 481-483.
Pendlebury, S. T. (2012). "Dementia in patients hospitalized with stroke: rates, time course, and clinico-pathologic factors." Int J Stroke **7**(7): 570-581.
Pendlebury, S. T. and P. M. Rothwell (2009). "Prevalence, incidence, and factors associated with pre-stroke and post-stroke dementia: a systematic review and meta-analysis." Lancet Neurol **8**(11): 1006-1018.
Penke, L., M. C. Valdes Hernandez, S. M. Maniega, A. J. Gow, C. Murray, J. M. Starr, M. E. Bastin, I. J. Deary and J. M. Wardlaw (2012). "Brain iron deposits are associated with general cognitive ability and cognitive aging." Neurobiol Aging **33**(3): 510-517 e512.
Peppiatt, C. M., C. Howarth, P. Mobbs and D. Attwell (2006). "Bidirectional control of CNS capillary diameter by pericytes." Nature **443**(7112): 700-704.

Peters, A. (2007). The Effects of Normal Aging on Nerve Fibers and Neuroglia in the Central Nervous System. Brain Aging: Models, Methods, and Mechanisms. D. R. Riddle. Boca Raton (FL).
Peters, A. and E. G. Jones (1984). Cellular Components of the Cerebral Cortex. New York, Plenum.
Petersen, M. A., J. K. Ryu and K. Akassoglou (2018). "Fibrinogen in neurological diseases: mechanisms, imaging and therapeutics." Nat Rev Neurosci **19**(5): 283-301.
Pinter, D., S. J. Ritchie, F. Doubal, T. Gattringer, Z. Morris, M. E. Bastin, C. V. H. M. Del, N. A. Royle, J. Corley, S. Munoz Maniega, A. Pattie, D. A. Dickie, J. Staals, A. J. Gow, J. M. Starr, I. J. Deary, C. Enzinger, F. Fazekas and J. Wardlaw (2017). "Impact of small vessel disease in the brain on gait and balance." Sci Rep **7**: 41637.
Pitsikas, N., A. E. Rigamonti, S. G. Cella, N. Sakellaridis and E. E. Muller (2005). "The nitric oxide donor molsidomine antagonizes age-related memory deficits in the rat." Neurobiol Aging **26**(2): 259-264.
Poirier, J. and C. Derouesne (1984). "Cerebral lacunae. A proposed new classification." Clin Neuropathol **3**(6): 266.
Pollock, H., M. Hutchings, R. O. Weller and E. T. Zhang (1997). "Perivascular spaces in the basal ganglia of the human brain: their relationship to lacunes." J Anat **191 (Pt 3)**: 337-346.
Polvikoski, T. M., E. C. van Straaten, F. Barkhof, R. Sulkava, H. J. Aronen, L. Niinisto, M. Oinas, P. Scheltens, T. Erkinjuntti and R. N. Kalaria (2010). "Frontal lobe white matter hyperintensities and neurofibrillary pathology in the oldest old." Neurology **75**(23): 2071-2078.
Potter, G., F. Doubal, C. Jackson, C. Sudlow, M. Dennis and J. Wardlaw (2010). "Associations of clinical stroke misclassification ('clinical-imaging dissociation') in acute ischemic stroke." Cerebrovasc Dis **29**(4): 395-402.
Potter, G. M., F. N. Doubal, C. A. Jackson, F. M. Chappell, C. L. Sudlow, M. S. Dennis and J. M. Wardlaw (2010). "Counting cavitating lacunes underestimates the burden of lacunar infarction." Stroke **41**(2): 267-272.
Potter, G. M., F. N. Doubal, C. A. Jackson, F. M. Chappell, C. L. Sudlow, M. S. Dennis and J. M. Wardlaw (2015). "Enlarged perivascular spaces and cerebral small vessel disease." Int J Stroke **10**(3): 376-381.
Potter, G. M., F. J. Marlborough and J. M. Wardlaw (2011). "Wide variation in definition, detection, and description of lacunar lesions on imaging." Stroke **42**(2): 359-366.
Preece, P. and N. J. Cairns (2003). "Quantifying mRNA in postmortem human brain: influence of gender, age at death, postmortem interval, brain pH, agonal state and inter-lobe mRNA variance." Brain Res Mol Brain Res **118**(1-2): 60-71.
Promjunyakul, N. O., H. H. Dodge, D. Lahna, E. L. Boespflug, J. A. Kaye, W. D. Rooney and L. C. Silbert (2018). "Baseline NAWM structural integrity and CBF predict periventricular WMH expansion over time." Neurology **90**(24): e2119-e2126.
Pullicino, P. M., L. L. Miller, A. V. Alexandrov and P. T. Ostrow (1995). "Infraputaminal 'lacunes'. Clinical and pathological correlations." Stroke **26**(9): 1598-1602.

Quick, S., J. Moss, R. M. Rajani and A. Williams (2021). "A Vessel for Change: Endothelial Dysfunction in Cerebral Small Vessel Disease." Trends Neurosci **44**(4): 289-305.
Radomski, M. W., R. M. Palmer and S. Moncada (1991). "Modulation of platelet aggregation by an L-arginine-nitric oxide pathway." Trends Pharmacol Sci **12**(3): 87-88.
Rajan, A. M., R. C. Ma, K. M. Kocha, D. J. Zhang and P. Huang (2020). "Dual function of perivascular fibroblasts in vascular stabilization in zebrafish." PLoS Genet **16**(10): e1008800.
Rajani, R. M., S. Quick, S. R. Ruigrok, D. Graham, S. E. Harris, B. F. J. Verhaaren, M. Fornage, S. Seshadri, S. S. Atanur, A. F. Dominiczak, C. Smith, J. M. Wardlaw and A. Williams (2018). "Reversal of endothelial dysfunction reduces white matter vulnerability in cerebral small vessel disease in rats." Sci Transl Med **10**(448).
Rajashekhar, G., A. Willuweit, C. E. Patterson, P. Sun, A. Hilbig, G. Breier, A. Helisch and M. Clauss (2006). "Continuous endothelial cell activation increases angiogenesis: evidence for the direct role of endothelium linking angiogenesis and inflammation." J Vasc Res **43**(2): 193-204.
Rannikmae, K., G. Davies, P. A. Thomson, S. Bevan, W. J. Devan, G. J. Falcone, M. Traylor, C. D. Anderson, T. W. Battey, F. Radmanesh, R. Deka, J. G. Woo, L. J. Martin, J. Jimenez-Conde, M. Selim, D. L. Brown, S. L. Silliman, C. S. Kidwell, J. Montaner, C. D. Langefeld, A. Slowik, B. M. Hansen, A. G. Lindgren, J. F. Meschia, M. Fornage, J. C. Bis, S. Debette, M. A. Ikram, W. T. Longstreth, R. Schmidt, C. R. Zhang, Q. Yang, P. Sharma, S. J. Kittner, B. D. Mitchell, E. G. Holliday, C. R. Levi, J. Attia, P. M. Rothwell, D. L. Poole, G. B. Boncoraglio, B. M. Psaty, R. Malik, N. Rost, B. B. Worrall, M. Dichgans, T. Van Agtmael, D. Woo, H. S. Markus, S. Seshadri, J. Rosand, C. L. Sudlow, M. Consortium, C. W. Group, I. I. G. S. Collaboration, W. M. H. i. I. S. G. S. Collaboration and C. International Stroke Genetics (2015). "Common variation in COL4A1/COL4A2 is associated with sporadic cerebral small vessel disease." Neurology **84**(9): 918-926.
Rashid, P. A., A. Whitehurst, N. Lawson and P. M. Bath (2003). "Plasma nitric oxide (nitrate/nitrite) levels in acute stroke and their relationship with severity and outcome." J Stroke Cerebrovasc Dis **12**(2): 82-87.
Ratelade, J., N. R. Klug, D. Lombardi, M. Angelim, F. Dabertrand, V. Domenga-Denier, R. Al-Shahi Salman, C. Smith, J. F. Gerbeau, M. T. Nelson and A. Joutel (2020). "Reducing Hypermuscularization of the Transitional Segment Between Arterioles and Capillaries Protects Against Spontaneous Intracerebral Hemorrhage." Circulation **141**(25): 2078-2094.
Reina-De La Torre, F., A. Rodriguez-Baeza and J. Sahuquillo-Barris (1998). "Morphological characteristics and distribution pattern of the arterial vessels in human cerebral cortex: a scanning electron microscope study." Anat Rec **251**(1): 87-96.
Revesz, T., C. P. Hawkins, E. P. du Boulay, R. O. Barnard and W. I. McDonald (1989). "Pathological findings correlated with magnetic resonance imaging in subcortical arteriosclerotic encephalopathy (Binswanger's disease)." Journal of Neurology, Neurosurgery & Psychiatry **52**(12): 1337-1344.

Revesz, T., J. L. Holton, B. Doshi, B. H. Anderton, F. Scaravilli and G. T. Plant (1999). "Cytoskeletal pathology in familial cerebral amyloid angiopathy (British type) with non-neuritic amyloid plaque formation." Acta Neuropathologica **97**(2): 170-176.
Reyahi, A., A. M. Nik, M. Ghiami, A. Gritli-Linde, F. Ponten, B. R. Johansson and P. Carlsson (2015). "Foxf2 Is Required for Brain Pericyte Differentiation and Development and Maintenance of the Blood-Brain Barrier." Dev Cell **34**(1): 19-32.
Rice, G., W. G. Newman, J. Dean, T. Patrick, R. Parmar, K. Flintoff, P. Robins, S. Harvey, T. Hollis, A. O'Hara, A. L. Herrick, A. P. Bowden, F. W. Perrino, T. Lindahl, D. E. Barnes and Y. J. Crow (2007). "Heterozygous mutations in TREX1 cause familial chilblain lupus and dominant Aicardi-Goutieres syndrome." Am J Hum Genet **80**(4): 811-815.
Richardson, W. D., K. M. Young, R. B. Tripathi and I. McKenzie (2011). "NG2-glia as multipotent neural stem cells: fact or fantasy?" Neuron **70**(4): 661-673.
Ringstad, G., L. M. Valnes, A. M. Dale, A. H. Pripp, S. S. Vatnehol, K. E. Emblem, K. A. Mardal and P. K. Eide (2018). "Brain-wide glymphatic enhancement and clearance in humans assessed with MRI." JCI Insight **3**(13).
Ringstad, G., S. A. S. Vatnehol and P. K. Eide (2017). "Glymphatic MRI in idiopathic normal pressure hydrocephalus." Brain **140**(10): 2691-2705.
Ritchie, S. J., D. A. Dickie, S. R. Cox, C. Valdes Hernandez Mdel, J. Corley, N. A. Royle, A. Pattie, B. S. Aribisala, P. Redmond, S. Munoz Maniega, A. M. Taylor, R. Sibbett, A. J. Gow, J. M. Starr, M. E. Bastin, J. M. Wardlaw and I. J. Deary (2015). "Brain volumetric changes and cognitive ageing during the eighth decade of life." Hum Brain Mapp **36**(12): 4910-4925.
Robinson, K. A., C. A. Stewart, Q. N. Pye, X. Nguyen, L. Kenney, S. Salzman, R. A. Floyd and K. Hensley (1999). "Redox-sensitive protein phosphatase activity regulates the phosphorylation state of p38 protein kinase in primary astrocyte culture." J Neurosci Res **55**(6): 724-732.
Rodrigues, M. A., N. Samarasekera, C. Lerpiniere, C. Humphreys, M. O. McCarron, P. M. White, J. A. R. Nicoll, C. L. M. Sudlow, C. Cordonnier, J. M. Wardlaw, C. Smith and R. Al-Shahi Salman (2018). "The Edinburgh CT and genetic diagnostic criteria for lobar intracerebral haemorrhage associated with cerebral amyloid angiopathy: model development and diagnostic test accuracy study." Lancet Neurol **17**(3): 232-240.
Rodriguez-Arellano, J. J., V. Parpura, R. Zorec and A. Verkhratsky (2016). "Astrocytes in physiological aging and Alzheimer's disease." Neuroscience **323**: 170-182.
Rosenberg, G. A., N. Sullivan and M. M. Esiri (2001). "White matter damage is associated with matrix metalloproteinases in vascular dementia." Stroke **32**(5): 1162-1168.
Rosenblum, W. I. (2008). "Fibrinoid necrosis of small brain arteries and arterioles and miliary aneurysms as causes of hypertensive hemorrhage: a critical reappraisal." Acta Neuropathol **116**(4): 361-369.
Rosenstein, J. M., J. M. Krum and C. Ruhrberg (2010). "VEGF in the nervous system." Organogenesis **6**(2): 107-114.

Russ, T. C., M. A. Parra, A. E. Lim, E. Law, P. J. Connelly and J. M. Starr (2015). "Prediction of general hospital admission in people with dementia: cohort study." Br J Psychiatry **206**(2): 153-159.
Sagare, A. P., R. D. Bell, Z. Zhao, Q. Ma, E. A. Winkler, A. Ramanathan and B. V. Zlokovic (2013). "Pericyte loss influences Alzheimer-like neurodegeneration in mice." Nat Commun **4**: 2932.
Sagare, A. P., M. D. Sweeney, J. Makshanoff and B. V. Zlokovic (2015). "Shedding of soluble platelet-derived growth factor receptor-beta from human brain pericytes." Neurosci Lett **607**: 97-101.
Salat, D. H., R. L. Buckner, A. Z. Snyder, D. N. Greve, R. S. Desikan, E. Busa, J. C. Morris, A. M. Dale and B. Fischl (2004). "Thinning of the cerebral cortex in aging." Cereb Cortex **14**(7): 721-730.
Sam, K., A. P. Crawley, J. Conklin, J. Poublanc, O. Sobczyk, D. M. Mandell, L. Venkatraghavan, J. Duffin, J. A. Fisher, S. E. Black and D. J. Mikulis (2016). "Development of White Matter Hyperintensity Is Preceded by Reduced Cerebrovascular Reactivity." Ann Neurol **80**(2): 277-285.
Samarasekera, N., A. Fonville, C. Lerpiniere, A. J. Farrall, J. M. Wardlaw, P. M. White, C. Smith, R. Al-Shahi Salman and C. Lothian Audit of the Treatment of Cerebral Haemorrhage (2015). "Influence of intracerebral hemorrhage location on incidence, characteristics, and outcome: population-based study." Stroke **46**(2): 361-368.
Samarasekera, N., C. Lerpiniere, A. F. Fonville, A. J. Farrall, J. M. Wardlaw, P. M. White, A. Torgersen, J. W. Ironside, C. Smith, R. Al-Shahi Salman and c. Lothian Audit of the Treatment of Cerebral Haemorrhage (2015). "Consent for Brain Tissue Donation after Intracerebral Haemorrhage: A Community-Based Study." PLoS One **10**(8): e0135043.
Samarasekera, N., C. Smith and R. Al-Shahi Salman (2012). "The association between cerebral amyloid angiopathy and intracerebral haemorrhage: systematic review and meta-analysis." J Neurol Neurosurg Psychiatry **83**(3): 275-281.
Scarpelli, M., U. Salvolini, L. Diamanti, R. Montironi, L. Chiaromoni and M. Maricotti (1994). "MRI and pathological examination of post-mortem brains: the problem of white matter high signal areas." Neuroradiology **36**(5): 393-398.
Schafer, K. A., J. Eighmy, J. D. Fikes, W. G. Halpern, R. R. Hukkanen, G. G. Long, E. K. Meseck, D. J. Patrick, M. S. Thibodeau, C. E. Wood and S. Francke (2018). "Use of Severity Grades to Characterize Histopathologic Changes." Toxicol Pathol **46**(3): 256-265.
Scheltens, P., F. Barkhof, D. Leys, E. C. Wolters, R. Ravid and W. Kamphorst (1995). "Histopathologic correlates of white matter changes on MRI in Alzheimer's disease and normal aging." Neurology **45**(5): 883-888.
Schini, V. B., W. Durante, E. Elizondo, T. Scott-Burden, D. C. Junquero, A. I. Schafer and P. M. Vanhoutte (1992). "The induction of nitric oxide synthase activity is inhibited by TGF-beta 1, PDGFAB and PDGFBB in vascular smooth muscle cells." Eur J Pharmacol **216**(3): 379-383.
Schmidt, H., M. Zeginigg, M. Wiltgen, P. Freudenberger, K. Petrovic, M. Cavalieri, P. Gider, C. Enzinger, M. Fornage, S. Debette, J. I. Rotter, M. A. Ikram, L. J. Launer, R. Schmidt and C. c. N. w. group (2011). "Genetic variants of the NOTCH3 gene in the

elderly and magnetic resonance imaging correlates of age-related cerebral small vessel disease." Brain **134**(Pt 11): 3384-3397.
Schmidt, R., S. Seiler and M. Loitfelder (2016). "Longitudinal change of small-vessel disease-related brain abnormalities." J Cereb Blood Flow Metab **36**(1): 26-39.
Schonfelder, U., A. Hofer, M. Paul and R. H. Funk (1998). "In situ observation of living pericytes in rat retinal capillaries." Microvasc Res **56**(1): 22-29.
Schrag, M., G. McAuley, J. Pomakian, A. Jiffry, S. Tung, C. Mueller, H. V. Vinters, E. M. Haacke, B. Holshouser, D. Kido and W. M. Kirsch (2010). "Correlation of hypointensities in susceptibility-weighted images to tissue histology in dementia patients with cerebral amyloid angiopathy: a postmortem MRI study." Acta Neuropathol **119**(3): 291-302.
Schroeder, A., O. Mueller, S. Stocker, R. Salowsky, M. Leiber, M. Gassmann, S. Lightfoot, W. Menzel, M. Granzow and T. Ragg (2006). "The RIN: an RNA integrity number for assigning integrity values to RNA measurements." BMC Mol Biol **7**: 3.
Schweser, F., A. Deistung, B. W. Lehr and J. R. Reichenbach (2010). "Differentiation between diamagnetic and paramagnetic cerebral lesions based on magnetic susceptibility mapping." Med Phys **37**(10): 5165-5178.
Sengillo, J. D., E. A. Winkler, C. T. Walker, J. S. Sullivan, M. Johnson and B. V. Zlokovic (2013). "Deficiency in mural vascular cells coincides with blood-brain barrier disruption in Alzheimer's disease." Brain Pathol **23**(3): 303-310.
Serlin, Y., I. Shelef, B. Knyazer and A. Friedman (2015). "Anatomy and physiology of the blood-brain barrier." Semin Cell Dev Biol **38**: 2-6.
Sharif, Y., F. Jumah, L. Coplan, A. Krosser, K. Sharif and R. S. Tubbs (2018). "Blood brain barrier: A review of its anatomy and physiology in health and disease." Clin Anat **31**(6): 812-823.
Shepro, D. and N. M. Morel (1993). "Pericyte physiology." FASEB J **7**(11): 1031-1038.
Shi, Y., M. J. Thrippleton, G. W. Blair, D. A. Dickie, I. Marshall, I. Hamilton, F. N. Doubal, F. Chappell and J. M. Wardlaw (2020). "Small vessel disease is associated with altered cerebrovascular pulsatility but not resting cerebral blood flow." J Cereb Blood Flow Metab **40**(1): 85-99.
Shi, Y., M. J. Thrippleton, S. D. Makin, I. Marshall, M. I. Geerlings, A. J. M. de Craen, M. A. van Buchem and J. M. Wardlaw (2016). "Cerebral blood flow in small vessel disease: A systematic review and meta-analysis." J Cereb Blood Flow Metab **36**(10): 1653-1667.
Shi, Y. and J. M. Wardlaw (2016). "Update on cerebral small vessel disease: a dynamic whole-brain disease." Stroke Vasc Neurol **1**(3): 83-92.
Shiga, A., H. Nozaki, A. Yokoseki, M. Nihonmatsu, H. Kawata, T. Kato, A. Koyama, K. Arima, M. Ikeda, S. Katada, Y. Toyoshima, H. Takahashi, A. Tanaka, I. Nakano, T. Ikeuchi, M. Nishizawa and O. Onodera (2011). "Cerebral small-vessel disease protein HTRA1 controls the amount of TGF-beta1 via cleavage of proTGF-beta1." Hum Mol Genet **20**(9): 1800-1810.
Shimizu, F., Y. Sano, O. Tominaga, T. Maeda, M. A. Abe and T. Kanda (2013). "Advanced glycation end-products disrupt the blood-brain barrier by stimulating the release of transforming growth factor-beta by pericytes and vascular endothelial

growth factor and matrix metalloproteinase-2 by endothelial cells in vitro." Neurobiol Aging **34**(7): 1902-1912.
Shoamanesh, A., C. S. Kwok and O. Benavente (2011). "Cerebral microbleeds: histopathological correlation of neuroimaging." Cerebrovasc Dis **32**(6): 528-534.
Shokri-Kojori, E., G. J. Wang, C. E. Wiers, S. B. Demiral, M. Guo, S. W. Kim, E. Lindgren, V. Ramirez, A. Zehra, C. Freeman, G. Miller, P. Manza, T. Srivastava, S. De Santi, D. Tomasi, H. Benveniste and N. D. Volkow (2018). "beta-Amyloid accumulation in the human brain after one night of sleep deprivation." Proc Natl Acad Sci U S A **115**(17): 4483-4488.
Siegenthaler, J. A., Y. Choe, K. P. Patterson, I. Hsieh, D. Li, S. C. Jaminet, R. Daneman, T. Kume, E. J. Huang and S. J. Pleasure (2013). "Foxc1 is required by pericytes during fetal brain angiogenesis." Biol Open **2**(7): 647-659.
Sierra, A., J. M. Encinas, J. J. Deudero, J. H. Chancey, G. Enikolopov, L. S. Overstreet-Wadiche, S. E. Tsirka and M. Maletic-Savatic (2010). "Microglia shape adult hippocampal neurogenesis through apoptosis-coupled phagocytosis." Cell Stem Cell **7**(4): 483-495.
Simpson, I. A., S. J. Vannucci, M. R. DeJoseph and R. A. Hawkins (2001). "Glucose transporter asymmetries in the bovine blood-brain barrier." J Biol Chem **276**(16): 12725-12729.
Simpson, J. E., M. S. Fernando, L. Clark, P. G. Ince, F. Matthews, G. Forster, J. T. O'Brien, R. Barber, R. N. Kalaria, C. Brayne, P. J. Shaw, C. E. Lewis, S. B. Wharton, M. R. C. C. Function and G. Ageing Neuropathology Study (2007). "White matter lesions in an unselected cohort of the elderly: astrocytic, microglial and oligodendrocyte precursor cell responses." Neuropathology & Applied Neurobiology **33**(4): 410-419.
Simpson, J. E., P. G. Ince, C. E. Higham, C. H. Gelsthorpe, M. S. Fernando, F. Matthews, G. Forster, J. T. O'Brien, R. Barber, R. N. Kalaria, C. Brayne, P. J. Shaw, K. Stoeber, G. H. Williams, C. E. Lewis, S. B. Wharton, M. R. C. C. Function and G. Ageing Neuropathology Study (2007). "Microglial activation in white matter lesions and nonlesional white matter of ageing brains." Neuropathology & Applied Neurobiology **33**(6): 670-683.
Simpson, J. E., S. B. Wharton, J. Cooper, C. Gelsthorpe, L. Baxter, G. Forster, P. J. Shaw, G. Savva, F. E. Matthews, C. Brayne and P. G. Ince (2010). "Alterations of the blood-brain barrier in cerebral white matter lesions in the ageing brain." Neurosci Lett **486**(3): 246-251.
Sironi, L., U. Guerrini, E. Tremoli, I. Miller, P. Gelosa, A. Lascialfari, I. Zucca, I. Eberini, M. Gemeiner, R. Paoletti and E. Gianazza (2004). "Analysis of pathological events at the onset of brain damage in stroke-prone rats: a proteomics and magnetic resonance imaging approach." J Neurosci Res **78**(1): 115-122.
Sironi, L., E. Tremoli, I. Miller, U. Guerrini, A. M. Calvio, I. Eberini, M. Gemeiner, M. Asdente, R. Paoletti and E. Gianazza (2001). "Acute-phase proteins before cerebral ischemia in stroke-prone rats: identification by proteomics." Stroke **32**(3): 753-760.
Skrobot, O. A., J. Attems, M. Esiri, T. Hortobagyi, J. W. Ironside, R. N. Kalaria, A. King, G. A. Lammie, D. Mann, J. Neal, Y. Ben-Shlomo, P. G. Kehoe and S. Love (2016). "Vascular cognitive impairment neuropathology guidelines (VCING): the contribution of cerebrovascular pathology to cognitive impairment." Brain.

Smallwood, A., A. Oulhaj, C. Joachim, S. Christie, C. Sloan, A. D. Smith and M. Esiri (2012). "Cerebral subcortical small vessel disease and its relation to cognition in elderly subjects: a pathological study in the Oxford Project to Investigate Memory and Ageing (OPTIMA) cohort." Neuropathol Appl Neurobiol **38**(4): 337-343.
Smith, C. D., D. Snowdon and W. R. Markesbery (2000). "Periventricular white matter hyperintensities on MRI: correlation with neuropathologic findings." Journal of Neuroimaging **10**(1): 13-16.
Smith, C. D., D. A. Snowdon, H. Wang and W. R. Markesbery (2000). "White matter volumes and periventricular white matter hyperintensities in aging and dementia." Neurology **54**(4): 838-842.
Smith, E. E. and F. Eichler (2006). "Cerebral amyloid angiopathy and lobar intracerebral hemorrhage." Arch Neurol **63**(1): 148-151.
Smith, E. E., J. A. Schneider, J. M. Wardlaw and S. M. Greenberg (2012). "Cerebral microinfarcts: the invisible lesions." Lancet Neurology **11**(3): 272-282.
Sobel, R. A., J. M. Greer, J. Isaac, G. Fondren and M. B. Lees (1994). "Immunolocalization of proteolipid protein peptide 103-116 in myelin." J Neurosci Res **37**(1): 36-43.
Sohet, F., C. Lin, R. N. Munji, S. Y. Lee, N. Ruderisch, A. Soung, T. D. Arnold, N. Derugin, Z. S. Vexler, F. T. Yen and R. Daneman (2015). "LSR/angulin-1 is a tricellular tight junction protein involved in blood-brain barrier formation." J Cell Biol **208**(6): 703-711.
Sorokin, L. (2010). "The impact of the extracellular matrix on inflammation." Nat Rev Immunol **10**(10): 712-723.
Sperling, R., S. Salloway, D. J. Brooks, D. Tampieri, J. Barakos, N. C. Fox, M. Raskind, M. Sabbagh, L. S. Honig, A. P. Porsteinsson, I. Lieberburg, H. M. Arrighi, K. A. Morris, Y. Lu, E. Liu, K. M. Gregg, H. R. Brashear, G. G. Kinney, R. Black and M. Grundman (2012). "Amyloid-related imaging abnormalities in patients with Alzheimer's disease treated with bapineuzumab: a retrospective analysis." Lancet Neurol **11**(3): 241-249.
Staals, J., T. Booth, Z. Morris, M. E. Bastin, A. J. Gow, J. Corley, P. Redmond, J. M. Starr, I. J. Deary and J. M. Wardlaw (2015). "Total MRI load of cerebral small vessel disease and cognitive ability in older people." Neurobiol Aging **36**(10): 2806-2811.
Staals, J., S. D. Makin, F. N. Doubal, M. S. Dennis and J. M. Wardlaw (2014). "Stroke subtype, vascular risk factors, and total MRI brain small-vessel disease burden.[Summary for patients in Neurology. 2014 Sep 30;83(14):e138-40; PMID: 25267990]." Neurology **83**(14): 1228-1234.
Stam, A. H., P. H. Kothari, A. Shaikh, A. Gschwendter, J. C. Jen, S. Hodgkinson, T. A. Hardy, M. Hayes, P. A. Kempster, K. E. Kotschet, I. M. Bajema, S. G. van Duinen, M. L. C. Maat-Schieman, P. de Jong, M. D. de Smet, D. de Wolff-Rouendaal, G. Dijkman, N. Pelzer, G. R. Kolar, R. E. Schmidt, J. Lacey, D. Joseph, D. R. Fintak, M. G. Grand, E. M. Brunt, H. Liapis, R. A. Hajj-Ali, M. C. Kruit, M. A. van Buchem, M. Dichgans, R. R. Frants, A. van den Maagdenberg, J. Haan, R. W. Baloh, J. P. Atkinson, G. M. Terwindt and M. D. Ferrari (2016). "Retinal vasculopathy with cerebral leukoencephalopathy and systemic manifestations." Brain **139**(11): 2909-2922.

Stan, A. D., S. Ghose, X. M. Gao, R. C. Roberts, K. Lewis-Amezcua, K. J. Hatanpaa and C. A. Tamminga (2006). "Human postmortem tissue: what quality markers matter?" Brain Res **1123**(1): 1-11.
Stanimirovic, D. B. and A. Friedman (2012). "Pathophysiology of the neurovascular unit: disease cause or consequence?" J Cereb Blood Flow Metab **32**(7): 1207-1221.
Stern, Y. (2012). "Cognitive reserve in ageing and Alzheimer's disease." Lancet Neurol **11**(11): 1006-1012.
Sternberger, N. H., Y. Itoyama, M. W. Kies and H. D. Webster (1978). "Myelin basic protein demonstrated immunocytochemically in oligodendroglia prior to myelin sheath formation." Proc Natl Acad Sci U S A **75**(5): 2521-2524.
Sternberger, N. H., R. H. Quarles, Y. Itoyama and H. D. Webster (1979). "Myelin-associated glycoprotein demonstrated immunocytochemically in myelin and myelin-forming cells of developing rat." Proc Natl Acad Sci U S A **76**(3): 1510-1514.
Stetson, D. B., J. S. Ko, T. Heidmann and R. Medzhitov (2008). "Trex1 prevents cell-intrinsic initiation of autoimmunity." Cell **134**(4): 587-598.
Streit, W. J., Q. S. Xue, J. Tischer and I. Bechmann (2014). "Microglial pathology." Acta Neuropathol Commun **2**: 142.
Strozyk, D., D. W. Dickson, R. B. Lipton, M. Katz, C. A. Derby, S. Lee, C. Wang and J. Verghese (2010). "Contribution of vascular pathology to the clinical expression of dementia." Neurobiol Aging **31**(10): 1710-1720.
Summers, P. M., D. A. Hartmann, E. S. Hui, X. Nie, R. L. Deardorff, E. T. McKinnon, J. A. Helpern, J. H. Jensen and A. Y. Shih (2017). "Functional deficits induced by cortical microinfarcts." J Cereb Blood Flow Metab **37**(11): 3599-3614.
Swartz, R. H., D. T. Stuss, F. Gao and S. E. Black (2008). "Independent cognitive effects of atrophy and diffuse subcortical and thalamico-cortical cerebrovascular disease in dementia." Stroke **39**(3): 822-830.
Tagami, M., Y. Nara, A. Kubota, H. Fujino and Y. Yamori (1990). "Ultrastructural changes in cerebral pericytes and astrocytes of stroke-prone spontaneously hypertensive rats." Stroke **21**(7): 1064-1071.
Tallini, Y. N., J. F. Brekke, B. Shui, R. Doran, S. M. Hwang, J. Nakai, G. Salama, S. S. Segal and M. I. Kotlikoff (2007). "Propagated endothelial Ca2+ waves and arteriolar dilation in vivo: measurements in Cx40BAC GCaMP2 transgenic mice." Circ Res **101**(12): 1300-1309.
Tan, R. Y. and H. S. Markus (2015). "Monogenic causes of stroke: now and the future." J Neurol **262**(12): 2601-2616.
Tanaka, A., Y. Ueno, Y. Nakayama, K. Takano and S. Takebayashi (1999). "Small chronic hemorrhages and ischemic lesions in association with spontaneous intracerebral hematomas." Stroke **30**(8): 1637-1642.
Tao, G., P. C. Kahr, Y. Morikawa, M. Zhang, M. Rahmani, T. R. Heallen, L. Li, Z. Sun, E. N. Olson, B. A. Amendt and J. F. Martin (2016). "Pitx2 promotes heart repair by activating the antioxidant response after cardiac injury." Nature **534**(7605): 119-123.
Taoka, T., Y. Masutani, H. Kawai, T. Nakane, K. Matsuoka, F. Yasuno, T. Kishimoto and S. Naganawa (2017). "Evaluation of glymphatic system activity with the

diffusion MR technique: diffusion tensor image analysis along the perivascular space (DTI-ALPS) in Alzheimer's disease cases." Jpn J Radiol **35**(4): 172-178.
Tatsumi, S., M. Shinohara and T. Yamamoto (2008). "Direct comparison of histology of microbleeds with postmortem MR images: a case report." Cerebrovasc Dis **26**(2): 142-146.
Tay, T. L., M. Carrier and M. È. Tremblay (2019). Physiology of Microglia. In: Neuroglia in Neurodegenerative Diseases. Advances in Experimental Medicine and Biology. A. Verkhratsky, M. Ho, R. Zorec and V. Parpura. Singapore, Springer. **1175**.
Tay, T. L., J. C. Savage, C. W. Hui, K. Bisht and M. E. Tremblay (2017). "Microglia across the lifespan: from origin to function in brain development, plasticity and cognition." J Physiol **595**(6): 1929-1945.
ten Dam, V. H., D. M. van den Heuvel, A. J. de Craen, E. L. Bollen, H. M. Murray, R. G. Westendorp, G. J. Blauw and M. A. van Buchem (2007). "Decline in total cerebral blood flow is linked with increase in periventricular but not deep white matter hyperintensities." Radiology **243**(1): 198-203.
Thal, D. R., L. T. Grinberg and J. Attems (2012). "Vascular dementia: different forms of vessel disorders contribute to the development of dementia in the elderly brain." Exp Gerontol **47**(11): 816-824.
Thal, D. R., U. Rub, M. Orantes and H. Braak (2002). "Phases of A beta-deposition in the human brain and its relevance for the development of AD." Neurology **58**(12): 1791-1800.
Thomas, T., S. Miners and S. Love (2015). "Post-mortem assessment of hypoperfusion of cerebral cortex in Alzheimer's disease and vascular dementia." Brain **138**(Pt 4): 1059-1069.
Thomas TL, M. S., Kehoe PG, Love S (2015). "Correlation between levels of VEGF and insoluble A beta(1-42) in the cerebral cortex in Alzheimer's disease (conference paper)." Neuropathology and Applied Neurobiology **41**: 22.
Thomsen, M. S., L. J. Routhe and T. Moos (2017). "The vascular basement membrane in the healthy and pathological brain." J Cereb Blood Flow Metab **37**(10): 3300-3317.
Thyboll, J., J. Kortesmaa, R. Cao, R. Soininen, L. Wang, A. Iivanainen, L. Sorokin, M. Risling, Y. Cao and K. Tryggvason (2002). "Deletion of the laminin alpha4 chain leads to impaired microvessel maturation." Mol Cell Biol **22**(4): 1194-1202.
Tomimoto, H., I. Akiguchi, T. Suenaga, M. Nishimura, H. Wakita, S. Nakamura and J. Kimura (1996). "Alterations of the blood-brain barrier and glial cells in white-matter lesions in cerebrovascular and Alzheimer's disease patients." Stroke **27**(11): 2069-2074.
Tomimoto, H., I. Akiguchi, H. Wakita, J. X. Lin and H. Budka (2000). "Cyclooxygenase-2 is induced in microglia during chronic cerebral ischemia in humans." Acta Neuropathol **99**(1): 26-30.
Tomita, H., M. P. Vawter, D. M. Walsh, S. J. Evans, P. V. Choudary, J. Li, K. M. Overman, M. E. Atz, R. M. Myers, E. G. Jones, S. J. Watson, H. Akil and W. E. Bunney, Jr. (2004). "Effect of agonal and postmortem factors on gene expression profile: quality control in microarray analyses of postmortem human brain." Biol Psychiatry **55**(4): 346-352.

Topakian, R., T. R. Barrick, F. A. Howe and H. S. Markus (2010). "Blood-brain barrier permeability is increased in normal-appearing white matter in patients with lacunar stroke and leucoaraiosis." Journal of Neurology, Neurosurgery & Psychiatry **81**(2): 192-197.
Torres, J., C. Loomis, B. Cucchiara, M. Smith and S. Messe (2016). "Diagnostic Yield and Safety of Brain Biopsy for Suspected Primary Central Nervous System Angiitis." Stroke **47**(8): 2127-2129.
Traylor, M., L. C. Rutten-Jacobs, V. Thijs, E. G. Holliday, C. Levi, S. Bevan, R. Malik, G. Boncoraglio, C. Sudlow, P. M. Rothwell, M. Dichgans and H. S. Markus (2016). "Genetic Associations With White Matter Hyperintensities Confer Risk of Lacunar Stroke." Stroke **47**(5): 1174-1179.
Traylor, M., C. R. Zhang, P. Adib-Samii, W. J. Devan, O. E. Parsons, S. Lanfranconi, S. Gregory, L. Cloonan, G. J. Falcone, F. Radmanesh, K. Fitzpatrick, A. Kanakis, T. R. Barrick, B. Moynihan, C. M. Lewis, G. B. Boncoraglio, R. Lemmens, V. Thijs, C. Sudlow, J. Wardlaw, P. M. Rothwell, J. F. Meschia, B. B. Worrall, C. Levi, S. Bevan, K. L. Furie, M. Dichgans, J. Rosand, H. S. Markus, N. Rost and C. International Stroke Genetics (2016). "Genome-wide meta-analysis of cerebral white matter hyperintensities in patients with stroke." Neurology **86**(2): 146-153.
Tsai, H. H., J. Niu, R. Munji, D. Davalos, J. Chang, H. Zhang, A. C. Tien, C. J. Kuo, J. R. Chan, R. Daneman and S. P. Fancy (2016). "Oligodendrocyte precursors migrate along vasculature in the developing nervous system." Science **351**(6271): 379-384.
Tschudi, M. R., M. Barton, N. A. Bersinger, P. Moreau, F. Cosentino, G. Noll, T. Malinski and T. F. Luscher (1996). "Effect of age on kinetics of nitric oxide release in rat aorta and pulmonary artery." J Clin Invest **98**(4): 899-905.
Tsim, S., C. A. Humphreys, G. W. Cowell, D. B. Stobo, C. Noble, R. Woodward, C. A. Kelly, L. Alexander, J. E. Foster, C. Dick and K. G. Blyth (2018). "Early Contrast Enhancement: A novel magnetic resonance imaging biomarker of pleural malignancy." Lung Cancer **118**: 48-56.
Tsukita, S., T. Katsuno, Y. Yamazaki, K. Umeda, A. Tamura and S. Tsukita (2009). "Roles of ZO-1 and ZO-2 in establishment of the belt-like adherens and tight junctions with paracellular permselective barrier function." Ann N Y Acad Sci **1165**: 44-52.
Uemura, M., H. Nozaki, T. Kato, A. Koyama, N. Sakai, S. Ando, M. Kanazawa, N. Hishikawa, Y. Nishimoto, K. Polavarapu, A. Nalini, A. Hanazono, D. Kuzume, A. Shindo, M. El-Ghanem, A. Abe, A. Sato, M. Yoshida, T. Ikeuchi, I. Mizuta, T. Mizuno and O. Onodera (2020). "HTRA1-Related Cerebral Small Vessel Disease: A Review of the Literature." Front Neurol **11**: 545.
Ueno, M., Y. Fujita, T. Tanaka, Y. Nakamura, J. Kikuta, M. Ishii and T. Yamashita (2013). "Layer V cortical neurons require microglial support for survival during postnatal development." Nat Neurosci **16**(5): 543-551.
Uiterwijk, R., M. Huijts, J. Staals, A. Duits, E. Gronenschild, A. A. Kroon, P. W. de Leeuw and R. J. van Oostenbrugge (2014). "Subjective cognitive failures in patients with hypertension are related to cognitive performance and cerebral microbleeds." Hypertension **64**(3): 653-657.

Uspenskaia, O., M. Liebetrau, J. Herms, A. Danek and G. F. Hamann (2004). "Aging is associated with increased collagen type IV accumulation in the basal lamina of human cerebral microvessels." BMC Neurosci **5**: 37.
Vahedi, K. and S. Alamowitch (2011). "Clinical spectrum of type IV collagen (COL4A1) mutations: a novel genetic multisystem disease." Curr Opin Neurol **24**(1): 63-68.
Valdes Hernandez Mdel, C., P. A. Armitage, M. J. Thrippleton, F. Chappell, E. Sandeman, S. Munoz Maniega, K. Shuler and J. M. Wardlaw (2015). "Rationale, design and methodology of the image analysis protocol for studies of patients with cerebral small vessel disease and mild stroke." Brain Behav **5**(12): e00415.
van Dalen, J. W., E. E. Scuric, S. J. van Veluw, M. W. Caan, A. J. Nederveen, G. J. Biessels, W. A. van Gool and E. Richard (2015). "Cortical microinfarcts detected in vivo on 3 Tesla MRI: clinical and radiological correlates." Stroke **46**(1): 255-257.
van der Holst, H. M., I. W. van Uden, A. M. Tuladhar, K. F. de Laat, A. G. van Norden, D. G. Norris, E. J. van Dijk, R. A. Esselink, B. Platel and F. E. de Leeuw (2015). "Cerebral small vessel disease and incident parkinsonism: The RUN DMC study." Neurology **85**(18): 1569-1577.
van der Veen, P. H., M. Muller, K. L. Vincken, J. Hendrikse, W. P. Mali, Y. van der Graaf, M. I. Geerlings and S. S. Group (2015). "Longitudinal relationship between cerebral small-vessel disease and cerebral blood flow: the second manifestations of arterial disease-magnetic resonance study." Stroke **46**(5): 1233-1238.
van der Veen, P. H., M. Muller, K. L. Vincken, T. D. Witkamp, W. P. Mali, Y. van der Graaf, M. I. Geerlings and S.-M. S. Group (2014). "Longitudinal changes in brain volumes and cerebrovascular lesions on MRI in patients with manifest arterial disease: the SMART-MR study." Journal of the Neurological Sciences **337**(1-2): 112-118.
van Dijk, E. J., M. M. Breteler, R. Schmidt, K. Berger, L. G. Nilsson, M. Oudkerk, A. Pajak, S. Sans, M. de Ridder, C. Dufouil, R. Fuhrer, S. Giampaoli, L. J. Launer, A. Hofman and C. Consortium (2004). "The association between blood pressure, hypertension, and cerebral white matter lesions: cardiovascular determinants of dementia study." Hypertension **44**(5): 625-630.
van Dijk, E. J., N. D. Prins, H. A. Vrooman, A. Hofman, P. J. Koudstaal and M. M. Breteler (2008). "Progression of cerebral small vessel disease in relation to risk factors and cognitive consequences: Rotterdam Scan study." Stroke **39**(10): 2712-2719.
Van Itallie, C. M. and J. M. Anderson (2006). "Claudins and epithelial paracellular transport." Annu Rev Physiol **68**: 403-429.
van Leijsen, E. M. C., I. W. M. van Uden, M. Ghafoorian, M. I. Bergkamp, V. Lohner, E. C. M. Kooijmans, H. M. van der Holst, A. M. Tuladhar, D. G. Norris, E. J. van Dijk, L. C. A. Rutten-Jacobs, B. Platel, C. J. M. Klijn and F. E. de Leeuw (2017). "Nonlinear temporal dynamics of cerebral small vessel disease: The RUN DMC study." Neurology **89**(15): 1569-1577.
van Norden, A. G., K. F. de Laat, R. A. Gons, I. W. van Uden, E. J. van Dijk, L. J. van Oudheusden, R. A. Esselink, B. R. Bloem, B. G. van Engelen, M. J. Zwarts, I. Tendolkar, M. G. Olde-Rikkert, M. J. van der Vlugt, M. P. Zwiers, D. G. Norris and F.

E. de Leeuw (2011). "Causes and consequences of cerebral small vessel disease. The RUN DMC study: a prospective cohort study. Study rationale and protocol." BMC Neurol **11**: 29.
van Swieten, J. C., J. H. van den Hout, B. A. van Ketel, A. Hijdra, J. H. Wokke and J. van Gijn (1991). "Periventricular lesions in the white matter on magnetic resonance imaging in the elderly. A morphometric correlation with arteriolosclerosis and dilated perivascular spaces." Brain **114 (Pt 2)**: 761-774.
van Veluw, S. J., K. Arfanakis and J. A. Schneider (2022). "Neuropathology of Vascular Brain Health: Insights From Ex Vivo Magnetic Resonance Imaging-Histopathology Studies in Cerebral Small Vessel Disease." Stroke **53**(2): 404-415.
van Veluw, S. J., G. J. Biessels, W. H. Bouvy, W. G. Spliet, J. J. Zwanenburg, P. R. Luijten, E. A. Macklin, A. J. Rozemuller, M. E. Gurol, S. M. Greenberg, A. Viswanathan and S. Martinez-Ramirez (2016). "Cerebral amyloid angiopathy severity is linked to dilation of juxtacortical perivascular spaces." Journal of Cerebral Blood Flow & Metabolism **36**(3): 576-580.
van Veluw, S. J., G. J. Biessels, C. J. Klijn and A. J. Rozemuller (2016). "Heterogeneous histopathology of cortical microbleeds in cerebral amyloid angiopathy." Neurology.
van Veluw, S. J., A. Charidimou, A. J. van der Kouwe, A. Lauer, Y. D. Reijmer, I. Costantino, M. E. Gurol, G. J. Biessels, M. P. Frosch, A. Viswanathan and S. M. Greenberg (2016). "Microbleed and microinfarct detection in amyloid angiopathy: a high-resolution MRI-histopathology study." Brain **139**(Pt 12): 3151-3162.
van Veluw, S. J., Y. D. Reijmer, A. J. van der Kouwe, A. Charidimou, G. A. Riley, A. Leemans, B. J. Bacskai, M. P. Frosch, A. Viswanathan and S. M. Greenberg (2019). "Histopathology of diffusion imaging abnormalities in cerebral amyloid angiopathy." Neurology **92**(9): e933-e943.
van Veluw, S. J., A. Y. Shih, E. E. Smith, C. Chen, J. A. Schneider, J. M. Wardlaw, S. M. Greenberg and G. J. Biessels (2017). "Detection, risk factors, and functional consequences of cerebral microinfarcts." Lancet Neurol **16**(9): 730-740.
van Veluw, S. J., J. J. Zwanenburg, J. Engelen-Lee, W. G. Spliet, J. Hendrikse, P. R. Luijten and G. J. Biessels (2013). "In vivo detection of cerebral cortical microinfarcts with high-resolution 7T MRI." Journal of Cerebral Blood Flow & Metabolism **33**(3): 322-329.
van Veluw, S. J., J. J. Zwanenburg, A. J. Rozemuller, P. R. Luijten, W. G. Spliet and G. J. Biessels (2015). "The spectrum of MR detectable cortical microinfarcts: a classification study with 7-tesla postmortem MRI and histopathology." J Cereb Blood Flow Metab **35**(4): 676-683.
Vanlandewijck, M., L. He, M. A. Mae, J. Andrae, K. Ando, F. Del Gaudio, K. Nahar, T. Lebouvier, B. Lavina, L. Gouveia, Y. Sun, E. Raschperger, M. Rasanen, Y. Zarb, N. Mochizuki, A. Keller, U. Lendahl and C. Betsholtz (2018). "A molecular atlas of cell types and zonation in the brain vasculature." Nature **554**(7693): 475-480.
Venkat, P., M. Chopp, A. Zacharek, C. Cui, L. Zhang, Q. Li, M. Lu, T. Zhang, A. Liu and J. Chen (2017). "White matter damage and glymphatic dysfunction in a model of vascular dementia in rats with no prior vascular pathologies." Neurobiol Aging **50**: 96-106.

Verbeek, E., M. E. Meuwissen, F. W. Verheijen, P. P. Govaert, D. J. Licht, D. S. Kuo, C. J. Poulton, R. Schot, M. H. Lequin, J. Dudink, D. J. Halley, R. I. de Coo, J. C. den Hollander, R. Oegema, D. B. Gould and G. M. Mancini (2012). "COL4A2 mutation associated with familial porencephaly and small-vessel disease." European Journal of Human Genetics **20**(8): 844-851.
Verbeek, M. M., R. M. de Waal, J. J. Schipper and W. E. Van Nostrand (1997). "Rapid degeneration of cultured human brain pericytes by amyloid beta protein." J Neurochem **68**(3): 1135-1141.
Verdura, E., D. Herve, F. Bergametti, C. Jacquet, T. Morvan, C. Prieto-Morin, A. Mackowiak, E. Manchon, H. Hosseini, C. Cordonnier, I. Girard-Buttaz, S. Rosenstingl, C. Hagel, G. Kuhlenbaumer, E. Leca-Radu, D. Goux, L. Fleming, T. Van Agtmael, H. Chabriat, F. Chapon and E. Tournier-Lasserve (2016). "Disruption of a miR-29 binding site leading to COL4A1 upregulation causes pontine autosomal dominant microangiopathy with leukoencephalopathy." Ann Neurol **80**(5): 741-753.
Verhaaren, B. F., S. Debette, J. C. Bis, J. A. Smith, M. K. Ikram, H. H. Adams, A. H. Beecham, K. B. Rajan, L. M. Lopez, S. Barral, M. A. van Buchem, J. van der Grond, A. V. Smith, K. Hegenscheid, N. T. Aggarwal, M. de Andrade, E. J. Atkinson, M. Beekman, A. S. Beiser, S. H. Blanton, E. Boerwinkle, A. M. Brickman, R. N. Bryan, G. Chauhan, C. P. Chen, V. Chouraki, A. J. de Craen, F. Crivello, I. J. Deary, J. Deelen, P. L. De Jager, C. Dufouil, M. S. Elkind, D. A. Evans, P. Freudenberger, R. F. Gottesman, V. Guethnason, M. Habes, S. R. Heckbert, G. Heiss, S. Hilal, E. Hofer, A. Hofman, C. A. Ibrahim-Verbaas, D. S. Knopman, C. E. Lewis, J. Liao, D. C. Liewald, M. Luciano, A. van der Lugt, O. O. Martinez, R. Mayeux, B. Mazoyer, M. A. Nalls, M. Nauck, W. J. Niessen, B. A. Oostra, B. M. Psaty, K. M. Rice, J. I. Rotter, B. von Sarnowski, H. Schmidt, P. J. Schreiner, M. Schuur, S. S. Sidney, S. Sigurdsson, P. E. Slagboom, D. J. Stott, J. C. van Swieten, A. Teumer, A. M. Toglhofer, M. Traylor, S. Trompet, S. T. Turner, C. Tzourio, H. W. Uh, A. G. Uitterlinden, M. W. Vernooij, J. J. Wang, T. Y. Wong, J. M. Wardlaw, B. G. Windham, K. Wittfeld, C. Wolf, C. B. Wright, Q. Yang, W. Zhao, A. Zijdenbos, J. W. Jukema, R. L. Sacco, S. L. Kardia, P. Amouyel, T. H. Mosley, W. T. Longstreth, Jr., C. C. DeCarli, C. M. van Duijn, R. Schmidt, L. J. Launer, H. J. Grabe, S. S. Seshadri, M. A. Ikram and M. Fornage (2015). "Multi-Ethnic Genome-Wide Association Study of Cerebral White Matter Hyperintensities on MRI." Circ Cardiovasc Genet.
Vermeer, S. E., W. T. Longstreth, Jr. and P. J. Koudstaal (2007). "Silent brain infarcts: a systematic review." Lancet Neurol **6**(7): 611-619.
Vermeer, S. E., N. D. Prins, T. den Heijer, A. Hofman, P. J. Koudstaal and M. M. Breteler (2003). "Silent brain infarcts and the risk of dementia and cognitive decline." N Engl J Med **348**(13): 1215-1222.
Vermeer, S. E., E. J. van Dijk, P. J. Koudstaal, M. Oudkerk, A. Hofman, R. Clarke and M. M. Breteler (2002). "Homocysteine, silent brain infarcts, and white matter lesions: The Rotterdam Scan Study." Ann Neurol **51**(3): 285-289.
Vernooij, M. W., A. van der Lugt, M. A. Ikram, P. A. Wielopolski, W. J. Niessen, A. Hofman, G. P. Krestin and M. M. Breteler (2008). "Prevalence and risk factors of cerebral microbleeds: the Rotterdam Scan Study." Neurology **70**(14): 1208-1214.

Vinters, H. V. (1987). "Cerebral amyloid angiopathy. A critical review." Stroke **18**(2): 311-324.
Vinters, H. V. and J. J. Gilbert (1983). "Cerebral amyloid angiopathy: incidence and complications in the aging brain. II. The distribution of amyloid vascular changes." Stroke **14**(6): 924-928.
Vinters, H. V., C. Zarow, E. Borys, J. D. Whitman, S. Tung, W. G. Ellis, L. Zheng and H. C. Chui (2018). "Review: Vascular dementia: clinicopathologic and genetic considerations." Neuropathol Appl Neurobiol **44**(3): 247-266.
Vuksanovic, V., R. T. Staff, T. Ahearn, A. D. Murray and C. M. Wischik (2019). "Cortical Thickness and Surface Area Networks in Healthy Aging, Alzheimer's Disease and Behavioral Variant Fronto-Temporal Dementia." Int J Neural Syst **29**(6): 1850055.
Wahlund, L. O., F. Barkhof, F. Fazekas, L. Bronge, M. Augustin, M. Sjogren, A. Wallin, H. Ader, D. Leys, L. Pantoni, F. Pasquier, T. Erkinjuntti, P. Scheltens and C. European Task Force on Age-Related White Matter (2001). "A new rating scale for age-related white matter changes applicable to MRI and CT." Stroke **32**(6): 1318-1322.
Walhout, R., H. J. Westeneng, E. Verstraete, J. Hendrikse, J. H. Veldink, M. P. van den Heuvel and L. H. van den Berg (2015). "Cortical thickness in ALS: towards a marker for upper motor neuron involvement." J Neurol Neurosurg Psychiatry **86**(3): 288-294.
Waller, R., L. Baxter, D. J. Fillingham, S. Coelho, J. M. Pozo, M. Mozumder, A. F. Frangi, P. G. Ince, J. E. Simpson and J. R. Highley (2019). "Iba-1-/CD68+ microglia are a prominent feature of age-associated deep subcortical white matter lesions." PLoS One **14**(1): e0210888.
Wang, F., J. Flanagan, N. Su, L. C. Wang, S. Bui, A. Nielson, X. Wu, H. T. Vo, X. J. Ma and Y. Luo (2012). "RNAscope: a novel in situ RNA analysis platform for formalin-fixed, paraffin-embedded tissues." J Mol Diagn **14**(1): 22-29.
Wang, J., D. W. Dickson, J. Q. Trojanowski and V. M. Lee (1999). "The levels of soluble versus insoluble brain Abeta distinguish Alzheimer's disease from normal and pathologic aging." Exp Neurol **158**(2): 328-337.
Wang, M., F. Ding, S. Deng, X. Guo, W. Wang, J. J. Iliff and M. Nedergaard (2017). "Focal Solute Trapping and Global Glymphatic Pathway Impairment in a Murine Model of Multiple Microinfarcts." J Neurosci **37**(11): 2870-2877.
Wardlaw, J., P. M. W. Bath, F. Doubal, A. Heye, N. Sprigg, L. J. Woodhouse, G. Blair, J. Appleton, V. Cvoro, T. England, A. Hassan, D. John Werring, A. Montgomery and L.-T. Investigators (2020). "Protocol: The Lacunar Intervention Trial 2 (LACI-2). A trial of two repurposed licenced drugs to prevent progression of cerebral small vessel disease." Eur Stroke J **5**(3): 297-308.
Wardlaw, J. M. (2008). "What is a lacune?" Stroke **39**(11): 2921-2922.
Wardlaw, J. M. (2011). "Post-mortem MR brain imaging comparison with macro- and histopathology: useful, important and underused." Cerebrovasc Dis **31**(5): 518-519.
Wardlaw, J. M., M. Allerhand, F. N. Doubal, M. Valdes Hernandez, Z. Morris, A. J. Gow, M. Bastin, J. M. Starr, M. S. Dennis and I. J. Deary (2014). "Vascular risk

factors, large-artery atheroma, and brain white matter hyperintensities." Neurology **82**(15): 1331-1338.
Wardlaw, J. M., M. E. Bastin, M. C. Valdes Hernandez, S. M. Maniega, N. A. Royle, Z. Morris, J. D. Clayden, E. M. Sandeman, E. Eadie, C. Murray, J. M. Starr and I. J. Deary (2011). "Brain aging, cognition in youth and old age and vascular disease in the Lothian Birth Cohort 1936: rationale, design and methodology of the imaging protocol." Int J Stroke **6**(6): 547-559.
Wardlaw, J. M., H. Benveniste, M. Nedergaard, B. V. Zlokovic, H. Mestre, H. Lee, F. N. Doubal, R. Brown, J. Ramirez, B. J. MacIntosh, A. Tannenbaum, L. Ballerini, R. L. Rungta, D. Boido, M. Sweeney, A. Montagne, S. Charpak, A. Joutel, K. J. Smith, S. E. Black and D. colleagues from the Fondation Leducq Transatlantic Network of Excellence on the Role of the Perivascular Space in Cerebral Small Vessel (2020). "Perivascular spaces in the brain: anatomy, physiology and pathology." Nat Rev Neurol **16**(3): 137-153.
Wardlaw, J. M., F. M. Chappell, M. D. C. Valdes Hernandez, S. D. J. Makin, J. Staals, K. Shuler, M. J. Thrippleton, P. A. Armitage, S. Munoz-Maniega, A. K. Heye, E. Sakka and M. S. Dennis (2017). "White matter hyperintensity reduction and outcomes after minor stroke." Neurology **89**(10): 1003-1010.
Wardlaw, J. M., S. Debette, H. Jokinen, F. E. De Leeuw, L. Pantoni, H. Chabriat, J. Staals, F. Doubal, S. Rudilosso, S. Eppinger, S. Schilling, R. Ornello, C. Enzinger, C. Cordonnier, M. Taylor-Rowan and A. G. Lindgren (2021). "ESO Guideline on covert cerebral small vessel disease." Eur Stroke J **6**(2): IV.
Wardlaw, J. M., M. S. Dennis, C. P. Warlow and P. A. Sandercock (2001). "Imaging appearance of the symptomatic perforating artery in patients with lacunar infarction: occlusion or other vascular pathology?" Ann Neurol **50**(2): 208-215.
Wardlaw, J. M., F. Doubal, P. Armitage, F. Chappell, T. Carpenter, S. M. Maniega, A. Farrall, C. Sudlow, M. Dennis and B. Dhillon (2009). "Lacunar stroke is associated with diffuse blood-brain barrier dysfunction." Ann Neurol **65**(2): 194-202.
Wardlaw, J. M., F. Doubal, P. Armitage, F. Chappell, T. Carpenter, S. Munoz Maniega, A. Farrall, C. Sudlow, M. Dennis and B. Dhillon (2009). "Lacunar stroke is associated with diffuse blood-brain barrier dysfunction." Ann Neurol **65**(2): 194-202.
Wardlaw, J. M., F. N. Doubal, M. Valdes-Hernandez, X. Wang, F. M. Chappell, K. Shuler, P. A. Armitage, T. C. Carpenter and M. S. Dennis (2013). "Blood-brain barrier permeability and long-term clinical and imaging outcomes in cerebral small vessel disease." Stroke **44**(2): 525-527.
Wardlaw, J. M., S. J. Makin, M. C. Valdés Hernández, P. A. Armitage, A. K. Heye, F. M. Chappell, S. Muñoz-Maniega, E. Sakka, K. Shuler, M. S. Dennis and M. J. Thrippleton (2017). "Blood-brain barrier failure as a core mechanism in cerebral small vessel disease and dementia: evidence from a cohort study." Alzheimer's & Dementia **13**: 634-643.
Wardlaw JM, M. S., Valdés Hernández MC, Armitage PA, Heye AK, Chappell FM, Muñoz-Maniega S, Sakka E, Shuler K, Dennis MS, Thrippleton MJ (2017). "Blood-brain barrier failure as a core mechanism in cerebral small vessel disease and dementia: evidence from a cohort study." Alzheimer's & Dementia **13**: 634-643.

Wardlaw, J. M., P. A. Sandercock, M. S. Dennis and J. Starr (2003). "Is breakdown of the blood-brain barrier responsible for lacunar stroke, leukoaraiosis, and dementia?" Stroke **34**(3): 806-812.
Wardlaw, J. M. and R. Sellar (1994). "A simple practical classification of cerebral infarcts on CT and its interobserver reliability." AJNR Am J Neuroradiol **15**(10): 1933-1939.
Wardlaw, J. M., C. Smith and M. Dichgans (2013). "Mechanisms of sporadic cerebral small vessel disease: insights from neuroimaging." Lancet Neurology **12**(5): 483-497.
Wardlaw, J. M., C. Smith and M. Dichgans (2019). "Small vessel disease: mechanisms and clinical implications." Lancet Neurol **18**(7): 684-696.
Wardlaw, J. M., E. E. Smith, G. J. Biessels, C. Cordonnier, F. Fazekas, R. Frayne, R. I. Lindley, J. T. O'Brien, F. Barkhof, O. R. Benavente, S. Black, C. Brayne, M. Breteler, H. Chabriat, C. DeCarli, F.-E. de Leeuw, F. Doubal, M. Duering, N. Fox, S. Greenberg, V. Hachinski, I. Kilimann, V. Mok, R. van Oostenbrugge, L. Pantoni, O. Speck, B. C. Stephan, S. Teipel, A. Viswanathan, D. Werring, C. Chen, C. Smith, M. van Buchem, B. Norrving, P. B. Gorelick and M. Dichgans (2013). "Neuroimaging standards for research into small vessel disease and its contribution to ageing and neurodegeneration: a united approach." Lancet Neurol **12**(8): 822-838.
Wardlaw, J. M., E. E. Smith, G. J. Biessels, C. Cordonnier, F. Fazekas, R. Frayne, R. I. Lindley, J. T. O'Brien, F. Barkhof, O. R. Benavente, S. E. Black, C. Brayne, M. Breteler, H. Chabriat, C. Decarli, F. E. de Leeuw, F. Doubal, M. Duering, N. C. Fox, S. Greenberg, V. Hachinski, I. Kilimann, V. Mok, R. Oostenbrugge, L. Pantoni, O. Speck, B. C. Stephan, S. Teipel, A. Viswanathan, D. Werring, C. Chen, C. Smith, M. van Buchem, B. Norrving, P. B. Gorelick, M. Dichgans and S. T. f. R. V. c. o. nEuroimaging (2013). "Neuroimaging standards for research into small vessel disease and its contribution to ageing and neurodegeneration." Lancet Neurol **12**(8): 822-838.
Wardlaw, J. M., M. C. Valdes Hernandez and S. Munoz Maniega (2015). "What are white matter hyperintensities made of? Relevance to vascular cognitive impairment." J Am Heart Assoc **4**: e001140.
Wardlaw, J. M., M. C. Valdes Hernandez and S. Munoz-Maniega (2015). "What are white matter hyperintensities made of? Relevance to vascular cognitive impairment." J Am Heart Assoc **4**(6): 001140.
Wasserman, J. K. and L. C. Schlichter (2007). "Minocycline protects the blood-brain barrier and reduces edema following intracerebral hemorrhage in the rat." Exp Neurol **207**(2): 227-237.
Weber, T., R. J. Seitz, U. G. Liebert, E. Gallasch and W. Wechsler (1985). "Affinity cytochemistry of vascular endothelia in brain tumors by biotinylated Ulex europaeus type I lectin (UEA I)." Acta Neuropathol **67**(1-2): 128-135.
Weinhard, L., P. d'Errico and T. L. Tay (2018). "Headmasters: microglial regulation of learning and memory in health and disease." AIMS Molecular Science **5**: 63-89.
Weller, R. O., E. Djuanda, H. Y. Yow and R. O. Carare (2009). "Lymphatic drainage of the brain and the pathophysiology of neurological disease." Acta Neuropathol **117**(1): 1-14.

Weller, R. O., M. Subash, S. D. Preston, I. Mazanti and R. O. Carare (2008). "Perivascular drainage of amyloid-beta peptides from the brain and its failure in cerebral amyloid angiopathy and Alzheimer's disease." Brain Pathol **18**(2): 253-266.
Wharton, S. B., J. E. Simpson, C. Brayne and P. G. Ince (2015). "Age-Associated White Matter Lesions: The MRC Cognitive Function and Ageing Study." Brain Pathol **25**(1): 35-43.
White, K., P. Yang, L. Li, A. Farshori, A. E. Medina and H. R. Zielke (2018). "Effect of Postmortem Interval and Years in Storage on RNA Quality of Tissue at a Repository of the NIH NeuroBioBank." Biopreserv Biobank **16**(2): 148-157.
Wilkins, A., S. Chandran and A. Compston (2001). "A role for oligodendrocyte-derived IGF-1 in trophic support of cortical neurons." Glia **36**(1): 48-57.
Wilson, H., F. Niccolini, C. Pellicano and M. Politis (2019). "Cortical thinning across Parkinson's disease stages and clinical correlates." J Neurol Sci **398**: 31-38.
Winkler, E. A., R. D. Bell and B. V. Zlokovic (2011). "Central nervous system pericytes in health and disease." Nat Neurosci **14**(11): 1398-1405.
Wiseman, S. J., M. E. Bastin, C. L. Jardine, G. Barclay, I. F. Hamilton, E. Sandeman, D. Hunt, E. N. Amft, S. Thomson, J. F. Belch, S. H. Ralston and J. M. Wardlaw (2016). "Cerebral Small Vessel Disease Burden Is Increased in Systemic Lupus Erythematosus." Stroke **47**(11): 2722-2728.
Wong, A., A. Y. Lau, E. Lo, M. Tang, Z. Wang, W. Liu, N. Tanner, N. Chau, L. Law, L. Shi, W. C. Chu, J. Yang, Y. Y. Xiong, B. Y. Lam, L. Au, A. Y. Chan, Y. Soo, T. W. Leung, L. K. Wong, L. C. Lam and V. C. Mok (2016). "Relations between Recent Past Leisure Activities with Risks of Dementia and Cognitive Functions after Stroke." PLoS One **11**(7): e0159952.
Wong, A. D., M. Ye, A. F. Levy, J. D. Rothstein, D. E. Bergles and P. C. Searson (2013). "The blood-brain barrier: an engineering perspective." Front Neuroeng **6**: 7.
Wu, C., F. Ivars, P. Anderson, R. Hallmann, D. Vestweber, P. Nilsson, H. Robenek, K. Tryggvason, J. Song, E. Korpos, K. Loser, S. Beissert, E. Georges-Labouesse and L. M. Sorokin (2009). "Endothelial basement membrane laminin alpha5 selectively inhibits T lymphocyte extravasation into the brain." Nat Med **15**(5): 519-527.
Wuerfel, J., M. Haertle, H. Waiczies, E. Tysiak, I. Bechmann, K. D. Wernecke, F. Zipp and F. Paul (2008). "Perivascular spaces--MRI marker of inflammatory activity in the brain?" Brain **131**(Pt 9): 2332-2340.
Xie, L., H. Kang, Q. Xu, M. J. Chen, Y. Liao, M. Thiyagarajan, J. O'Donnell, D. J. Christensen, C. Nicholson, J. J. Iliff, T. Takano, R. Deane and M. Nedergaard (2013). "Sleep drives metabolite clearance from the adult brain." Science **342**(6156): 373-377.
Xiong, Y., A. Wong, M. Cavalieri, R. Schmidt, W. W. Chu, X. Liu, K. S. Wong and V. Mok (2014). "Prestroke statins, progression of white matter hyperintensities, and cognitive decline in stroke patients with confluent white matter hyperintensities." Neurotherapeutics **11**(3): 606-611.
Xu, L., A. Nirwane and Y. Yao (2019). "Basement membrane and blood-brain barrier." Stroke Vasc Neurol **4**(2): 78-82.

Yamori, Y., R. Horie, H. Handa, M. Sato and M. Fukase (1976). "Pathogenetic similarity of strokes in stroke-prone spontaneously hypertensive rats and humans." Stroke **7**(1): 46-53.
Yamori, Y., R. Horie, M. Sato, S. Sasagawa and K. Okamoto (1975). "Experimental studies on the pathogenesis and prophylaxis of stroke in stroke-prone spontaneously hypertensive rats (SHR).(1) Quantitative estimation of cerebrovascular permeability." Jpn Circ J **39**(5): 611-615.
Yang, Y. G., T. Lindahl and D. E. Barnes (2007). "Trex1 exonuclease degrades ssDNA to prevent chronic checkpoint activation and autoimmune disease." Cell **131**(5): 873-886.
Young, V. G., G. M. Halliday and J. J. Kril (2008). "Neuropathologic correlates of white matter hyperintensities." Neurology **71**(11): 804-811.
Yu, L., R. J. Dawe, A. S. Buchman, P. A. Boyle, J. A. Schneider, K. Arfanakis and D. A. Bennett (2017). "Ex vivo MRI transverse relaxation in community based older persons with and without Alzheimer's dementia." Behav Brain Res **322**(Pt B): 233-240.
Yuen, T. J., J. C. Silbereis, A. Griveau, S. M. Chang, R. Daneman, S. P. J. Fancy, H. Zahed, E. Maltepe and D. H. Rowitch (2014). "Oligodendrocyte-encoded HIF function couples postnatal myelination and white matter angiogenesis." Cell **158**(2): 383-396.
Zagaglia, S., C. Selch, J. R. Nisevic, D. Mei, Z. Michalak, L. Hernandez-Hernandez, S. Krithika, K. Vezyroglou, S. M. Varadkar, A. Pepler, S. Biskup, M. Leao, J. Gartner, A. Merkenschlager, M. Jaksch, R. S. Moller, E. Gardella, B. S. Kristiansen, L. K. Hansen, M. S. Vari, K. L. Helbig, S. Desai, C. L. Smith-Hicks, N. Hino-Fukuyo, T. Talvik, R. Laugesaar, P. Ilves, K. Ounap, I. Korber, T. Hartlieb, M. Kudernatsch, P. Winkler, M. Schimmel, A. Hasse, M. Knuf, J. Heinemeyer, C. Makowski, S. Ghedia, G. M. Subramanian, P. Striano, R. H. Thomas, C. Micallef, M. Thom, D. J. Werring, G. J. Kluger, J. H. Cross, R. Guerrini, S. Balestrini and S. M. Sisodiya (2018). "Neurologic phenotypes associated with COL4A1/2 mutations: Expanding the spectrum of disease." Neurology **91**(22): e2078-e2088.
Zaitout, Z., C. Romanowski, K. Karunasaagarar, D. Connolly and R. Batty (2014). "A review of pathologies associated with high T1W signal intensity in the basal ganglia on Magnetic Resonance Imaging." Pol J Radiol **79**: 126-130.
Zbesko, J. C., T. V. Nguyen, T. Yang, J. B. Frye, O. Hussain, M. Hayes, A. Chung, W. A. Day, K. Stepanovic, M. Krumberger, J. Mona, F. M. Longo and K. P. Doyle (2018). "Glial scars are permeable to the neurotoxic environment of chronic stroke infarcts." Neurobiol Dis **112**: 63-78.
Zhang, C. E., S. M. Wong, H. J. van de Haar, J. Staals, J. F. Jansen, C. R. Jeukens, P. A. Hofman, R. J. van Oostenbrugge and W. H. Backes (2017). "Blood-brain barrier leakage is more widespread in patients with cerebral small vessel disease." Neurology **88**(5): 426-432.
Zhang, E. T., C. B. Inman and R. O. Weller (1990). "Interrelationships of the pia mater and the perivascular (Virchow-Robin) spaces in the human cerebrum." J Anat **170**: 111-123.

Zhang, J., A. F. Defelice, J. P. Hanig and T. Colatsky (2010). "Biomarkers of endothelial cell activation serve as potential surrogate markers for drug-induced vascular injury." Toxicol Pathol **38**(6): 856-871.
Zhang, Y., K. Chen, S. A. Sloan, M. L. Bennett, A. R. Scholze, S. O'Keeffe, H. P. Phatnani, P. Guarnieri, C. Caneda, N. Ruderisch, S. Deng, S. A. Liddelow, C. Zhang, R. Daneman, T. Maniatis, B. A. Barres and J. Q. Wu (2014). "An RNA-sequencing transcriptome and splicing database of glia, neurons, and vascular cells of the cerebral cortex." J Neurosci **34**(36): 11929-11947.
Zhu, Y. C., C. Tzourio, A. Soumare, B. Mazoyer, C. Dufouil and H. Chabriat (2010). "Severity of dilated Virchow-Robin spaces is associated with age, blood pressure, and MRI markers of small vessel disease: a population-based study." Stroke **41**(11): 2483-2490.